The University Of Sheffield.

Debonding failure of RC beams retrofitted with Near Surface Mounted FRP Reinforcement

A thesis presented for the degree of

Doctor of Philosophy in Civil and Structural Engineering

at The University of Sheffield

by

NGUYEN VAN HIEN

April 2016

This page is left intentionally blank

ABSTRACT

Near Surface Mounted (NSM) Fibre Reinforced Polymer (FRP) reinforcement is an effective rehabilitation solution to strengthen RC structures, as it can enable higher load carrying capacity and ductility than conventional Externally Bonded Reinforcement (EBR). However, the performance of elements strengthened in flexure is still controlled by bond failure between the NSMR system and the concrete substrate. This can reduce both the effectiveness and safety of NSMR systems and should be accounted for in design. The development of high stresses due to the abrupt termination of NSMR is the main cause for the dominant end debonding failure. This type of failure is not well understood and needs to be examined in detail. The aim of this work is to achieve a comprehensive understanding of bond behaviour and debonding mechanisms of the NSMR in flexural strengthening applications both experimentally and theoretically so as to enable the development of practical and reliable design methods for RC beams strengthened in flexure with NSMR.

An analytical elastic model is developed to facilitate a fundamental understanding of the distribution of bond stresses along the NSMR, especially in the region around the termination point. The model identifies differences of stress states between EBR and NSMR. However, since it is based on elastic analysis and continuum mechanics, it is unable to represent bond behaviour of NSMR at high load levels. This issue can only be examined in detail via specially developed experimental work.

A total of ten RC beams, including two control beams and eight beams strengthened in flexure with CFRP and BFRP bars or strips, are tested to examine the overall structural behaviour of RC beams retrofitted with NSMR of different embedment lengths. Tested beams are heavily instrumented to examine the influence of yield penetration along the internal steel bars on the bond behaviour of the NSM reinforcement within the shear spans and the resulting debonding mechanisms. NSMR enhanced flexural capacity by up to 50% and the dominant failure mode was end debonding after yielding. The experimental results show that yielding of the steel reinforcement penetrates in the shear span much further than predicted through classic section analysis, reaching near or even beyond the termination point. The experimental evidence is used to develop a new simple, yet effective methodology to estimate the minimum embedment length. The new design method is validated against an extensive database collected from literature and is found to provide more accurate and reliable results.

ACKNOWLEDGEMENTS

I acknowledge the financial support of the Ministry of Education and Training and the University of Sheffield for the research programme.

I would like to express my gratitude and deep appreciation for the help, guidance and endless support of **Professor Kypros Pilakoutas**. Your understanding and kindness helped me to stand up and fight for hopes during my hard time.

I would like also to thank **Dr Maurizio Guadagnini** for his patient and dedicated supervision and valuable guidance of my work.

Special thanks go to

Laboratory staffs: Shane, Paul, Chris and Jonathan, Kieran, Dave. Their expertise and experience really make a big difference.

All friends of CEE group. I am highly appreciated useful discussions and your un-conditional supports, friendships, especially great supports from Harris to finalise the thesis.

Specialists and staffs of Royal Hallamshire hospital. Your great expertise and dedication gave me a great chance to win the battle of life.

My parents. Great lessons of your great devotion for whole family during hard time of Vietnam war and post-war inspired me and gave me a robust motivation during my hard time. I wish you keep watching me and are proud of your son.

My wife, Mai Khoi and Huy Khiem and members of great Family

Finally, my deepest thanks to my wife, Diem Chau and children Mai Khoi and Huy Khiem and members of the Great family for their encouragement, understanding and patience over the years.

.

Table of contents

List of abbreviations

BFRP *- Basalt Fiber Reinforced Polymer*

CFRP*- Carbon Fiber Reinforced Polymer*

EBR *- Externally Bonded Reinforcement*

FRP *- Fiber Reinforced Polymer*

IC *- Intermediate Crack*

NSMR *- Near Surface Mounted Reinforcement*

RC *- Reinforced Concrete*

List of figures

List of Tables

Chapter 1

INTRODUCTION

1.1 Background

Near Surface Mounted Reinforcement (NSMR) is a strengthening technique for which Fibre Reinforced Polymer (FRP) bars or strips are inserted into pre-cut grooves on the concrete cover of structures (Figure 1-1). In recent years, it has emerged as a valid alternative to externally bonded FRP reinforcement (EBR) which bonds plates directly onto the concrete surface.

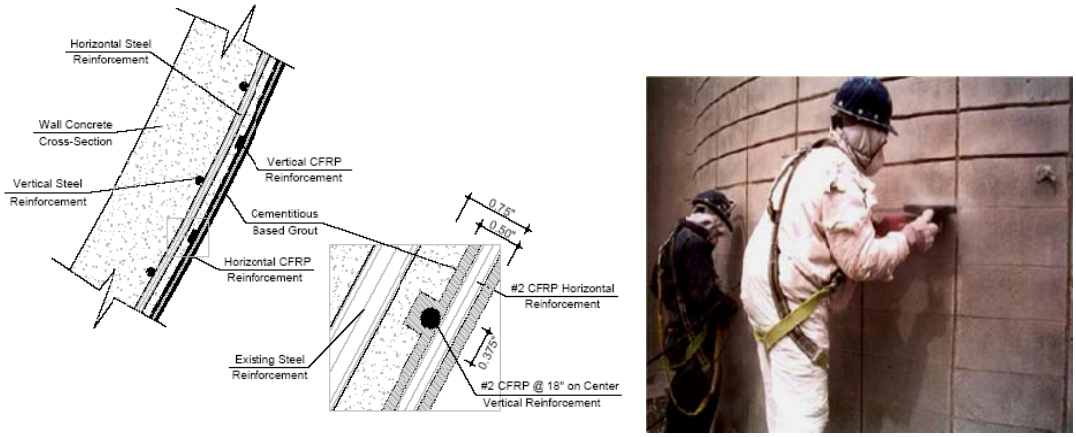

a) **b)**

Figure 1-1 Near surface mounted reinforcement application for silo strengthening (Andrea Prota 2003)

The use of NSM FRP reinforcement has been adopted by the construction industry for strengthening of RC structures (Alkhrdaji and Nanni 2000; Irwin and Rahman 2002; Andrea Prota 2003; Co-Force America 2005; Tumialan 2007) and initial design guidelines have already been published (ACI-440-Commitee 2008; Cement and Concrete Industry Publiccation 2012). Bond tests demonstrate the superior bond behaviour of NSMR to that of EBR (De Lorenzis and Antonio 2001; De Lorenzis and Nanni 2002; De Lorenzis et al. 2002; Seracino et al. 2007; Kotynia 2010; Bilotta et al. 2011), both in terms of bond performance and post-peak behaviour. NSMR can help develop high bond strength even with short

embedment lengths and was found to outperform EBR in terms of debonding load in flexural tests (Quattlebaum et al. 2005; Cruz et al. 2006). The superior performance of the NSMR over EBR can be explained by the fact that the embedment of NSMR in the concrete substrate provides a higher ratio of bond area to cross section area and improves peeling resistance. The use of NSMR can also reduce the risk of vandalism and provide extra UV and fire protection.

Failure modes of beams strengthened with NSMR are similar to those observed in beams strengthened with EBR, including flexural failure, concrete cover separation, intermediate crack-induced debonding (Barros and Fortes 2005; Quattlebaum et al. 2005; Cruz et al. 2006; Teng et al. 2006). Similar to EBR, the presence of epoxy bonded FRP materials can change the failure mode from ductile to brittle, due to debonding caused by high bond stress concentration at the termination points of FRP. This causes sudden concrete cover separation and debonding before the full flexural capacity of the composite member is reached. As a result, the performance of structures strengthened with NSMR is limited by the bond developed between the FRP and the concrete substrate. Thus, understanding bond behaviour of the NSMR, both theoretically and experimentally is a crucial aspect that needs to be examined in detail so as to develop practical and reliable design guidelines.

Analytical solutions can provide a fundamental understanding of bond behaviour of NSMR in strengthened RC structures, but are limited by their inability to accurately model sources of singularity and nonlinearity that govern concrete behaviour, such as cracks and interaction of steel reinforcement and FRP (Smith 2006, Hassan 2005, Hien Nguyen 2009). Experimental work is therefore needed to understand the real structural behaviour of NSMR and help develop more accurate analytical models.

Bond behaviour of NSMR is generally examined mostly through small scale bond tests and only few studies have been conducted on large scale flexural tests. Bond tests are generally simple to undertake, but can reveal bond behaviour only at the local level. The absence of the true mechanisms that typically develop in flexural elements, such as bending effects, cracks and the interaction between flexural steel rebars and the NSMR system (particularly after yielding of the steel reinforcement), limits the use of bond test results when characterising the real stress states and failure mechanisms of NSMR in real structures (Teng et al. 2006). In addition, large scatter in bond strength results, partly due to lack of standard tests (De Lorenzis and Nanni 2002; De Lorenzis et al. 2002; Cruz et al. 2006; Teng et al. 2006; Novidis et al. 2007; Kotynia 2010), has led to unreliable design guidelines.

Beam tests, though more demanding, can provide a more accurate representation of bond behaviour and debonding mechanism of NSMR in real flexural strengthening applications.

However, the current understanding on bond behaviour and the debonding mechanism of NSMR in beam tests is limited due to lack of published data, as well as insufficient experimental details. For example, the lack of data on the distribution of strains along the entire length of both steel and FRP reinforcement prevents the understanding of the interaction between the internal and the external reinforcement around the termination points, as well as the impact of the yielding penetration of steel reinforcement in shear spans on the end debonding failure of NSMR. Although the likely failure modes of NSMR have been identified, the existing knowledge on the NSM FRP method is still very limited compared to that already exist for the EBR method. The designers are still not offered an efficient design method that would cover all possible failure modes that the strengthened RC elements need to be guarded against and this is a significant barrier for the wider adoption of the NSMR method.

1.2 Aims and objectives

The main aim of this research programme is to achieve a comprehensive understanding of bond behaviour and debonding mechanisms of the NSMR in flexural strengthening applications, both experimentally and theoretically, so as to enable the development of practical and reliable design methods for RC beams strengthened in flexure with NSMR. For this purpose, the following objectives have been identified:

- Derive an analytical method to gain fundamental understanding of bond stress concentration along the NSMR, especially in the vicinity of the termination point.
- Undertake an extensive experimental study to (a) characterise the mechanical properties of the materials that can be used in the development of numerical and analytical models and (b) to examine the overall structural performance of pre-damaged RC beams strengthened with NSMR. Examine strain and bond stress distributions along the NSMR and the steel reinforcement to evaluate effects of interaction between the steel reinforcement and the NSMR; shear, crack pattern.
- Propose a simple, yet efficient, design method to estimate the required embedment length of NSMR to avoid end debonding.
- Validate the proposed design method against an extensive database collected from literature.
- Provide step-by-step guidance and design examples that can be used by researchers and consulting engineers to design the structures flexurally strengthened with NSM FRP reinforcement.

1.3 Thesis layout

The thesis is organised in six chapters. Chapters 2, 3, 4 and 5 are based on four journal papers (to be submitted). A brief overview of each chapter is given in the following.

Chapter 1 introduces the use of NSM FRP reinforcement for flexural strengthening applications and discusses problems that need further research. In this chapter, the main aims and objectives of this research programme are presented along with a brief discussion on the methodology implemented.

Chapter 2 (paper was published in FRPRCS9 proceeding, 2009. Extended version will be submitted to *Composites Part B: Engineering*, Elsevier)
The paper presents the derivation of a closed-form analytical solution to compute the interfacial bond stress distribution between FRP, adhesive and concrete. The effect of various parameters is discussed including the area and yield strength of steel; Young's modulus of FRP; adhesive and its thickness; concrete matrix; thickness, height, embedded length and number of FRP strips; beam geometry and loading condition. Special attention is paid to the stress concentration in the vicinity of the cut-off point where both vertical and longitudinal shear stresses reach their maximum values.

Chapter 3 (paper to be submitted to *Composites Part B: Engineering*, Elsevier)
The paper presents the experimental work undertaken and it is divided in two main parts: material testing and beam testing. In the first testing series, materials used in the beam tests: concrete, structural adhesive, steel reinforcement, CFRP and BFRP are tested to obtain their mechanical properties. In the second test series sixteen tests are carried out on eight beams, strengthened in flexure by CFRP and BFRP. A brief description of test set-up, specimen preparation, instrumentation and testing is included. The structural behaviour of tested beams is presented and discussed in detail. Special attention is paid on the analysis of strain and bond stress distribution along the NSMR and the steel reinforcement, in the region near the termination point.

Chapter 4 (paper prepared for the Journal of Composites in Construction, ASCE)
The paper presents experimental evidence of deep yielding penetration of the steel reinforcement towards the termination points at high load levels and discusses its impact on bond behaviour and end debonding failure mechanisms.

Chapter 5 (paper prepared for the Journal of Composites for Construction, ASCE)
In this chapter, a new design method based on experimental findings is presented along with validation against an extensive database collected from literature.

Chapter 6, general conclusions from the study are drawn, together with recommendations for further research in the area of study.

Chapter 2

BOND STRESS CONCENTRATION: AN ANALYTICAL MODEL

Hien V. Nguyen[1], Maurizio Guadagnini[1], Kypros Pilakoutas[1], Nam V. Le[2]
[1]Department of Civil and Structural Engineering
The University of Sheffield, UK. Email: n.hien@sheff.ac.uk
[2] Department of Civil and Structural Engineering
HCMC University of Technology, Vietnam National University, Vietnam

(Paper published in FRPRCS9 Proceeding, Sydney 2009)

2.1 Introduction

The strengthening of RC structures using near surface mounted Reinforcement (NSMR) has emerged as a very attractive and promising technique. Previous experimental results indicate that this technique can enhance significantly the bond performance between FRP and concrete substrate, delay premature debonding and improve the load carrying capacity of RC concrete structures [1, 2]. Despite the fact that NSMR exhibits a better bond behaviour than plate bonding, debonding remains a crucial issue that needs to be further examined. Existing models developed to predict debonding failures of NSMR FRPs ignore the effects of axial deformation of the beam and flexural deformation of FRP strips [3]. These simplifications yield rather conservative predictions when the flexural effect and the flexural rigidity FRP bars/strips are significant. This paper proposes a new close-form analytical solution to compute the interfacial stresses between FRP, adhesive and concrete materials in beams retrofitted with NSMR. In this model, a 3-D state of stress is considered including normal stress, shear stress in both longitudinal and vertical directions. The influence of various parameters is discussed including the area of steel,

Young modulus of FRP, adhesive and concrete, number, thickness and height of FRP strips, the thickness of adhesive, yield strength of steel, loading condition, geometry of a beam and the embedded length of FRP strips. Special attention is paid to the stress concentration in the vicinity of the cut-off point where both shear stresses reach their maximum values.

2.2 Analytical solution

2.2.1 Geometry and loading

A typical RC beam retrofitted with NSMR which is loaded by four-point bending is shown in Fig.1. The RC beam has a height, width and effective depth equal to b, h and d respectively (Figure 2-1). The beam is strengthened by n strips with the length of L_f. Distance from the cut-off point to the support is a. The thickness, the height and Young modulus of the strips are t_f, h_f and E_f. The adhesive has a thickness ta and shear modulus Ga. The beam is reinforced with steel bars, the area of which is A_s. The modulus of concrete is E_c and the yield strength of steel is f_y.

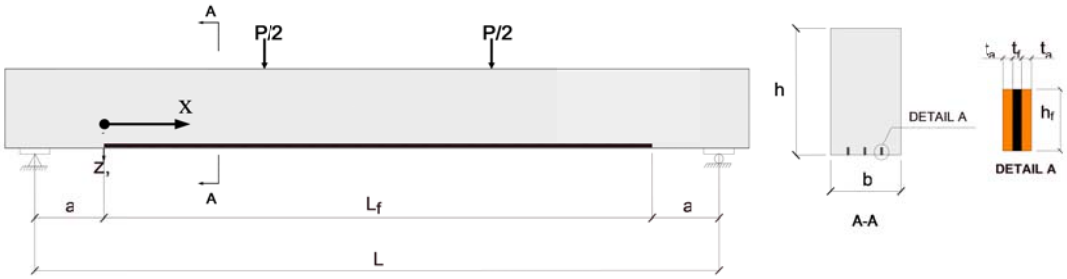

Figure 2-1 Typical configuration of the selected EBR FRP-RC beams

2.2.2 Assumptions

The following key assumptions are adopted in the model. Firstly, during the derivation of longitudinal shear stress, the adhesive layers are subjected only to shear stress and the deformation of the adhesive layers is negligible. As a result, curvature of the FRP strips and RC beam at the interface is assumed to be the same. This assumption is not applicable during the determination of vertical shear stress. Secondly, the longitudinal deformation varies linearly and the shear stress is uniform across the adhesive thickness. Thirdly, the stress arising due to the difference of flexural rigidity between FRP strips and RC beam is carried only by vertical shear stress. Finally, the deformation of the RC beam and FRP strips is caused by bending moment, axial and shear force.

2.2.3 Mathematical model, equilibrium equations

A differential segment of the RC beam retrofitted with NSMR, as shown in Fig. 2-2, is considered in the following. The Figures 2-2a and 2-2b present the full model and the simplified model, respectively. The longitudinal, vertical shear stresses and the normal stress are denoted as τ_{yx} , τ_{yz} and σ_y. The sign convention for bending moment, shear force, axial force and loading is also indicated in Figure 2-2.

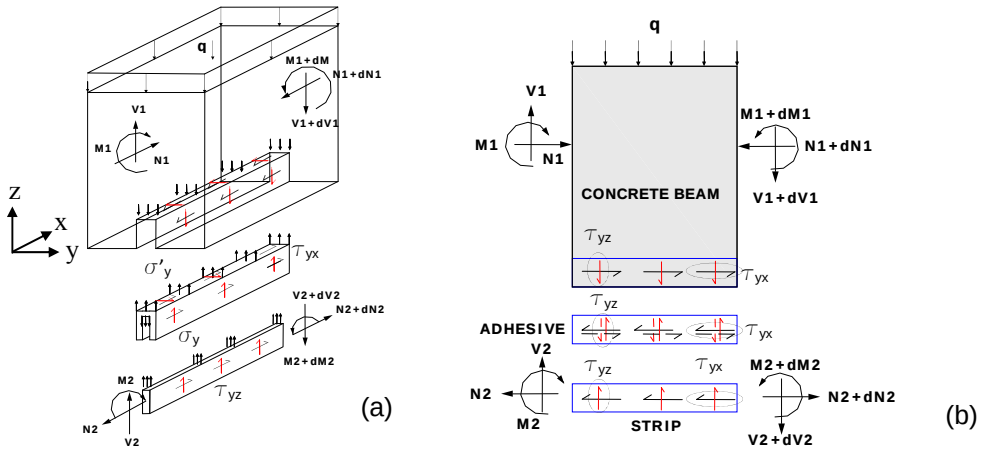

Figure 2-2 Differential segment of beam retrofitted with NSMR (a) full model (b) simplified model

Equilibrium and compatibility conditions of the beam, FRP strips and their interfaces are imposed for the derivation of the close-form solution. The derivation leads to the system of differential equations of longitudinal and vertical shear stress as shown in equations 1 and 2.

$$\frac{d\tau_{yx}^2(x)}{dx} - \frac{G_a 2nh_f}{t_a}\left[\frac{(y_{eff}-\frac{h_f}{2})^2}{E_cI_{eff}+E_fI_f}+\frac{1}{E_cA_{eff}}+\frac{1}{E_fA_f}\right]\tau_{yx}(x) = \frac{G_a}{t_a}\frac{(y_{eff}-\frac{h_f}{2})}{E_cI_{eff}+E_fI_f}V_T(x) -$$

$$-\frac{G_a}{t_a}\frac{(y_{eff}-h_f)}{G_cA_{ff}}\frac{dq}{dx} + 2nh\left(\frac{y_{eff}-h_f}{G_cA_{eff}}+\frac{h_f b}{2G_fA_f}\right)\frac{d\,\tau_{yz}(x)}{dx} \qquad \text{(Eq. 1)}$$

$$\frac{d^4\,\tau_{yz}(x)}{dx^4} - \frac{2G_a nh_f}{t_a}\left(\frac{1}{G_cA_{eff}}+\frac{1}{G_fA_f}\right)\frac{d^2\,\tau_{yz}(x)}{dx^2} + \frac{G_a 2nh_f}{t_a}\left(\frac{1}{E_cA_{eff}}+\frac{1}{E_fA_f}\right)\tau_{yz}(x)$$

$$= \frac{G_a 2nh_f}{t_a E_c I_{eff}} \left(y_{eff} - \frac{h_f}{2}\right) \frac{\tau_{yx}(x)}{dx} + \frac{G_a}{t_a} \frac{b}{G_1 A_{eff}} \frac{d^2 q}{dx^2} - \frac{G_a q}{t_a E_c I_{eff}} \quad \text{(Eq. 2)}$$

Where

$$\mathbf{y_{eff} = h - C_{eff}} \quad \text{(Eq. 3)}$$

$$C_{eff} = \left(\frac{M_{cr}}{M_a}\right)^{2.5} C_g - \left(1 - \left(\frac{M_{cr}}{M_a}\right)^{2.5}\right) C_{cr}; \quad A_{eff} = bC_{eff}; \quad I_{eff} = \left(\frac{M_{cr}}{M_a}\right)^{3} I_g - \left(1 - \left(\frac{M_{cr}}{M_a}\right)^{3}\right) I_{cr} \quad \text{(Eq. 4)}$$

M_{cr}, I_{cr}, C_{cr} are the cracking bending moment, moment of inertia and the neutral axis depth of the cracked RC beam, respectively.

I_g, C_g are gross moment of inertia and the neutral axis depth of the un-cracked RC beam, respectively.

M_a is the imposed bending moment.

y_{eff} is distance from the bottom fibre to the effective neutral axis.

C_{eff}, A_{eff}, I_{eff} are effective neutral axis depth, area and moment of inertia of RC beam, respectively.

2.3 Solution and discussion

Since these equations are coupled form, their solution is rather complicated. To solve the system, a simplification is made by assuming that the shear deformation in RC beam, FRP strips and normal stress are negligible. In this paper, only the four-point bending case is considered when imposing the boundary conditions (P is a concentrated load). The solution for the longitudinal shear stress and the vertical shear stress for this case are shown in equations (5) - (10) as follows

$$\tau_{yx}(x) = \frac{\alpha}{\beta} P a e^{-\beta x} + \gamma P \quad \text{(Eq. 5)}$$

$$\beta = \sqrt{\frac{2G_a A_f}{t_a t_f}\left[\frac{\left(y_{eff} - \frac{h_f}{2}\right)^2}{E_c I_{eff} + E_f I_f} + \frac{1}{E_c A_{eff}} + \frac{1}{E_f A_f}\right]} \quad \text{(Eq. 6)}$$

$$\alpha = \frac{G_a}{t_a \beta^2} \frac{y_{eff} - \frac{h_f}{2}}{E_c I_{eff} + E_f f} \qquad \gamma = \frac{G_a}{t_a} \frac{y_{eff}}{E_c I_{eff}} \quad \text{(Eq. 7)}$$

$$\tau_{yz}(x) = e^{-\omega x}[A\cos(\omega x) + B\sin(\omega x)] \quad \text{(Eq. 8)}$$

where

$$\omega = \sqrt[4]{\frac{G_a n h_f}{2 t_a}\left[\frac{1}{E_f I_f} + \frac{1}{E_c I_{eff}}\right]} \quad \text{(Eq. 9)}$$

$$A = \frac{G_a P}{2E_c I_{eff}\omega^3 t_a}\left[1 + \omega a - 2nh_f\left(\frac{\alpha}{\beta}a + \gamma\right)(y_{eff} - h_f)\right] \quad B = -\frac{G_a P a}{2\omega^2 t_a E_c I_{eff}} \qquad \text{(Eq. 10)}$$

The derivation of the equations and the analysis of the results were performed with the aid of software packages such as MATHCAD and MAPLE. The results were used to calculate longitudinal and vertical shear interfacial stresses along the FRP strips. The distribution of longitudinal and vertical shear interfacial stresses is shown in

Figure 2-3a and

Figure 2-3b, respectively, for values of **a** of 60mm, 90mm, 120mm. For the examined beam, both peak stresses increase sharply when the location of the cut-off point changes from 90mm to 120mm from the support.

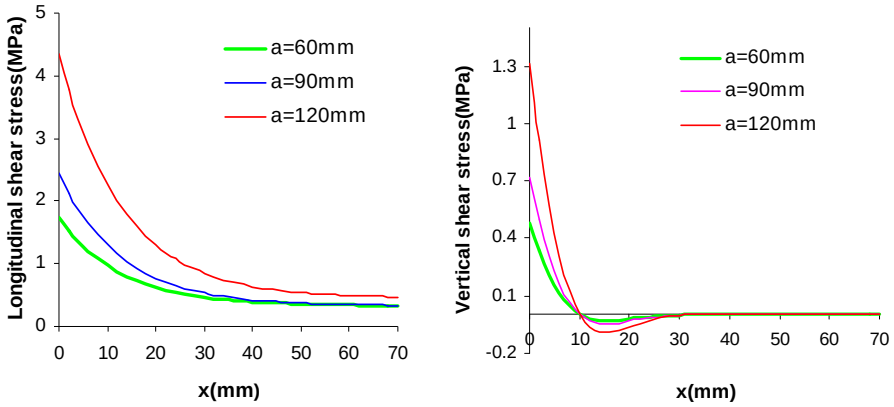

x: distance from the termination point of the NSM FRP

Figure 2-3 Interfacial shear stress (a) longitudinal shear stress (b) vertical shear stress.

Figure 2-3 presents the distribution of the longitudinal shear stress (Figure 2-4a) and the vertical shear stress (Figure 2-4b) along the FRP strips as a function of the position of the cut-off point. From the 3-D plots, it can be observed that when the value of ***a*** increases, so does the peak interfacial shear stress. This increase is more significant when the cut-off point moves from un-cracked section to a cracked section. This transition occurs for a value of ***a*** equal to 109mm (L_{cr}) of the examined beam. When the cut-off point is in a non-cracked zone, the peak stresses rise steadily with the increase of **a**. However, when ***a*** is greater than L_{cr}, the peak stress rises suddenly and the slope of the curves at the cut-off point becomes much steeper.

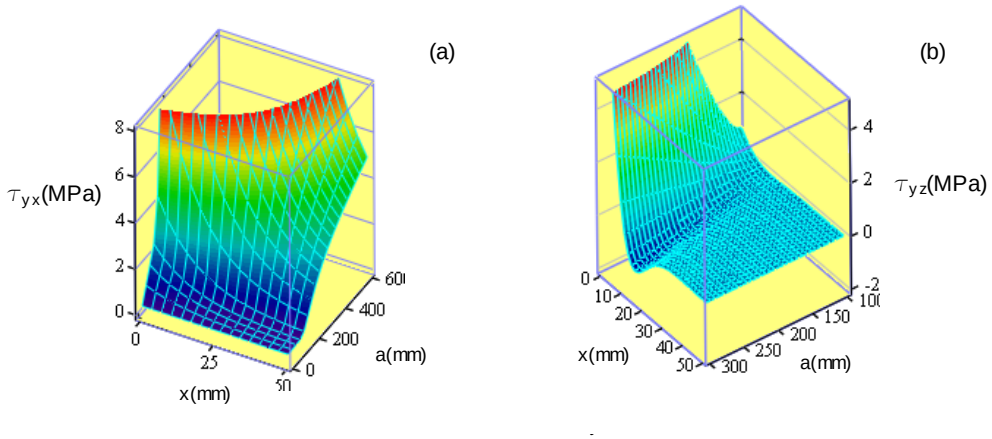

Figure 2-4. Variation of distribution of interfacial shear stresses along FRP strips as a function of location of the cut-off point (a) longitudinal shear stress (b) vertical shear stress

2.4 Conclusions

This paper presents a new closed-form analytical solution for interfacial stresses that can be used to predict the failure load of beam retrofitted with NSMR. The solution takes into account axial deformation of RC beam and flexural effect of FRP strips. The following conclusions are deduced from the present study:

- The flexural effects influence noticeably on interfacial shear behaviour at the FRP.
- The magnitude of longitudinal shear stress is approximately four times higher than that of vertical shear stress.
- The results from the model also indicate that when the cut-off point is located in the non-cracked zone, shear stresses are rather small. Beyond this point, shear stresses rise noticeably and the load carrying capacity of the strengthened beam reduces sharply.

Future work will examine the proposed solution parametrically and make comparisons with experimental work and other analytical methods.

2.5 Further discussion

The analytical model developed, has enabled a more fundamental understanding of the bond stress development along the NSMR, especially in the region around the termination point. The model accounts for differences in stress states between EBR and NSMR induced by shifting the FRP from the surface, into the concrete. Details of the derivations as well as a parametric study are given in appendix A. This additional work and the conference paper will be included in a new paper to be submitted in Journal of composite: part B. Some of the most significant findings are discussed below:

- The longitudinal shear resulting from the variation of strains along the NSMR, reduces about twofold compared to that developed in the EBR system. The peak shear stress concentrates in a very narrow zone approximately 20mm from the termination point and reduces sharply towards mid-span.
- The vertical shear stress (τ_{yz}), a result of the difference of flexural stiffness of the NSMR and the beam, peaks around the termination point and decreases sharply towards mid span. The vertical shear stress developed in the NSMR is approximately twice the normal stress developed in EBR (σ_y). This can be explained by the fact that the stiffness of the vertical NSMR system is much higher than that of the EBR. The peak vertical shear stress is approximately 25%-30% of the peak longitudinal shear stress (τ_{yx}).
- The vertical shear stress is more dominant in NSMR placed vertically than the normal stress in EBR system. As a result, the failure modes of NSMR are the combination of fracture mode II (sliding mode with a shear stress acting parallel to the plane of the crack and perpendicular to the crack front) and III (tearing mode with a shear stress acting parallel to the plane of the crack and parallel to the crack front), instead of mode I (a tensile stress normal to the plane of the crack) and II typical of EBR. Despite the higher vertical shear stress developed, NSMR is not affected by peeling, as the fracture energy of mode 2 in NSMR is much greater than the fracture energy of mode 1 in EBR.
- The bond stress concentration reduces significantly when the termination point of the NSMR is located in the un-cracked region.

Even though the analytical model provides useful information (both qualitative and quantitative) and helps to understand bond behaviour along the FRP in NSMR applications, it still has several limitations as it is based on elastic analysis and continuum mechanics. At high load levels, both the concrete and the steel reinforcement exhibit a highly nonlinear behaviour, while the bond along the NSMR is affected by severe discontinuities (eg. flexural-shear cracks, tributary shear cracks). This leads to inaccuracies in the analytical solution. Moreover, bond stress concentration zones near the termination point can significantly affect bond behaviour and trigger debonding failure of the NSMR.

To complement this study, some initial numerical analysis using commercial FEM software (ABAQUS) was also carried out to examine the bond behaviour of NSMR in

strengthened beams. The results of the numerical analysis are given in appendix A. Similar to the analytical solutions, the basic numerical method has significant limitations.

Therefore, a focused experimental investigation was designed with the aim to examine the strain development along NSMR and steel reinforcement in concrete elements subjected to combinations of external actions that are representative of real life structures. The experimental phase of this research programme, which is described in the next chapter, will be used to gain extra insight into bond behaviour of NSMR in flexural strengthening applications, overall structural behaviour as well as to inform possible improvements to the above analytical model. Understanding bond behaviour of NSMR, both theoretically and experimentally, can provide the foundation for the development of a simple, yet effective design method.

ACKNOWLEDGEMENTS

The authors gratefully acknowledge the financial support from the Ministry of Education and Training of Vietnam and the University of Sheffield.

REFERENCES

[1] De Lorenzis, L. and Teng, J.G., "Near-surface mounted FRP reinforcement: An emerging technique for strengthening structures", *Composites Part B: Engineering*, 38(2), 2006, pp 119-143.

[2] Harrison, R. R., Rasheed H. R., Peterman, R. J. and Alkhrdaji, T., "Comparison of Four Techniques for Strengthening Concrete Beams Using Performance and Practicality Criteria", *Structures Congress 2006,* St. Louis, Missouri, USA, 2006, pp 70-70.

[3] Hassan T. and Rizkalla S., "Investigation of Bond in Concrete Structures Strengthened with Near Surface Mounted Carbon Fiber Reinforced Polymer Strips", *Journal of Composites for Construction*, 7(3), 2003, pp 248-257.

Chapter 3

PERFORMANCE OF RC BEAMS STRENGTHENED IN FLEXURE WITH NSMR

Hien V. Nguyen[1], Maurizio Guadagnini[1], Kypros Pilakoutas[1], Nam V. Le[2]

[1]Department of Civil and Structural Engineering

The University of Sheffield, UK. Email: n.hien@sheff.ac.uk

[2] Department of Civil and Structural Engineering

HCMC University of Technology, Vietnam National University, Vietnam

(Paper to be submitted to Composites part B: Engineering)

ABSTRACT

Debonding of near surface mounted (NSM) FRP reinforcement remains an important issue that needs to be better understood and controlled as it can prevent strengthened structures from developing their full flexural capacity. This paper presents an experimental study that examines the overall structural behaviour of RC beams retrofitted with NSMR of different embedment lengths. Special attention is paid to the influence of yield penetration along the internal steel bars on the bond behavior of the NSM reinforcement within the shear spans and the resulting debonding mechanisms. The experimental results show that yielding of the steel reinforcement penetrates in the shear spans much further than predicted according to classic section analysis, reaching near or even beyond the cut-off point (termination point). The existence of yielding intensifies bond stresses in the vicinity of the cut-off points and eventually leads to debonding. This work will assist in the development of more efficient design guidelines for flexural strengthening using NSM FRP reinforcement.

Keywords: NSMR, debonding, BFRP, CFRP, yielding

3.1 Introduction

The use of NSM FRP reinforcement has been widely adopted by the construction industry for the strengthening of RC structures [1-5] and initial design guidelines have already been published [6, 7]. Similarly to externally bonded reinforcement (EBR) applications, the design of NSMR strengthening systems is limited by bond performance. Previous research on bond behaviour and debonding failure of NSM FRP reinforcement in flexural strengthening applications has concluded that:

(1) Failure modes of beams strengthened with NSMR are similar to those observed in beams strengthened with EBR, including flexural failure, concrete cover separation, intermediate crack-induced debonding [8-11].

(2) The high ratio of bond area to cross section area along with the deeper embedded position of the NSMR, results in a bond behaviour that is superior to that of EBR, both in terms of bond strength and post-peak residual strength behaviour. NSMR can develop high bond strength even with short embedment length and can outperform EBR in terms of debonding load [12-17].

(3) Debonding failure of NSMR is affected by various parameters including shape, size, surface finish of FRP, properties of the adhesive, concrete and FRP, and geometry of the grooves (location, size, shape, spacing etc.) [13, 15, 18-20].

The bond behaviour of NSM FRP reinforcement has been examined mostly through bond tests and only a few studies have included tests on large scale flexural specimens. Although bond tests are generally simple to undertake, these can be used to examine bond behaviour only at the local level. In fact, typical bond tests cannot account for the effect of critical aspects that are typical of flexural structures, such as bending effects and the interaction between flexural steel rebars and the NSMR system, particularly after yielding of the steel reinforcement. In addition, the scatter in bond strength results, partly due to lack of standard tests [10, 16, 20-22] can lead to conservative design guidelines. In contrast, though more complex, beam tests can represent more adequately the bond behaviour and the debonding mechanisms of NSMR in real strengthening applications. However, the current knowledge on the bond behaviour and debonding mechanisms of NSMR in beam tests, is limited due to lack of sufficiently detailed experimental data in the literature. For example, the absence of data on the distribution of strains along the entire length of both steel and FRP reinforcement can hinder the understanding of the interaction between the internal and the external reinforcement around the termination points as well as the impact of the penetration of yielding of the steel reinforcement on end debonding failure mechanisms.

The experimental programme presented in this paper aims to gain a better understanding of bond behaviour and debonding failures in RC structures strengthened in flexure with NSMR. Special attention is paid to the development of yielding along the steel reinforcement and its effect on the bond behaviour and debonding mechanisms of NSMR. The main parameters examined in this study are embedment length and type of FRP. The details of the experimental work are presented and discussed in this paper, including the overall structural behaviour of the tested RC specimens, observed failure modes and failure mechanisms.

3.2 Experimental details

A total of ten RC beams, including two control beams and eight beams strengthened in flexure with CFRP and BFRP bars or strips, were tested. All the materials used in the beam tests (structural adhesive, reinforcing steel, CFRP, BFRP and concrete matrix) were tested prior to structural testing to characterise their mechanical properties.

3.2.1 Materials characterisation

A total of 31 concrete cylinders (150x300mm) and seven concrete prisms (150x150x500mm) were prepared and tested in accordance to BS EN12390 series: 2001-2009[23] to obtain the compressive strength, splitting tensile strength and flexural tensile strength. Three steel rebar specimens were tested in accordance to BS EN-6892-1:2009[24] to obtain elastic modulus, yield strain, yield stress, ultimate strain, and ultimate stress. Three CFRP strips and three BFRP strips were tested in accordance to ASTM D7565/D7565M-10[(D7565/D7565M-10 2010) to determine their elastic modulus, tensile strength and ultimate strain. The properties of the CFRP round bars were determined as a part of a previously run research programme and are reported elsewhere [26](Al-Sunna 2006). Seven specimens, including five cylinders (30x60mm) and two 30mm cubes, were tested to determine the shear modulus of the structural adhesive. A total of 4 - 6 strain gauges were bonded to the side faces of each adhesive specimen to measure the vertical and horizontal strains (Figures 3-1a and 3-1b).

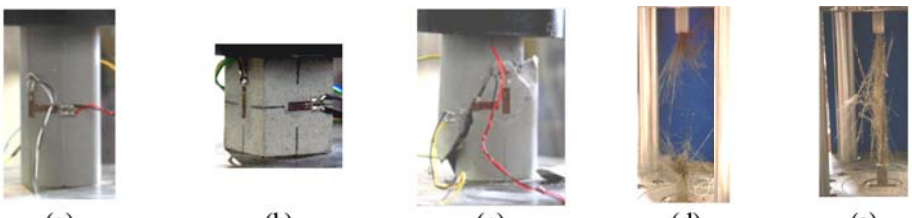

Figure 3-1 Material characterisation: structural adhesive specimens (a, b); typical failure of structural adhesive (c); typical failure of CFRP (d) and BFRP (e) bars

Figures 3-1c, 3-1d and 3-1e show the damaged specimens of adhesive, CFRP and BFRP bars, respectively. The mechanical properties of concrete, reinforcing materials and adhesive are summarised in Tables 3-1, 3-2 and 3-3, respectively. Typical stress-strain relationship of the tested structural adhesive, steel reinforcement, CFRP and BFRP bars are shown in Figures 3-2a and 3-2b.

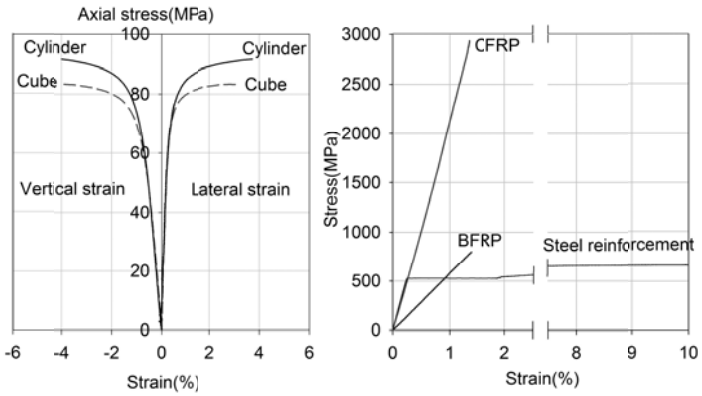

Figure 3-2 Stress-strain relationships (a) adhesive and (b) steel and FRP reinforcement

Table 3-1.Concrete properties

Type	Mean compressive strength (MPa)	Mean splitting tensile strength (MPa)	Mean flexural tensile strength (MPa)	Used in beam(s)
Mix1	23.9(1.1) *	---	---	NSM2Aa
Mix2	50.2(3.6) *	3.7(0.32) *	4.2(0.2) *	REF0, NSM3Aa
Mix3	32.3(2.5) *	2.8(0.23) *	3.9(0.11) *	REF1, EBR, NSM4Aa- NSM9Ba

Table 3-2 Reinforcing material properties

Reinforcing materials	Elastic modulus (GPa)	Yield strain (%)	Yield stress (GPa)	Ultimate strain (%)	Ultimate stress (GPa)
Steel	210	0.25	525	4.3	600
CFRP(strips)	214	---	---	1.3	2804
CFRP(D6)**	133	---	---	1.1	1450
CFRP(D12)**	119	---	---	1.2	1477
BFRP	57	---	---	1.4	800

Table 3-3 Structural adhesive properties

	Elastic modulus (GPa)	Poisson ratio	Shear modulus (GPa)	Compressive strength (MPa)
Cylinde	9.7 (1.4) *	0.4(0.02) *	3.7(0.6) *	84(5.3) *
Cubes	8.4	0.3	3.3	93

*Values in brackets are standard deviations; **Results were reported from previous research (Al-Sunna 2006)

3.2.2 Beam specimens

A total of ten RC beams were cast, including two control beams (B0 and B1) and eight retrofitted with MSM carbon and basalt FRP bars/strips. Beams were tested in two groups:

Group A included six beams NSM2Aa-NSM7Aa retrofitted with CFRP bars/strips with long embedment lengths; and group B included beams retrofitted with BFRP bars with short embedment lengths. For comparison purposes, beam EBR, which had similar type, amount and bond length of FRP as beam NSM4Aa was also tested (Serbescu 2014). Figure 3-3 shows the overall dimensions of the tested beams along with typical cross sections showing the position of the steel and NSM reinforcement. All beams were 2.5m long and had a rectangular cross section of 150 mm by 250 mm.

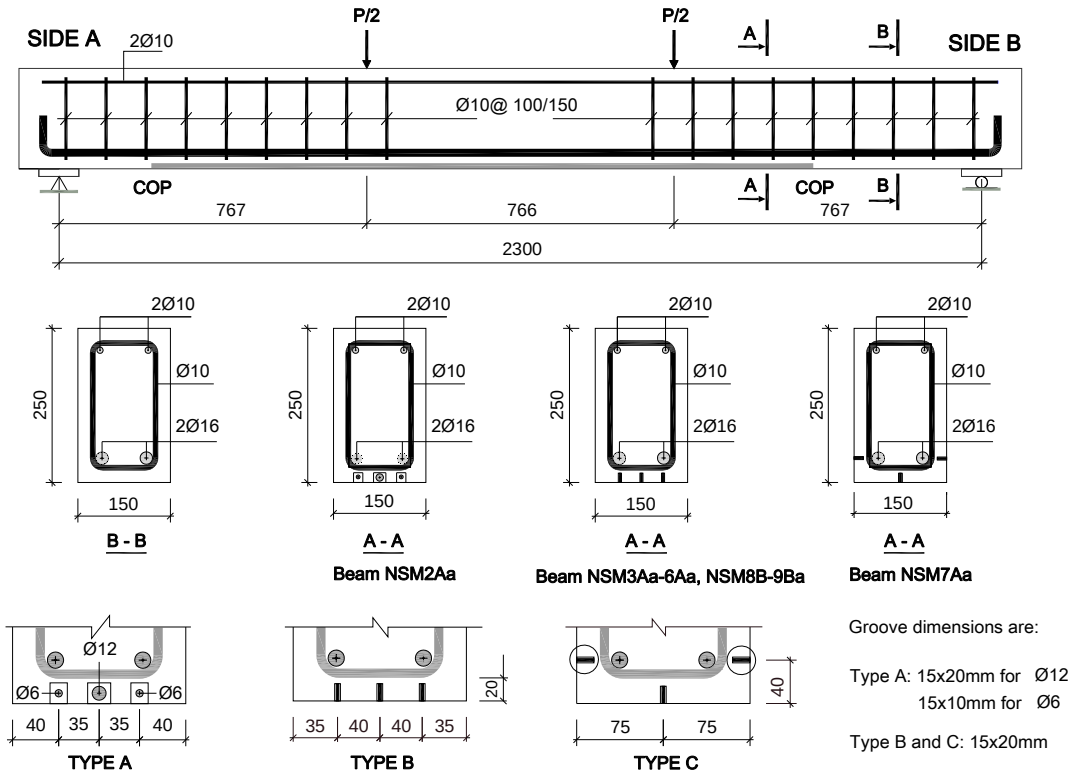

Figure 3-3 Design of beam specimens and details of reinforcement

The beams were simply supported and tested in four point bending, with a clear span of 2.3m and shear spans of 0.767m. Table 3-4 summarises the design details for each of the tested beams. All specimens were under-reinforced, with the ratio of flexural steel reinforcement being 1.3%. The ratio between the area of the NSMR and the steel rebars varied from 12.5% (beams NSM3Aa-NSM7Aa) to 42% (beam NSM2Aa) (Table 3-4). The shear reinforcement was designed to prevent shear failure of the fully strengthened beams and comprised 10 mm diameter steel stirrups at spacing of 100 mm or 150mm. Except for beam NSM2Aa, which was retrofitted with CFRP round bars, the remaining beams, were retrofitted with BFRP and CFRP strips. Three types of grooves were cut in the concrete soffit as shown in Figure 3-3. Type A grooves were used to accommodate CFRP round bars on the bottom face of beam NSM2Aa; type B grooves were used in combination with rectangular FRP strips on the bottom face of beams NSM3Aa- NSM9Ba, and type C grooves

were cut on the side faces of beam NSM7Aa. The ratio of bonded length and shear span (L_a/L_s and L_b/L_s, see Figure 3-4) of the NSMR varied from 0.54 to 1 for the beams retrofitted with CFRP, and from 0.22 to 0.35 for BFRP (Table 3-5). Except for beam NSM2Aa for which the bond length of the CFRP bars were symmetrical (L_a= L_b), the remaining beams were strengthened with asymmetric embedment length (L_a> L_b). The strengthening scheme and details of the bonded length of the NSMR are given in Figure 3-4 and Table 3-5. The asymmetric arrangement of embedment lengths of the NSMR bars/strips was designed to force debonding failure on the side with a shorter embedment length (side B) and enabled the examination of the bond behaviour of the NSMR at different bond lengths as these beams could be re-tested.

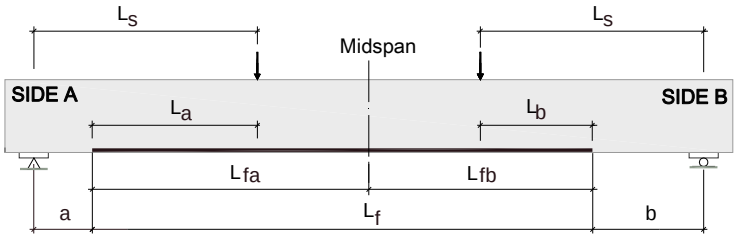

Figure 3-4 Scheme of embedment length of the beam specimens

Table 3-4 Details of tested beams

Beam	Concret	Steel reinforcement			FRP				
		Flexure		Shear					
	f_c (MPa)	A_s (mm^2)	ρ_s (%)	s (mm)	Cross section	E_f (GPa)	A_f (mm^2)	ρ_f (%)	ρ_f/ρ_s
B0	50.2	402	1.3	100	---	---	---	---	---
B1	32.3	402	1.3	100	---	---	---	---	---
EBR	32.3	402	1.3	100	36x1.4mm*	214	50	0.15	0.13
NSM2Aa	23.9	402	1.3	100	2D6+D12*	133/119	170	0.54	0.42
NSM3Aa	50.2	402	1.3	100	3x12x1.4mm*	214	50	0.16	0.13
NSM4Aa	32.3	402	1.3	100	3x12x1.4mm*	214	50	0.16	0.13
NSM5Aa	32.3	402	1.3	100	3x12x1.4mm*	214	50	0.16	0.13
NSM6Aa	32.3	402	1.3	150	3x12x1.4mm*	214	50	0.16	0.13
NSM7Aa	32.3	402	1.3	100	3x12x1.4mm*	214	50	0.16	0.13
NSM8Ba	32.3	402	1.3	150	3x 14x2mm**	57	84	0.27	0.21
NSM9Ba	32.3	402	1.3	100	3x 14x2mm**	57	84	0.27	0.21

Note: * CFRP ** BFRP

Table 3-5 Embedment length of NSMR

Beam	L_f (mm)	a (mm)	L_{fa} (mm)	L_a (mm)	L_a/L_s	b (mm)	L_{fb} (mm)	L_b (mm)	L_b/L_s
EBR	1800	200	950	567	0.74	300	850	467	0.61
NSM2Aa	2000	150	1000	617	0.80	150	1000	617	0.80
NSM3Aa	2150	0	1150	767	1.00	150	1000	617	0.80
NSM4Aa	1800	200	950	567	0.74	300	850	467	0.61
NSM5Aa	1700	250	900	517	0.67	350	800	417	0.54
NSM6Aa	1700	250	900	517	0.67	350	800	417	0.54
NSM7Aa	1700	250	900	517	0.67	350	800	417	0.54
NSM8Ba	1200	500	650	267	0.35	600	550	167	0.22
NSM9Ba	1200	500	650	267	0.35	600	550	167	0.22

3.2.3 Instrumentation

A total of 60-89 strain gauges were bonded to the FRP bars/strips, the tension and compression steel rebars and the stirrups of each beam. In the vicinity of the termination points, strain gauges were typically bonded at intervals of 15-35 mm on the FRP bars/ strips and at 30-50 mm on the tensile steel bars. Figure 3-5a illustrates typical strain gauge arrangement for the tested beams. Figure 3-5b illustrates a typical layout of LVDTs for the tested beams. A total of 15-20 LVDTs were installed, to monitor beam deflection profiles, end displacement of NSMR and formation and development of tributary shear cracks and bridging cracks in the vicinity of the cut-off points (COPs) (Figure 3.5b). The first set of seven LVDTs (D1-D7) was mounted along the beam specimens to record deflection profiles. The second set of four to six LVDTs (E1a- E3a, E1b-E3b) was installed at the ends of the NSMR strips to measure their end displacement; and the third set including four to six LVDTs (C1f- C3f, C1b-C3b) was mounted in the region between cracks near the COPs on the side faces to detect the formation and to monitor the propagation of tributary shear cracks and bridging cracks.

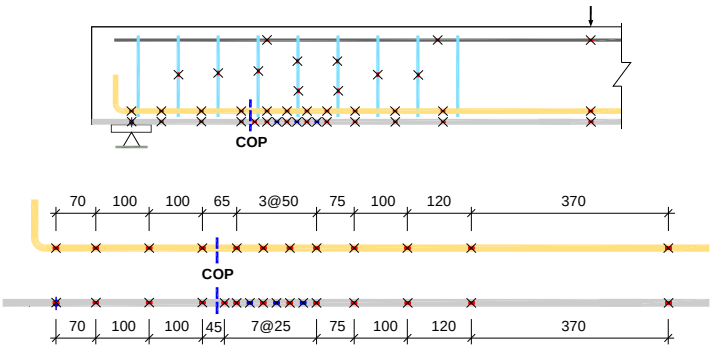

(a) Location of strain gauges on shear links, steel and NSMR reinforcements

(b) Layout of LVDTs **Note (C1f/b f-front face; b-bottom face)**

Figure 3-5 Instrumentation of beam NSM4Aa

3.2.4 Testing procedure

With the exception of beams NSM2Aa and NSM3Aa, which were not pre-cracked before strengthening, the remaining beams were loaded up to a load Po that induced a stable flexural crack pattern before strengthening (Table 3-6). The beams were loaded in displacement control at a rate of 0.2mm/min. The strengthened beam specimens were also

loaded at a rate of 0.2mm/min up to the yielding load and then at 0.4mm/min until failure. Loading-unloading cycles were carried out at 20kN, 40kN, and 60kN and just before steel yielding. Several cameras, microscopes and camcorders were used during the tests to document the initiation and development of cracks and failure at both cut-off regions.

3.3 Results

Table 3-6 summarises the main test results including pre-cracking load (P_o), yield load (P_y), peak load (P_p), ultimate load (P_u), and failure modes, as well as the theoretical flexural failure load (P_{cal}) predicted according to the section analysis approach.

Table 3-6 Summary of test results

Beam	P_o (kN)	P_y (kN)	P_p (kN)	P_p/P_0	P_{cal} (kN)	P_{exp}/P_{cal}	d_p/d_0	P_u (kN)	P_u/P_y	Failure modes
NSM2Aa	---	139	146	1.35	145	1.01	---	123	1.05	C
B0	---	106	116	1.07	109	1.06	---	107	1.09	C
B1	---	94	100	1.05	105	0.95	---	92	1.06	C
EBR	50	---	98	---	149	0.66	0.27	98	---	D
NSM2Aa	---	140	146	1.35	145	1.01	---	123	1.04	C
NSM3Aa	56	136	174	1.53	176	0.99	1.08	174	1.28	C, D*, F*
NSM4Aa	51	122	149	1.25	146	1.02	0.64	149	1.22	D
NSM5Aa	40	122	141	1.30	146	0.97	0.62	141	1.16	D
NSM6Aa	41	122	130	1.32	146	0.89	0.54	130	1.07	D
NSM7Aa	40	121	138	1.25	142	1.00	0.7	138	1.14	D
NSM8Ba	41	105	113	1.09	126	0.90	0.76	106	1.08	C**,S*
NSM9Ba	40	103	111	1.07	126	0.88	0.63	109	1.08	C**,S*

Note : *Secondary failure mode; ** Crushing of concrete after high rotation developed

C: Concrete crushing following steel yielding, D: end debonding; S: Shear failure

3.3.1 Failure of beam specimens

The two control beams (B0, B1) and beams NSM2Aa failed in pure flexure following concrete crushing. Two beams NSM8Ba and NSM9Ba also failed in flexure after developing excessive rotation around the termination points. The remaining beams failed by end debonding of the NSMR and mixed modes (Table 6). There was no visual evidence of intermediate crack induced debonding in any of the tested specimens. Each of the different mode of failure is discussed briefly in the following section.

3.3.1.1 Concrete crushing

Figure 3-6 shows the failure of beam NSM2Aa, which failed in flexure due to crushing of concrete shortly after yielding of the steel reinforcement at 138.5kN. The load then gradually dropped to 122.6kN before abrupt failure. There was no visual evidence of debonding of the NSMR. This beam behaved like an over-reinforced beam due to having an un-expected weak concrete and relatively high amount of total reinforcement.

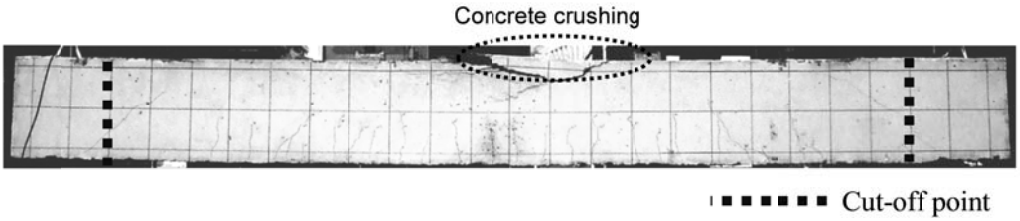

Figure 3-6 Failure of beam NSM2Aa

3.3.1.2 Mixed flexural failure mode

Figure 3-7a shows the failure of beam NSM3Aa due to end debonding and rupture of the NSMR. The concrete below the point load began to crush at a load of 170kN without any visual evidence of debonding of the NSMR (Figure 3-7b). At 174 kN, debonding of the side strips and rupture of the middle strip occurred suddenly and almost simultaneously on side B (Figure 3-7c). This beam failed very close to its theoretical flexural capacity, 176kN, which confirms that the FRP strips were fully utilised.

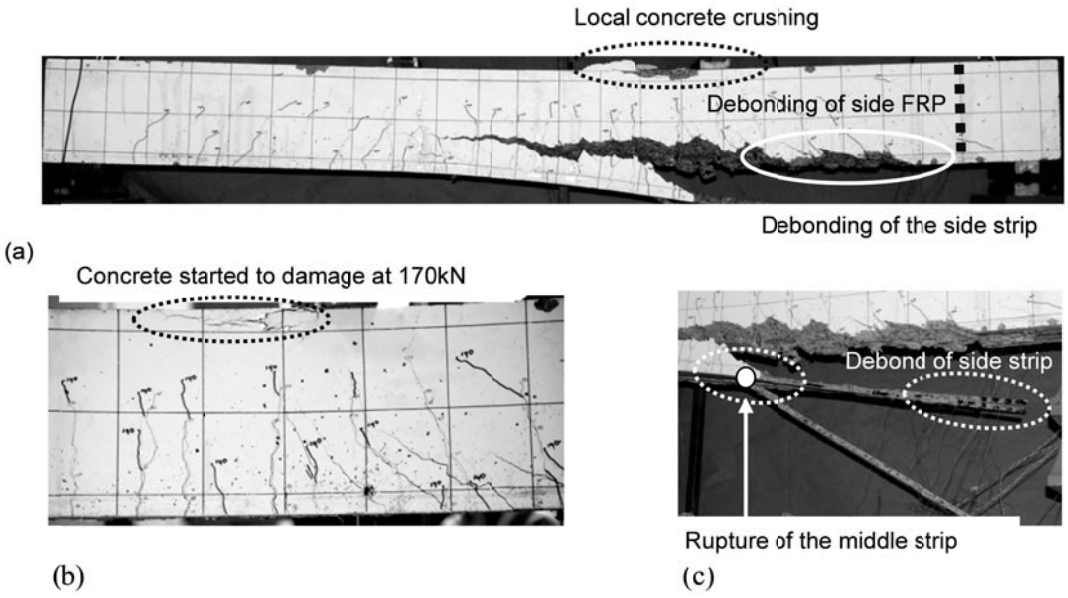

Figure 3-7 Failure of beam NSM3Aa

3.3.1.3 End debonding failure

Figure 3-8 shows the end debonding failure of all four beams NSM4Aa-NSM7Aa. As expected, end debonding occurred in the vicinity of the termination point on side B following the formation of extensive tributary shear cracks within the shear spans. After the yield load, a significant increase in the number of tributary shear cracks between the already formed flexural-shear cracks reduced the crack spacing. Debonding failure occurred when the cracks spacing decreased to the critical value of 30mm-50mm (Figure 3-8a) followed by the abrupt formation of bridging cracks which develops horizontally at the steel reinforcement level (Figure 3-8b). In addition to the bridging cracks, splitting

cracks were always observed along the NSMR of beams NSM4Aa-7Aa. The FRP strips placed on the side faces prevented the tributary shear cracks from developing downwards through the concrete cover. Instead, splitting in the concrete around the side strips (Figure 3-8d) was observed. Except for beam NSM6Aa, which failed earlier than expected (90% of P_{cal}), debonding failure at beams NSM4Aa, NSM5Aa and NSM7Aa occurred close to their predicted flexural capacity (Table 3-6).

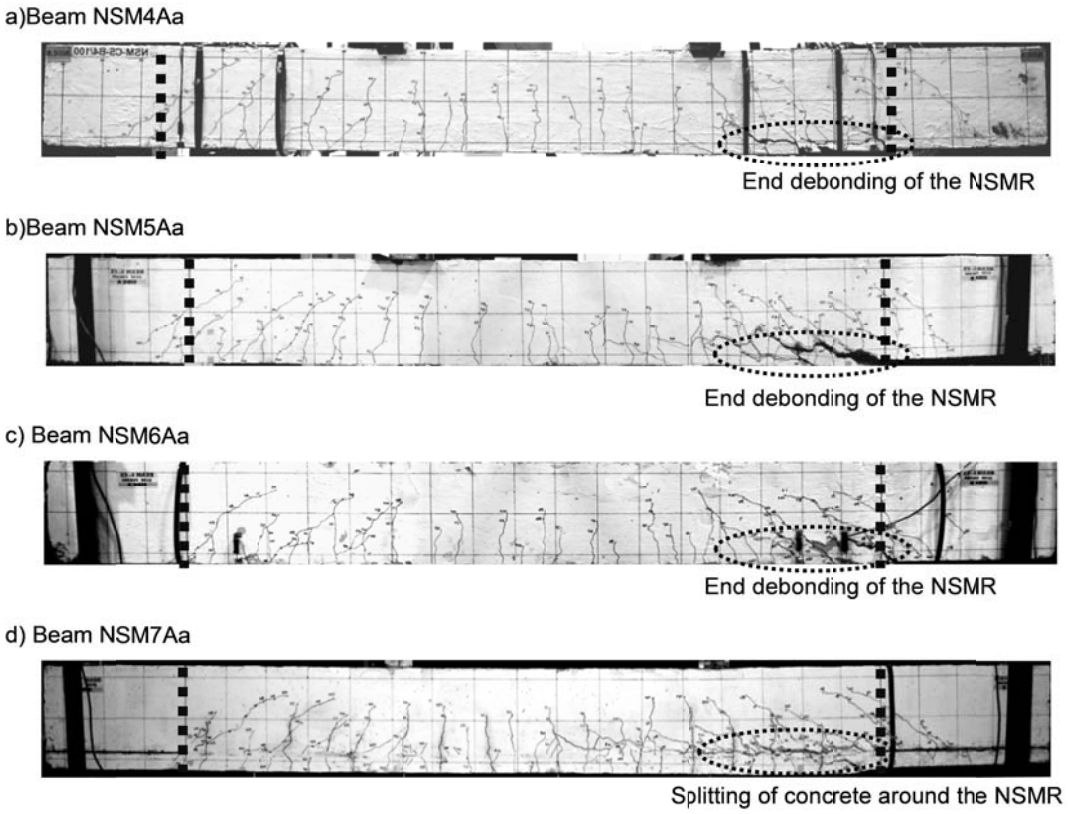

Figure 3-8 End debonding failure of beams NSM4Aa-NSM7Aa

3.3.1.4 Flexural failure with excessive local rotation around the termination point

Figure 3-9 shows the failure of beams NSM8Ba and NSM9Ba which failed by concrete crushing in the region near the loading point on side B after developing excessive rotation around the termination point region. This was due to highly yielding of the steel reinforcement near the termination point.

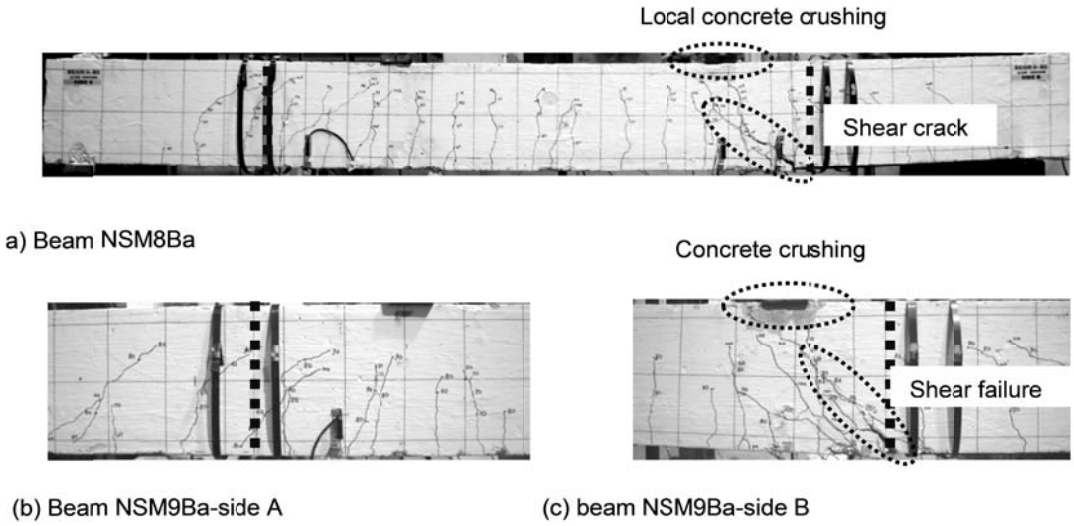

Figure 3-9 End debonding failure of beams NSM8Ba-NSM9Ba

3.3.2 Load enhancement

Figure 3-10 shows the yield load and maximum load enhancement of the tested beams as well as the change in the ultimate deflection load (d_p) with respect to the control specimen. Compared to the un-strengthened beams, the yield loads of the six beams retrofitted with CFRP increased approximately by 26%-28% while their maximum loads increased by 30-50%. The yield and maximum loads of the two beams retrofitted with BFRP increased by only about 10% and 11-12%, respectively. All beams failed after yielding of the rebars and the ratio of the maximum load to the yield load (P_p/P_y) varied in the range of 1.04-1.28 for beams retrofitted with CFRP and approximately 1.08 for beams retrofitted with BFRP. The superior performance of beams strengthened with CFRP over BFRP can be explained by the fact that the elastic modulus of CFRP is almost four times higher than that of BFRP and the embedment length of CFRP bars/strips were longer than those of BFRP. Compared with the similar beam retrofitted with EBR, the peak load of beam NSM4Aa was approximately 50% higher than that of beam EBR (Figure 3-10). With the exception of beam NSM6Aa and beams in group B, which failed rather early, all other beams almost attained their predicted flexural capacity, even when debonding failure occurred.

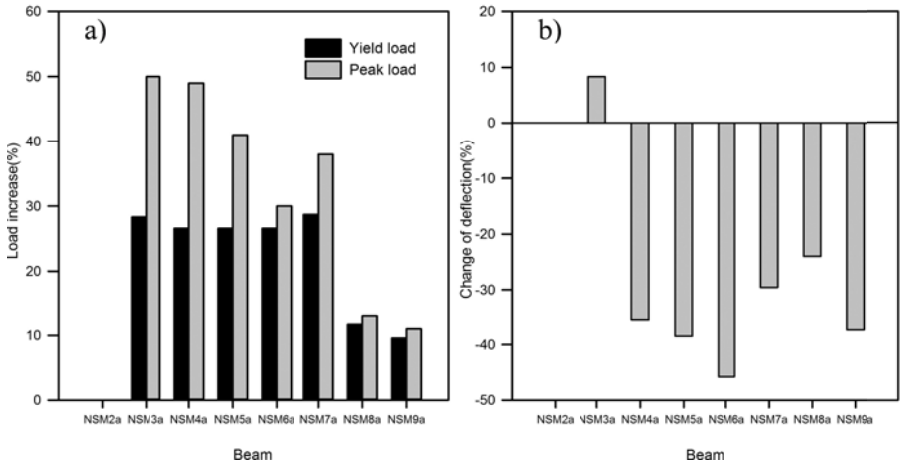

Figure 3-10 (a) Load enhancement due to strengthening (b) difference in deflection at the ultimate load of the strengthened beams when compared to the control beam B1

3.3.3 Load-deflection response

Figure 3-10b shows the change in maximum deflection compared to the reference beam. Figure 3-11 shows the mid-span deflection of the tested beams. Beam NSM3Aa exhibited high ductility performance whilst attaining the highest increase in load carrying capacity. In all other beams, ductility reduced noticeably, with a deflection at mid-span smaller than 50% of that of the reference beam. The deflection of the strengthened beams increased slowly up to a load of 60-80kN, corresponding to the occurrence of the first inclined cracks; then increased more rapidly due to the loss of stiffness caused by the development of inclined cracks (point S) along the shear spans. After yield load (point Y), deflection increased more rapidly up to failure. Only beam NSM2Aa exhibited softening behaviour in the post peak stage due to crushing of the low strength concrete in compression once the flexural capacity had been achieved. Beams NSM8Ba-9Ba exhibited good plasticity in the post-yield stage. Figure 3-12 shows the deflection profiles of beams NSM4Aa and NSM9Ba as representatives of the beams tested in groups A and B, respectively.

The deflection profile of beam NSM4Aa was nearly symmetrical up to failure (Figure 3-12a). This behaviour was observed for beam NSM9Ba only up to the yielding load (Figure 3-12b). Subsequently, the deflection in the region near the termination point on side B increased more rapidly and caused significant asymmetry in the deflection profile. The deflection measured under the loading point in the damaged side was approximately 50% higher than that at the opposite side (Figure 3-12b), indicating that a plastic hinge developed in this region.

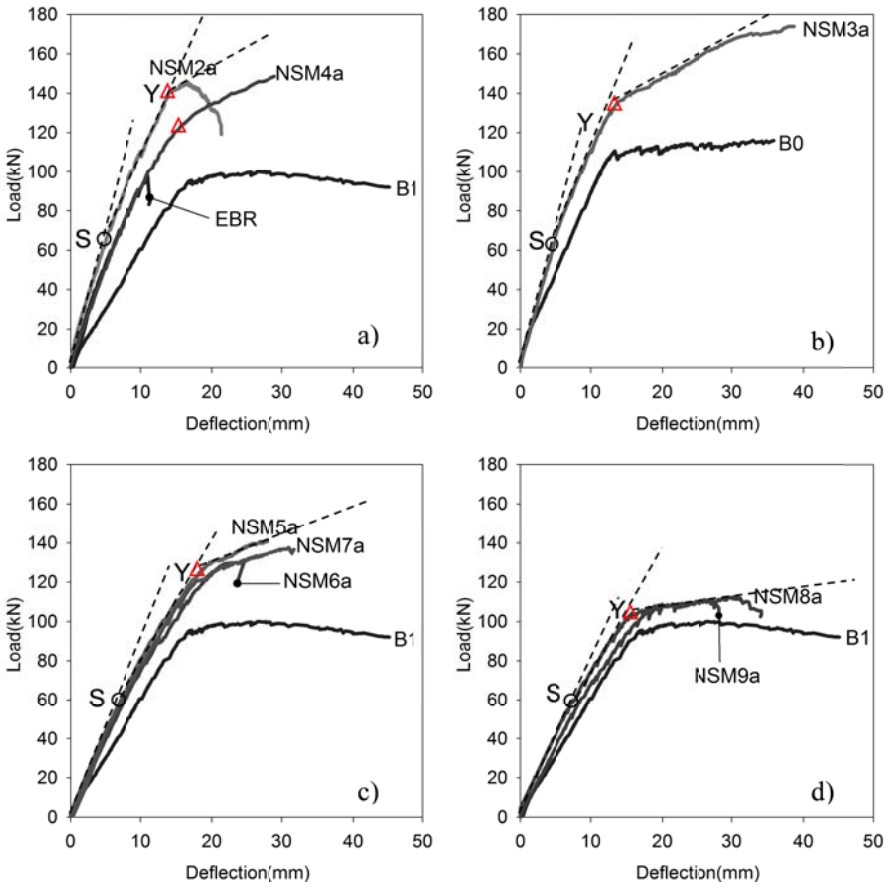

Figure 3-11 Load versus deflection at the mid-span of tested beams

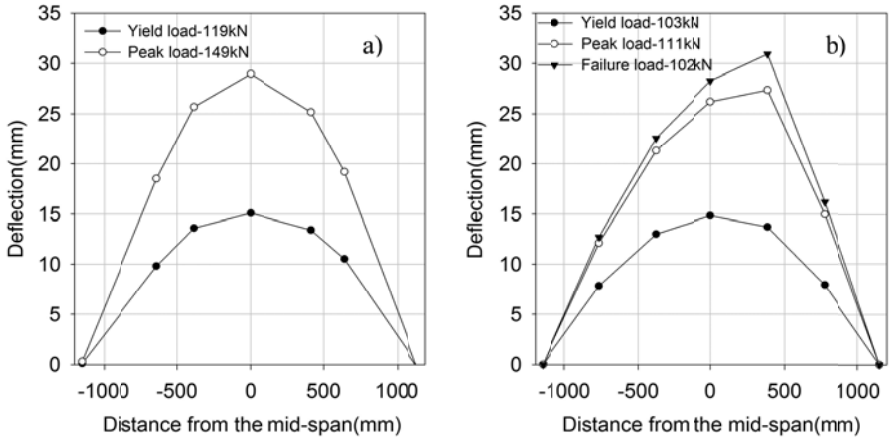

Figure 3-12 Deflection profile of (a) beam NSM4Aa and (b) of beam NSM9Ba

3.3.4 Strain in the steel reinforcement and NSM FRP reinforcement

Table 3-7 summarises the maximum strain measured in the tension (ε_{st}) and compression reinforcement (ε_{sc}) and in the NSMR (ε_{fmax}). The maximum strain in the NSMR varied from 0.52% to 1.18% corresponding to 36-92 % of their ultimate strains. Figure 3-13 shows load versus strain measured in (a,b) the tension steel rebars, and (c,d) the NSM FRP reinforcement. As expected, yielding occurred in all specimens. Beam NSM2Aa, however, just reached yield strain at peak load.

Table 3-7 Summary of maximum strain in tension steel reinforcement and NSMR

Beam	ε_{st} (‰)	ε_{fmax} (‰)	$\varepsilon_{fmax}/\varepsilon_{fu}$ (%)
B0	13.8	---	---
B1	15.2*	---	---
NSM2Aa	2.6	6.5	54
NSM3Aa	5.0*	11.8	92
NSM4Aa	18.1*	7.2	55
NSM5Aa	4.3	8.0	62
NSM6Aa	5.9	5.2	40
NSM7Aa	8.1	8.5	65
NSM8Ba	4.6	4.9	36
NSM9Ba	12.1	7.3	62

* Strain gauge failed before the ultimate load

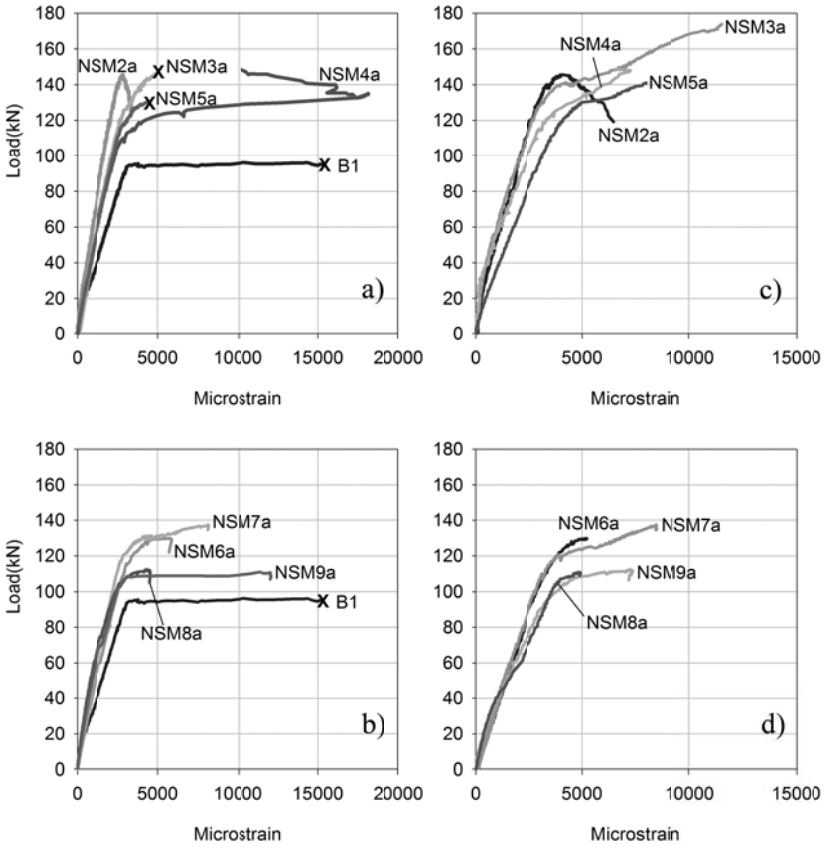

Figure 3-13 Maximum strain in the reinforcement (a, b) tension steel bars (c, d) FRP

3.3.5 Strain in steel and NSM FRP reinforcement bond stress profiles

Figures 3-14a and 3-14b show the strain profiles along the steel and FRP NSM reinforcements of beam NSM5Aa. Typically, three distinct zones can be identified along the strengthened beams: zone I, which extends from the support to the termination point, is the un-strengthened region; zone II is the transition zone, along which the strain in the NSMR develops from zero to the value corresponding to the full composite action; and zone III is the full composite action zone, which comprises the remaining length of the beam specimen. In zone 1, the strain in the steel reinforcement develops rapidly as only the internal steel

reinforcement contributes to the total flexural resistance. In zone 2, which spans approximately 200mm, the strain in the steel reinforcement increases rather moderately whilst strain increases rapidly in the NSMR as stress is shared progressively between the two reinforcement systems. In zone 3, the strains in the NSMR are higher than those in the steel reinforcement as expected from plane strain section.

After yielding of the steel reinforcement, the strain in both the steel reinforcement and the NSMR increased rapidly. With the exception of local effects, strains along the mid strip and side strips were almost similar. At peak load, yielding of the steel reinforcement almost reached the termination point on side B, whilst it developed 220mm away from the termination point on side A. The strain readings in the NSMR were also much higher than those in the steel reinforcement (Figure 3-14b), possibly due to the smaller contribution of the concrete surrounding the NSMR as well as the confinement effects caused by the shear links on the steel reinforcement.

At yield load, bond stress along the NSMR (Figures 3-14c and 3-14d) attained the highest value around the termination point (zone 2), then decreased rapidly in zone 3 (Figure 3-14d). In contrast, bond stress along the steel reinforcement attained the highest magnitude in zone 1 then decreased rapidly in zones 2 and 3. Subsequently, the yield penetration into the shear spans increased strain gradient in the NSMR, creating a high bond stress concentration zone along the yield length of the shear spans (zone 3). When yielding approached to the termination point region, this zone expanded and merged with high bond stress concentration in zone 2, creating a critical zone of bond stress and triggering end debonding failure. In the steel reinforcement, yield penetration within the shear span caused the bond stress to drop to zero in the yield region while increased sharply in adjacent regions (Figure 3-14d). At failure, the maximum bond stresses in the steel reinforcement and the NSMR were 10.5MPa and 6.3 MPa, respectively.

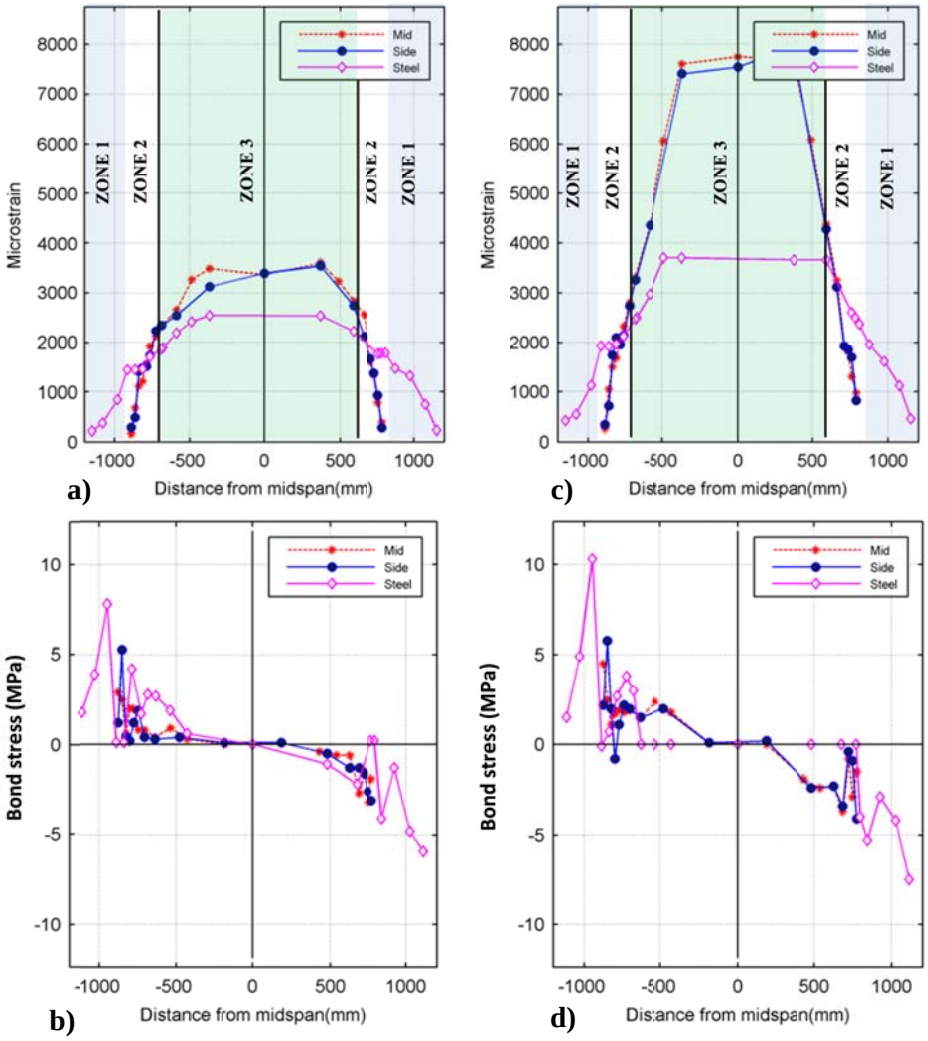

Figure 3-14 Strain and bond stress distribution of steel and NSM reinforcement along the span of beam NSM5Aa (a, b) at the yield load and (c, d) at the peak load

Figures 3-15a and 3-15c show the strain profiles along the steel reinforcement and the NSMR of beam NSM8Ba. Before the yield load, the distribution of strain along the NSMR and the rebars is similar to those of beams with a long embedment length of NSMR with a transition zone of approximately 250mm. After the yield load, the strain distribution along the steel reinforcement was noticeably different from that of beams in groups A. Yielding initiated at a crack formed in the pre-cracked stage, approximately 100mm away from the termination points of side B, and then spread along the entire strengthened section. At 109 kN, (Figure 3-15b) strains in the steel increased intensively around point P1, whilst developing steadily in the mid-span region and yielding penetrated 50mm beyond the termination point on side B. At the peak load of 113 kN, yielding continued to penetrate 100mm beyond the termination 3-15b and 3-15c). This may implies that the NSMR remains well bonded at both ends during the development of the plastic hinge around the termination points.

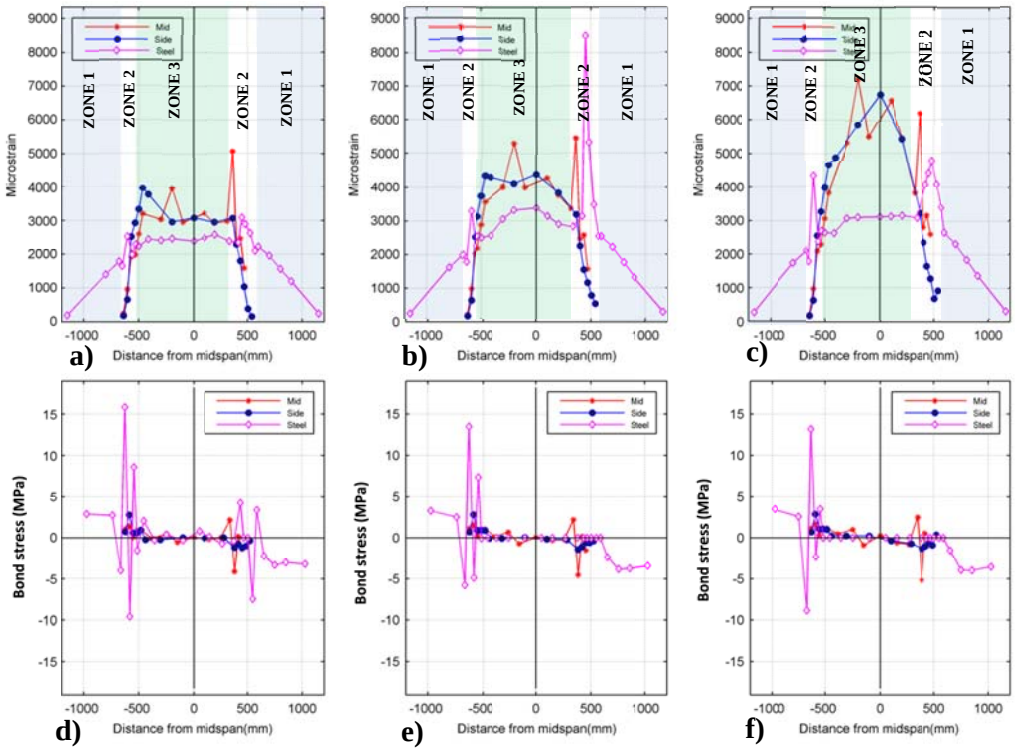

Figure 3-15 Strain distribution (a) 90kN (b) 109 kN (c) 112 kN (at failure) and bond stress distribution of the steel and NSM reinforcement along the span of beam NSM8Ba (d) 90kN (e) 109 kN (f) 112 kN (at failure)

Figures 3-15d-f show the bond stress profiles along the steel reinforcement and NSMR at the yield, maximum and ultimate loads of beam NSM8Ba, respectively. In contrast to beams in group A, which exhibit high values of bond stress in zone 1, bond stresses in the steel reinforcement in zone 1 are rather small, only 3MPa at yield load when compared to the values achieved in zone 2 of side B around the termination point (17MPa). This high bond stress in zone 2 implies potential local debonding of the steel reinforcement in the highly yielded region within zone 2 (although the steel rebars are still well anchored at the two ends). While high bond stresses developed along the steel reinforcement, those in the NSMR were rather small, with a maximum magnitude of about 2.5MPa, possibly due to the relatively low stiffness of the NSMR.

3.4 Discussion

On the basis of the results presented above, the differences in the formation and development of yielding of the steel reinforcement of beams in groups A and B are discussed in this section.

Beams in groups A and B exhibited different yielding patterns in term of both initiation and development. For beams in group A, yielding formed initially along the entire maximum moment zone and then expanded rapidly into the shear spans at higher loads, increasing the yield length significantly (Figure 3-16). At failure load, yielding spread to the region near

the termination point, creating a yield length about 1.3-1.8 d (effective beam depth) longer than predicted by conventional section analysis. This can be attributed to the formation and development of inclined cracks caused by high shear-bending interaction. Deep penetration of steel yielding inside the shear span greatly affected the bond stress distribution due to the higher strain gradient induced in the NSMR. As a result, this caused significant increase in bond stresses not only around the termination point, but also in the yield zone. At the ultimate load, yielding of the steel reinforcement around the termination point led to a significant increase in the bond stress in both curtailment and yield zones and promoted the development of two stress concentration zones, which eventually merged creating a wider bond stress concentration zone covering the entire embedment length in the shear span. Such substantial increase of bond stresses caused the formation of a large number of tributary shear cracks, particularly near the termination point, weakening the concrete soffit and eventually leading to the development of splitting, bridging cracks and ultimately debonding failure.

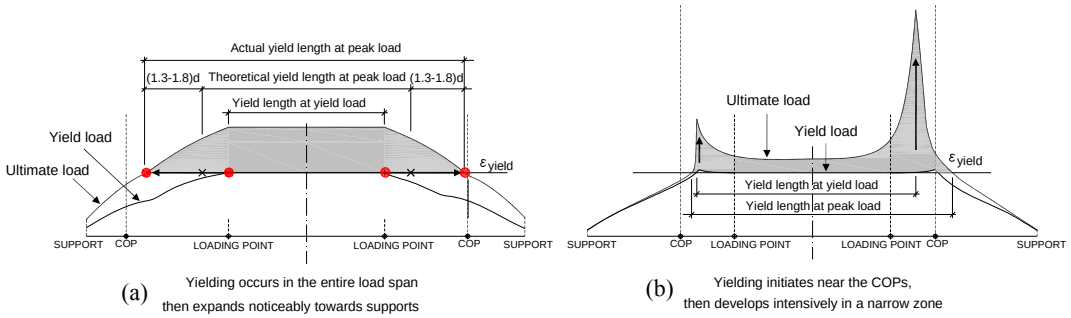

Figure 3-16 Progressive yielding of the steel reinforcement (a) in the beam group A (b) in the beams group B

In contrast, for beams in group B, yielding initiated around the termination point, then developed rapidly within a narrow zone of about 150mm, especially around the termination point on side B (shortest embedment length - Figure 3-16b). The development of very high yielding strains within a narrow zone tends to cause high curvatures, creating a plastic hinge around the termination point region. Although yielding of the steel reinforcement did not cause a noticeable change in the bond behaviour of the NSMR, it did affect significantly the bond stress distribution along the steel reinforcement. At failure, strains in the NSMR remained high at mid-span whilst bond stress around the termination point remained stable. This confirms that NSMR is still well bonded at termination points while bond stresses along the steel reinforcement increase significantly before decreasing, indicating local debonding of the steel reinforcement around the termination point.

3.5 Conclusions

This paper presented an experimental study that examined the overall behaviour of pre-damaged RC beams retrofitted with CFRP and BFRP NSMR. The discussion mainly

focused on the impact of progressive yielding of the internal steel reinforcement on the bond behaviour of the NSMR, and the resulting debonding failure mechanisms. From the experimental results and discussion presented above, the following conclusions can be drawn:

1. End debonding is the most dominant failure mode and none of the tested beams failed by intermediate crack induced debonding.

2. Yielding of the internal steel reinforcement at failure loads was detected near the termination point in the beams in group A and even penetrated beyond the termination point in the beams in group B. The yield length of the steel reinforcement is longer than that calculated by theoretical predictions, approximately 1-1.4 times the effective beam depth.

3. The steel reinforcement of the beams in groups A and B exhibited distinctive yielding patterns. For beams in group A, yield initiated in the maximum moment region and subsequently spread into the shear spans. For beams in group B, yielding initiated and developed within a narrow region around the termination points, creating a plastic hinge.

4. Yielding of the steel reinforcement affected significantly the bond behaviour and failure mechanism of the NSMR. In beams of group A, a significant increase of bond stress due to the yield penetration near the termination point triggered the formation of tributary shear cracks and weakened the concrete, eventually leading to debonding of the NSMR. In beams of group B, the plastic hinge formed in the vicinity of the termination point and, while this did not cause a significant change in bond stress along the NSMR, it caused a severe increase in bond stress along the steel reinforcement, leading to local debonding of the steel reinforcement around the termination point.

5. End debonding failure followed the development of significant cracking near the termination point, which caused the formation of concrete blocks delimited by splitting cracks surrounding the NSMR, bridging cracks and tributary shear cracks.

ACKNOWLEDGMENTS

The first author gratefully acknowledges the financial support provided by the Ministry of Education and Training of Vietnam and the University of Sheffield.

REFERENCES

[1] Alkhrdaji T, Nanni A. Flexural Strengthening of Bridge Piers Using FRP Composites. In: Mohamed E, editor.: ASCE; 2000. p. 174.

[2] Prota A. RP, Antonio Nanni. Upgrade of RC Silos Using Near Surface Mounted FRP Composites(unpublished). Industria Italiana del Cemento. 2003;LXXIII(784):170-83.

[3] Co-Force America I. Old Keys bridge repairs, negative moment strengthening of the Rockland Channel Bridge. Technical report. 2005.

[4] Tumialan JG, Vatovec, M., and Kelley, P.L. Case Study: Strengthening of Parking Garage Decks with Near-Surface-Mounted CFRP Bars. Journal of Composites for Construction. 2007;11(5):523-30.

[5] Irwin R, Rahman A. FRP strengthening of concrete structures-Design constrains and practical effects on construction detailing. New Zealand Concrete Society Conference, Wairakei. 2002.

[6] ACI-440-Commitee. ACI 440.2R-08 Guide for the Design and Construction of Externally Bonded FRP Systems for Strengthening Concrete Structures. Farmington Hills, MI, USA2008.

[7] Cement and Concrete Industry Publiccation. Technical report No. 55: Design guidance for strengthening concrete structures using fibre composite materials. 2012(CCIP-56).

[8] Quattlebaum J, B. , Harries K, A. , Petrou M, F. . Comparison of Three Flexural Retrofit Systems under Monotonic and Fatigue Loads. Journal of Bridge Engineering. 2005;10(6):731-40.

[9] Teng JG, De Lorenzis L, Wang B, Li R, Wong TN, Lam L. Debonding Failures of RC Beams Strengthened with Near Surface Mounted CFRP Strips. Journal of Composites for Construction. 2006;10(2):92-105.

[10] Cruz JMS, Barros JAO, Gettu R, Azevedo AFM. Bond Behavior of Near-Surface Mounted CFRP Laminate Strips under Monotonic and Cyclic Loading. Journal of Composites for Construction. 2006;10(4):295-303.

[11] Barros JAO, Fortes AS. Flexural strengthening of concrete beams with CFRP laminates bonded into slits. Cement and Concrete Composites. 2005;27(4):471-80.

[12] Oehlers D, Haskett M, Wu C, Seracino R. Embedding NSM FRP Plates for Improved IC Debonding Resistance. Journal of Composites for Construction. 2008;12(6):635-42.

[13] De Lorenzis L, Antonio N. Characterization of FRP Rods as Near-Surface Mounted Reinforcement. Journal of Composites for Construction. 2001;5(2):114-21.

[14] Jose MSC, Joaquim AOB, Ravindra G, Alvaro FMA. Bond Behavior of Near-Surface Mounted CFRP Laminate Strips under Monotonic and Cyclic Loading. Journal of Composites for Construction. 2006;10(4):295-303.

[15] Kalupahana WKKG, Ibell TJ, Darby AP. Bond characteristics of near surface mounted CFRP bars. Construction and Building Materials. 2013;43(0):58-68.

[16] Kotynia R. Bond between FRP and concrete in reinforced concrete beams strengthened with near surface mounted and externally bonded reinforcement. Construction and Building Materials. 2010; 32: 41-54.

[17] Blaschko M, Zilch K. Rehabilitation of concrete structures with CFRP strips glued into slits. Proceedings of the 12th International Conference on Composite Materials, Paris, July 5-9, 1999. 1999.

[18] Wu G, Dong Z, Wu Z, Zhang L. Performance and Parametric Analysis of Flexural Strengthening for RC Beams with NSM-CFRP Bars. Journal of Composites for Construction. 2013:04013051.

[19] Hassan T, Rizkalla S. Investigation of Bond in Concrete Structures Strengthened with Near Surface Mounted Carbon Fiber Reinforced Polymer Strips. Journal of Composites for Construction. 2003;7(3):248-57.

[20] De Lorenzis L, Rizzo A, La Tegola A. A modified pull-out test for bond of near-surface mounted FRP rods in concrete. Composites Part B: Engineering. 2002;33(8):589-603.

[21] Novidis D, Pantazopoulou SJ, Tentolouris E. Experimental study of bond of NSM-FRP reinforcement. Construction and Building Materials. 2007;21(8):1760-70.

[22] De Lorenzis L, Nanni A. Bond between near-surface mounted fiber-reinforced polymer rods and concrete in structural strengthening. ACI structural journal. 2002;99(2):123-32.

[23] British Standard. BS EN 12390 series:Testing of hardened concrete,2000/2009. BSI.

[24] British Standard. BS EN ISO 6892-1:2009. Tensile testing of metallic materials Method of test at ambient temperature.

[25] D7565/D7565M-10 A. Standard Test Method for Determining Tensile Properties of Fiber Reinforced Polymer Matrix Composites Used for Strengthening of Civil Structures. ASTM International, West Conshohocken, PA; 2010.

[26] Al-Sunna RAS. Deflection Behaviour of FRP Reinforced Concrete Flexural Members. Doctoral thesis, The University of Sheffield. 2006.

[27] Serbescu A. Doctoral thesis: Strengthening of RC Beams with basalt FRPs. The University of Sheffield. 2014.

Chapter 4

IMPACT OF YIELD PENETRATION ON DEBONDING FAILURE OF NSMR

Hien V. Nguyen[1], Maurizio Guadagnini[1], Kypros Pilakoutas[1], Nam V. Le[2]

[1] Department of Civil and Structural Engineering

The University of Sheffield, UK. Email: n.hien@sheffield.ac.uk

[2] Department of Civil and Structural Engineering

HCMC University of Technology, Vietnam National University, Vietnam

(Paper to be submitted to the Journal of Composites for Construction, ASCE)

Abstract

RC structures strengthened in flexure with NSMR are generally designed to reach their capacity after considerable yielding of the steel reinforcement to maintain ductility and to take advantage of the high strength of the FRP. However, yield penetration inside the shear span can cause (a) complex bond interactions between the reinforcements and (b) a significant change in bond behaviour of NSMR in the termination and yield region, triggering the premature debonding of the FRP. Understanding the impact of yield penetration inside the shear span on bond performance of NSMR and debonding failure mechanism can lead to more accurate predictions of the debonding load. This paper presents experimental evidence of deep yield penetration into the termination region and investigates its impact on bond performance and debonding failure of NSMR. This is the first such work to show that the yield penetration can reach the termination region and this understanding can lead to the development of simpler and more efficient design methods to predict debonding load of RC beams strengthened in flexure with NSMR system.

Keywords: NSMR, yielding, experimental, design method.

4.1 Introduction

Lightweight, high strength-weight ratio and corrosion resistance (Task Group 9.3 2001) make FRP an attractive option for repairing and retrofitting RC structures. Two main strengthening techniques using bonded FRP are adopted in construction (a) externally bonded reinforcement (EBR) and (b) NSMR. Bond tests provide solid evidence that NSMR is superior to EBR in terms of bond strength and post peak performance (Barros and Fortes 2005; Quattlebaum et al. 2005; Kotynia 2010; Nguyen et al. 2016)). Beam tests also confirm that beams retrofitted with NSMR can attain much higher debonding loads and ductility compared to those retrofitted with EBR (Hassan and Rizkalla 2003; Barros and Fortes 2005; Quattlebaum et al. 2005; Teng et al. 2006; Barros et al. 2007; Bonaldo et al. 2008; Soliman et al. 2008; Soliman et al. 2010; Sharaky et al. 2014; Sharaky et al. 2015; Nguyen et al. 2016). Although NSMR outperforms EBR, it still can suffer from the premature failure (Hassan and Rizkalla 2003; Barros and Fortes 2005; Quattlebaum et al. 2005; Teng et al. 2006; Barros et al. 2007; Bonaldo et al. 2008; Sharaky et al. 2014; Nguyen et al. 2016). Debonding failure of NMSR is influenced by various parameters including: shape, size and surface finish of FRP, properties of the adhesive, concrete and FRP, and geometry of the grooves (location, size, shape, spacing etc.) as well as end treatments (De Lorenzis and Antonio 2001; De Lorenzis et al. 2002; Hassan and Rizkalla 2003; Kotynia 2010; Kalupahana et al. 2013; Wu et al. 2013).

Strengthened beams are designed to attain ultimate loads much higher than the yield load, to take advantage of the high strength of FRP and to maintain adequate ductility. As a consequence, yielding of the steel reinforcement may penetrate into the shear span towards the termination point. This can cause a complex interaction between the steel reinforcement and the NSMR. In the yield region, strains in both the steel reinforcement and the NSMR increase rapidly. The bond stress in the steel reinforcement drops dramatically to zero due to its plastic behaviour, whilst that in the NSMR increases significantly to create a new bond stress concentration zone. This zone tends to expand along with yield penetration and may interact with other high bond stress regions developed around the termination point and flexural cracks. Moreover, shear-bending interaction also increases strains in the steel reinforcement and FRP, intensifying yielding as well as the bond stress in the NSMR along the shear span. These issues have not been reported in the literature and need to be highlighted and examined in detail to further our understanding of NSMR debonding. Bond tests are not able to examine such issues due to the absence of key features of flexural structures (such as bending, shear-bending interaction and the interaction of the two reinforcements) and beam tests are necessary for this purpose.

This paper presents and discusses experimental evidence, from eight RC beams, of yield penetration around the termination point. It then elaborates on its impact on bond behaviour and debonding failure mechanism of the NSMR on beam specimens.

4.2 Experimental work

A total eight RC beams retrofitted with carbon and basalt FRP bars/strips NSM reinforcement (NSM2a-NSM9a) and two control beams (B0 and B1) were tested. Details of dimensions, the layout of the steel and NSM reinforcements of the tested beams are shown in Figure 4-1. All beams were 2.5m long with a rectangular cross section of 150 mm by 250 mm. The beams were simply supported and tested using the four point bending scheme, with a clear span of 2.3m and a shear span of 0.767m. Table 4-1 summaries details of concrete; flexure and shear rebars and the FRP NSMR. Full details of mechanical properties of materials used in the tests are reported elsewhere (Nguyen et al. 2016).With the exception of beam NSM2a which was retrofitted with CFRP round bars, the remaining beams were retrofitted with BFRP and CFRP strips. Beam NSM7Aa was retrofitted with two NSM strips placed along the side faces and one placed along the bottom face. Details of test set up and instrumentation are reported elsewhere (Nguyen et al. 2016).

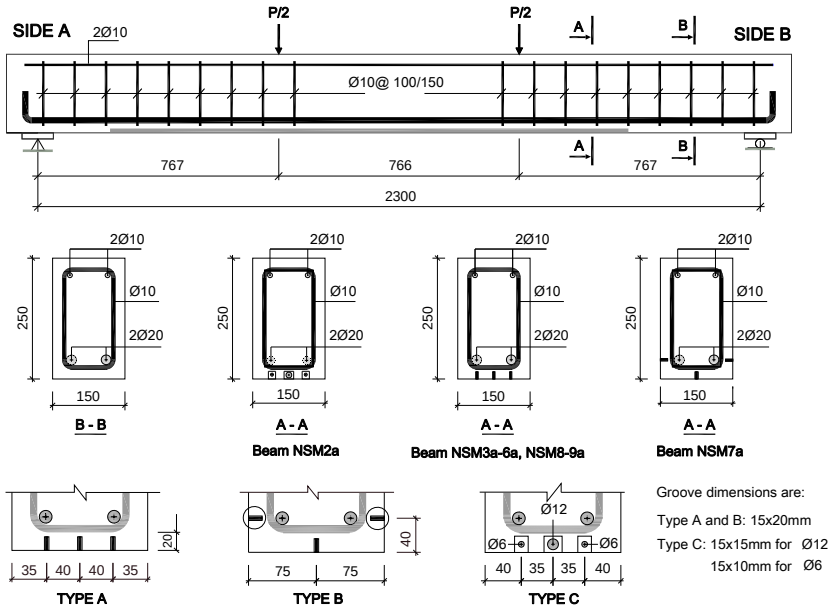

Figure 4-1 Design of beam specimens and details of reinforcement

Table 4-1 Details of tested beams

Beam	Concrete	Steel reinforcement			FRP				ρ_f/ρ_s
		Flexure		Shea					
	f_c (MPa)	A_s (mm^2)	ρ_s (%)	s (mm)	Cross section	E_f (GPa)	A_f (mm^2)	ρ_f (%)	
B0	50.2	402	1.3	100	---	---	---	---	---
B1	32.3	402	1.3	100	---	---	---	---	---
EBR	32.3	402	1.3	100	36x1.4mm	214	50	0.15	0.13
NSM2Aa	23.9	402	1.3	100	2D6+D12	133/119	170	0.54	0.42
NSM3Aa	50.2	402	1.3	100	3x12x1.4mm*	214	50	0.16	0.13
NSM4Aa	32.3	402	1.3	100	3x12x1.4mm*	214	50	0.16	0.13
NSM5Aa	32.3	402	1.3	100	3x12x1.4mm*	214	50	0.16	0.13
NSM6Aa	32.3	402	1.3	150	3x12x1.4mm*	214	50	0.16	0.13
NSM7Aa	32.3	402	1.3	100	3x12x1.4mm*	214	50	0.16	0.13
NSM8Ba	32.3	402	1.3	150	3x 14x2mm**	57	84	0.27	0.21
NSM9Ba	32.3	402	1.3	100	3x 14x2mm**	57	84	0.27	0.21

The ratio of bonded length and shear span (L_a/L_s) of the NSMR varied from 0.7-1 for the beams retrofitted with CFRP, and 0.22-0.35 for BFRP. Except for beam NSM2a which had a symmetric bond length, the remaining beams were strengthened un-symmetrically. The un-symmetric arrangement of embedment lengths of NSMR bars/strips was designed to force debonding failure to occur at the side with the shorter embedment length (side B). The scheme and details of the bond length of the NSMR are given in Figure 4-2 and Table 4-2.

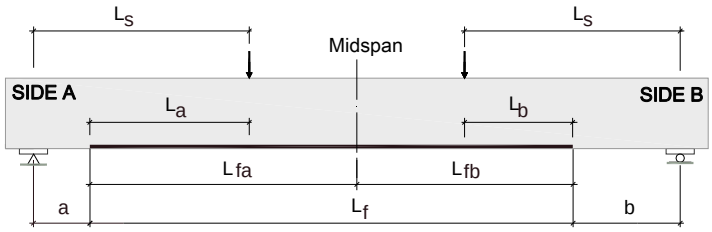

Figure 4-2 Scheme of embedment length of the beam specimens

Table 4-2 Embedment length of NSMR

Beam	L_f (mm)	a (mm)	L_{fa} (mm)	L_a (mm)	L_a/L_s	b (mm)	L_{fb} (mm)	L_b (mm)	L_b/L_s
EBR	1800	200	950	567	0.74	300	850	467	0.61
NSM2Aa	2000	150	1000	617	0.80	150	1000	617	0.80
NSM3Aa	2150	0	1150	767	1.00	150	1000	617	0.80
NSM4Aa	1800	200	950	567	0.74	300	850	467	0.61
NSM5Aa	1700	250	900	517	0.67	350	800	417	0.54
NSM6Aa	1700	250	900	517	0.67	350	800	417	0.54
NSM7Aa	1700	250	900	517	0.67	350	800	417	0.54
NSM8Ba	1200	500	650	267	0.35	600	550	167	0.22
NSM9Ba	1200	500	650	267	0.35	600	550	167	0.22

4.3 Results and discussion

Beam NSM2Aa failed in pure flexure following concrete crushing and two other beams NSM8Ba and NSM9Ba also failed in flexure, but after developing substantial rotation around the termination points. The remaining beams failed by end debonding of the NSMR and mixed modes. Intermediate crack induced debonding was not observed in any of the tested specimens. Figure 4-3 shows the deflection at mid-span versus load of tested beams. Table 4-3, summarises the test results. The overall behaviour including more extensive test data are presented in (Nguyen et al. 2016). This section presents and discusses the impact of yield penetration on bond distribution.

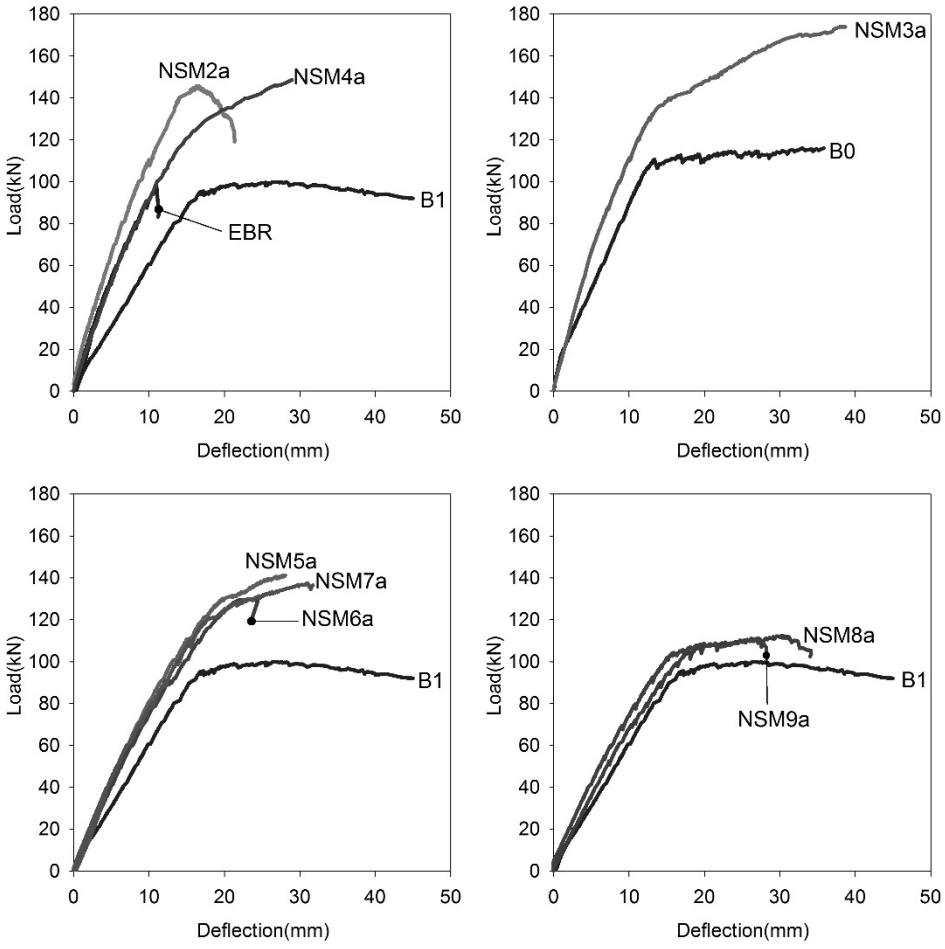

Figure 4-3 Load-deflection of tested beams

Table 4-3 Summary of test results

Beam	P_o (kN)	P_y (kN)	P_p (kN)	P_p/P_0	P_{cal} (kN)	P_{exp}/P_{cal}	d_p/d_0	P_u (kN)	P_u/P_y	Failure modes
NSM2Aa	---	139	146	1.35	145	1.01	---	123	1.05	C
B0	---	106	116	1.07	109	1.06	---	107	1.09	C
B1	---	94	100	1.05	105	0.95	---	92	1.06	C
EBR	50	---	98	---	149	0.66	0.27	98	---	D
NSM2Aa	---	140	146	1.35	145	1.01	---	123	1.04	C
NSM3Aa	56	136	174	1.53	176	0.99	1.08	174	1.28	C, D*, F*
NSM4Aa	51	122	149	1.25	146	1.02	0.64	149	1.22	D
NSM5Aa	40	122	141	1.30	146	0.97	0.62	141	1.16	D
NSM6Aa	41	122	130	1.32	146	0.89	0.54	130	1.07	D
NSM7Aa	40	121	138	1.25	142	1.00	0.7	138	1.14	D
NSM8Ba	41	105	113	1.09	126	0.90	0.76	106	1.08	C**,S*
NSM9Ba	40	103	111	1.07	126	0.88	0.63	109	1.08	C**,S*

Note : *Secondary failure mode; ** Crushing of concrete after high rotation developed

C: Concrete crushing following steel yielding, D: end debonding; S: Shear failure

4.3.1 Yield penetration

Figures 4-4a-d and 4-4e-h show strain profiles for the steel reinforcement and the NSMR of beams of group A at failure load around the termination points on side A and side B, respectively. Table 4-4 summaries the yield lengths of tested specimens, the ratios of yield length over embedment length and shear span of each side of the tested beams along with yield lengths calculated using the section analysis approach. As expected, yielding of beams in group A initiated in the pure flexure span then developed rapidly towards the termination point after yield load. This rapid development of yielding increased significantly the strain in the FRP in the yield zone as well as in the vicinity of the termination point. At failure, yielding almost reached the termination point; 95-100% of the embedment length on side B and 78-83% on side A. For beam NSM2Aa which failed in flexure, yielding penetrates only 50% of the embedment length. In contrast, for beams in group B, steel initially yielded around the termination point then strain developed intensively in a narrow region around the termination point. Despite that yielding in the pure flexure span was rather moderate (approximately 3000με). The intensive yielding around the termination point produced a plastic hinge with high local curvature. At failure yielding was observed to develop 100-150mm beyond the termination point on side B.

The yield lengths recorded at the ultimate load in the tested beams failing by end debonding were longer than those predicted by section analysis in the range of 260mm-270mm corresponding to 1.3-1.8 of the effective depth. The deeper yield penetration than expected may be contributed to inclined shear cracks in the shear span that tend to add extra strain on both steel and NSMR reinforcement, as a result of the truss effect (or shear shift).

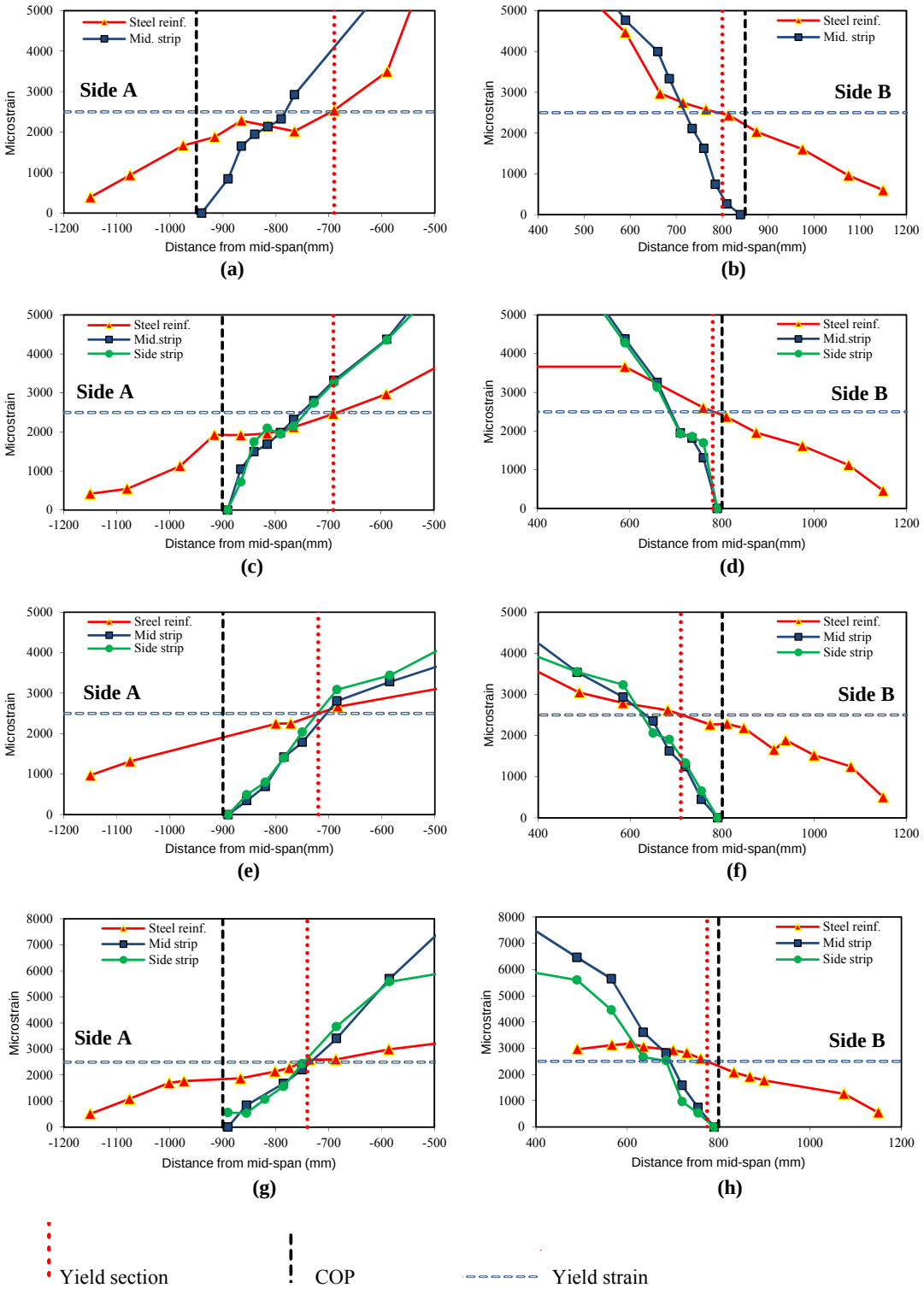

Figure 4-4 Strain profiles of steel reinforcement and NSMR around the termination points of beam group A (a,b)beam NSM4Aa, (c,d) beam NSM5Aa, (e,f) beam NSM6Aa and (g,h) beam NSM7Aa

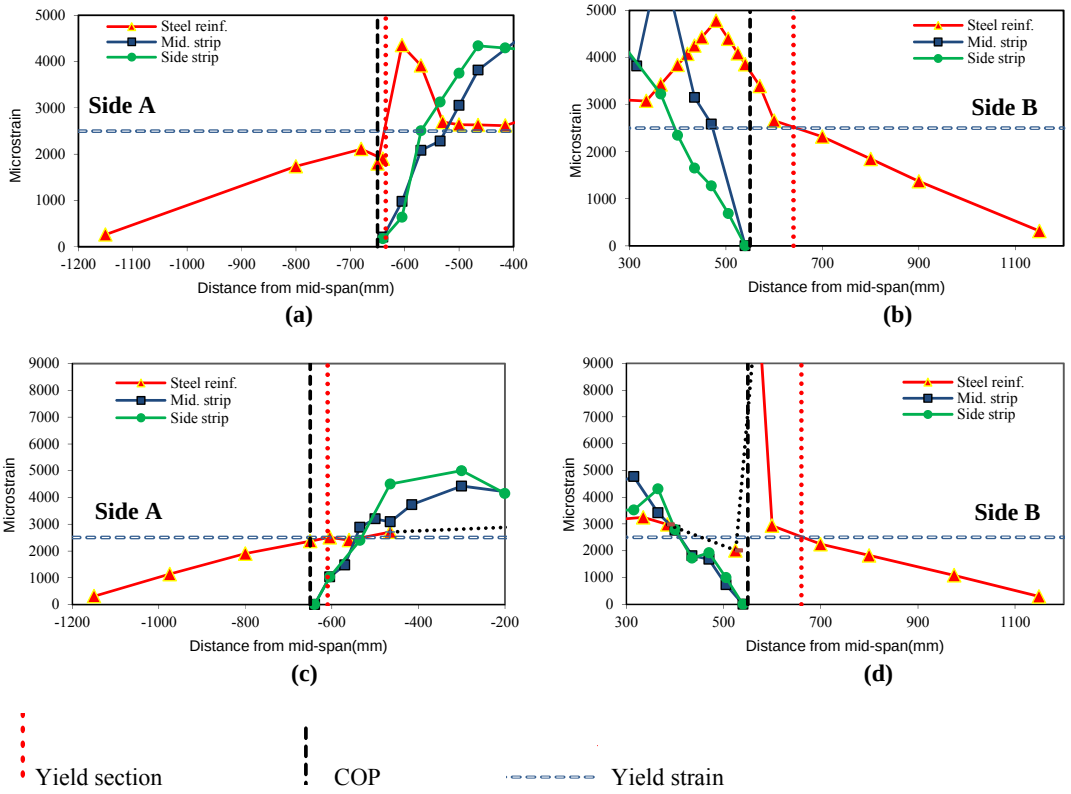

Figure 4-5 Strain profiles of steel reinforcement and NSMR around the termination points of beam group B (a,b)beam NSM8Ba and (c, d) beam NSM9Ba.

Table 4-4 Penetration of yielding at failure load of the beam specimens

Beam ID.	Side B (Damaged side)					Side A(Non-damaged side)				
	a	a_y	y_A	(y_A/L_s)	(y_A/L_a)	b	b_y	y_B	(y_B/L_s)	(y_B/L_b)
NSM2Aa	150	380(520)*	387	50%	50%	150	380	387	50%	50%
NSM3Aa	150	---	---	---	---	0	---	---	---	---
NSM4Aa	300	45	422	55%	95%	200	250	317	41%	74%
NSM5Aa	350	18	399	52%	98%	250	218	299	39%	76%
NSM6Aa	350	0	417	54%	100%	250	190	327	43%	79%
NSM7Aa	350	25	392	51%	97%	250	155	362	47%	83%
NSM8Aa	600	-100	202	26%	106%	500	12	255	33%	98%
NSM9Aa	600	-150	317	41%	127%	500	40	227	30%	94%

a,b : distance from termination point to the support on side A and side B, respectively

y_A and y_B: yield lengths on sides A and B, respectively

a_y and b_y: distances from yield point to the termination points of sides A and B, respectively

4.4 Discussion

4.4.1 Catch-up length and transition length in beams of group A

Within zone 2, strains in the NSMR develop rapidly, while those in the steel reinforcement develop rather moderately or even decrease as a result of progressive force distribution between the two sets of reinforcement.

Strain in the NSMR catches-up and matches that in the steel reinforcement at some section within zone 2, hereafter referred to as the 'catch-up' section. The 'catch-up' length is determined as the distance between the termination point and the 'catch-up' section. Along this length, the classical assumption that plane sections remain plane is not valid; strains in the NSMR are smaller than (or equal to) those in the steel reinforcement, but are characterised by a much steeper gradient, thus resulting in higher bond stresses. Moreover, the penetration of yielding into the catch up length intensifies bond stresses thus promoting end debonding within this zone. The catch up lengths measured in the tested beams were in the range of 200-250mm, equivalent to approximately 1-1.1 times the effective depth of the beam. Strain in the NSMR and the steel reinforcement at the catch-up section ranged between 1 to 1.3 times the yield strain.

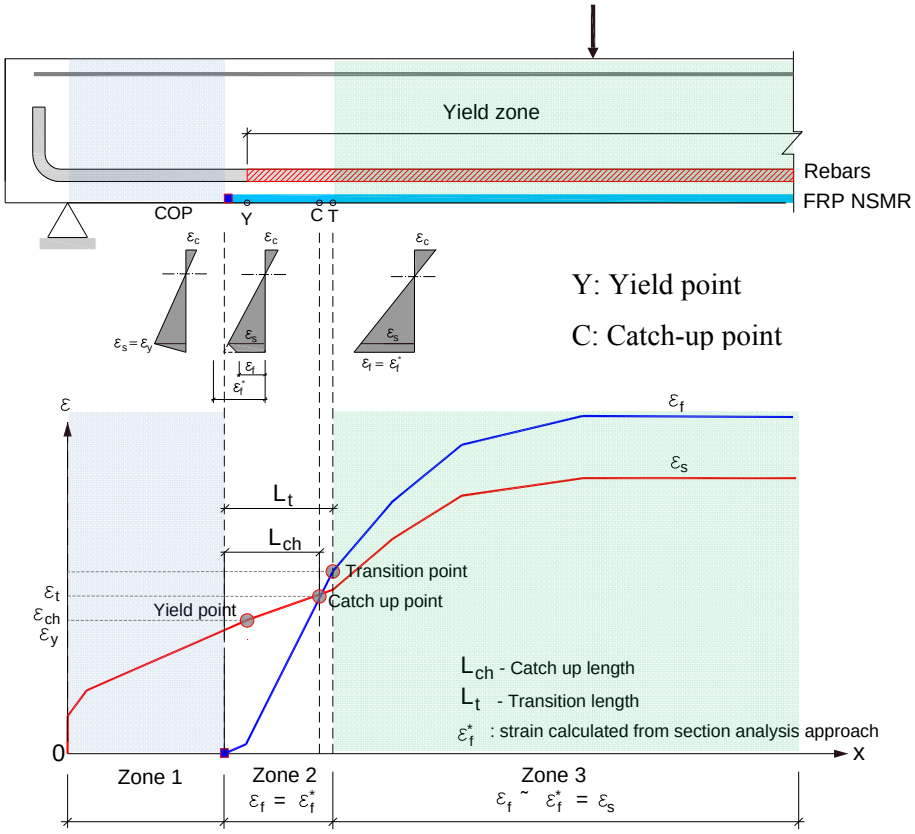

Figure 4-6 Transition length and catch up length at failure.

Transition length is an extended version of the 'catch-up' length. Within this length, the plane sections assumption is still not valid. The transition length for NSMR is approximately 1.1 times greater than the catch-up length (Figure 4-6). It is worth distinguishing between the anchorage length calibrated from bond tests and the transition length obtained from beam tests. The anchorage length is calibrated from pure shear tests to evaluate the bond strength between FRP and concrete substrate. In contrast, the transition length is determined via

strain profiles of both steel and FRP in flexure tests and reflects the mutual interaction between the steel reinforcement and the NSMR.

4.4.2 Yield patterns

As expected, yielding in beams of group A initiated in the pure bending zone and then spread rapidly into the shear spans at higher loads, expanding the yield region significantly (Figure 4-7a).

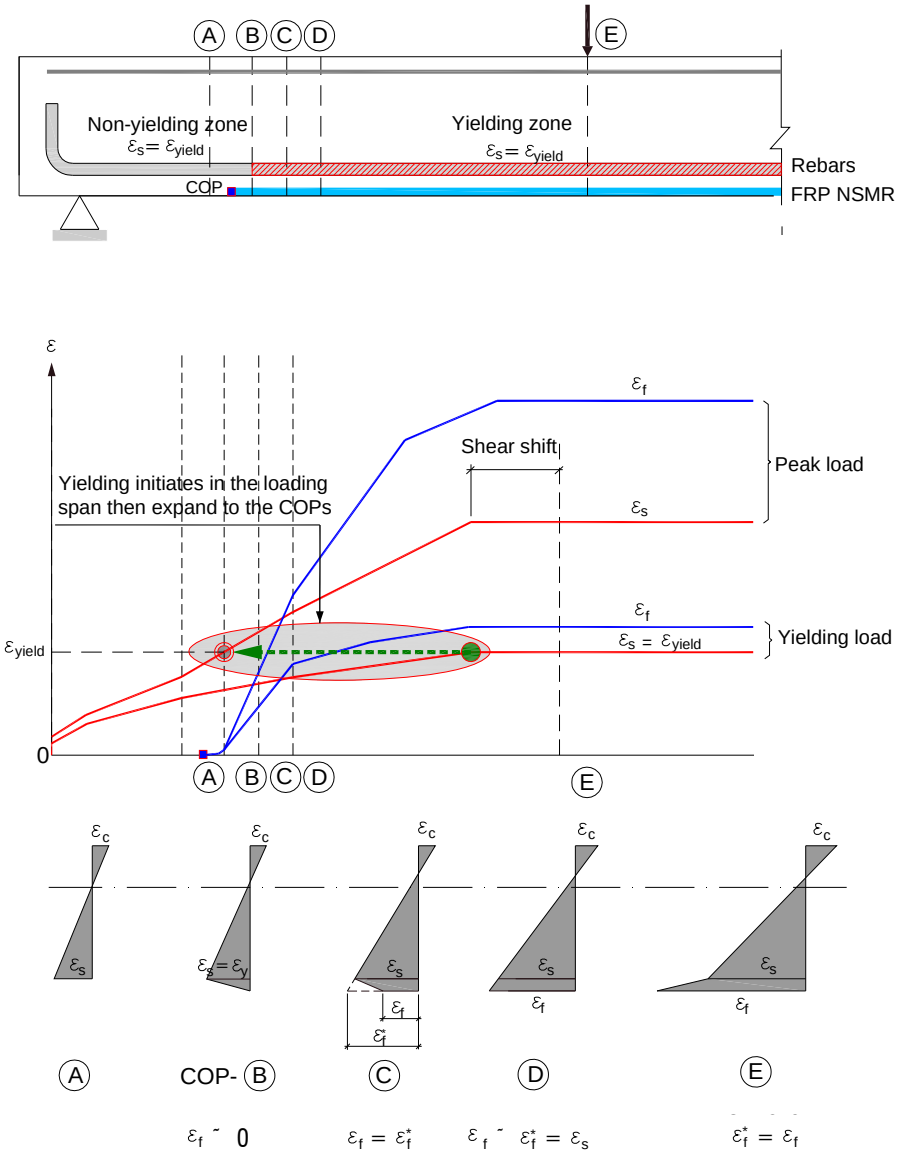

Figure 4-7 Formation and development of yielding of beams in group B

At failure yielding penetrated into the region near the COP, creating a yield length about 1.3-1.8 d (effective beam depth) longer than predicted by conventional section analysis. This can be attributed to the formation and development of inclined cracks caused by high shear-bending interaction. At high load levels, strains in the NSMR can be much higher than those in the steel reinforcement as in section D due to curvature or even much higher as in section

E in between pre-existing cracks (Figure 4-7b). This can be explained by the fact that the contribution of concrete surrounding the steel reinforcement is much more significant than that near the NSMR where cracks move uniformly. At failure, yielding penetrates into the 'catch-up length' with strain in the reinforcement at the catch-up section being in the range of 1.1-1.2 times yield strain.

Yielding in beams in group B (Figure 4-8), initiated around the COP, then developed intensively within a narrow zone of about 150mm. Yielding in the mid-span was rather moderate. Intensive yielding within a narrow zone caused high curvatures, creating a plastic hinge around the COP region. Yielding developed within the catch-up length, and was even found to develop 100-150mm in the un-strengthened section of the beam. The strain in the steel reinforcement within the 'catch up' length was up to five times higher than the yield strain, much higher than that in beams in group A (gauge 67) (Figure 4-9a).

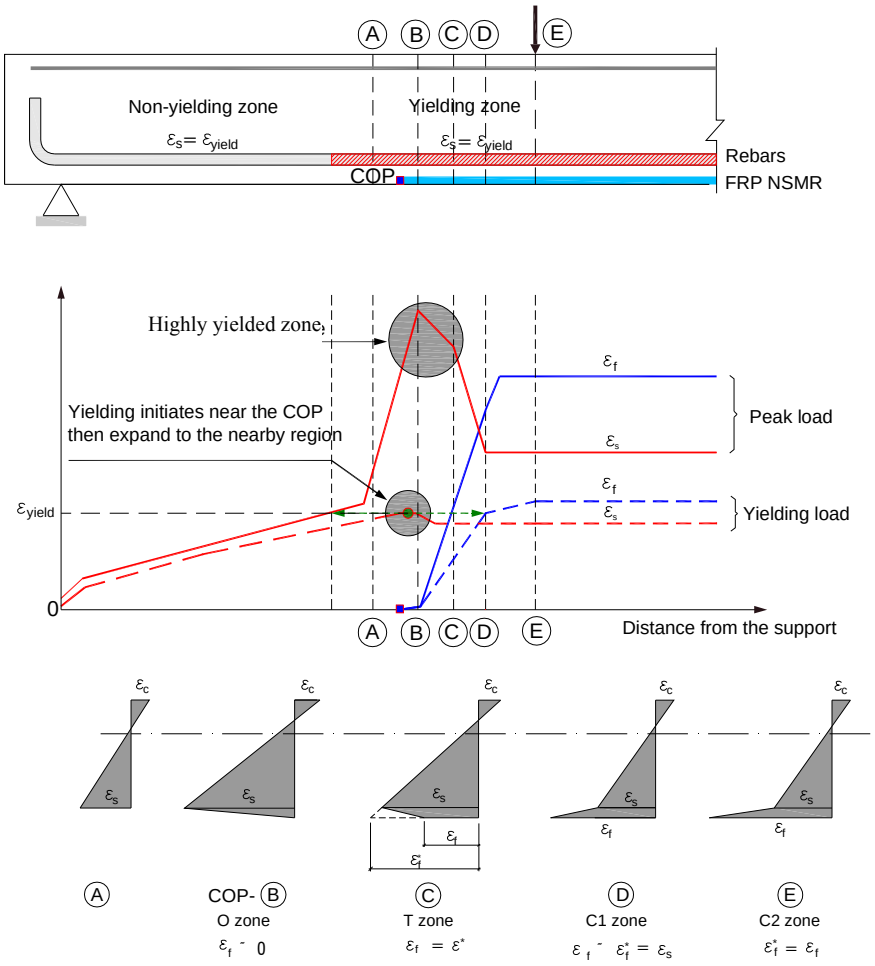

Figure 4-8 Formation and development of yielding in beams group B

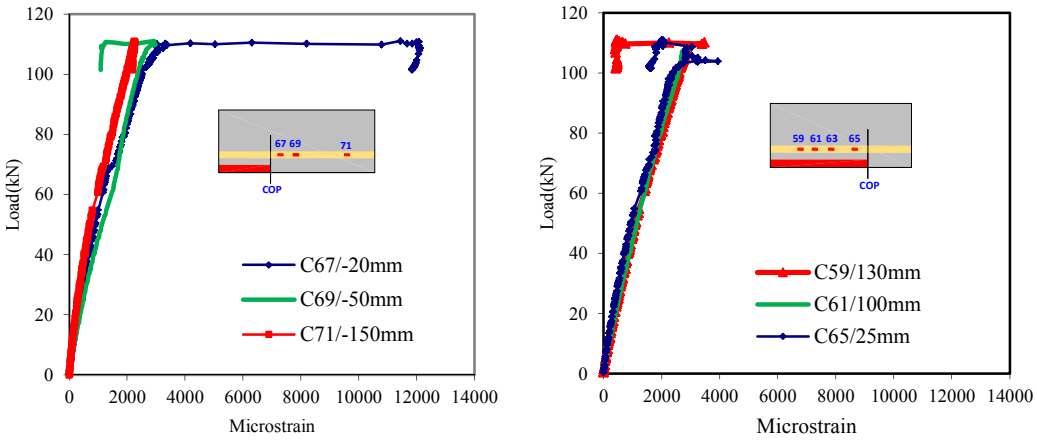

Figure 4-9 Strain in steel reinforcement around the termination point (a) un-strengthen region (b) strengthened region

4.4.3 Effects of steel yielding on the bond stress along the NSMR

4.4.3.1 Beams in group A

Figures 4-10 a-b and c-d show the strain and bond stress around the termination point of the NSMR of beams NSM4Aa and NSM7Aa, respectively. Up to the yield load, high bond stresses developed in a narrow region within approximately 50mm from the termination point; these then decreased significantly away from the termination point (Figure 4-10b). It is worth noting that by the yield load, the peak of bond stress can shift 50-70 mm away from the termination point, as in NSM7Aa, due to loss of stress in the FRP (existence of stress-free zone) in the FRP (Figures 4.10 c and d).

At failure load, the deep yield penetration in the vicinity of the termination point increases significantly the strain along the NSMR, causing higher average bond stress along the entire shear span (Figures 4-10 b and d). In beam NSM4Aa, bond stresses decreased significantly after reaching the maximum magnitude of 5.8MPa around the termination point, indicating local debonding of NSMR. Consequently, bond stresses increased substantially in the yield zone (starting at 50mm from the termination point) (Figure 4-10b). Despite the lower bond stress very near the termination point, a significant increase in bond stress in the shear span was also observed in beam NSM7Aa (Figure 4-10d).

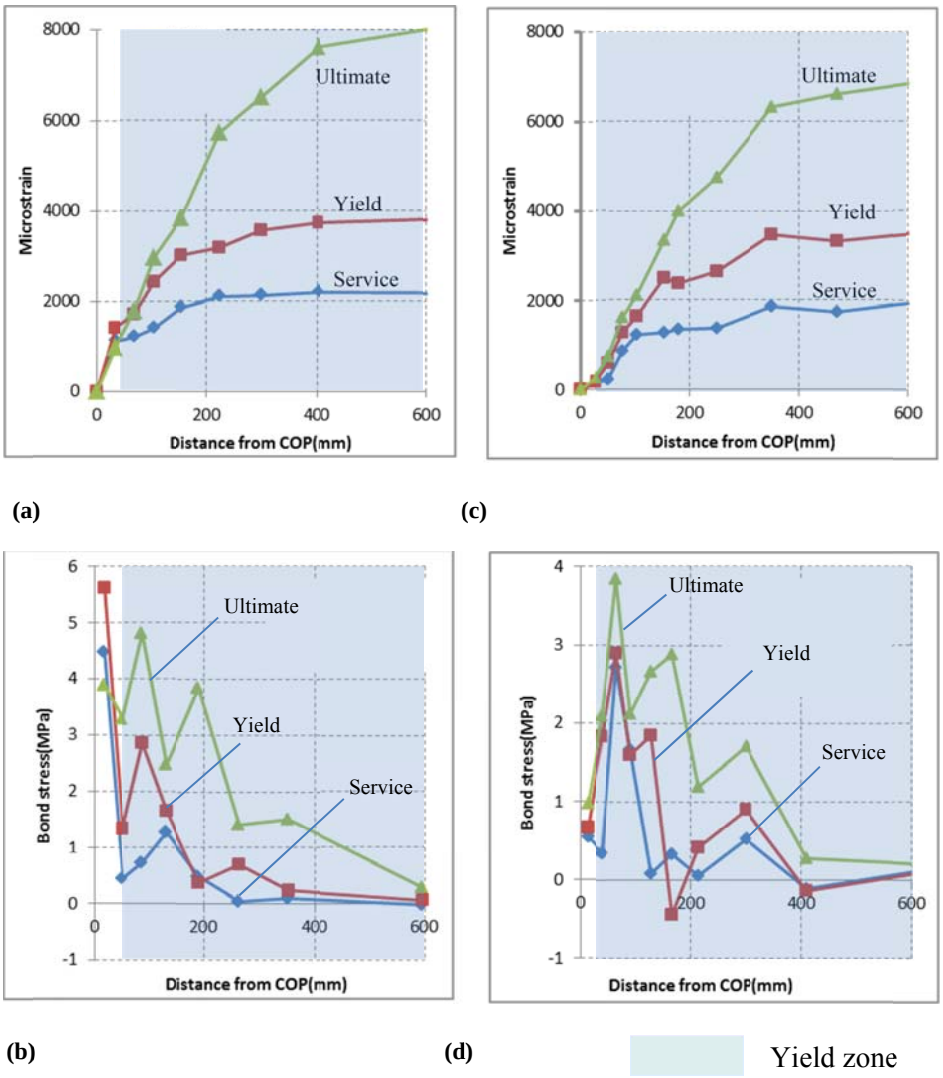

Figure 4-10 Evolution of strain and bond stress around the termination point at different load level on side B (a, b) beam NSM4Aa (c, d) beam NSM7Aa

Along the embedment length, the region between the termination point and the adjacent crack is the most critical region for end debonding, due to the overlapping of high bond stress concentration zones. In this region, the bending and pull-out actions simultaneously influence the strain and bond stress along the NSMR. Bending creates average shear, (τ_a) along the shear span. Stiffness discontinuity causes a bond stress around the termination point, τ_c, whilst the pull-out action causes bond stress concentration around the adjacent crack (τ_{cr}) (Figures 4-11).

At yield load, the bond stress around the termination point, τ_c increases rapidly, whilst τ_{cr} remains small, as only a small amount of additional strain develops around the crack near to the termination point. Both bond stress concentrations, τ_c and τ_{cr} , develop in separate narrow regions. After yielding, the average bond stress, τ_a, which is considered to be uniform within the shear span for point loaded structures, increases significantly as a high strain gradient develops in the yield zone of the shear span (since the steel picks up no

significant additional load). As yield penetrates near the termination point, all bond stresses τ_c, τ_{cr} and τ_a are intensified. This promotes local debonding around the termination point and the adjacent cracks and causes the shift of the two bond stress concentration zones close together. Furthermore, yield penetration into the region promotes the formation and development of tributary shear cracks, reducing significantly crack spacing in the region (only 35-50mm at failure). The development of these cracks makes the interaction between the two high bond stress zones more intensive, ultimately leading to end debonding failure (Figure 4-12).

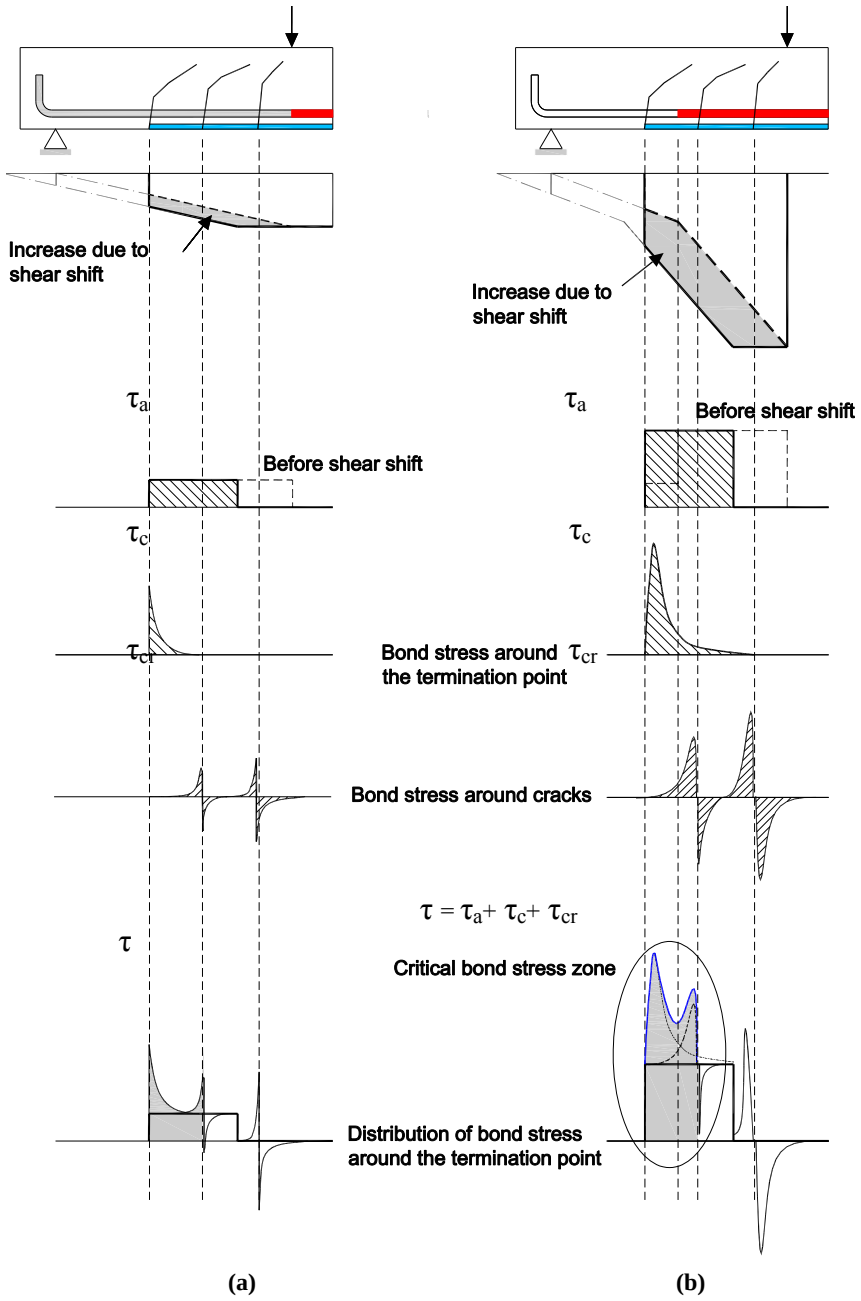

Figure 4-11 Evolution of bond stress along the NSMR in beams in group A(a) at yield load (b) at ultimate load

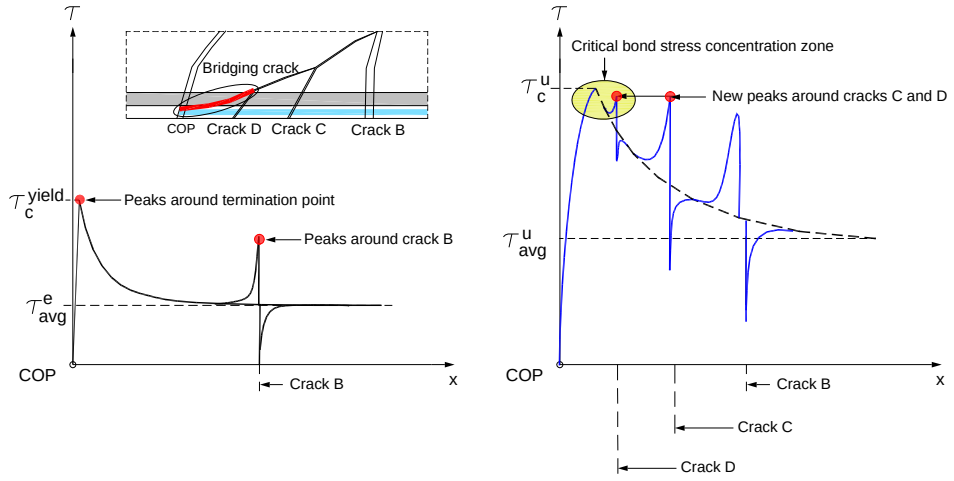

Figure 4-12 Formation of critical zone of bond stress in the vicinity of the termination point following the formation of tributary shear cracks

4.4.3.1 Beams in group B

Figures 4-13a and b show the strain and bond stress distribution, respectively, along the steel reinforcement and NSMR at failure. Intensive yielding at the COP did not cause a noticeable change in the bond behaviour of the NSMR, but it did affect significantly the local bond stress distribution along the steel reinforcement even though this is a very localised effect due to the high yielding strains and local debonding. This confirms that NSMR are still well bonded at COPs (Figure 4-13).

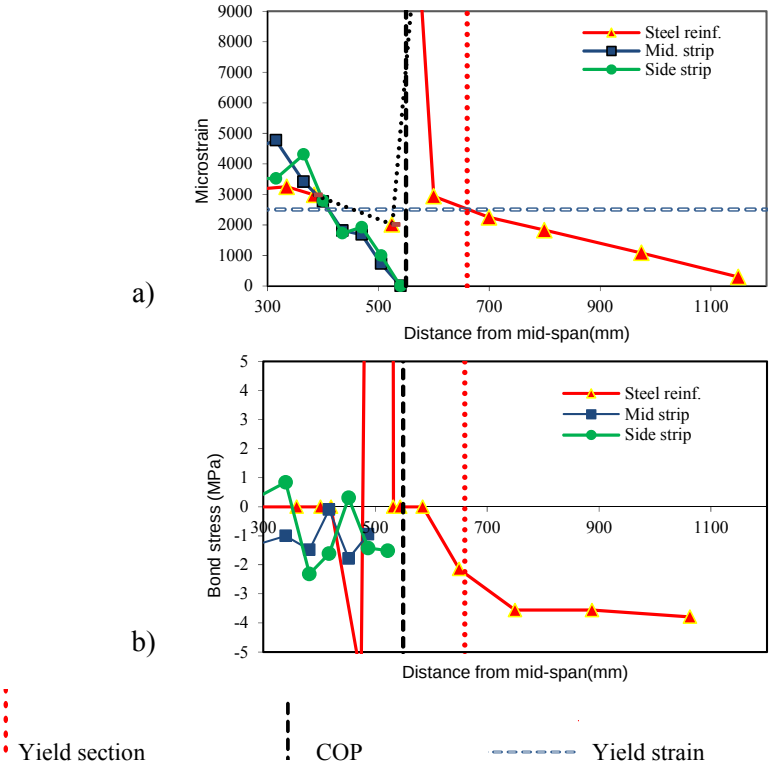

Figure 4-13. Profile of strain (a) and bond stress (b) of NSMR and the steel reinforcement along the span on side B at failure

4.5 Conclusions

The work presented here has provided experimental evidence that yielding of the flexural steel reinforcement can develop deeply into the shear span and can reach close or even beyond the COP when failure occurs. From the discussion presented above the following conclusions can be drawn:

- At failure, the yield length in the tested beams was longer than predicted by section analysis.
- The penetration of yielding near the termination point not only increases remarkably the average bond stress along the NSMR, but also intensifies the bond stress concentration around the termination point and adjacent cracks.
- The interaction between bond stress concentration zones increases with increasing the load. These zones eventually merge together to create the critical bond stress concentration zone between the termination point and the adjacent crack (crack B).
- Yielding around the COP promotes the development of debonding from the local scale to the global scale (i.e. failure).

The findings of this experimental work can be used to develop more effective design methodologies to prevent end debonding failure for NSMR.

ACKNOWLEDGMENTS

The first author gratefully acknowledges the financial support provided by the Ministry of Education and Training of Vietnam and the University of Sheffield.

REFERENCES

Al-Mahmoud, F., A. Castel, et al. (2009). "Strengthening of RC members with near-surface mounted CFRP rods." Composite Structures **91**(2): 138-147.

Al-Mahmoud, F., A. Castel, et al. (2010). "RC beams strengthened with NSM CFRP rods and modeling of peeling-off failure." Composite Structures 92(8): 1920-1930.

Barros, J. A. O., S. J. E. Dias, et al. (2007). "Efficacy of CFRP-based techniques for the flexural and shear strengthening of concrete beams." Cement and Concrete Composites 29(3): 203-217.

Bilotta, A., F. Ceroni, et al. (2011). "Bond Efficiency of EBR and NSM FRP Systems for Strengthening Concrete Members." Journal of Composites for Construction 15(5): 757-772.

Bonaldo, E., J. A. O. Barros, et al. (2005). "Concrete slabs strips reinforced with epoxy-bonded carbon laminates into slits." International conference on construction materials 3 “Construction materials : performance, innovations and structural implications (ConMat'05) proceedingsVancouver, Canada [CD-ROM].

Bonaldo, E., J. de Barros, et al. (2008). "Efficient Strengthening Technique to Increase the Flexural Resistance of Existing RC Slabs." Journal of Composites for Construction 12(2): 149-159.

Ceroni, F. (2010). "Experimental performances of RC beams strengthened with FRP materials." Construction and Building Materials 24(9): 1547-1559.

Cruz, J. M. S., J. A. O. Barros, et al. (2006). "Bond Behavior of Near-Surface Mounted CFRP Laminate Strips under Monotonic and Cyclic Loading." Journal of Composites for Construction 10(4): 295-303.

De Lorenzis, L. and N. Antonio (2001). "Characterization of FRP Rods as Near-Surface Mounted Reinforcement." Journal of Composites for Construction 5(2): 114-121.

De Lorenzis, L. and A. Nanni (2002). "Bond between near-surface mounted fiber-reinforced polymer rods and concrete in structural strengthening." ACI structural journal 99(2): 123-132.

De Lorenzis, L., A. Rizzo, et al. (2002). "A modified pull-out test for bond of near-surface mounted FRP rods in concrete." Composites Part B: Engineering 33(8): 589-603.

fib-TG9.3. 2001. Design and Use of Externally Bonded Fiber Polymer Reinforcement (FRP EBR) for Reinforced Concrete Structures. Technical Report Prepared by EBR Task Group 9.3, Bulletin 14, Lausanne, Swiss.

Hassan, T. and S. Rizkalla (2003). "Investigation of Bond in Concrete Structures Strengthened with Near Surface Mounted Carbon Fiber Reinforced Polymer Strips." Journal of Composites for Construction 7(3): 248-257.

Kalupahana, W. K. K. G., T. J. Ibell, et al. (2013). "Bond characteristics of near surface mounted CFRP bars." Construction and Building Materials 43(0): 58-68.

Kotynia, R. (2010). "Bond between FRP and concrete in reinforced concrete beams strengthened with near surface mounted and externally bonded reinforcement." Construction and Building Materials 32: 41-54.

Nguyen, V., Hien, M. Guadagnini, et al. (2016a). "Performance of RC beams strengthened in flexure with FRP NSMR." Composite part B: (to be submitted).

Quattlebaum, J., B. , K. Harries, A. , et al. (2005). "Comparison of Three Flexural Retrofit Systems under Monotonic and Fatigue Loads." Journal of Bridge Engineering 10(6): 731-740.

Seracino, R., M. Raizal Saifulnaz, et al. (2007). "Generic Debonding Resistance of EB and NSM Plate-to-Concrete Joints." Journal of Composites for Construction 11(1): 62-70.

Sharaky, I. A., L. Torres, et al. (2014). "Flexural response of reinforced concrete (RC) beams strengthened with near surface mounted (NSM) fibre reinforced polymer (FRP) bars." Composite Structures 109(0): 8-22.

Sharaky, I. A., L. Torres, et al. (2015). "Experimental and analytical investigation into the flexural performance of RC beams with partially and fully bonded NSM FRP bars/strips." Composite Structures 122(0): 113-126.

Soliman, S. M., E. El-Salakawy, et al. (2010). "Flexural behaviour of concrete beams strengthened with near surface mounted fibre reinforced polymer bars." Canadian Journal of Civil Engineering 37(10): 1371-1382.

Teng, J. G., L. De Lorenzis, et al. (2006). "Debonding Failures of RC Beams Strengthened with Near Surface Mounted CFRP Strips." Journal of Composites for Construction 10(2): 92-105.

Wang, B., J. G. Teng, et al. (2008). "Strain monitoring of RC members strengthened with smart NSM FRP bars." Construction and Building Materials In Press, Corrected Proof.

Wu, G., Z. Dong, et al. (2013). "Performance and Parametric Analysis of Flexural Strengthening for RC Beams with NSM-CFRP Bars." Journal of Composites for Construction: 04013051.

Chapter 5

NEW DESIGN METHOD FOR EMBEDMENT LENGTH OF NSMR

Hien V. Nguyen[1], Maurizio Guadagnini[1], Kypros Pilakoutas[1], Nam V. Le [2]

[1,]Department of Civil and Structural Engineering

The University of Sheffield, UK. Email: n.hien@sheffield.ac.uk

[2] Department of Civil and Structural Engineering

HCMC University of Technology, Vietnam National University, Vietnam

(Paper to be submitted to the Journal of Composites for Construction, ASCE)

ABSTRACT

Premature end debonding is the most common failure mode of RC structures strengthened in flexure with Near Surface Mounted Reinforcement (NSMR), which prevents structures from developing their full flexural capacity. The failure can be avoided by providing a sufficient embedment length for NSMR. Embedment length models proposed by existing design guidelines are currently unable to provide a consistent level of safety. This paper presents a new simple, yet effective design method based on experimental evidence which shows that yielding of the steel reinforcement in the termination region intensifies stresses and triggers end debonding failure. The proposed design method is validated against an extensive database of results reported in the literature and is compared against existing design guidelines. It is shown that that the new design method preforms better than existing models and provides more reliable predictions.

Keywords: NSMR, end debonding, yielding, design guidelines.

5.1 Introduction

The superior bond behaviour of NSMR guarantees an overall better performance of this strengthening solution when compared to the more conventional externally bonded reinforcement (EBR) (Barros and Fortes 2005; Quattlebaum et al. 2005; Kotynia 2010; Nguyen et al. 2016b). However, performance of NSMR is still controlled by the bond strength between FRP and the concrete substrate and premature debonding is still a crucial issue in strengthening applications. The stress concentration that develops at the termination point of the FRP can cause end debonding. The magnitude of developed stresses around the termination point can be affected by several parameters, such as, embedment length; FRP and steel reinforcement ratios; shapes, size and surface finish of FRP and mechanical properties of steel and FRP reinforcement, structural adhesive and concrete; concrete cover, spacing between NSMR and distance to the edge, etc. Of all these parameters, the embedment length of NSMR is one of the most important parameters in controlling end debonding. The use of adequate embedment length for the NSMR can reduce sufficiently the stresses around the termination point and help to prevent end debonding (Hassan and Rizkalla 2003; Barros and Fortes 2005; Quattlebaum et al. 2005; Teng et al. 2006; Barros et al. 2007; Bonaldo et al. 2008; Soliman et al. 2008; Soliman et al. 2010; Sharaky et al. 2014; Sharaky et al. 2015; Nguyen et al. 2016).

Analytical solutions can provide explicit fundamental understanding of the development of stresses in various parts of a strengthened structure, especially around the termination point and are useful to understand effects of various parameters on stress development. However, since they rely either on (a) linear analysis or (b) continuum mechanics, or both, they are unable to predict accurately the structural behaviour at higher load levels when a significant amount of material nonlinearity and geometrical discontinuities arise.

Significant attempts were made to develop models to determine the required embedment length by calibrating results obtained from small scale bond tests (De Lorenzis and Antonio 2001; De Lorenzis and Nanni 2001; Cruz and Barros 2002; De Lorenzis and Nanni 2002; De Lorenzis et al. 2002; Cruz and Barros 2004; De Lorenzis 2004; De Lorenzis et al. 2004; Bonaldo et al. 2005; Chen and Pan 2006; Novidis et al. 2007; Seracino et al. 2007; Kotynia 2010; Bilotta et al. 2011; Kalupahana et al. 2013). Despite the fact that bond tests are simple to carry out and provide fundamental understanding of bond performance and debonding failure of a strengthening system, they have key limitations: (a) the bond length used in the bond tests are far too short when compared to those used in strengthened beams tests (De Lorenzis and Antonio 2001; De Lorenzis and Nanni 2001; Cruz and Barros 2002; De Lorenzis and Nanni 2002; De Lorenzis et al. 2002; Cruz and Barros 2004; De Lorenzis 2004; De Lorenzis et al. 2004; Bonaldo et al. 2005; Chen and Pan 2006; Seracino et al.

2007; Kotynia 2010; Bilotta et al. 2011; Kalupahana et al. 2013) (b) the absence of key flexural features in pure shear tests (cracks, bending, bending-shear interaction; and interaction of steel-FRP) and (c) inconsistent results due to lack of testing standards (De Lorenzis and Antonio 2001; De Lorenzis and Nanni 2001; Cruz and Barros 2002; De Lorenzis and Nanni 2002; De Lorenzis et al. 2002; Cruz and Barros 2004; De Lorenzis 2004; De Lorenzis et al. 2004; Bonaldo et al. 2005; Chen and Pan 2006; Seracino et al. 2007; Kotynia 2010; Bilotta et al. 2011; Kalupahana et al. 2013). These limitations do not allow bond tests to represent accurately the bond performance of the NSMR system in flexural elements, thus these tests cannot be directly used to predict debonding failure and calculate the embedment length in flexural elements.

Furthermore, most design guidelines use different provisions for determining the theoretical termination section and corresponding anchorage length (L_f) and tensile force T_f, for example: section with maximum tensile force (point D, $L_f = L_{fmax}$ and $T_f = T_{fmax}$ in Figure 5-1); yield section (point C, $L_f = L_{fy}$ and $T_f = T_{fy}$ in Figure 5-1), section where the FRP is 'no longer needed' (point B, $L_f = L^*$ and $T_f = T^*$ in Figure 5-1); and cracking section (point A, $L_f = L_{fc}$ and $T_f = T_{fc}$ in Figure 5-1).

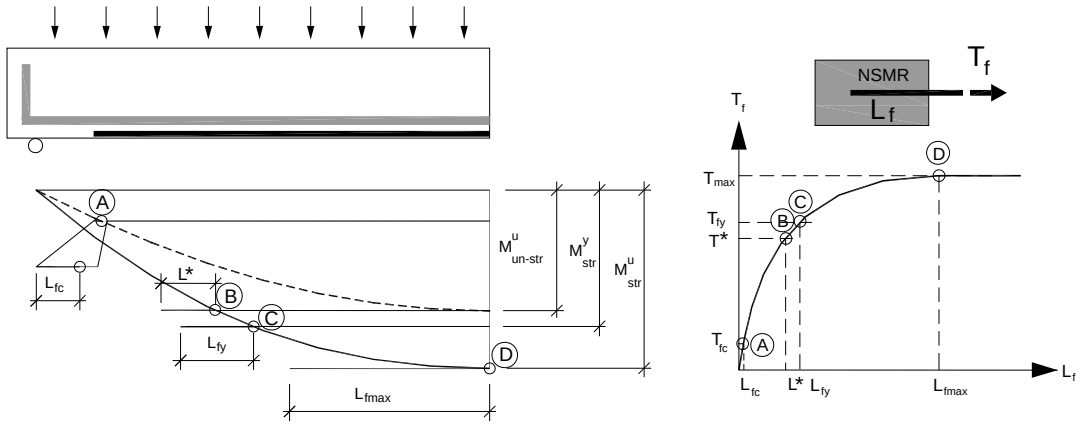

Figure 5-1 Theoretical termination section for fracture mechanics based models

The experimental work presented in Chapters 4 and 5 shows that end debonding occurs following yield penetration near the COP. The yielding of steel reinforcement in the termination region intensifies bond stresses along the NSMR at COP and at the nearest crack (crack B) (Figure 5-2), triggering limited local debonding at these regions. At the ultimate load, these local debonding zones tend to migrate towards the COP leading them to merge together to form a critical bond stress zone. Furthermore, yielding stimulates the formation and development of tributary shear cracks in the region, weakening the concrete cover.

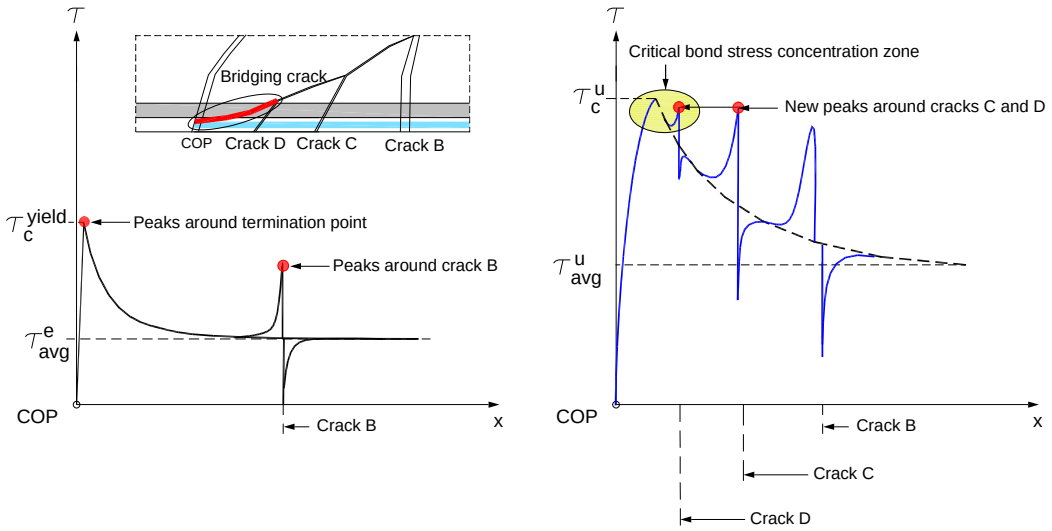

Figure 5-2 Formation of critical zone of bond stress between the termination point and the nearest crack following the formation of tributary shear cracks

5.2 Calculation of embedment length of NSMR for RC structures strengthened in flexure

A new design method to estimate the minimum embedment length, l_f, to prevent end debonding is developed based on the fact that yielding near the termination promotes the interaction of bond stress zones and intensifies bond stresses, eventually leading to end debonding failure (Nguyen et al. 2016a; Nguyen et al. 2016b). Hence, end debonding failure can be avoided by limiting yielding to a certain distance, *t*, away from the termination point (Figure 5-3). l_f can be taken as the sum of the theoretical yield length L_y, increased by s (shear shift) to account for the additional tensile force in the reinforcement induced by shear, and *t* (Eq. 5.1).

$$l_f = L_y + s + t \qquad \text{(Eq. 5.1)}$$

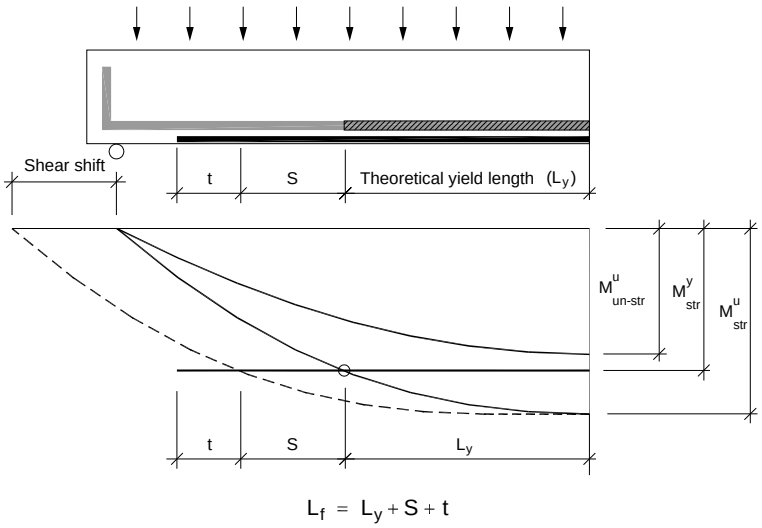

Figure 5-3 Scheme for bond length calculation.

A value of t equal to 50mm was determined from the analysis of the experimental results (Nguyen et al. 2016, c). The shear shift, s, of the bending diagram can be determined from the analysis of the experimental results (Nguyen et al. 2016, b), given in Eqs.5.2-5.5.

$$s = z.m \approx (0.45.d).m \quad \text{(Eq. 5.2)}$$

- $\frac{L_s}{d} \leq 2.5 \qquad m = 2.5$ (Eq. 5.3)
- $2.5 \leq \frac{L_s}{d} \leq 6.5 \qquad m = 1 + 0.375\left(6.5 - \frac{L_s}{d}\right)$ (Eq. 5.4)
- $\frac{L_s}{d} \geq 6.5 \qquad m = 1$ (Eq. 5.5)

5.3 Validation against experimental database

The new design method is compared against a large number of data obtained from published literature (El-Hacha et al. 2004; Bonaldo et al. 2005; Quattlebaum et al. 2005; Teng et al. 2006; Bonaldo et al. 2008; Wang et al. 2008; Al-Mahmoud et al. 2009; Al-Mahmoud et al. 2010; Ceroni 2010; Soliman et al. 2010; Wu et al. 2013; Sharaky et al. 2014; Sharaky et al. 2015; Nguyen et al. 2016) to confirm its reliability, consistency and accuracy. Predictions calculated from two other methods ACI 440-2R 2008, TR55 (ACI-440-Commitee 2008; Cement and Concrete Industry Publiccation 2012) are also included for comparison purposes.

Data of seventy two beam and slab tests were collected and the influence of various parameters was accessed. The main parameters include: geometry (rectangular, T sections), concrete strengths (16.8MPa to 50.2MPa), type of FRP(CFRP, BFRP, GRRP), shapes of FRP (round bars, strips), ratio of steel (0.24% to 1.33%) and FRP (0.12% to 0.56%), types of adhesive, groove configurations (side, bottom face), surface treatment of FRP (sand coating, ribbed), concrete cover (23-80mm), etc. (Table 5-1). Although the full data included a total of 135 specimens (see appendix D), only beams specimens in which the NSMR were not embedded at or beyond the supports were used to examine the performance of the proposed model. Continuous beams and slabs were also excluded from the database.

Figure 5.4 and Table 5.2 show the predicted values versus the experimental results for the proposed model. The model overall predicts safely the experimental results with a mean value of 0.97 and a standard error of 0.04.

Table 5-1 Data collected from seventy two beam and slab tests

References	Beam ID	Span			Geometry		Concrete	Steel			FRP					Groove					
		L	L_s	L_o	b	h	f_c	As	f_y	d_s	A_f	E_f	σ_f	d_f	n	ϕ	t	h	a	h_g
		m	m	mm	mm	mm	MPa	mm^2	MPa	mm	mm^2	GPa	MPa	mm		mm	mm	mm	mm	mm
Teng (2006)	B0	3	1.20		150	300	35.2	226.2	532	256										
	B500	3	1.20	1250	150	300	35.2	226.2	532	256	64.0	131.0	2068	290	1	----	4	16	8	22
	B1200	3	1.20	900	150	300	35.2	226.2	532	256	64.0	131.0	2068	290	1	----	4	16	8	22
	B1800	3	1.20	600	150	300	35.2	226.2	532	256	64.0	131.0	2068	290	1	----	4	16	8	22
	B2900	3	1.20	50	150	300	35.2	226.2	532	256	64.0	131.0	2068	290	1	----	4	16	8	22
Nguyen(2009)	B0	2.3	0.77		150	250	50.2	402.1	525	212										
	B1	2.3	0.77		150	250	32.3	402.1	525	212										
	NSM2	2.3	0.77	150	150	250	23.9	402.1	525	212	169.6	142.3	1477	241	3	2ϕ6+ϕ12			15	15
	NSM3/B0	2.3	0.77	150	150	250	50.2	402.1	525	212	50.4	214.0	2804	242	3	---	1.4	12	4	15
	NSM4/B1	2.3	0.77	300	150	250	32.3	402.1	525	212	50.4	214.0	2804	242	3	---	1.4	12	4	15
	NSM5/B1	2.3	0.77	350	150	250	32.3	402.1	525	212	50.4	214.0	2804	242	3	---	1.4	12	4	15
	NSM6/B1	2.3	0.77	350	150	250	32.3	402.1	525	212	50.4	214.0	2804	242	3	---	1.4	12	4	15
	NSM7/B1	2.3	0.77	350	150	250	32.3	402.1	525	212	50.4	214.0	2804	220	3	---	1.4	12	4	15
	NSM8/B1	2.3	0.77	600	150	250	32.3	402.1	525	212	84.0	51.7	800	242	3	---	2	14	4	15
	NSM9/B1	2.3	0.77	600	150	250	32.3	402.1	525	212	84.0	51.7	800	242	3	---	2	14	4	15
Barros(2004)	V1	1.5	0.50		100	178	45.3	56.5	800	154										
	V1R1	1.5	0.50	50	100	170	45.3	56.5	770	146	14.3	158.8	2740	170	1	---	1.45	9.6	4	12
	V2	1.5	0.50		100	173	48.9	84.8	800	149										
	V2R2	1.5	0.50	50	100	177	48.9	84.8	770	153	28.5	158.8	2740	170	2	---	1.45	9.6	4	12
	V3	1.5	0.50		100	175	48.9	106.8	700	150										
	V3R2	1.5	0.50	50	100	175	48.9	106.8	700	150	28.5	158.8	2740	170	2	---	1.45	9.6	4	12
	V4	1.5	0.50		100	175	46.4	150.8	554	150										
	V4R3	1.5	0.50	50	100	180	46.4	150.8	554	155	42.8	158.8	2740	170	3	---	1.45	9.6	4	12

Table 5-1 Data collected from seventy two beam and slab tests (cont.)

References	Beam ID	Span			Geometry		Concrete	Steel			FRP					Groove					
		L	L_s	L_o	b	h	f_c	As	f_y	d_s	A_f	E_f	σ_f	d_f	n	ϕ	t	h	a	h_g
		m	m	mm	mm	mm	MPa	mm^2	MPa	mm	mm^2	GPa	MPa	mm		mm	mm	mm	mm	mm
Al-Mahmoud(2009)	Controlbeam	2.8	0.80		150	280	37.4	226.2	600	238										
	S-C6(270-R)	2.8	0.80	50	150	280	36.5	226.2	600	238	56.6	145.9	1875	274	2	6	-----	-----	12	12
	S-C6(210-R)	2.8	0.80	350	150	280	36.7	226.2	600	238	56.6	145.9	1875	274	2	6	-----	-----	12	12
	S-C6(2VC60)	2.8	0.80	50	150	280	66.5	226.2	600	238	56.6	145.9	1875	274	2	6	-----	-----	12	12
	S-C6(270-M) -Motar	2.8	0.80	50	150	280	38.1	226.2	600	238	56.6	145.9	1875	274	2	6	-----	-----	12	12
	S-C12(VC30)	2.8	0.80	0	150	280	37.5	226.2	600	238	113.1	145.9	1875	274	1	12	-----	-----	24	24
	S-C12(VC60)	2.8	0.80	0	150	280	66.5	226.2	600	238	113.1	145.9	1875	274	1	12	-----	-----	24	24
Al-Mahmoud(2010)	C	2.8	1.20		150	280	35.2	226.2	600	238										
	S-C(CR)(240)	2.8	1.20	0	150	280	36.9	226.2	600	238	56.6	145.9	1875	274	2	6	-----	-----	12	12
	S-C(CR)(190)	2.8	1.20	0	150	280	36.5	226.2	600	238	56.6	145.9	1875	274	2	6	-----	-----	12	12
	S-C(CR)(150)	2.8	1.20	0	150	280	37.4	226.2	600	238	56.6	145.9	1875	274	2	6	-----	-----	12	12
	C(FPT)	2.8	0.80	50	150	280	36.7	226.2	600	238	56.6	145.9	1875	274	2	6	-----	-----	12	12
	S-C(FPT)(270)	2.8	0.80	50	150	280	36.5	226.2	600	238	56.6	145.9	1875	274	2	6	-----	-----	12	12
	S-C(FPT)(210)	2.8	0.80	50	150	280	36.7	226.2	600	238	56.6	145.9	1875	274	2	6	-----	-----	12	12
Bonaldo (2008)	SL1	1.8	0.60	50	300	80	26.0	150.8	466	56										
	SL4s	1.8	0.60	50	300	80	26.4	150.8	557	56	52.8	156.1	2879	73	4	-----	1.4	9.4	4	15
E. Bonaldo	SL2	1.8	0.60	50	300	80	26.0	150.8	557	56										
	SL3s	1.8	0.60	50	300	80	26.4	150.8	557	56	52.8	156.1	2879	73	4	-----	1.4	9.4	4	15
Bonaldo(2005)	SL01	1.8	0.60	50	300	80	45.7	56.5	494.1	57										
E. Bonaldo	SL06	1.8	0.60	50	300	80	49.4	56.5	494.1	57										
	SL03S	1.8	0.60	50	300	80	43.1	56.5	494.1	57	26.3	156.1	2879	76	2	-----	1.4	9.4	5	15
	SL04S	1.8	0.60	50	300	80	32.4	56.5	494.1	57	26.3	156.1	2879	77	2	-----	1.4	9.4	5	15
	SL08S	1.8	0.60	50	300	80	49.4	56.5	494.1	57	26.3	156.1	2879	78	2	-----	1.4	9.4	5	15

Table 5-1 Data collected from seventy two beam and slab tests (cont.)

References	Beam ID	Span			Geometry		Concrete	Steel			FRP				Groove					
		L	L_s	L_o	b	h	f_c	As	f_y	d_s	A_f	E_f	σ_f	d_f	n	ϕ	t	h	a	h_g
		m	m	mm	mm	mm	MPa	mm^2	MPa	mm	mm^2	GPa	MPa	mm		mm	mm	mm	mm	mm
A. Balsamo	Ref_d_no_1	2.1		50	120	160	16.8	157.1	540	115										
	NSM_d_2x1.4x10_1	2.1	1.05	50	120	160	16.8	157.1	540	115	28.0	171.0	2052	153	2	-----	1.4	10	5	15
	NSM_d_3x1.4x10_1	2.1	1.05	50	120	160	16.8	157.1	540	115	42.0	171.0	2052	153	3	-----	1.4	10	5	15
Quattlebaum(2005)	U-S	4.6	2.29	153	152	254	29.5	398.2	466	222										
	N-S	4.6	2.29	153	152	254	29.5	398.2	466	222	70.0	216.0	3900	241	2	-------	2	25	6.4	32
Wu(2014)	Control	1.8	0.60		150	300	34.4	461.8	510	253										
	B11	1.8	0.60	50	150	300	34.4	461.8	510	253	53.3	170.0	2629	290	1	7.9	-----	-----	20	20
	B21	1.8	0.60	50	150	300	34.4	461.8	510	253	106.6	170.0	2629	290	2	7.9	-----	-----	20	20
	B22	1.8	0.60	50	150	300	34.4	461.8	510	253	106.6	170.0	2629	290	2	7.9	-----	-----	20	20
Sharaky(2014)	CB	2.4	0.80	200	160	280	32.4	226.2	545	236										
	LB1C1	2.4	0.80	200	160	280	32.4	226.2	545	236	50.3	165.0	2350	268	1	8	---	---	16	16
	LB1G1	2.4	0.80	200	160	280	32.4	226.2	545	236	50.3	64.0	1350	268	1	8	---	---	16	16
	LB2C1	2.4	0.80	200	160	280	32.4	226.2	545	236	100.5	165.0	2350	268	2	8	---	---	16	16
	LB2G1	2.4	0.80	200	160	280	32.4	226.2	545	236	100.5	64.0	1350	268	2	8	---	---	16	16
	LA2C1	2.4	0.80	200	160	280	32.4	226.2	545	236	100.5	165.0	2350	268	2	8	---	---	16	16
	LA2G1	2.4	0.80	200	160	280	32.4	226.2	545	236	100.5	64.0	1350	268	2	8	---	---	16	16
	LB1G2	2.4	0.80	200	160	280	32.4	226.2	545	236	113.1	64.0	1350	268	1	12	---	---	24	24
Sharaky(2015)	CB	2.4	0.80	200	160	280	30.5	226.2	540	236										
	F2C1	2.4	0.80	201	160	280	30.5	226.2	540	236	100.5	170.0	2350	272	2	8	---	---	16	16
	F2S1	2.4	0.80	202	160	280	30.5	226.2	540	236	56.0	170.0	2350	268	2	---	1.4	20	5	25
	F2G1	2.4	0.80	203	160	280	30.5	226.2	540	236	100.5	64.0	1350	272	2	8	---	---	16	16
	F1G2	2.4	0.80	204	160	280	30.5	226.2	540	236	113.1	64.0	1350	268	1	12	---	---	24	24

Table 5-1 Data collected from seventy two beam and slab tests (cont.)

References	Beam ID	Span			Geometry		Concrete	Steel			FRP				Groove					
		L	L_s	L_o	b	h	f_c	As	f_y	d_s	A_f	E_f	σ_f	d_f	n	ϕ	t	h	a	h_g
		m	m	mm	mm	mm	MPa	mm^2	MPa	mm	mm^2	GPa	MPa	mm		mm	mm	mm	mm	mm
Soliman(2010)	A0	2.6	0.80		200	300	41.0	200.0	454	250										
	AC1	2.6	0.80	686	200	300	41.0	200.0	454	250	71.0	124.0	1596	294	1	9.5	-----	-----	19	19
	AC2	2.6	0.80	572	200	300	41.0	200.0	454	250	71.0	124.0	1596	294	1	9.5	-----	-----	19	19
	AC3	2.6	0.80	344	200	300	41.0	200.0	454	250	71.0	124.0	1596	294	1	9.5	-----	-----	19	19
	AC4	2.6	0.80	230	200	300	41.0	200.0	454	250	71.0	124.0	1596	294	1	9.5	-----	-----	19	19
	AC5	2.6	0.80	572	200	300	41.0	200.0	454	250	71.0	124.0	1596	294	1	9.5	-----	-----	14.3	14.3
	AC6	2.6	0.80	344	200	300	41.0	200.0	454	250	71.0	124.0	1596	294	1	9.5	-----	-----	14.3	14.3
	AC7	2.6	0.80	230	200	300	41.0	200.0	454	250	71.0	124.0	1596	294	1	9.5	-----	-----	19	19
	AC8	2.6	0.80	495.2	200	300	41.0	200.0	454	250	127.0	134.0	1250	294	1	12.7	-----	-----	25.4	25.4
	AC9	2.6	0.80	190.4	200	300	41.0	200.0	454	250	127.0	134.0	1250	294	1	12.7	-----	-----	25.4	25.4
	AG10	2.6	0.80	495.2	200	300	41.0	200.0	454	250	127.0	45.0	756	294	1	12.7	-----	-----	25.4	25.4
	AG11	2.6	0.80	190.4	200	300	41.0	200.0	454	250	127.0	45.0	756	294	1	12.7	-----	-----	25.4	25.4
	B0	2.6	0.80		200	300	41.0	400.0	460	250										
	BC1	2.6	0.80	572	200	300	41.0	400.0	460	250	71.0	124.0	1596	294	1	9.5	-----	-----	19	19
	BC2	2.6	0.80	344	200	300	41.0	400.0	460	250	71.0	124.0	1596	294	1	9.5	-----	-----	19	19
	C0	2.6	0.80		200	300	41.0	800.0	460	250										
	CC1	2.6	0.80	686	200	300	41.0	800.0	460	250	71.0	124.0	1596	294	1	9.5	-----	-----	19	19
	CC2	2.6	0.80	629	200	300	41.0	800.0	460	250	71.0	124.0	1596	294	1	9.5	-----	-----	19	19
	CC3	2.6	0.80	572	200	300	41.0	800.0	460	250	71.0	124.0	1596	294	1	9.5	-----	-----	19	19
	CC4	2.6	0.80	344	200	300	41.0	800.0	460	250	71.0	124.0	1596	294	1	9.5	-----	-----	19	19
Ceroni(2010)	A1	2	0.88		100	180	33.6	157.1	441	150				172	1					
	A9(crossed support)	2	0.88	0	100	180	33.6	157.1	441	150	100.5	109.0	1020	172	2	8	---	---	15	15
	A10	2	0.88	200	100	180	33.6	157.1	441	150	100.5	109.0	1020	172	2	8	---	---	15	15

Table 5-1 Data collected from seventy two beam and slab tests (cont.)

References	Beam ID	Span			Geometry		Concrete	Steel			FRP					Groove				
		L	L_s	L_o	b	h	f_c	As	f_y	d_s	A_f	E_f	σ_f	d_f	n	ϕ	t	h	a	h_g
		m	m	mm	mm	mm	MPa	mm^2	MPa	mm	mm^2	GPa	MPa	mm		mm	mm	mm	mm	mm
Wang(2008)	B0	3	1.20		150	300	37.5	226.2	576.3	254				192.5					15	15
	B2600	3	1.20	200	150	300	37.5	226.2	576.3	254	157.1	40.8	760	192.5	1	10	-----	-----	15	15
	B2800	3	1.20	100	150	300	37.5	226.2	576.3	254	157.1	40.8	760	192.5	1	10	-----	-----	15	15
	B3200	3	1.20	0	150	300	37.5	226.2	576.3	254	157.1	40.8	760	192.5	1	10	-----	-----	15	15
EL-Hacha(2004)	B0	2.5	1.25	50	150	300	45.0	650.5	400	220										
	B1	2.5	1.25	50	150	300	45.0	650.5	400	220	71.3	122.5	1408	285	1	9.5	----	----	18	30
	B2	2.5	1.25	50	150	300	45.0	650.5	400	220	64.0	140.0	1525	290	2	----	2	16	6.4	19
	B3	2.5	1.25	50	150	300	45.0	650.5	400	220	60.0	150.0	2000	288	2	----	1.2	25	6.4	25
	B4	2.5	1.25	50	150	300	45.0	650.5	400	220	200.0	45.0	1000	288	5	----	2	20	6.4	25
	B2a	2.5	1.25	50	150	300	45.0	650.5	400	220	64.0	140		301	2	----	2	16	----	----
	B2b	2.5	1.25	50	150	300	45.0	650.5	400	220	64.0	140		301	2	----	2	16	----	----
	B4a	2.5	1.25	50	150	300	45.0	650.5	400	220	200.0	45		301	5	----	2	20	----	----

Table 5-2 Predicted values versus the experimental results for the proposed model and existing design guidelines

No.	References	Beam ID	Experimental	TR-55		ACI		NGUYEN		Theoretical	
										Yielding	Ultimate
			P_{exp}	P_{TR-55}	P_{TR-55}/P_{exp}	P_{ACI}	P_{ACI}/P_{exp}	P_{NGUYEN}	P_{NGUYEN}/P_{exp}	P_y	$P_{the.}$
			(kN)	(kN)		(kN)		(kN)		(kN)	(kN)
24	Al-Mahmoud(2009)	Controlbeam	73.75							73.7	76.6
25		S-C6(270-R)	133.3	91.5	0.69	134.9	1.01	143.1	1.07	91.0	143.1
26		S-C6(210-R)	110.0	63.2	0.57	110.0	1.00	93.1	0.85	91.0	143.5
27		S-C6(VC60)	133.25	62.7	0.47	139.0		188.3		91.7	188.3
28		S-C6(270-M) -Mota	109.75		0.00	135.3	1.23			91.1	145.9
29		S-C12(VC30)				168.4				108.4	178.1
30		S-C12(VC60)				210.3				109.1	239.7
31	Al-Mahmoud(2010)	C	36.1							24.5	25.5
32		S-C(CR)(240)	71.4	61.1	0.86	45.5	0.64	47.9	0.67	30.3	47.9
33		S-C(CR)(190)	62.0	61.0	0.98	45.3	0.73	47.7	0.77	30.3	47.7
34		S-C(CR)(150)	43.2	61.1	1.41	45.8	1.06	48.2	1.12	30.3	48.2
35		C(FPT)	43.2	90.8	2.10	134.9		143.5		91.0	143.5
36		S-C(FPT)(270)	133.3	91.5	0.69	134.9	1.01	143.1	1.07	91.0	143.1
37		S-C(FPT)(210)	110	91.6	0.83	134.9	1.23	143.5	1.30	91.0	143.5
38	Bonaldo (2008)	SL1	14.3							11.8	12.1
39		SL4s	37.7	18.8	0.50	25.1	0.66	26.3	0.70	21.3	26.3
40	E. Bonaldo	SL2	15.1							14.1	14.2
41		SL3s	35.6	18.8	0.53	15.5	0.43	26.3	0.74	21.0	26.3
42	Bonaldo(2005)	SL01	5.4							5.0	5.2
43	E. Bonaldo	SL06	4.7							5.0	5.2

Table 5--2 Predicted values versus the experimental results for the proposed model and existing design guidelines (cont.)

No.	References	Beam ID	Experimental	TR-55		ACI		NGUYEN		Theoretical	
										Yielding	Ultimate
			P_{exp}	P_{TR-55}	P_{TR-55}/P_{exp}	P_{ACI}	P_{ACI}/P_{exp}	P_{NGUYEN}	P_{NGUYEN}/P_{exp}	P_y	$P_{the.}$
			(kN)	(kN)		(kN)		(kN)		(kN)	(kN)
44		SL03S	24.4	6.5	0.27	21.5	0.88	25.3	1.04	8.3	25.3
45		SL04S	24.9	6.6	0.26	20.6	0.83	22.0	0.89	8.4	22.0
46		SL08S	24.2	6.5	0.27	23.8	0.98	28.2	1.16	8.5	28.2
47	A. Balsamo	Ref_d_no_1	46.1							31.1	31.9
48		NSM_d_2x1.4x10_1	71.3	18.3	0.26	19.0	0.27	41.1	0.58	40.3	41.1
49		NSM_d_3x1.4x10_1	67.6	18.9	0.28	20.2	0.30	44.0	0.65	45.0	44.0
50	Quattlebaum(2005)	U-S	37.1							31.8	32.7
51		N-S	49.4	38.3	0.77	47.9	0.97	49.9	1.01	38.6	49.9
52	Wu(2014)	Control	168.7							176.0	180.7
53		B11	256.7	212.7	0.83	239.9	0.93	248.6	0.97	199.6	248.6
54		B21	260.9	206.6	0.79	250.9	0.96	274.6	1.05	223.2	287.8
55		B22	288.3	206.6	0.72	250.9	0.87	274.6	0.95	223.2	287.8
56	Sharaky(2014)	CB	70.4							66.9	69.1
57		LB1C1	109.1	91.3	0.84	126.3	1.16	111.4	1.02	82.5	133.1
58		LB1G1	99.2	83.3	0.84	99.4	1.00	111.4	1.12	72.9	100.9
59		LB2C1	117.2	90.9	0.78	127.6	1.09	111.4	0.95	98.1	163.5
60		LB2G1	112.2	82.9	0.74	117.9	1.05	111.4	0.99	79.0	123.8
61		LA2C1	114.5	90.9	0.79	127.6	1.11	111.4	0.97	98.1	163.5
62		LA2G1	110.6	82.9	0.75	117.9	1.07	111.4	1.01	79.0	123.8

Table 5--2 Predicted values versus the experimental results for the proposed model and existing design guidelines (cont.)

No.	References	Beam ID	Experimental	TR-55		ACI		NGUYEN		Theoretical	
										Yielding	Ultimate
			P_{exp}	P_{TR-55}	P_{TR-55}/P_{exp}	P_{ACI}	P_{ACI}/P_{exp}	P_{NGUYEN}	P_{NGUYEN}/P_{exp}	P_y	$P_{the.}$
			(kN)	(kN)		(kN)		(kN)		(kN)	(kN)
63		LB1G2	105.8	91.7	0.87	121.7	1.15	111.4	1.05	80.5	128.0
64	Sharaky(2015)	CB	70.4							66.1	68.2
65		F2C1	117.2	90.7	0.77	127.2	1.09	109.9	0.94	66.1	162.1
66		F2S1	111.7	86.4	0.77	146.2	1.31	109.7	0.98	66.1	134.3
67		F2G1	122.2	82.3	0.67	115.9	0.95	109.5	0.90	66.1	121.8
68		F1G2	105.8	90.8	0.86	118.2	1.12	109.3	1.03	66.1	124.3
69	Soliman(2010)	A0	55.0							52.8	55.5
70		AC1	67.0	88.5	1.32	67.9	1.01	55.5	0.83	69.2	181.0
71		AC2	73.0	88.5	1.21	85.2	1.17	55.5	0.76	69.2	181.0
72		AC3	94.0	88.5	0.94	118.6	1.26	65.4	0.70	69.2	181.0
73		AC4	96.0	88.5	0.92	132.8	1.38	79.5	0.83	69.2	181.0
74		AC5	88.0	81.5	0.93	85.2	0.97	55.5	0.63	69.2	181.0
75		AC6	94.0	81.5	0.87	118.6	1.26	65.4	0.70	69.2	181.0
76		AC7	102.0	88.5	0.87	132.8	1.30	79.5	0.78	69.2	181.0
77		AC8	74.0	100.9	1.36	109.5	1.48	55.5	0.75	84.6	231.7
78		AC9	109.0	100.9	0.93	162.3	1.49	85.9	0.79	84.6	231.7
79		AG10	75.0	82.2	1.10	121.5	1.62	55.5	0.74	63.5	154.3
80		AG11	112.0	82.2	0.73	121.5	1.08	85.9	0.77	63.5	154.3
81		B0	130.0							104.2	109.8

Table 5--2 Predicted values versus the experimental results for the proposed model and existing design guidelines (cont.)

No.	References	Beam ID	Experimental	TR-55		ACI		NGUYEN		Theoretical	
										Yielding	Ultimate
			P_{exp}	P_{TR-55}	P_{TR-55}/P_{exp}	P_{ACI}	P_{ACI}/P_{exp}	P_{NGUYEN}	P_{NGUYEN}/P_{exp}	P_y	$P_{the.}$
			(kN)	(kN)		(kN)		(kN)		(kN)	(kN)
82		BC1	135.0	140.3	1.04	136.3	1.01	109.8	0.81	120.7	207.1
83		BC2	154.0	140.3	0.91	170.4	1.11	129.2	0.84	120.7	207.1
84		C0	233.0							201.6	209.4
85		CC1	227.0	237.1	1.04	209.6	0.92	209.4	0.92	217.9	268.3
86		CC2	229.0	237.1	1.04	221.8	0.97	209.4	0.91	217.9	268.3
87		CC3	234.0	237.1	1.01	232.2	0.99	209.4	0.89	217.9	268.3
88		CC4	254.0	237.1	0.93	266.3	1.05	249.7	0.98	217.9	268.3
89	Ceroni(2010)	A1						0.0		21.1	22.0
90		A9	50.7	30.0	0.59	45.0	0.89	47.4	0.94	31.0	47.4
91		A10				45.0		47.4		0.0	47.4
91	Wang(2008)	B0	59.7							50.5	52.7
92		B2600	81.5	61.9	0.76	70.2	0.86	72.5	0.89	53.6	72.5
93		B2800	80.6	52.5	0.65	70.2	0.87	72.5	0.90	53.6	72.5
94		B3200	81.9	52.5	0.64	70.2	0.86	72.5	0.89	53.6	72.5
95	EL-Hacha(2004)	B0	55.4							79.5	83.6
96		B1	93.8	99.4	1.06	117.0	1.25	121.8	1.30	89.7	121.8
97		B2	99.3	92.2	0.93	118.9	1.20	124.0	1.25	90.5	124.0
98		B3	110.2	92.2	0.84	118.5	1.08	123.5	1.12	90.3	123.5
99		B4	102.7	85.6	0.83	118.5	1.15	123.5	1.20	90.3	123.5

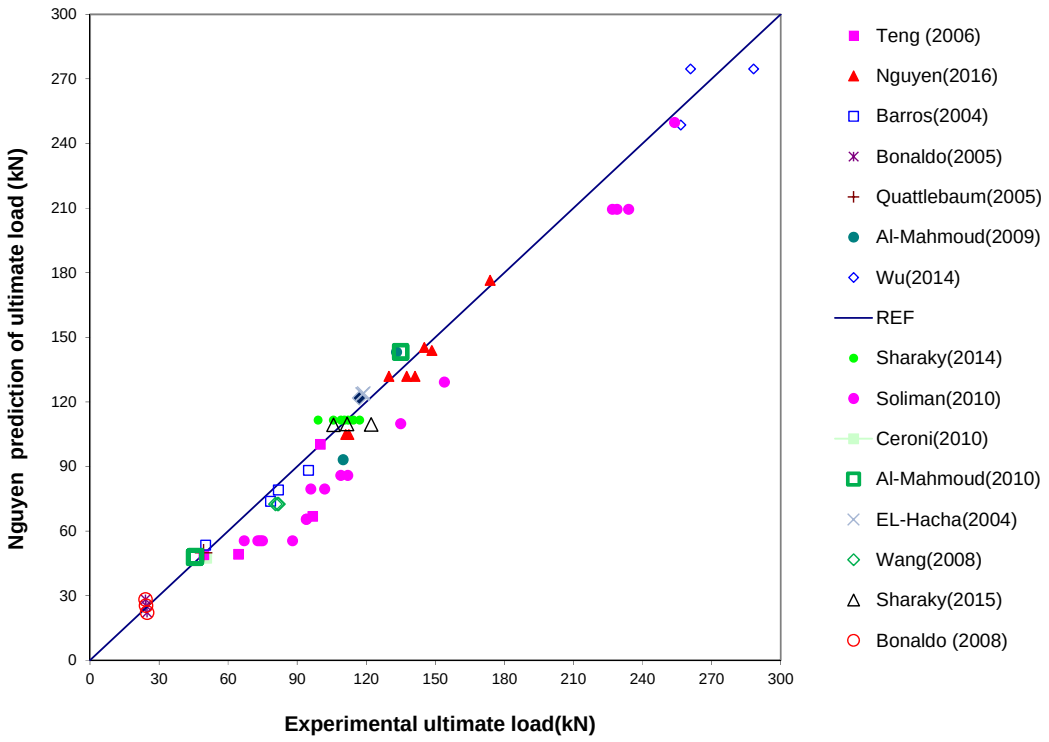

Figure 5-4 Comparison between the results calculated according to the proposed method and experimental results

5.4 Comparison to available design guidelines

5.4.1 TR55 design guidelines

The anchorage design proposed by TR55 (Cement and Concrete Industry Publiccation 2012) based on fracture mechanics based method is summarised below (Eq. 5.2-5.9). NSM separation failure design includes several checks of bond stress concentration arising from a) bond stress due to termination of the FRP b) Bond stress due to yielding of the steel reinforcement c) bond stress due to crack. The maximum bond stress must not exceed the bond strength of the NSMR to avoid end debonding.

The allowable force and the required embedment length of FRP are given in (Eq.5.5) and (Eq. 5.9), respectively. Advantages of TR55 are that all potential high bond stress zones along the NSMR (at cracks in the yielding zone and at termination point of the FRP) and failure modes (cover separation, concrete splitting, failure in adhesive layer) are checked. However, the application of the design guidelines requires the implementation of a rather complex methodology.

To avoid concrete splitting failure, maximum ultimate anchorage force, $T_{nsm,max}$ and corresponding maximum anchorage length, $l_{nsm,max}$ need to be calculated from the following equations:

$$T_{nsm,max} = 10 b_{fnotthperim} \sqrt{E_{fd} A_f f_{ctk}} \quad \text{(Eq. 5.2)}$$

$$l_{nsm,max} = 0.135\sqrt{\frac{E_{fd}A_f}{f_{ctk}}} \quad \text{(Eq. 5.3)}$$

$b_{fnotthperim}$: effective perimeter of a groove

$E_{fd,}\ A_f$: elastic modulus and area of FRP, respectively

$If\ l_{nsm} < l_{nsm,max}, T_{nsm}$

$$T_{nsm} = T_{nsm,max} = T_{nsm,max}\frac{l_{nsm}}{l_{nsm,max}}\left(2 - \frac{l_{nsm}}{l_{nsm,max}}\right) \quad \text{(Eq. 5.4)}$$

T_{nsm} should be checked with $T_{nsm,ad}$, $T_{nsm,lim}$ and $T_{rupture}$ to satisfy (Eq. 5.5)

$$T_{nsm} = \min(T_{nsm,ad}, T_{nsm,lim}, T_{rupture}) \quad \text{(Eq. 5.5)}$$

$T_{nsm,ad}$: characteristic adhesive bond failure force (N)

$$T_{nsm,ad} = 0.3 f_{at} b_{barperim} l_{nsm} \quad \text{(Eq. 5.6)}$$

$T_{nsm,lim}$: limiting maximum achievable anchorage force (N)

$$T_{nsm,lim} = 38\sqrt{\frac{b}{n_{nsm}} E_{fd} A_f f_{ctk}} \quad \text{(Eq. 5.7)}$$

$T_{rupture}$: rupture force (N)

$$T_{rupture} = A_f \sigma_f \quad \text{(Eq. 5.8)}$$

The required embedment length, corresponding to T_{nsm}

$$l_{nsm} = l_{nsm,max}\left(1 - \sqrt{1 - \frac{T_{nsm}}{T_{nsm,max}}}\right) \quad \text{(Eq. 5.9)}$$

Comparison of experimental results and prediction proposed by TR.55 are shown in Figure 5.5 and Table 5.2. The results show that the predictions are rather conservative (mean=0.82, STD=0.03)

5.4.2 ACI-440.2R-08

To avoid the end debonding failure, the ACI 440 (ACI-440-Commitee 2008) proposes a minimum embedment length of NSMR (Eq.5.10), starting from the maximum moment section. It can be seen that the predictive method of ACI.2R-08 is relatively simple. However, it does not consider the bond stress concentration around the termination point, crack, yielding of the steel reinforcement and shear-bending interaction.

- $l_{db} = \frac{A_f}{p_f}\frac{f_{fd}}{\tau_b}$ (Eq. 5.10)
- A_f and p_f are area and perimeter of the NSMR, respectively
- f_{fd} : the tensile strength of FRP
- τ_b : the bond strength of FRP and concrete substrate, equals to $6.9MPa$ for all cases

Comparison of experimental results and predictions of the ultimate load of ACI 440-2R-08 is shown in Figure 5-6 and Table 5.2. Despite its simplicity, predictions of ACI-440.2R are reasonably good, however, they still have high scatter and are unsafe (mean=1.06, SE=0.06).

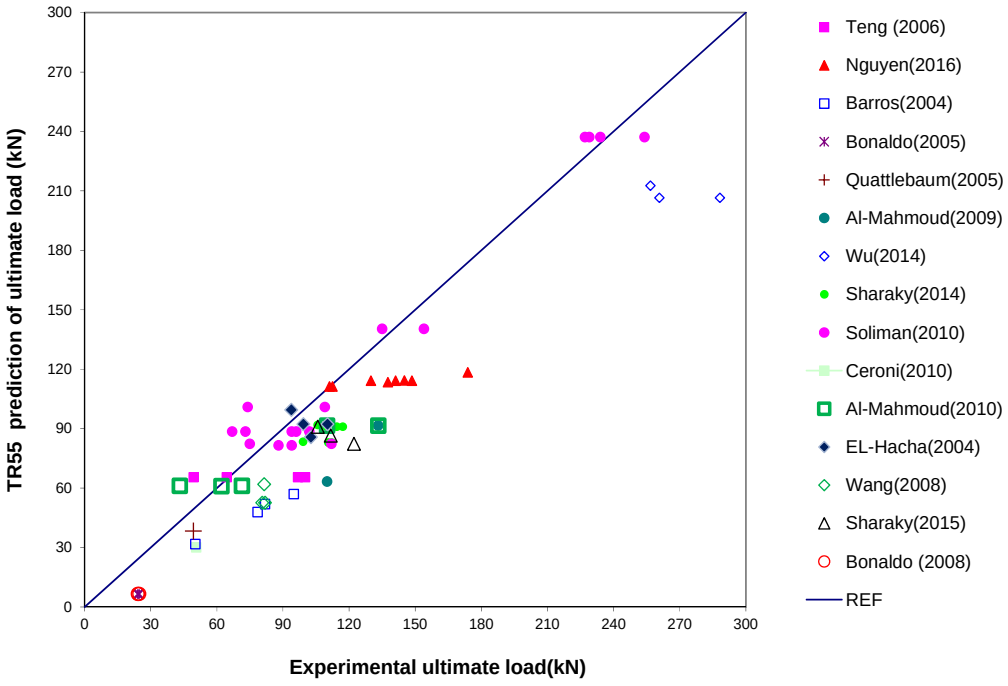

Figure 5-5 Comparison between the experimental results and TR55 prediction of the flexural strength

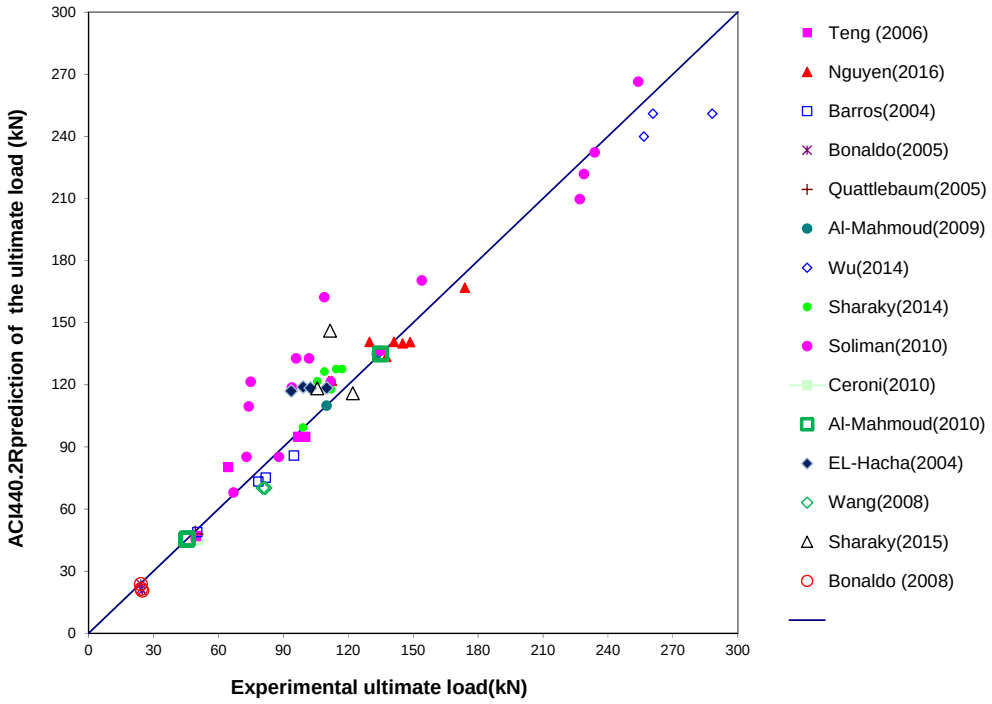

Figure 5-6 Comparison between the experimental results and ACI440 prediction of the ultimate load.

It can be explained by the fact that the constant value of bond strength used in prediction does not cover wide ranges of concrete strengths; types of adhesive; surface finishes, shapes and sizes of FRP. In other words, by using an average bond strength the code eliminates the effects of various parameters affecting the NSMR system.

5.5 Conclusions

Experimental evidence confirms that end debonding failure occurs following deep yield penetration in the proximity of the termination point. This finding is adopted in a new design methodology which provides a simple tool to predict the debonding load or to calculate the embedment length corresponding to a desired strengthening level to avoid debonding. The new design method is validated against a large number of data obtained from published literature, representing a wide range of parameters of materials, geometry and test configurations of elements. For comparison purposes, the results calculated by the proposed method are compared with those of ACI-440.2R, TR-55. The comparative work shows that the new design method provides more accurate predictions and a more reliable performance over a wide range of RC beams retrofitted with NSMR. The new design method provides a simple, yet effective tool for engineers to predict the debonding load with adequate safety margins.

ACKNOWLEDGEMENTS

The authors gratefully acknowledge the financial support from the Ministry of Education and Training of Vietnam and the University of Sheffield.

REFERENCES

ACI-440-Commitee (2008). ACI 440.2R-08 Guide for the Design and Construction of Externally Bonded FRP Systems for Strengthening Concrete Structures. Farmington Hills, MI, USA.

Al-Mahmoud, F., A. Castel, et al. (2009). "Strengthening of RC members with near-surface mounted CFRP rods." Composite Structures 91(2): 138-147.

Al-Mahmoud, F., A. Castel, et al. (2010). "RC beams strengthened with NSM CFRP rods and modeling of peeling-off failure." Composite Structures 92(8): 1920-1930.

Barros, J. A. O., S. J. E. Dias, et al. (2007). "Efficacy of CFRP-based techniques for the flexural and shear strengthening of concrete beams." Cement and Concrete Composites 29(3): 203-217.

Bilotta, A., F. Ceroni, et al. (2011). "Bond Efficiency of EBR and NSM FRP Systems for Strengthening Concrete Members." Journal of Composites for Construction 15(5): 757-772.

Bonaldo, E., J. de Barros, et al. (2008). "Efficient Strengthening Technique to Increase the Flexural Resistance of Existing RC Slabs." Journal of Composites for Construction 12(2): 149-159.

Cement and Concrete Industry Publiccation. Technical report No. 55: Design guidance for strengthening concrete structures using fibre composite materials. 2012(CCIP-56).

Ceroni, F. (2010). "Experimental performances of RC beams strengthened with FRP materials." Construction and Building Materials 24(9): 1547-1559.

Cruz, J. M. S., J. A. O. Barros, et al. (2006). "Bond Behavior of Near-Surface Mounted CFRP Laminate Strips under Monotonic and Cyclic Loading." Journal of Composites for Construction 10(4): 295-303.

El-Hacha, R., J. S. Filho, et al. (2004). "Effectiveness of near surface mounted FRP reinforcement for flexural strengthening of reinforced concrete beams." Advanced Composite Materials in Bridges and Structures 4th International Conference, Calgary, Canada.

Kalupahana, W. K. K. G., T. J. Ibell, et al. (2013). "Bond characteristics of near surface mounted CFRP bars." Construction and Building Materials 43(0): 58-68.

Nguyen, V., Hien, M. Guadagnini, et al. (2016). "Performance of RC beams strengthened in flexure with FRP NSMR." Composite part B: (to be published).

Novidis, D., S. J. Pantazopoulou, et al. (2007). "Experimental study of bond of NSM-FRP reinforcement." Construction and Building Materials 21(8): 1760-1770.

Quattlebaum, J., B. , K. Harries, A. , et al. (2005). "Comparison of Three Flexural Retrofit Systems under Monotonic and Fatigue Loads." Journal of Bridge Engineering 10(6): 731-740.

Seracino, R., M. Raizal Saifulnaz, et al. (2007). "Generic Debonding Resistance of EB and NSM Plate-to-Concrete Joints." Journal of Composites for Construction 11(1): 62-70.

Sharaky, I. A., L. Torres, et al. (2014). "Flexural response of reinforced concrete (RC) beams strengthened with near surface mounted (NSM) fibre reinforced polymer (FRP) bars." Composite Structures 109(0): 8-22.

Sharaky, I. A., L. Torres, et al. (2015). "Experimental and analytical investigation into the flexural performance of RC beams with partially and fully bonded NSM FRP bars/strips." Composite Structures 122(0): 113-126.

Soliman, S. M., E. El-Salakawy, et al. (2010). "Flexural behaviour of concrete beams strengthened with near surface mounted fibre reinforced polymer bars." Canadian Journal of Civil Engineering 37(10): 1371-1382.

Teng, J. G., L. De Lorenzis, et al. (2006). "Debonding Failures of RC Beams Strengthened with Near Surface Mounted CFRP Strips." Journal of Composites for Construction 10(2): 92-105.

Wang, B., J. G. Teng, et al. (2008). "Strain monitoring of RC members strengthened with smart NSM FRP bars." Construction and Building Materials In Press, Corrected Proof.

Wu, G., Z. Dong, et al. (2013). "Performance and Parametric Analysis of Flexural Strengthening for RC Beams with NSM-CFRP Bars." Journal of Composites for Construction: 04013051.

Chapter 6

CONCLUSIONS AND RECOMMENDATIONS FOR FUTURE RESEARCH

The main aim of this study was to achieve a better understanding of bond behaviour and debonding mechanisms of NSMR in flexural strengthening applications. The aim was achieved through an extensive experimental programme, analytical solution and the assessment of a comprehensive database of tests available in the literature.

A brief summary of the main conclusions drawn from each part of this study is presented below followed by a set of recommendations for future research.

6.1 Conclusions

Analytical modelling

- An analytical model based on elastic principles was developed to examine in detail the bond stress distribution along the NSMR, especially in the vicinity of the termination point. The following conclusions are drawn:
- The bond stress concentration at the COP of NSMR can be reduced significantly by terminating the external reinforcement in the un-cracked zone of the element.
- The maximum longitudinal bond stress in NSMR is significantly lower (up to 100%) compared to that developed in EBR systems.
- Vertical shear stress is dominant in NSMR placed vertically, instead of the normal stress in EBR system. As a result, the failure modes of NSMR are the combination of fracture mode 2 and 3, instead of mode 1 and 2 typical of EBR. Despite of the

higher vertical shear stress developed, NSMR is not affected by peeling, as fracture energy of mode 2 in NSMR is much greater than fracture energy of mode 1 in EBR.

- Large bond stresses develop within a narrow zone at the termination point of NSMR and then reduce sharply towards the mid-span.

Performance of beams retrofitted with the NSMR

- The most dominant failure mode observed in tested beams was end debonding initiating from the termination point. Intermediate crack induced debonding was not observed.
- The use of NSMR enhanced significantly the load carrying capacity of the deficient beams up to 50%, but also caused the loss of ductility (50%) compared to the un-strengthened beams.
- Beams retrofitted with BFRP increased the load carrying capacity marginally due to low stiffness of BFRP.
- At end debonding the maximum strain developed in the NSMR was in the range of 0.52%-1.18%.
- Maximum bond stress as developed in the FRP for beams with long and short embedment lengths were approximately 6.5MPa and 2.5MPa, respectively.
- In beams retrofitted with short embedment lengths, local debonding occurred in the steel reinforcement around the termination.

Yield penetration of the steel reinforcement in the shear span

Two different yield patterns were observed in tested beams in beams retrofitted with long and short length:

- In beams with long embedment length, yield penetrated deeply into the termination region when end debonding occurred. Yielding around the termination region intensified the bond stresses in the entire region and promoted the interaction between bond stress concentration zones, triggering end debonding failure.
- In beams with short embedment length, yielding developed in a narrow region around the termination point. Yielding even penetrated beyond the termination into the un-strengthened region. Intensive yielding creates a plastic hinge around the termination point and high local curvature.

- At failure, for beams failing by end debonding, yielding was found to penetrate near the termination point. The yield length found is longer than predicted by section analysis between 1.3 and 1.8 of the effective depth.

Catch-up length

- The concept of catch-up length, the length along which the strain in the NSMR catches up with the strain in the steel reinforcement, is introduced. The transition length is an extended version of the catch-up length.
- In the tested beams, the catch-up lengths were in the range of 200-250mm, equivalent to 1-1.1 times the effective depth.
- The strain at catch-up section was 1.1-1.3 times greater than the yield strain.

New design method

Based on the experimental evidence, a new simple, yet effective method was developed to calculate the minimum effective length of the NSMR in flexural strengthening applications.

The design method is based on the fact that debonding occurs following yield penetration in the termination region. The new method was validated against extensive database of beams and slabs in the published literature. The results show that the new method is more accurate than existing design guidelines such as TR55 and ACI440.

6.2 Recommendations for future work

Based on the work conducted in this study, a series of recommendations for future research work are identified and presented in the following:

- *Modified analytical model*

- The analytical model developed in chapter 2 is based on elastic analysis and continuum mechanics. This has several limitations and requires improvements to include sources of high nonlinearity and discontinuity to better reflect the structural response at high load levels. The modified model should include: (a) the effect of yielding on stress development along the termination region (b) effects of cracks adjacent to the termination point.
- The experimental evidence of this work can be used to identify more realistic boundary conditions to be used in the solution of the governing differential

equations. For example, effects of the nearest crack from the termination point on bond stress concentration can be included in the existing model.

- More work should be carried out to account for the interaction between longitudinal and vertical shear stress.

- *Experimental work*

- More experimental work should be carried out to examine (a) performance of heavily damaged beams retrofitted with NSMR and the pre-tensioned steel strapping technique to improve both the ultimate load and ductility and (b) impact of steel strapping on bond behaviour and debonding failure of NSMR and potential applications.
- More experimental work should be done on flexural elements having wide ranges of parameters of materials and geometry to evaluate (a) the catch-up and the transition length of the NSMR (b) bending-shear effects (c) ductility (d) yield penetration.
- Techniques based on fibre optics and digital image analysis could be used to capture more effectively the variations of stress and strain in various components which can provide better understanding of structural behaviour.

- *Numerical analysis*

- Nonlinear FEM can be used to examine the impact of yield penetration on the development of bond stresses in the region between the termination point and the nearest crack.
- Different models to simulate the interfacial bond between concrete-FRP, concrete-steel, concrete-adhesive, FRP-adhesive can be explored and validated against the experimental work presented here.

REFERENCES

ACI-440-Commitee (2008). ACI 440.2R-08 Guide for the Design and Construction of Externally Bonded FRP Systems for Strengthening Concrete Structures. Farmington Hills, MI, USA.

Al-Mahmoud, F., A. Castel, et al. (2009). "Strengthening of RC members with near-surface mounted CFRP rods." Composite Structures 91(2): 138-147.

Al-Mahmoud, F., A. Castel, et al. (2010). "RC beams strengthened with NSM CFRP rods and modeling of peeling-off failure." Composite Structures 92(8): 1920-1930.

Al-Sunna, R. A. S. (2006). "Deflection Behaviour of FRP Reinforced Concrete Flexural Members." Doctoral thesis, The University of Sheffield.

Alkhrdaji, T. and A. Nanni (2000). Flexural Strengthening of Bridge Piers Using FRP Composites, ASCE.

Andrea Prota, R. P., Antonio Nanni (2003). "Upgrade of RC Silos Using Near Surface Mounted FRP Composites(unpublished)." Industria Italiana del Cemento LXXIII(784): 170-183.

Barros, J. A. O., S. J. E. Dias, et al. (2007). "Efficacy of CFRP-based techniques for the flexural and shear strengthening of concrete beams." Cement and Concrete Composites 29(3): 203-217.

Barros, J. A. O. and A. S. Fortes (2005). "Flexural strengthening of concrete beams with CFRP laminates bonded into slits." Cement and Concrete Composites 27(4): 471-480.

Bilotta, A., F. Ceroni, et al. (2011). "Bond Efficiency of EBR and NSM FRP Systems for Strengthening Concrete Members." Journal of Composites for Construction 15(5): 757-772.

Bonaldo, E., J. A. O. Barros, et al. (2005). "Concrete slabs strips reinforced with epoxy-bonded carbon laminates into slits." International conference on construction materials 3 “Construction materials : performance, innovations and structural implications (ConMat'05) proceedingsVancouver, Canada [CD-ROM].

Bonaldo, E., J. de Barros, et al. (2008). "Efficient Strengthening Technique to Increase the Flexural Resistance of Existing RC Slabs." Journal of Composites for Construction 12(2): 149-159.

Cement and Concrete Industry Publiccation (2012). "Technical report No. 55: Design guidance for strengthening concrete structures using fibre composite materials." (CCIP-56).

Ceroni, F. (2010). "Experimental performances of RC beams strengthened with FRP materials." Construction and Building Materials 24(9): 1547-1559.

Chen, J. F. and W. K. Pan (2006). "Three dimensional stress distribution in FRP-to-concrete bond test specimens." Construction and Building Materials 20(1-2): 46-58.

Co-Force America, I. (2005). "Old Keys bridge repairs, negative moment strengthening of the Rockland Channel Bridge." Technical report.

Cruz, J. M. S. and J. A. O. Barros (2002). "Bond behavior of carbon laminate strips into concrete by pull-out bending tests." Proceedings Bond in Concrete: From Research to Standards, Budapest, Nov. 20-22, 2002: 614-621.

Cruz, J. M. S., J. A. O. Barros, et al. (2006). "Bond Behavior of Near-Surface Mounted CFRP Laminate Strips under Monotonic and Cyclic Loading." Journal of Composites for Construction 10(4): 295-303.

Cruz, J. S. and J. Barros (2004). "Modeling of bond between near-surface mounted CFRP laminate strips and concrete." Computers & Structures 82(17-19): 1513-1521.

D7565/D7565M-10, A. (2010). Standard Test Method for Determining Tensile Properties of Fiber Reinforced Polymer Matrix Composites Used for Strengthening of Civil Structures, ASTM International, West Conshohocken, PA.

De Lorenzis, L. (2004). "Anchorage length of near-surface mounted fiber-reinforced polymer rods for concrete strengthening - Analytical modeling." ACI Structural Journal 101(3): 375-386.

De Lorenzis, L. and N. Antonio (2001). "Characterization of FRP Rods as Near-Surface Mounted Reinforcement." Journal of Composites for Construction 5(2): 114-121.

De Lorenzis, L., K. Lundgren, et al. (2004). "Anchorage Length of Near-Surface Mounted Fiber-Reinforced Polymer Bars for Concrete Strengthening - Experimental Investigation and Numerical Modeling." ACI structural journal 101(2): 269-278.

De Lorenzis, L. and A. Nanni (2001). "Characterization of FRP Rods as Near-Surface Mounted Reinforcement." Journal of Composites for Construction 5(2): 114-121.

De Lorenzis, L. and A. Nanni (2002). "Bond between near-surface mounted fiber-reinforced polymer rods and concrete in structural strengthening." ACI structural journal 99(2): 123-132.

De Lorenzis, L., A. Rizzo, et al. (2002). "A modified pull-out test for bond of near-surface mounted FRP rods in concrete." Composites Part B: Engineering 33(8): 589-603.

El-Hacha, R., J. S. Filho, et al. (2004). "Effectiveness of near surface mounted FRP reinforcement for flexural strengthening of reinforced concrete beams." Advanced Composite Materials in Bridges and Structures 4th International Conference, Calgary, Canada.

fib-TG9.3. 2001. Design and Use of Externally Bonded Fiber Polymer Reinforcement (FRP EBR) for Reinforced Concrete Structures. Technical Report Prepared by EBR Task Group 9.3, Bulletin 14, Lausanne, Swiss.

Hassan, T. and S. Rizkalla (2003). "Investigation of Bond in Concrete Structures Strengthened with Near Surface Mounted Carbon Fiber Reinforced Polymer Strips." Journal of Composites for Construction 7(3): 248-257.

Irwin, R. and A. Rahman (2002). "FRP strengthening of concrete structures-Design constrains and practical effects on construction detailing." New Zealand Concrete Society Conference, Wairakei.

Kalupahana, W. K. K. G., T. J. Ibell, et al. (2013). "Bond characteristics of near surface mounted CFRP bars." Construction and Building Materials 43(0): 58-68.

Kotynia, R. (2010). "Bond between FRP and concrete in reinforced concrete beams strengthened with near surface mounted and externally bonded reinforcement." Construction and Building Materials 32: 41-54.

Nguyen, V., Hien, M. Guadagnini, et al. (2016). "Impact of yield penetration on debonding failure of NSMR." Journal of Composites for Construction, ASCE (to be published).

Nguyen, V., Hien, M. Guadagnini, et al. (2016). "Performance of RC beams strengthened in flexure with FRP NSMR." Composite part B: (on publishcation).

Novidis, D., S. J. Pantazopoulou, et al. (2007). "Experimental study of bond of NSM-FRP reinforcement." Construction and Building Materials 21(8): 1760-1770.

Quattlebaum, J., B. , K. Harries, A. , et al. (2005). "Comparison of Three Flexural Retrofit Systems under Monotonic and Fatigue Loads." Journal of Bridge Engineering 10(6): 731-740.

Seracino, R., M. Raizal Saifulnaz, et al. (2007). "Generic Debonding Resistance of EB and NSM Plate-to-Concrete Joints." Journal of Composites for Construction 11(1): 62-70.

Serbescu, A. (2014). "Doctoral thesis: Strengthening of RC Beams with basalt FRPs." The University of Sheffield.

Sharaky, I. A., L. Torres, et al. (2014). "Flexural response of reinforced concrete (RC) beams strengthened with near surface mounted (NSM) fibre reinforced polymer (FRP) bars." Composite Structures 109(0): 8-22.

Sharaky, I. A., L. Torres, et al. (2015). "Experimental and analytical investigation into the flexural performance of RC beams with partially and fully bonded NSM FRP bars/strips." Composite Structures 122(0): 113-126.

Soliman, S. M., E. El-Salakawy, et al. (2010). "Flexural behaviour of concrete beams strengthened with near surface mounted fibre reinforced polymer bars." Canadian Journal of Civil Engineering 37(10): 1371-1382.

Soliman, S. M., E. F. El-Salakawy, et al. (2008). "Flexural behaviour of concrete beams strengthened with near surface mounted FRP bars." Proceeding, 4th Int. Conference on FRP Composites in Civil Engineering (CICE2008).

Teng, J. G., L. De Lorenzis, et al. (2006). "Debonding Failures of RC Beams Strengthened with Near Surface Mounted CFRP Strips." Journal of Composites for Construction 10(2): 92-105.

Tumialan, J. G., Vatovec, M., and Kelley, P.L. (2007). "Case Study: Strengthening of Parking Garage Decks with Near-Surface-Mounted CFRP Bars." Journal of Composites for Construction 11(5): 523-530.

Wang, B., J. G. Teng, et al. (2008). "Strain monitoring of RC members strengthened with smart NSM FRP bars." Construction and Building Materials In Press, Corrected Proof.

Wu, G., Z. Dong, et al. (2013). "Performance and Parametric Analysis of Flexural Strengthening for RC Beams with NSM-CFRP Bars." Journal of Composites for Construction: 04013051.

APPENDICES

A.APPENDIX A.1

APPENDIX A.1 – A PARTIAL INTERFACIAL MODEL

From equilibrium equation:

Due to such simplifications, set of equilibrium equations reduces from three to only one of lateral force of equilibrium

$$\tau.(2h+t).dx = d\sigma_f.(h.t) \qquad \textbf{(A-1)}$$

For a strip:

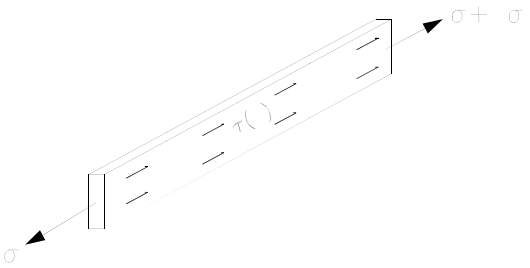

Figure 0.1: Equilibrium of NSMR strip

$$\tau = \frac{d\sigma_f}{dx}.\frac{h.t_f}{2h+t_f} \qquad \textbf{(A-2)}$$

In practical, if tf <<h, $\frac{t_f}{h_f}$ can be eliminable

$$\tau = \frac{d\sigma_f}{dx}.\frac{t_f}{2+\frac{t_f}{h_f}} \qquad \textbf{(A-3)}$$

$$\tau = \frac{d\sigma_f}{dx}.\frac{t_f}{2} \qquad \textbf{(A-4)}$$

For a round bar: $\tau = \frac{d\sigma_f}{dx}.\frac{d_f}{2}$ **(A-5)**

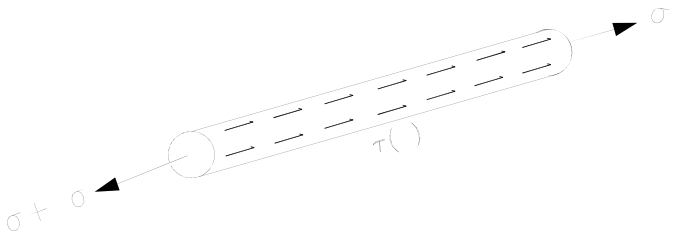

Figure 0.2: Equilibrium of NSMR round bar

Shear strain:

$$\tau = G_a.\gamma \qquad \textbf{(A-6)}$$

$$\gamma = \left(\frac{du}{dy} + \frac{dw}{dx} + \frac{du}{dx}.\frac{du}{dy} + \frac{dw}{dx}.\frac{dw}{dy} \right) \qquad \textbf{(A-7)}$$

$$\frac{du}{dy}, \frac{dw}{dx} << 1 \quad , \quad \frac{du}{dy}\frac{dw}{dx} \to 0 \qquad \textbf{(A-8)}$$

Because of $\frac{du}{dy}, \frac{dw}{dx} << 1$, the second order term can be negligible and shear strain can be written:

$$\gamma = \left(\frac{du}{dy} + \frac{dw}{dx} \right) \qquad \textbf{(A-9)}$$

$$\frac{d\sigma_f}{dx} = 2.\frac{\tau}{t_f} = \frac{2}{t_f}.G_a.\left(\frac{du}{dy} + \frac{dw}{dx} \right) \qquad \textbf{(A-10)}$$

$$\frac{d^2\sigma_f}{dx} = 2.\frac{\tau}{t_f} = \frac{2}{t_f}.G_a.\left(\frac{d^2u}{dydx} + \frac{d^2w}{d^2x} \right) \qquad \textbf{(A-11)}$$

The term $\frac{d^2w}{d^2x} = \rho = \frac{M}{EI} = \frac{\varepsilon}{x}$ <<1 and can be omitted and (3-11) becomes

$$\frac{d^2\sigma_f}{dx} = 2.\frac{\tau}{t_f} = \frac{2G_a}{t_f}.\frac{d^2u}{dydx} \qquad \textbf{(A-12)}$$

$$\frac{d^2\sigma_f}{dx} = 2.\frac{\tau}{t_f} = \frac{2G_a}{t_f}.\frac{d^2u}{dydx} = \frac{2G_a}{t_f}\frac{du}{dy}\left(\frac{du}{dx} \right) \qquad \textbf{(A-13)}$$

$$\frac{du}{dx} = \varepsilon_f - \varepsilon_c \tag{A-14}$$

Assume that the shear stress is linear distribution in adhesive layer

$$\frac{du}{dy}\left(\frac{du}{dx}\right) = \frac{1}{t_a}\left(\varepsilon_f - \varepsilon_c\right) \tag{A-15}$$

ε_c is calculated includes the normal force and the moment $-\frac{\sigma_c}{E_c} + \frac{M_x}{E.I}$ and (3-16) can be written

$$\frac{d^2\sigma_f}{dx^2} = 2.\frac{\tau}{t_f} = \frac{2G_a}{Tt_f}.\left(\frac{\sigma_f}{E_f} - \frac{\sigma_c}{E_c} + \frac{M_x}{E.I}\right) \tag{A-16}$$

$$\frac{d^2\sigma_f}{dx^2} - \frac{2G_a}{t_a.t_f}.\left(\frac{\sigma_f}{E_f} - \frac{\sigma_c}{E_c} + \frac{M_x}{E.I}\right) = 0 \tag{A-17}$$

$$\frac{d^2\sigma_f}{dx^2} - \frac{2G_a}{t_a.t_f}.\frac{\sigma_f}{E_f} = \frac{2G_a}{t_a.t_f}.\frac{\sigma_c}{E_f} \tag{A-18}$$

$$\frac{d^2\sigma_f}{dx^2} - \frac{2G_a}{t_a.t_f}.\sigma_f = \frac{2G_a}{t_a.t_f}.\frac{E_f}{E_f}\sigma_c \tag{A-19}$$

$$\frac{d^2\sigma_f}{dx^2} - \alpha^2.\sigma_f = \alpha^2.n\sigma_c \tag{A-20}$$

The characteristic(homogenous) solution of (3-21)

$$\sigma_f^h = C_1.\cosh(\alpha.x) + C_2.\sinh(\alpha.x) \tag{A-21}$$

Assume applied load on the beam is uniform distribution, thus the bending moment at point x is in quadratic form

$$\sigma_c = a_0 + a_1.x + a_2.x^2 \tag{A-22}$$

The particular solution for the differential equation corresponding to σ_c given above is

$$\sigma_f^p = -n\left(a_2.x^2 + a_1.x + 2.\frac{a_2}{\alpha^2} + a_0\right) \tag{A-23}$$

Thus, the general solution for the differential equation:

$$\sigma_f = \sigma_f^h + \sigma_f^p = C_1.\cosh(\alpha.x) + C_2.\sinh(\alpha.x) - n\left(a_2.x^2 + a_1.x + 2.\frac{a_2}{\alpha^2} + a_0\right) \tag{A-24}$$

Appendix A – Analytical solution

General solution for the differential equation:

$$\tau_f = \sigma_f^h + \sigma_f^p = C_1.\alpha.\sinh(\alpha.x) + C_2.\alpha.\cosh(\alpha.x) - 2n.a_2.x - n.a_1 \quad \textbf{(A-25)}$$

Boundary conditions:

$$x = 0 \rightarrow \sigma_f = 0 \quad \sigma_f = C_1 - n\left(2.\frac{a_2}{\alpha^2} + a_0\right) = 0 \rightarrow C_1 = n\left(2.\frac{a_2}{\alpha^2} + a_0\right) \quad \textbf{(A-26)}$$

$$x = X_c \rightarrow \tau_f = \tau_o$$

Replace stress values at boundary to equation ()

$$\tau_f = C_1.\alpha.\sinh(\alpha.X_c) + C_2.\alpha.\cosh(\alpha.X_c) - 2n.a_2.X_c - n.a_1 = 0$$
$$\rightarrow C_2 = \frac{\tau_0 + 2n.a_2.X_c + n.a_1 - C_1.\alpha.\sinh(\alpha.X_c)}{\alpha.\cosh(\alpha.X_c)} \quad \textbf{(A-27)}$$

$$C_2 = \frac{2n.a_2.X_c + n.a_1 - n\left(2.\frac{a_2}{\alpha^2} + a_0\right).\alpha.\sinh(\alpha.X_c)}{\alpha.\cosh(\alpha.X_c)} \quad \textbf{(A-28)}$$

Replace C1 and C2 to the general solution:

$$\sigma_f = \sigma_f^h + \sigma_f^p = n\left(2.\frac{a_2}{\alpha^2} + a_0\right).\cosh(\alpha.x) + \frac{\tau_0 + 2n.a_2.X_c + n.a_1 - n\left(2.\frac{a_2}{\alpha^2} + a_0\right).\alpha.\sinh(\alpha.X_c)}{\alpha.\cosh(\alpha.X_c)}.\sinh(\alpha.x) - n\left(a_2.x^2 + a_1.x + 2.\frac{a_2}{\alpha^2} + a_0\right) \quad \textbf{(A-29)}$$

$$\tau_f = n\left(2.\frac{a_2}{\alpha^2} + a_0\right).\sinh(\alpha.x) + \frac{\tau_0 + 2n.a_2.X_c + n.a_1 - n\left(2.\frac{a_2}{\alpha^2} + a_0\right).\alpha.\sinh(\alpha.X_c)}{\alpha.\cosh(\alpha.X_c)}.\sinh(\alpha.x) - n\left(a_2.x^2 + a_1.x + 2.\frac{a_2}{\alpha^2} + a_0\right) \quad \textbf{(A-30)}$$

A.1 BOUNDARY CONDITIONS

Four point bending test

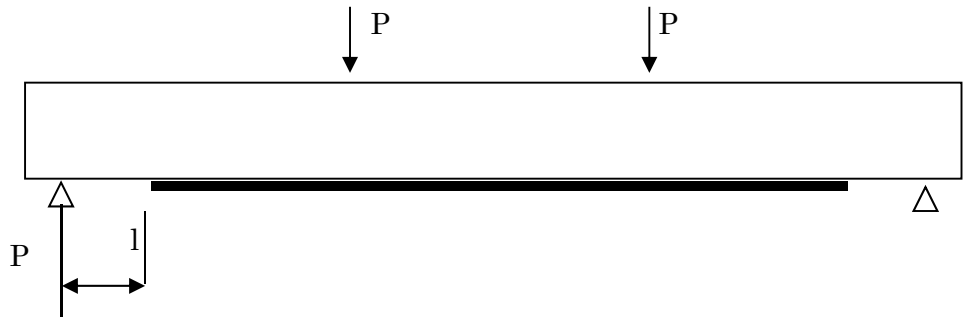

Bending moment of beam at x mm from cut-off point

$$M = \frac{P}{2}(l_0 + x) \quad \textbf{(A-31)}$$

$$\sigma_c = \frac{M}{I_{eff}} y_{eff} = \frac{P}{2}\frac{y_{eff}}{I_{eff}} x + \frac{Pl_0}{2}\frac{y_{eff}}{I_{eff}} \quad \textbf{(A-32)}$$

$$a_0 = \frac{Pl_0}{2}\frac{y_{eff}}{I_{eff}}$$

$$a_1 = \frac{P}{2}\frac{y_{eff}}{I_{eff}} \quad \textbf{(A-33)}$$

$$a_2 = 0$$

$$C_1 = n\left(2.\frac{a_2}{\alpha^2} + a_0\right) = n\frac{Pl_0}{2}\frac{y_{eff}}{I_{eff}} \quad \textbf{(A-34)}$$

$$\tau_f = n\frac{Pl_0}{2}\frac{y_{eff}}{I_{eff}}.\alpha.\sinh(\alpha.x) + C_2.\alpha.\cosh(\alpha.x) - n.\frac{P}{2}\frac{y_{eff}}{I_{eff}} \quad \textbf{(A-35)}$$

$$y_{eff} = d_f - c_{eff} \quad \textbf{(A-36)}$$

$$c_{eff} = \left(\frac{M_{cr}}{M}\right)^{2.5} c_{cr} + \left(1 - \left(\frac{M_{cr}}{M}\right)^{2.5}\right) c_g \quad \textbf{(A-37)}$$

$$I_{eff} = \left(\frac{M_{cr}}{M}\right)^{3} I_{cr} + \left(1 - \left(\frac{M_{cr}}{M}\right)^{3}\right) I_g \quad \textbf{(A-38)}$$

$$\frac{M_{cr}}{M(x)} = \lambda(x) \quad \textbf{(A-39)}$$

$$c_{eff} = (\lambda(x))^{2.5} c_{cr} + \left(1 - (\lambda(x)^{2.5}\right) c_g \quad \textbf{(A-40)}$$

$$I_{eff} = (\lambda(x))^3 I_{cr} + \left(1 - \lambda(x)^3\right) I_g \quad \textbf{(A-41)}$$

$$\sigma_f = n\frac{Pl_0}{2}\frac{y_{eff}}{I_{eff}}.\cosh(\alpha.x) + \frac{\tau_0 + n.\frac{P}{2}\frac{y_{eff}}{I_{eff}} - n\left(a_0\right)\alpha.\sinh(\alpha.X_c)}{\alpha.\cosh(\alpha.X_c)}.\sinh(\alpha.x) - n\left(\frac{P}{2}\frac{y_{eff}}{I_{eff}}x + \frac{Pl_0}{2}\frac{y_{eff}}{I_{eff}}\right)$$

(A-42)

$$\tau_f = \sigma_f^h + \sigma_f^p = n\frac{Pl_0}{2}\frac{y_{eff}}{I_{eff}}.\alpha.\sinh(\alpha.x) + \frac{\tau_0 + n.\frac{P}{2}\frac{y_{eff}}{I_{eff}} - n\frac{Pl_0}{2}\frac{y_{eff}}{I_{eff}}.\alpha.\sinh(\alpha.X_c)}{\alpha.\cosh(\alpha.X_c)}.\alpha.\cosh(\alpha.x) - n.\frac{P}{2}\frac{y_{eff}}{I_{eff}}$$

(A-43)

$$\tau_f = \sigma_f^h + \sigma_f^p = n\frac{Pl_0}{2}\frac{P}{2}\frac{\left[d_f - (\lambda(X_c))^{2.5} c_{cr} + \left[1 - (\lambda(X_c)^{2.5}\right] c_g\right]}{(\lambda(X_c))^3 I_{cr} + \left(1 - \lambda(X_c)^3\right) I_g}.\alpha.\sinh(\alpha.x) +$$

$$\frac{\tau_0 + n.\frac{P}{2}\frac{P}{2}\frac{\left[d_f - (\lambda(X_c))^{2.5} c_{cr} + \left[1 - (\lambda(X_c)^{2.5}\right] c_g\right]}{(\lambda(X_c))^3 I_{cr} + \left(1 - \lambda(X_c)^3\right) I_g} - n\frac{Pl_0}{2}\frac{y_{eff}}{I_{eff}}.\alpha.\sinh(\alpha.X_c)}{\alpha.\cosh(\alpha.X_c)}.\alpha.\cosh(\alpha.x) -$$

$$- n.\frac{P}{2}\frac{P}{2}\frac{\left[d_f - (\lambda(X_c))^{2.5} c_{cr} + \left[1 - (\lambda(X_c)^{2.5}\right] c_g\right]}{(\lambda(X_c))^3 I_{cr} + \left(1 - \lambda(X_c)^3\right) I_g} \quad \textbf{(A-44)}$$

Uniform distribution load

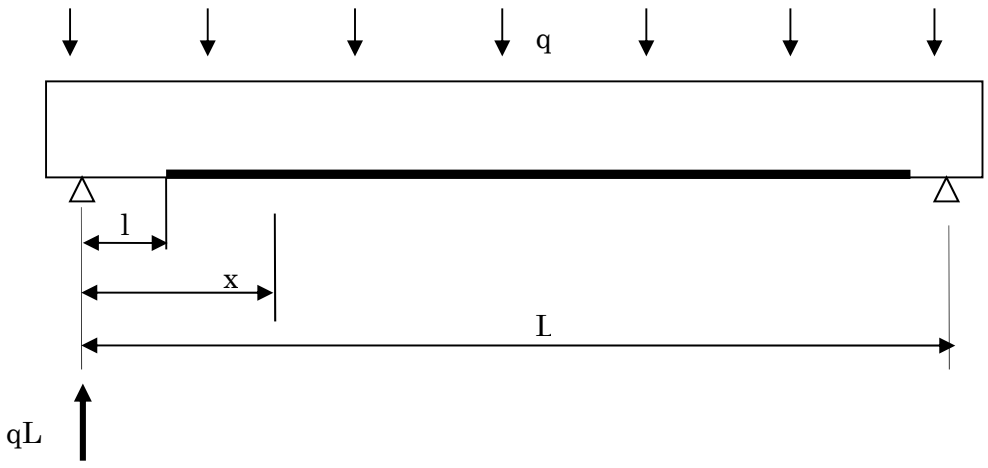

$$M = \frac{qL}{2}(l_0 + x) - q\frac{(l_0 + x)^2}{2} = \frac{q}{2}x^2 + \frac{q}{2}(2l_0 + L).x + q\left(l_o^{\,2} + L.l_o\right) \quad \textbf{(A-45)}$$

$$\sigma_c = \frac{M}{I_{eff}} y_{eff} = \frac{q}{2}\frac{y_{eff}}{I_{eff}} x^2 + \frac{q}{2}(2l_0 + L)\frac{y_{eff}}{I_{eff}} x + q\left(l_0{}^2 + L.l_0\right) \quad \textbf{(A-46)}$$

$$a_0 = q\left(l_0{}^2 + L.l_0\right)$$

$$a_1 = \frac{q}{2}(2l_0 + L) \quad \textbf{(A-47)}$$

$$a_2 = \frac{q}{2}\frac{y_{eff}}{I_{eff}}$$

$$\sigma_f = \sigma_f^h + \sigma_f^p = n\left(2.\frac{\frac{q}{2}\frac{y_{eff}}{I_{eff}}}{\alpha^2} + q\left(l_0{}^2 + L.l_0\right)\right).\cosh(\alpha.x) +$$

$$+\frac{\tau_0 + 2n.\frac{q}{2}\frac{y_{eff}}{I_{eff}}.X_c + n.\frac{q}{2}(2l_0 + L) - n\left(2.\frac{\frac{q}{2}\frac{y_{eff}}{I_{eff}}}{\alpha^2} + q\left(l_0{}^2 + L.l_0\right)\right).\alpha.\sinh(\alpha.X_c)}{\alpha.\cosh(\alpha.X_c)}.\sinh(\alpha.x) - \quad \textbf{(A-48)}$$

$$-n\left(\frac{q}{2}\frac{y_{eff}}{I_{eff}}.x^2 + \frac{q}{2}(2l_0 + L).x + 2.\frac{\frac{q}{2}\frac{y_{eff}}{I_{eff}}}{\alpha^2} + q\left(l_0{}^2 + L.l_0\right)\right)$$

$$\tau_f = \sigma_f^h + \sigma_f^p = n\left(2.\frac{\frac{q}{2}\frac{y_{eff}}{I_{eff}}}{\alpha^2} + a_0\right).\alpha.\sinh(\alpha.x) +$$

$$+\frac{\tau_0 + 2n.\frac{q}{2}\frac{y_{eff}}{I_{eff}}.X_c + n.\frac{q}{2}(2l_0 + L) - n\left(2.\frac{\frac{q}{2}\frac{y_{eff}}{I_{eff}}}{\alpha^2} + a_0\right).\alpha.\sinh(\alpha.X_c)}{\alpha.\cosh(\alpha.X_c)}.\alpha.\cosh(\alpha.x) - 2n.\frac{q}{2}\frac{y_{eff}}{I_{eff}}.x - n.\frac{q}{2}(2l_0 + L) \quad \textbf{(A-49)}$$

$$\tau_f = \sigma_f^h + \sigma_f^p = n\left(2.\frac{\frac{q}{2}\frac{\left[d_f - \left[\left(\lambda_2(x)\right)^{2.5} c_{cr} + \left[1-\left(\lambda_2(x)\right)^{2.5}\right].c_g\right]\right]}{\left(\lambda_2(x)\right)^3 I_{cr} + \left(1-\lambda_2(x)^3\right).I_g}}{\alpha^2} + a_0\right).\alpha.\sinh(\alpha.x) +$$

$$\tau_0 + 2n.\frac{q}{2}\frac{\left[d_f - \left[\left(\lambda_2(x)\right)^{2.5} c_{cr} + \left[1-\left(\lambda_2(x)\right)^{2.5}\right].c_g\right]\right]}{\left(\lambda_2(x)\right)^3 I_{cr} + \left(1-\lambda_2(x)^3\right).I_g}.X_c + n.\frac{q}{2}\left(2l_0 + L\right) -$$

$$-n\left(2.\frac{\frac{q}{2}\frac{\left[d_f - \left[\left(\lambda_2(x)\right)^{2.5} c_{cr} + \left[1-\left(\lambda_2(x)\right)^{2.5}\right].c_g\right]\right]}{\left(\lambda_2(x)\right)^3 I_{cr} + \left(1-\lambda_2(x)^3\right).I_g}}{\alpha^2} + a_0\right).\alpha.\sinh(\alpha.X_c)$$

$$+\frac{}{\alpha.\cosh(\alpha.X_c)}.\alpha.\cosh(\alpha.x) \qquad \textbf{(A-50)}$$

$$-2n.\frac{q}{2}\frac{\left[d_f - \left[\left(\lambda_2(x)\right)^{2.5} c_{cr} + \left[1-\left(\lambda_2(x)\right)^{2.5}\right].c_g\right]\right]}{\left(\lambda_2(x)\right)^3 I_{cr} + \left(1-\lambda_2(x)^3\right).I_g}.x - n.\frac{q}{2}\left(2l_0 + L\right)$$

$$\sigma_f = C_1.\alpha.\sinh(\alpha.x) + C_2.\alpha.\cosh(\alpha.x) - n.q.\left[\frac{\left[d_f - \left[\left(\lambda_2(x)\right)^{2.5} c_{cr} + \left[1-\left(\lambda_2(x)\right)^{2.5}\right].c_g\right]\right]}{\left(\lambda_2(x)\right)^3 I_{cr} + \left(1-\lambda_2(x)^3\right)I_g}\right].\left(\frac{1}{2}x^2 + \frac{1}{2}\left(2l_0 + L\right)x + {l_0}^2.L\right)$$

(A-51)

$$\tau_f = C_1.\alpha.\sinh(\alpha.x) + C_2.\alpha.\cosh(\alpha.x) - n.q\left[\frac{\left[d_f - \left[\left(\lambda(x)\right)^{2.5} c_{cr} + \left[1-\left(\lambda(x)\right)^{2.5}\right].c_g\right]\right]}{\left(\lambda(x)\right)^3 I_{cr} + \left(1-\lambda(x)^3\right)I_g}\right].\left(x + \frac{L}{2} + l_0\right) \qquad \textbf{(A-52)}$$

A.2 INTERFACIAL MODEL FOR BEAM RETROFITTED WITH FRP BY NEAR SURFACE MOUNTED TECHNIQUE

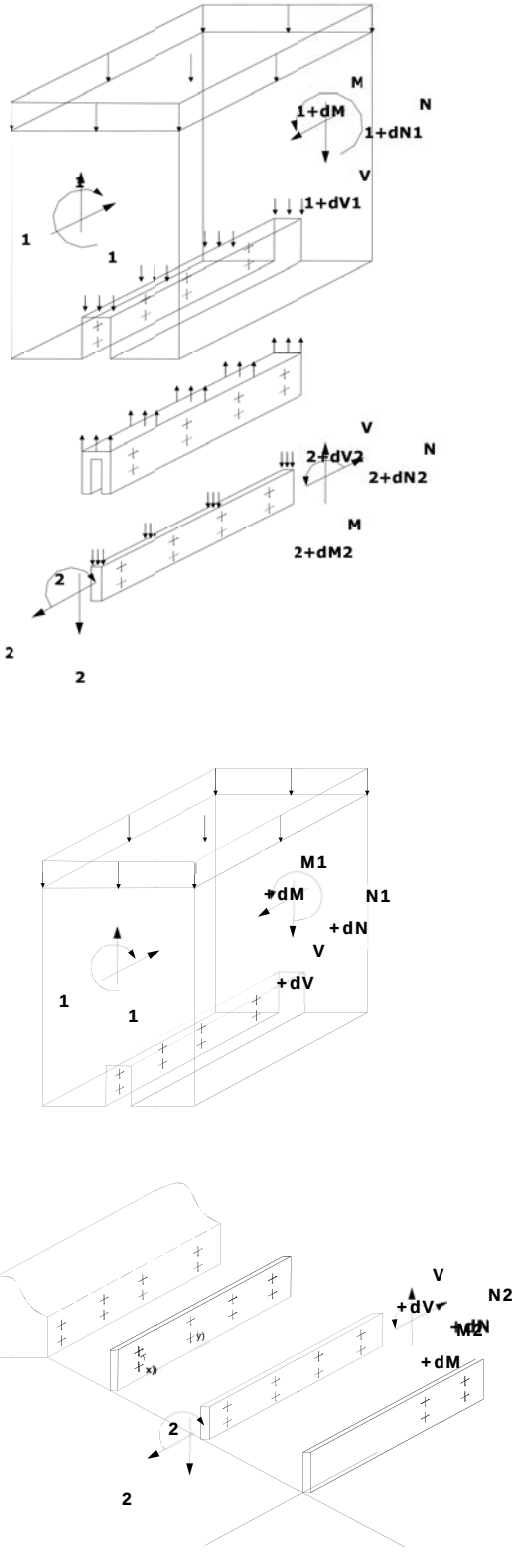

Figure 0.3: 3D differential segment for beam retrofitted with FRP by NSMR technique

2D INTERFACIAL SHEAR STRESS

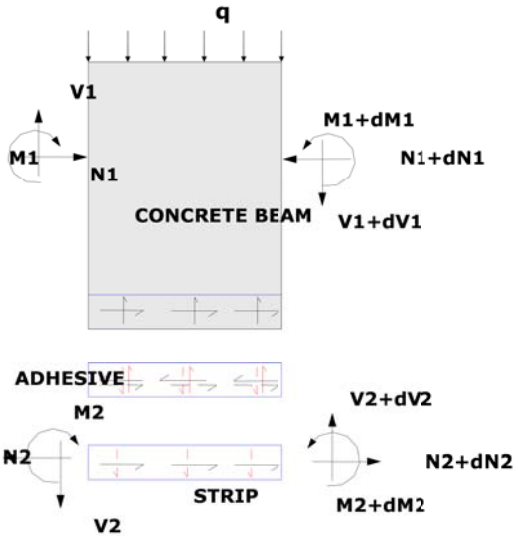

Figure 0.4: 2D differential segment for beam retrofitted with FRP by NSMR technique

The Figure 4.1 shows the force equilibrium of separate sections in the beam with NSMR and stress transferred between them. Between adherents and adhesive, there have shear stress $\tau(x)$ and normal stress $\sigma(x)$

The shear strain can be expressed in general form of Green's tensor

$$\gamma_{yx} = \frac{\partial u}{\partial y} + \frac{\partial v}{\partial x} + \frac{\partial u}{\partial x}\frac{\partial u}{\partial y} + \frac{\partial v}{\partial x}\frac{\partial v}{\partial y} \quad \textbf{(A-53)}$$

However, the beam is considered stiff enough and the second order can be omitted. Thus, shear stress can be written

$$\tau_{yx}(x) = G_a\left(\frac{\partial u}{\partial y} + \frac{\partial v}{\partial x}\right) \quad \textbf{(A-54)}$$

The first differential of $\tau(x)$

$$\frac{\tau_{yx}(x)}{dx} = G_a\left(\frac{\partial^2 u}{\partial y \partial x} + \frac{\partial^2 v}{\partial x^2}\right) \quad \textbf{(A-55)}$$

$\frac{\partial^2 v}{\partial x^2} = \frac{M_T(x)}{(EI)_t} \ll 1$ can be omitted **(A-56)**

Assume that the shear distribution in adhesive layer is linear and constant along the plate width. Thus

$$\frac{\partial u(x,y)}{\partial y} = \frac{1}{t_a}[u_2(x) - u_1(x)] \quad \textbf{(A-57)}$$

$$\frac{d^2u(x)}{dydx} = \frac{1}{t_a}\left[\frac{du_2(x)}{dx} - \frac{du_1(x)}{dx}\right] \quad \textbf{(A-58)}$$

$$\frac{\tau_{yx}(x)}{dx} = G_a\left[\frac{1}{t_a}\left[\frac{du_2(x)}{dx} - \frac{du_1(x)}{dx}\right] - \frac{M_T(x)}{(EI)_t}\right]\left[\frac{du_2(x)}{dx} - \frac{du_1(x)}{dx}\right] \quad \textbf{(A-59)}$$

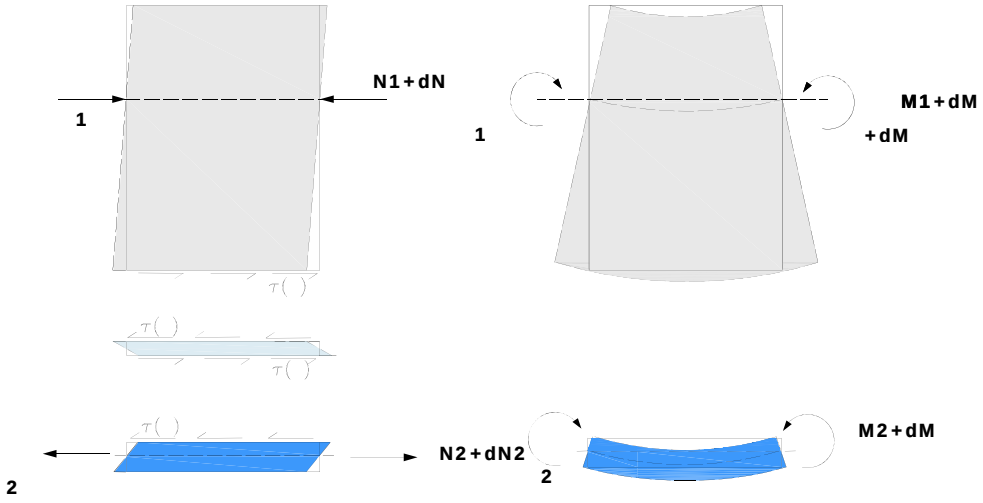

Figure 0.5 Deformation of elements of the segment for shear interfacial stress

The longitudinal strain at the bottom of adherent 1:

For the top point

$$\varepsilon_1 = \frac{du_1(x)}{dx} = -\frac{N_1(x)}{E_1A_1} + \frac{M_1(x)}{E_1I_1}(y_{eff} - h_f) + \frac{q+b\sigma(x)+2nh\,\tau_{yz}(x)}{G\alpha}(y_{eff} - h_f) \quad \textbf{(A-60)}$$

The longitudinal strain at the top of adherent 2

$$\varepsilon_2 = \frac{du_2(x)}{dx} = \frac{N_2(x)}{E_2A_2} - \frac{M_2(x)}{E_2I_2}\frac{h_f}{2} + \frac{b\sigma(x)+2nh\tau_{yz}(x)}{G\alpha}\frac{h_f}{2} \quad \textbf{(A-61)}$$

Take equilibrium of the adherent 1 and adherent 2

$$\frac{dN_1(x)}{dx} = \frac{dN_2(x)}{dx} = 2nh\,\tau_{yx}(x) \quad \textbf{(A-62)}$$

$$N_1(x) = N_2(x) = N(x) = 2nh\int_0^x \tau_{yx}(x)dx \quad \textbf{(A-63)}$$

Hence two adherents have similar deflection and curvature

$$M_1(x) = RM_2(x) \quad \textbf{(A-64)}$$

Place

$$R = \frac{E_1 I_1}{E_2 I_2} \quad \textbf{(A-65)}$$

The total moment on the plated beam includes moments contributed from adherents and shear force of adhesive

$$M_T(x) = M_1(x) + M_2(x) + N(x)(y_{eff} - \frac{h_f}{2}) \quad \textbf{(A-66)}$$

From (4.12), (4.13) and (4.14), $M_1(x)$ can be expressed

$$M_1(x) = \frac{R}{R+1}\left[M_T(x) - 2nh \int_0^x \tau_{yx}(x)(y_{eff} - \frac{h_f}{2})dx\right] \quad \textbf{(A-67)}$$

And $M_2(x)$

$$M_2(x) = \frac{1}{R+1}\left[M_T(x) - 2nh \int_0^x \tau_{yx}(x)(y_{eff} - \frac{h_f}{2})dx\right] \quad \textbf{(A-68)}$$

Differentiate (0.1) and (0.2) leading to

$$\frac{dM_1(x)}{dx} = V_1(x) = \frac{R}{R+1}\left[V_T(x) - 2nh\, \tau_{yx}(x)(y_{eff} - \frac{h_f}{2})\right] \quad \textbf{(A-69)}$$

$$\frac{dM_2(x)}{dx} = V_2(x) = \frac{1}{R+1}\left[V_T(x) - 2nh\, \tau_{yx}(x)(y_{eff} - \frac{h_f}{2})\right]$$

Differentiate (4.7), (4.8) and (4.9) and then them replace into (4.10), (4.17), (4.18) leading to the differential equation for shear stress along the strip

$$\frac{d\tau_{yx}^2(x)}{dx} = \frac{G_a}{t_a}\left[\begin{array}{c} \frac{1}{E_2A_2}2nh\,\tau_{yx}(x) + \frac{\frac{h_f}{2}}{E_2I_2}\frac{1}{R+1}\left[V_T(x) - 2nh\,\tau_{yx}(x)(y_{eff} - \frac{h_f}{2})\right] + \\ + \frac{b}{G_2A_2}\frac{d\sigma(x)}{dx}\frac{h_f}{2} + \frac{2nhb}{G_2\alpha A_2}\frac{h_f}{2}\frac{d\tau_{yz}(x)}{dx} + \frac{1}{E_1A_1}2nh\,\tau_{yx}(x) - \frac{(y_{eff}-h_f)}{E_1I_1}\frac{R}{R+1}\left[V_T(x) - 2nh\,\tau_{yx}(x)(y_{eff} - \frac{h_f}{2})\right] + \\ - \frac{(y_{eff}-h_f)}{G_1A_1}\frac{dq}{dx} - \frac{b(y_1-h_f)}{G_1A_1}\frac{d\sigma(x)}{dx} - \\ - \frac{2nh(y_{eff}-h_f)}{G_1A_1}\frac{d\tau_{yz}(x)}{dx} \end{array}\right] \quad \textbf{(A-70)}$$

$$\frac{d\tau_{yx}^2(x)}{dx} = \frac{G_a}{t_a}\left[\begin{array}{c} \frac{2nh}{E_2A_2}\,\tau_{yx}(x) - \frac{h_f}{2}\frac{1}{E_1I_1+E_2I_2}\left[V_T(x) - 2nh\,\tau_{yx}(x)(y_{eff}-\frac{h_f}{2})\right] + \\ +\frac{\frac{h_f}{2}b}{G_2A_2}\frac{d\sigma(x)}{dx} + \frac{nh_fh_fb}{G_2A_2}\frac{d\tau_{yz}(x)}{dx} + \frac{1}{E_1A_1}2nh_f\,\tau_{yx}(x) \\ -\frac{y_{eff}-h_f}{E_1I_1+E_2I_2}\left[V_T(x) - 2nh\,\tau_{yx}(x)(y_{eff}-\frac{h_f}{2})\right] - \frac{(y_{eff}-h_f)}{G_1A_1}\frac{dq}{dx} - \frac{b(y_{eff}-h_f)}{G_1A_1}\frac{d\sigma(x)}{dx} + \\ -\frac{2nh(y_{eff}-h_f)}{G_1A_1}\frac{d\tau_{yz}(x)}{dx} \end{array}\right]$$

$$\frac{d\tau_{yx}^2(x)}{dx} - \frac{G_a 2nh}{t_a}\left[\frac{(y_{eff}-\frac{h_f}{2})^2}{E_cI_{eff}+E_2I_2} + \frac{1}{E_1A_1} + \frac{1}{E_2A_2}\right]\tau_{yx}(x)$$

$$= -\frac{\mathrm{G_a}}{\mathrm{t_a}}\frac{(y_{eff}-\frac{h_f}{2})}{\mathrm{E_1I_{eff}+E_2I_2}}\mathrm{V_T(x)} - \frac{(y_{eff}-h_f)}{G_1A_1}\frac{dq}{dx} + \frac{\mathrm{G_a b}}{\mathrm{t_a}}\left(\frac{\mathrm{y_2}}{\mathrm{G_2A_f}} - \frac{y_{eff}-h_f}{\mathrm{G_1A_{eff}}}\right)\frac{\mathrm{d\sigma(x)}}{\mathrm{dx}}$$
$$-\frac{2\mathrm{nh}}{}\left(\frac{y_{eff}-\mathrm{h}}{\mathrm{G_1A_1}} - \frac{h_f\mathrm{b}}{2\mathrm{G_2A_2}}\right)\frac{\mathrm{d}\,\tau_{\mathrm{yz}}(\mathrm{x})}{\mathrm{dx}}$$

(A-71)

It can be observed that this differential equation is in coupled form of $\tau(x)$ and $\sigma(x)$. The next section is devoted to derive the remaining one of differential equation system of bond stress and normal stress distribution along the strip(bar).

A.3 INTERFACIAL VERTICAL SHEAR STRESS

The normal stress that causes peel -off of plate from the beam. This stress arises due to the difference of deflection of two adherents.

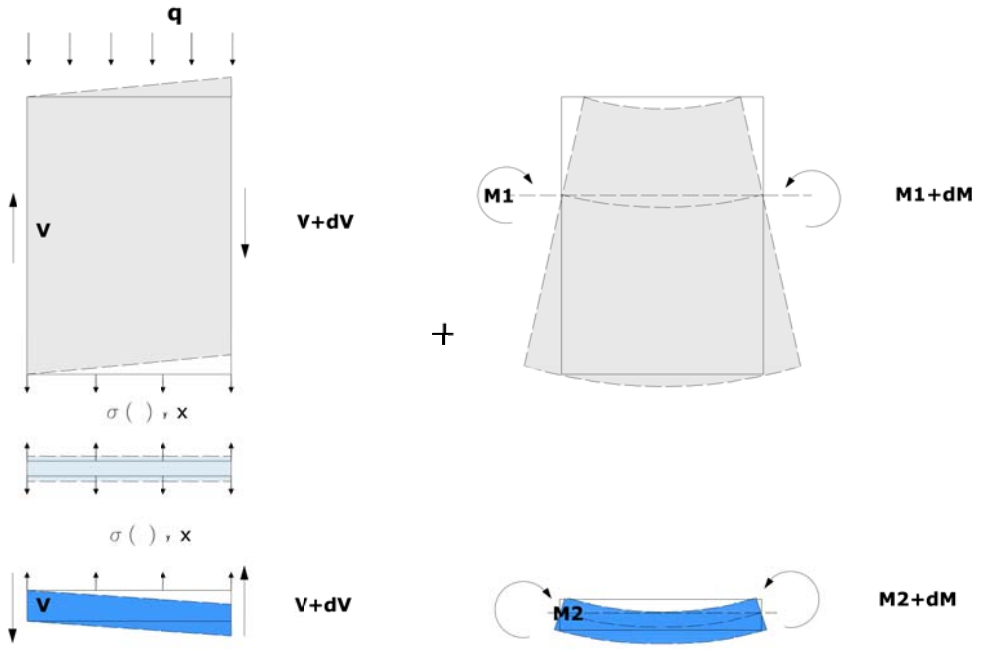

Figure 0.6 Deformation of elements of the differential segment for normal interfacial stress

$$\tau_{yz}(x) = \frac{G_a}{t_a}[v_2(x) - v_1(x)] \quad \textbf{(A-72)}$$

Adherent 1

The relationship of $v_1(x)$, $M_1(x)$ and shear force can be written as following. The first part is a contribution from moment and the second one is from the shear force

$$\frac{\partial^2 v_1(x)}{\partial x^2} = -\frac{M_1(x)}{E_1 I_1} - \frac{q + b\sigma(x) + 2nh\,\tau_{yz}(x)}{G_1 \alpha A_1} \quad \textbf{(A-73)}$$

From the moment equilibrium of the adherent 1. Eliminate the second order terms

$$\frac{dM_1(x)}{dx} = V_1(x) - 2nh\,\tau_{yx}(x)\left(y_1 - \frac{h}{2}\right) \quad \textbf{(A-74)}$$

Vertical force equilibrium of adherent 1

$$\frac{dV_1(x)}{dx} = -nb_t\sigma(x) - q - 2nh\,\tau_{yz}(x) \quad \textbf{(A-75)}$$

$$\frac{d^2M_1(x)}{dx^2} = -b\sigma(x) - q - 2nh\,\tau_{yz}(x) - 2nh\left(y_1 - \frac{h}{2}\right)\frac{\tau_{yx}(x)}{dx} \quad \textbf{(A-76)}$$

Replace (4.24) and (4.25) into double differentiated (4.23)

Appendix A – Analytical solution

$$\frac{\partial^4 v_1(x)}{\partial x^4} = \left[-b\sigma(x) - q - 2nh\,\tau_{yz}(x) - 2nh\left(y_1 - \frac{h}{2}\right)\frac{\tau_{yx}(x)}{dx}\right]\frac{1}{E_1 I_1} - \frac{b}{G_1 \alpha A_1}\frac{d^2 q}{dx^2}$$

$$-\frac{b}{G_1 \alpha A_1}\frac{d^2\sigma(x)}{dx^2} - \frac{2nh}{G_1 \alpha A_1}\frac{d^2\,\tau_{yz}(x)}{dx^2} \quad \textbf{(A-77)}$$

Adherent 2

$$\frac{\partial^2 v_2(x)}{\partial x^2} = -\frac{M_2(x)}{E_2 I_2} + \frac{2nh\,\tau_{yz}(x)}{G_2 A_2 \alpha} \quad \textbf{(A-78)}$$

From the moment equilibrium of the adherent2

$$\frac{dM_2(x)}{dx} = V_2(x) \quad \textbf{(A-79)}$$

Vertical force equilibrium

$$\frac{dV_2(x)}{dx} = 2nh\,\tau_{yz}(x) \quad \textbf{(A-80)}$$

$$\frac{d^2 M_2(x)}{dx^2} = 2nh\frac{d\tau_{yz}(x)}{dx} \quad \textbf{(A-81)}$$

Adherent 2

Apply similarly concept for the adherent 2

$$\frac{\partial^4 v_2(x)}{\partial x^4} = -\frac{2nh}{E_f I_f}\frac{d\tau_{yz}(x)}{dx} + \frac{2nh}{G_2 A_2 \alpha}\frac{d^2\,d\tau_{yz}(x)}{dx^2} \quad \textbf{(A-82)}$$

Replace (4.29) and (4.30) into (4.22)

$$\frac{d^4\,\tau_{yz}(x)}{dx^4} = \frac{G_a}{t_a}\left[\begin{array}{c} -\frac{2nh}{E_2 I_2}\frac{d\tau_{yz}(x)}{dx} + \frac{2nh}{G_2 A_2 \alpha}\frac{d^2\,d\tau_{yz}(x)}{dx^2} + \frac{q}{E_1 I_1} + \frac{b\sigma(x)}{E_1 I_1} + \frac{2nh\,d\tau_{yz}(x)}{E_1 I_1} \\ +\frac{2nh}{E_1 I_1}\left(y_1 - \frac{h}{2}\right)\frac{\tau_{yx}(x)}{dx} + \frac{b}{G_1 \alpha A_1}\frac{d^2 q}{dx^2} + \frac{b}{G_1 \alpha A_1}\frac{d^2\sigma(x)}{dx^2} + \frac{2nh}{G_1 \alpha A_1}\frac{d^2\,d\tau_{yz}(x)}{dx^2} \end{array}\right] \quad \textbf{(A-83)}$$

$$\frac{d^4\,\tau_{yz}(x)}{dx^4} - \frac{2G_a nh}{\alpha t_a}\left(\frac{1}{G_c A_{eff}} - \frac{1}{G_f A_f}\right)\frac{d^2\,\tau_{yz}(x)}{dx^2} + \frac{G_a 2nh}{t_a}\left(\frac{1}{E_c A_{eff}} + \frac{1}{E_f A_f}\right)\tau_{yz}(x)$$

$$= \frac{2nh}{E_c I_{eff}}\left(y_{eff} - \frac{h}{2}\right)\frac{\tau_{yx}(x)}{dx} + \frac{b}{G_1 \alpha A_{eff}}\frac{d^2 q}{dx^2} + \frac{b}{G_c \alpha A_{eff}}\frac{d^2\sigma(x)}{dx^2} + \frac{G_a}{t_a}\frac{q}{E_c I_{eff}} + \frac{G_a}{t_a}\frac{b\sigma(x)}{E_c I_{eff}} \quad \textbf{(A-84)}$$

The homogeneous solution for equation (5.31)

$$\tau_{yz}^h(x) = C_1 e^{\alpha x} + C_2 e^{-\alpha x} + C_3 e^{\beta x} + C_4 e^{-\beta x} \quad \textbf{(A-85)}$$

The second order term $\left[\frac{G_a nh}{\alpha t_a}\left(\frac{1}{G_1 A_1} - \frac{1}{G_2 A_2}\right)\right]^2$ can be eliminated

Appendix A – Analytical solution

The characteristic of t, when x become large, t tends to zero; α and β are positive. Thus C1 and C3 approach to zero.

$$\tau_{xy}^{h}(x) = C_2 e^{-\alpha x} + C_4 e^{-\beta x} \quad \textbf{(A-86)}$$

If eliminate influence of shear deformation, the homogenous solution becomes

$$\tau_{xy}^{h}(x) = (C_1 e^{-\beta x} + C_2 e^{\beta x})\sin(\beta x) + \left[C_3 e^{\beta x} + C_4 e^{-\beta x}\right]\cos(\beta x) \quad \textbf{(A-87)}$$

$$\tau_{xy}^{h}(x) = C_1 e^{-\beta x}\sin(\beta x) + C_4 e^{-\beta x}\cos(\beta x) \quad \textbf{(A-88)}$$

$$\beta = \sqrt[4]{\frac{G_a n h}{2\alpha t_a}\left(\frac{1}{G_1 A_1} - \frac{1}{G_2 A_2}\right)} \quad \textbf{(A-89)}$$

APPENDIX A.2 – MAPLE CODE TO SOLVE DIFFERENTIAL EQUATIONS

```
> ode:=diff(y(x),x,x) =lambda^2*y(x)-a;
```

$$ode := \frac{d^2}{dx^2} y(x) = \lambda^2 y(x) - a$$

```
> dsolve(ode,y(x),type=h);
```

$$y(x) = e^{-\lambda x} \_C2 + e^{\lambda x} \_C1 + \frac{a}{\lambda^2}$$

```
> expsols(ode, y(x), output=solution);
```

$$\left[[e^{\lambda x}, e^{-\lambda x}], -\frac{a}{\lambda^2} \right]$$

```
> dsolve(ode,y(x),[exact]);

> taylor( sinh(x), x=0, 10 ):
> R := simplify( series(1/2*exp(10)-1/2/exp(10)+(1/2*exp
  (10)+1/2/exp(10))*(x-10)+(1/4*exp(10)-1/4/exp(10))*
  (x-10)^2+(1/12/exp(10)+1/12*exp(10))*(x-10)^3+(1/48*
  exp(10)-1/48/exp(10))*(x-10)^4+(1/240*exp(10)
  +1/240/exp(10))*(x-10)^5+O((x-10)^6),x = 10,6) ):
> taylor( cosh(x), x=0, 6 );
```

$$1 + \frac{1}{2} x^2 + \frac{1}{24} x^4 + O(x^6)$$

```
> taylor( alpha*sinh(omega*x)+beta*cosh(omega*x), x=0, 6
  ):
> taylor((Mo/P/(x+Lo))^2.5, x=0, 6 );
```

$$\left(\frac{Mo}{P\,Lo}\right)^{5/2} - \frac{5}{2} \frac{\left(\frac{Mo}{P\,Lo}\right)^{5/2}}{Lo} x + \frac{35}{8} \frac{\left(\frac{Mo}{P\,Lo}\right)^{5/2}}{Lo^2} x^2 - \frac{105}{16} \frac{\left(\frac{Mo}{P\,Lo}\right)^{5/2}}{Lo^3} x^3 + \frac{1155}{128} \frac{\left(\frac{Mo}{P\,Lo}\right)^{5/2}}{Lo^4} x^4 - \frac{3003}{256} \frac{\left(\frac{Mo}{P\,Lo}\right)^{5/2}}{Lo^5} x^5 + O(x^6)$$

```
> taylor((1-(Mo/P/(x+Lo))^m), x=0, 6 ):
> collect(taylor((Mo/P/(0+Lo))^m*Ig+(1-(Mo/P/(0+Lo))^m)*
  Icr, x=0, 6 ),x):
```

```
> collect(taylor((Mo/P/(0+Lo))^2.5*Xg+(1-(Mo/P/(0+Lo))
  ^2.5)*Xcr, x=0, 6 ),x):
```

```
> taylor( exp(-lambda*x), x=0, 6 );
```

$$1-\lambda x+\frac{1}{2}\lambda^2 x^2-\frac{1}{6}\lambda^3 x^3+\frac{1}{24}\lambda^4 x^4-\frac{1}{120}\lambda^5 x^5+\mathrm{O}(x^6)$$

```
> taylor( alpha*exp(-lambda*x)+beta*exp(lambda*x), x=0,
  6 );
```

$$\alpha+\beta+(-\alpha\lambda+\beta\lambda)x+\left(\frac{1}{2}\alpha\lambda^2+\frac{1}{2}\beta\lambda^2\right)x^2+\left(\frac{1}{6}\beta\lambda^3-\frac{1}{6}\alpha\lambda^3\right)x^3$$
$$+\left(\frac{1}{24}\alpha\lambda^4+\frac{1}{24}\beta\lambda^4\right)x^4+\left(-\frac{1}{120}\alpha\lambda^5+\frac{1}{120}\beta\lambda^5\right)x^5+\mathrm{O}(x^6)$$

```
> taylor((a0+a1*x+a2*x^2+a3*x^3+a4*x^4+a5*x^5)/(b0+b1*x+
  b2*x^2+b3*x^3+b4*x^4+b5*x^5),x=0,6):
```

```
> simplify(coeff(taylor((a0-2.5*x+4.375*x^2-6.5625*
  x^3+9.023437*x^4-11.73046875*x^5)/(b0-3*x+6*x^2-10*
  x^3+15*x^4-21*x^5),x=0,6),x,5)):
```

```
> diff(y(x),x,x,x,x) = -4*alpha^4*y(x)+a*x^2+b*x+c:
```

```
> dsolve(%, y(x));
```

$$y(x)=\frac{1}{4}\,\frac{a x^2+b x+c}{\alpha^4}+\_C1\,\mathrm{e}^{\alpha x}\sin(\alpha x)+\_C2\,\mathrm{e}^{\alpha x}\cos(\alpha x)$$
$$+\_C3\,\mathrm{e}^{-\alpha x}\sin(\alpha x)+\_C4\,\mathrm{e}^{-\alpha x}\cos(\alpha x)$$

```
> plot([sinh(x),x+x^3/6+x^5/120+x^7/5040+x^9/9!+x^11/11!
  +x^13/13!+x^15/15!+x^17/17!], x=15..20, color=[red,
  blue], style=[point,line]):
```

```
> diff(y(x),x,x,x,x) = -4*alpha^4*y(x)+a;
```

$$\frac{\mathrm{d}^4}{\mathrm{d}x^4}y(x)=-4\,\alpha^4 y(x)+a$$

```
> dsolve(%, y(x));
```

$$y(x)=\frac{1}{4}\,\frac{a}{\alpha^4}+\_C1\,\mathrm{e}^{\alpha x}\sin(\alpha x)+\_C2\,\mathrm{e}^{\alpha x}\cos(\alpha x)+\_C3\,\mathrm{e}^{-\alpha x}\sin(\alpha x)$$
$$+\_C4\,\mathrm{e}^{-\alpha x}\cos(\alpha x)$$

```
> diff(y(x),x,x,x,x) = -4*alpha^4*y(x)+a*x+b;
```

$$\frac{\mathrm{d}^4}{\mathrm{d}x^4}y(x)=-4\,\alpha^4 y(x)+a\,x+b$$

```
> dsolve(%, y(x)):
```

```
> diff(y(x),x,x,x,x) = -4*beta^4*y(x)+a*x^5+b*x^4+c*x^3+
  d*x^2+e*x+f;
```

$$\frac{d^4}{dx^4} y(x) = -4\,\beta^4 y(x) + a\,x^5 + b\,x^4 + c\,x^3 + d\,x^2 + e\,x + f$$

```
> diff(y(x),x,x,x,x) = -4*alpha^4*y(x)+cosh(beta*x)+sinh
  (beta*x):
> dsolve(%, y(x)):
> diff(y(x),x,x,x,x) = -4*beta^4*y(x)+A*x^4+B*x^3+C*x^2+
  D*x+E;
```

$$\frac{d^4}{dx^4} y(x) = -4\,\beta^4 y(x) + A\,x^4 + B\,x^3 + C\,x^2 + \mathrm{D}\,x + E$$

```
> dsolve(%, y(x));
```

$$y(x) = \frac{1}{4}\,\frac{\beta^4 E - 6A + \mathrm{D}\,x\,\beta^4 + C\,x^2\beta^4 + B\,x^3\beta^4 + A\,x^4\beta^4}{\beta^8} + \_C1\,e^{\beta x}\sin(\beta x) + \_C2\,e^{\beta x}\cos(\beta x) + \_C3\,e^{-\beta x}\sin(\beta x) + \_C4\,e^{-\beta x}\cos(\beta x)$$

```
> diff(y(x),x,x,x,x)=(beta)^2*y(x)+a;
```

$$\frac{d^4}{dx^4} y(x) = \beta^2 y(x) + a$$

```
> dsolve(%, y(x));
```

$$y(x) = -\frac{a}{\beta^2} + \_C1\,\sin\left(\sqrt{\beta}\,x\right) + \_C2\,\cos\left(\sqrt{\beta}\,x\right) + \_C3\,e^{\sqrt{\beta}\,x} + \_C4\,e^{-\sqrt{\beta}\,x}$$

```
> with(DEtools):
  DEplot(cos(x)*diff(y(x),x,x,x)-diff(y(x),x)+Pi*diff(y
  (x),x,x)=y(x)-x,y(x),
  x=-10..1.4,[[y(0)=1,D(y)(0)=2,(D@@2)(y)(0)=1]],y=-4.
  .5,stepsize=.05):

> DEplot([diff(x(t),t)=x(t)*(1-y(t)),diff(y(t),t)=.3*y
  (t)+diff(x(t),t)],
  [x(t),y(t)],t=-5..5,x=-5..2,y=-1..2,arrows=LARGE,
  title=`Lotka-Volterra model`,color=[.3*y(t)*(x(t)-1),x
  (t)*(1-y(t)),.1]);
Error, empty plot

> ode:={diff(x(t),t,t)-x(t),diff(y(t),t,t)-0.3*y(t)*(x
```

```
(t)-1)}:
```

```
> dsolve(ode):
```

```
> Order := 6;
```

$$Order := 6$$

```
> sys1 := {diff(sigma(x),x,x,x,x)-A1*diff(sigma(x),x,x)=
  -A2*diff(tau(x),x)-A3*sigma(x)+a*x^3+b*x^2+c*x+d,diff
  (tau(x),x,x)+B1*tau(x)-B2*diff(sigma(x),x)-m*x^3+n*
  x^2+x+p};
```

$$sys1 := \left\{ \frac{d^4}{dx^4}\,\sigma(x) - A1\left(\frac{d^2}{dx^2}\,\sigma(x)\right) = -A2\left(\frac{d}{dx}\,\tau(x)\right) - A3\,\sigma(x) + a\,x^3 + b\,x^2 + c\,x + d,\ \frac{d^2}{dx^2}\,\tau(x) + B1\,\tau(x) - B2\left(\frac{d}{dx}\,\sigma(x)\right) - m\,x^3 + n\,x^2 + x + p \right\}$$

```
> with(DEtools):
```

```
> ans := dsolve(sys1 union {}, {sigma(x),tau(x)}, type=
  'series');
```

$$ans := \left\{ \sigma(x) = \sigma(0) + D(\sigma)(0)\,x + \frac{1}{2}\,D^{(2)}(\sigma)(0)\,x^2 + \frac{1}{6}\,D^{(3)}(\sigma)(0)\,x^3 + \left(\frac{1}{24}\,A1\,D^{(2)}(\sigma)(0) - \frac{1}{24}\,A2\,D(\tau)(0) - \frac{1}{24}\,A3\,\sigma(0) + \frac{1}{24}\,d\right)x^4 + \left(\frac{1}{120}\,A1\,D^{(3)}(\sigma)(0) + \frac{1}{120}\,A2\,B1\,\tau(0) - \frac{1}{120}\,A2\,B2\,D(\sigma)(0) + \frac{1}{120}\,A2\,p - \frac{1}{120}\,A3\,D(\sigma)(0) + \frac{1}{120}\,c\right)x^5 + O(x^6),\ \tau(x) = \tau(0) + D(\tau)(0)\,x + \left(-\frac{1}{2}\,B1\,\tau(0) + \frac{1}{2}\,B2\,D(\sigma)(0) - \frac{1}{2}\,p\right)x^2 + \left(-\frac{1}{6}\,B1\,D(\tau)(0) + \frac{1}{6}\,B2\,D^{(2)}(\sigma)(0) - \frac{1}{6}\right)x^3 + \left(\frac{1}{24}\,D^{(3)}(\sigma)(0)\,B2 + \frac{1}{24}\,B1^2\,\tau(0) - \frac{1}{24}\,B1\,B2\,D(\sigma)(0) + \frac{1}{24}\,B1\,p - \frac{1}{12}\,n\right)x^4 + \left(\frac{1}{120}\,B1^2\,D(\tau)(0) - \frac{1}{120}\,B1\,B2\,D^{(2)}(\sigma)(0) + \frac{1}{120}\,B1 + \frac{1}{120}\,B2\,A1\,D^{(2)}(\sigma)(0) - \frac{1}{120}\,B2\,A2\,D(\tau)(0) - \frac{1}{120}\,B2\,A3\,\sigma(0)\right) \right\}$$

$$+\frac{1}{120}\,B2\,d+\frac{1}{20}\,m\Big)\,x^5+\mathrm{O}(x^6)\Big\}$$

```
> peel_stress:=diff(sigma(x),x,x,x,x)=-4*A3^4*sigma(x)+
  diff(tau(x),x)+a*x^3+b*x^2+c*x+d;
```

$$peel\_stress := \frac{d^4}{dx^4}\,\sigma(x) = -4\,A3^4\,\sigma(x)+\frac{d}{dx}\,\tau(x)+a\,x^3+b\,x^2+c\,x+d$$

```
> ans := dsolve(peel_stress,sigma(x), type='series');
```

$$ans := \sigma(x) = \sigma(0)+\mathrm{D}(\sigma)(0)\,x+\frac{1}{2}\,\mathrm{D}^{(2)}(\sigma)(0)\,x^2+\frac{1}{6}\,\mathrm{D}^{(3)}(\sigma)(0)\,x^3$$
$$+\left(-\frac{1}{6}\,A3^4\,\sigma(0)+\frac{1}{24}\,\mathrm{D}(\tau)(0)+\frac{1}{24}\,d\right)x^4+\left(-\frac{1}{30}\,A3^4\,\mathrm{D}(\sigma)(0)\right.$$
$$\left.+\frac{1}{120}\,\mathrm{D}^{(2)}(\tau)(0)+\frac{1}{120}\,c\right)x^5+\mathrm{O}(x^6)$$

```
> ans := dsolve(B1*diff(tau(x),x,x)-B2*tau(x)-B3*diff
  (sigma(x),x)-m*x^3+n*x^2+x+p,tau(x), type='series');
```

$$ans := \tau(x) = \tau(0)+\mathrm{D}(\tau)(0)\,x+\frac{1}{2}\,\frac{B2\,\tau(0)+B3\,\mathrm{D}(\sigma)(0)-p}{B1}\,x^2$$
$$+\frac{1}{6}\,\frac{B3\,\mathrm{D}^{(2)}(\sigma)(0)-1+B2\,\mathrm{D}(\tau)(0)}{B1}\,x^3$$
$$-\frac{1}{24}\,\frac{1}{B1^2}\left(-B2^2\,\tau(0)-B2\,B3\,\mathrm{D}(\sigma)(0)+B2\,p+2\,n\,B1\right.$$
$$\left.-\mathrm{D}^{(3)}(\sigma)(0)\,B3\,B1\right)x^4+\mathrm{O}(x^5)$$

```
> shearstress:=B1*diff(tau(x),x,x)-B2*tau(x)-m*x^3+n*
  x^2+x+p;
```

$$shearstress := B1\left(\frac{d^2}{dx^2}\,\tau(x)\right)-B2\,\tau(x)-m\,x^3+n\,x^2+x+p$$

```
> t := dsolve(B1*diff(tau(x),x,x)-B2*tau(x)-m*x^3+n*x^2+
  x+p);
```

$$t := \tau(x) = e^{\frac{\sqrt{B2}\,x}{\sqrt{B1}}}\,\_C2+e^{-\frac{\sqrt{B2}\,x}{\sqrt{B1}}}\,\_C1$$
$$+\frac{\left(-m\,x^3+n\,x^2+x+p\right)B2+2\,B1\,(n-3\,m\,x)}{B2^2}$$

```
> taylor(exp(1/B1^(1/2)*B2^(1/2)*x)*_C2+exp(-1/B1^(1/2)*
  B2^(1/2)*x)*C1+((-m*x^3+n*x^2+x+p)*B2+2*B1*(n-3*m*x))
  /B2^2,x,5);
```

$$\_C2 + C1 + \frac{B2\,p + 2\,n\,B1}{B2^2} + \left(\frac{\sqrt{B2}\,\_C2}{\sqrt{B1}} - \frac{\sqrt{B2}\,C1}{\sqrt{B1}} + \frac{B2 - 6\,B1\,m}{B2^2} \right) x + \left(\frac{1}{2}\,\frac{B2\,\_C2}{B1} + \frac{1}{2}\,\frac{B2\,C1}{B1} + \frac{n}{B2} \right) x^2 + \left(\frac{1}{6}\,\frac{B2^{3/2}\,\_C2}{B1^{3/2}} - \frac{1}{6}\,\frac{B2^{3/2}\,C1}{B1^{3/2}} - \frac{m}{B2} \right) x^3 + \left(\frac{1}{24}\,\frac{B2^2\,\_C2}{B1^2} + \frac{1}{24}\,\frac{B2^2\,C1}{B1^2} \right) x^4 + \mathrm{O}(x^5)$$

```
> sys:=[diff(y1(x),x)-y1(x)+x*y2(x)=x^3,x*diff(y2(x),x)
  -2*y2(x)]:

> vars:=[y1(x),y2(x)]:

> dsolve({op(sys)} union {y1(0)=13},vars,'series'):

> f := x^6-5*x^4;
```

$$f := x^6 - 5\,x^4$$

```
> convert(f, ln);
```

$$x^6 - 5\,x^4$$

```
> convert(cosh(x)-sinh(x),exp);
```

$$\frac{1}{e^x}$$

```
> with(DEtools):
```

```
> DEplot([diff(x(t),t,t)=x(t)*(1-y(t)),diff(y(t),t)=.3*y
  (t)*(x(t)-1)],
  [x(t),y(t)],t=-7..7,[[x(0)=1.2,y(0)=1.2,D(x)(1)=0],[x
  (0)=1,y(0)=.7]],stepsize=.2,
  title=`Lotka-Volterra model`,color=[.3*y(t)*(x(t)-1),x
  (t)*(1-y(t)),.1],
  linecolor=t/2,arrows=MEDIUM,method=rkf45);
Error, (in DEtools/DEplot/CheckInitial) Too few
initial conditions: [x(0) = 1, y(0) = .7]
```

```
> T:=exp(-beta*x)*(C1*sin(beta*x)+C2*cos(beta*x));
```

$$T := e^{-\beta x} \left(C1 \sin(\beta x) + C2 \cos(\beta x) \right)$$

```
> simplify(taylor(T, x=0,6));
```

$$C2 + (C1\,\beta - \beta\,C2)\,x - \beta^2\,C1\,x^2 + \left(\frac{1}{3}\,C1\,\beta^3 + \frac{1}{3}\,\beta^3\,C2\right)x^3 - \frac{1}{6}\,C2\,\beta^4\,x^4 + \left(\frac{1}{30}\,\beta^5\,C2 - \frac{1}{30}\,C1\,\beta^5\right)x^5 + O(x^6)$$

```
> plot([[2*cos(s), sin(s), s=0..-Pi], [cos(t), sin(t),
  t=0..Pi]],
    color=[blue,yellow]):

> plot([2*cos(s), sin(s), s=0..2*Pi], color=[blue,
  yellow]):
> smartplot(cos(x) + sin(x)):

> with(plots):


> with(plots):
>
  animate( plot, [exp(-0.5*x)*(1*sin(0.5*x)+A*cos(0.5*x)
  ),x=0..15], A=1..40,frames=100,color=RED );
  animate( plot, [(x-A)^2-1,x=-4..4], A=0..1,frames=100
  ):
> with(plots):
>
  animate( plot, [exp(-0.5*x)*(A*sin(0.5*x)+1*cos(0.5*x)
  ),x=0..15], A=1..0.025,frames=100,color=RED );
  animate( plot, [(x-A)^2-1,x=-4..4], A=0..1,frames=100
  ):
>
  animate( plot, [sin(x)*exp(-x/5), x=0..t], t=0..10,
  frames=50 )
```

```
> animate( plot, [sin(x)*exp(-x/5), x=t-2*Pi..t], t=-2.
  .5, frames=50);
```

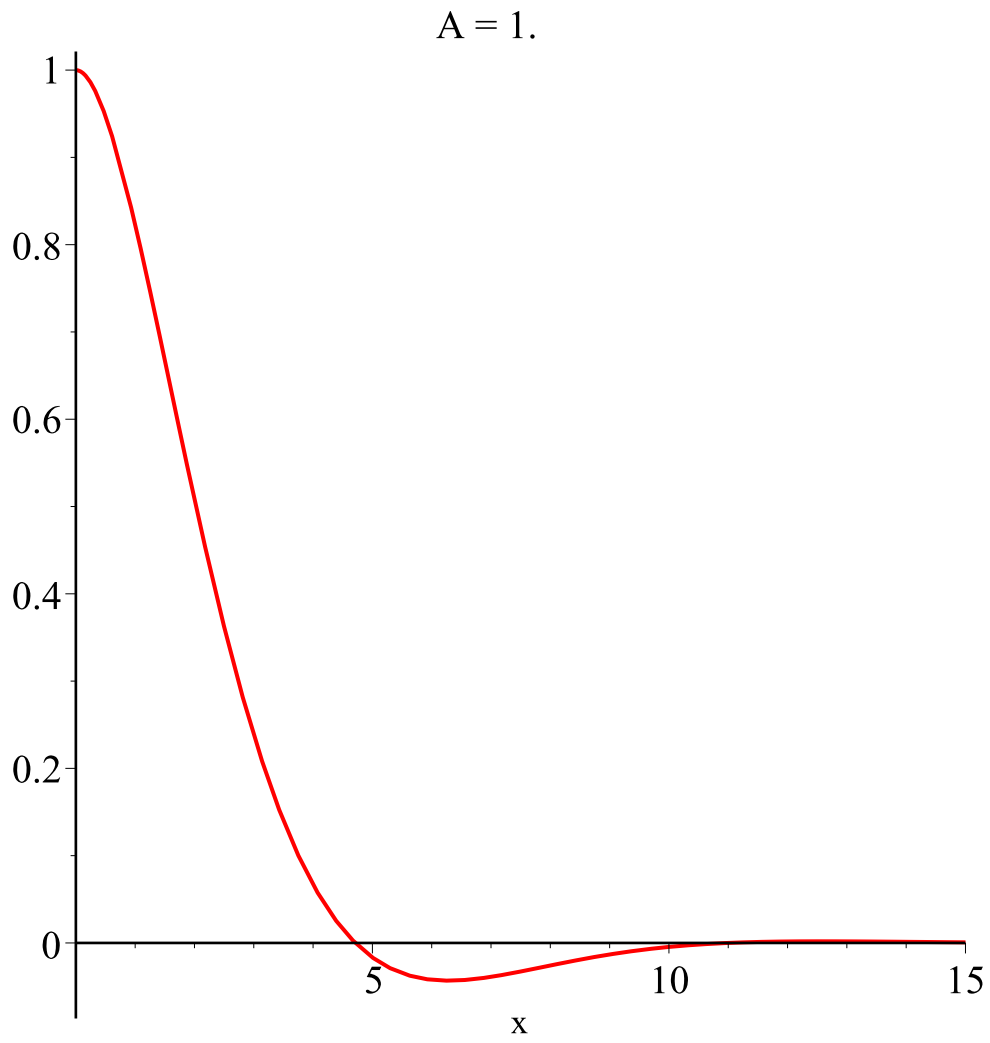


```
> opts := thickness=5, numpoints=100, color=black:
  animate( spacecurve, [[cos(t), sin(t), (2+sin(A))*t],
                        t=0..20, opts], A=0..2*Pi ):
> curve := implicitplot( exp(-0.5*x)*(sin(x)+C1*cos(x)),
  x=0..10, C1=0..4, color=blue ):
  animate( implicitplot, [exp(-0.5*x)*(C2*sin(x)+C1*cos
  (x)), x=0..10,C1=0..4],
           C2=0..3, background=curve,frames=100 ):
> curve := implicitplot( y-exp(-0.5*x)*(sin(x)+cos(x)),
  x=0..10, y=-1..4, color=blue ):
  animate( implicitplot, [y/C1-exp(-0.5*x)*(sin(x)+C1*
  cos(x)), x=0..10,y=-1..4],
           C1=1..2, background=curve,frames=100 );
```

C1 = 2.0000

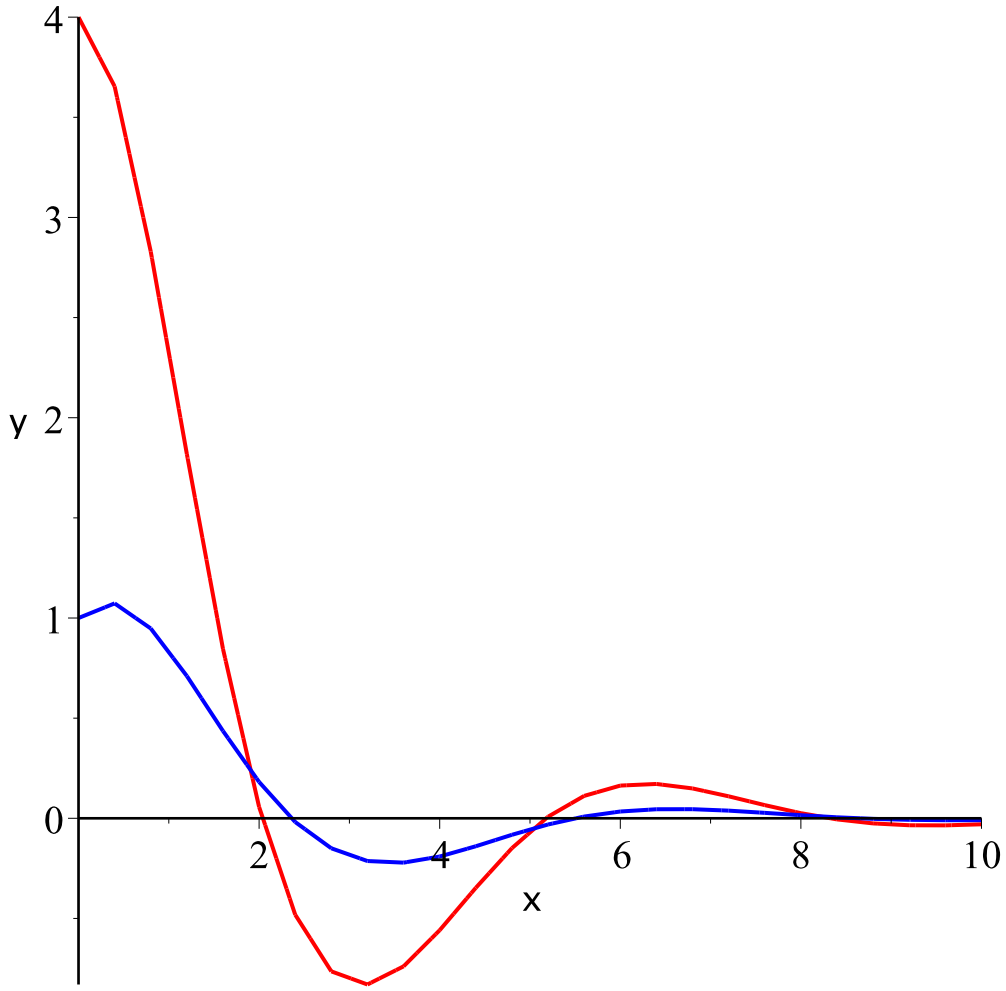


```
> beta=0.5;
```

$\beta = 0.5$

```
> curve := plot( [exp(-0.5*x)*(1*sin(0.5*x)+1*cos(0.5*x)
  ),exp(-0.5*x)*(1*sin(0.5*x)+5*cos(0.5*x))], x=0..10,
  color=[blue,green],thickness=[2,2] ):
  animate(plot,[exp(-0.5*x)*(1*sin(0.5*x)+A*cos(0.5*x)),
  x=0..10],A=0..5,background=curve,thickness=2, frames=
  200 ):
> curve := plot( [exp(-0.5*x)*(1*sin(0.5*x)+0.5*cos(0.5*
  x)),exp(-0.5*x)*(1*sin(0.5*x)+5*cos(0.5*x))], x=0..10,
  color=[blue,green],thickness=[2,2] ):
  animate(plot,[exp(-0.5*x)*(1*sin(0.5*x)+A*cos(0.5*x)),
  x=0..10] ,A=0..5,background=curve,thickness=2, frames=
  200 );
```

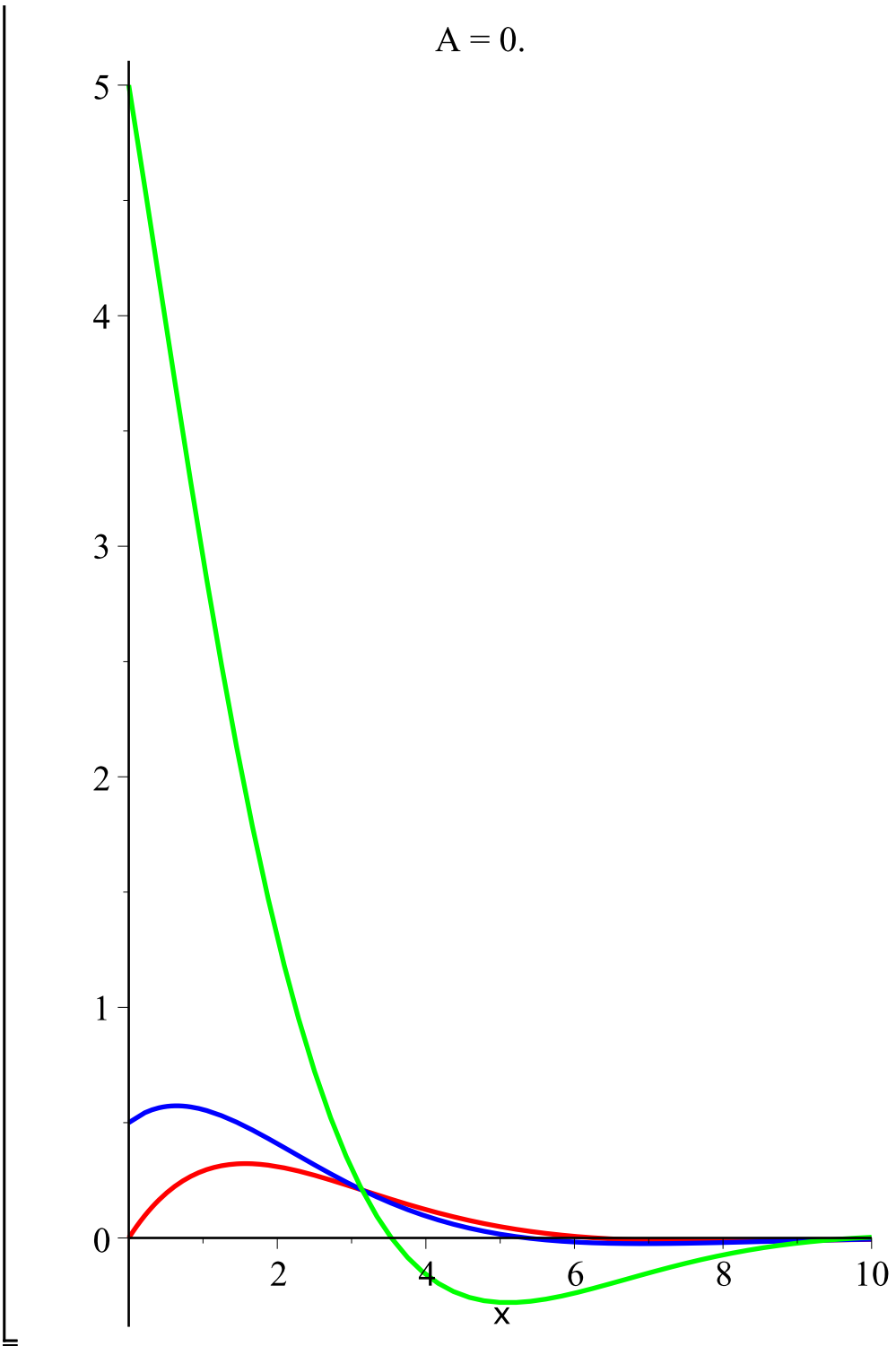


```
> :plots[interactive](animate(plot,[exp(-beta*x)*(A*sin
  (beta*x)+4*cos(beta*x))+exp(beta*x)*(.36e-3*sin(beta*
  x)+.9e-4*cos(beta*x))+.2e-1*x+.1, x = 0 .. 10],A = 0 .
  . 10,background = INTERFACE_PLOT(CURVES([[0.,
  4.1000009], [undefined, undefined]]),AXESLABELS("x",
  ""),COLOUR(RGB,0.,0.,1.00000000),VIEW(0. .. 10.,
  DEFAULT)),frames = 50));
Error, (in animate) background value must be a real
number or a plot structure
```

```
> animate( plot3d, [(-A*x^2-y^2+4)^0.5, x=-2..2, y=-2.
  .2], A=0..1,frames=10 ):
```

```
> animate( plot3d, [A*exp(-beta*x)*(sin(beta*x)+1.877*
  cos(beta*x)), x=0..10, beta=0.1..1],A=0..5,frames=100,
  axes=boxed, labels=[x,b,s],font=[SYMBOL,BOLD,10],
  titlefont=[times,bold,20],title=`PEEL STRESS
  DISTRIBUTION`);
```

$$animate(plot3d, [A\,e^{-\beta x}(\sin(\beta x) + 1.877\cos(\beta x)), x = 0..10, \beta = 0.1..1], A = 0..5, frames = 100, axes = boxed, labels = [x, b, s], font = [SYMBOL, BOLD, 10], titlefont = [times, bold, 20], title = PEEL\ STRESS\ DISTRIBUTION)$$

```
> curve := implicitplot( x^2+y^2, x=-3..1, y=-4..4,
  color=blue,thickness=2 ):
  animate( implicitplot, [x^3-A*y+y^2, x=-3..1, y=-4.
  .4],
           A=-2..2, background=curve,thickness=2,frames=
  100 ):
```

```
> plot( [exp(-0.5*x)*(10*sin(0.5*x)+10*cos(0.5*x)),x^2],
  x=0..10, color=[blue,green],thickness=[2,2] ):
```

```
> F:=plot(cos(x), x=-Pi..Pi, y=-Pi..Pi, style=line):
  G:=plot(tan(x), x=-Pi..Pi, y=-Pi..Pi, style=point):
  display({F, G}, axes=boxed, scaling=constrained,
  title=`Cosine and Tangent`):
```

```
> P := animate(plot, [exp(-0.5*x)*(sin(-0.5*x)+C*cos
  (-0.5*x)), x=0..50, color=blue,thickness=2], C=1..4,
  frames=100):
  Q := animate(plot, [exp(-0.2*x)*(sin(0.2*x)+C*cos(0.2*
  x)), x=0..50,thickness=2,style=point], C=1..4, frames=
  100):R := animate(plot, [exp(-0.35*x)*(sin(0.35*x)+C*
  cos(0.35*x)), x=0..50,thickness=2, color=green], C=1.
  .4, frames=100):T := animate(plot, [exp(-0.1*x)*(sin
  (0.1*x)+C*cos(0.1*x)), x=0..50,thickness=1,color=
  magenta], C=1..4, frames=100):
  display([P, Q, R, T ]);
```

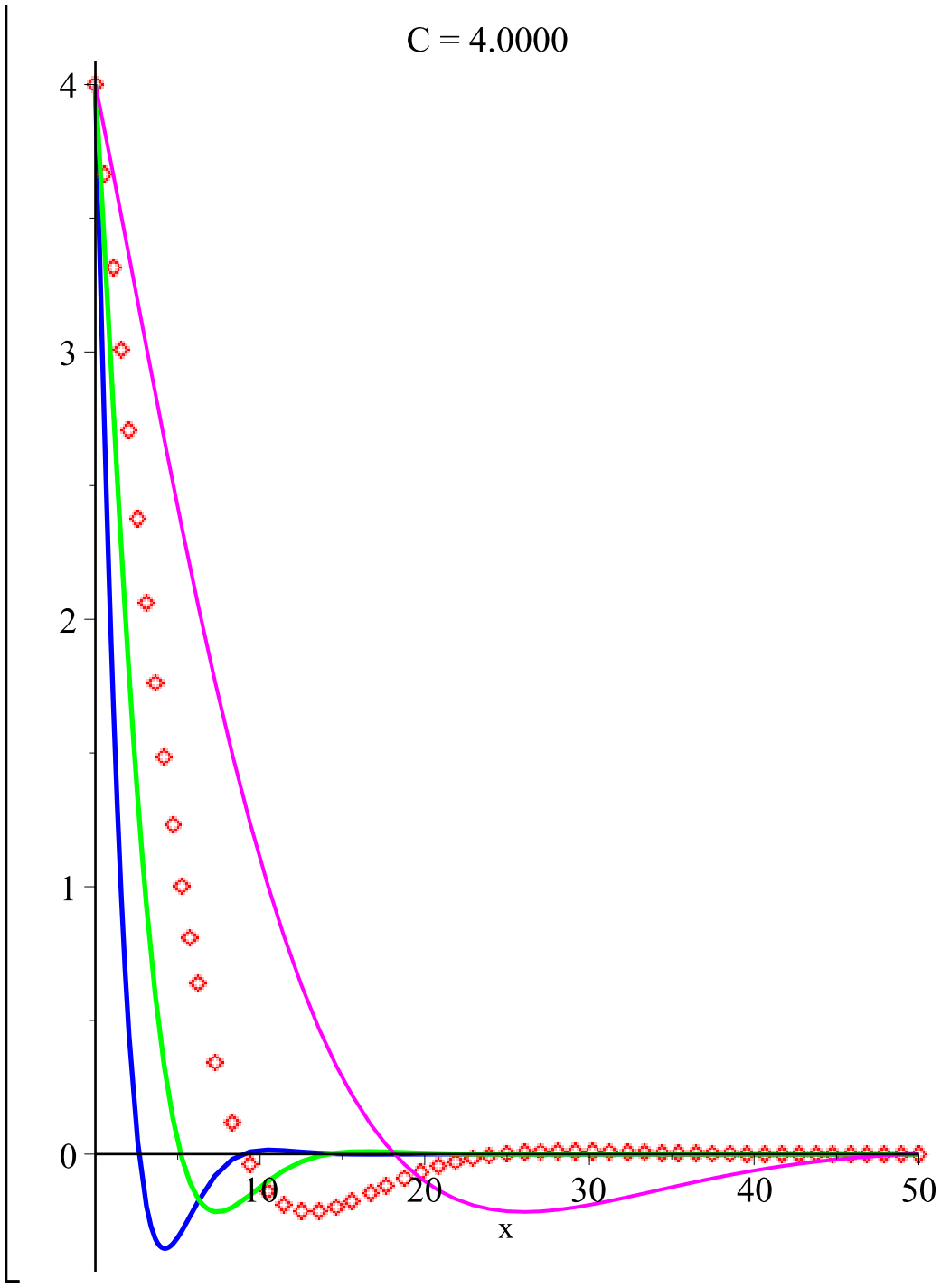


```
> P := animate(plot3d, [cos(t*x)*sin(t*y), x=-Pi..Pi, y=
  -Pi..Pi], t=1..2, frames=4):
  Q := animate(plot3d, [x*cos(t*u), x=1..3, t=1..4], u=
  2..4, coords=spherical, frames=4):
  display([P, Q], style=patch);
```

$$display\left(\left[animate\left(plot3d, \left[\cos(t\,x)\ \sin(t\,y), x=-\pi..\pi, y=-\pi..\pi\right], t=1..2,\right.\right.$$
$$\left.\left.frames=4\right), animate(plot3d, [x\cos(t\,u), x=1..3, t=1..4], u=2..4,\right.$$
$$\left.coords=spherical, frames=4\right)\left.\right], style=patch\left.\right)$$

```
> ode := (t)*diff(z(t),t$3) - (t^2- 2)*diff(z(t),t$2)
                - (t + 2)*diff(z(t),t) = 0:
```

```
expsols(ode, z(t) ):
```

```
> with(PDEtools):
```

```
> ode := diff(y(x),x,x) -lambda^2*y(x)-(a);
```

$$ode := \frac{d^2}{dx^2} y(x) - \lambda^2 y(x) - a$$

```
> expsols(ode,y(x));
```

$$\left[\left[e^{\lambda x}, e^{-\lambda x} \right], -\frac{a}{\lambda^2} \right]$$

```
> dsolve(ode, y(x));
```

$$y(x) = e^{\lambda x} \_C2 + e^{-\lambda x} \_C1 - \frac{a}{\lambda^2}$$

PARAMETRIC STUDY ON THE ANALYTICAL SOLUTION

Materials characteristics

$E_a := 4000$ $E_f := 300000$

$G_a := \frac{E_a}{2\cdot(1 + 0.36)}$ $G_a = 1.471 \times 10^3$ $G_f := \frac{E_f}{2\cdot(1 + 0.2)}$ $G_f = 1.25 \times 10^5$

$fcm := 44$ $E_c := 20\cdot\left(\frac{fcm}{10}\right)^{0.3}\cdot 1000$

$G_c := \frac{E_c}{2\cdot(1 + 0.2)}$ $G_c = 1.3 \times 10^4$

$A_s := 402$

Geometry properties

The span length $L := 3000$

The thickness of FRP $t_f := 2$

The height of the strips $h_f := 15$

Number of strips $n := 3$

The width of beam $b_1 := 150$

The height of beam $h := 300$ $d := 270$

The thickness of adhesive layer $t_a := 1$

$P := 85000$ $V_o := P$

$\rho_f := \frac{A_s}{b_1\cdot d}$ $\rho_f = 9.926 \times 10^{-3}$

$m := \frac{200000}{E_c}$ $m = 6.412$

$k := \sqrt{2\cdot\rho_f\cdot m + (\rho_f\cdot m)^2} - \rho_f\cdot m$ $k = 0.299$

$I_{cr} := \frac{1}{3}\cdot b_1\cdot(k\cdot d)^3 + A_s\cdot(h - k\cdot d)^2$ $I_{cr} = 4.558 \times 10^7$ $b := \frac{L}{3}$

Moment inertia of concrete beam

$Ig := \frac{b_1\cdot h^3}{12}$ $M_{cr} := \frac{0.62\cdot\sqrt{fcm}\cdot Ig}{0.5\cdot h}$ $Lcr := \frac{M_{cr}}{P}$ $Lcr = 108.863$

$I_f := n\frac{t_f\cdot h_f^3}{12}$

$A_f := n\cdot h_f\cdot t_f$

$$I_c(a) := \begin{cases} Ig \\ \left(\frac{M_{cr}}{P\cdot a}\right)^3\cdot Ig + \left[1 - \left(\frac{M_{cr}}{P\cdot a}\right)^3\right]\cdot I_{cr} \quad \text{if } a > Lcr \end{cases}$$

$$C_{eff}(a) := \begin{cases} \frac{h}{2} \\ \left(\frac{M_{cr}}{P\cdot a}\right)^{2.5}\cdot\frac{h}{2} + \left[1 - \left(\frac{M_{cr}}{P\cdot a}\right)^{2.5}\right]\cdot k\cdot d \quad \text{if } a > Lcr \end{cases}$$

$$y(a) := h - C_{eff}(a) - \frac{h_f}{2}$$

$$A_c(a) := \begin{cases} b_1 \cdot h \\ b_1 \cdot C_{eff}(a) \quad \text{if } a > Lcr \end{cases}$$

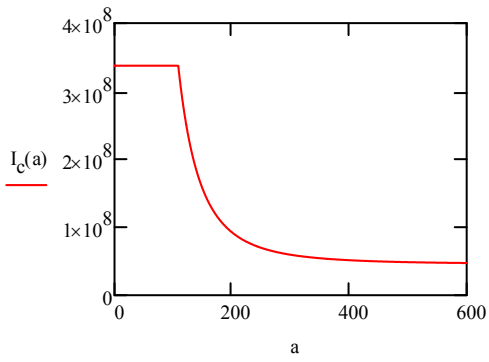

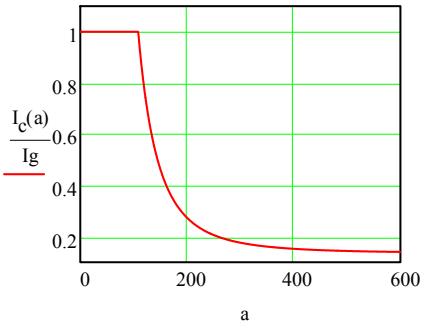

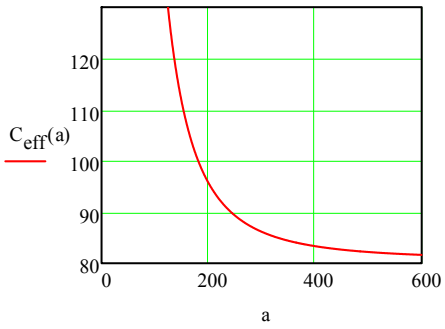

Shear stress

$$\lambda(a) := \sqrt{\frac{G_a \cdot 2.n \cdot h_f}{t_a} \left(\frac{y(a)^2}{E_c \cdot I_c(a) + E_f \cdot I_f} + \frac{1}{E_c \cdot A_c(a)} + \frac{1}{E_f \cdot A_f} \right)}$$

$$\lambda 1(a) := \sqrt{\frac{G_a \cdot (2.n \cdot h_f)}{t_a} \cdot \left(\frac{1}{E_f \cdot A_f} + \frac{y(a)^2}{E_c \cdot I_c(a)} \right)}$$

$$m1(a) := \frac{G_a}{t_a \cdot \lambda 1(a)^2} \cdot \frac{y(a)}{E_c \cdot I_c(a) + E_f \cdot I_f}$$

$$m2(a) := \frac{G_a \cdot y(a)}{t_a \cdot E_c \cdot I_c(a)}$$

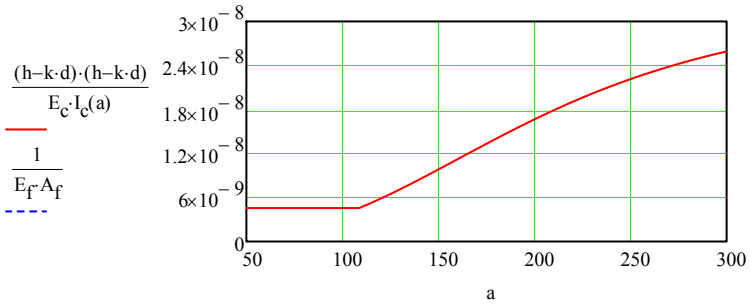

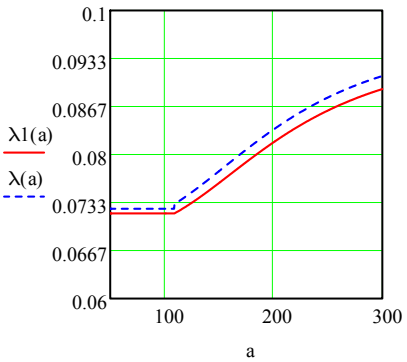

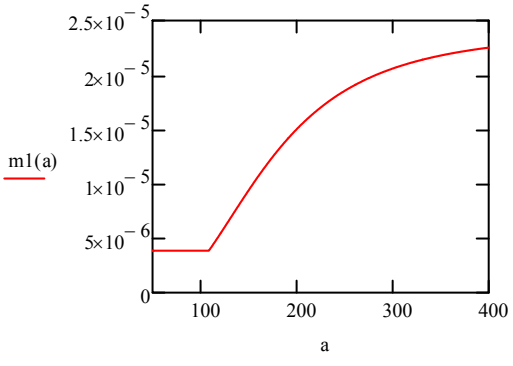

$$\left[\frac{G_a\cdot\left(h-C_{eff}(a)\right)}{t_a\cdot E_c\cdot I_c(a)}\right]$$

$$\frac{G_a}{t_a}\cdot\frac{\left(h-C_{eff}(a)\right)+\frac{t_f}{2}}{E_c\cdot I_c(a)+E_f\cdot I_f}$$

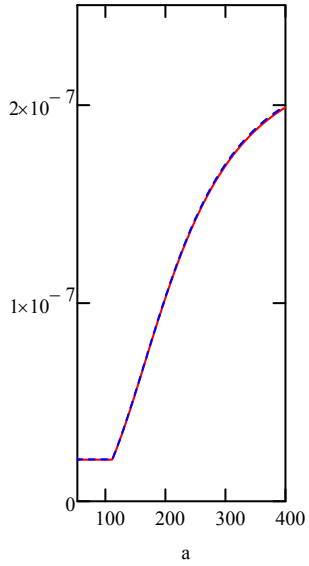

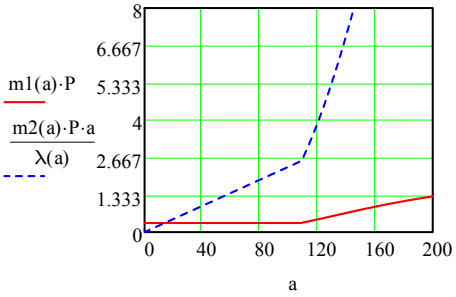

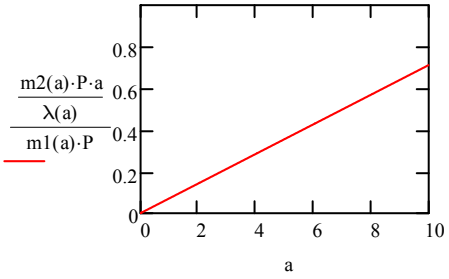

$$\tau(x,a) := \frac{m2(a)}{\lambda(a)}\cdot P\cdot a\cdot e^{-\lambda\left(C_{eff}(a)\right)\cdot x} + m1(a)\cdot P$$

$$\tau f(x,a) := \frac{\frac{G_a\cdot y(a)}{t_a\cdot E_c\cdot I_c(a)}}{\sqrt{\frac{G_a\cdot\left(2.n\cdot h_f\right)}{t_a}\cdot\left(\frac{1}{E_f\cdot A_f}+\frac{y(a)^2}{E_c\cdot I_c(a)}\right)}}\cdot P\cdot a + \frac{G_a}{t_a\cdot\lambda 1(a)^2}\cdot\frac{y(a)}{E_c\cdot I_c(a)+E_f\cdot I_f}\cdot P$$

$x := 0, 2 .. 70$

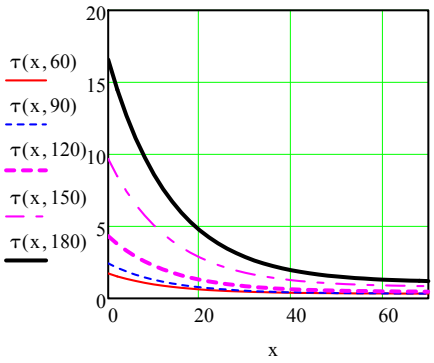

$\tau(x,90) =$

2.429
2.127
1.868
1.646
1.457
1.294
…

$\tau(x,120) =$

4.323
3.777
3.309
2.906
2.561
2.264
…

$\tau(x,250) =$

34.792
30.31
26.433
23.079
20.178
…

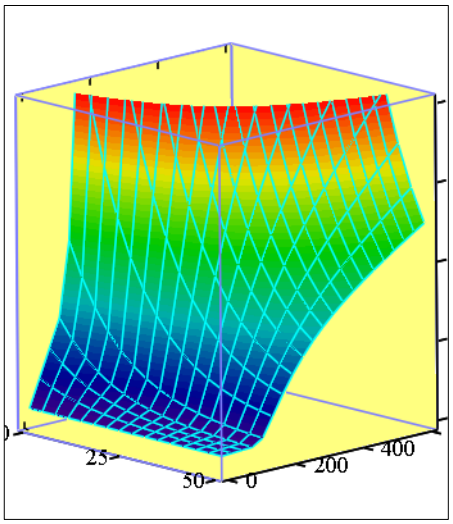

τ

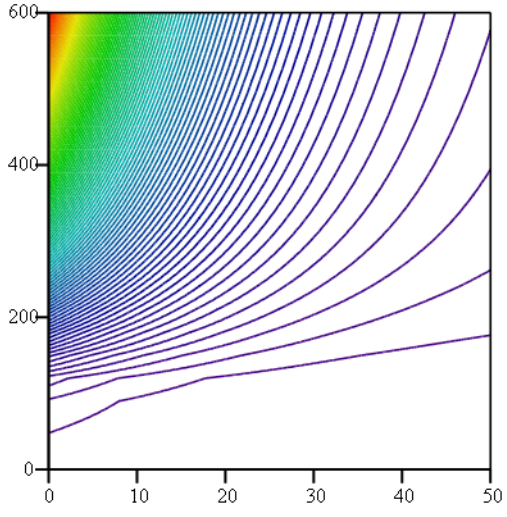

τ

INFLUENCE OF Ga

$$\lambda_G(a, G_a) := \sqrt{\frac{G_a \cdot 2.n \cdot h_f}{t_a}\left(\frac{y(a)^2}{E_c \cdot I_c(a) + E_f \cdot I_f} + \frac{1}{E_c \cdot A_c(a)} + \frac{1}{E_f \cdot A_f}\right)}$$

$$m1_G(a, G_a) := \frac{G_a}{t_a \cdot \lambda_G(a, G_a)^2} \cdot \frac{y(a)}{E_c \cdot I_c(a) + E_f \cdot I_f}$$

$$m2_G(a, G_a) := \frac{G_a \cdot y(a)}{t_a \cdot E_c \cdot I_c(a)}$$

$$\tau_G(a, G_a) := \frac{m2_G(a, G_a)}{\lambda_G(a, G_a)} \cdot P \cdot a + m1_G(a, G_a) \cdot P$$

$a := 0 .. 200$

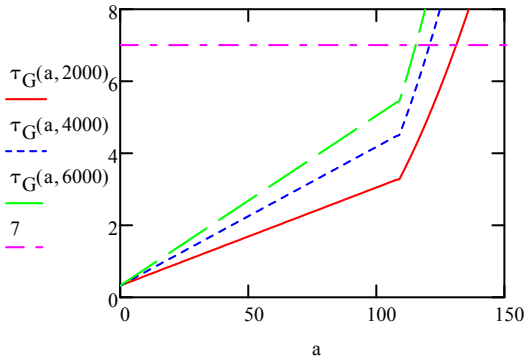

$\tau_G(a, 2000) =$

0.322
0.349
0.377
0.404
0.431
0.458
0.486
0.513
…

$\tau_G(a, 6000) =$

0.322
0.369
0.416
0.464
0.511
0.558
0.605
0.652
…

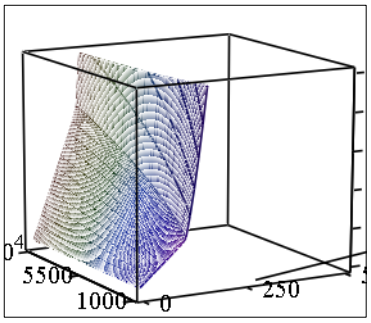

τ_G

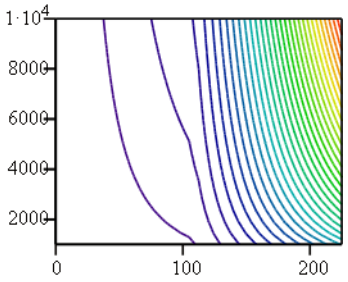

τ_G

INFLUENCE OF ta

$$\lambda_t(a, t_a) := \sqrt{\frac{G_a \cdot 2.n \cdot h_f}{t_a}\left(\frac{y(a)^2}{E_c \cdot I_c(a) + E_f \cdot I_f} + \frac{1}{E_c \cdot A_c(a)} + \frac{1}{E_f \cdot A_f}\right)}$$

$a := 0 .. 200$

$$m1_t(a, t_a) := \frac{G_a}{t_a \cdot \lambda_t(a, t_a)^2} \cdot \frac{y(a)}{E_c \cdot I_c(a) + E_f \cdot I_f}$$

$$m2_t(a, t_a) := \frac{G_a \cdot y(a)}{t_a \cdot E_c \cdot I_c(a)}$$

$$\tau_t(a, t_a) := \frac{m2_t(a, t_a)}{\lambda_t(a, t_a)} \cdot P \cdot a + m1_t(a, t_a) \cdot P$$

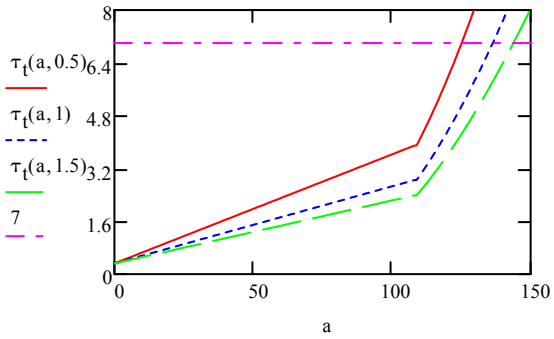

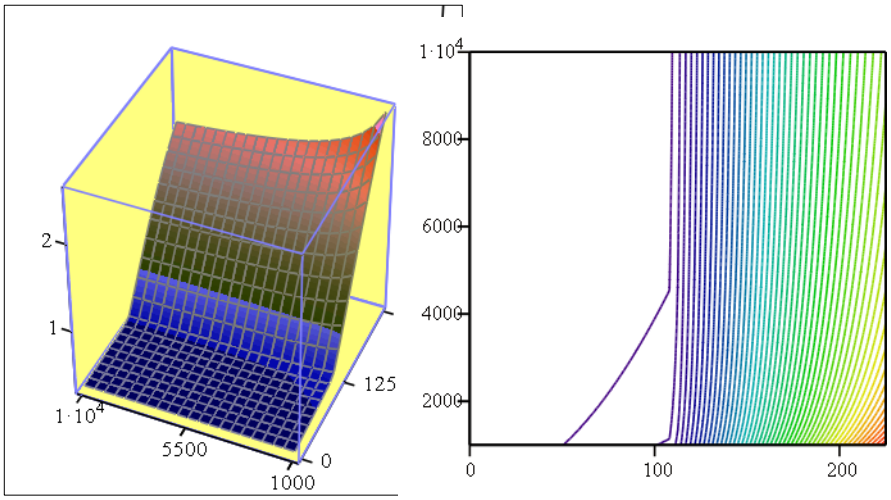

INFLUENCE OF Ef

$$\lambda_E(E_f, a) := \sqrt{\frac{G_a \cdot 2.n \cdot h_f}{t_a}\left(\frac{y(a)^2}{E_c \cdot I_c(a) + E_f \cdot I_f} + \frac{1}{E_c \cdot A_c(a)} + \frac{1}{E_f \cdot A_f}\right)}$$

$$m1_E(E_f, a) := \frac{G_a}{t_a \cdot \lambda_E(E_f, a)^2} \cdot \frac{y(a)}{E_c \cdot I_c(a) + E_f \cdot I_f} \qquad m2_E(E_f, a) := \frac{G_a \cdot y(a)}{t_a \cdot E_c \cdot I_c(a)}$$

$$\tau_E(E_f, a) := \frac{m2_E(E_f, a)}{\lambda_E(E_f, a)} \cdot P \cdot a + m1_E(E_f, a) \cdot P \qquad E_f := 50000, 100000 .. 300000$$

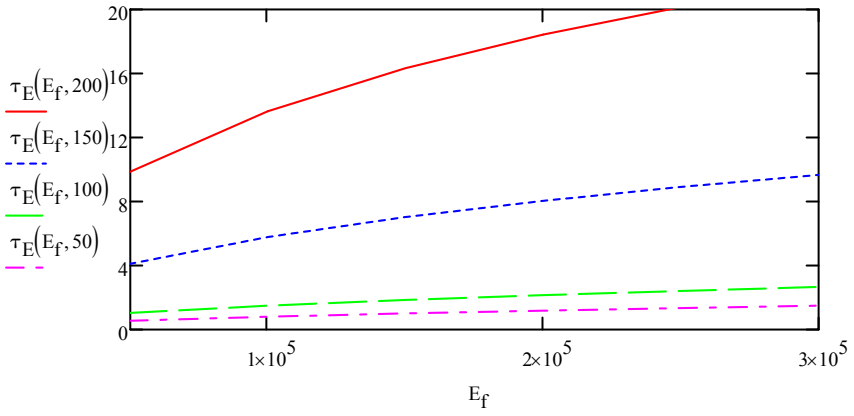

$E_f := 100000$

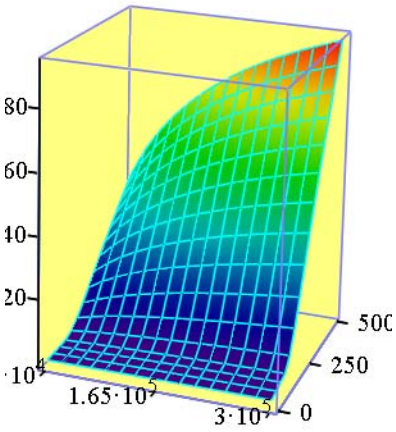

τ_E

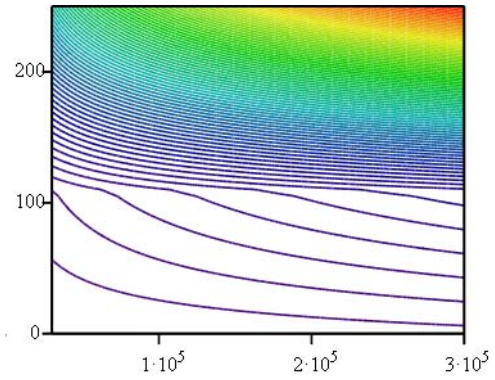

τ_E

VERTICAL SHEAR STRESS CALCULATION

$$\beta 1(a) := \sqrt[4]{\frac{E_a \cdot (2.n \cdot h_f)}{4 \cdot t_a} \left(\frac{1}{E_c \cdot I_c(a)} + \frac{1}{E_f \cdot I_f} \right)}$$

Due to $\frac{1}{E_c \cdot I_c(x)}$ is too small in the comparison with the remaining term, it can be ommited

$$\beta := \sqrt[4]{\frac{E_a \cdot (2.n \cdot h_f)}{4 \cdot t_a} \left(\frac{1}{E_f \cdot I_f} \right)}$$

Due to $\frac{E_{frp} \cdot I_{frp}}{E_c \cdot I_c(x)}$ is too small, n1(x) equals to -tf /2

$$n1(a) := \frac{\left[\left(h - C_{eff}(a) - h_f \right) \cdot \left(E_f \cdot I_f \right) \right] - \frac{t_f}{2} \cdot \left(E_c \cdot I_c(a) \right)}{E_c \cdot I_c(a) + E_f \cdot I_f}$$

$$n_2(a) := \frac{E_f \cdot I_f}{2.n \cdot h_f \cdot \left(E_c \cdot I_c(a) + E_f \cdot I_f \right)}$$

$$n1b(a) := \frac{\left(h - C_{eff}(a) - h_f \right) \cdot \left(E_f \cdot I_f \right)}{E_c \cdot I_c(a) + E_f \cdot I_f}$$

$$n1c(x) := \frac{-\left[\frac{t_f}{2} \cdot \left(E_c \cdot I_c(x) \right) \right]}{E_c \cdot I_c(x)}$$

$$n1b(x) := -\frac{t_f}{2}$$

$n1(100) = -0.998$

$n1c(100) = -1$

$$n3(a) := \frac{E_a \cdot (2.n \cdot h_f)}{t_a} \left(\frac{h - C_{eff}(a) - h_f}{E_c \cdot I_c(a)} - \frac{t_f}{2 \cdot E_f \cdot I_f} \right)$$

$n3(100) = -2.129 \times 10^{-3}$

$$n_{3b} := \frac{E_a \cdot (2.n \cdot h_f)}{t_a} \left(-\frac{t_f}{2 \cdot E_f \cdot I_f} \right)$$

$n_{3b} = -2.133 \times 10^{-3}$

$n3(200) = -2.11 \times 10^{-3}$

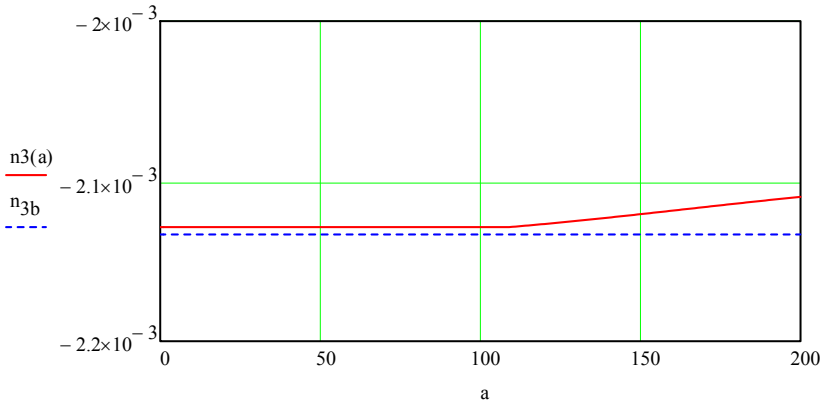

$n_1 := \frac{-t_f}{2}$ $\beta = 0.152$ $a_2 := 0$ $a_o(a) := \frac{m2(a)}{\lambda(a)} \cdot P \cdot a$ $a_1(a) := \frac{m2(a)}{\lambda(a)} \cdot P \cdot a \cdot (-\lambda(a))^4$

$a_2(a) := \frac{m2(a)}{\lambda(a)} \cdot P \cdot a \cdot (-\lambda(a))^3$

$$C1(a) := \frac{E_a}{2 \cdot \beta^3 \cdot t_a} \cdot \frac{1}{E_c \cdot I_c(a)} \cdot \left(V_o + \beta \cdot V_o \cdot a\right) - \frac{n_{3b}}{2 \cdot \beta^3} \cdot a_o(a) + \frac{n_1}{2 \cdot \beta^3}\left(a_1(a) + \beta \cdot a_2(a)\right)$$

$$C2(a) := -\frac{E_a}{2 \cdot \beta^2 \cdot t_a} \cdot \frac{1}{E_c \cdot I_c(a)} \cdot \left(\beta \cdot V_o \cdot a\right) - \frac{n_1}{2 \cdot \beta^2}\left(a_2(a)\right)$$

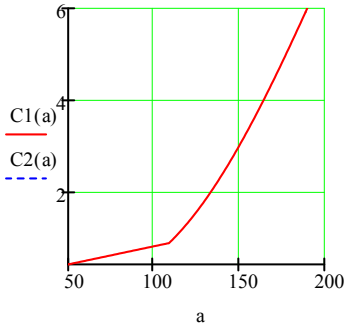

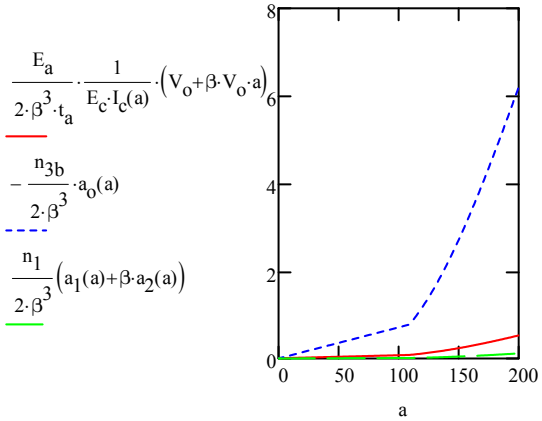

$\tau_{xy}(a, x) := e^{-\beta \cdot x} \cdot (C1(a) \cdot \cos(\beta \cdot x) + C2(a) \cdot \sin(\beta \cdot x))$

$x := 0, 2 .. 50$ $E_a := 4000$ $t_c := 2$ $t_a := 1$

$h := 300$ $b_1 := 150$ $P := 50000$ $E_f := 300000$

$$\tau_{Riz}(a) := \frac{P \cdot \left(h - C_{eff}(a) - h_f\right)}{E_c \cdot I_c(a)} \cdot \left(a \cdot \sqrt{\frac{E_f \cdot t_f \cdot G_a}{2 \cdot t_a}} + \frac{E_f \cdot t_f}{2}\right)$$

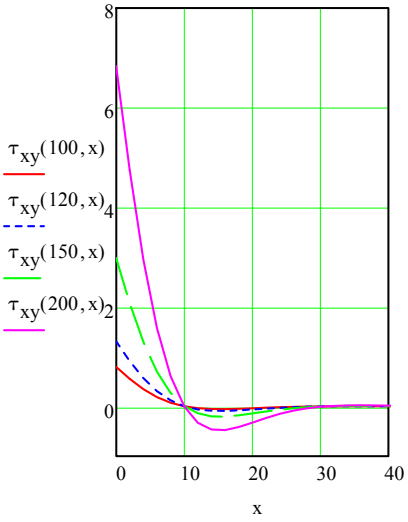

$\tau_{xy}(60,x)$ =

0.478
0.333
0.208
0.112
0.044
$1.433 \cdot 10^{-3}$
-0.022
-0.032
-0.033
...

$\tau_{xy}(90,x)$ =

0.715
0.498
0.311
0.167
0.066
$2.124 \cdot 10^{-3}$
-0.033
-0.048
...

$\tau_{xy}(200,x)$ =

6.836
4.739
2.951
1.576
0.612
$3.437 \cdot 10^{-3}$
-0.328
-0.464
...

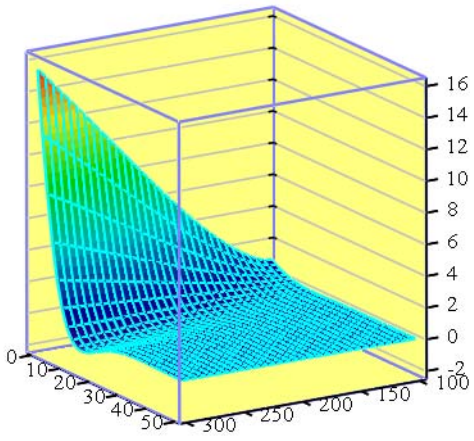

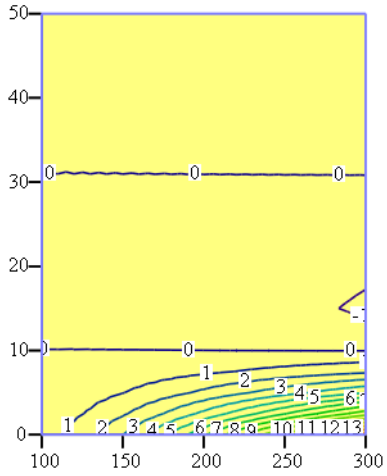

τ_{xy}

τ_{xy}

$$\tau(a) := \frac{\frac{G_a \cdot (h - C_{eff}(a) - h_f)}{t_a \cdot E_c \cdot I_c(a)}}{\sqrt{\frac{G_a \cdot (2.n \cdot h_f)}{t_a} \cdot \left[\frac{1}{E_f \cdot A_f} + \frac{(h - C_{eff}(a) - h_f) \cdot (h - C_{eff}(a) - h_f)}{E_c \cdot I_c(a)}\right]} + \frac{G_a}{t_a \cdot \lambda 1(a)^2} \cdot \frac{h - C_{eff}(a) - h_f}{E_c \cdot I_c(a) + E_f \cdot I_f}} \cdot P \cdot a \ ...$$

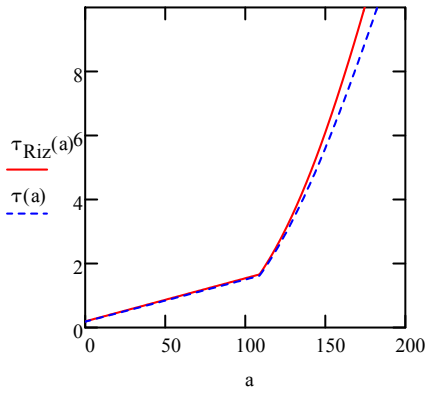

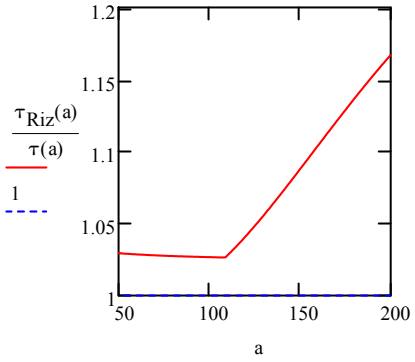

$$y(a) := h - C_{eff}(a) - h_f$$

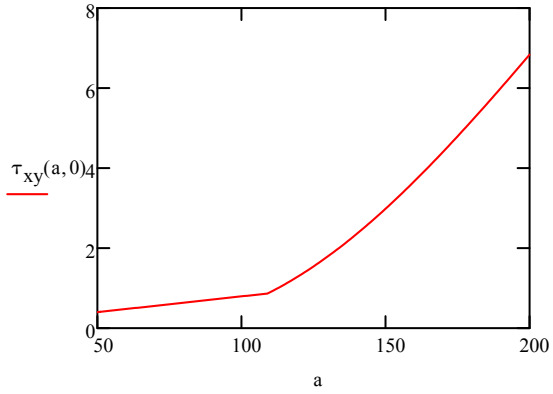

$$\frac{\frac{G_a\cdot\left(h-C_{eff}(a)-\frac{h_f}{2}\right)}{t_a\cdot E_c\cdot I_c(a)}}{\sqrt{\frac{G_a\cdot(2.n\cdot h_f)}{t_a}\cdot\left[\frac{1}{E_f\cdot A_f}+\frac{\left(h-C_{eff}(a)-\frac{h_f}{2}\right)\cdot\left(h-C_{eff}(a)-\frac{h_f}{2}\right)}{E_c\cdot I_c(a)}\right]}}\cdot P\cdot a \ldots$$

$$+\frac{G_a}{t_a\cdot\lambda 1(a)^2}\cdot\frac{h-C_{eff}(a)-\frac{h_f}{2}}{E_c\cdot I_c(a)+E_f\cdot I_f}\cdot P$$

$$TT(a) := \frac{\frac{G_a\cdot y(a)}{t_a\cdot E_c\cdot I_c(a)}}{\sqrt{\frac{G_a\cdot(2.n\cdot h_f)}{t_a}\cdot\left(\frac{1}{E_f\cdot A_f}+\frac{y(a)^2}{E_c\cdot I_c(a)}\right)}}\cdot P\cdot a+\frac{G_a}{t_a\cdot\lambda 1(a)^2}\cdot\frac{y(a)}{E_c\cdot I_c(a)+E_f\cdot I_f}\cdot P$$

$$\frac{\frac{G_a\cdot y(a)}{t_a\cdot E_c\cdot I_c(a)}}{\sqrt{\frac{G_a\cdot(2.n\cdot h_f)}{t_a}\cdot\left(\frac{1}{E_f\cdot A_f}+\frac{y(a)^2}{E_c\cdot I_c(a)}\right)}}\cdot P\cdot a+\frac{G_a}{t_a\cdot\lambda 1(a)^2}\cdot\frac{y(a)}{E_c\cdot I_c(a)}\cdot P$$

SIMPLIFICATION (VH SOLUTION)

$$Tsim1(a) := \left[\frac{a}{\sqrt{\frac{G_a\cdot(2.\cdot n\cdot h_f\cdot t_f)}{t_a\cdot t_f}\cdot\left(\frac{1}{E_f\cdot A_f}\right)}}+\frac{1}{\frac{G_a\cdot(2.\cdot n\cdot h_f\cdot t_f)}{t_a\cdot t_f}\cdot\left(\frac{1}{E_f\cdot A_f}\right)}\right]\cdot\frac{P\cdot G_a\cdot y(a)}{t_a\cdot E_c\cdot I_c(a)}$$

$$Tsim2(a) := \frac{P\cdot y(a)}{E_c\cdot I_c(a)}\cdot\left(a\sqrt{\frac{G_a\cdot E_f\cdot t_f}{2\cdot t_a}}+\frac{E_f\cdot t_f}{2}\right)$$

$$X(a) := \frac{a}{\sqrt{\frac{G_a\cdot(2.\cdot n\cdot h_f\cdot t_f)}{t_a\cdot t_f}\cdot\left(\frac{1}{E_f\cdot A_f}+\frac{y(a)^2}{E_c\cdot I_c(a)}\right)}}+\frac{1}{\frac{G_a\cdot(2.\cdot n\cdot h_f\cdot t_f)}{t_a\cdot t_f}\cdot\left(\frac{1}{E_f\cdot A_f}+\frac{y(a)^2}{E_c\cdot I_c(a)}\right)}$$

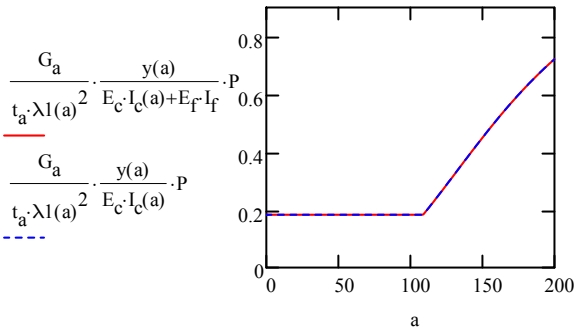

$$X\_a(a) := \frac{a}{\sqrt{\frac{G_a\cdot(2.\cdot n\cdot h_f\cdot t_f)}{t_a\cdot t_f}\cdot\left(\frac{1}{E_f\cdot A_f}\right)}}+\frac{1}{\frac{G_a\cdot(2.\cdot n\cdot h_f\cdot t_f)}{t_a\cdot t_f}\cdot\left(\frac{1}{E_f\cdot A_f}\right)}$$

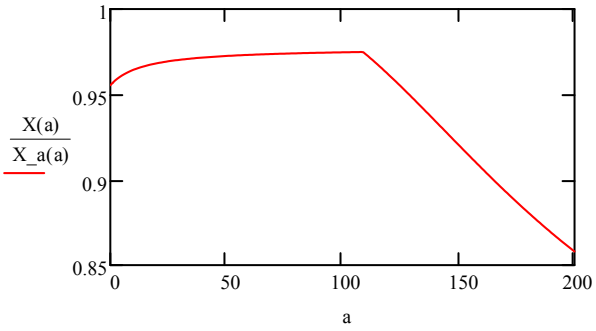

EXPANSION OF RIZKALLA SOLUTION

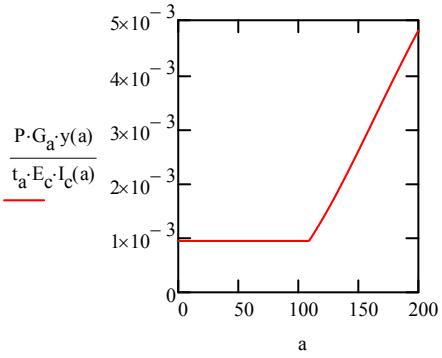

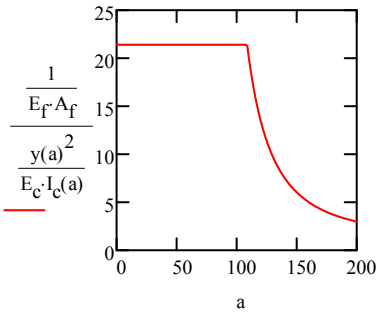

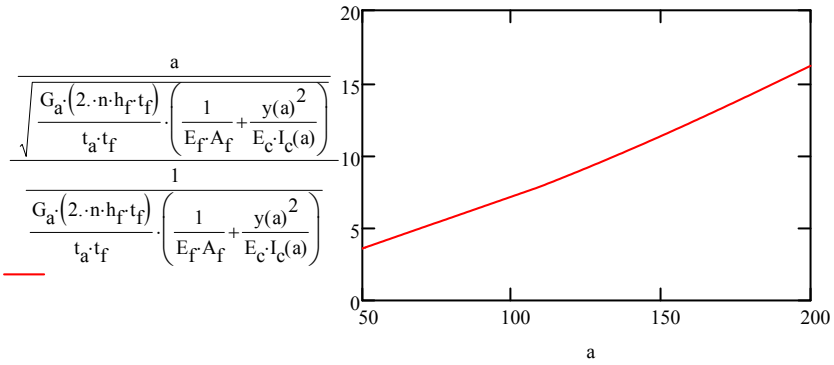

$$A1(a) := \frac{\frac{G_a \cdot y(a)}{t_a \cdot E_c \cdot I_c(a)}}{\sqrt{\frac{G_a \cdot (2. \cdot n \cdot h_f)}{t_a} \cdot \left(\frac{1}{E_f \cdot A_f} + \frac{y(a)^2}{E_c \cdot I_c(a)} \right)}} \cdot P \cdot a$$

$$A2(a) := \frac{G_a}{t_a \cdot \lambda 1(a)^2} \cdot \frac{y(a)}{E_c \cdot I_c(a) + E_f \cdot I_f} \cdot P$$

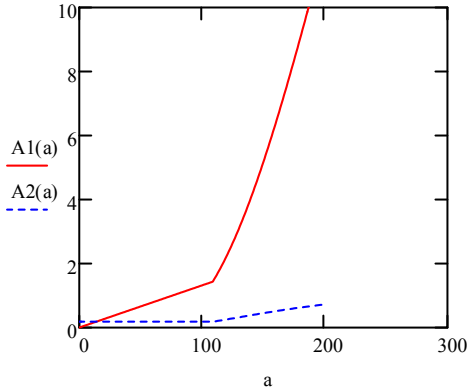

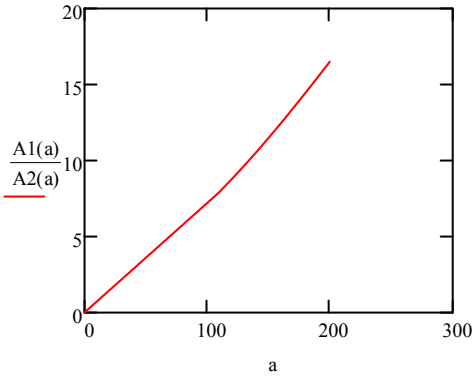

$$\left[\frac{1}{\sqrt{\frac{G_a\cdot\left(2.n\cdot h_f\cdot t_f\right)}{t_a\cdot t_f}\cdot\left(\frac{1}{E_f\cdot A_f}+\frac{y(a)^2}{E_c\cdot I_c(a)}\right)}}\cdot\frac{1}{t_a\cdot E_c\cdot I_c(a)}\right]\cdot P\cdot a\cdot G_a\cdot y(a)$$

$$\tau(a):=\left[\frac{1}{\sqrt{\frac{2G_a}{t_a\cdot t_f}\cdot\left[\frac{1}{E_f}+\frac{y(a)^2\cdot\left(n\cdot h_f\cdot t_f\right)}{E_c\cdot I_c(a)}\right]}}\cdot\frac{1}{t_a\cdot E_c\cdot I_c(a)}\right]\cdot P\cdot a\cdot G_a\cdot y(a)$$

$$\tau\tau 2(a):=\frac{P\cdot y(a)}{E_c\cdot I_c(a)}\cdot\left(a\cdot\sqrt{\frac{E_f\cdot t_f\cdot G_a}{2t_a}}+\frac{E_f\cdot t_f}{2}\right)$$

$$TTT(a):=\sqrt{TT(a)^2+\tau_{xy}(a,0)^2}$$

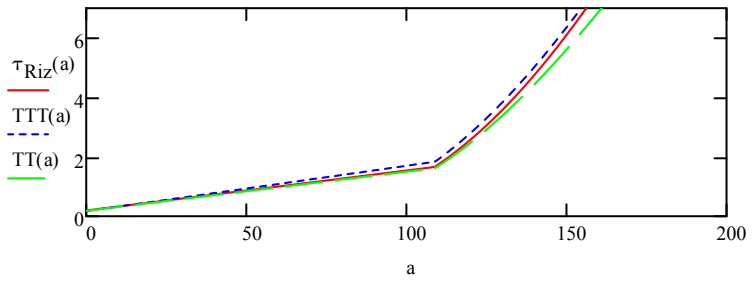

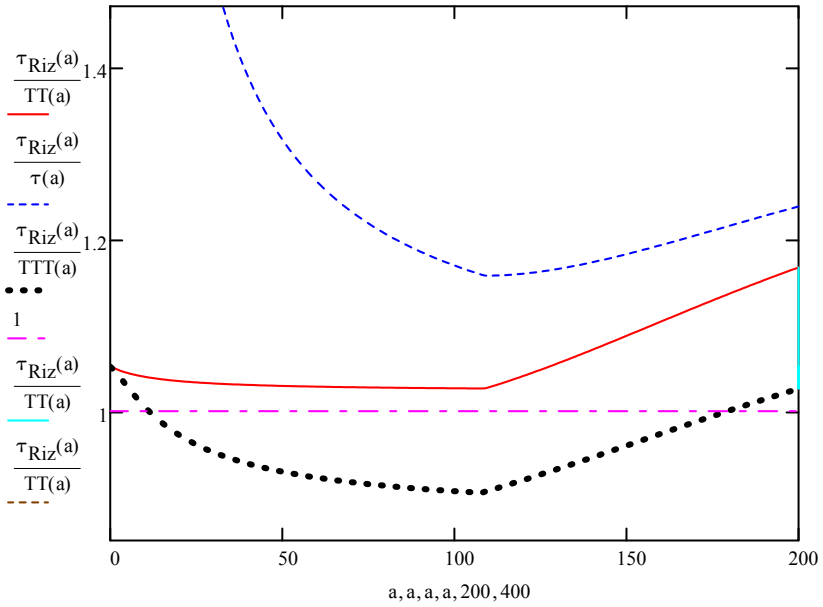

$$A(a):=E_c\cdot I_c(a)\qquad B:=E_f\cdot t_f\qquad \tau_{max}:=5\qquad C:=\frac{G_a}{t_a}$$

$$P(a):=\frac{\tau_{max}\cdot A(a)}{\frac{a}{2}\cdot\sqrt{B\cdot C}+\frac{B}{2}}\cdot\frac{1}{y(a)}$$

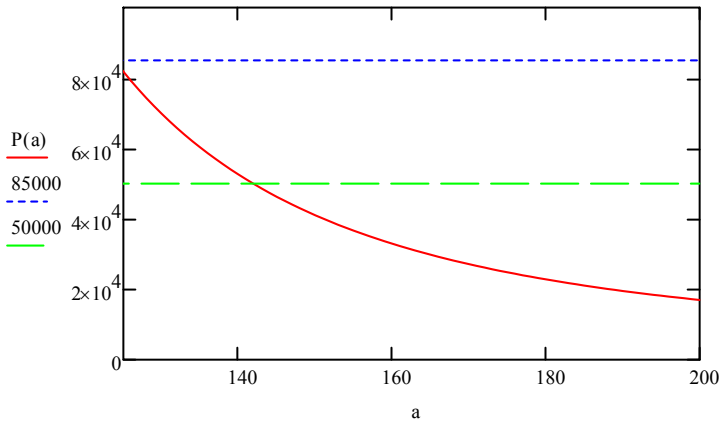

NUMERICAL ANALYSIS

GEOMETRY

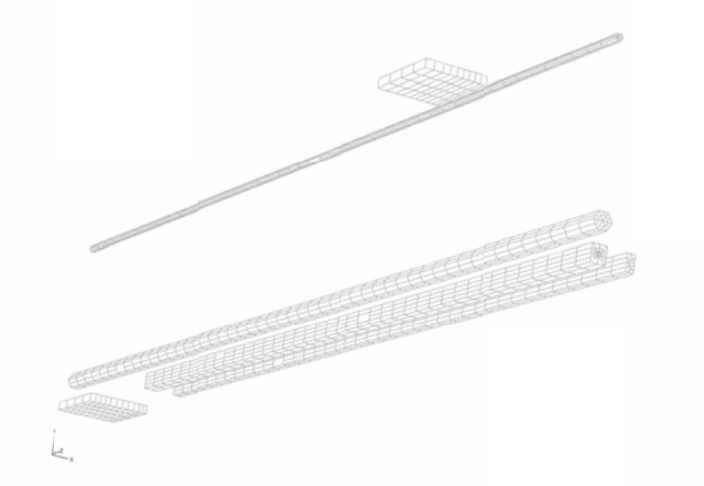

Figure A.4-1.Different parts of beam retrofitted with NSMR

ASSEMBLY

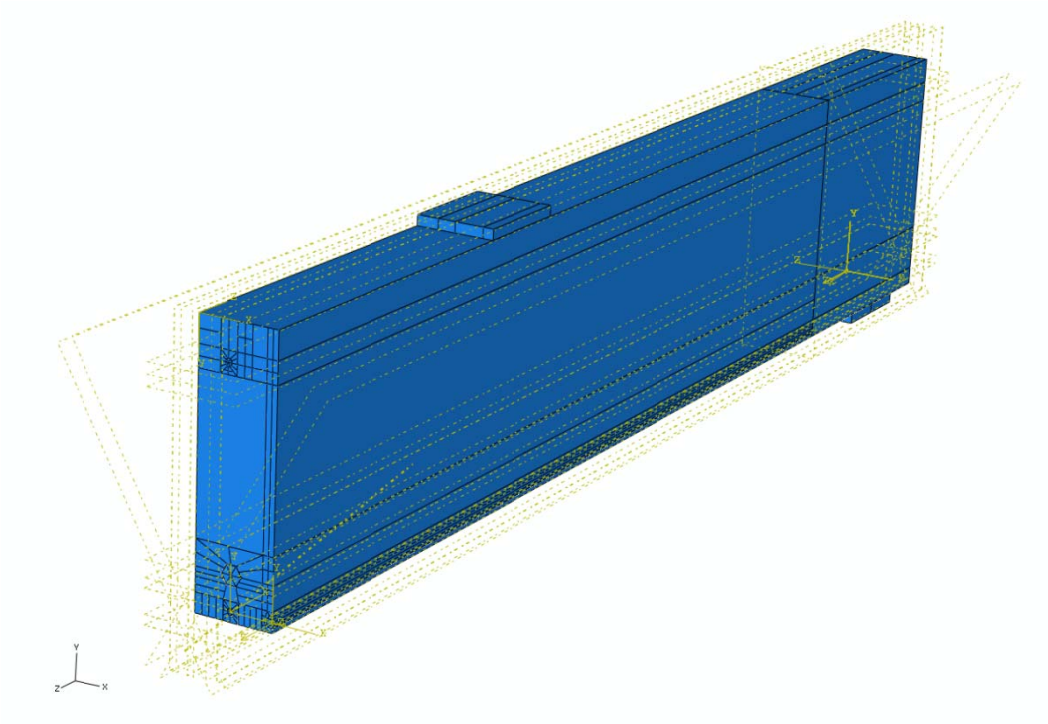

Figure A.4 – 2. Assembly of various parts in the retrofitted beam

MESH

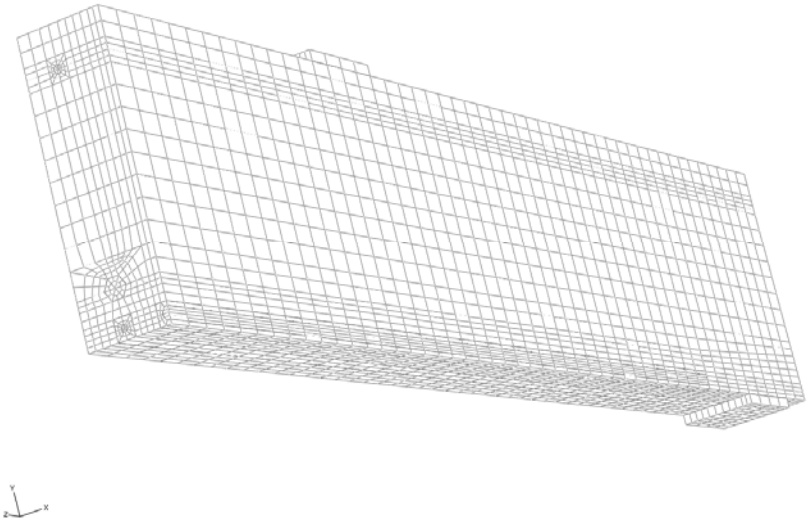

Figure A.4 –3. Mesh of the retrofitted beam.

RESULTS

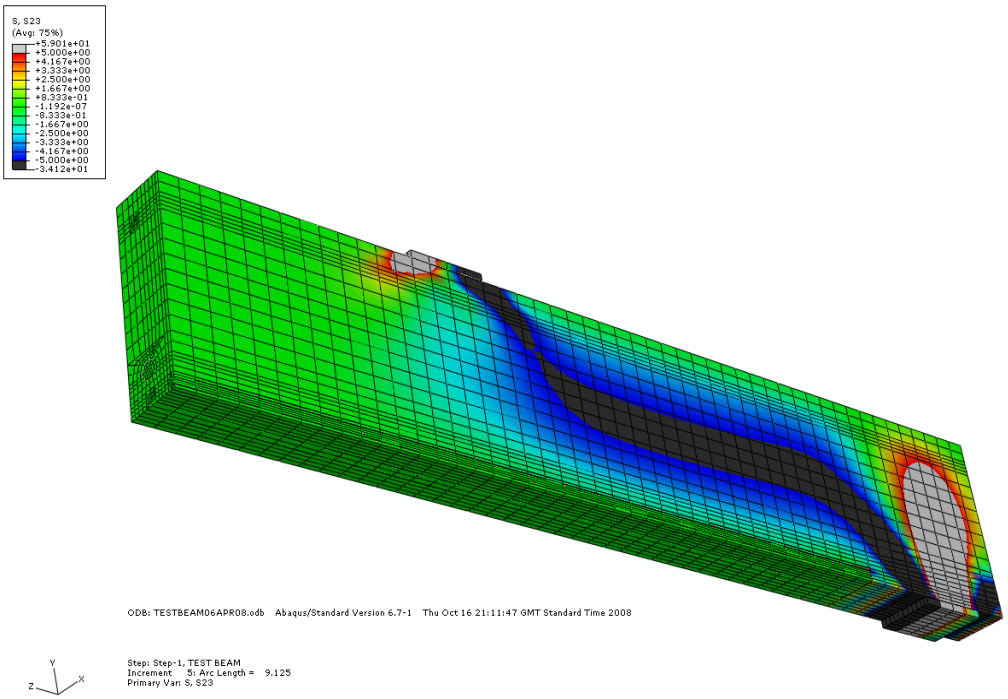

Figure A.4 –4. Shear stress along the retrofitted beam

VON-MISES STRESS

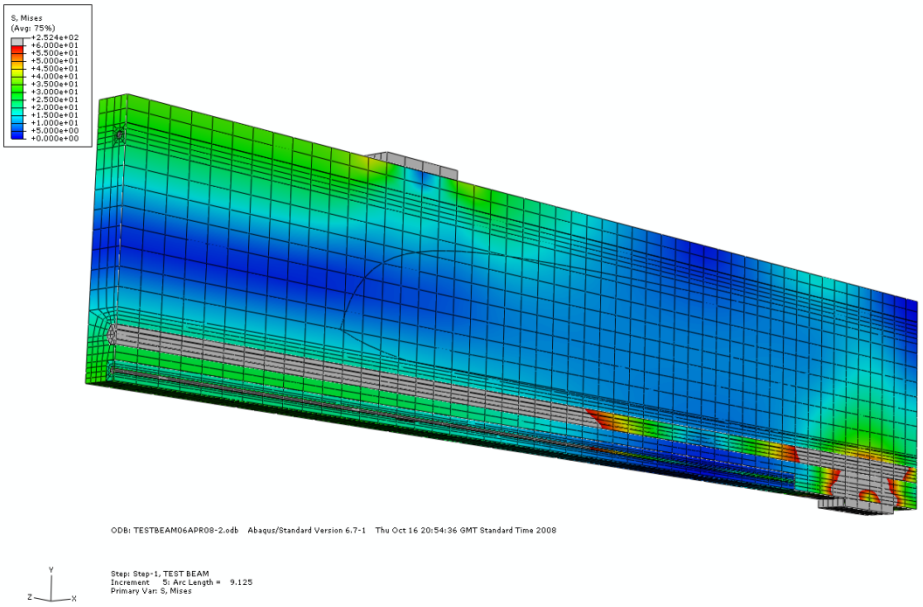

Figure A.4 –5. Von Mises stress along the retrofitted beam

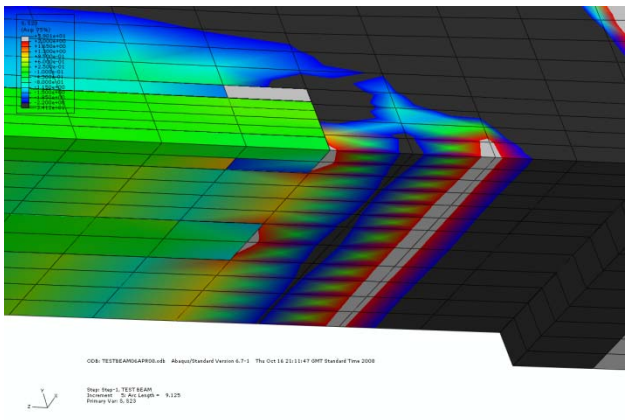

Figure A.4 –5. Stress concentration around the termination point

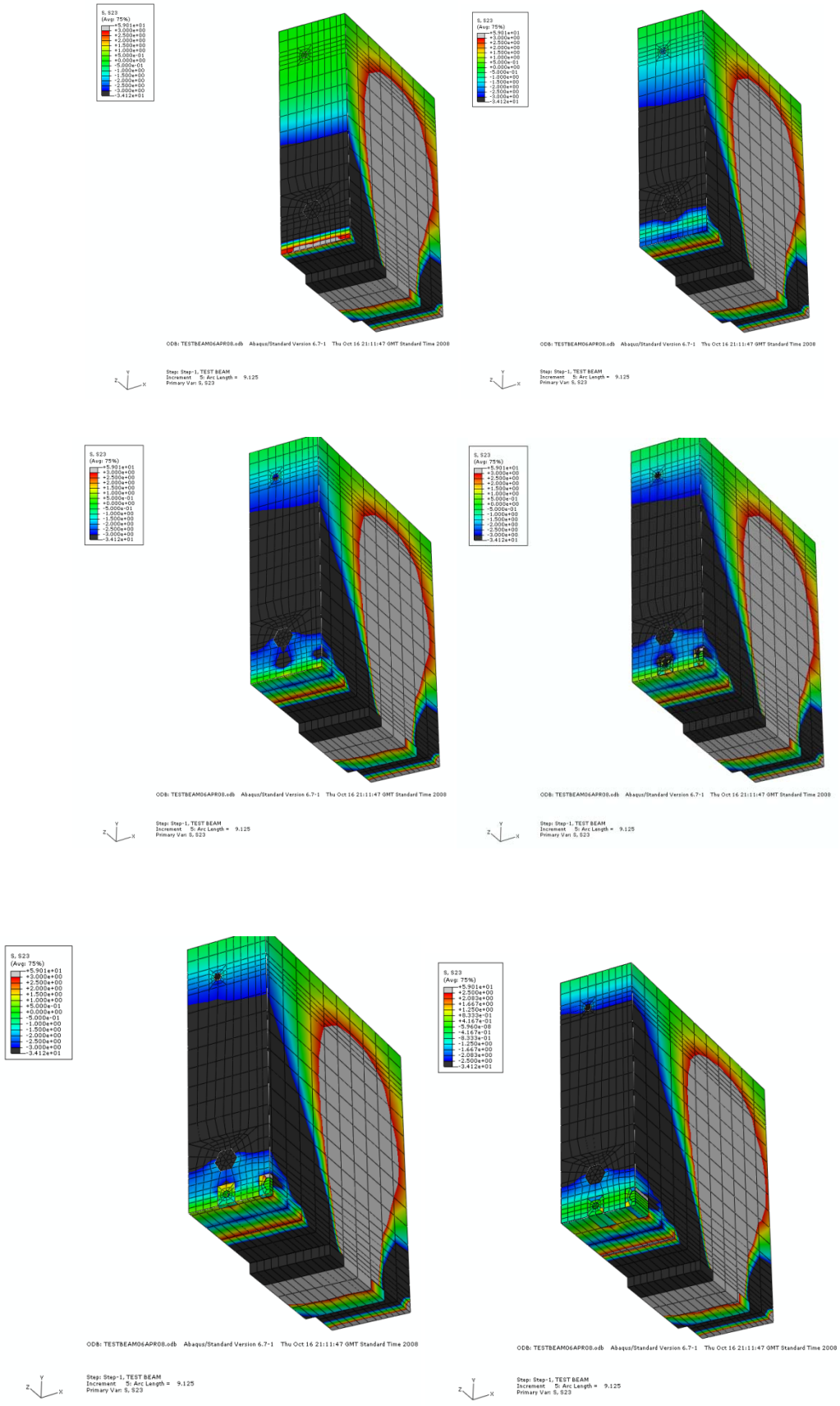

Figure A.4 –6. Shear stress in various cross sections along the beam

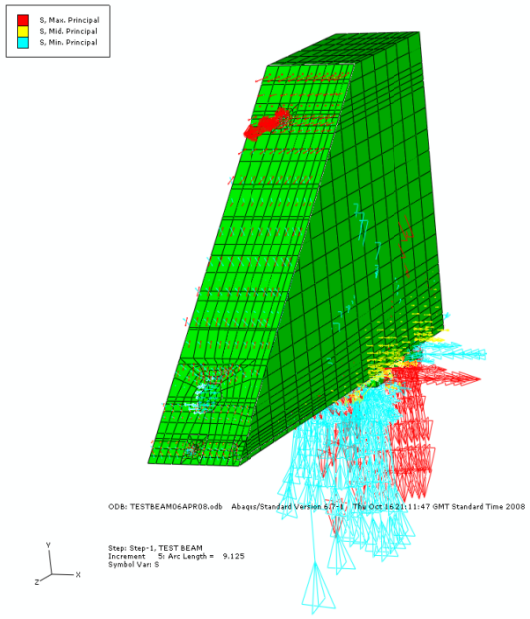

Figure A.4 –7. Principle stresses in cross section near the COP.

MODELLING FOR PULL OUT TEST

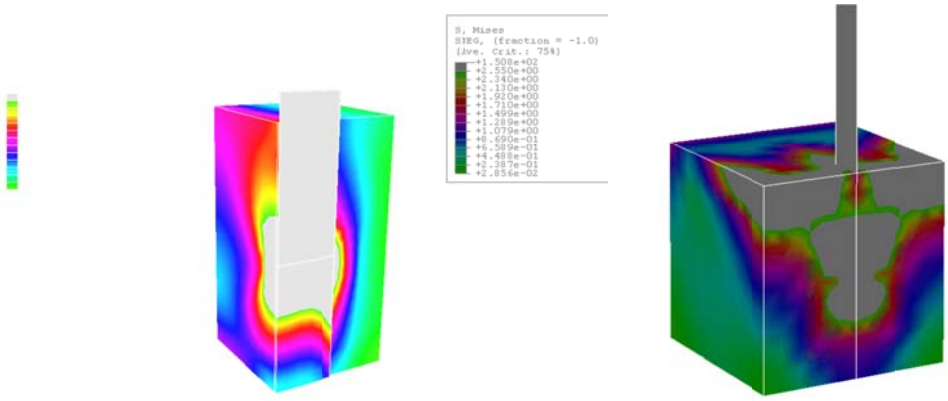

Figure A.4 –7. Stress distribution in the pull-out specimen with NSMR.

APPENDIX B – EXPERIMENTAL WORK

B.1 MATERIAL TESTS

B.1.1 CONCRETE

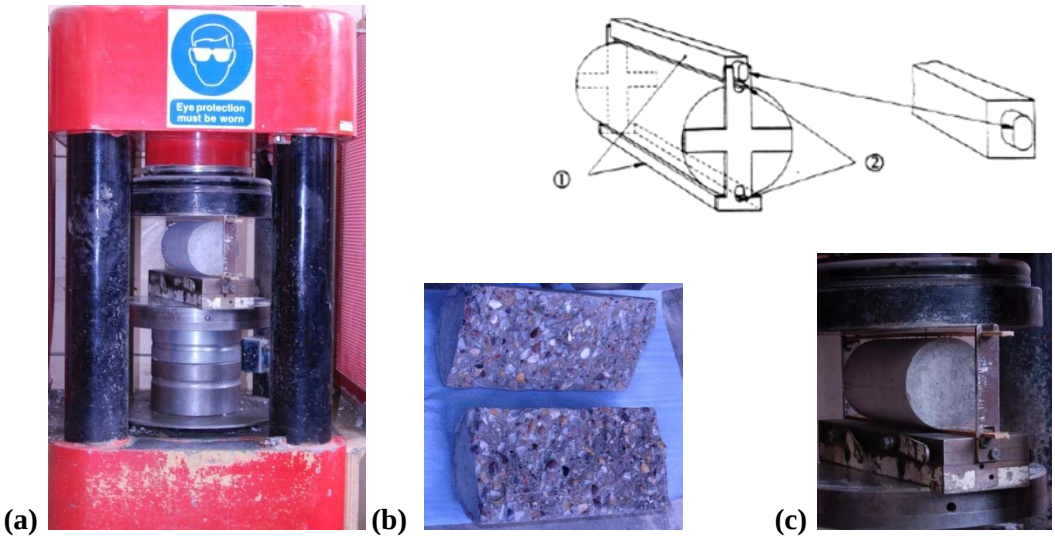

Fig. B - 1: Splitting tension test setup (a), (b), (c) and failure of specimen

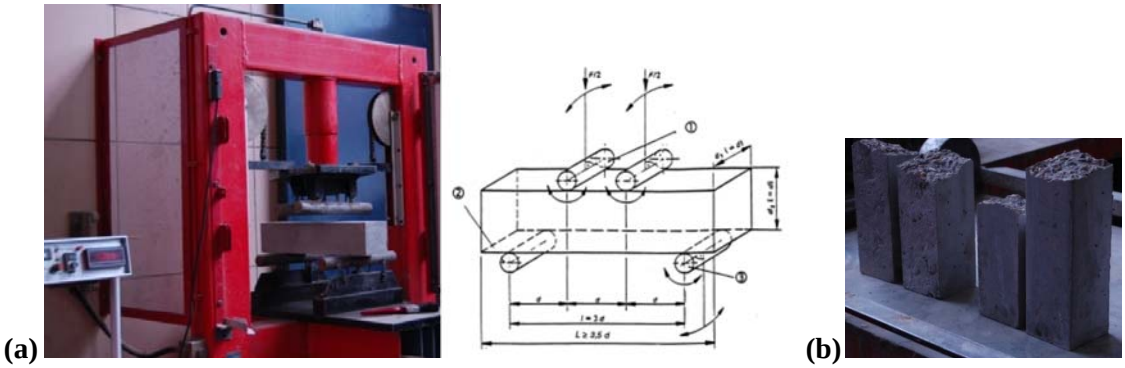

Fig. B - 2: Flexural tension test (a) test setup and (b) failure of specimens

B.1.2 FRP

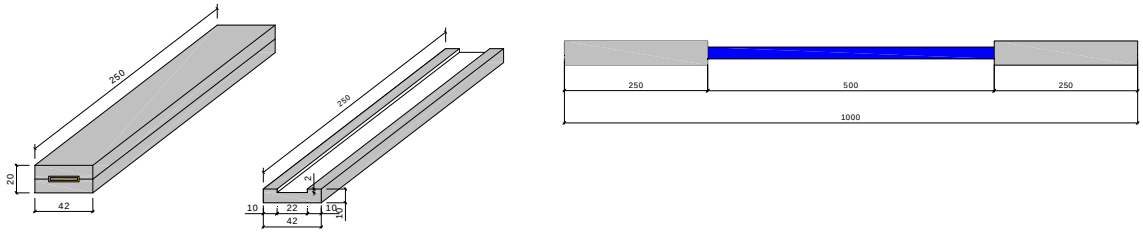

Fig. B - 3: Design of anchorage at the end of FRP specimens to avoid splitting of FRP

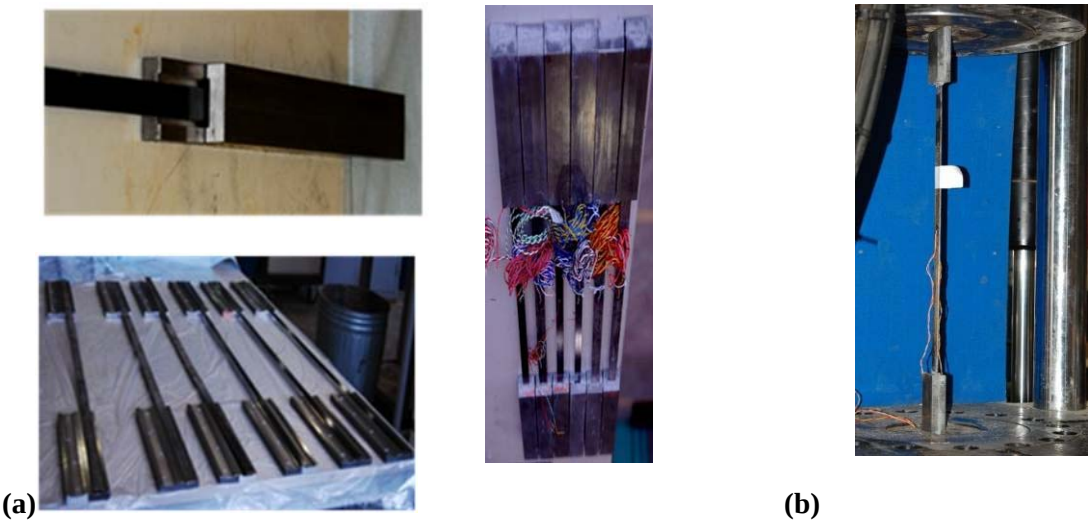

(a) **(b)**

Fig. B - 4: Preparation of tensile tests and FRPs (a) specimen preparation (b) test set up

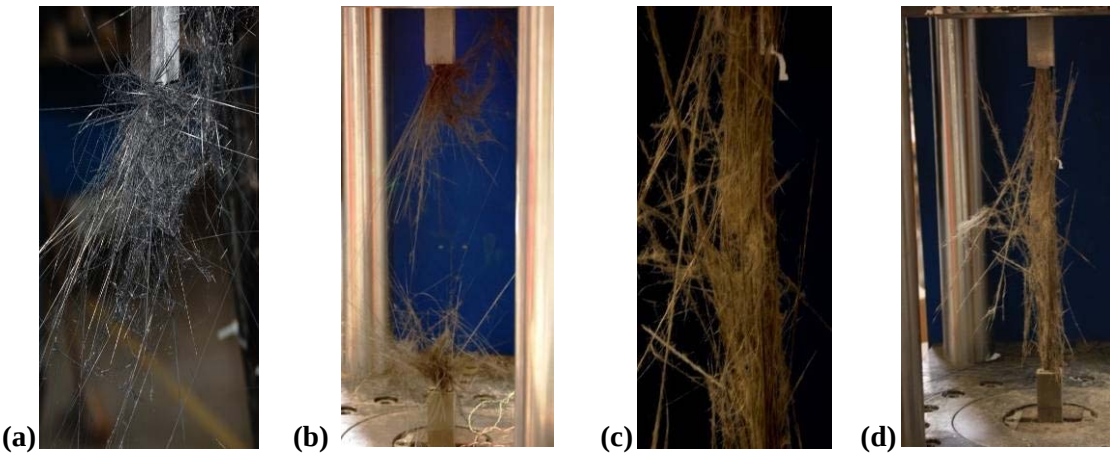

(a) **(b)** **(c)** **(d)**

Fig. B - 5: Failure of (a), (c) BFRP (b), (d) CFRP

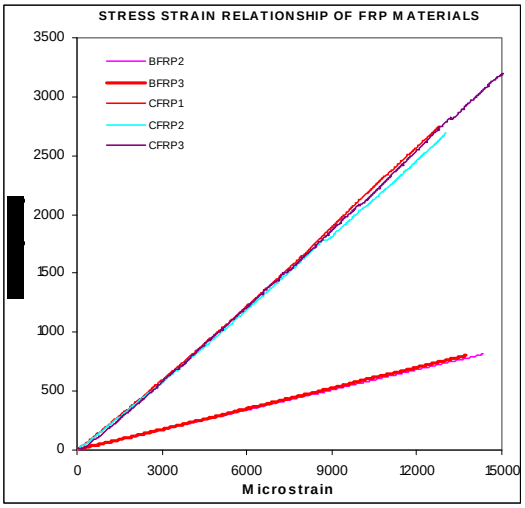

Fig. B - 6: Stress strain relationship of FRP materials

B.1.3 ENFORCE EP STRUCTURAL ADHESIVE

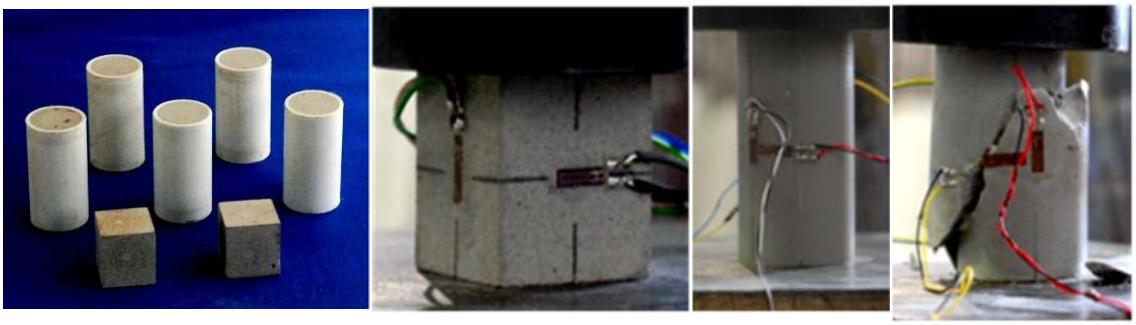

(a) **(b)** **(c)** **(d)**

Fig. B - 7: Adhesive specimens (a) specimen preparation (b),(c) instrumentation (d) failure

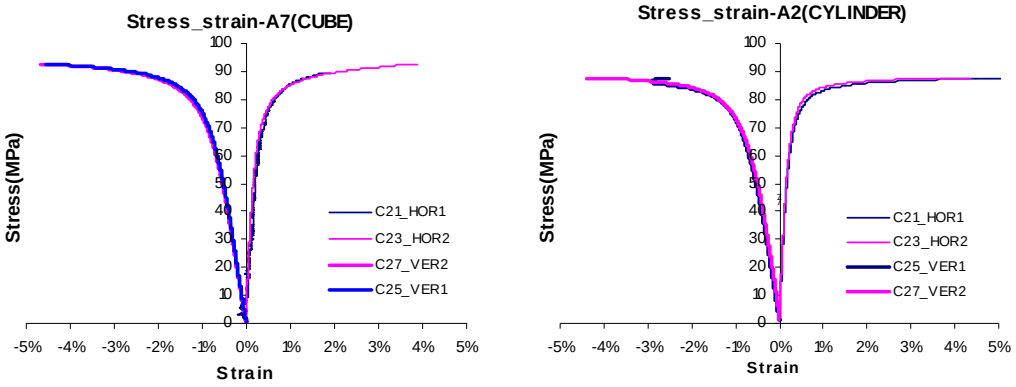

(a) **(b)**

Fig. B - 8: (a) Cubes specimens, (b) Cylinder specimens

B.1.4 STEEL REINFORCEMENT BAR

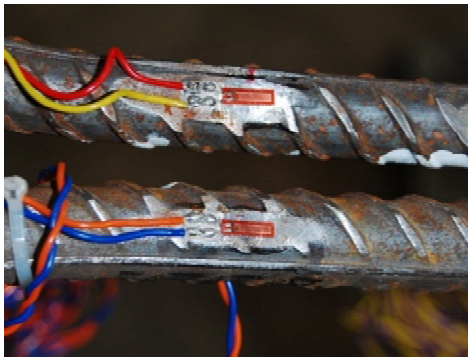

Fig. B - 9: Strain gauge attached on steel reinforcement

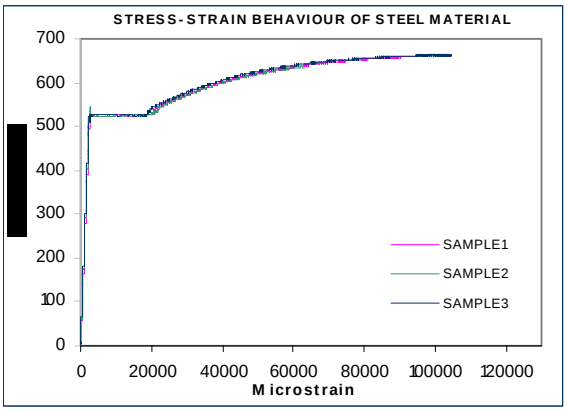

Fig. B - 10: Stress-strain relationship of steel speciments

B.1.5 INSTRUMENTATIONS

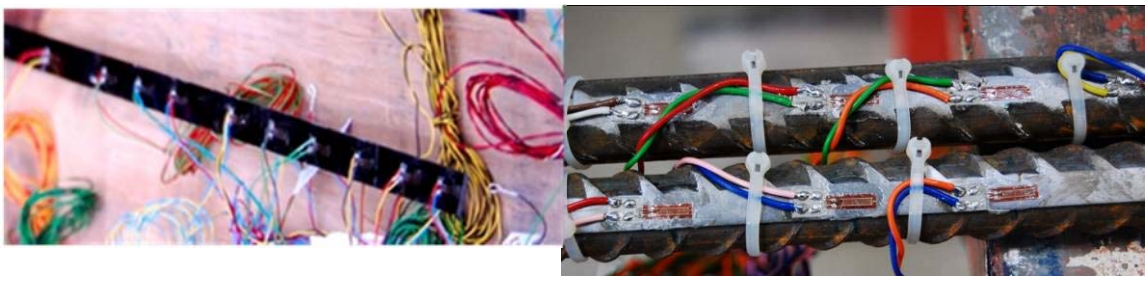

(a)

(b)

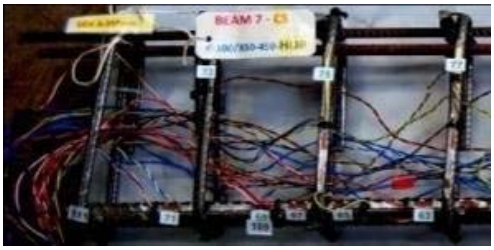

(c)

Fig. B - 11: Strain gauge bonded on FRP strips and steel reinforcement, (a) FRP, (b) Flexural steel bar, (c) Shear link

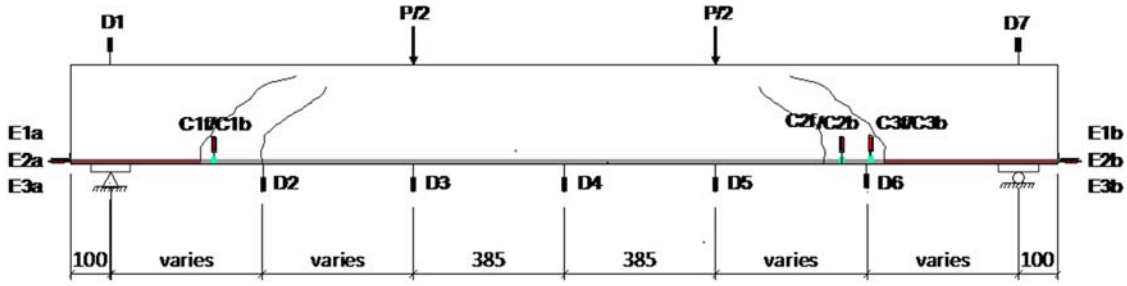

Fig. B - 12: Arrangement of LVDTs along the span

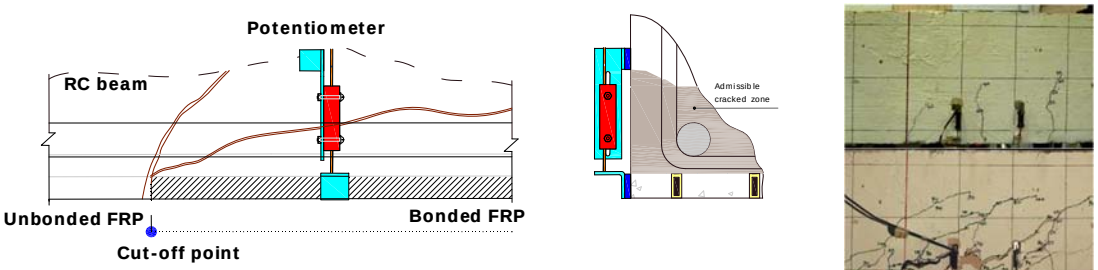

(a) **(b)**

Fig. B - 13: Details of (a) set up of LVDT group C, (b) LVDTs group C before and after debonding failure of the tested beam

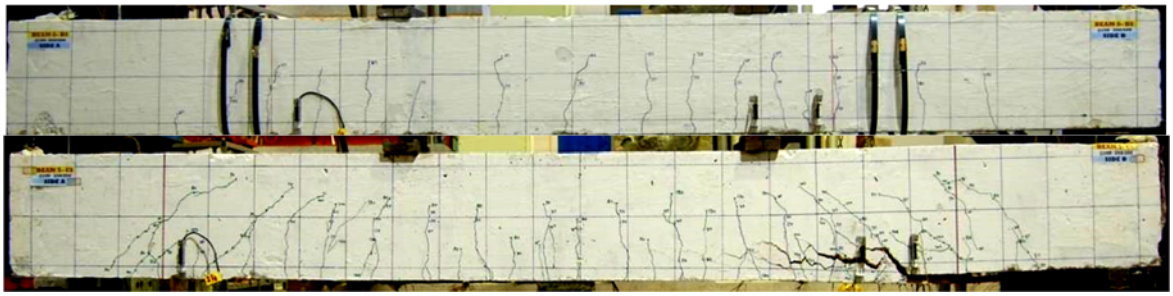

Fig. B - 14: Details of set up of LVDTs in the vicinity of the COPs

Fig. B - 15: Details of set up of LVDTs at the LVDT group C

B.2 BEAM FABRICATION

(a) **(b)**

Fig. B - 16: Steel cage preparation (a) preparation (b) before concrete casting

Fig. B - 17: Concrete casting and curing

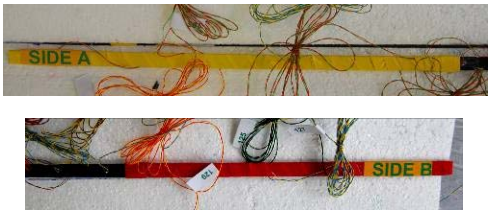

Fig. B - 18: Strain gauges bonded on strips before strengthening

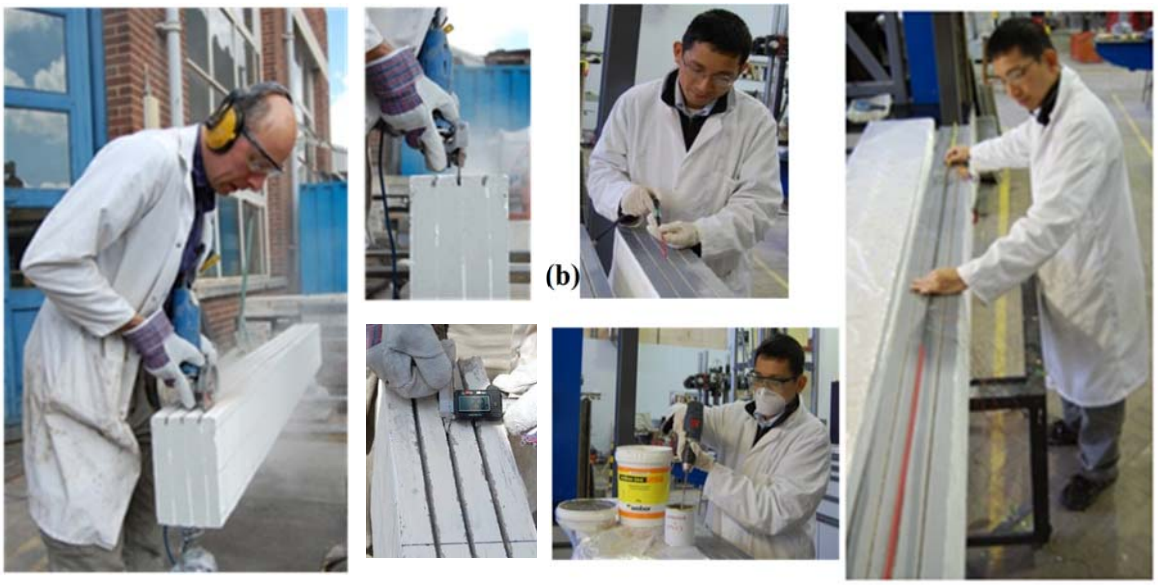

(a) **(c)** **(d)**

Fig. B - 19: NSMR preparation (a) Cutting groove, (b) Cleaning grooves using high compressed air, (c) Mixing structural adhesive and half fill into grooves, (d) Placing FRP into groove and fully fill adhesive

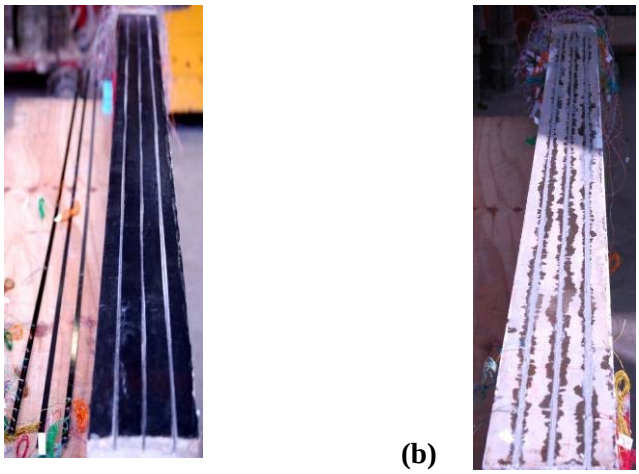

(a) **(b)**

Fig. B - 20: Restoration of partly failed beam for future testing, beams (a) before and (b) after strengthening

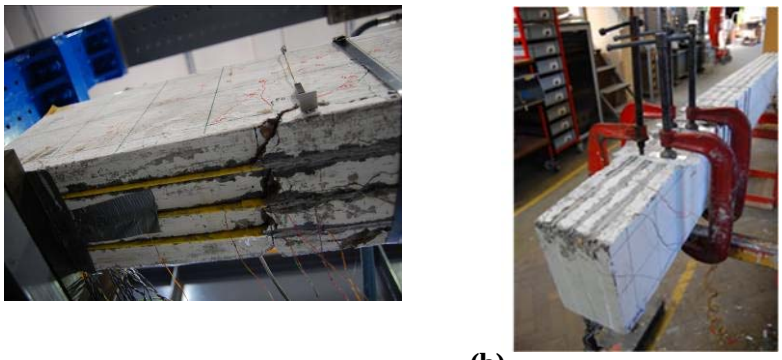

(a) **(b)**

Fig. B - 21: Repair and bond the damaged side, (a) beam after debonding, (b) fixing debonding NSMR by clamps and bond NSMR in the non-damaged side

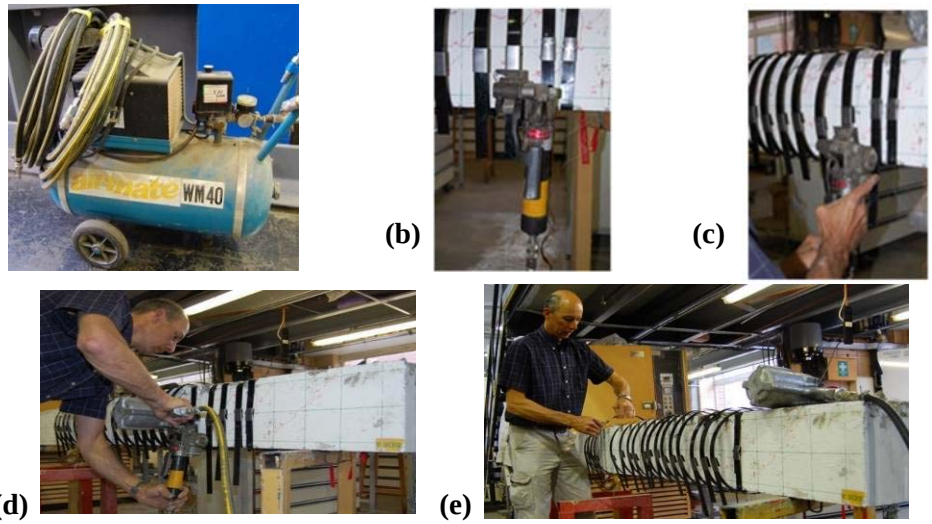

(a) **(b)** **(c)**

(d) **(e)**

Fig. B - 22: Preparation for steel strapping (a) air compressive, (b) pneumatic steel strapping tensioning, (c) strapping

B.3 TESTING PROCEDURES

B.3.1 PRE-CRACK AND RETROFIT NSMR

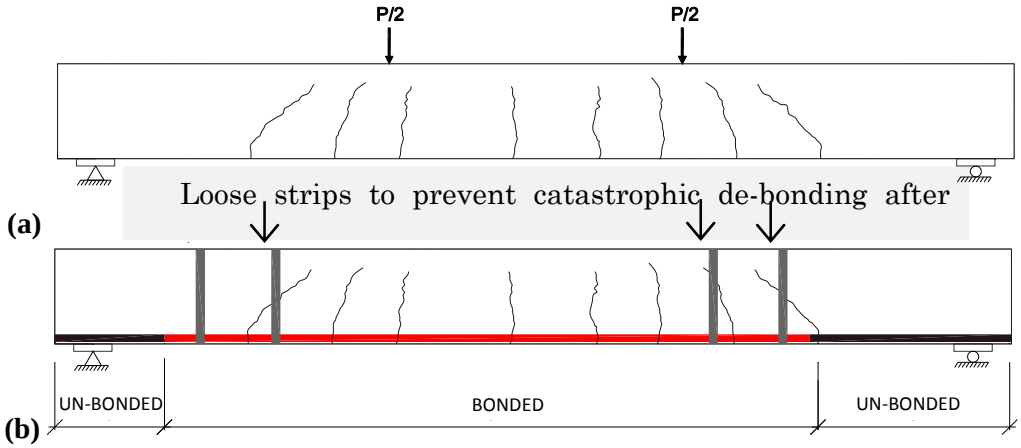

Fig. B - 23: (a) Pre-cracking beam (b) retrofitting NSMR

1.

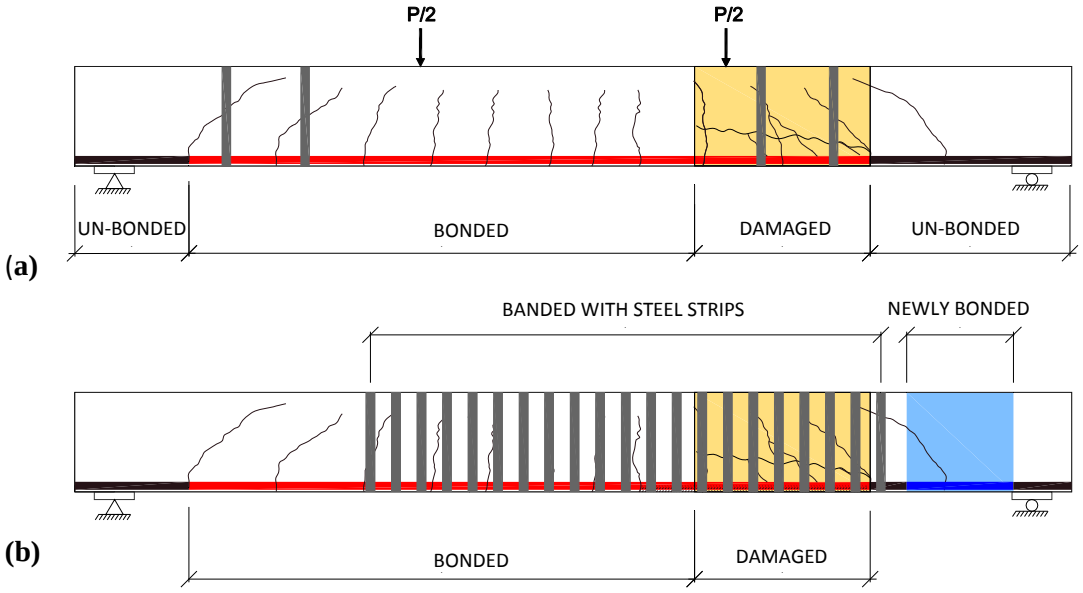

Fig. B - 24: Repair the damaged beam (a) beam after damage, (b) Restore the damaged in region B beam by steel straps in region B and bond FRP to the concrete substrate in section A

2. PHASE 2 OF TESTING-DE-BONDING FAILURE OF SIDE B

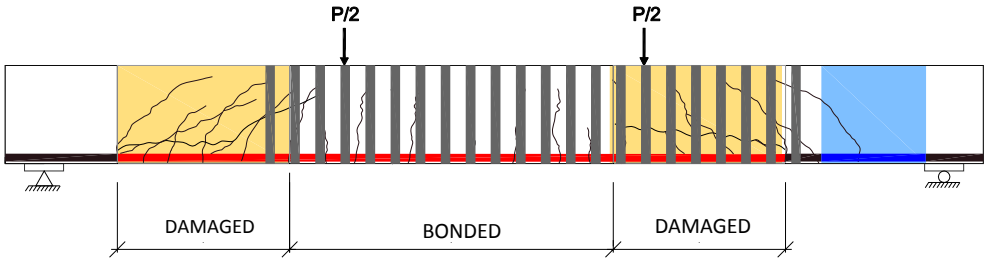

Fig. B - 25: Testing the restored beam debonding on the other side

3. PHASE 3 OF TESTING- FLEXURAL FAILURE

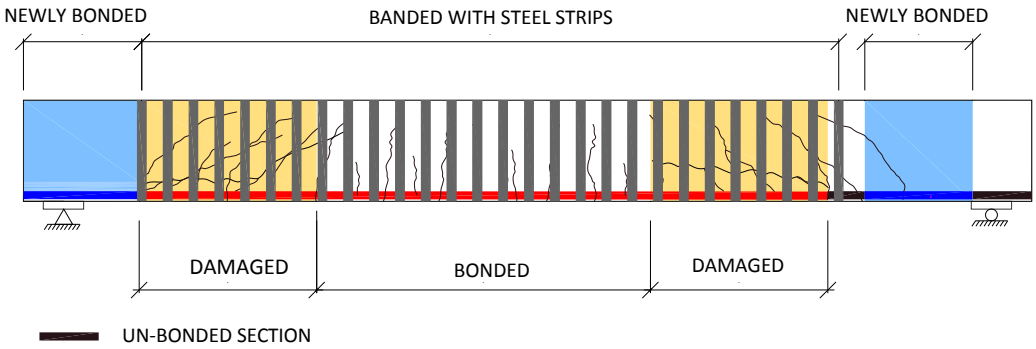

Fig. B - 26: Restoring beams after debonding on both sides by steel straps in zone C and bond FRP in zone B

4.

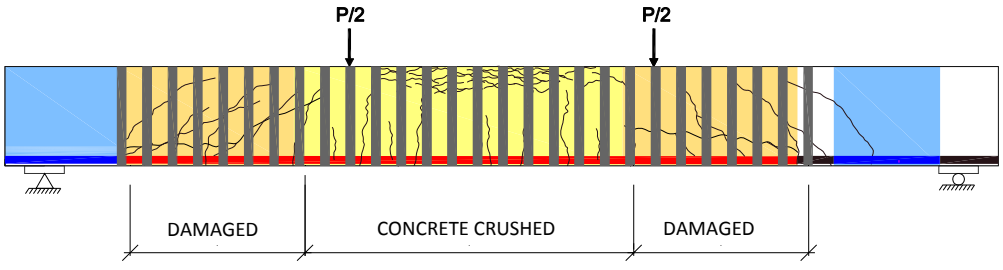

Fig. B - 27: Preparation for the damaged beam and testing for the final phase

(A)

(B)

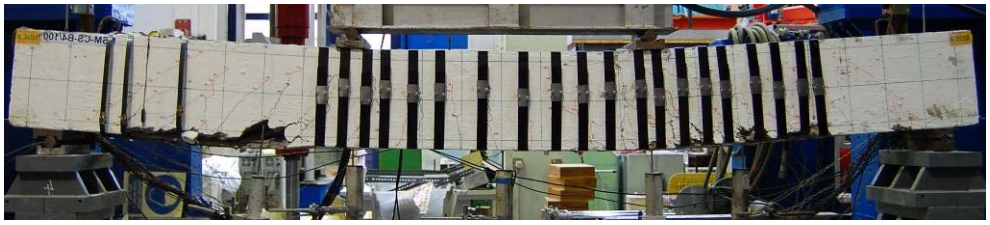

(C)

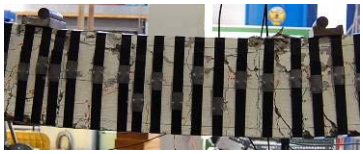

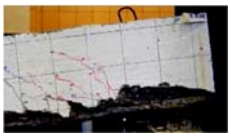

C.1.1 TYPICAL FAILURE OF REFERENCE BEAMS

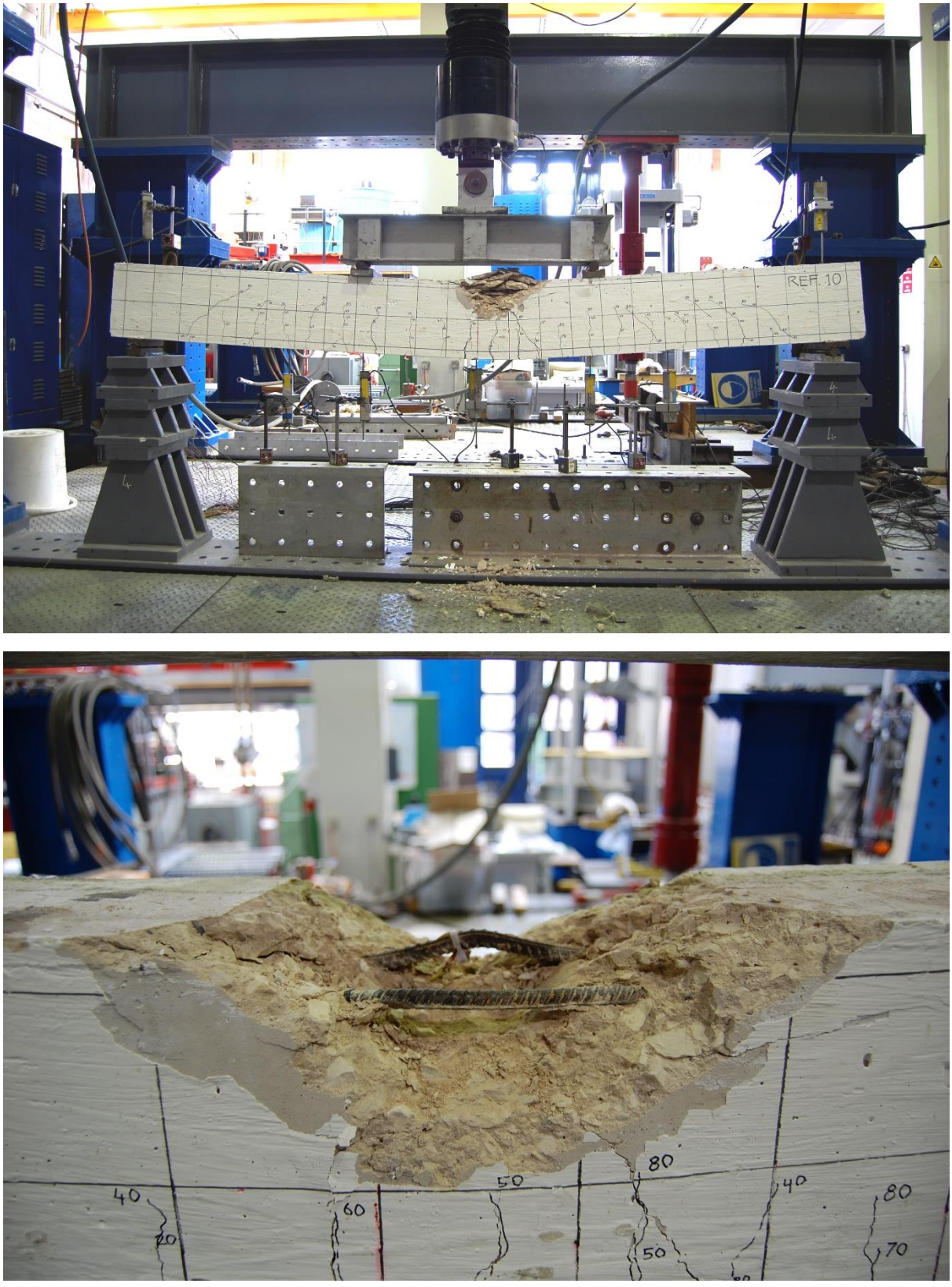

Fig. C1 - 1: Typical failure of reference beams

C.1.2 DEFLECTION GRAPHS FOR BEAM0

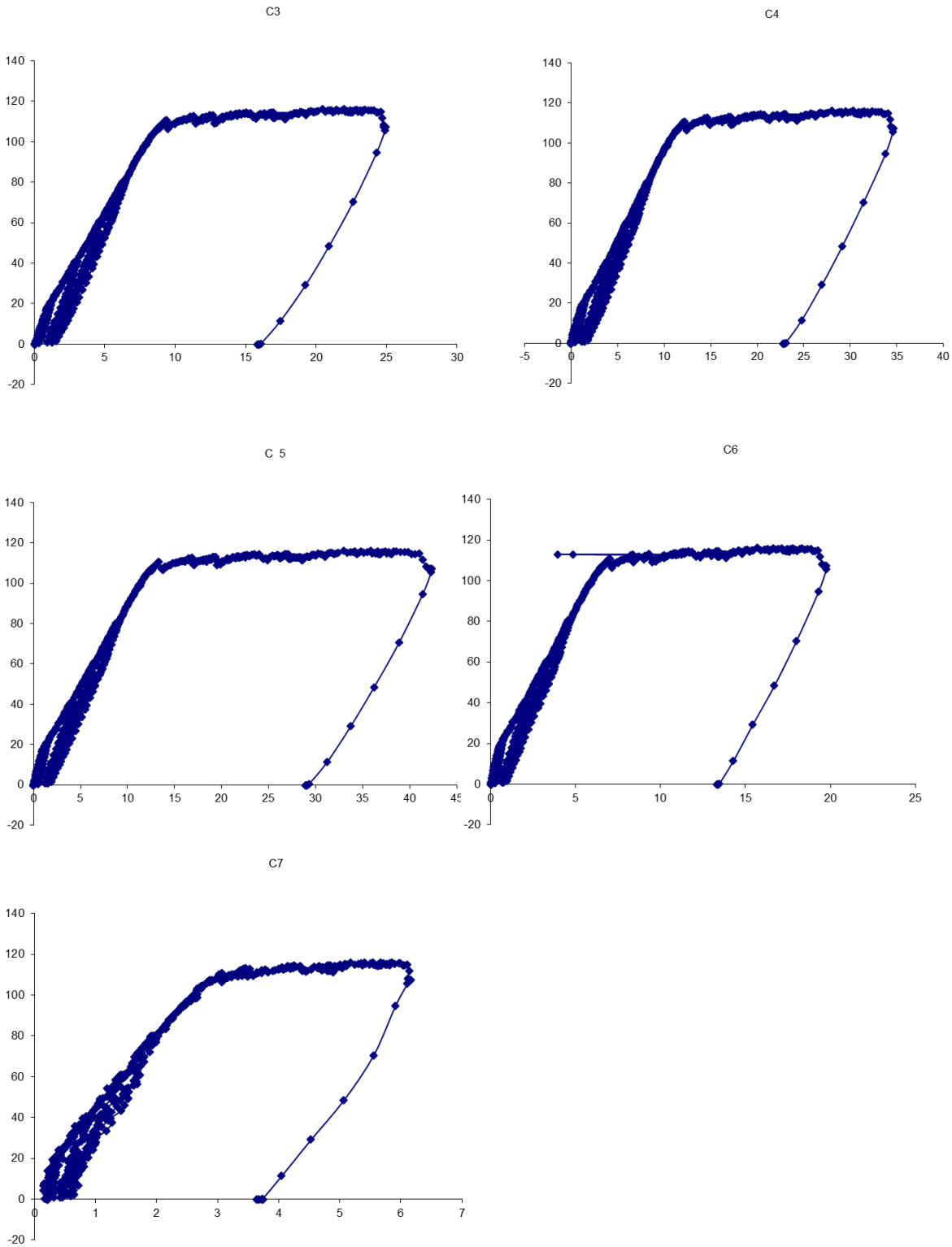

Fig. C1 - 2: Deflection graphs for beam0 (C3-C7)

C.1.3 STRAIN READINGS FOR BEAM0

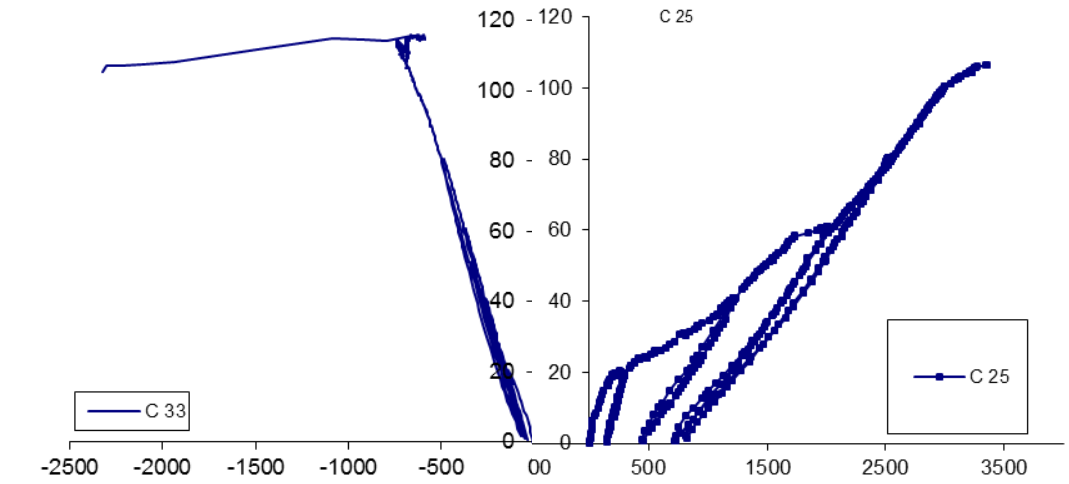

(a)

(b)

Fig. C1 - 3: (a) Strain in the compression steel reinforcement, (b) Strain in the tension steel reinforcement

C.1.4 DEFLECTION GRAPHS FOR BEAM1

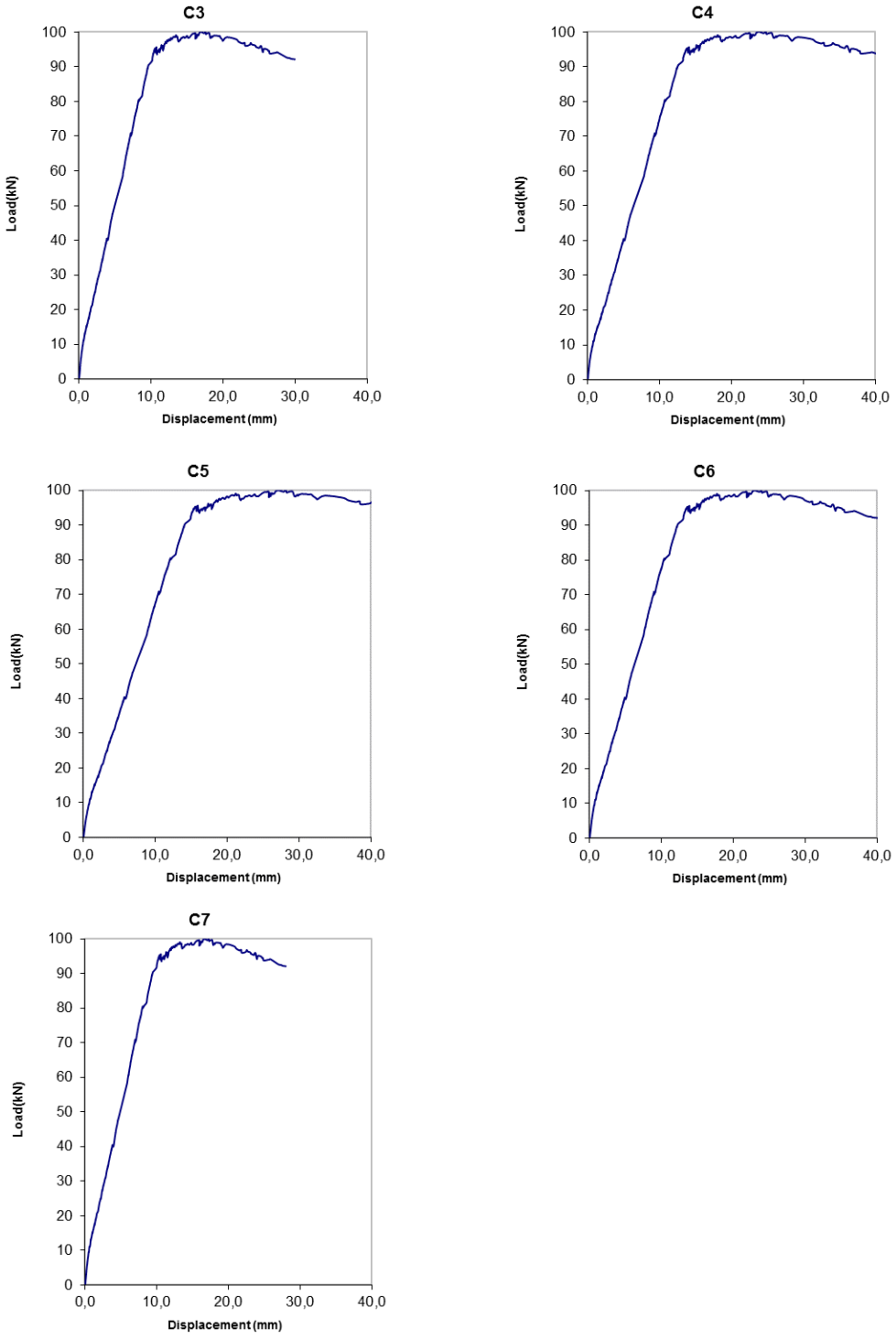

Fig. C1 - 4: Deflection graphs for beam1 (C3-C7)

C.1.5 STRAIN READINGS FOR BEAM1

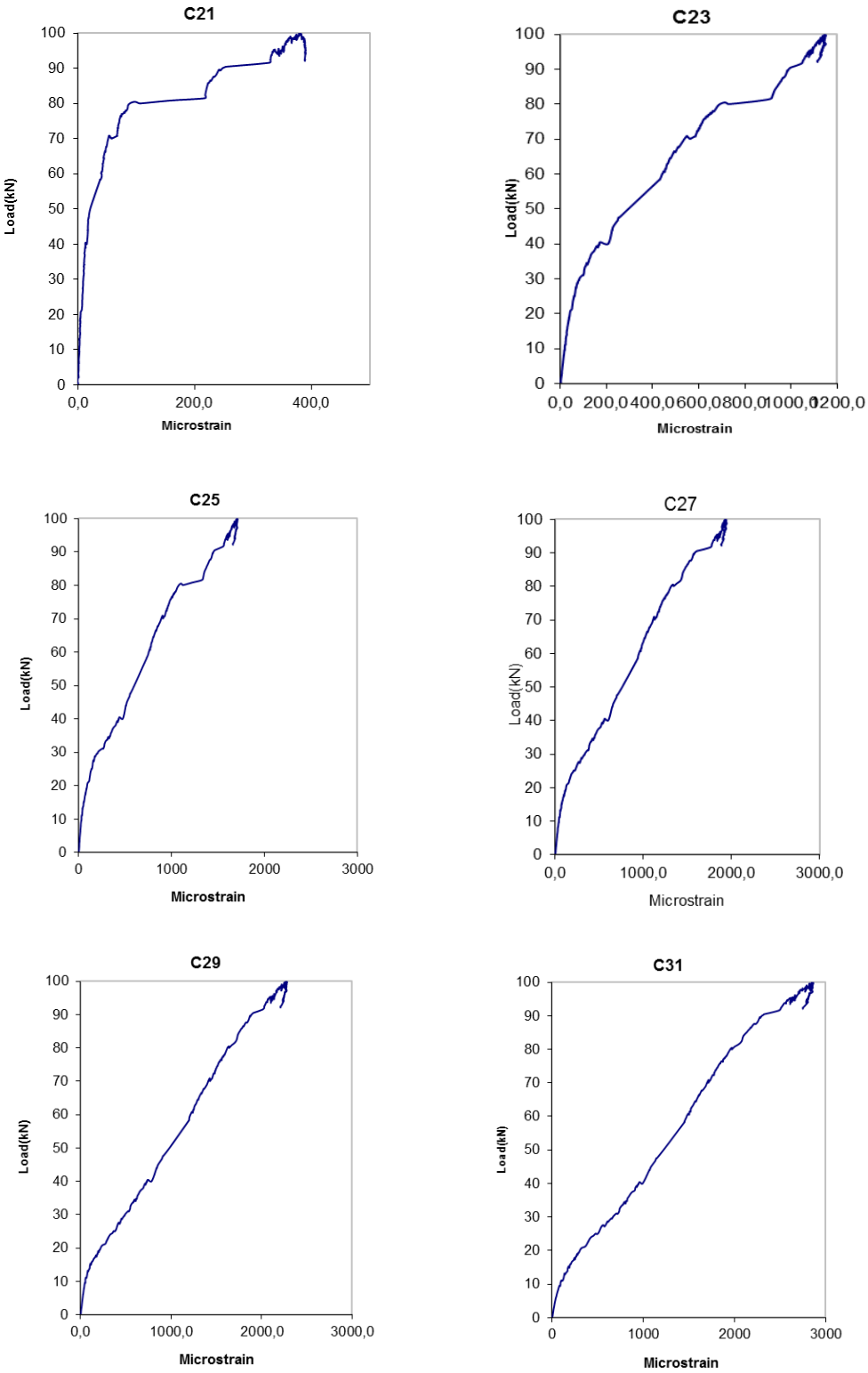

Fig. C1 - 5: Strain in the compression steel reinforcement (C21-C31)

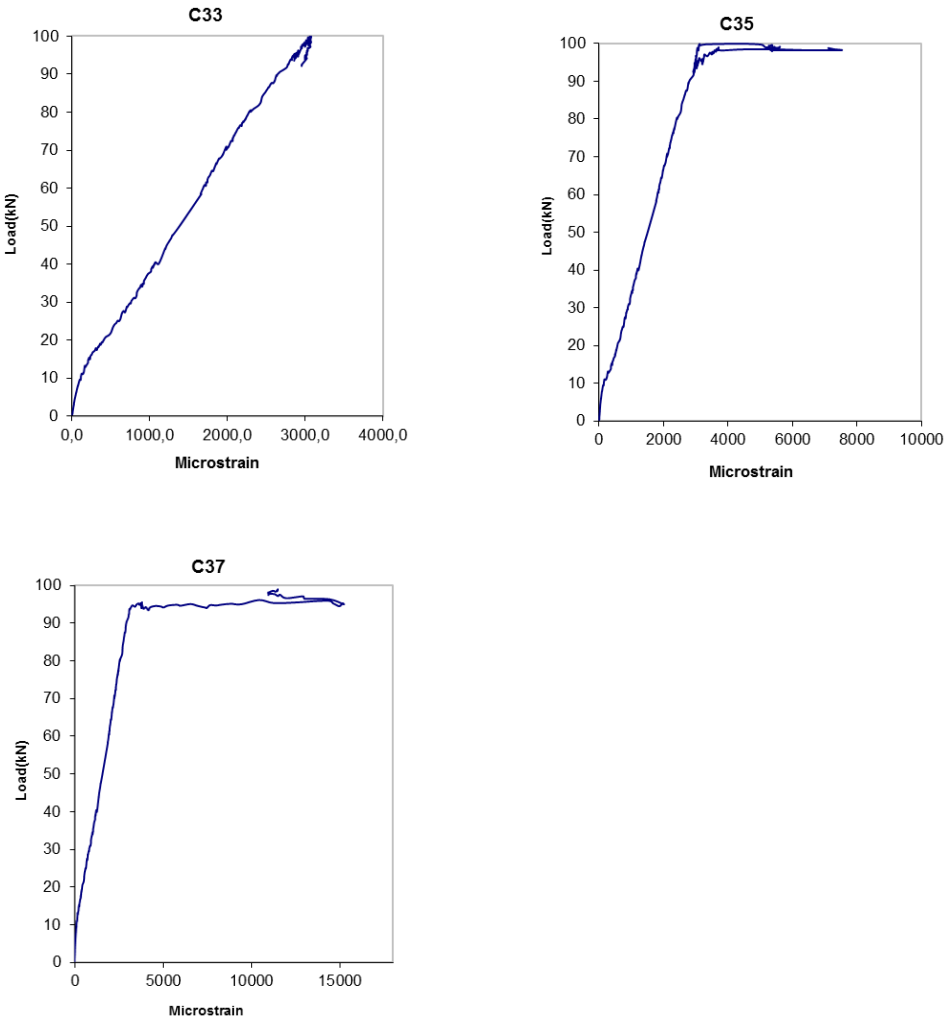

Fig. C1 - 6: Strain in the compression steel reinforcement (C33-C37)

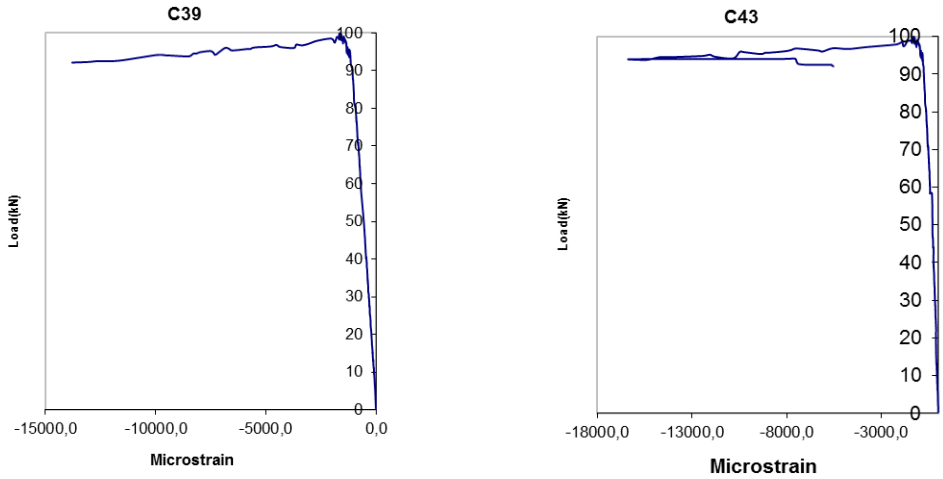

Fig. C1 - 7: Strain in the tension steel reinforcement (C39-C43)

C.2.1 BEAM DESIGN

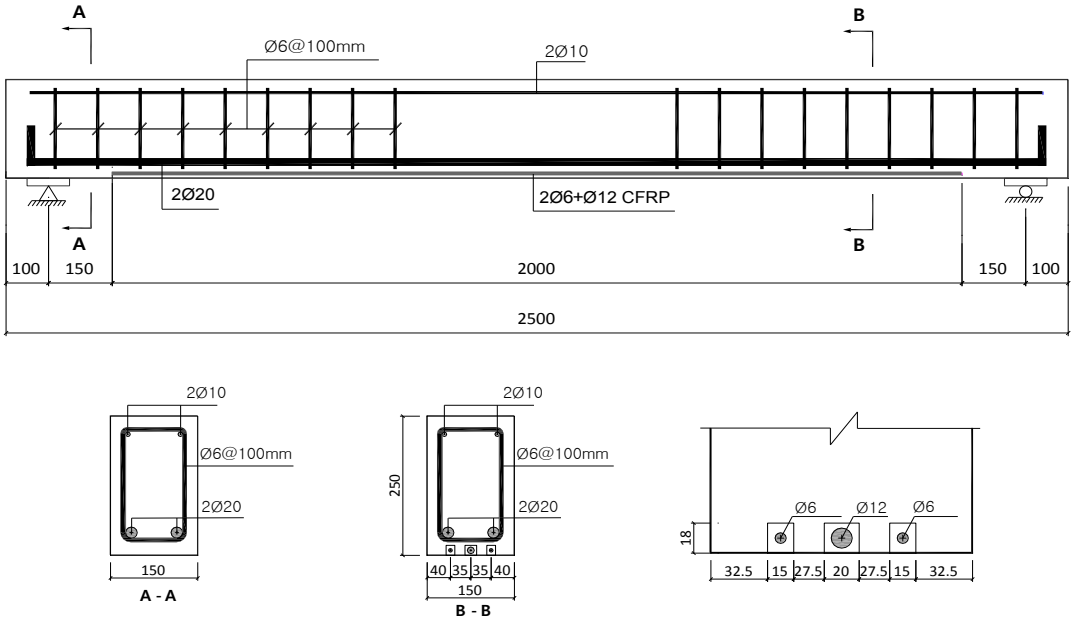

Fig. C2 - 1: Details of specimen

C.2.2 INSTRUMENTATION

(a)

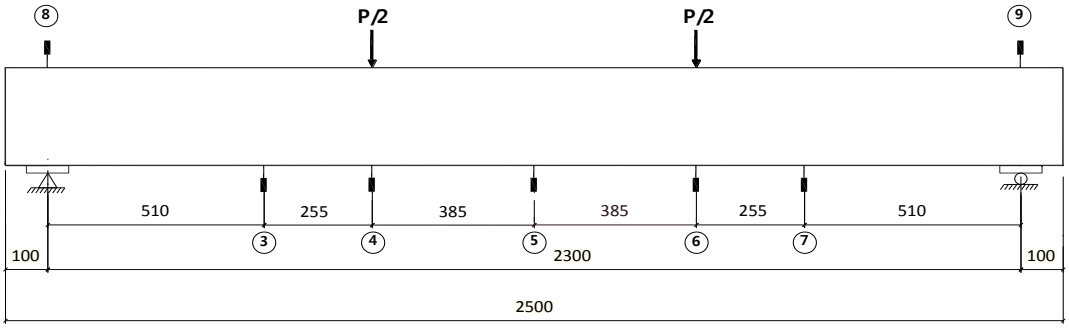

(b)

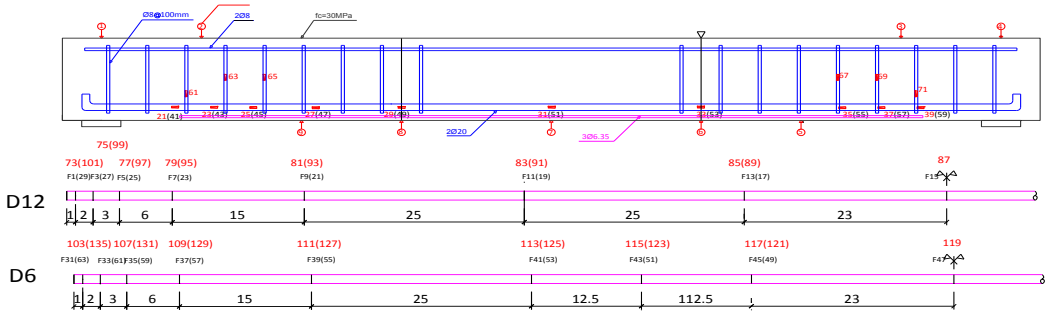

Fig. C2 - 2: (a): LVDTS arrangement along the beam - (b): Strain gauge arrangement in various components

C.2.3 FAILURE

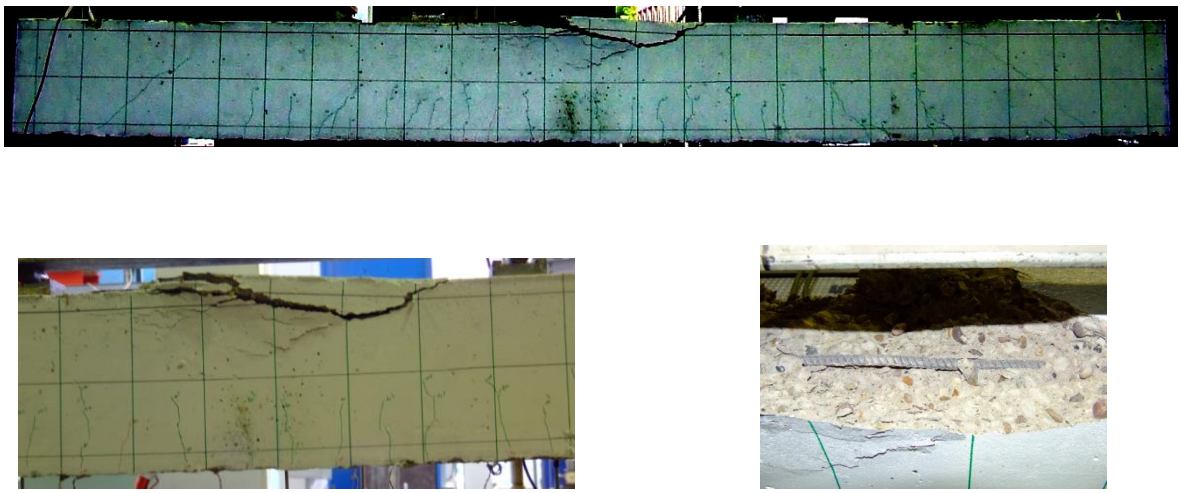

Fig. C2 - 3: Failure of beam NSM2A

C.2.4 READINGS OF LVDTs

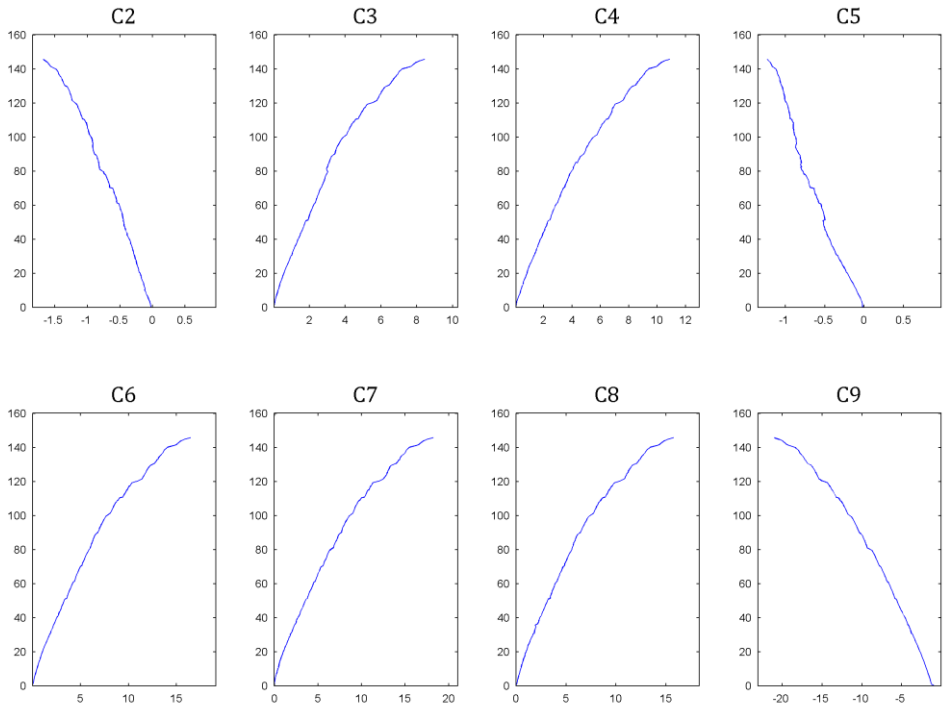

Fig. C2 - 4: Readings of LVDTs (C2 – C9)

C.2.5 STRAIN READINGS

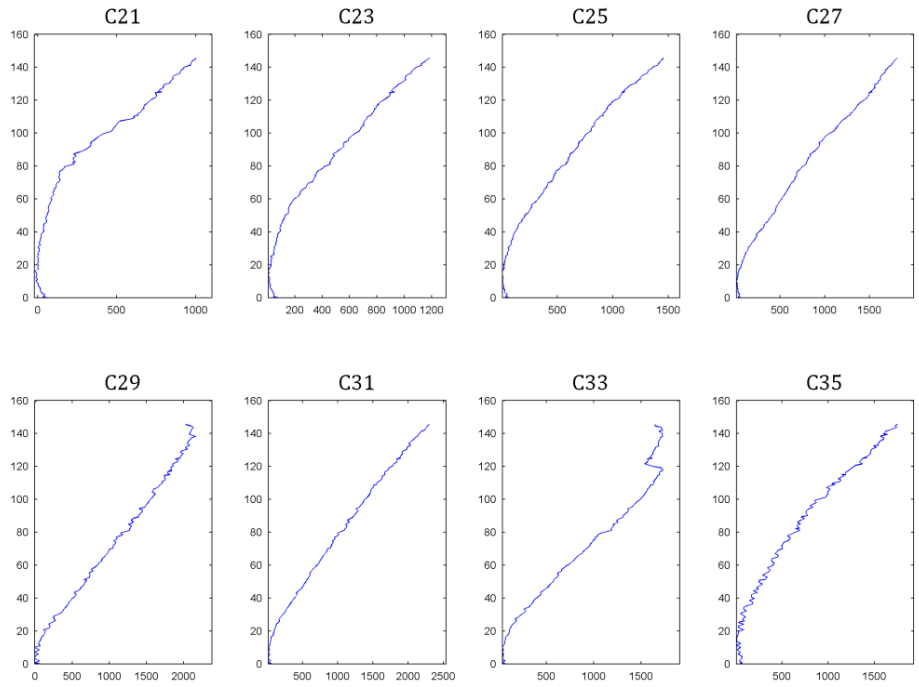

Fig. C2 - 5: Strain Readings (C21-C35)

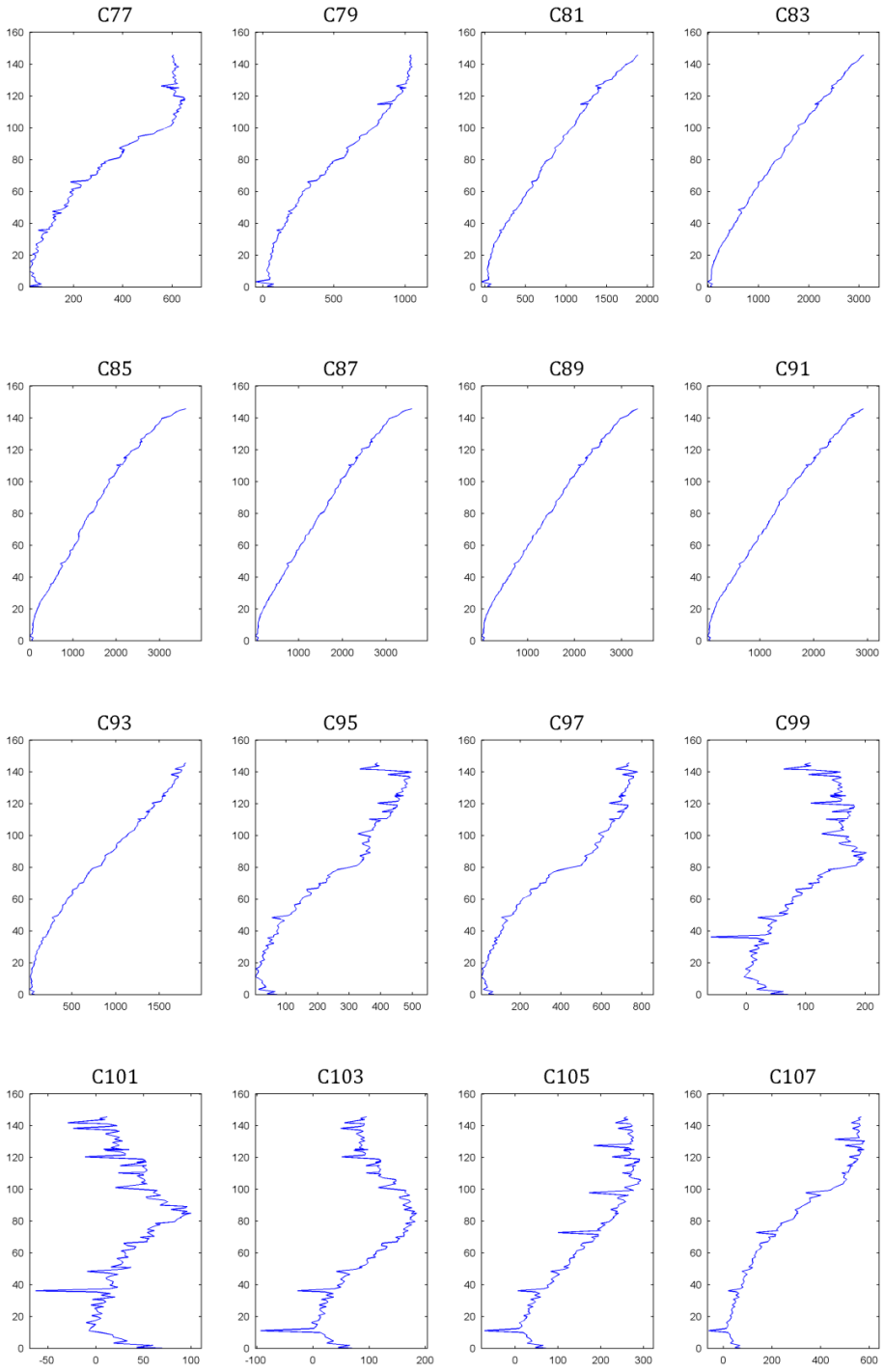

Fig. C2 - 6: Strain Readings (C77-C107)

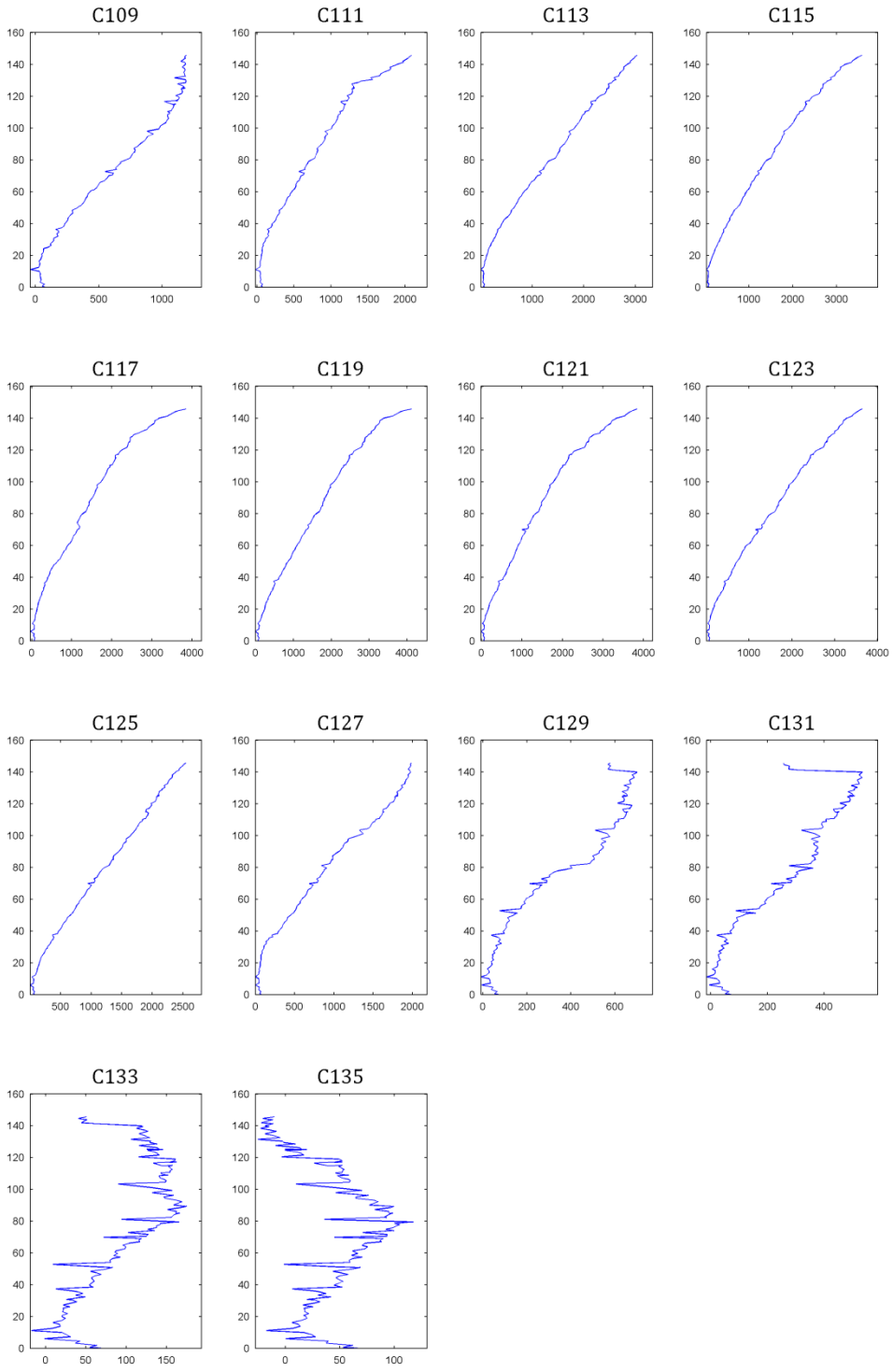

Fig. C2 - 7: Strain Readings (C109-C135)

C.2.6 DEFLECTION

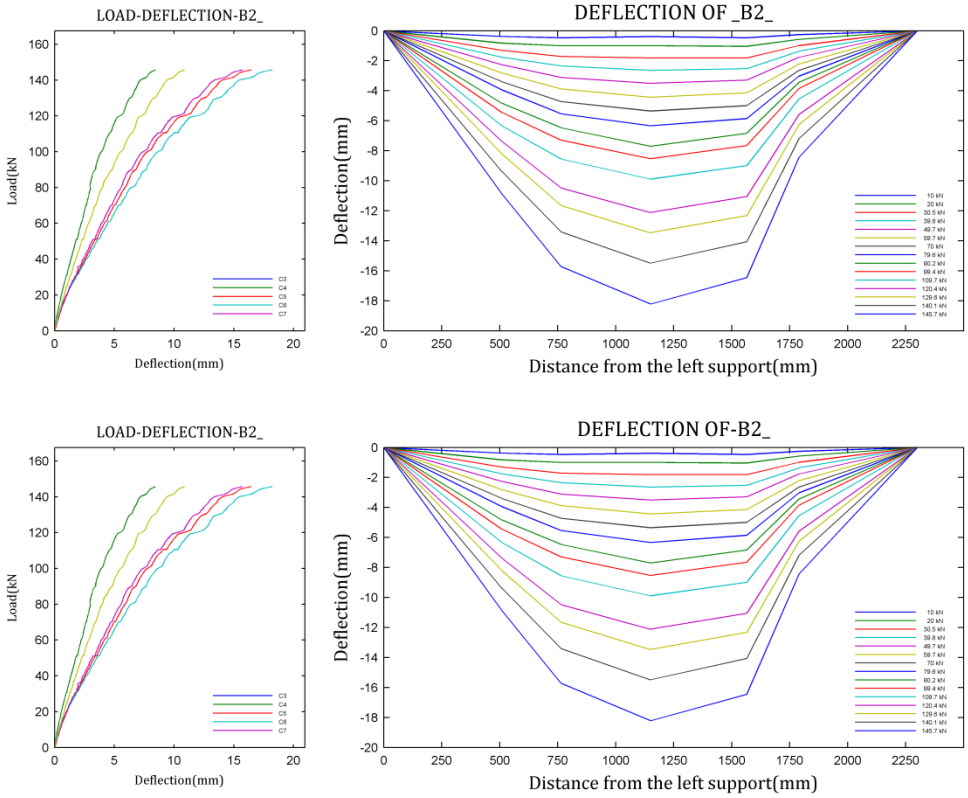

Fig. C2 - 8: Deflection profile

C.2.7 STRAINS IN THE STEEL REINFORCEMENT AND FRP ALONG THE SPAN

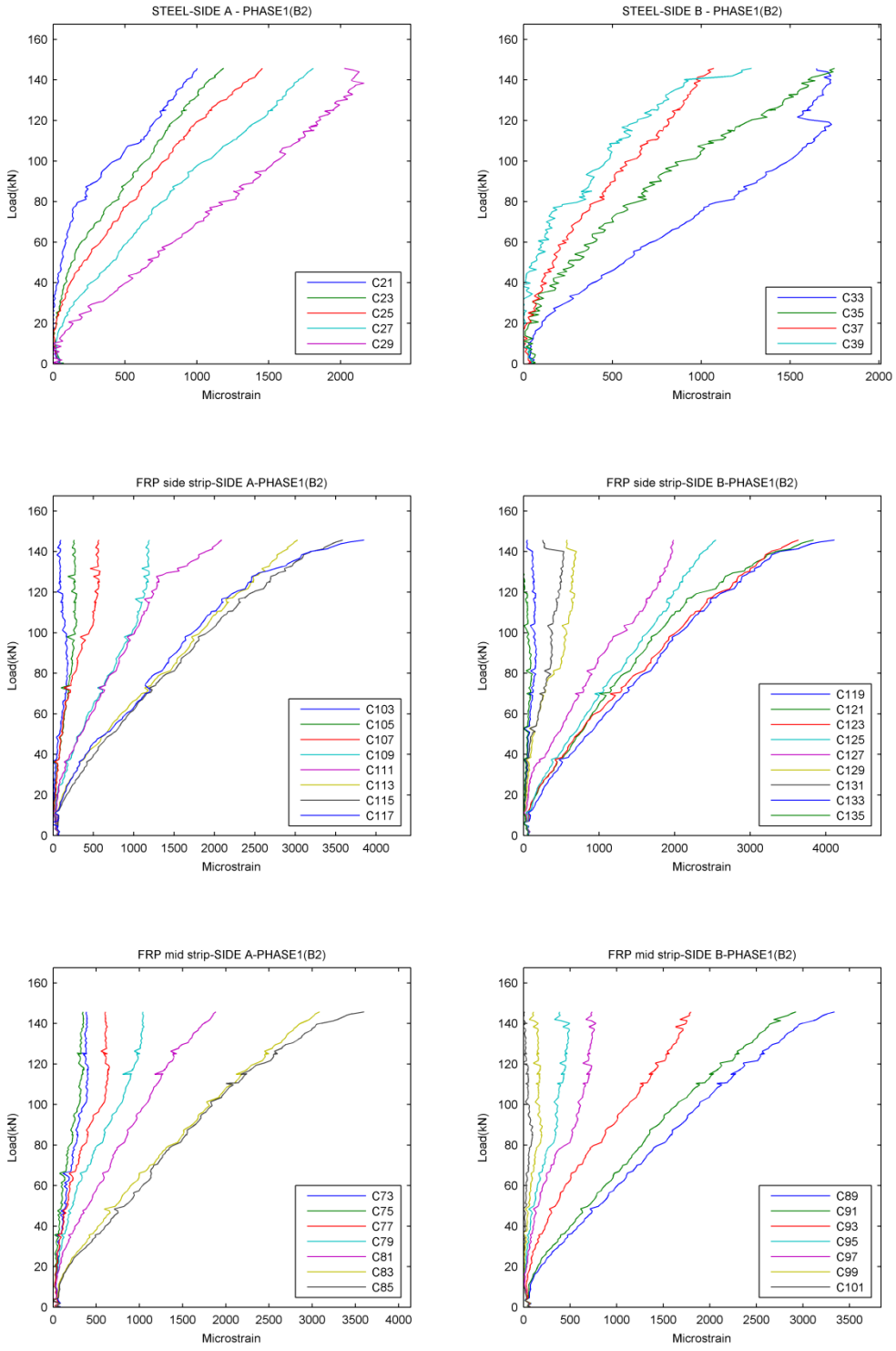

Fig. C2 - 9: Strains in the steel reinforcement and FRP along the span

C.2.8 STRAIN AND BOND STRESS PROFILES

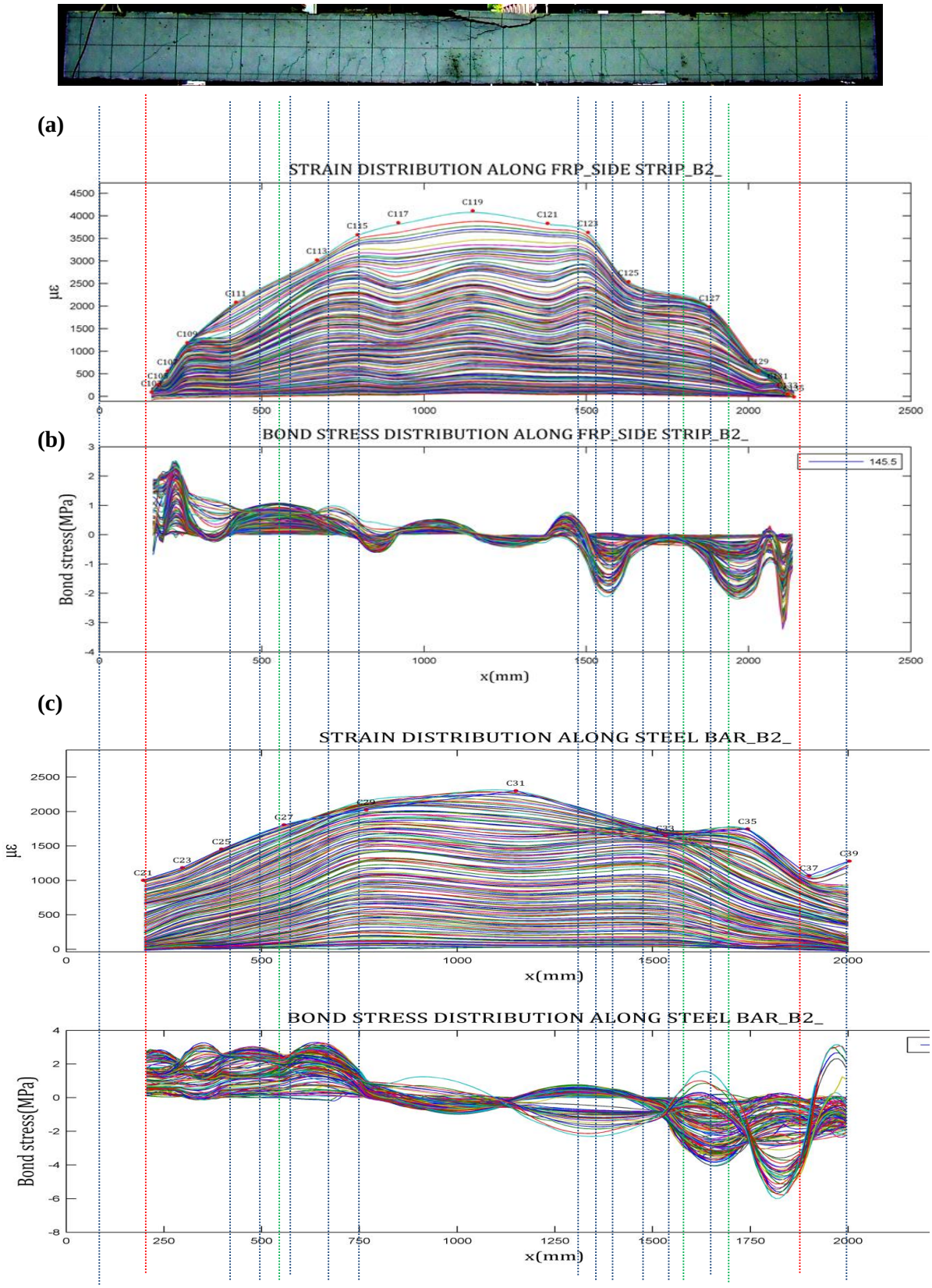

Fig. C2 - 10: Strain and bond stress profiles of (a) Crack pattern of beam NSM2A, (b) FRP, (c) The steel reinforcement

C.2.9 3D PROFILE OF STRAIN AND BOND STRESS

(a)

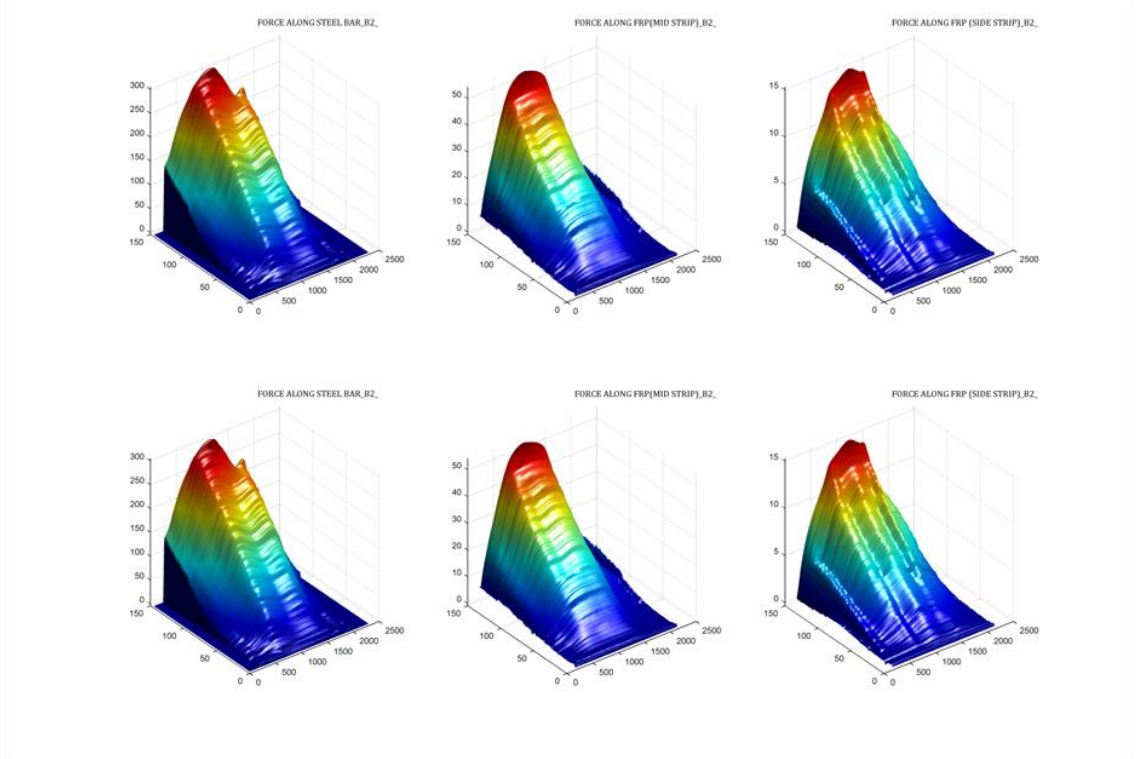

(b)

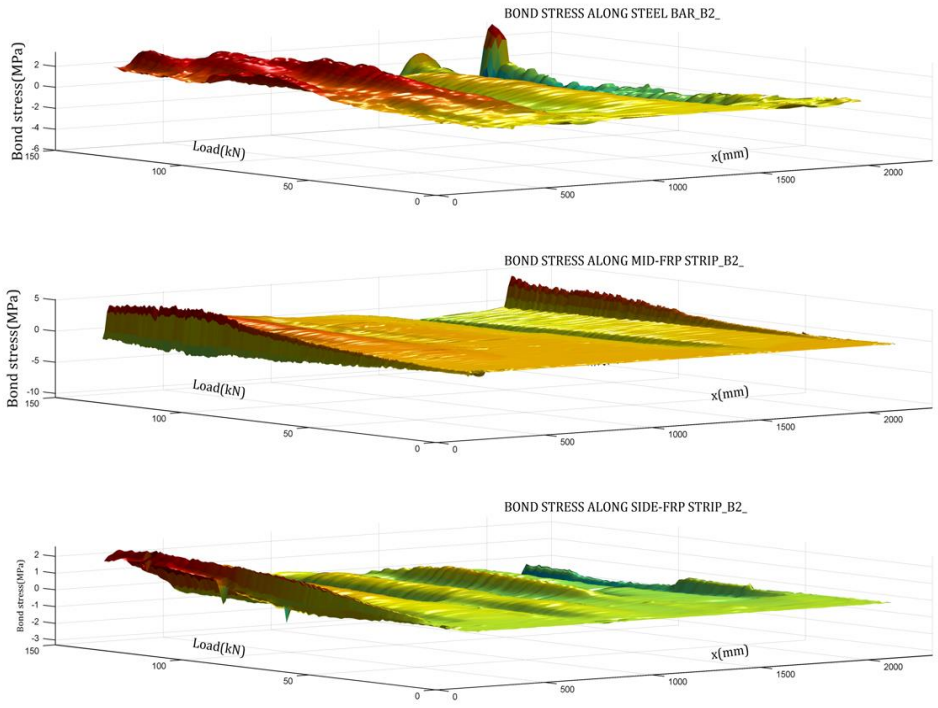

Fig. C2 - 11: Variation of (a) strains and (b) bond stress along the reinforcement and FRP at different load levels

C.3.1 BEAM DESIGN

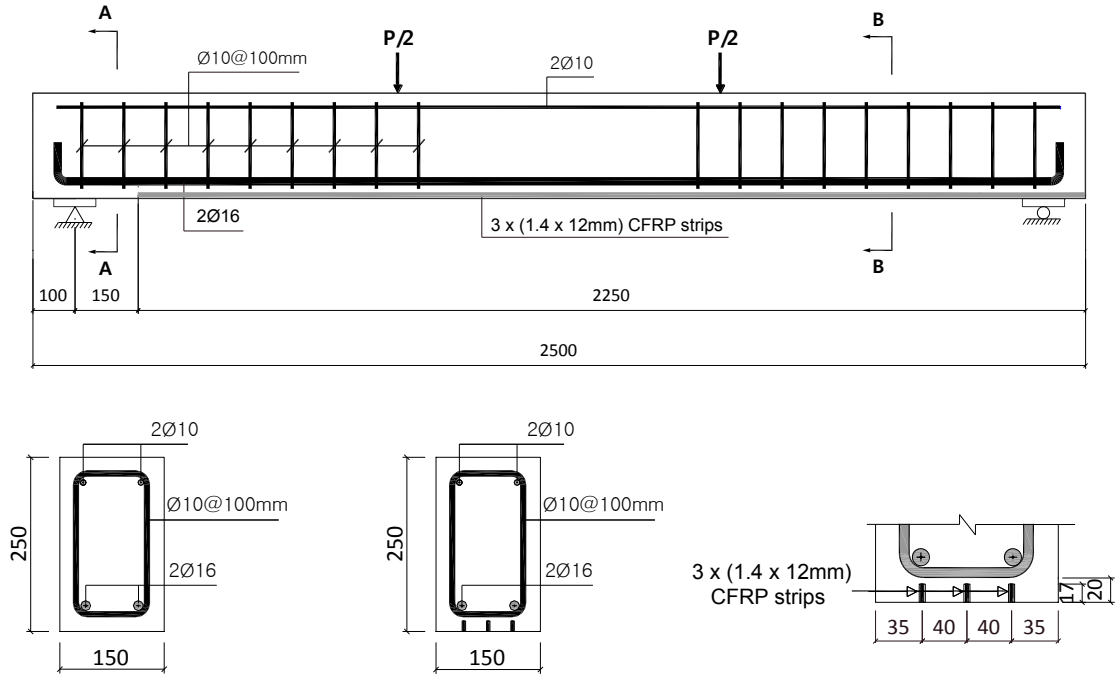

Fig. C3- 1: Details of specimen

C.3.2 INSTRUMENTATION

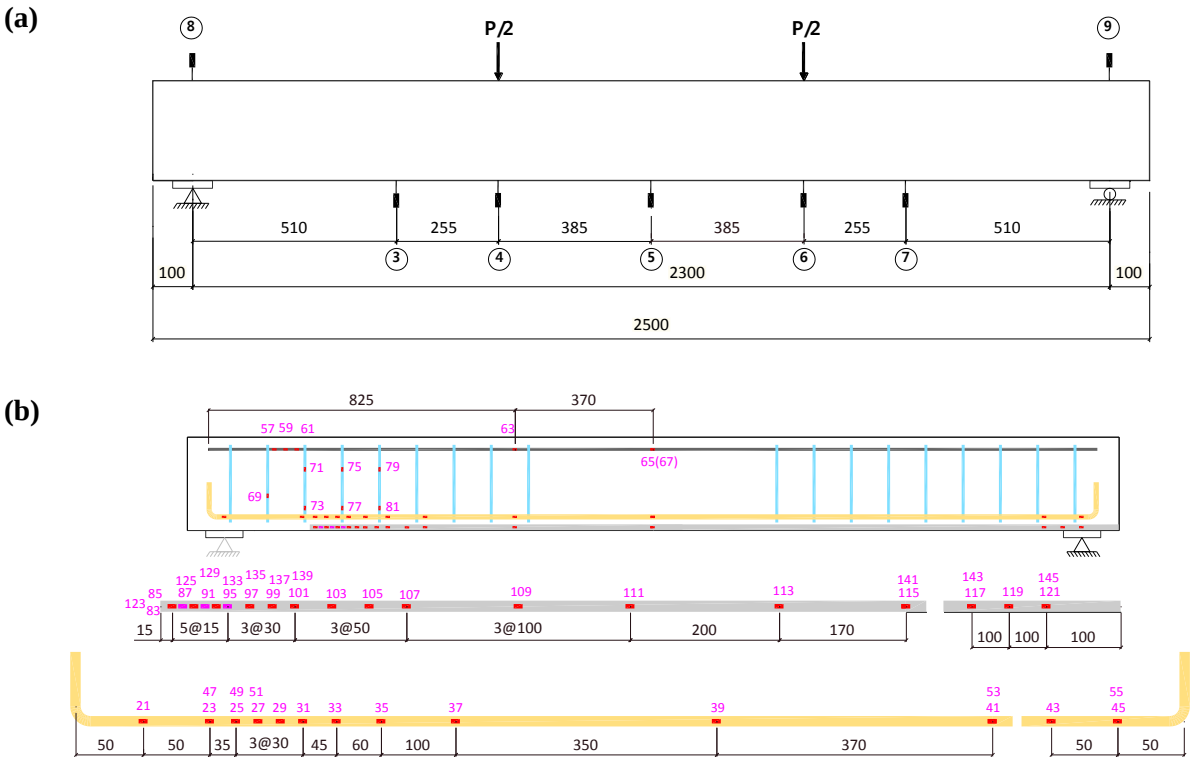

Fig. C3- 2: (a) LVDTs arrangement along the beam, (b) Strain gauge arrangement in various components

C.3.3 FAILURE

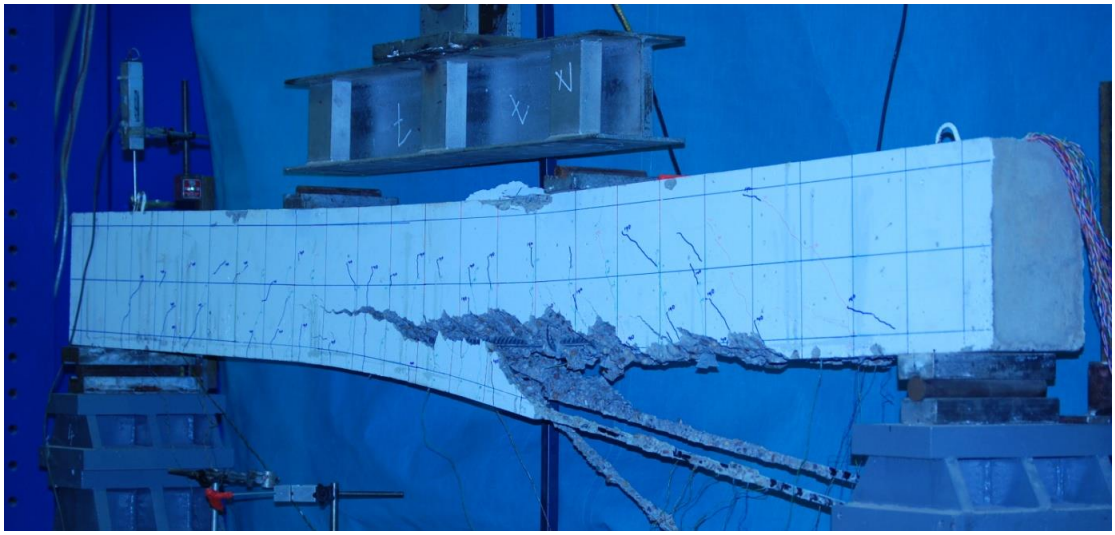

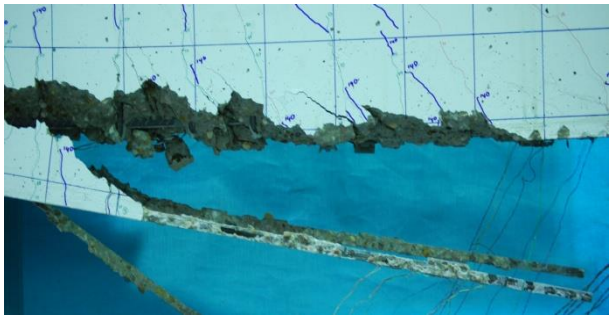

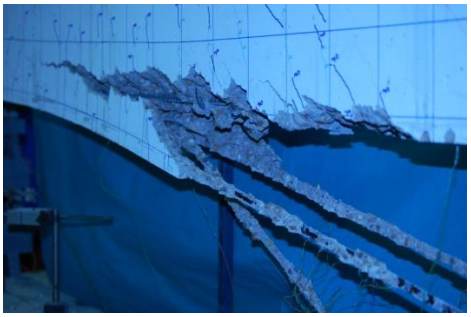

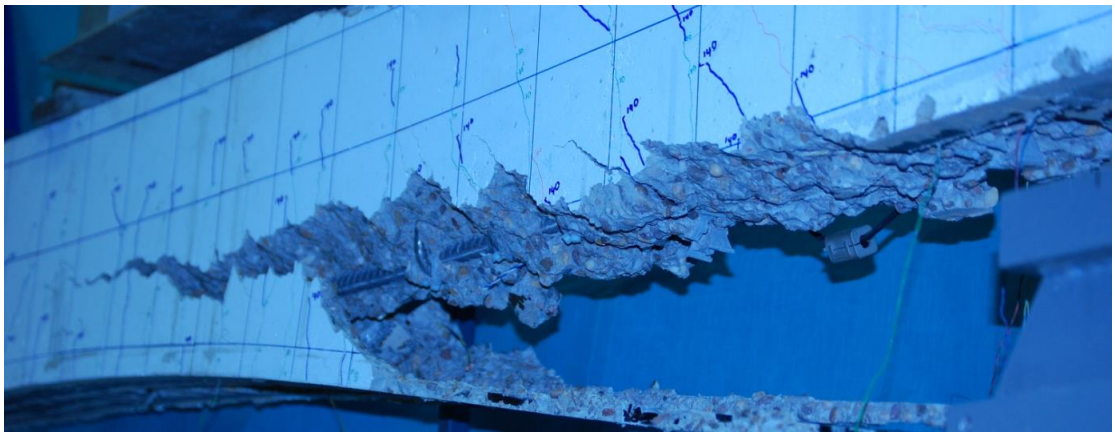

Fig. C3- 3: Failure of beam NSM3A

C.3.4 FIRST TESTING PHASE: PRE-CRACK STAGE

a. READINGS OF LVDTs

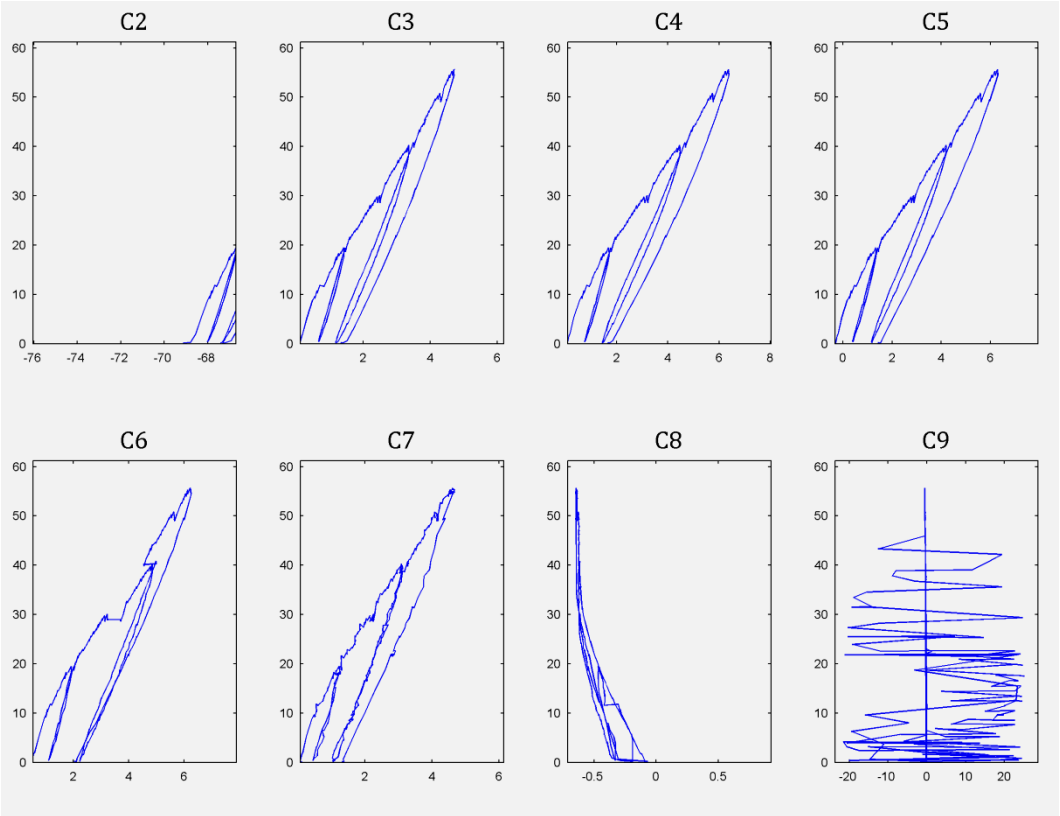

Fig. C3- 4: Readings of LVDTs (C2 – C9)

b. STRAIN READINGS

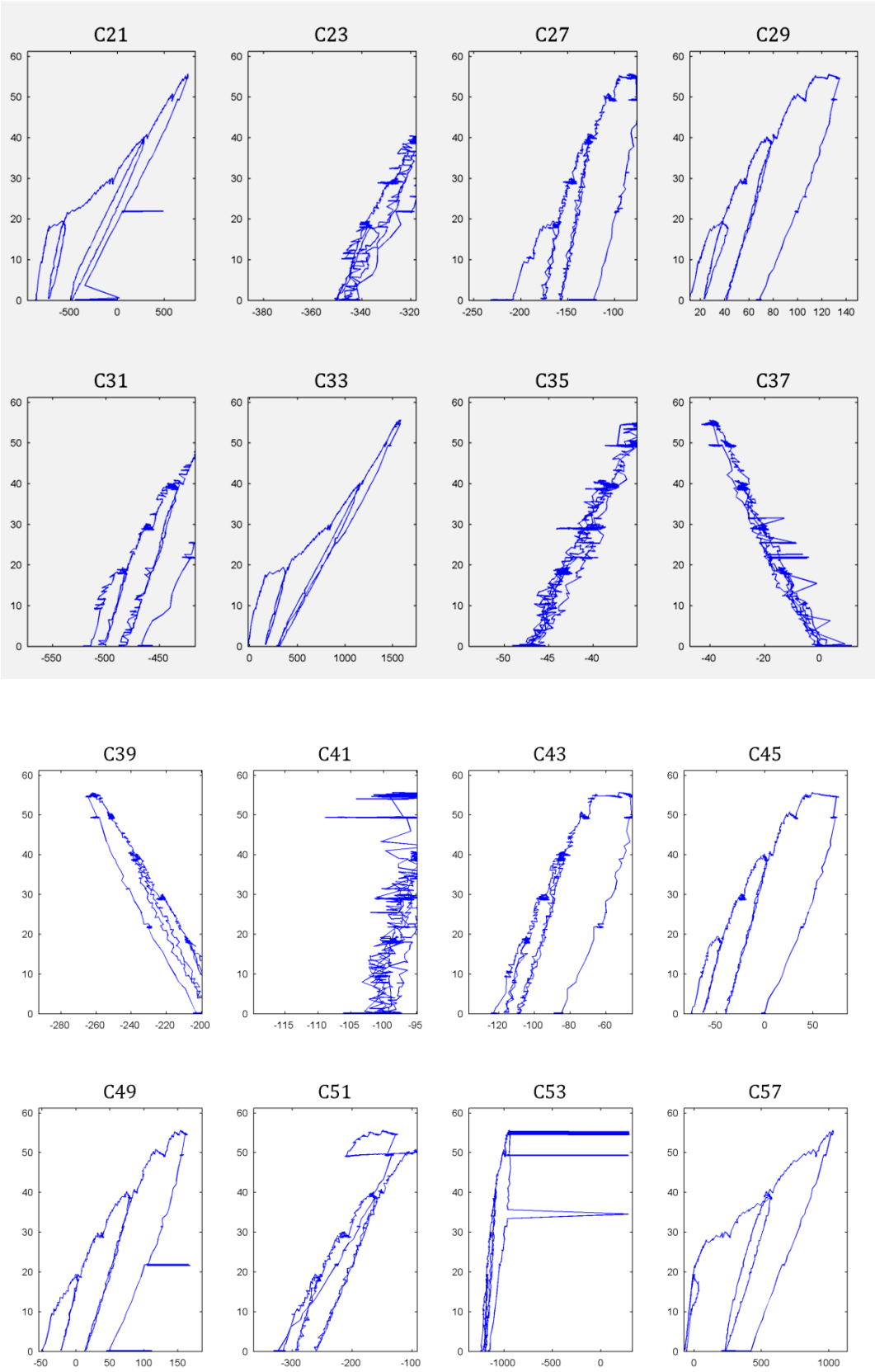

Fig. C3- 5: Strain readings (C21 – C57)

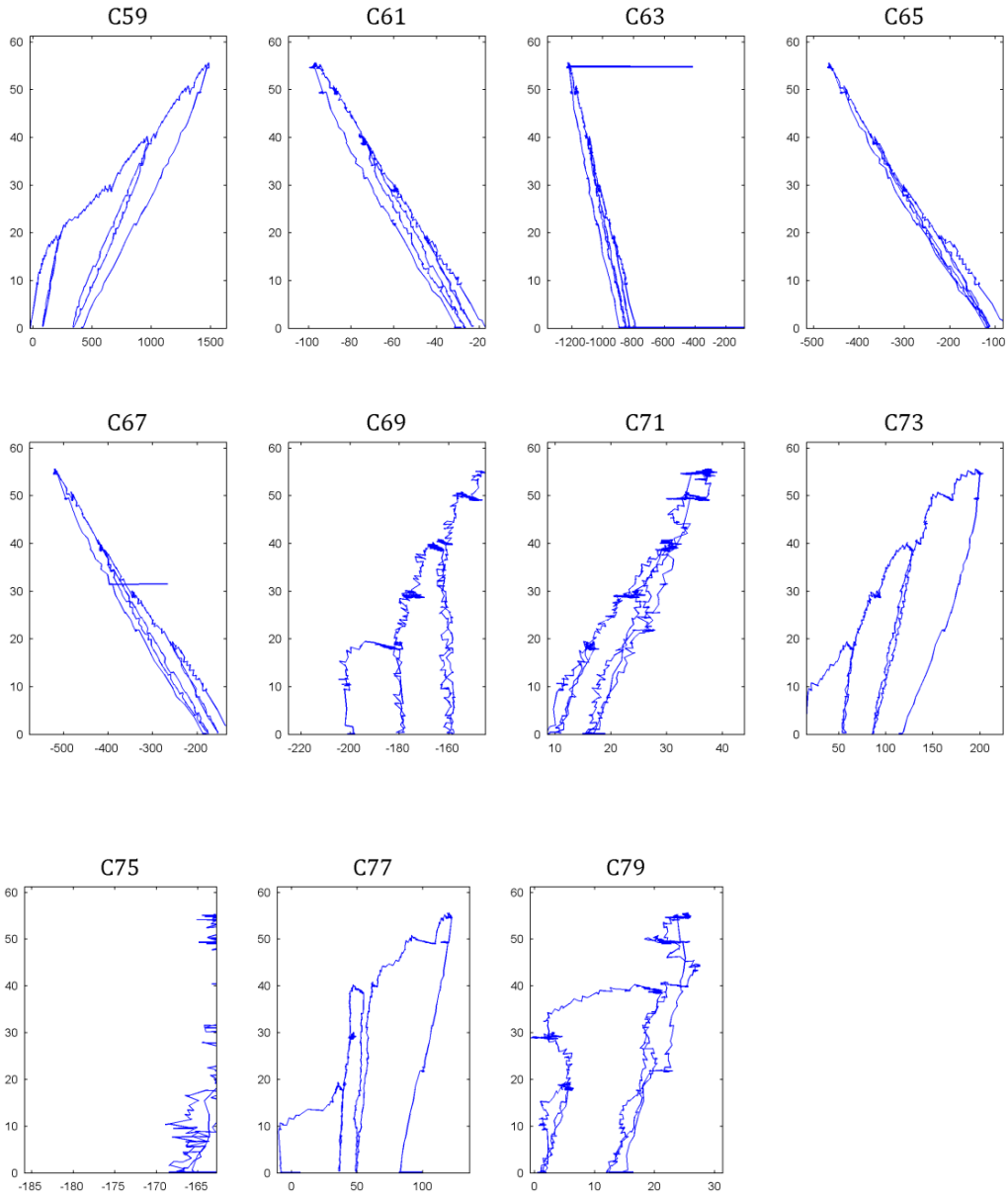

Fig. C3- 6: Strain readings (C21 – C79)

C.3.5 FINAL TESTING PHASE

a. READINGS OF LVDTs

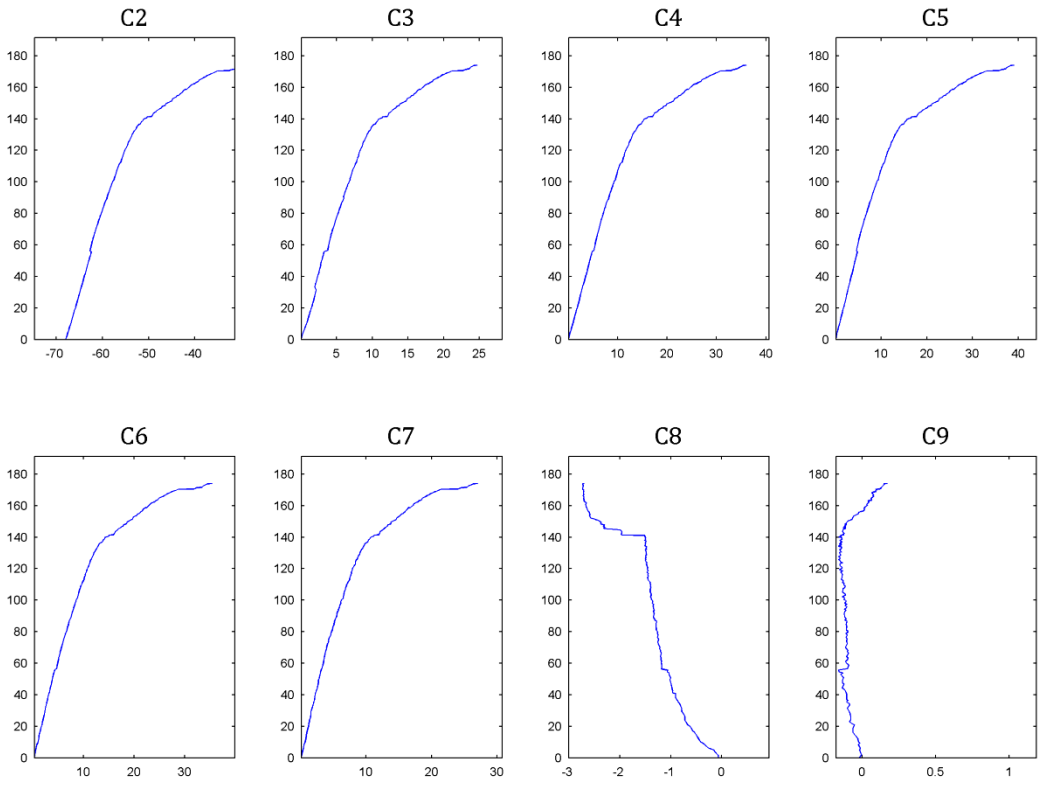

Fig. C3- 7: Readings of LVDTs (C2 – C9)

b. STRAIN READINGS

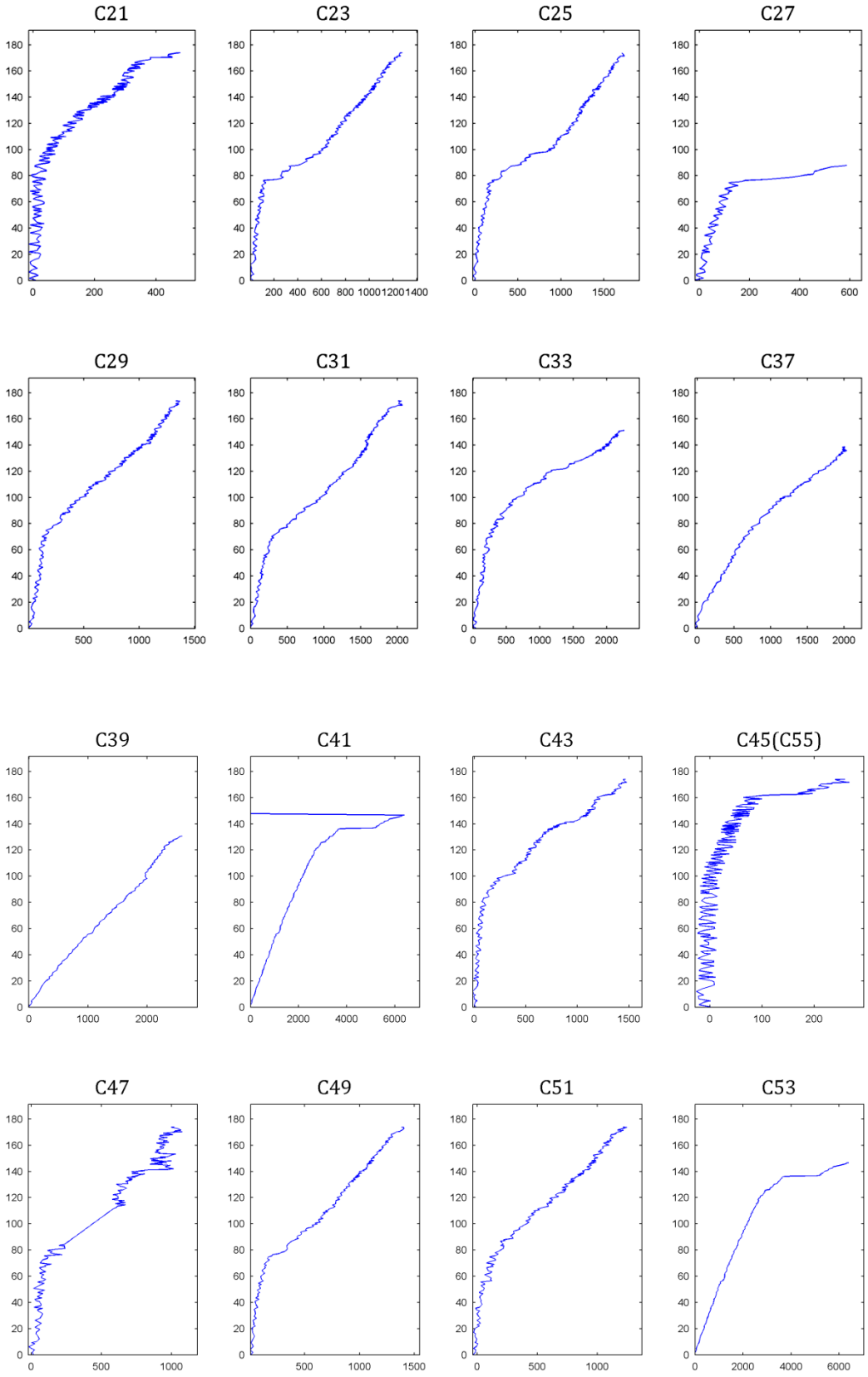

Fig. C3- 8: Strain readings (C21 – C53)

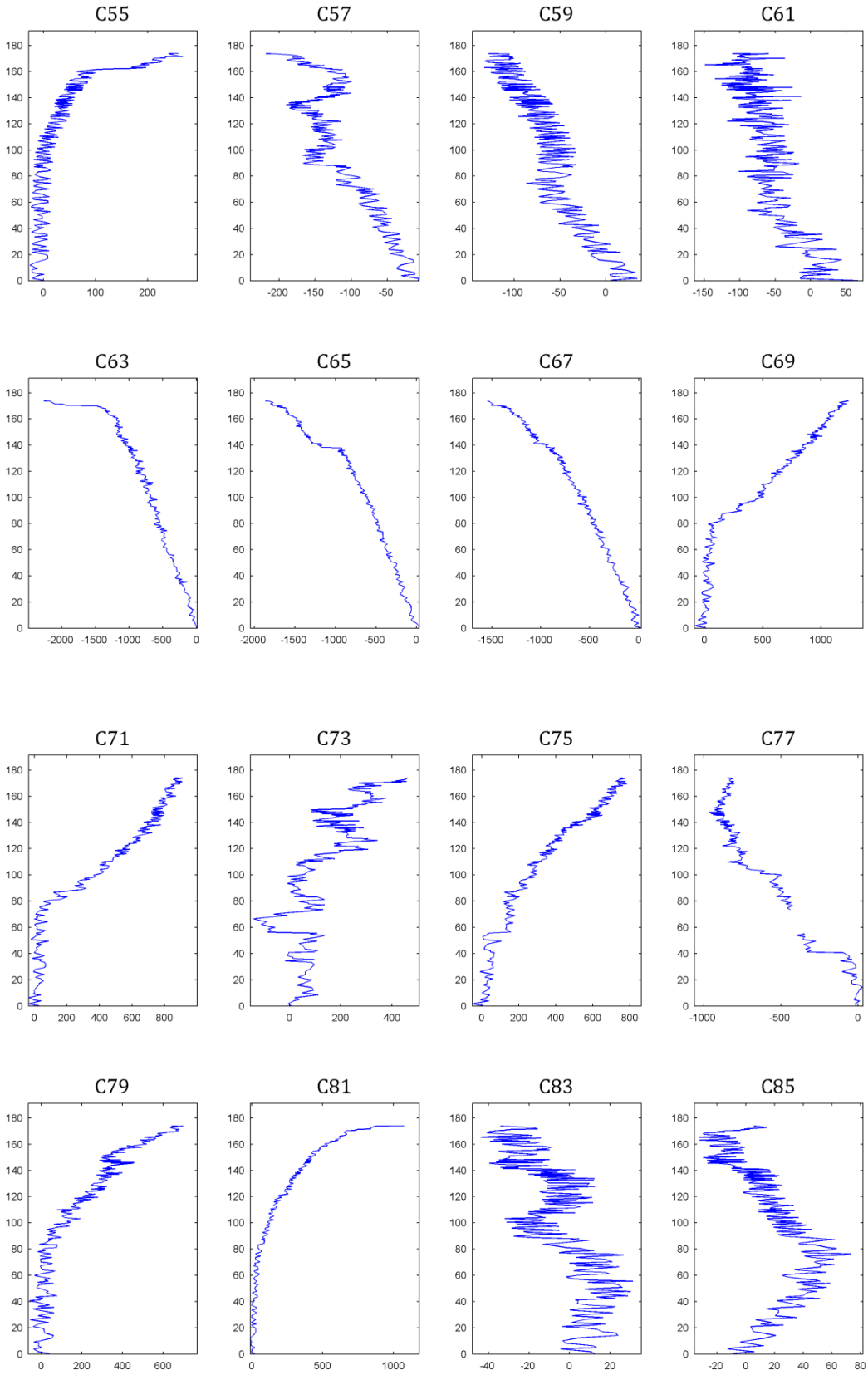

Fig. C3- 9: Strain readings (C55 – C85)

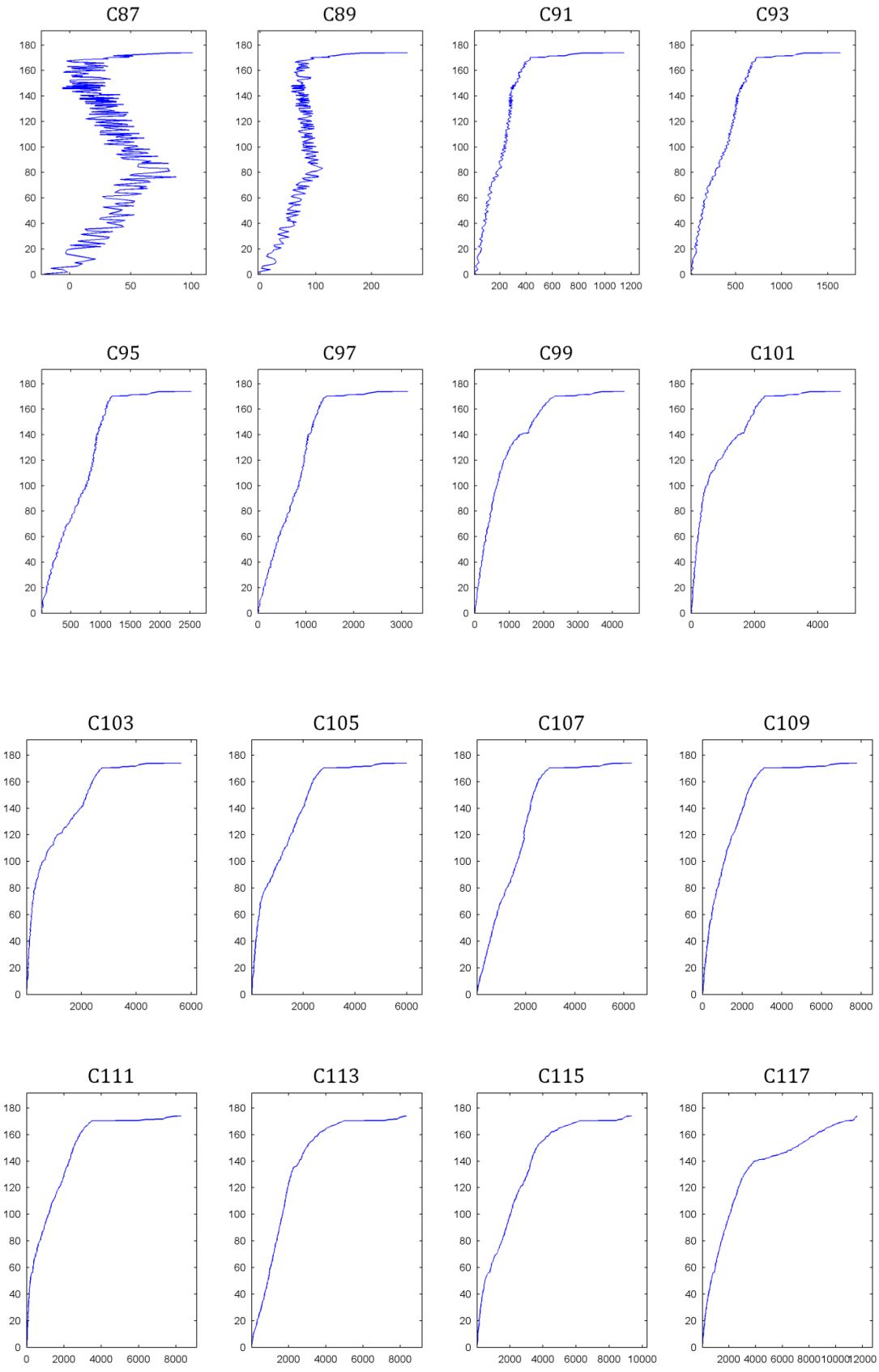

Fig. C3- 10: Strain readings (C87 – C117)

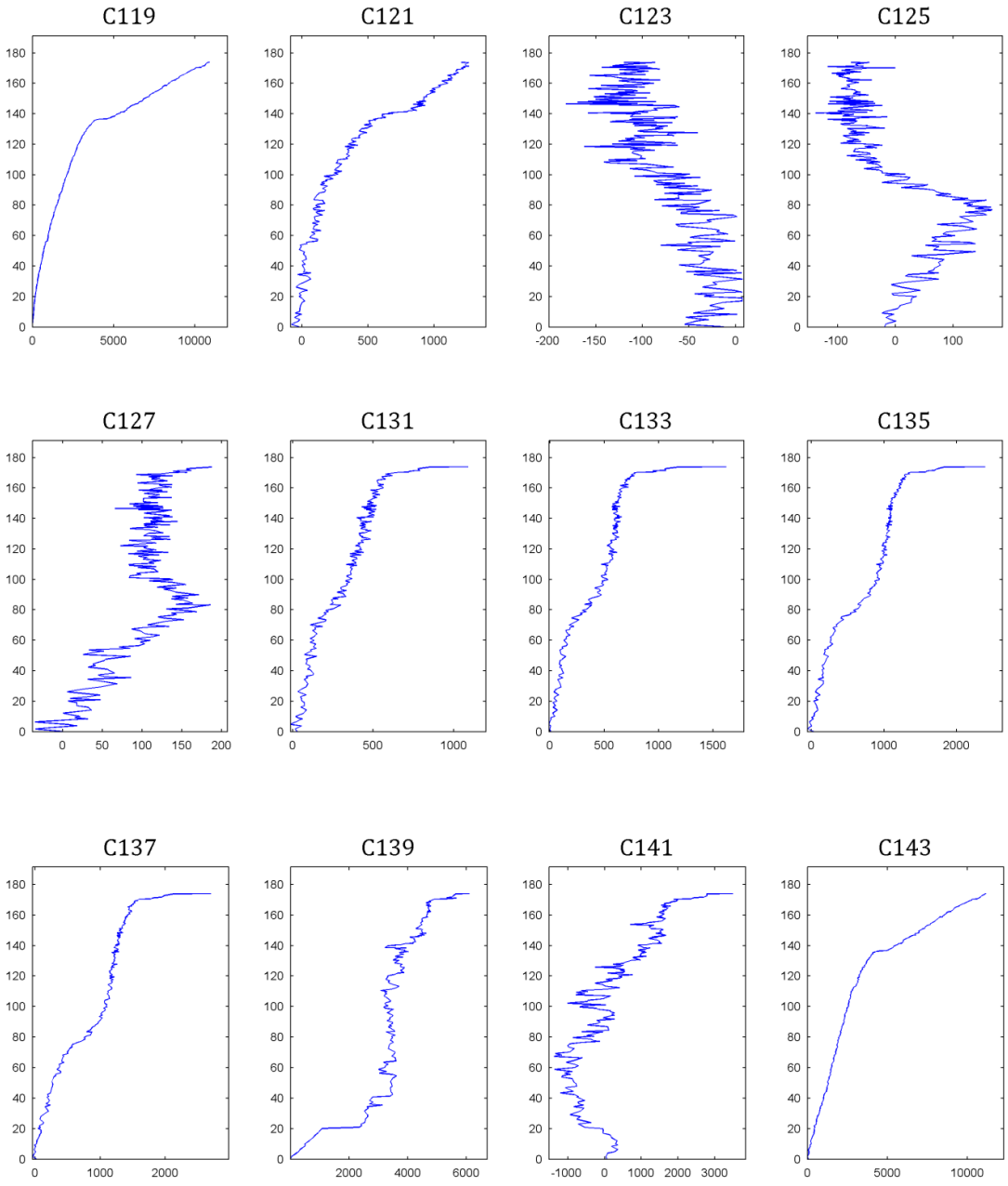

Fig. C3- 11: Strain readings (C119 – C143)

C.3.6 DEFLECTION

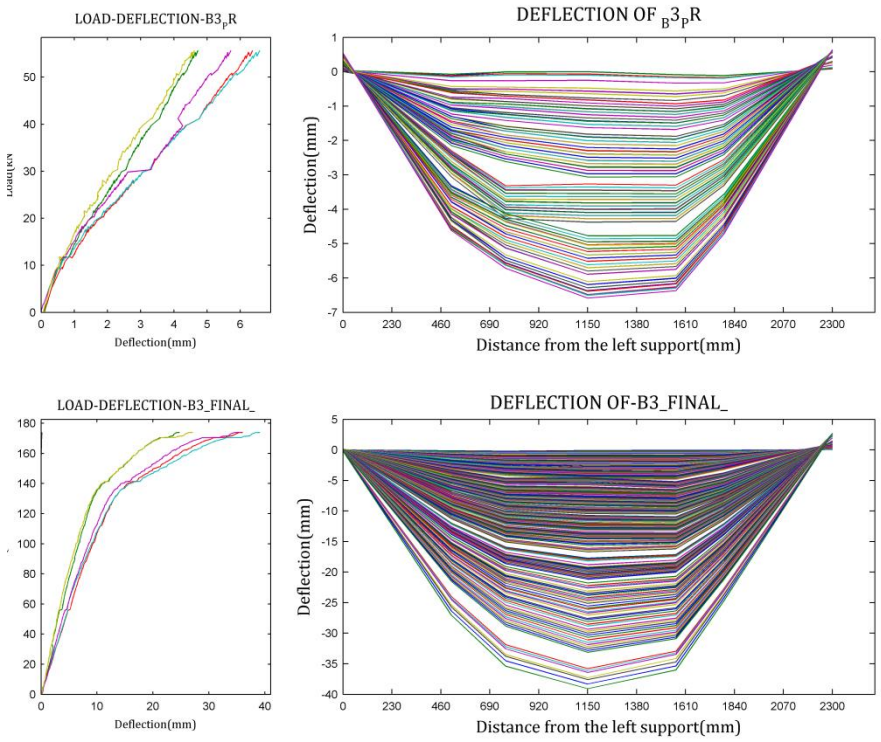

Fig. C3- 12: Deflection profile

C.3.7 STRAIN DISTRIBUTION AND BOND STRESS IN THE STEEL REINFORCEMENT AND FRP ALONG THE SPAN

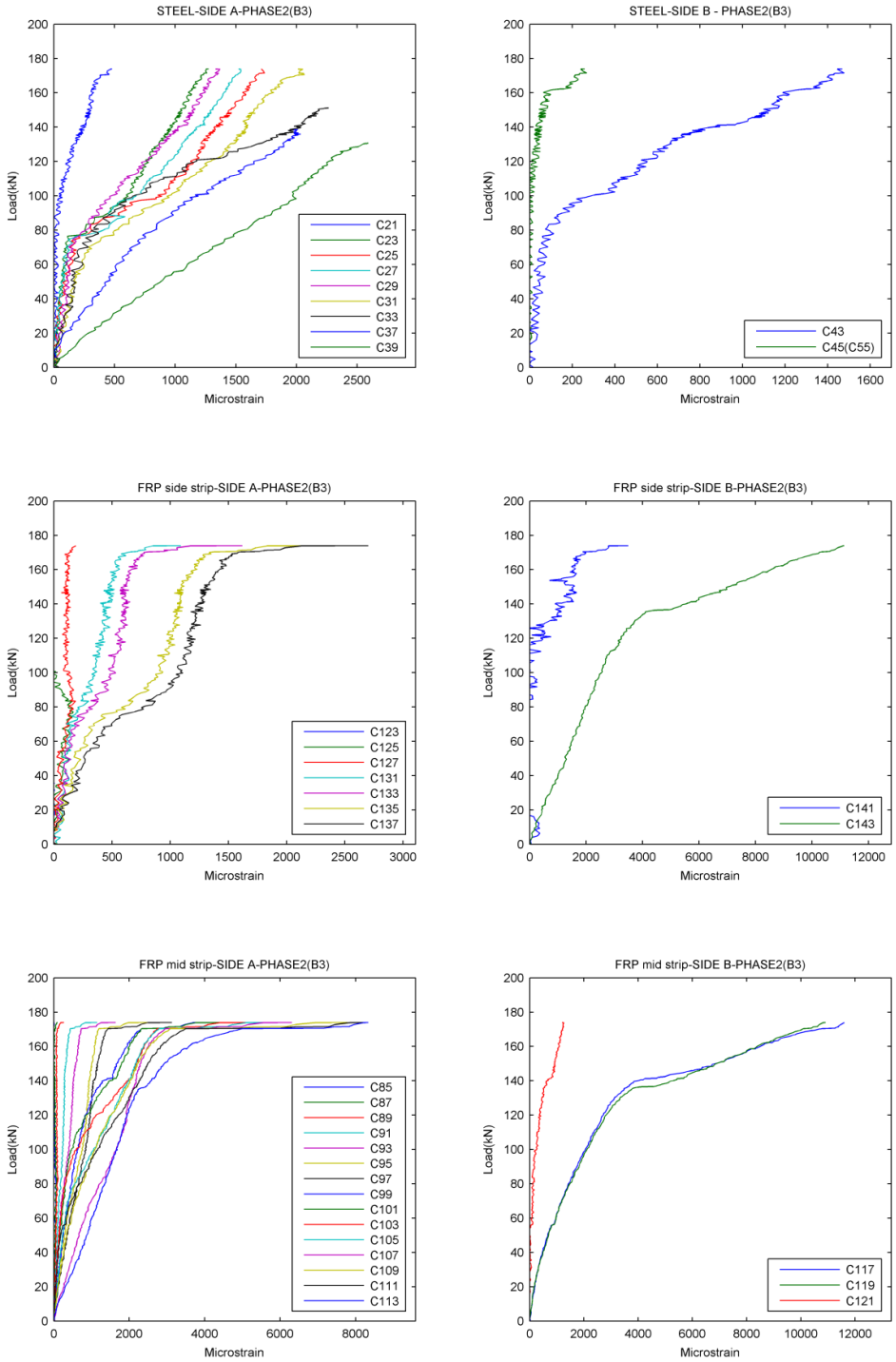

Fig. C3- 13: Strains in the steel reinforcement and FRP along the span

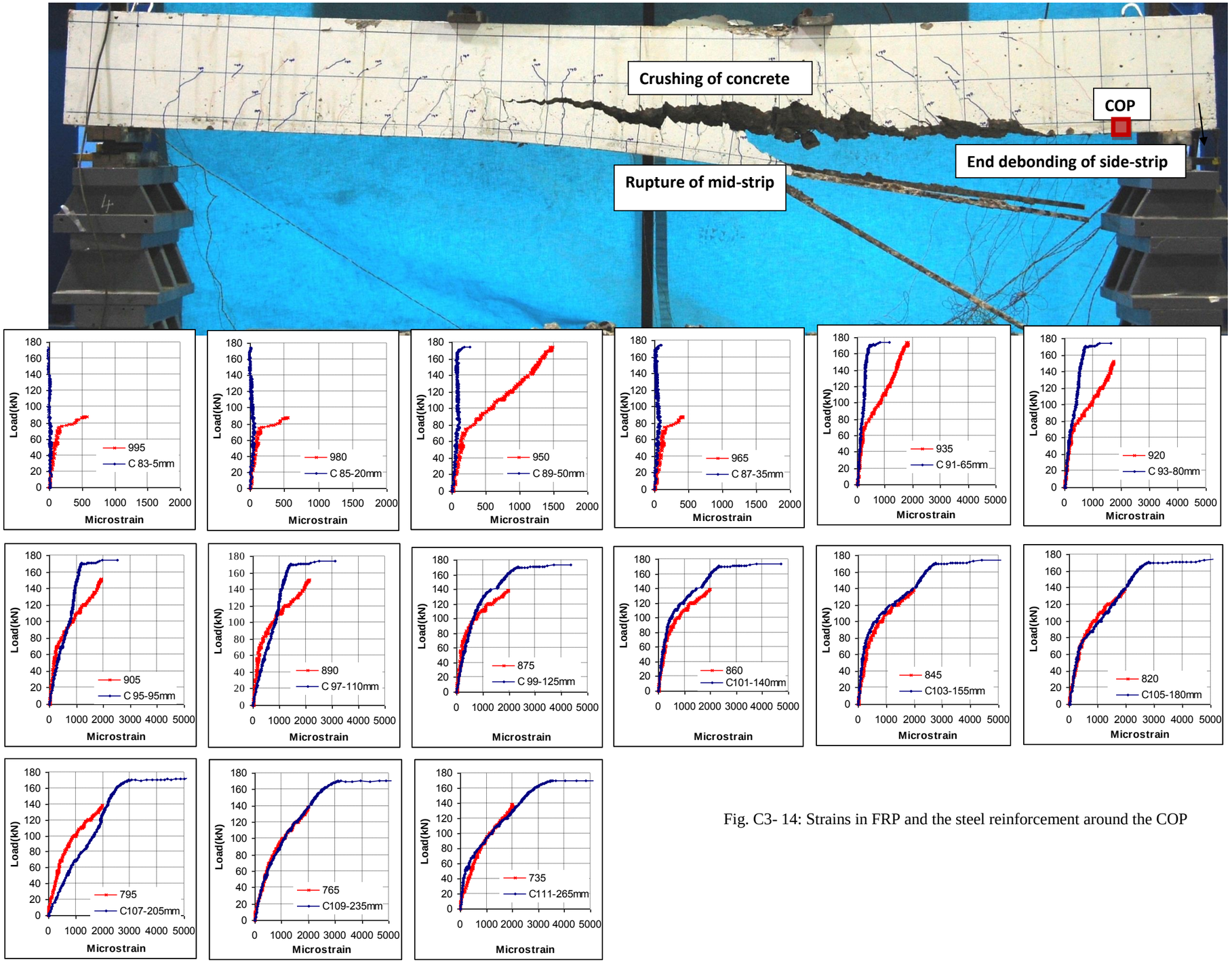

Fig. C3- 14: Strains in FRP and the steel reinforcement around the COP

C.4.1 BEAM DESIGN

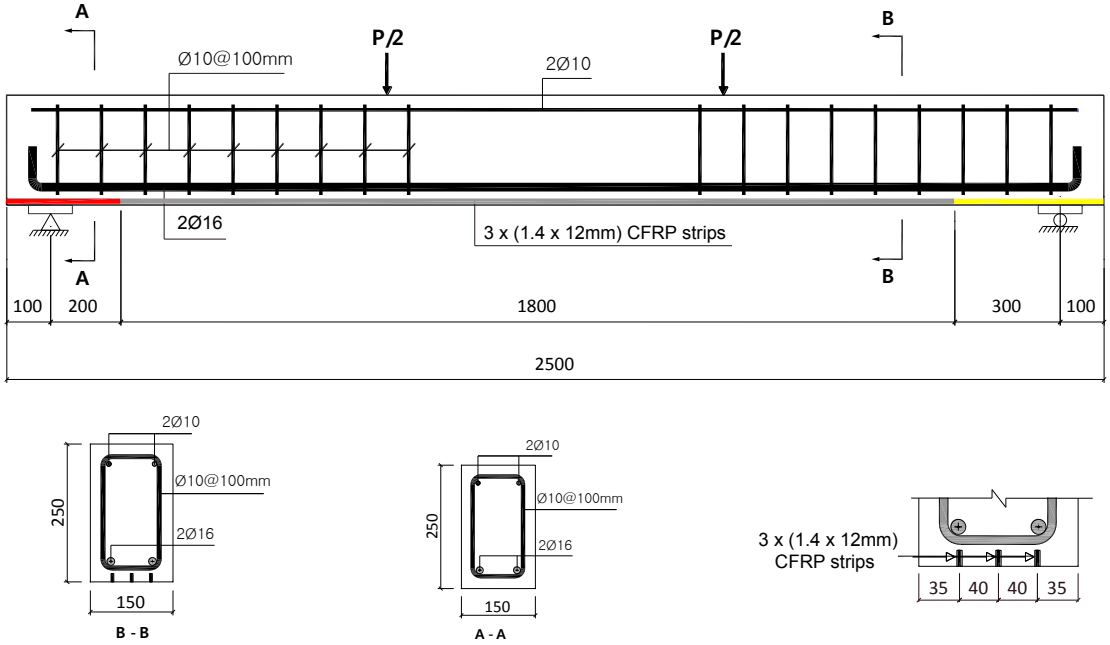

Fig. C4 - 1: Beam set-up.

C.4.2 INSTRUMENTATION

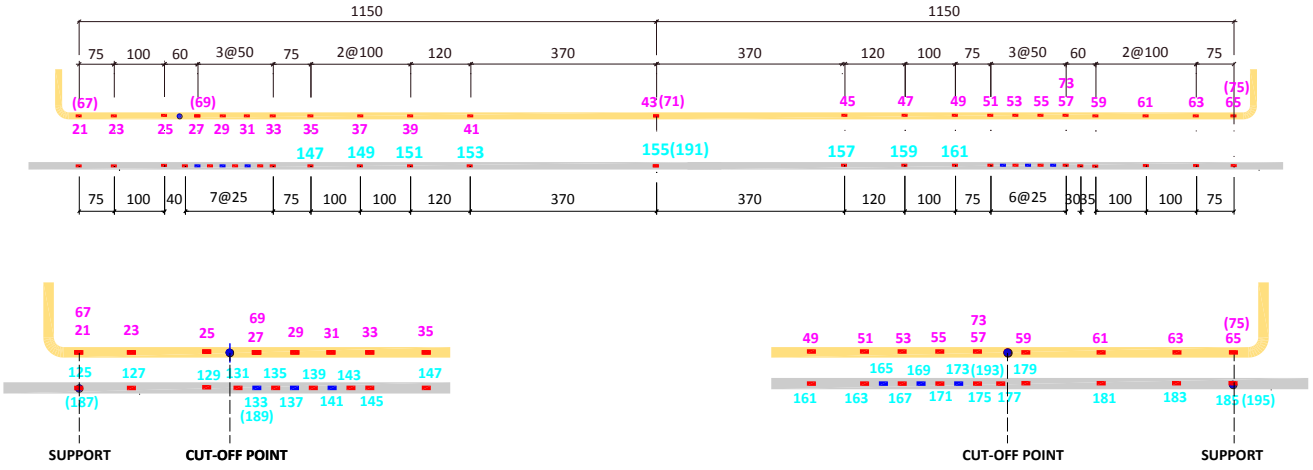

Fig. C4 - 2: Strain gauge arrangement in various components

C.4.3 HE FIRST PHASE OF TESTING-FAILURE AT SIDE A

(a)

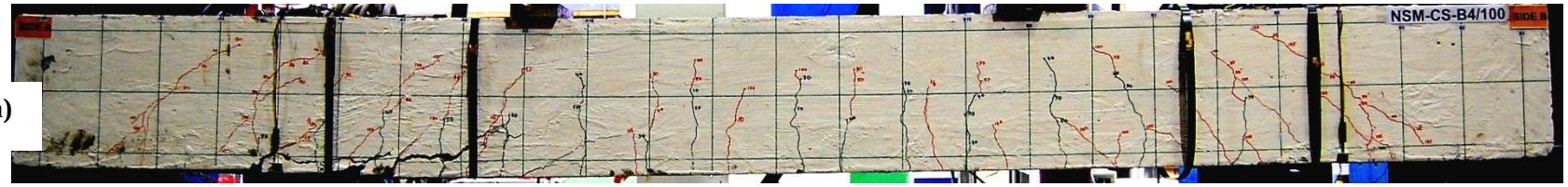

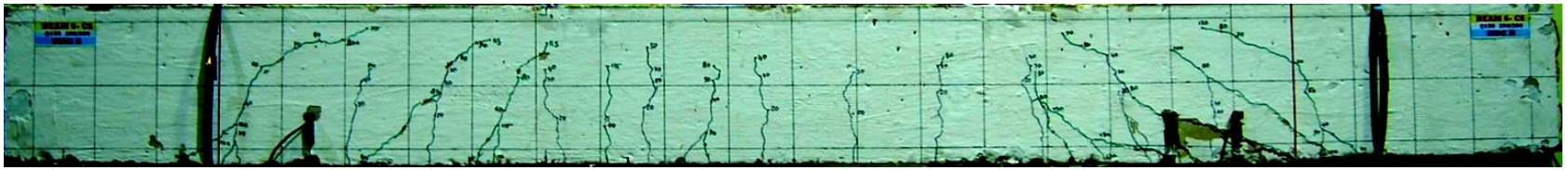

(b)

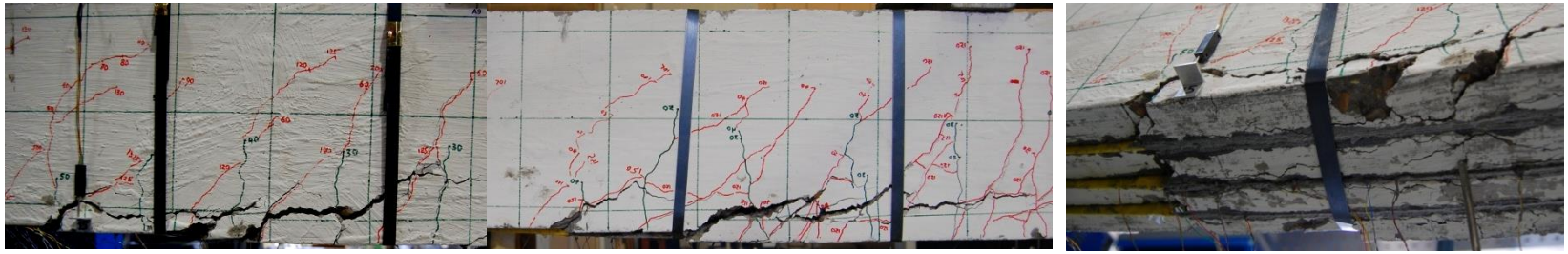

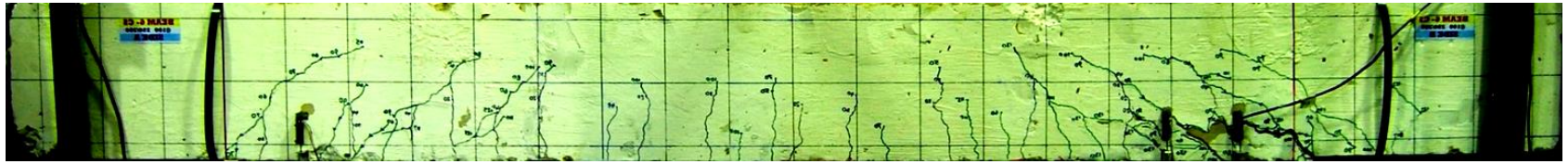

Fig. C4 - 3: : (a) Crack pattern and (b) Debonding of beam NSM5A.

C.4.4 THE SECOND PHASE(failure side A)

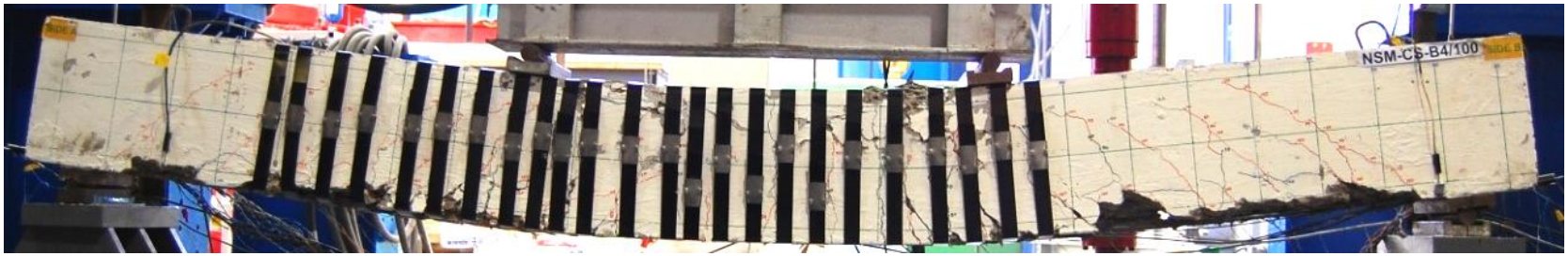

Fig. C4 - 4: Failure at the second phase.

C.4.5 THE FINAL PHASE

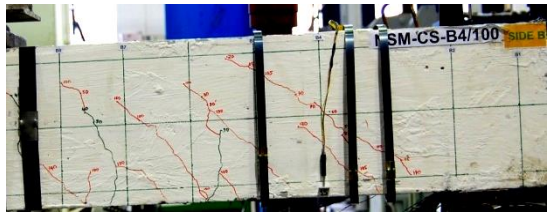

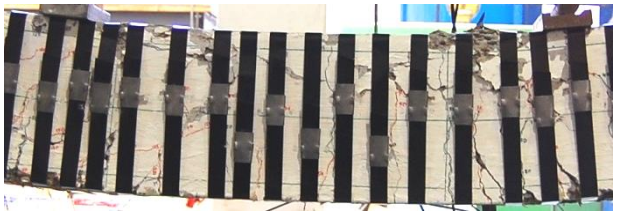

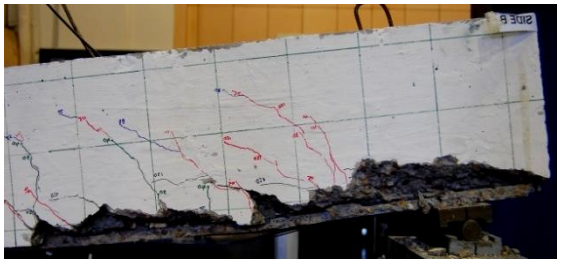

Fig. C4 - 5: Failure at the final phase.

C.4.6 FIRST TESTING PHASE: PRE-CRACK STAGE

a. READINGS OF LVDTs

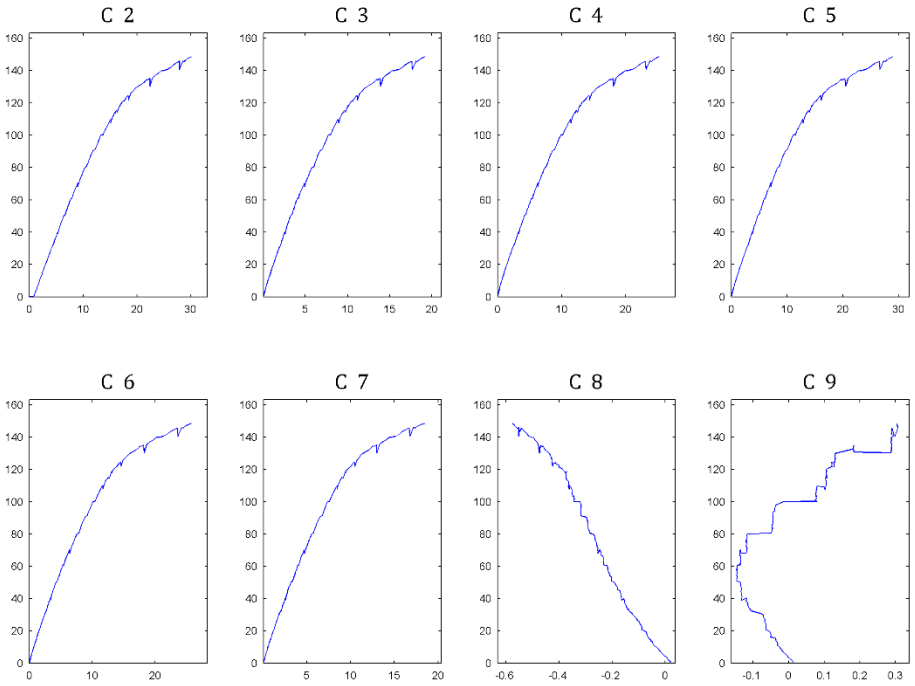

Fig. C4 - 6: Readings of LVDTs (C2 – C9)

b. STRAIN READINGS

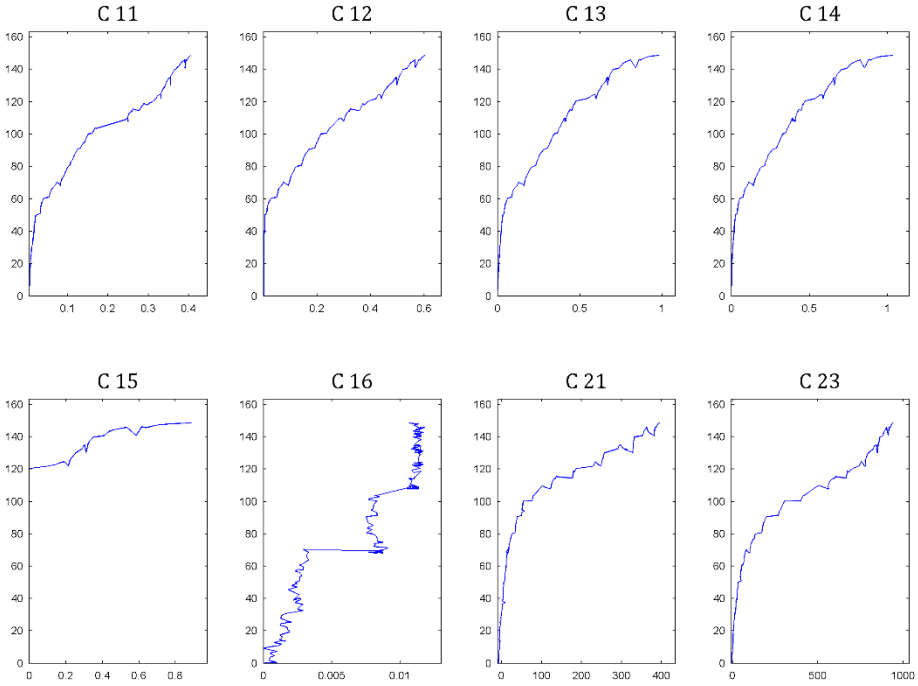

Fig. C4 - 7: Strain readings (C11 – C23)

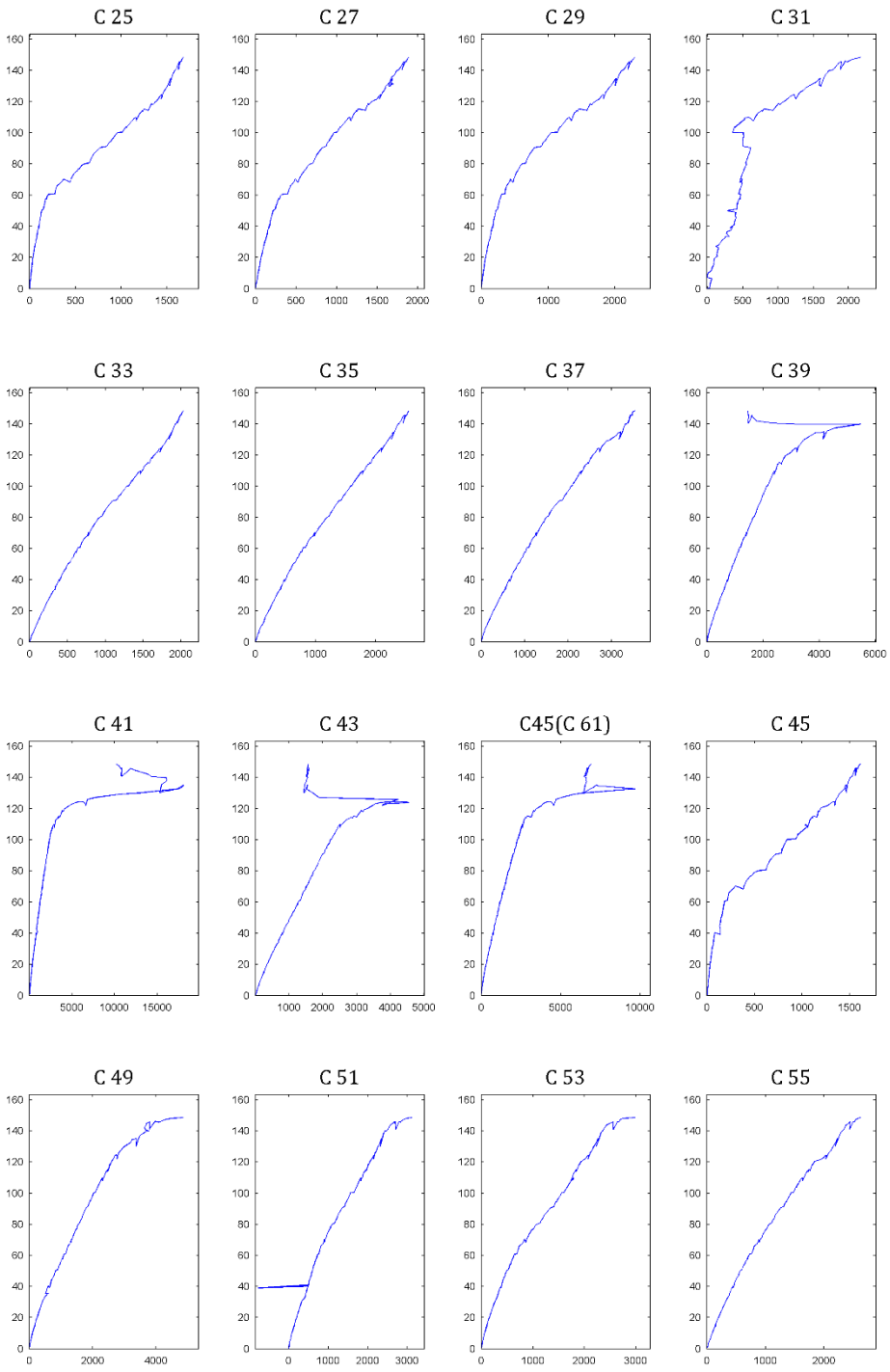

Fig. C4 - 8: Strain readings (C25 – C55)

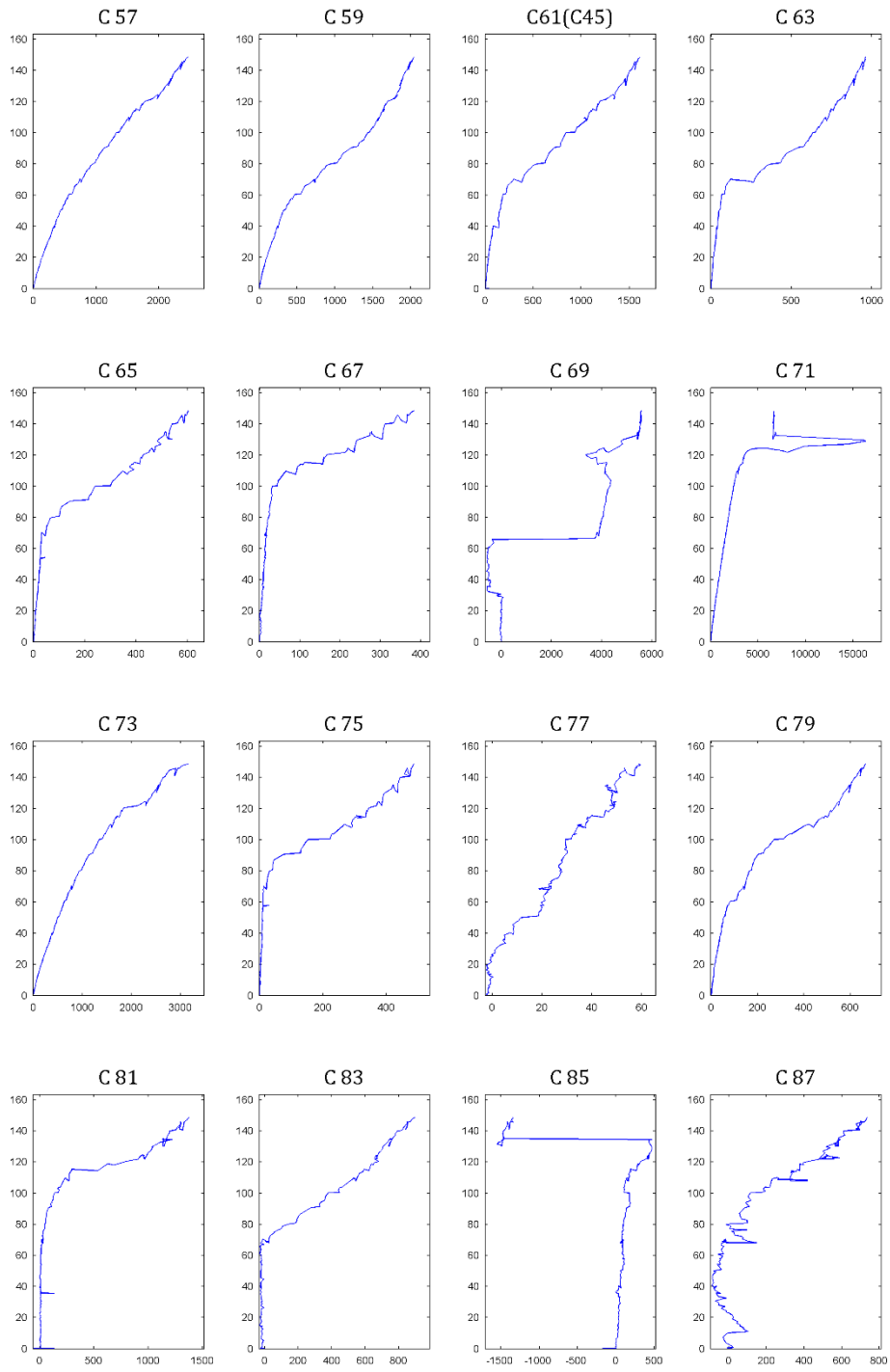

Fig. C4 - 9: Strain readings (C57 – C87)

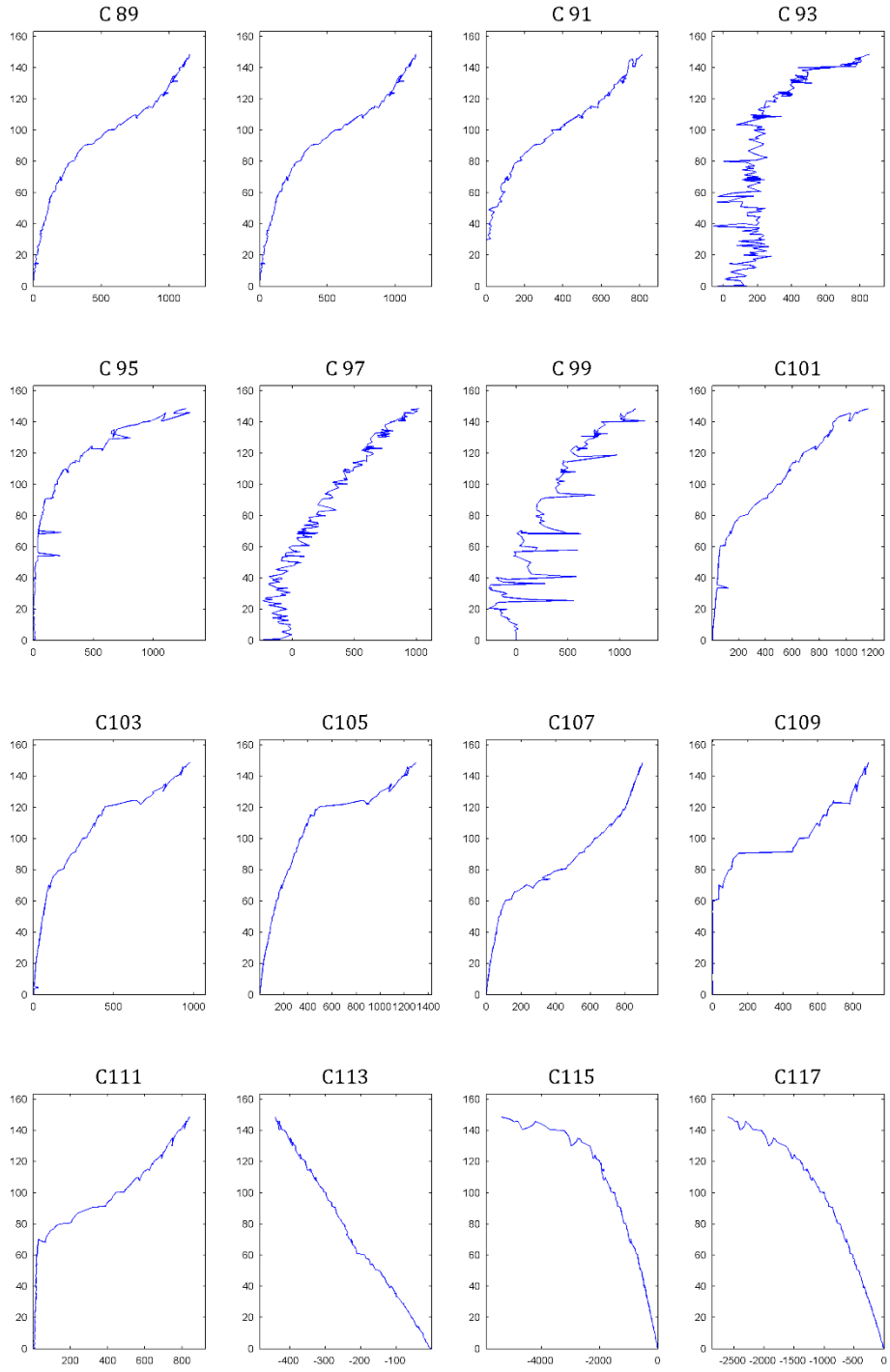

Fig. C4 - 10: Strain readings (C89 – C117)

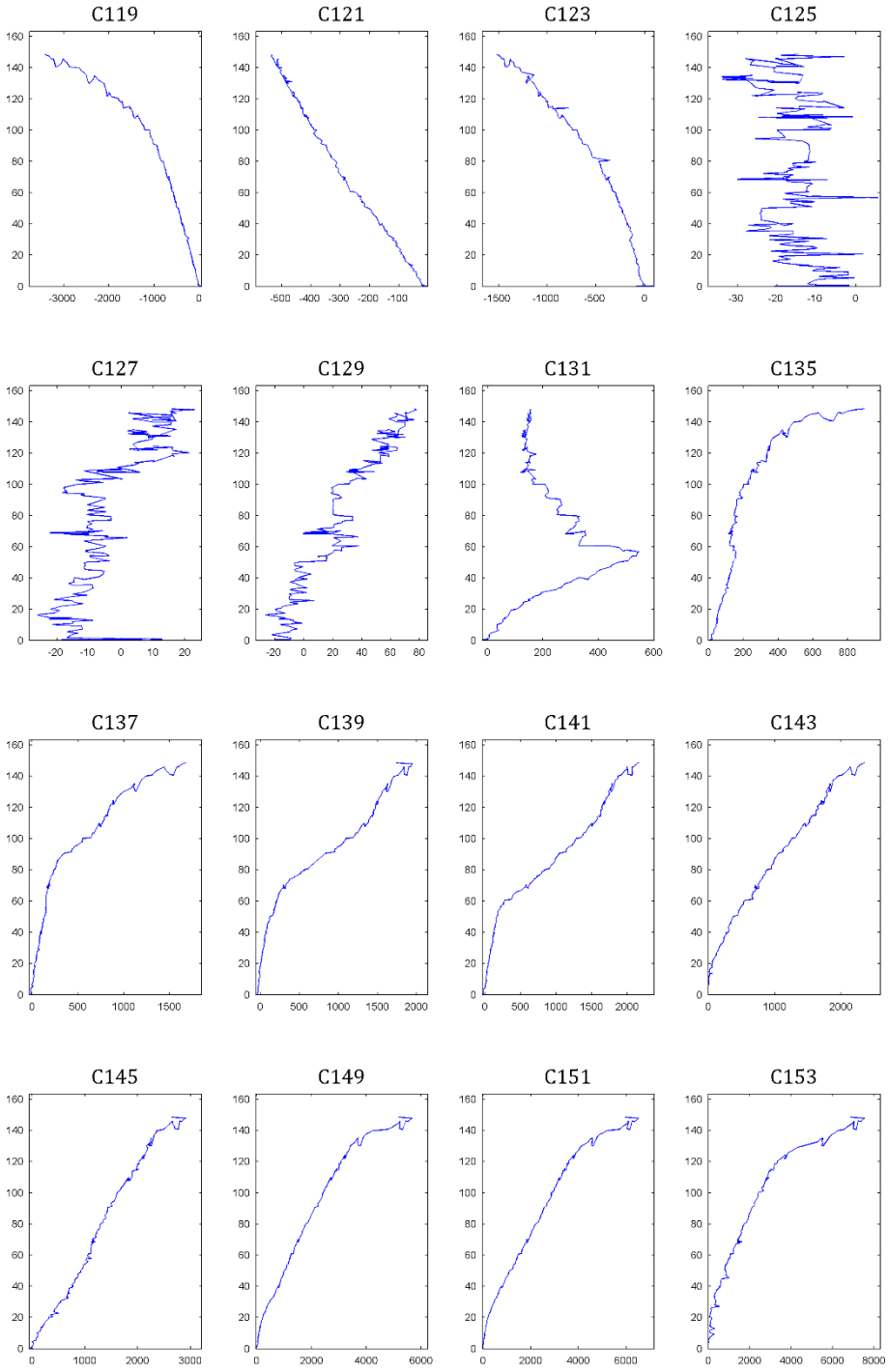

Fig. C4 - 11: Strain readings (C119 – C153)

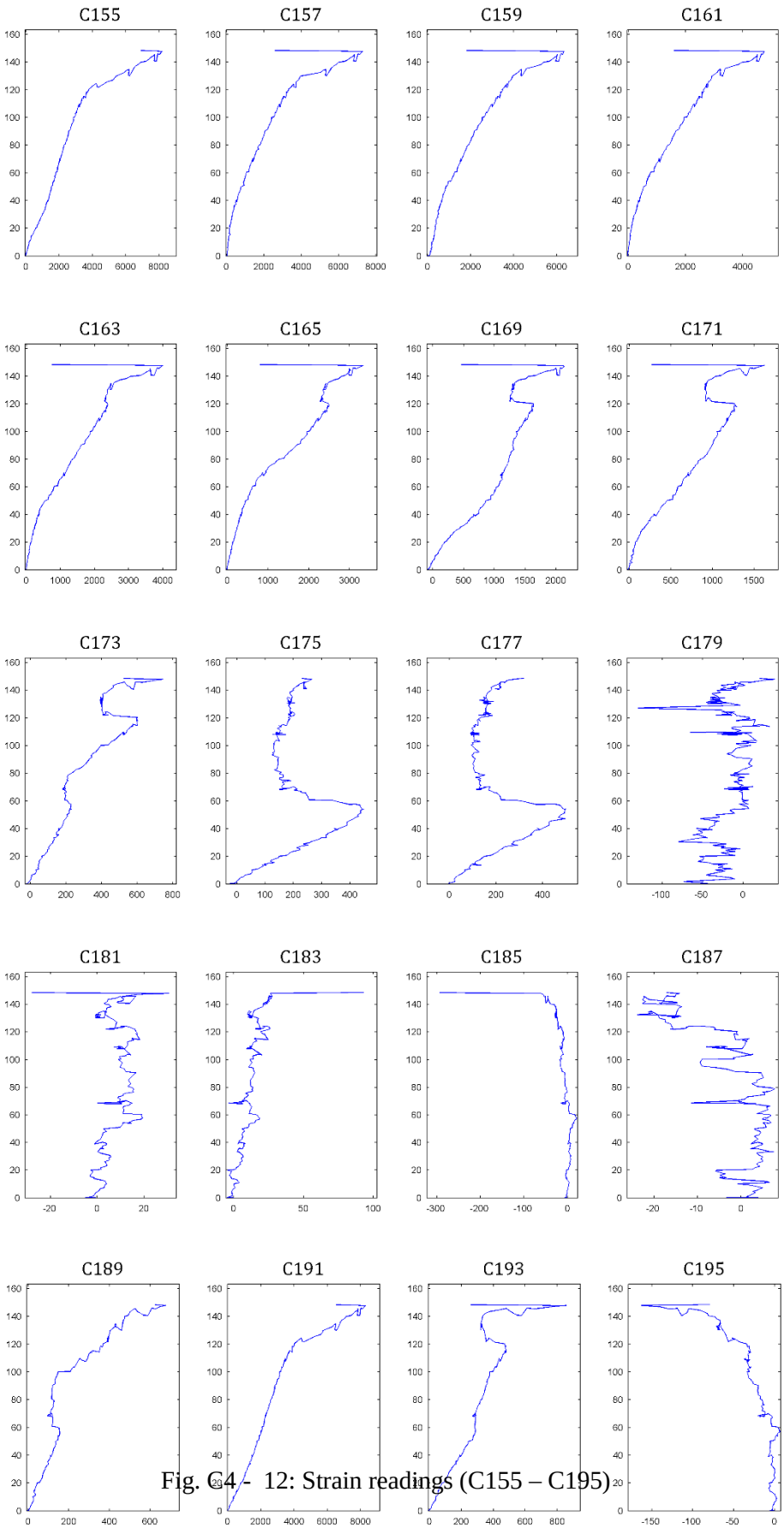

Fig. C4 - 12: Strain readings (C155 – C195)

C.4.7 LOAD-DEFLECTION

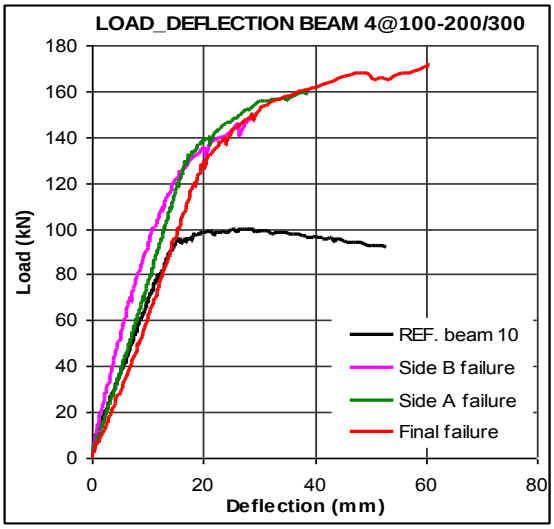

Fig. C4 - 13: Load deflection for Beam 4.

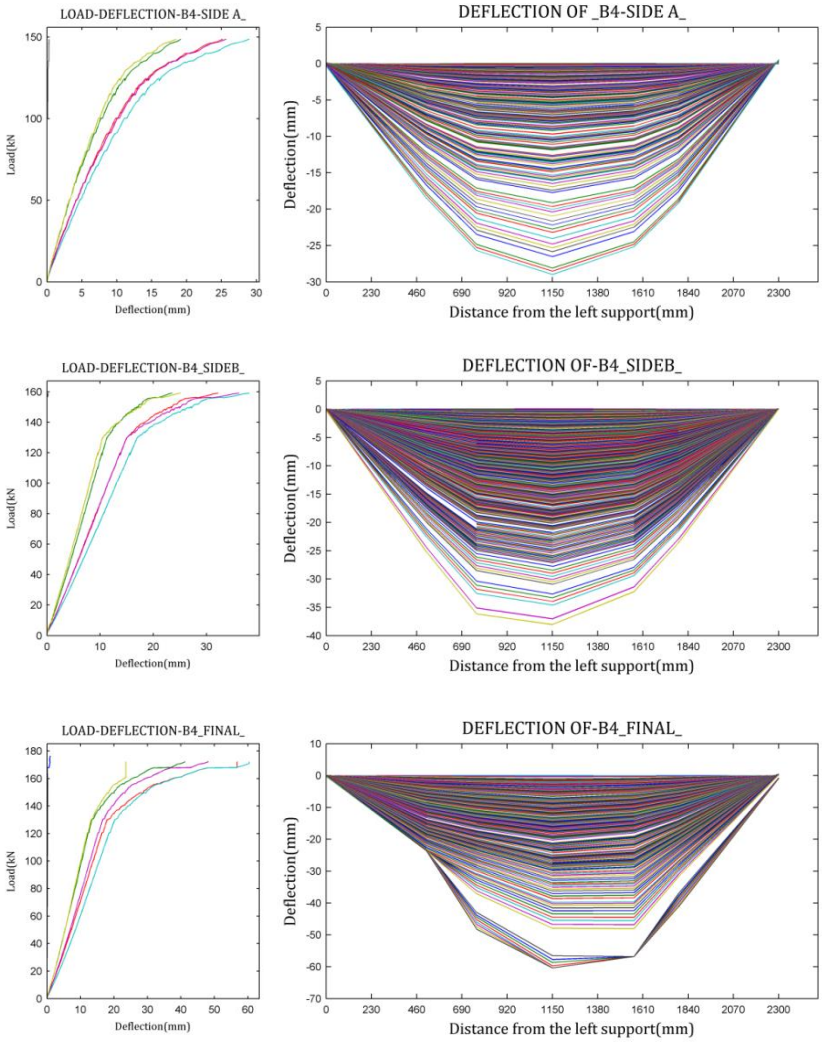

Fig. C4 - 14: Deflection profile

C.4.8 FIRST PHASE-SIDE A FAILURE

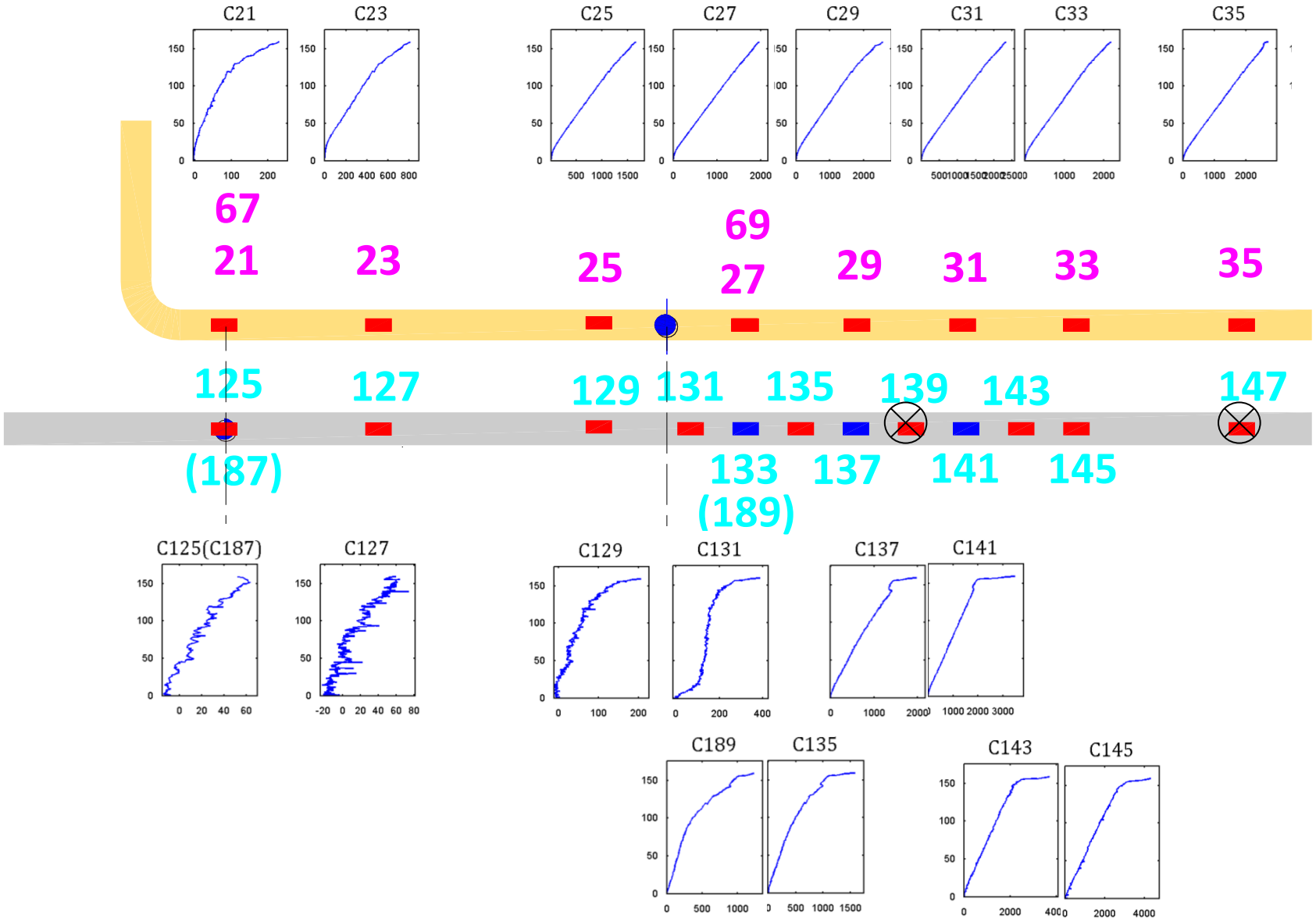

Fig. C4 - 15: Strains in FRP and the steel reinforcement along the side A and the end slips of FRP.

C.4.9 FIRST PHASE-SIDE B FAILURE

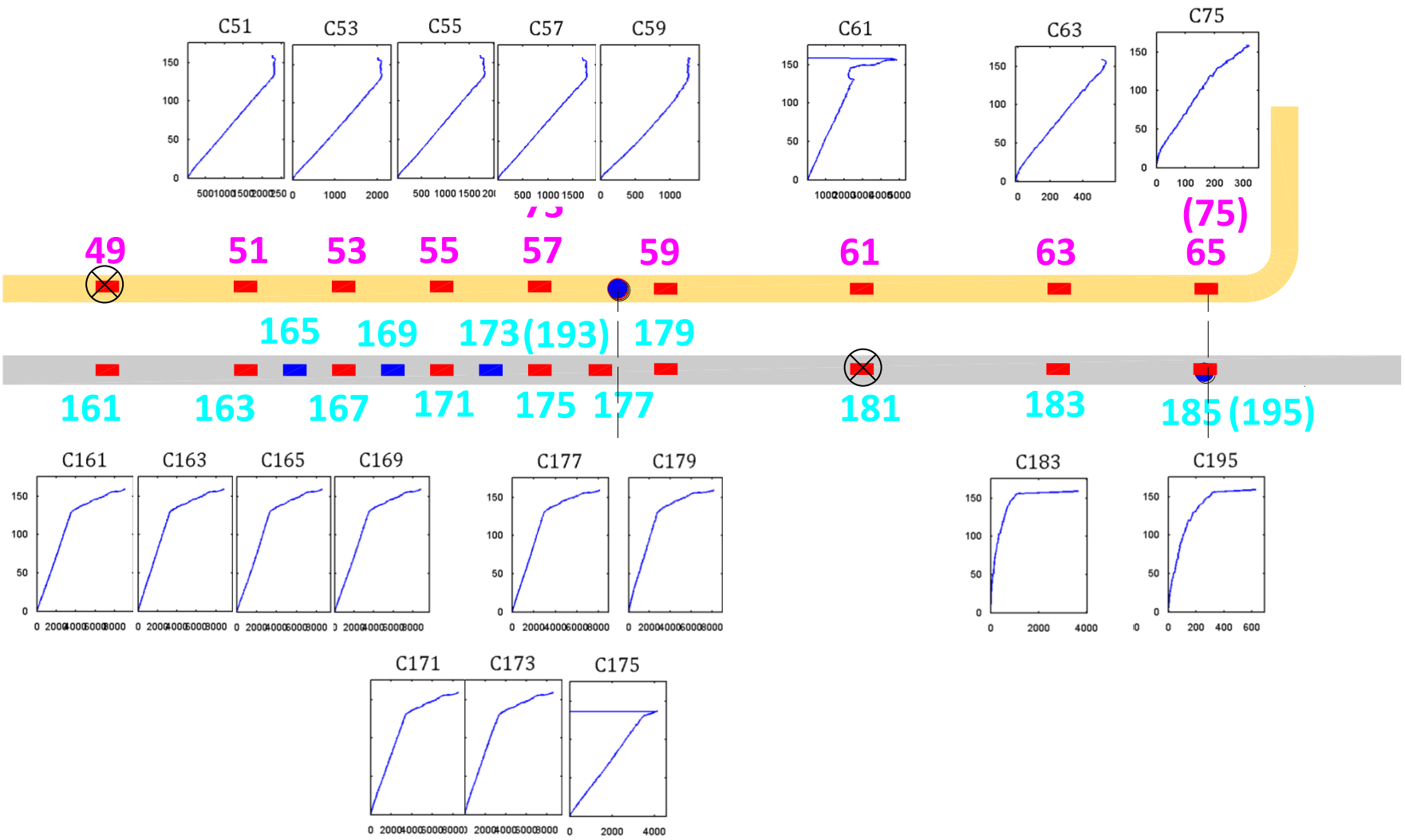

Fig. C4 - 16: Strains in FRP and the steel reinforcement along the side B and the end slips of FRP

C.4.10 3D PROFILE OF STRAIN AND BOND STRESS

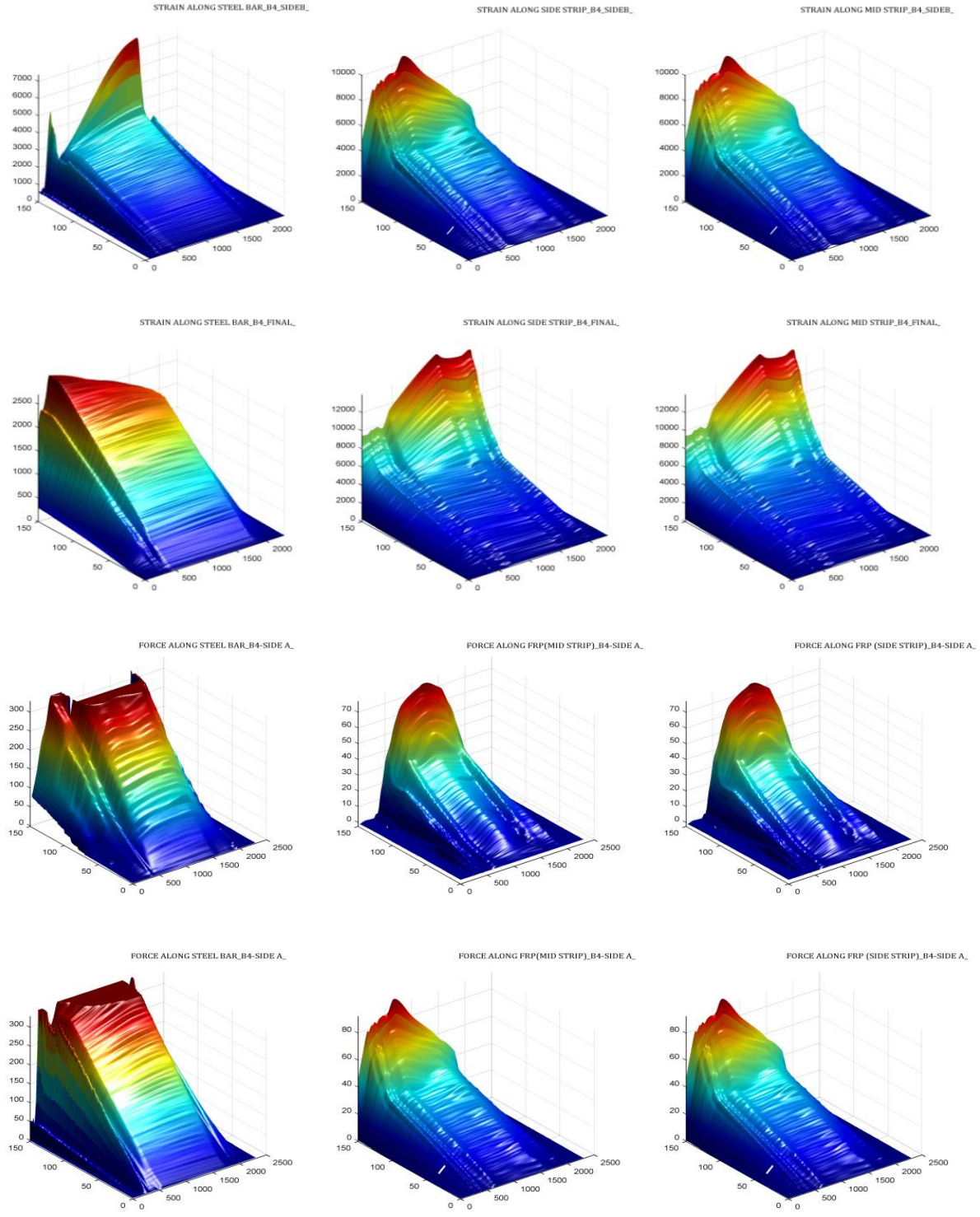

Fig. C4 - 17: Variation of forces and strain at different

C.4.11 STRAIN AND BOND STRESS PROFILES

(a)

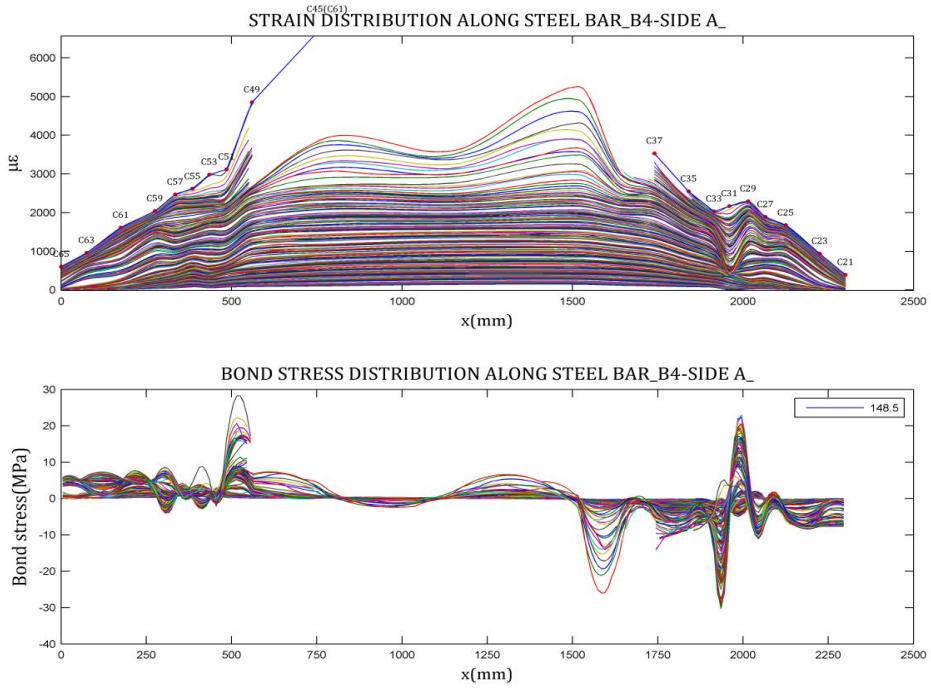

(b)

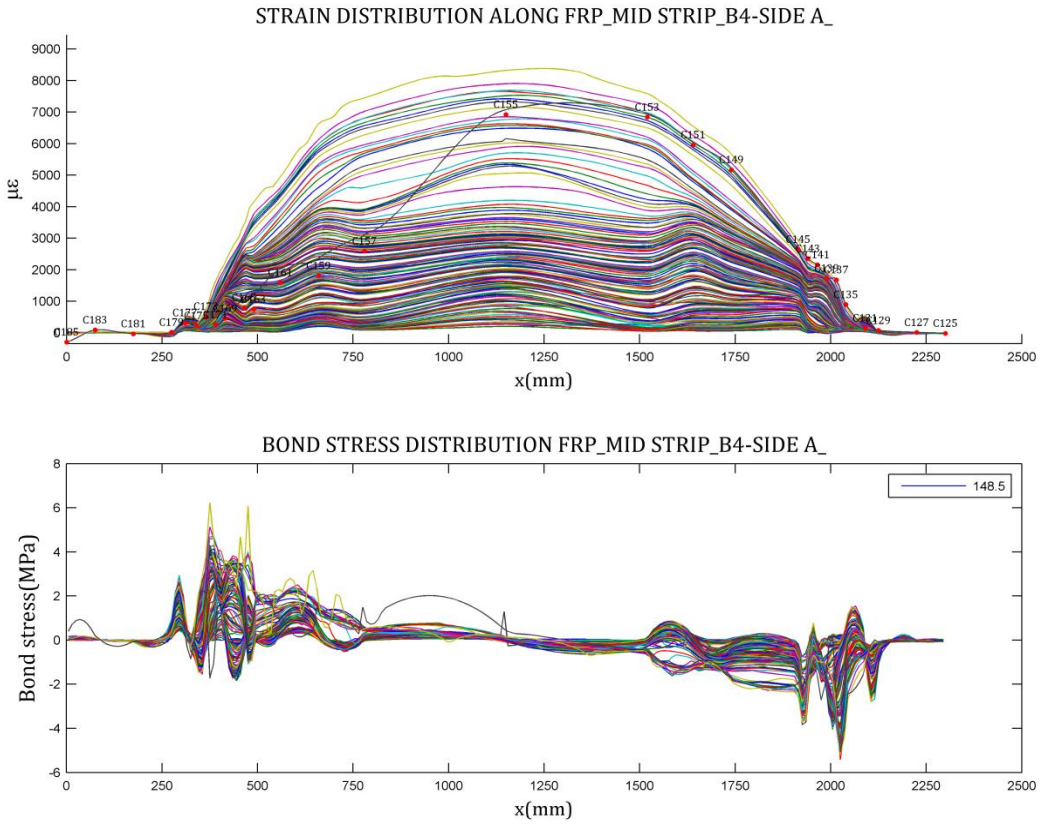

Fig. C4 - 18: Strain and bond stress profiles of (a) The steel reinforcement and (b) FRP.

C.4.12 STRAINS IN THE STEEL REINFORCEMENT AND FRP ALONG THE SPAN

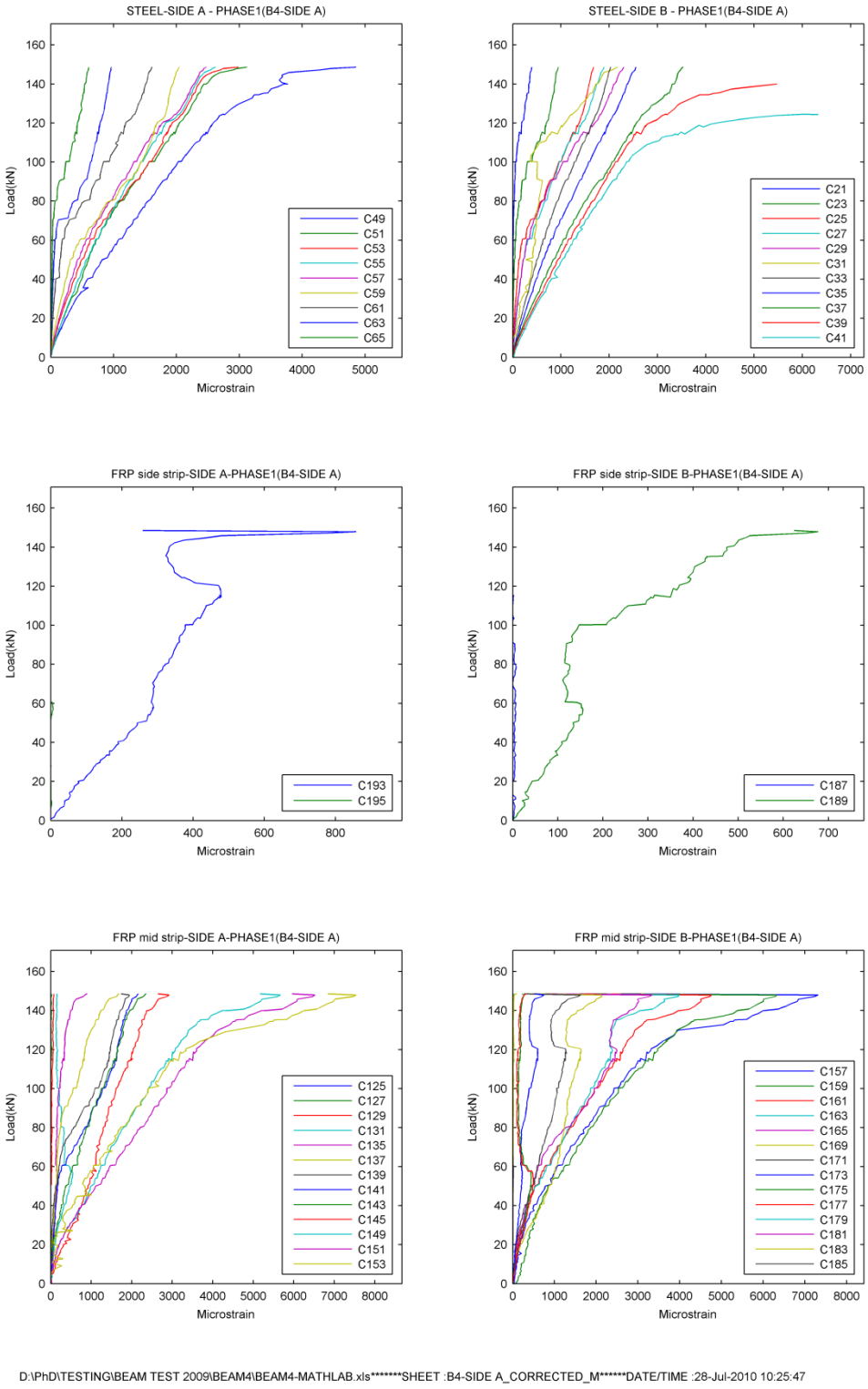

Fig. C4 - 19: Strains in the steel reinforcement and FRP along the span.

C.4.13 READINGS OF LVDTs

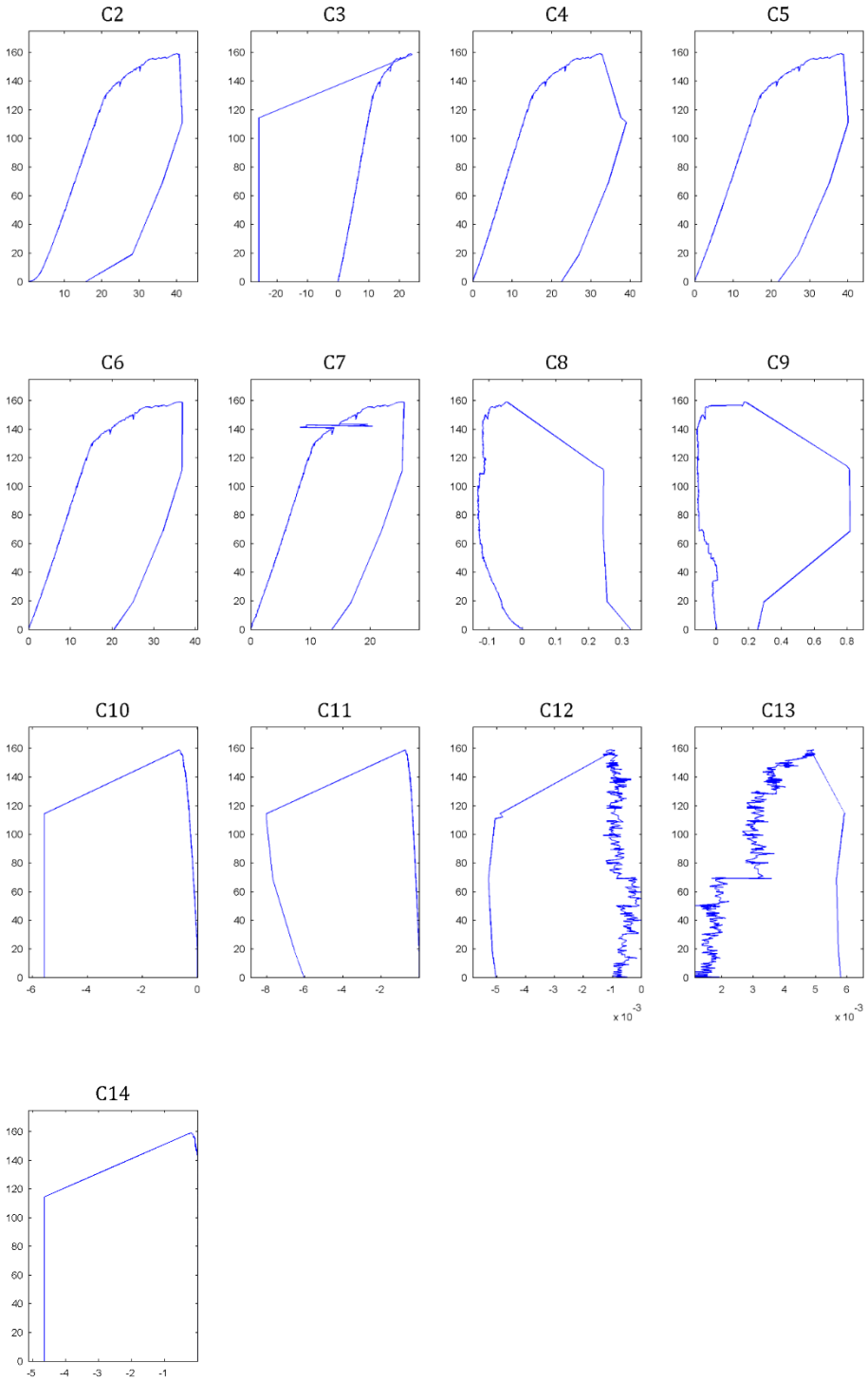

Fig. C4 - 20: Readings of LVDTs (C2 – C14)

C.4.14 SECOND PHASE – STRAIN READINGS

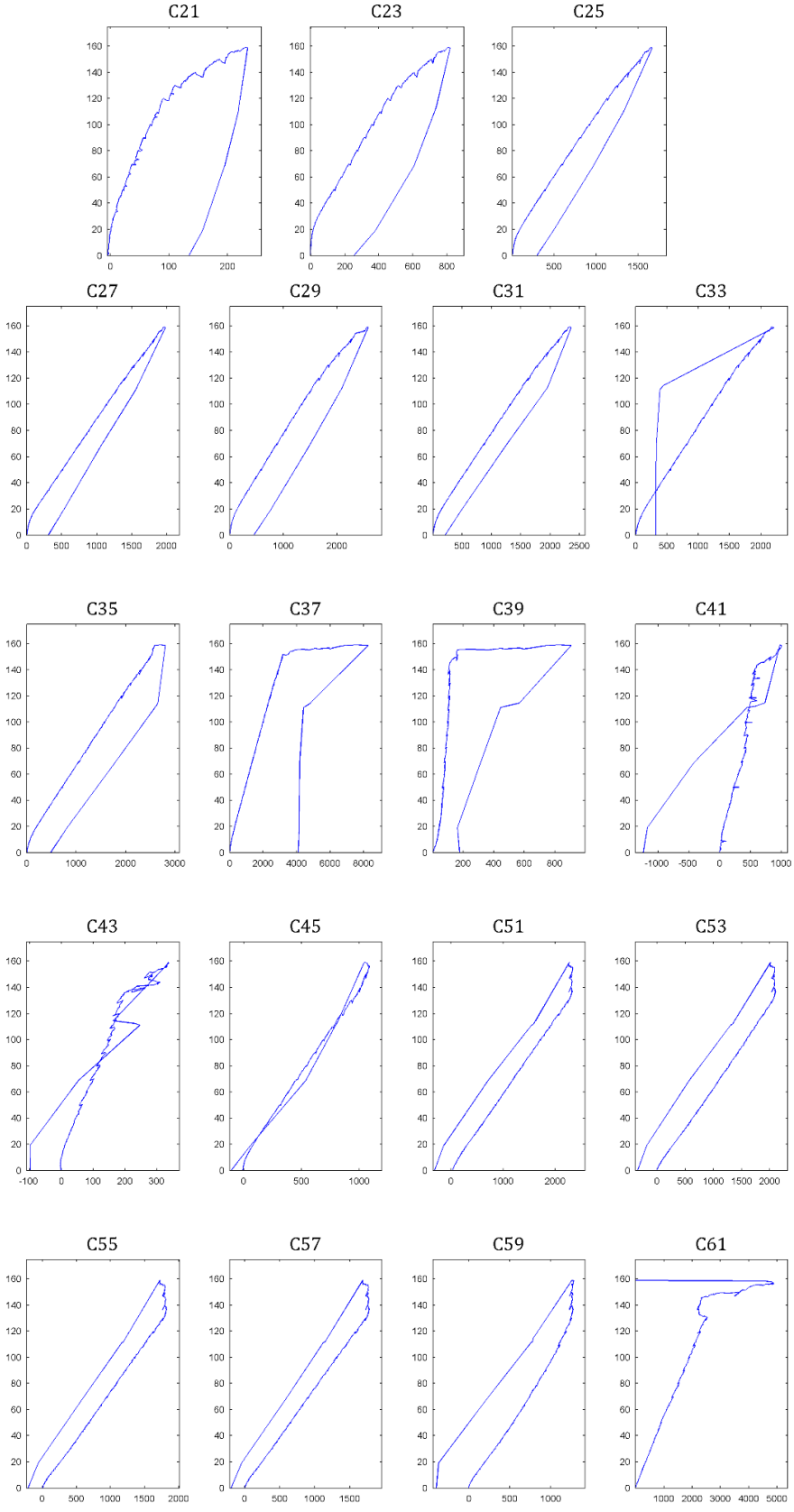

Fig. C4 - 21: Strain readings (C21-C61)

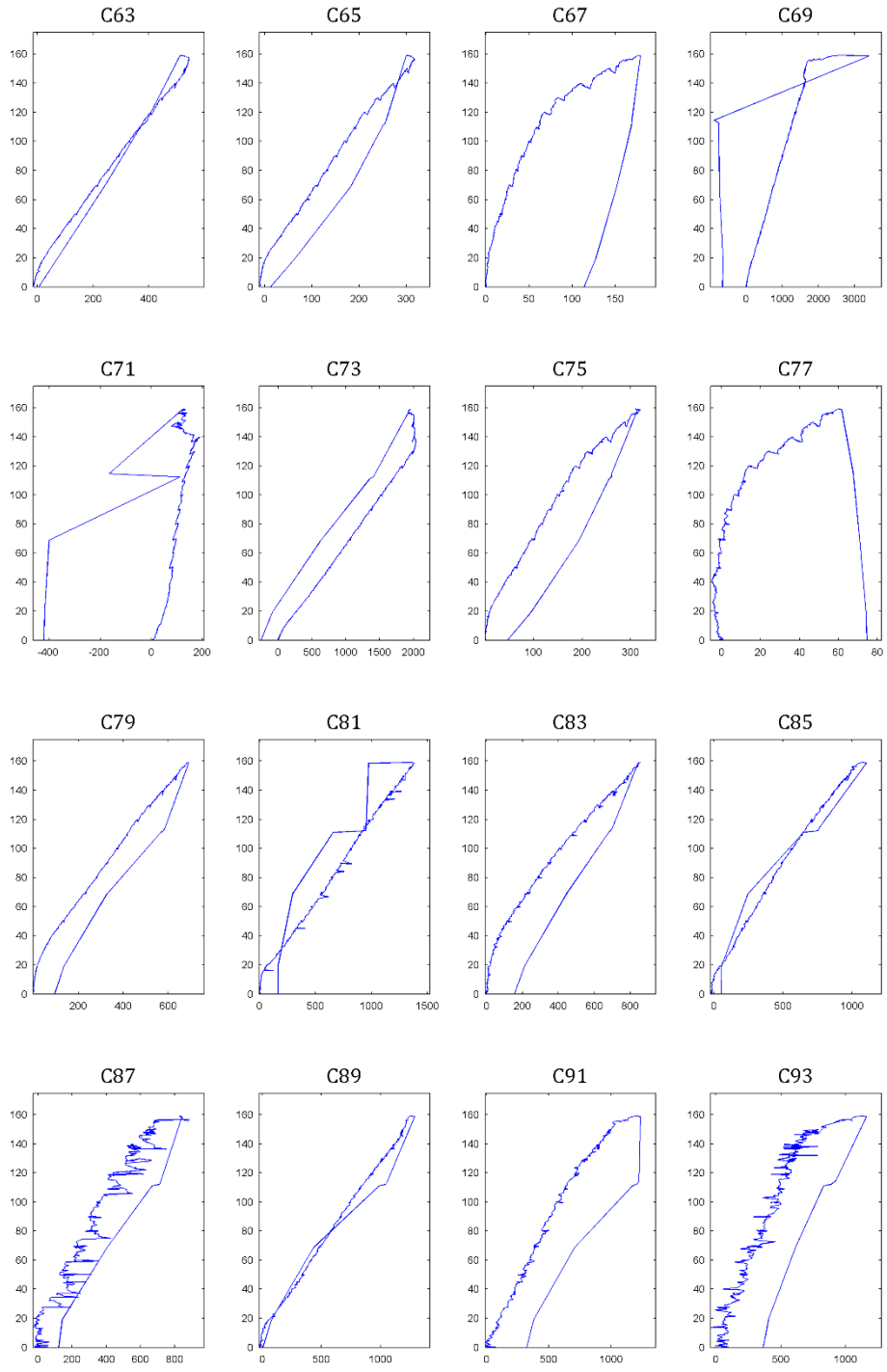

Fig. C4 - 22: Strain readings (C63-C93)

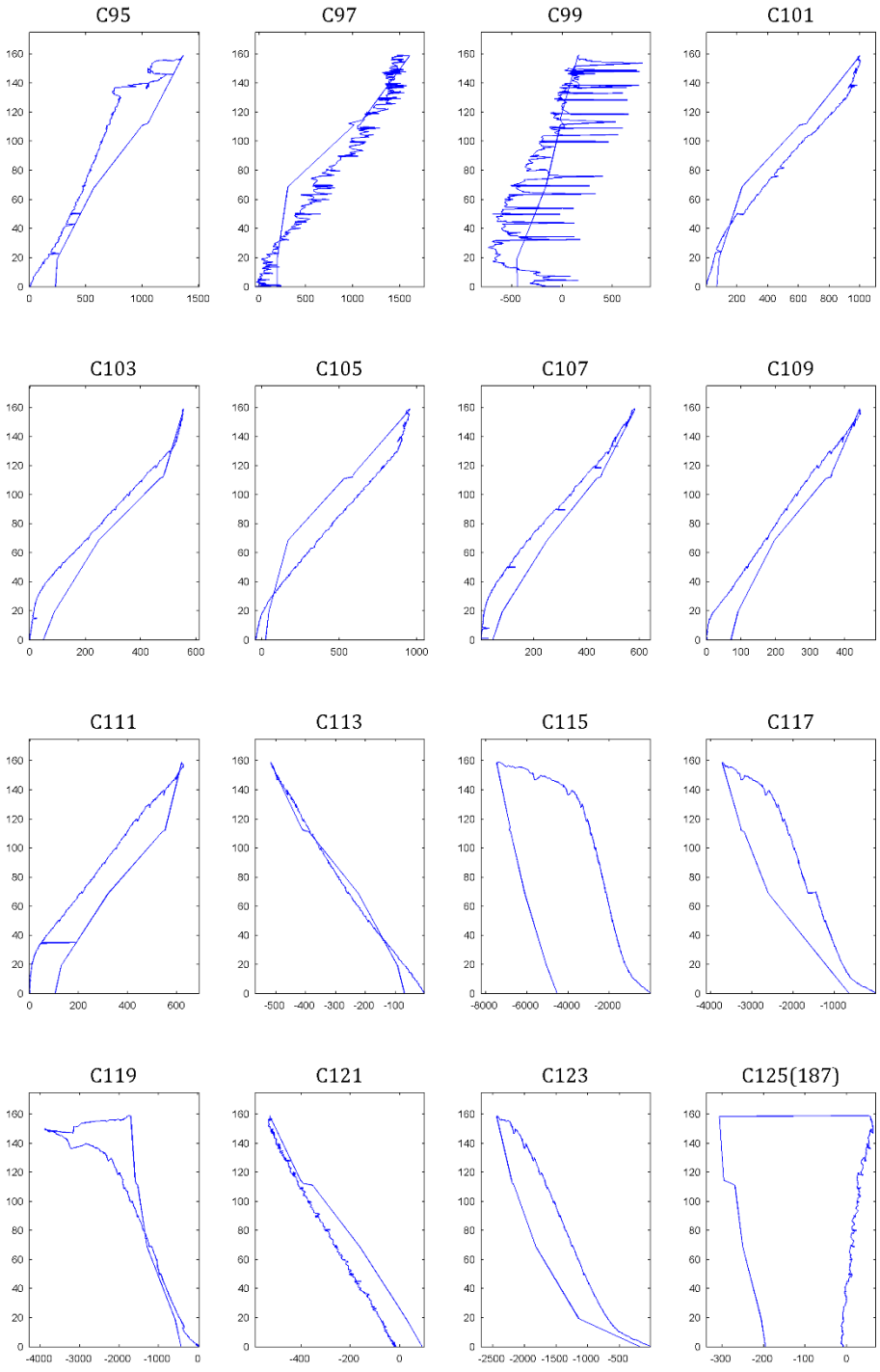

Fig. C4 - 23: Strain readings (C95-C125)

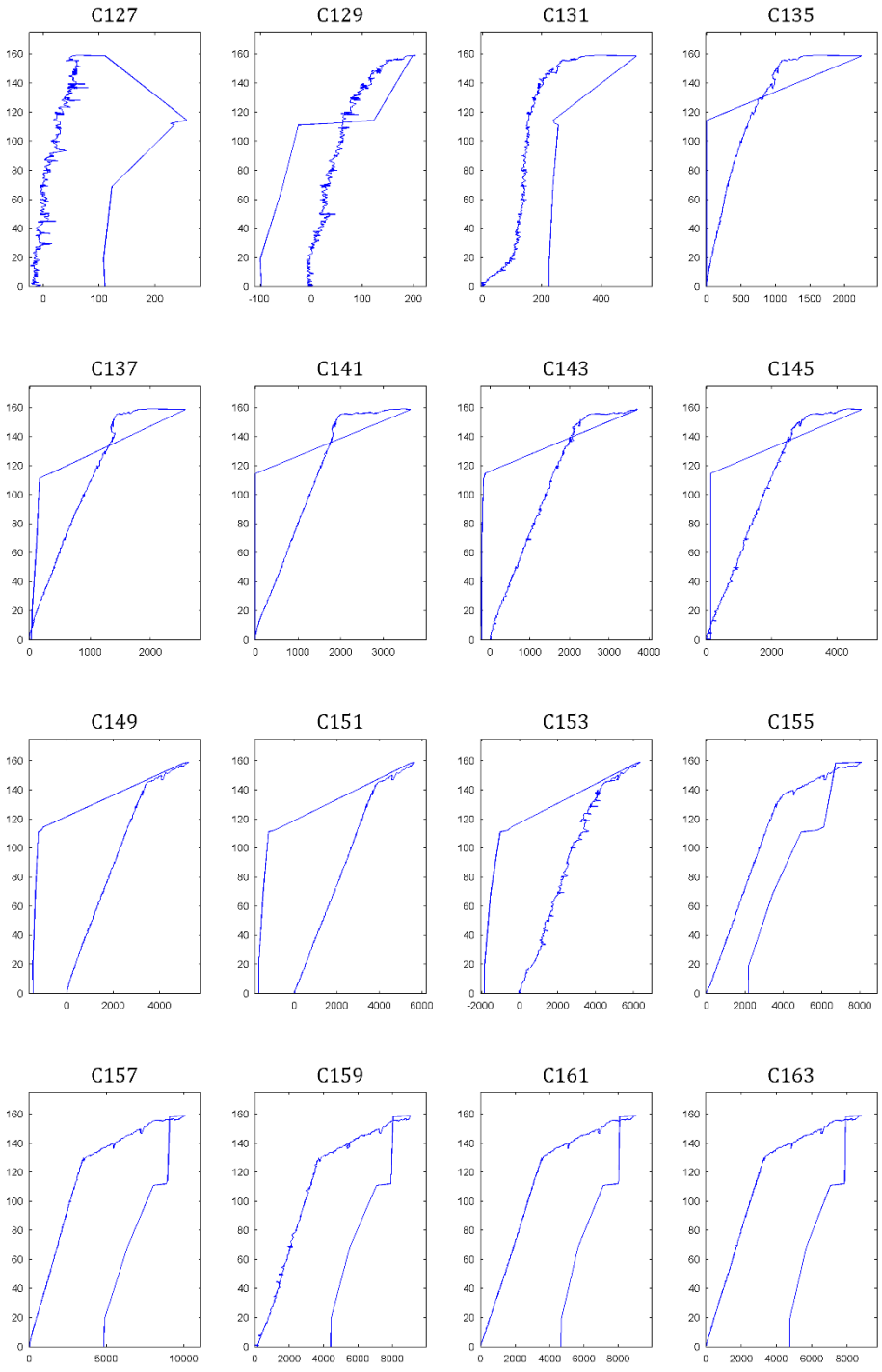

Fig. C4 - 24: Strain readings (C127-C163)

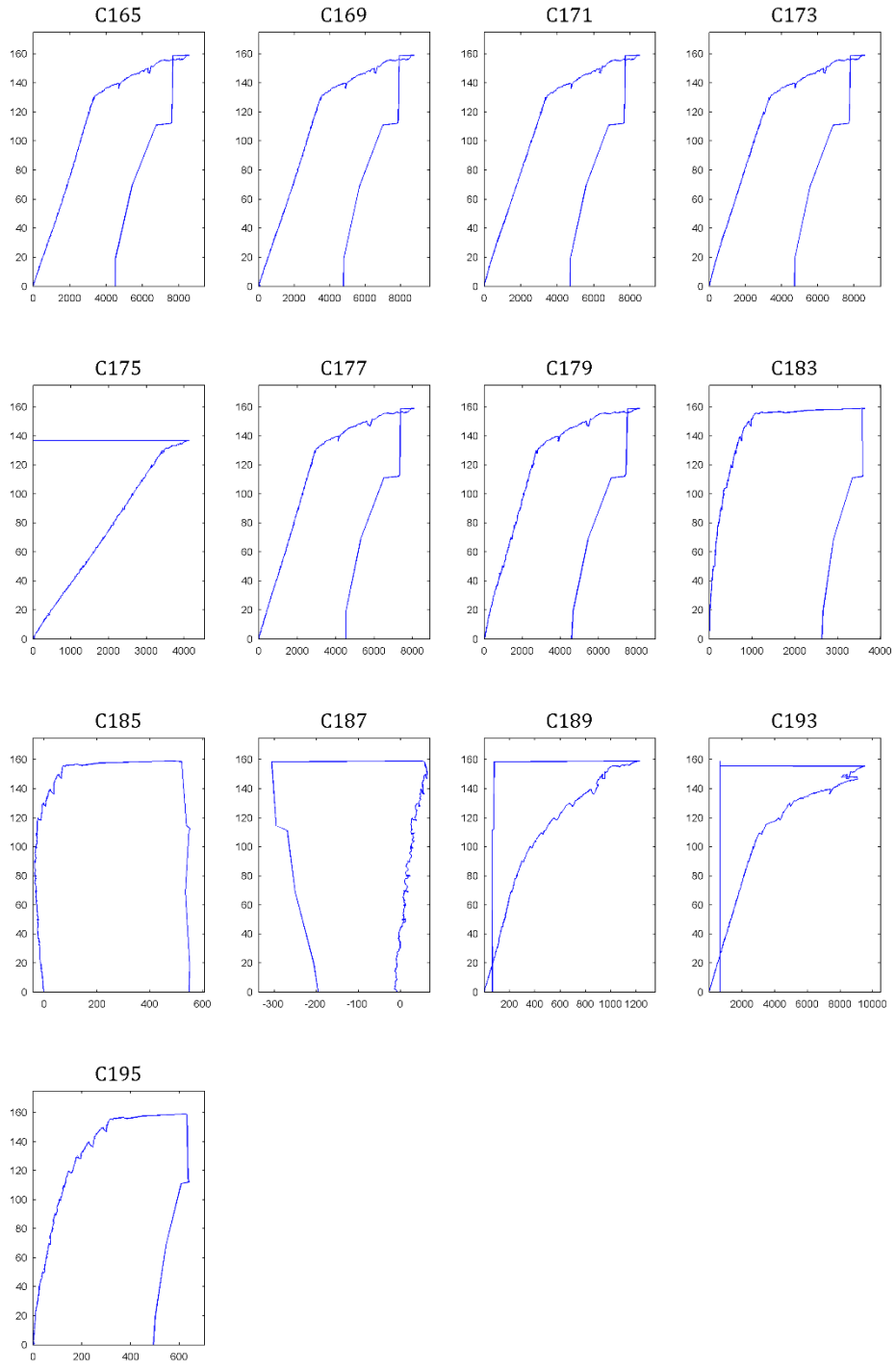

Fig. C4 - 25: Strain readings (C165-C195)

C.4.15 3D PROFILE OF STRAIN AND BOND STRESS

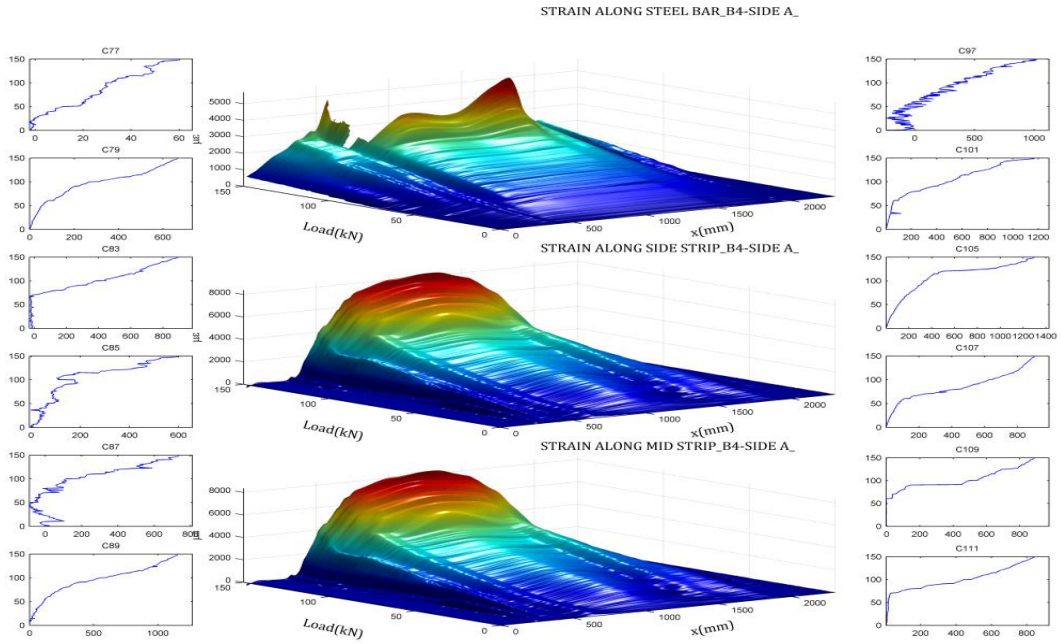

Fig. C4 - 26: Variation of strain along the side A.

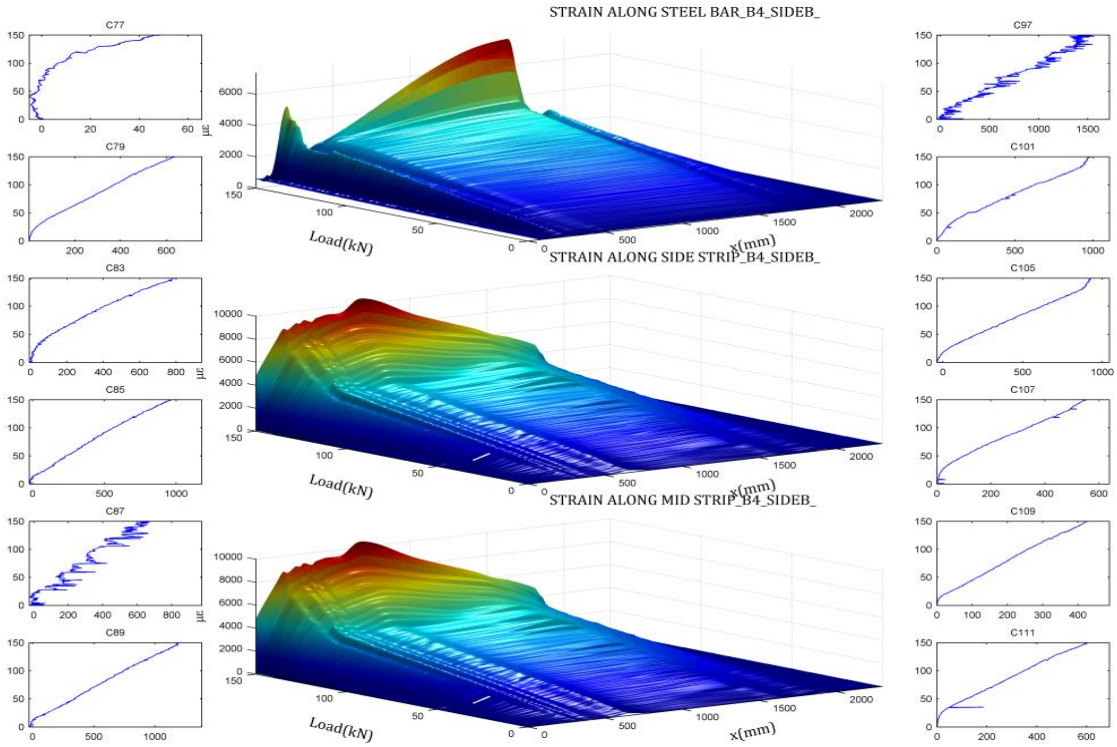

Fig. C4 - 27: Variation of strain along the side B.

C.4.16 STRAINS IN THE STEEL REINFORCEMENT AND FRP ALONG THE SPAN

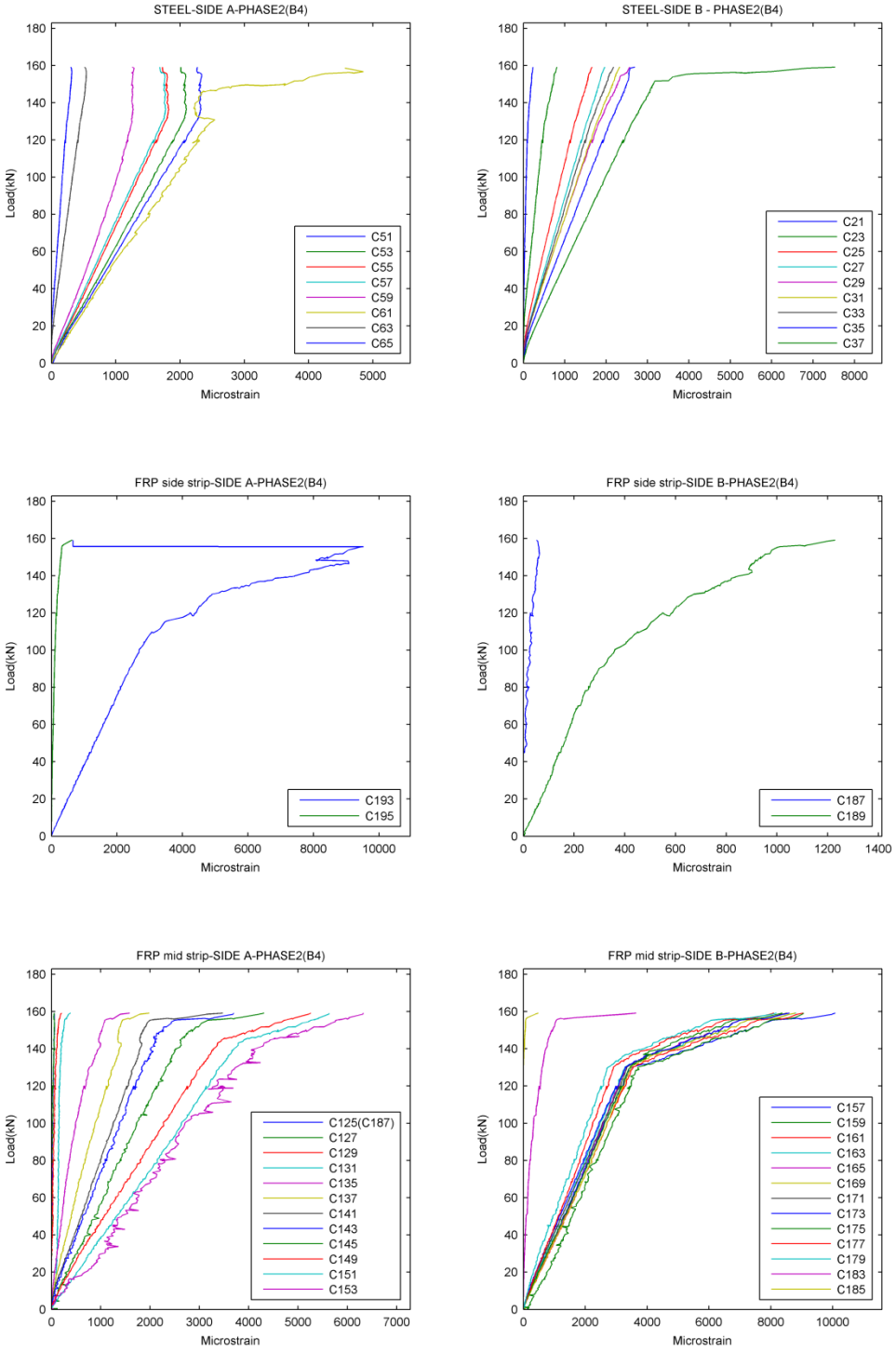

Fig. C4 - 28: Strains in the steel reinforcement and FRP along the span.

C.4.17 3D PROFILE OF STRAIN AND BOND STRESS

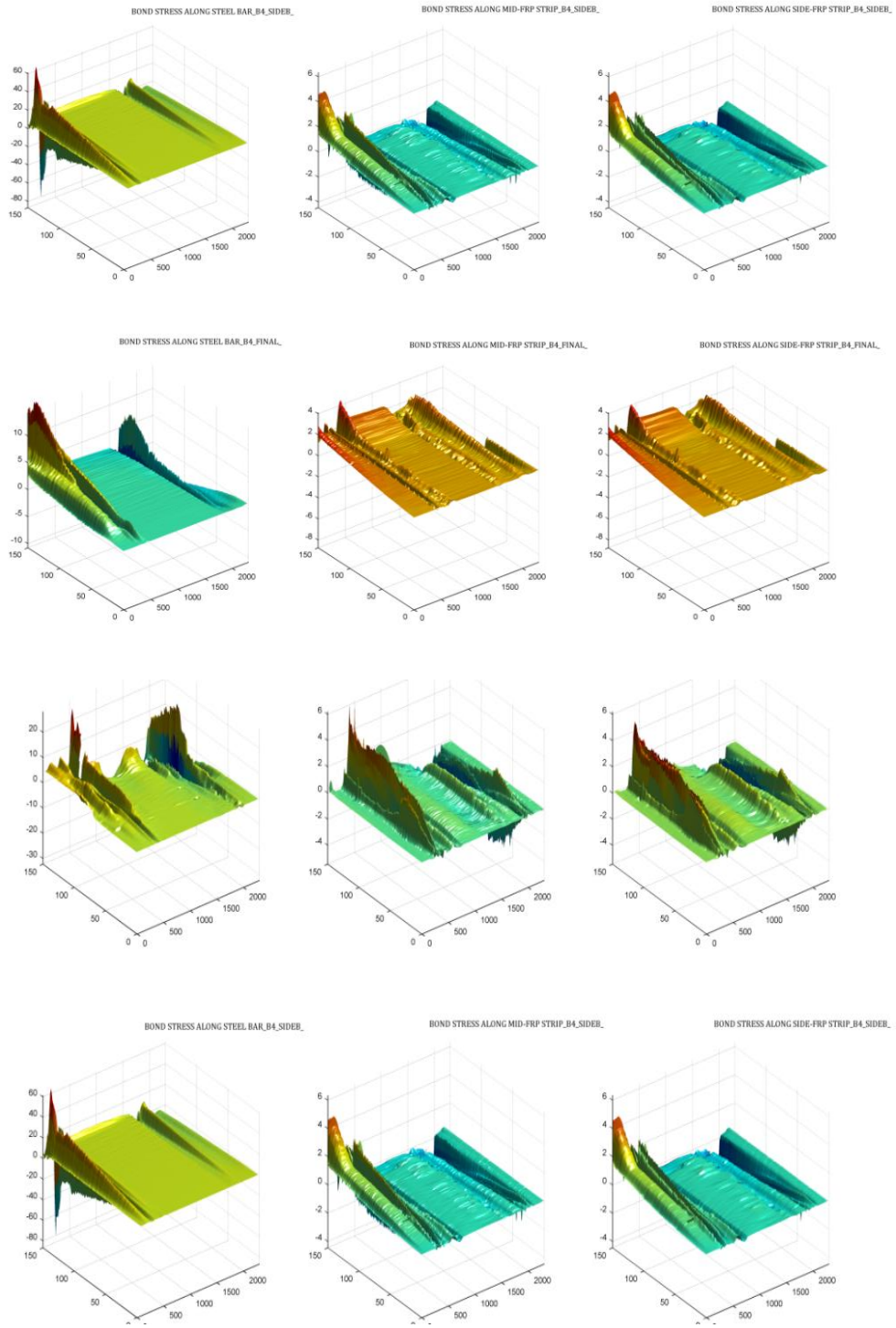

Fig. C4 - 29: Variation of strain and bond stress along the reinforcement and FRP at different load level.

C.4.18 STRAINS IN THE STEEL REINFORCEMENT AND FRP ALONG THE SPAN

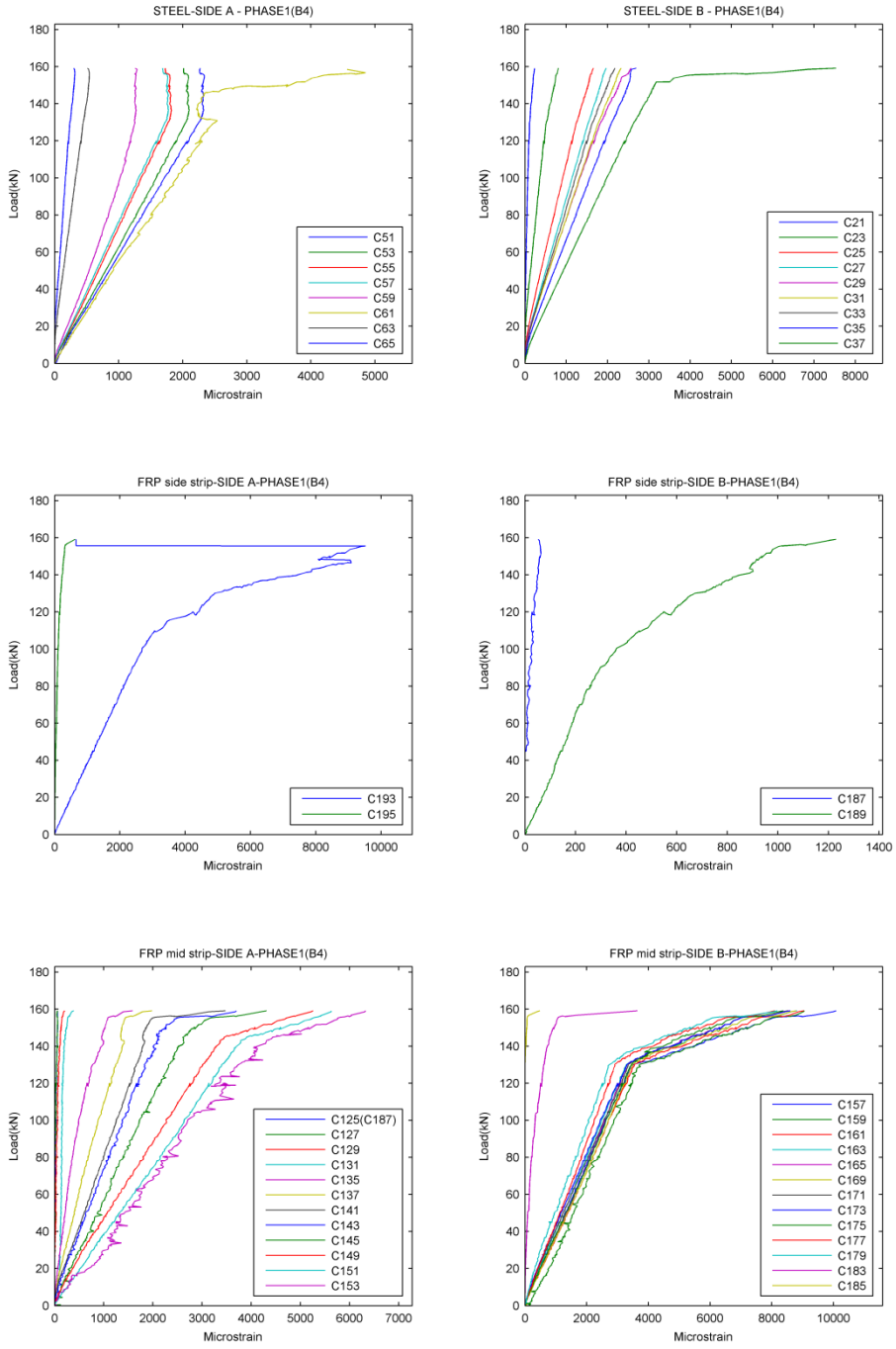

Fig. C4 - 30: Strains in the steel reinforcement and FRP along the span.

C.4.19 FINAL TESTING PHASE-READINGS OF LVDTs

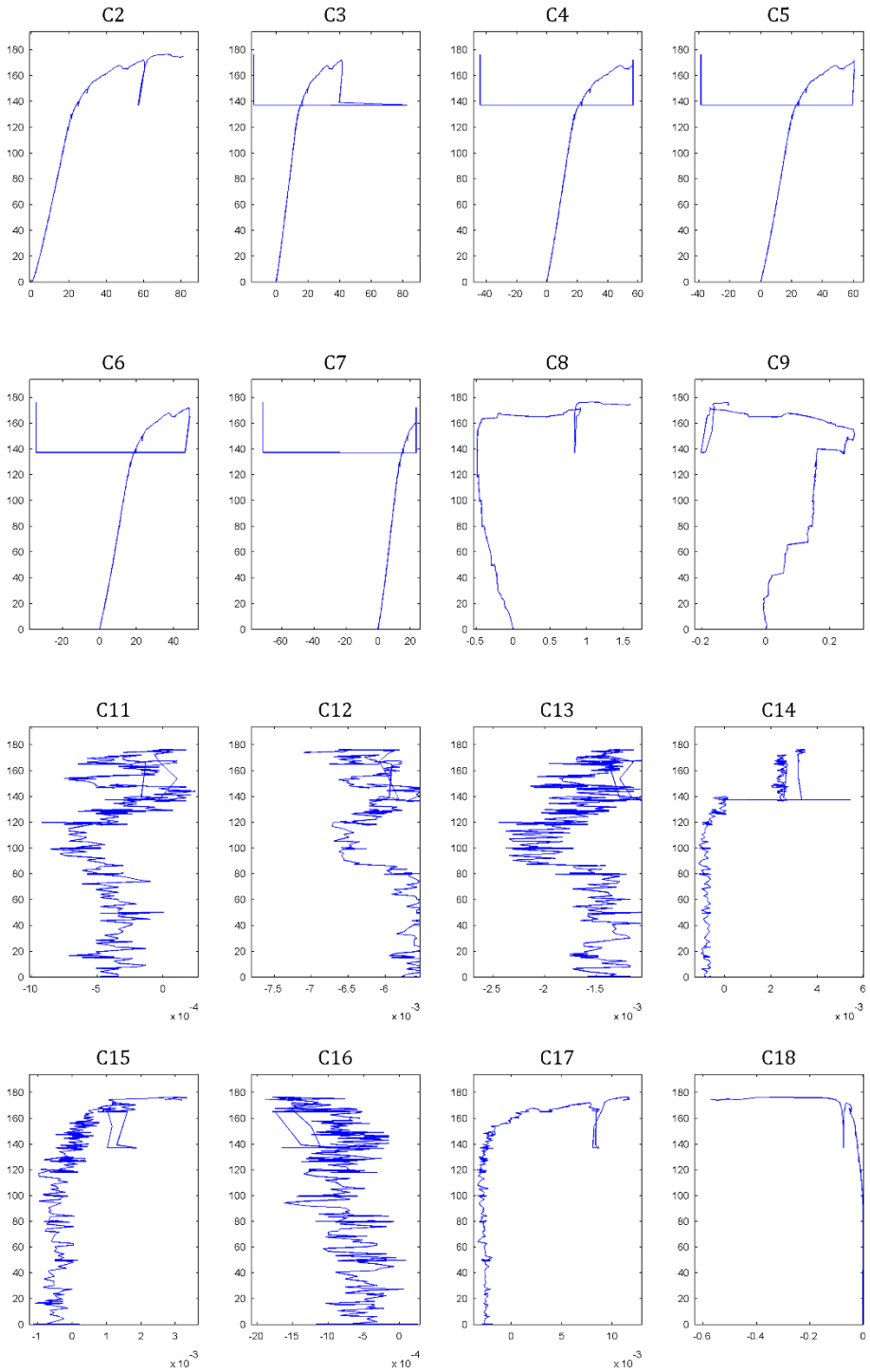

Fig. C4 - 31: Readings of LVDTs (C2 – C18)

C.4.20 FINAL TESTING PHASE-STRAIN READINGS

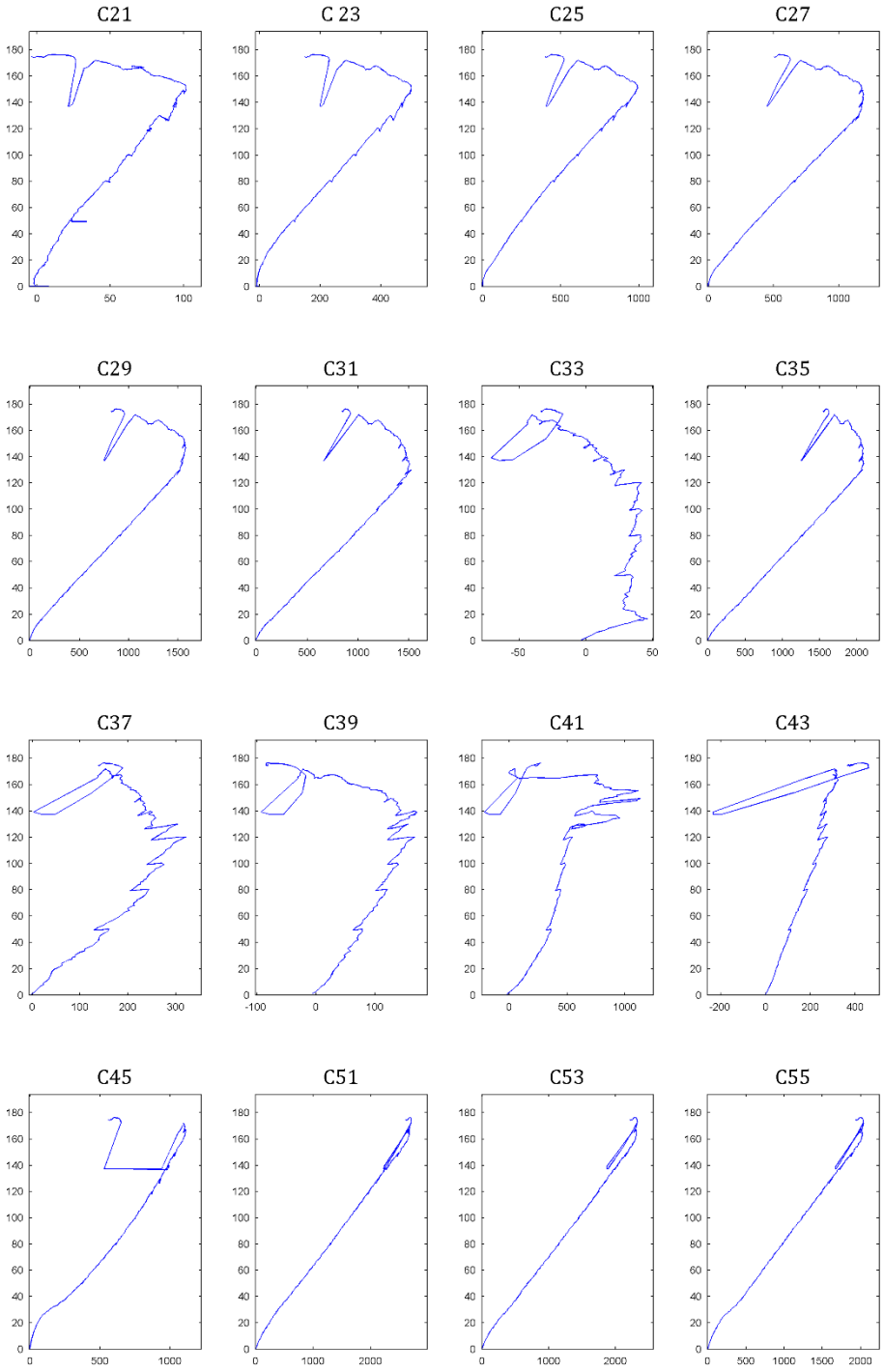

Fig. C4 - 32: Strain readings (C21-C55)

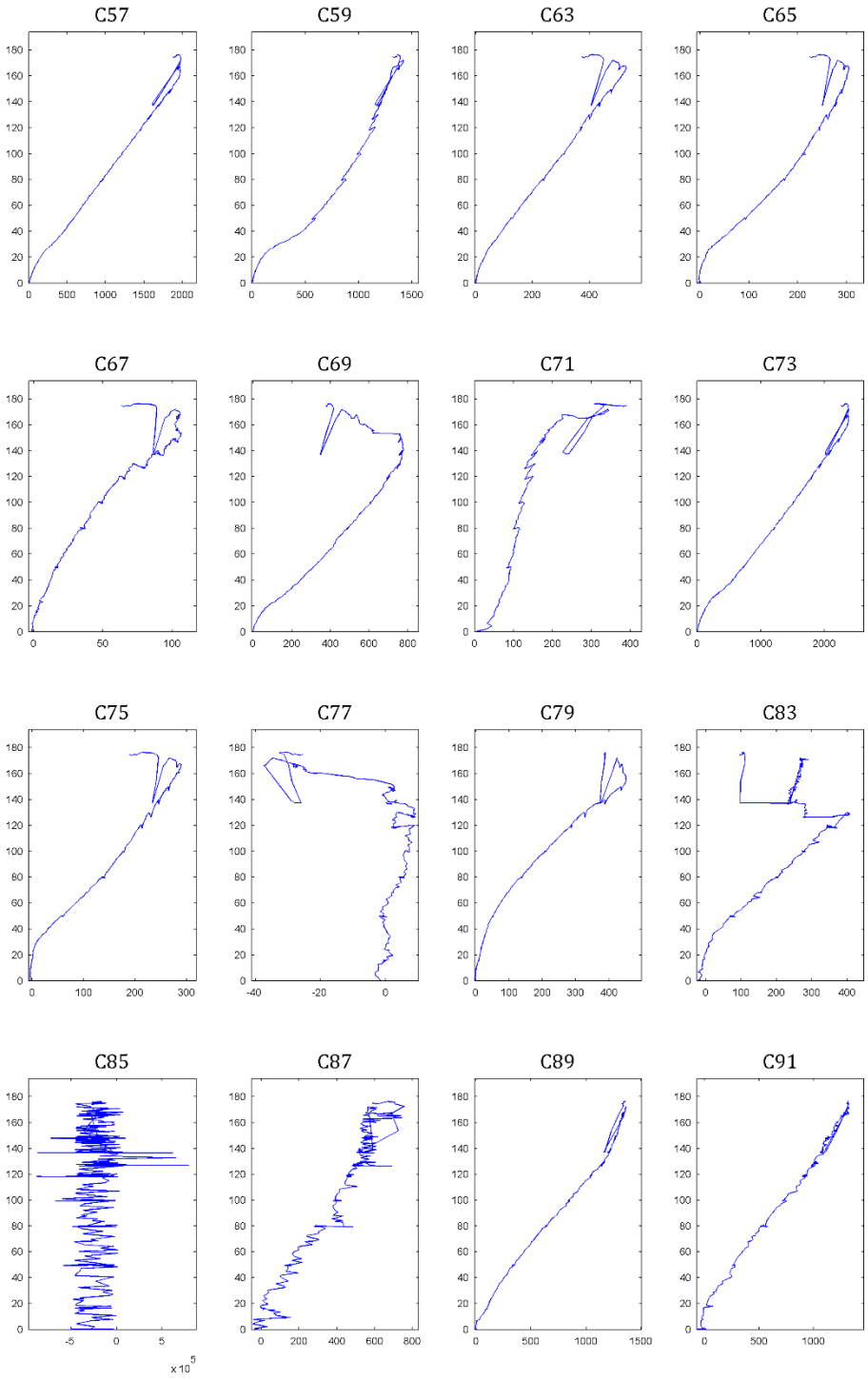

Fig. C4 - 33: Strain readings (C57-C91)

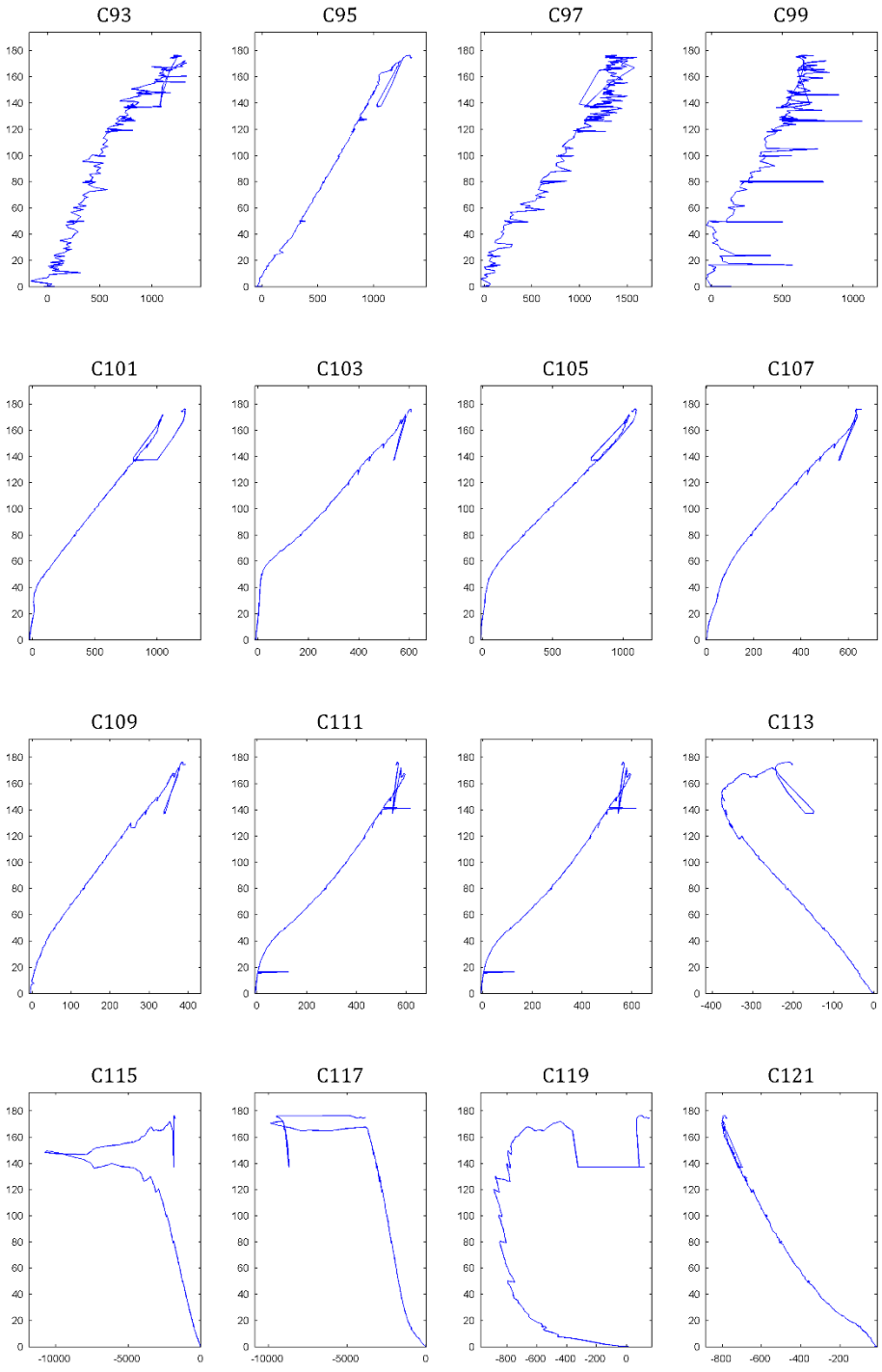

Fig. C4 - 34: Strain readings (C93-C121)

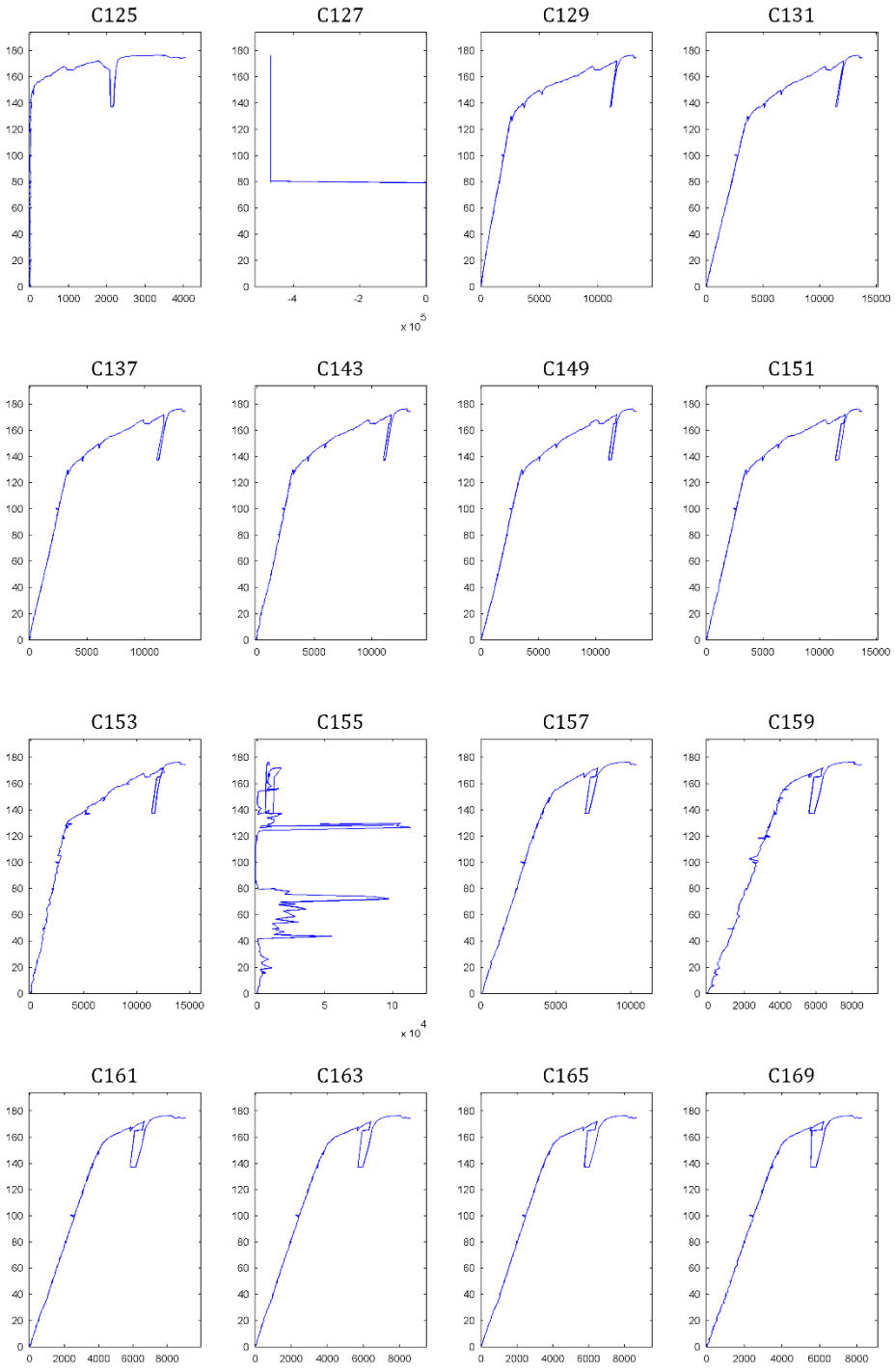

Fig. C4 - 35: Strain readings (C125-C169)

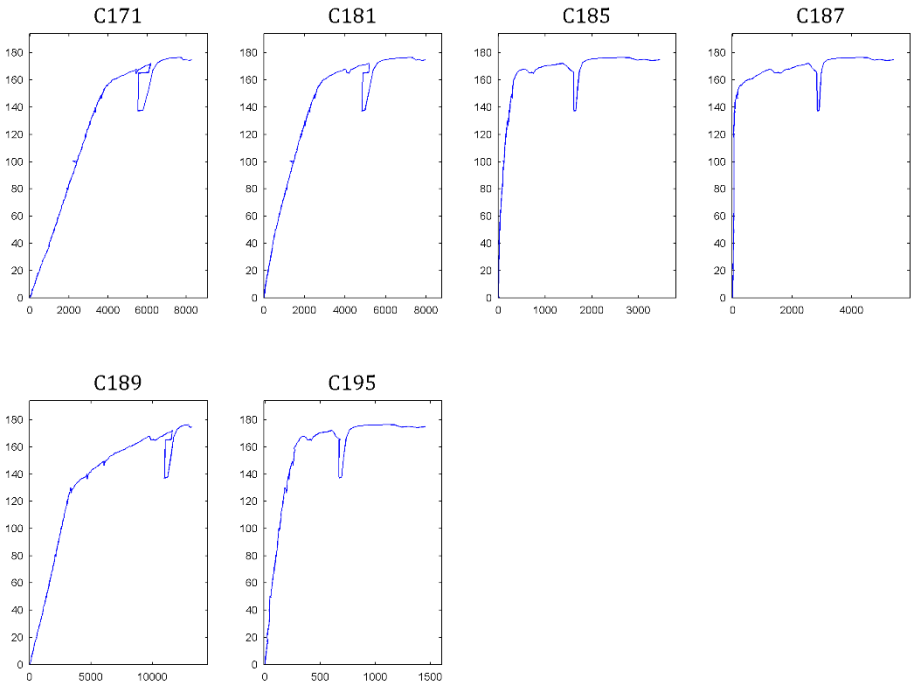

Fig. C4 - 36: Strain readings (C171-C195)

C.4.21 3D PROFILE OF FORCES

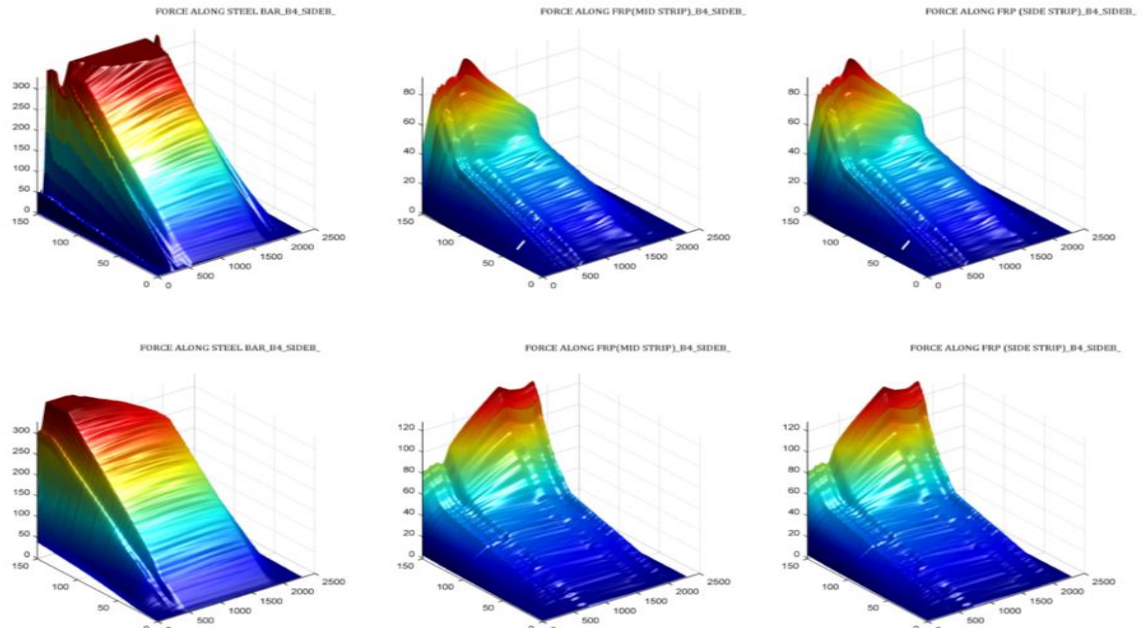

Fig. C4 - 37: Variations of forces along the steel reinforcement and FRP

C.4.22 STRAIN AND BOND STRESS PROFILES

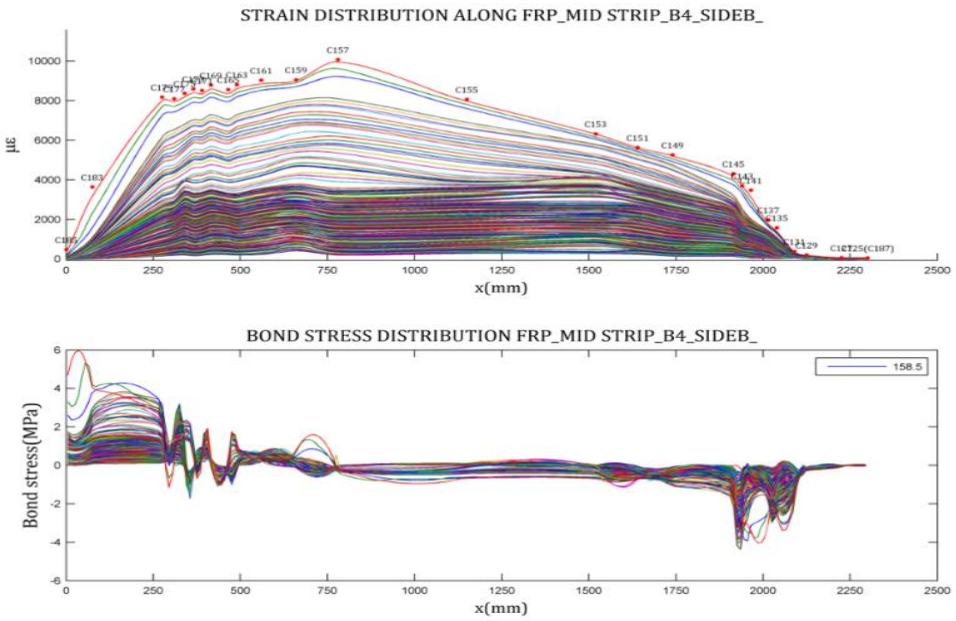

Fig. C4 - 38: Strain and bond stress profiles of FRP.

C.4.23 STRAINS IN THE STEEL REINFORCEMENT AND FRP ALONG THE SPAN

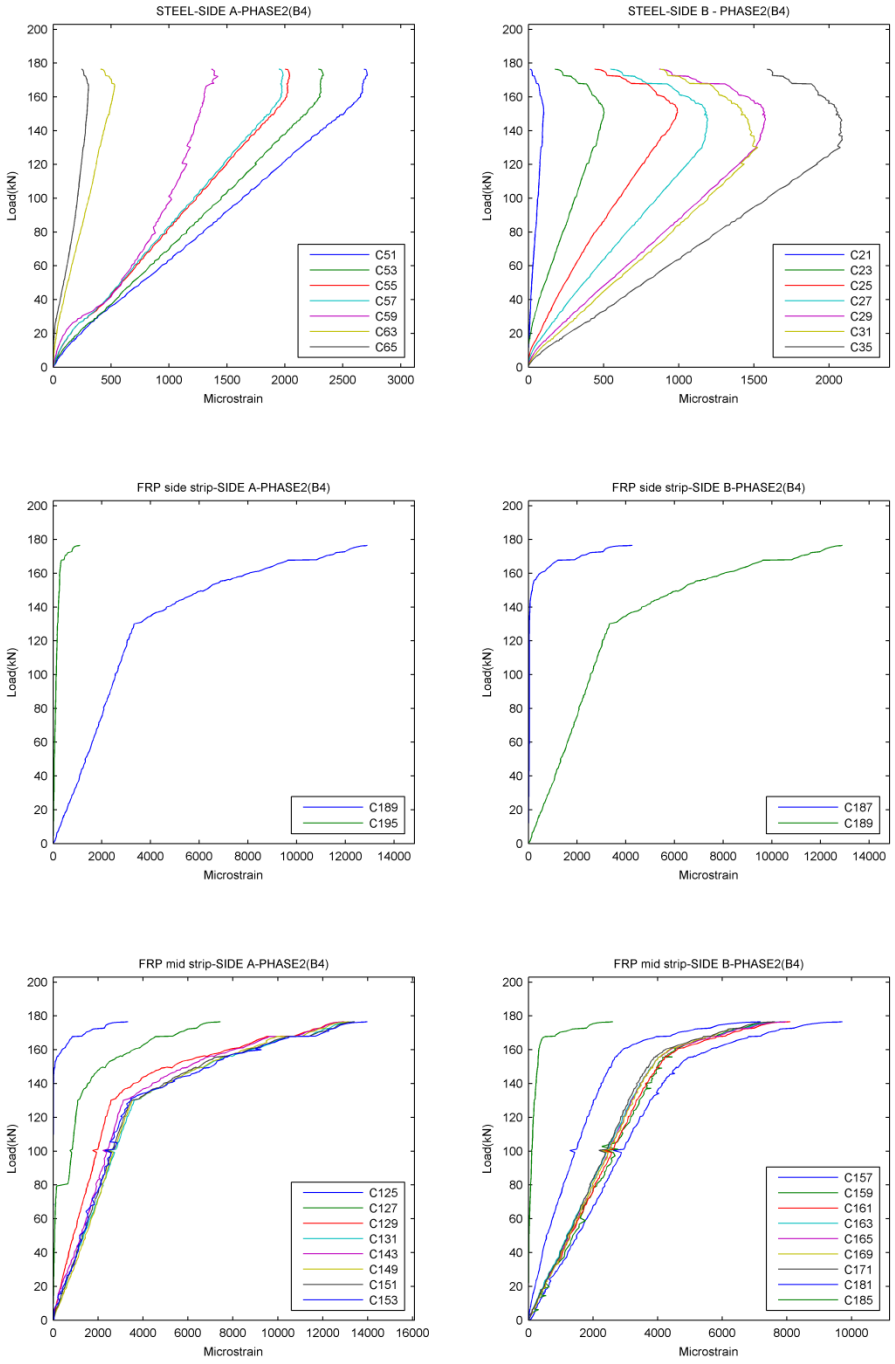

Fig. C4 - 39: Strains in the steel reinforcement and FRP along the span.

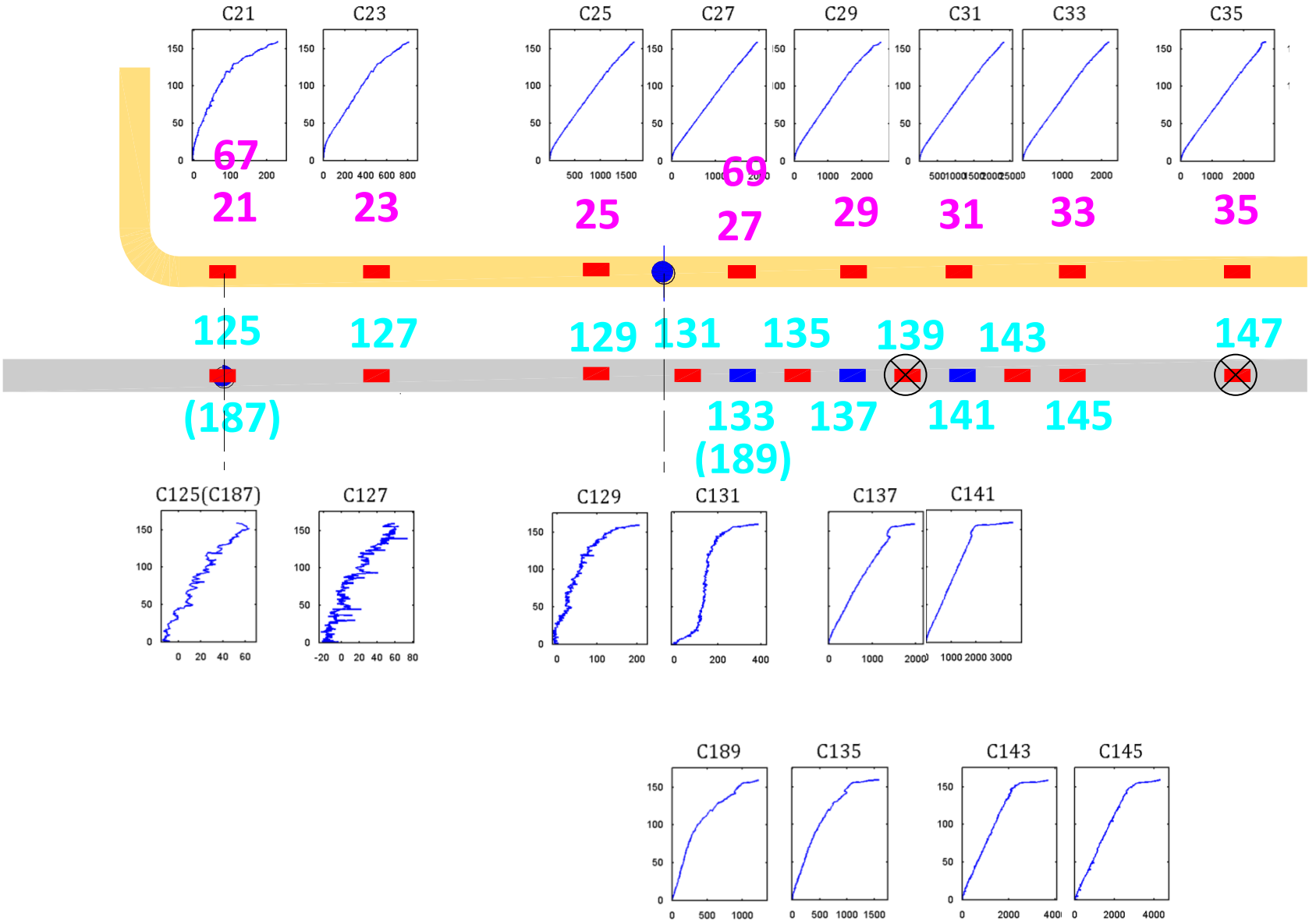

Fig. C4 - 40: Strain along the steel reinforcement and FRP in from the support to the region near the termination point on side B.

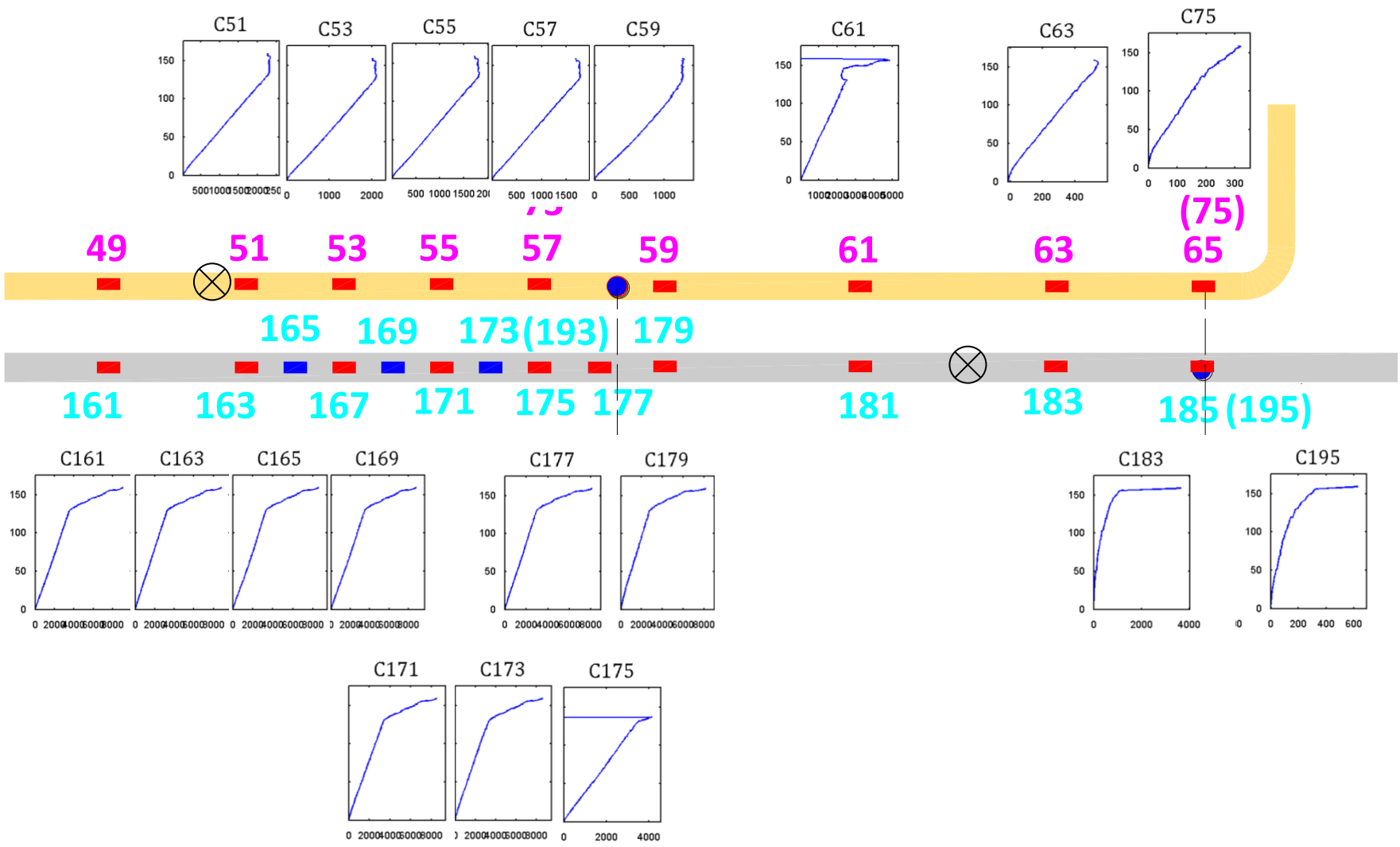

Fig. C4 - 41: Strain along the steel reinforcement and FRP in from the support to the region near the termination point on side A.

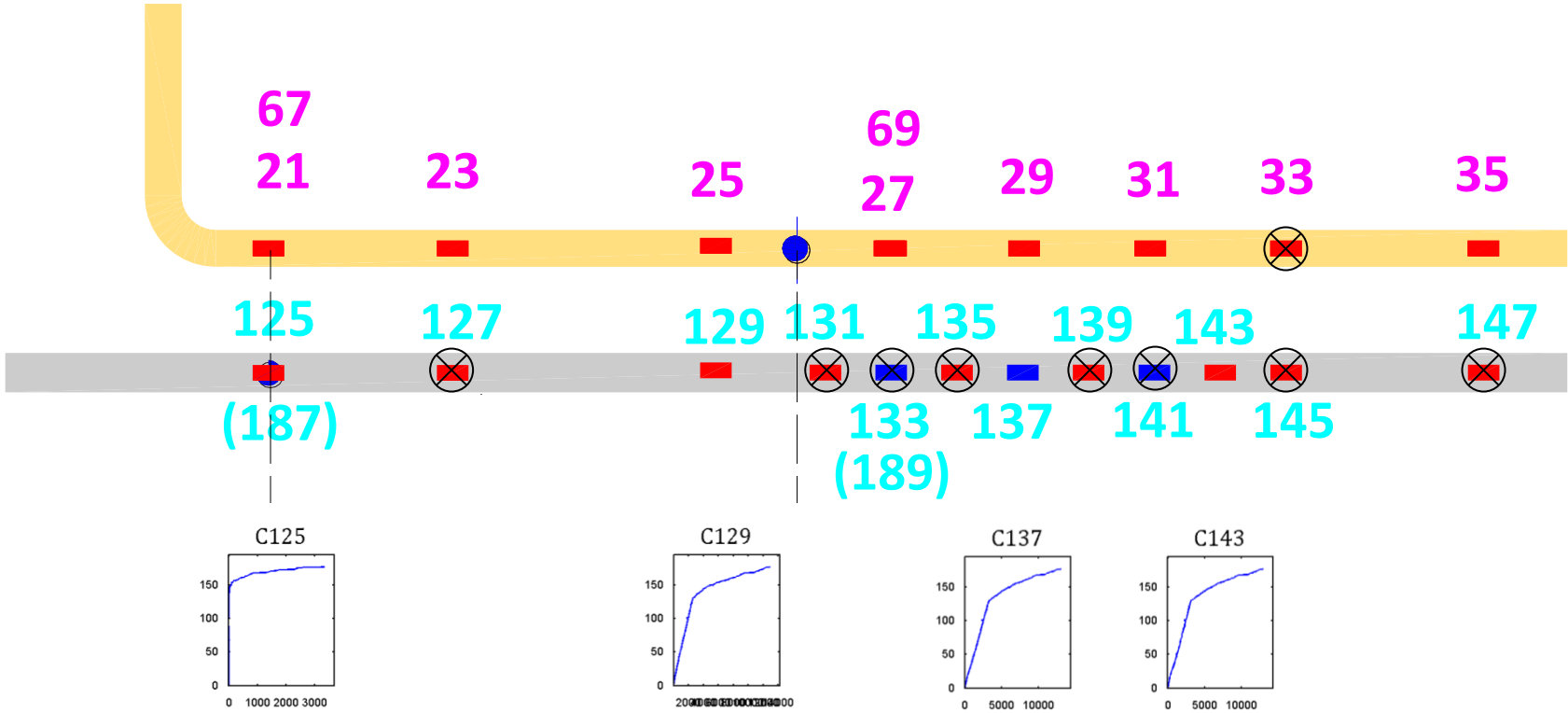

Fig. C4 - 42: Strain along the steel reinforcement and FRP (mid strip) in from the support to the region near the termination point on side B (phase 4).

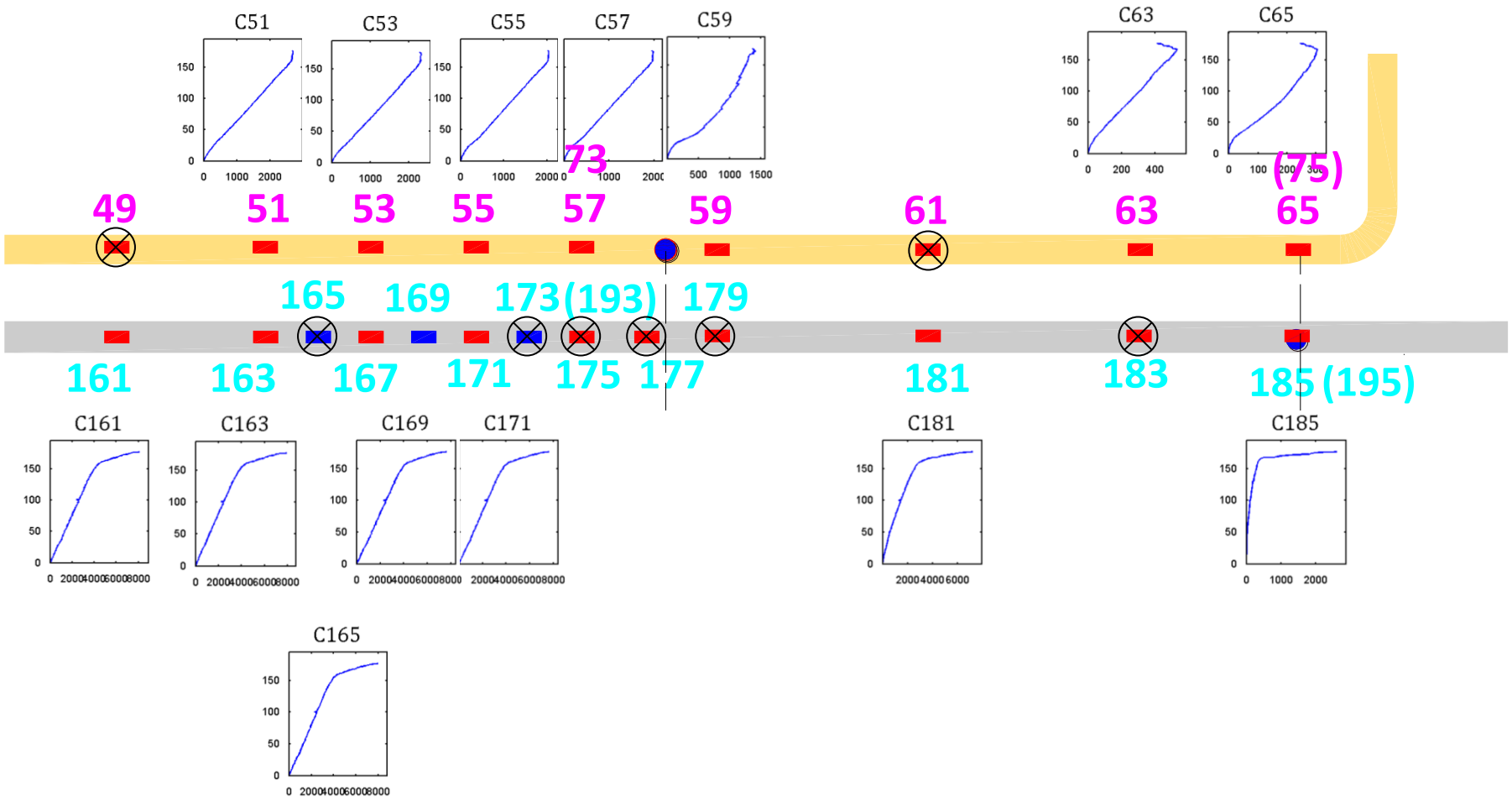

Fig. C4 - 43: Strain along the steel reinforcement and FRP (mid strip) in from the support to the region near the termination point on side A (phase 4).

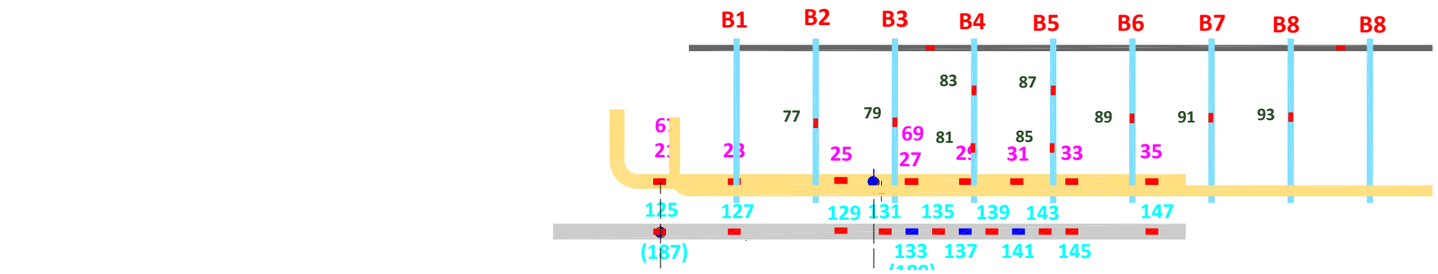

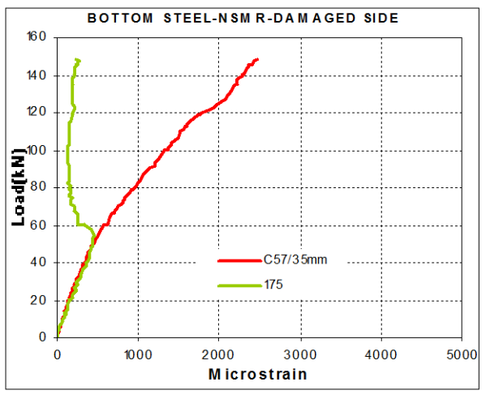

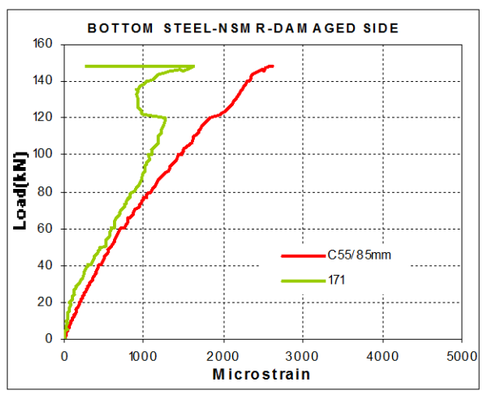

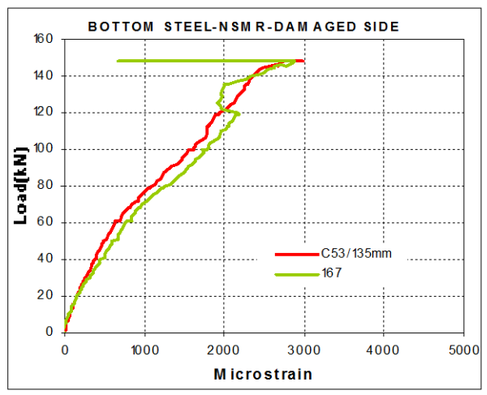

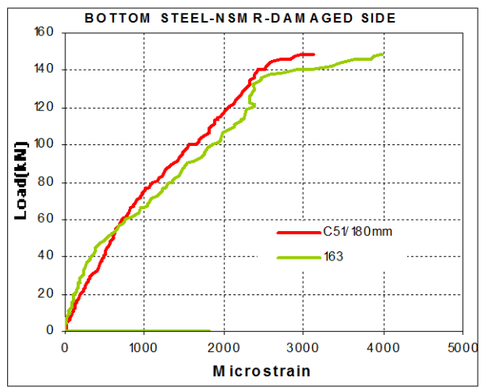

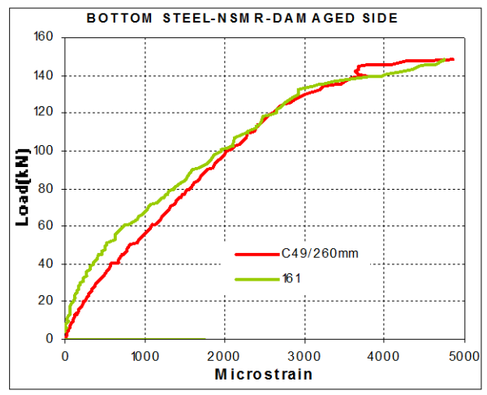

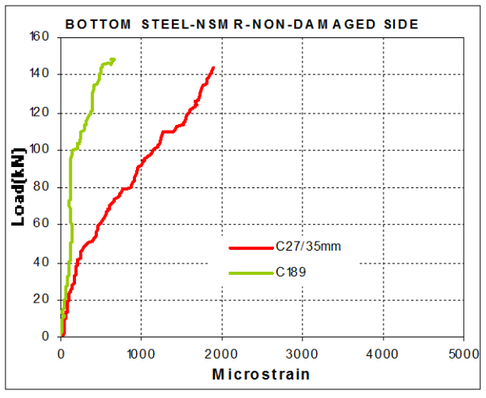

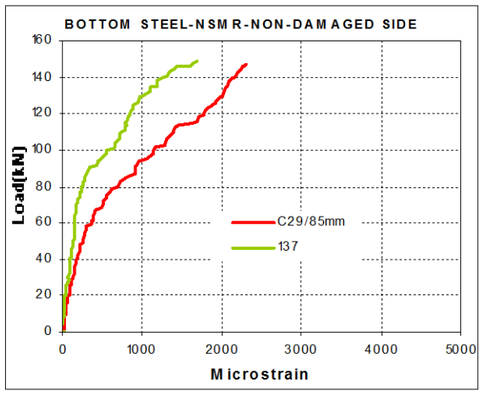

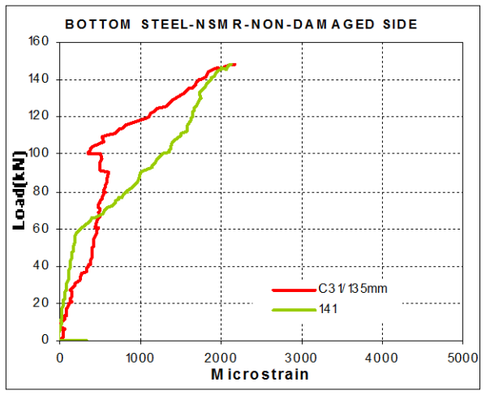

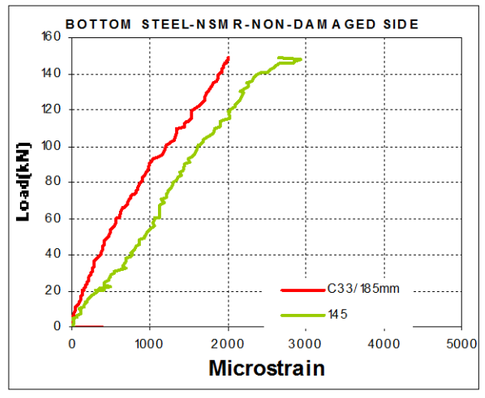

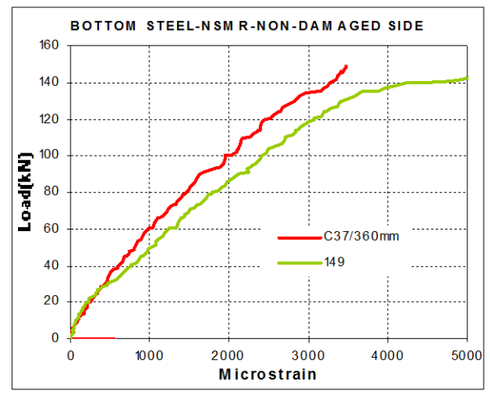

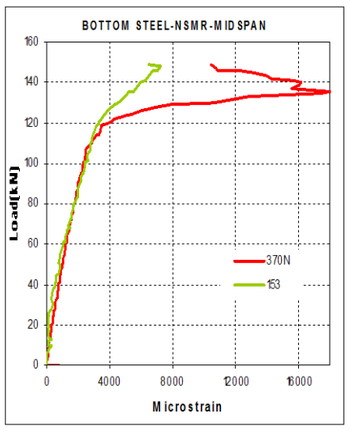

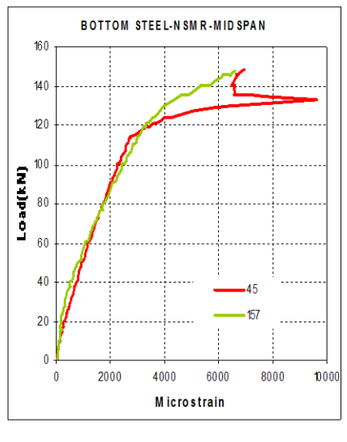

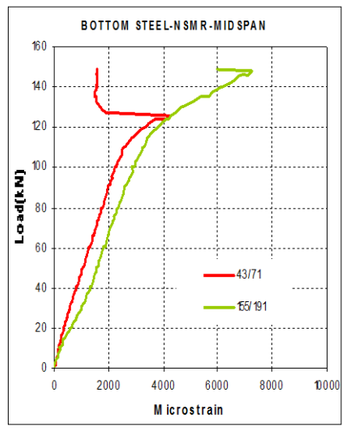

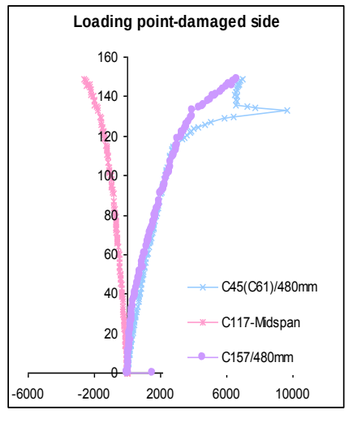

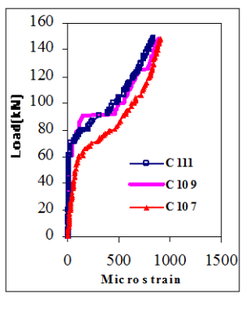

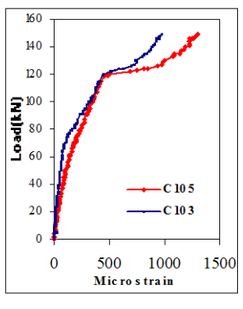

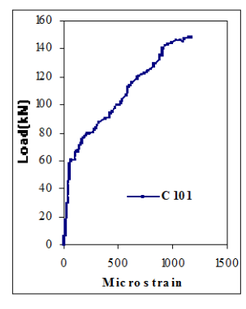

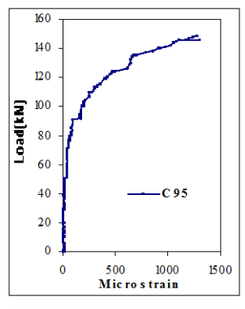

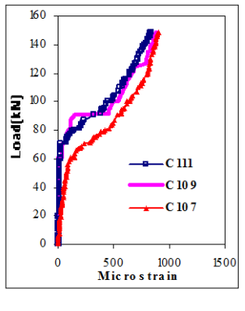

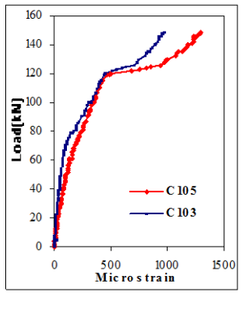

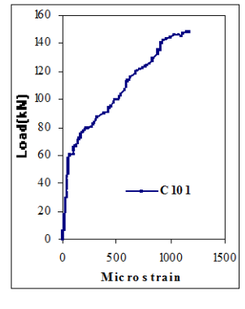

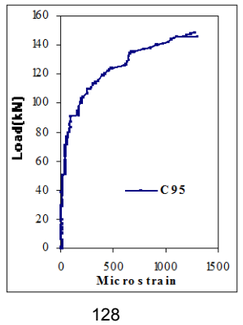

Fig. C4 - 44: The strains along FRP and the steel reinforcement around the COP

C.5.1 BEAM DESIGN

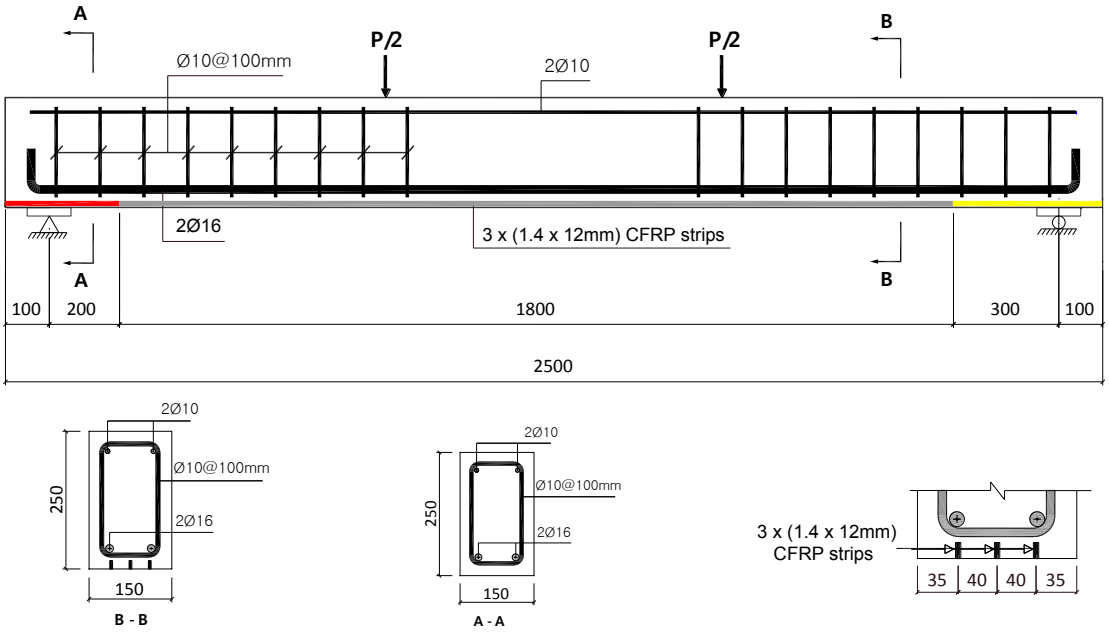

Fig. C5 - 1: Details of specimen

C.5.2 INSTRUMENTATION

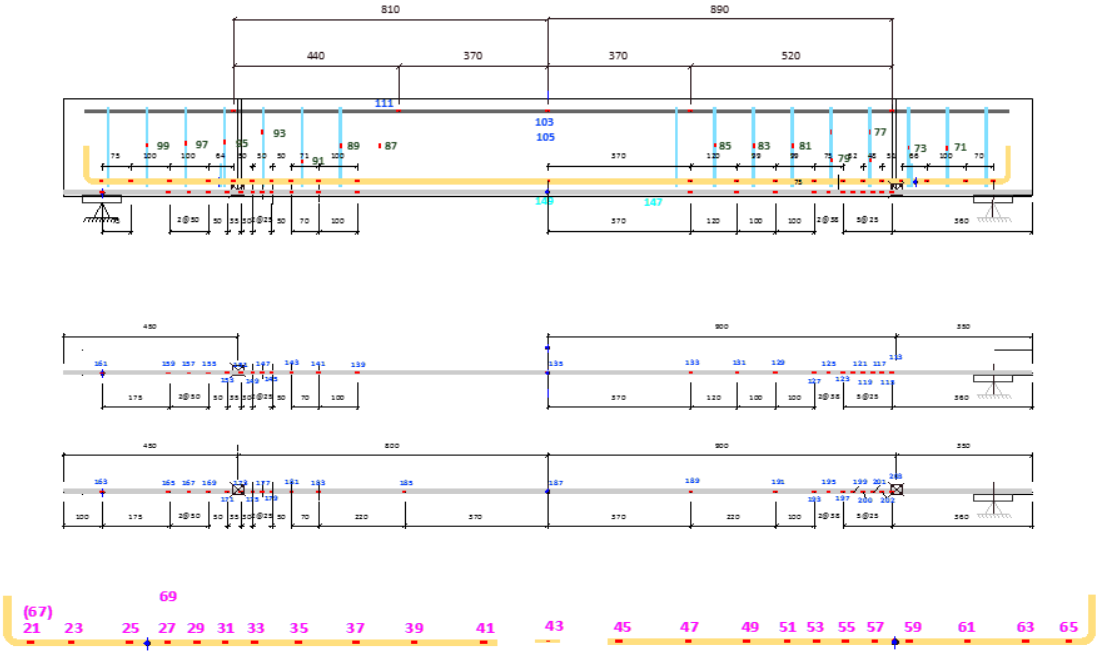

Fig. C5 - 2: Strain gauge arrangement in various components

C.5.3 FIRST TESTING PHASE: PRE-DAMAGING

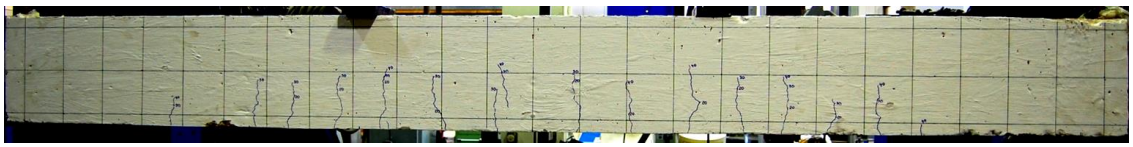

Fig. C5 - 3: Crack pattern of beam NSM5A

C.5.4 FIRST TESTING PHASE: FAILURE ON SIDE B

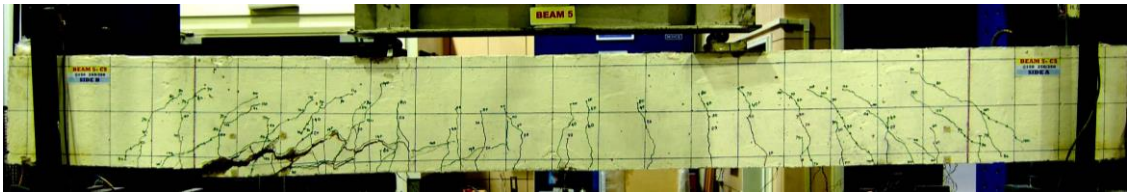

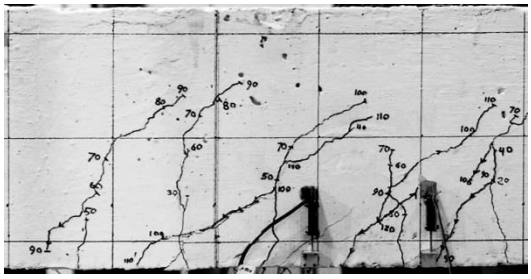

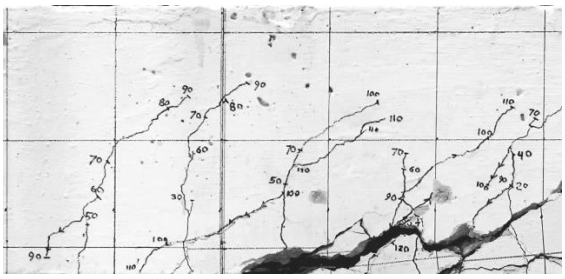

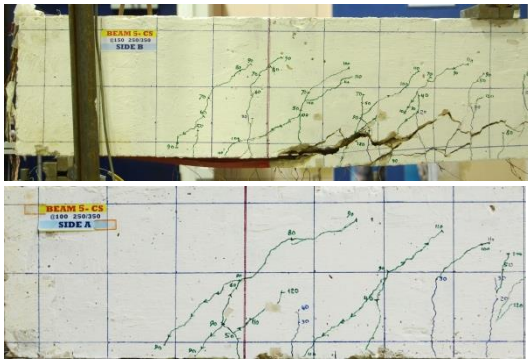

Fig. C5 - 4: Debonding of beam NSM5A

C.5.5 FIRST PHASE - DISPACEMENT READINGS OF LVDTS

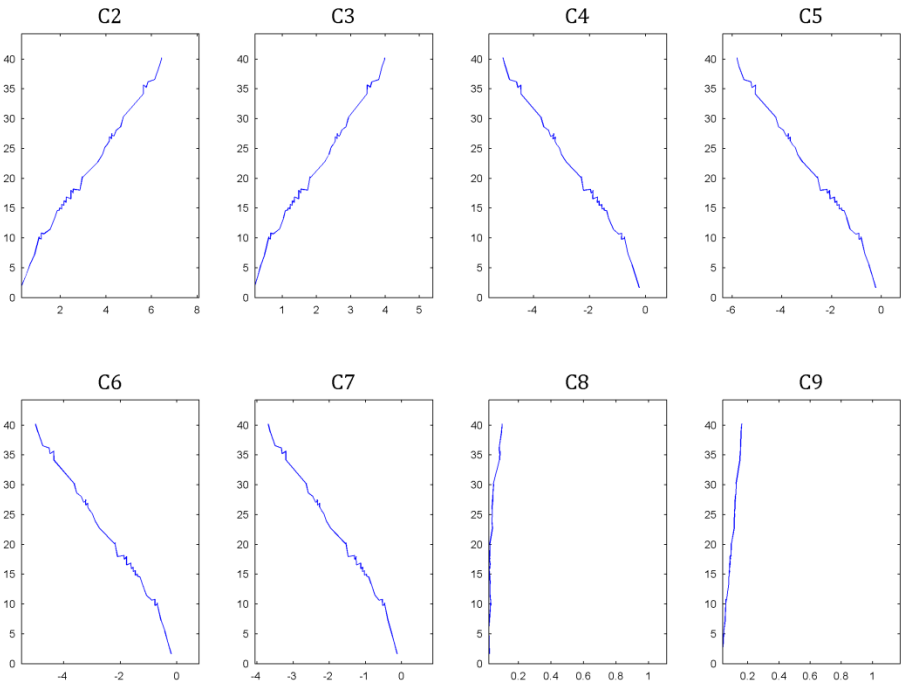

Fig. C5 - 5: Displacement readings of LVDTS (C2 - C9)

C.5.6 STRAIN READINGS

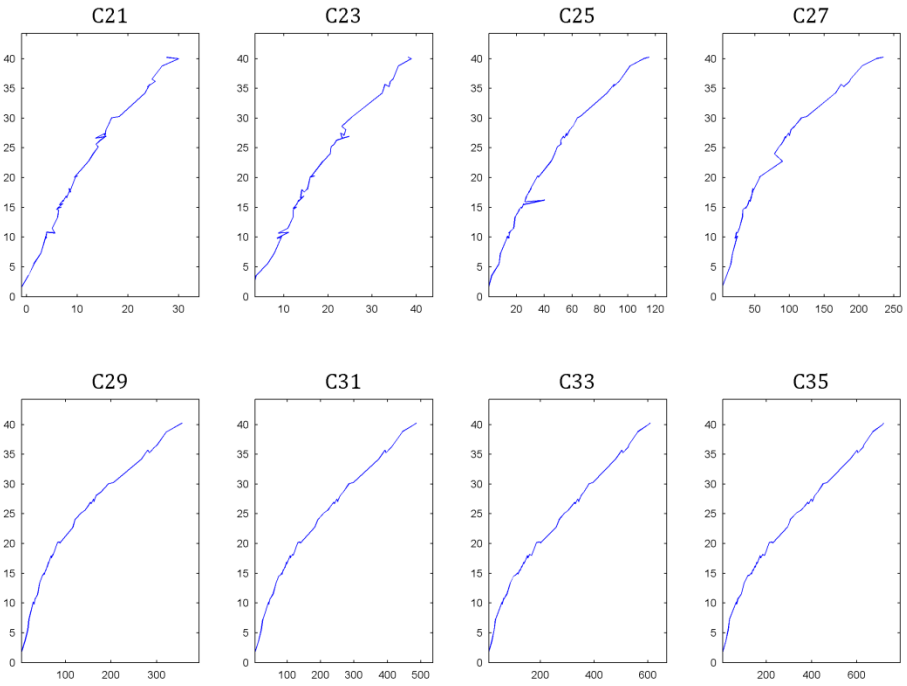

Fig. C5 - 6: Strain readings (C21-C35)

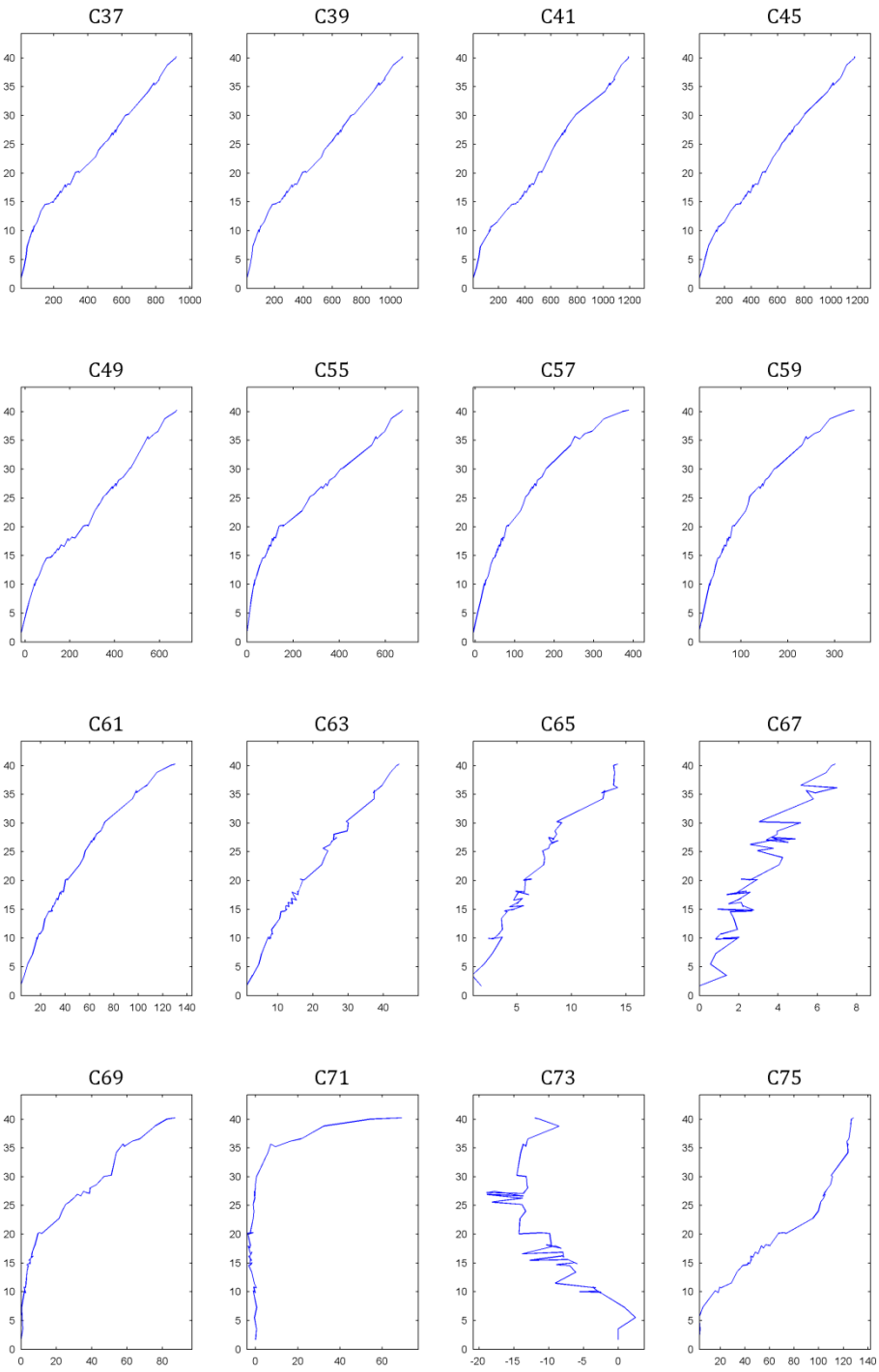

Fig. C5 - 7: Strain readings (C37-C75)

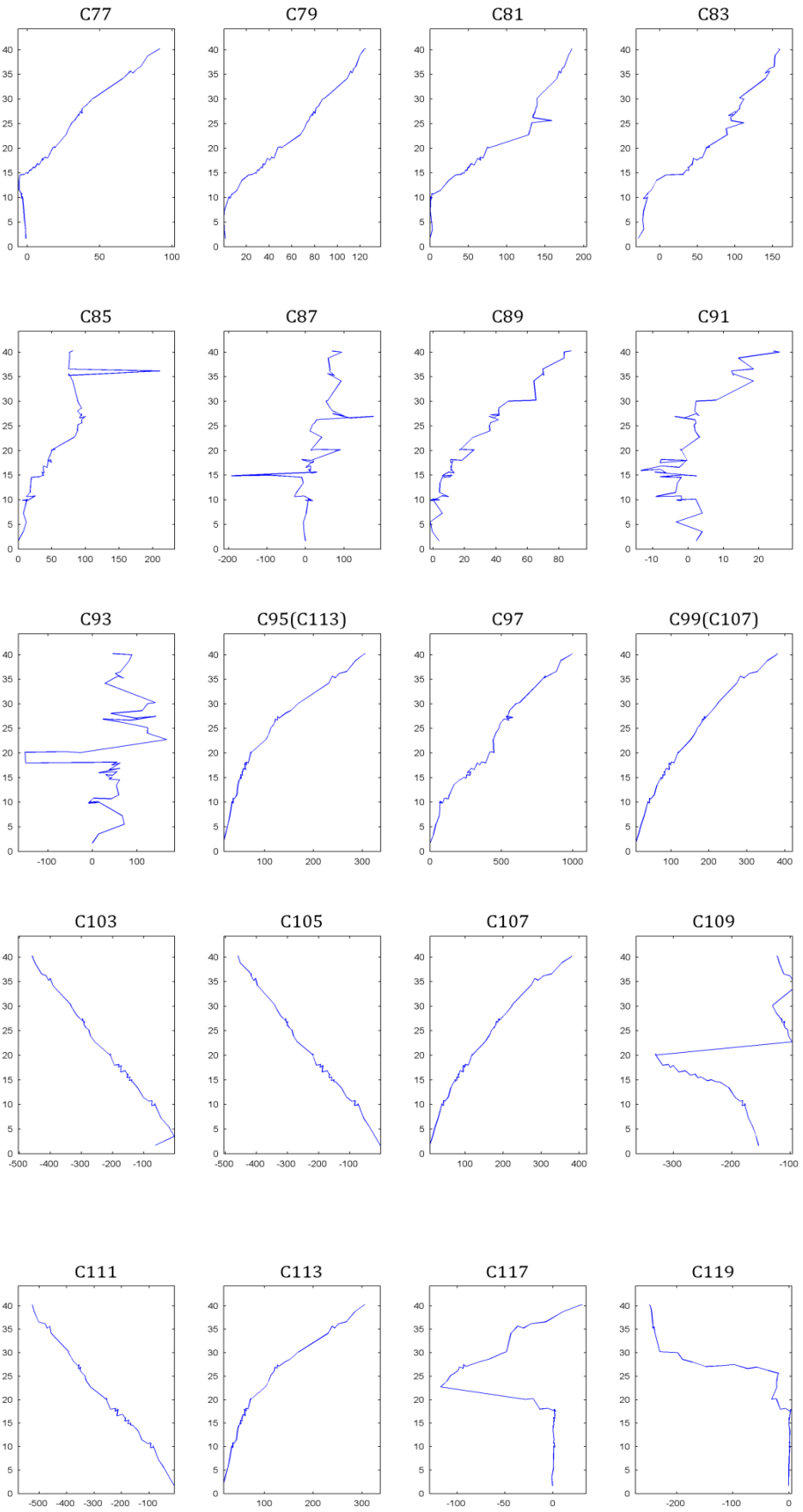

Fig. C5 - 8: Strain readings (C77 – C119)

C.5.7 DISPLACEMENT READINGS OF LVDTs

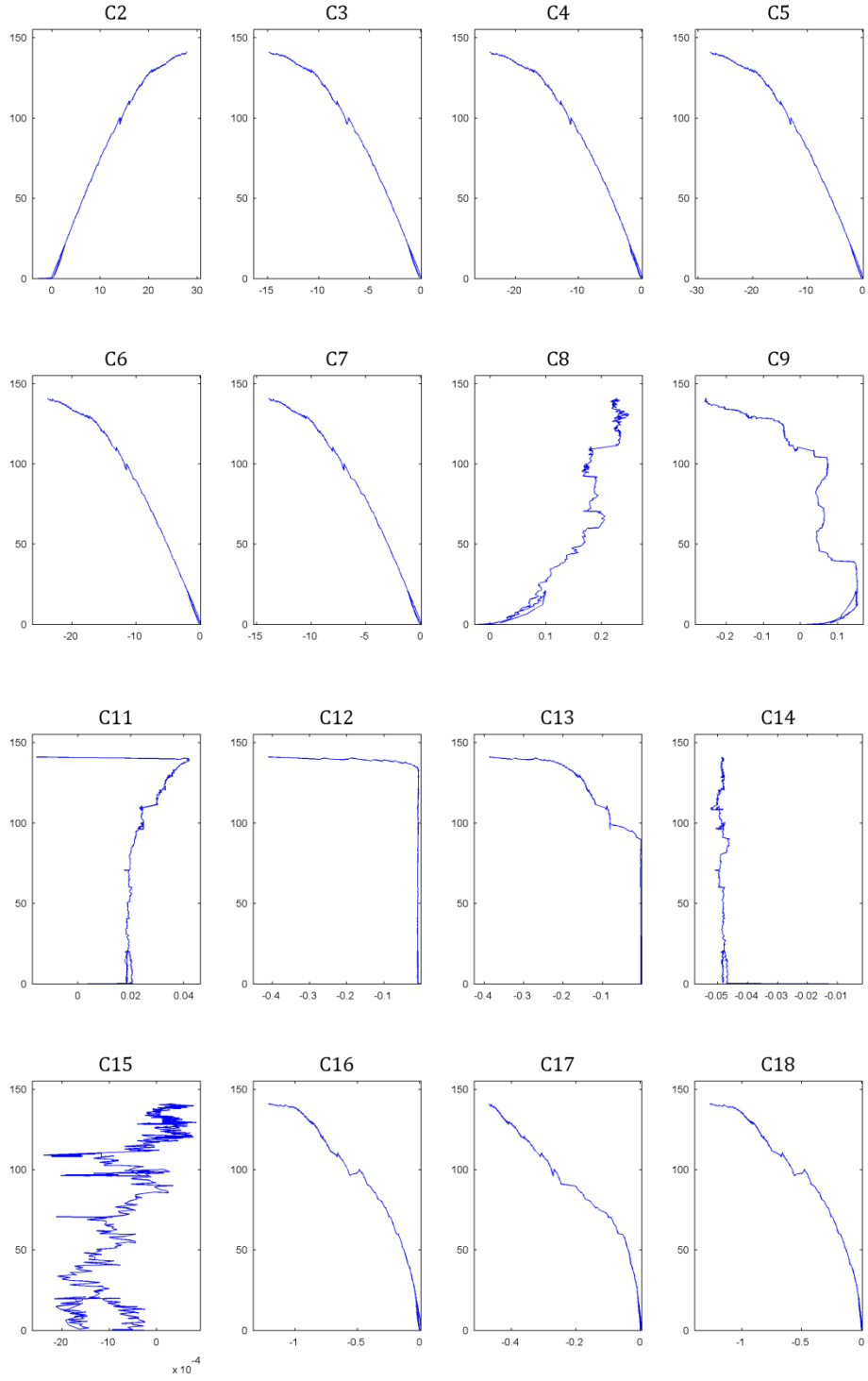

Fig. C5 - 9: Displacement readings of LVDTs (C2-C18)

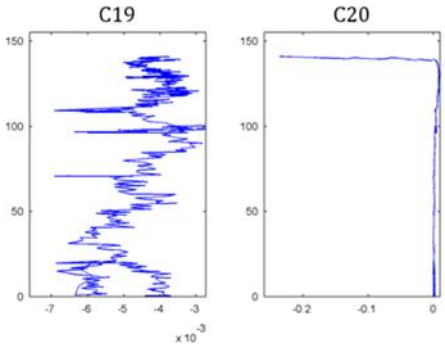

Fig. C5 - 10: Displacement readings (C19 – C20)

C.5.8 STRAIN READINGS

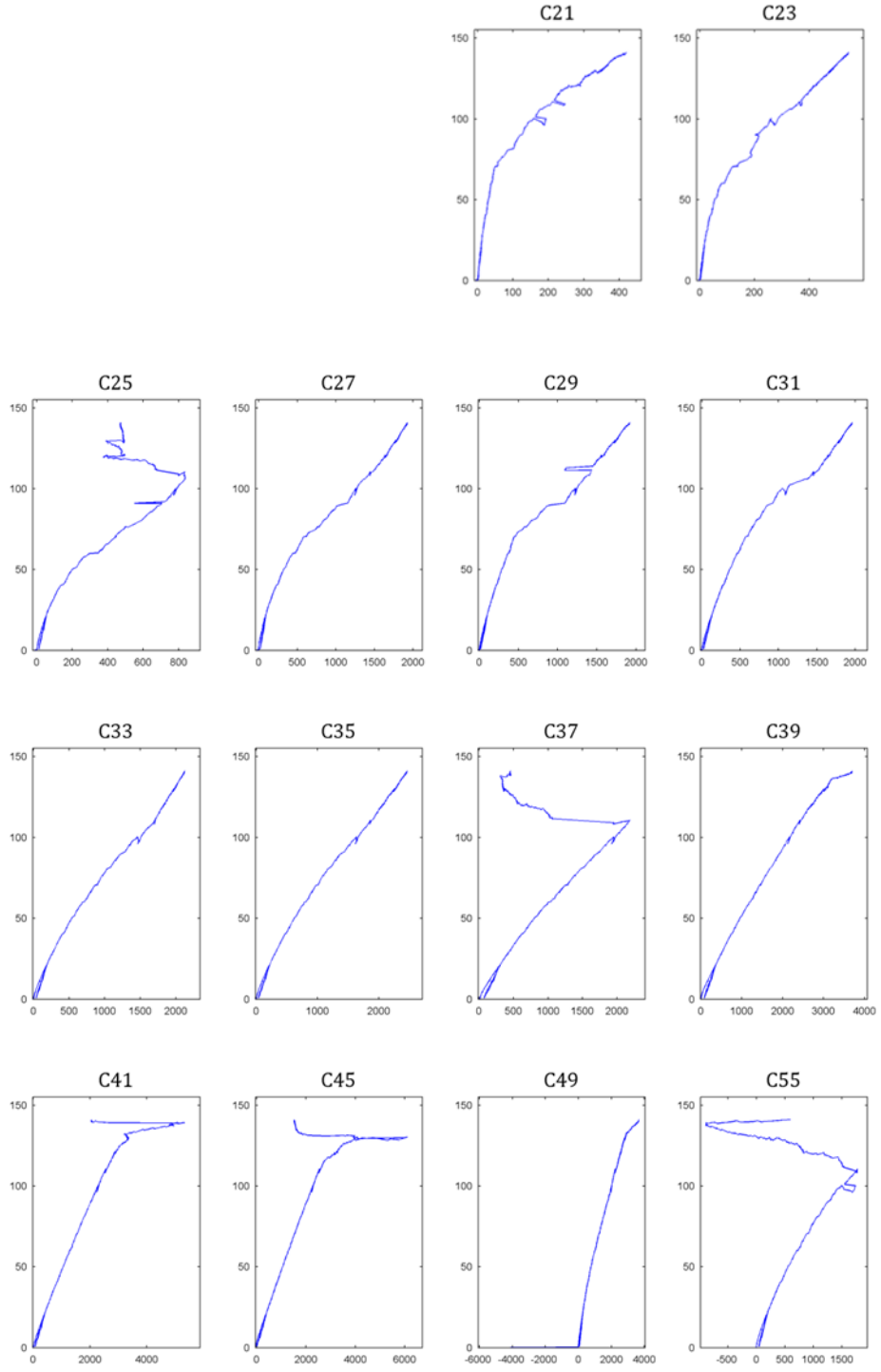

Fig. C5 - 11: Strain readings (C21-C55)

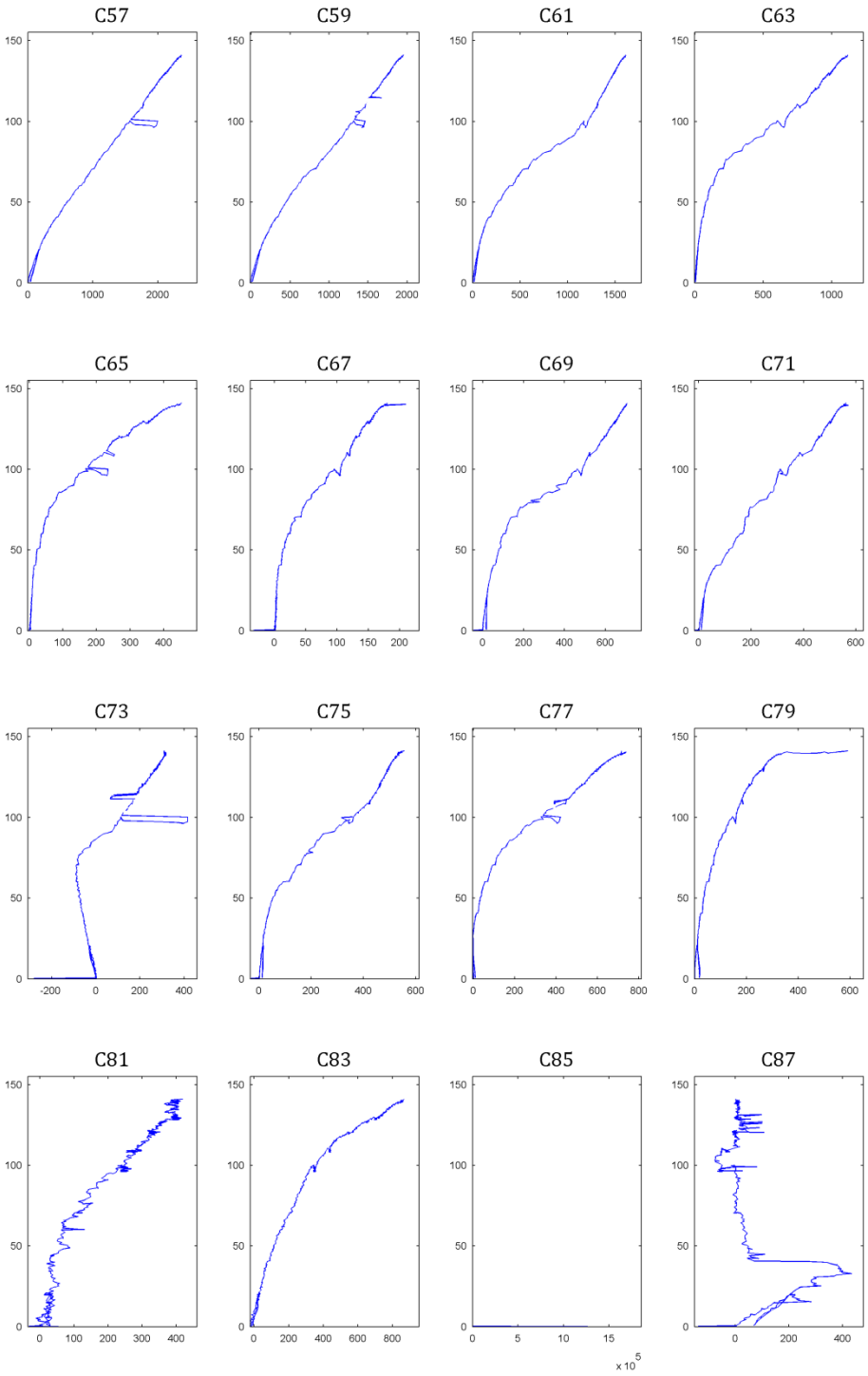

Fig. C5 - 12: Strain readings (C57-C87)

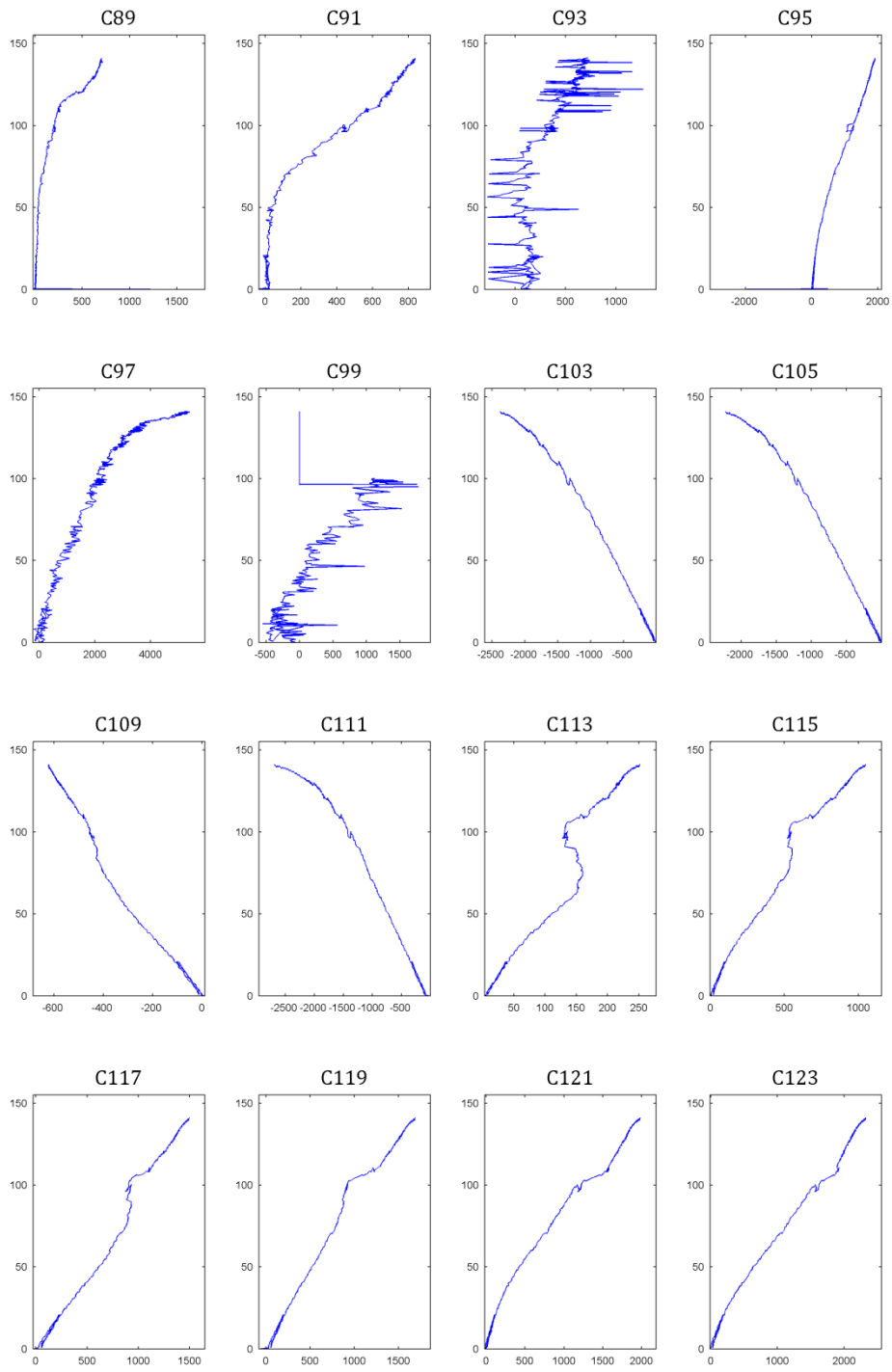

Fig. C5 - 13: Strain readings (C89-C123)

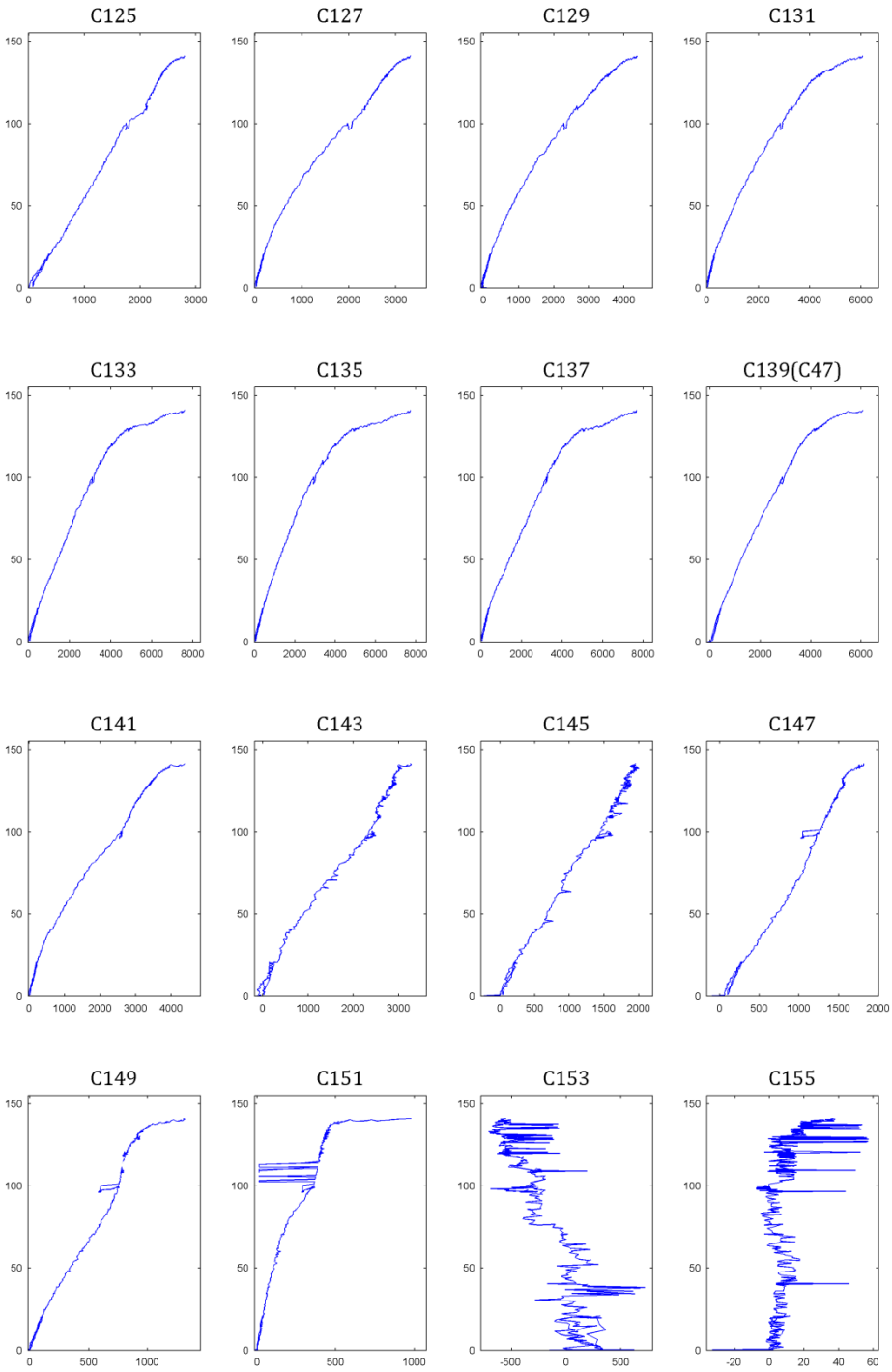

Fig. C5 - 14: Strain readings (C125-C155)

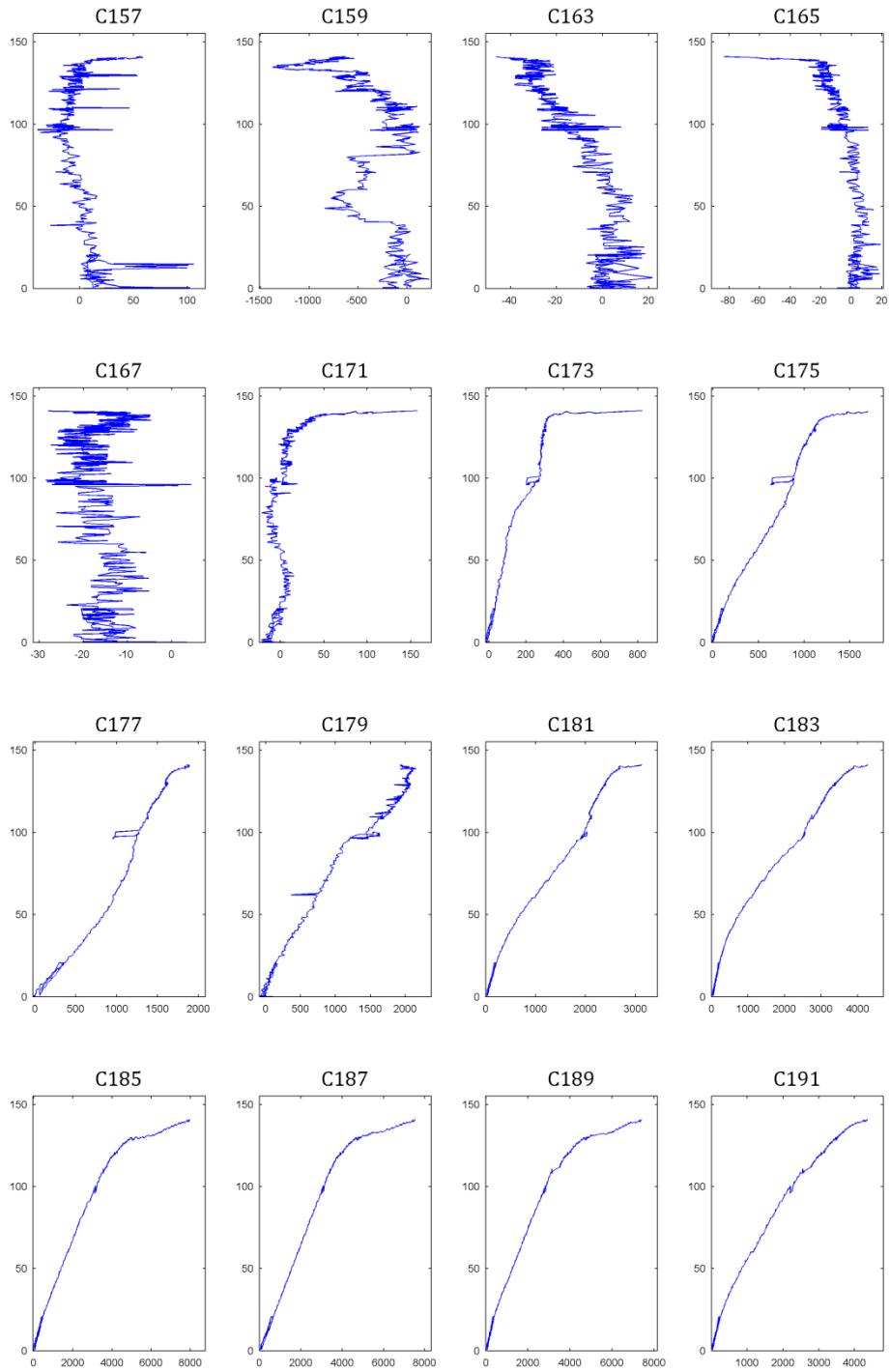

Fig. C5 - 15: Strain readings (C157-C191)

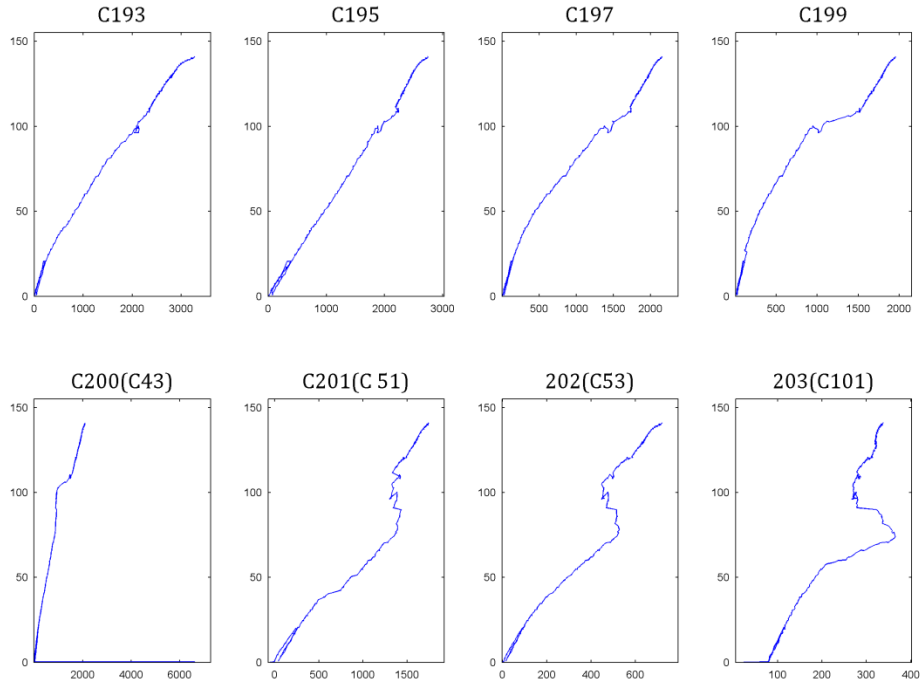

Fig. C5 - 16: Strain readings (C193 – 203(C101))

C.5.9 DEFLECTION

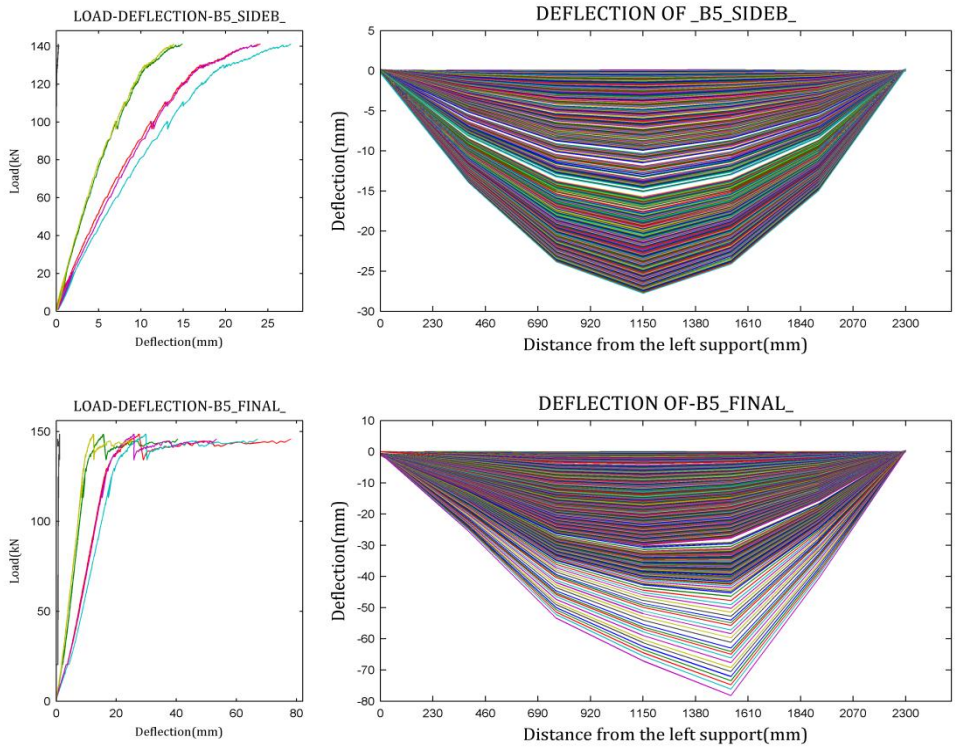

Fig. C5 - 17: Deflection profile

C.5.10 STRAINS IN THE STEEL REINFORCEMENT AND FRP ALONG THE SPAN

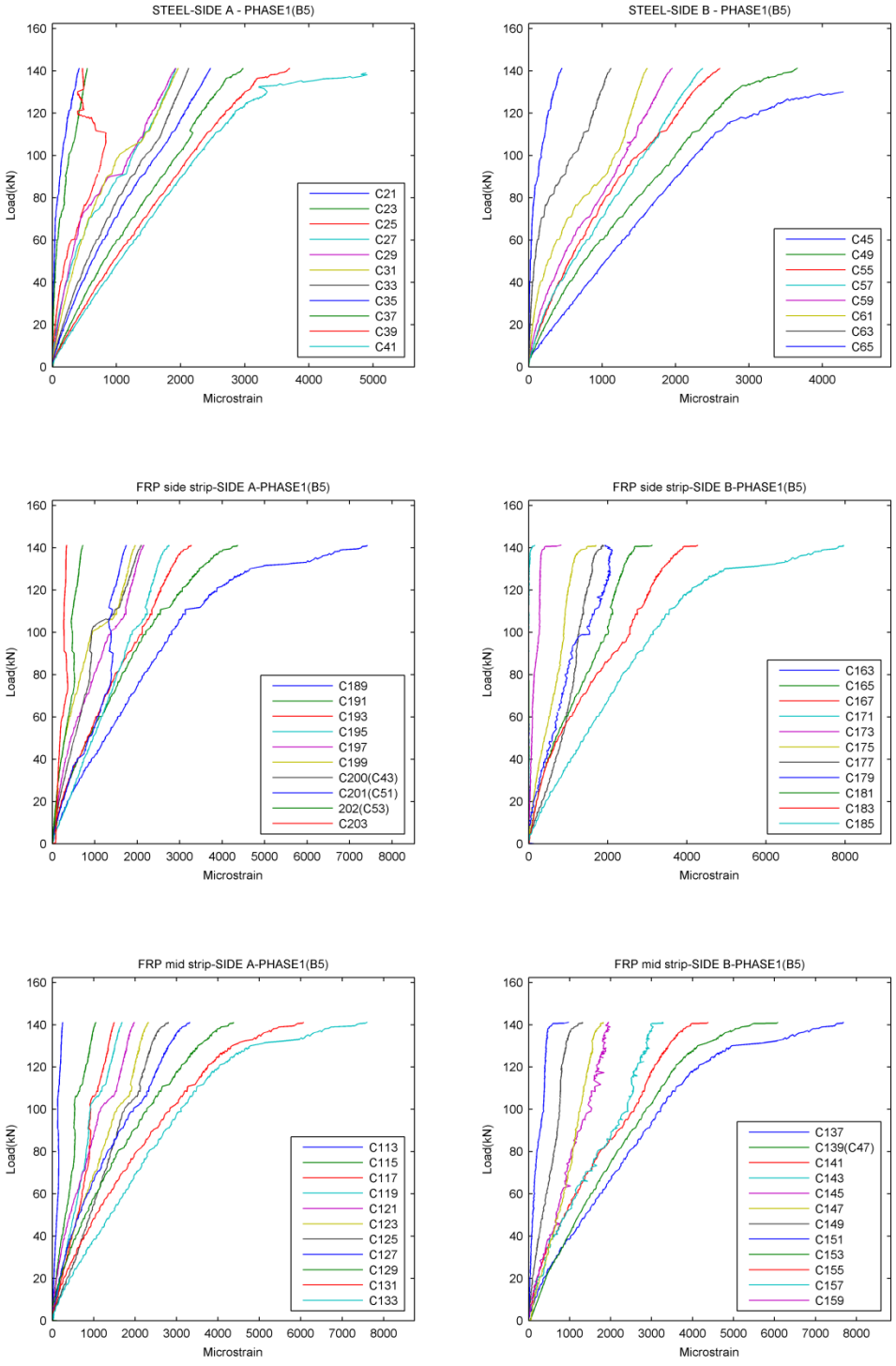

Fig. C5 - 18: Strains in the steel reinforcement and FRP along the span

C.5.11 STRAIN AND BOND STRESS PROFILES

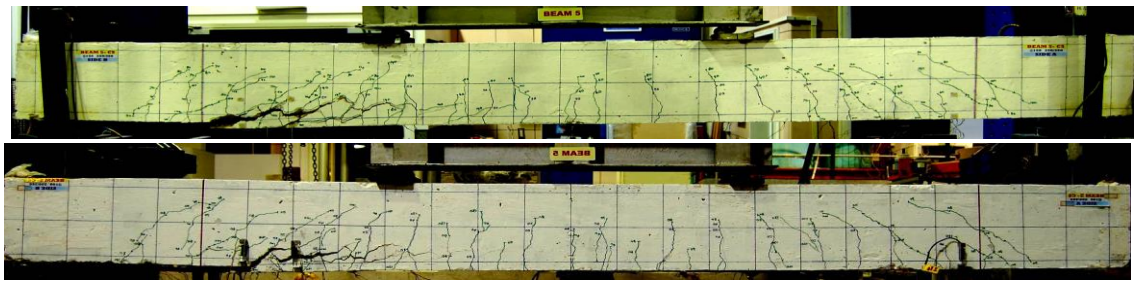

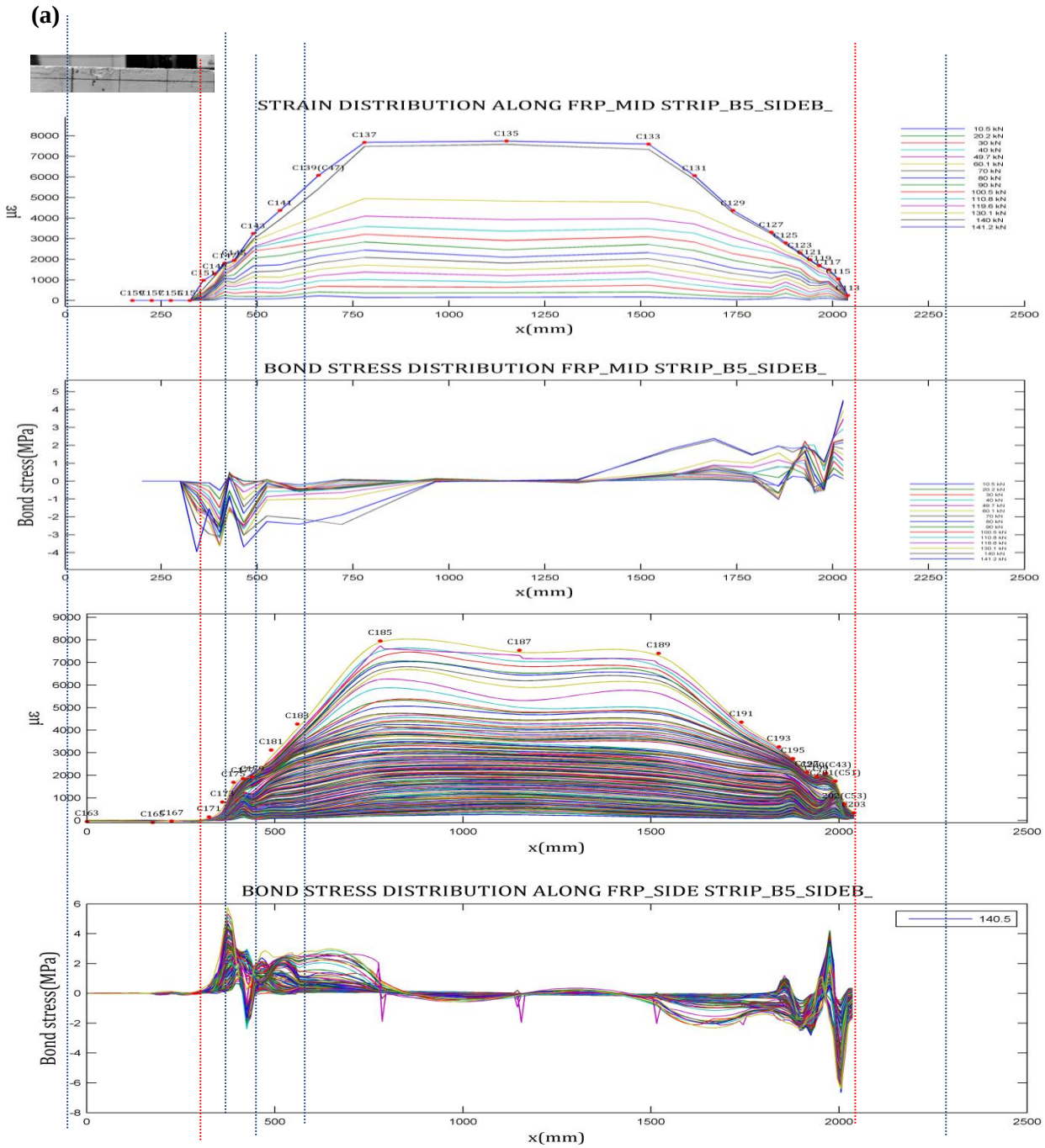

Fig. C5 - 19: Strain and bond stress profiles of (a) Crack pattern of beam NSM2A, (b) FRP, (c) The steel reinforcement

C.5.12 3D PROFILE OF STRAIN AND BOND STRESS

(a)

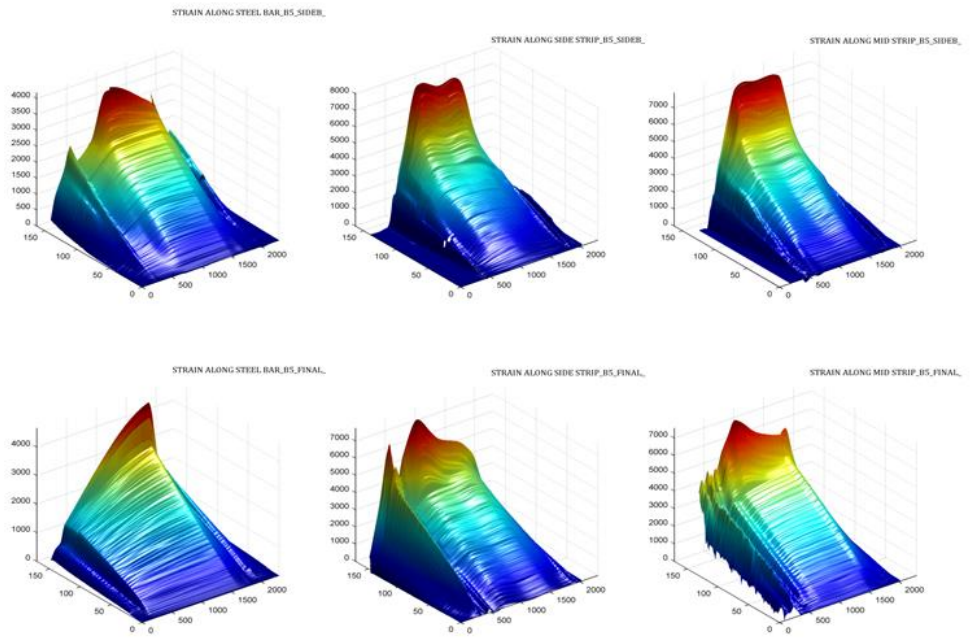

(b)

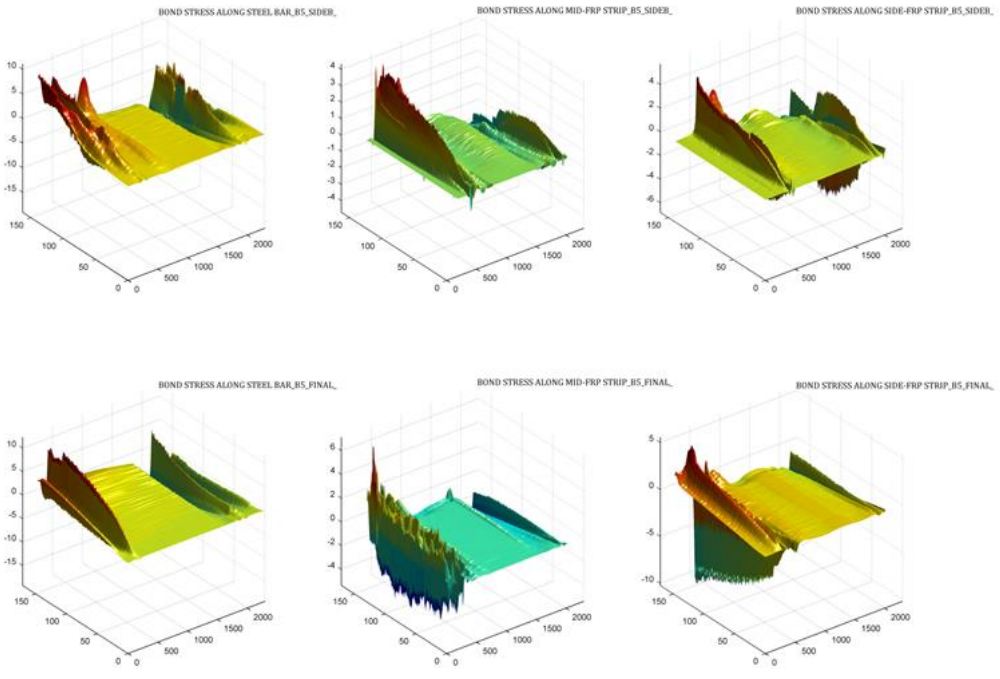

Fig. C5 - 20: Variation of (a) strains and (b) bond stress along the reinforcement and FRP at different load levels

C.5.13 FINAL TESTING PHASE

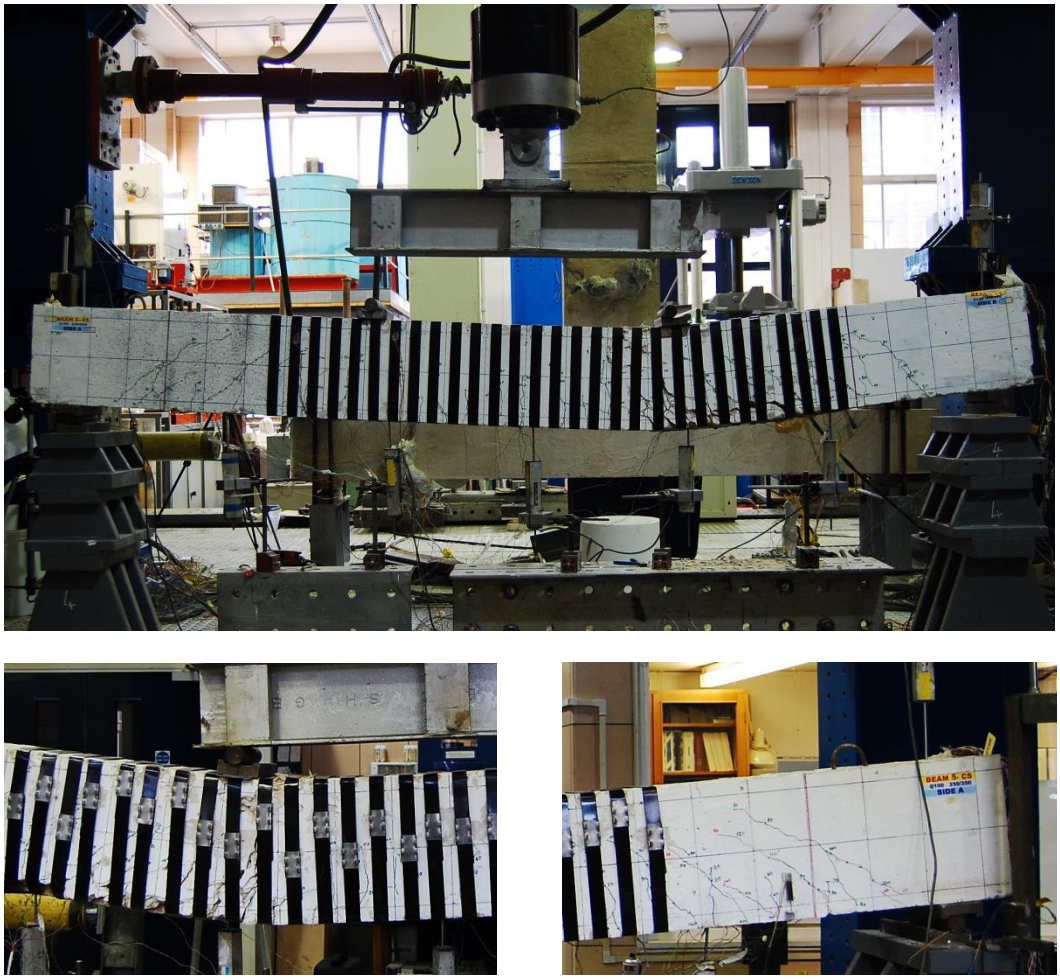

Fig. C5 - 21: Final testing phase of beam NSM5A

C.5.14 FINAL TESTING PHASE-READINGS OF LVDTs

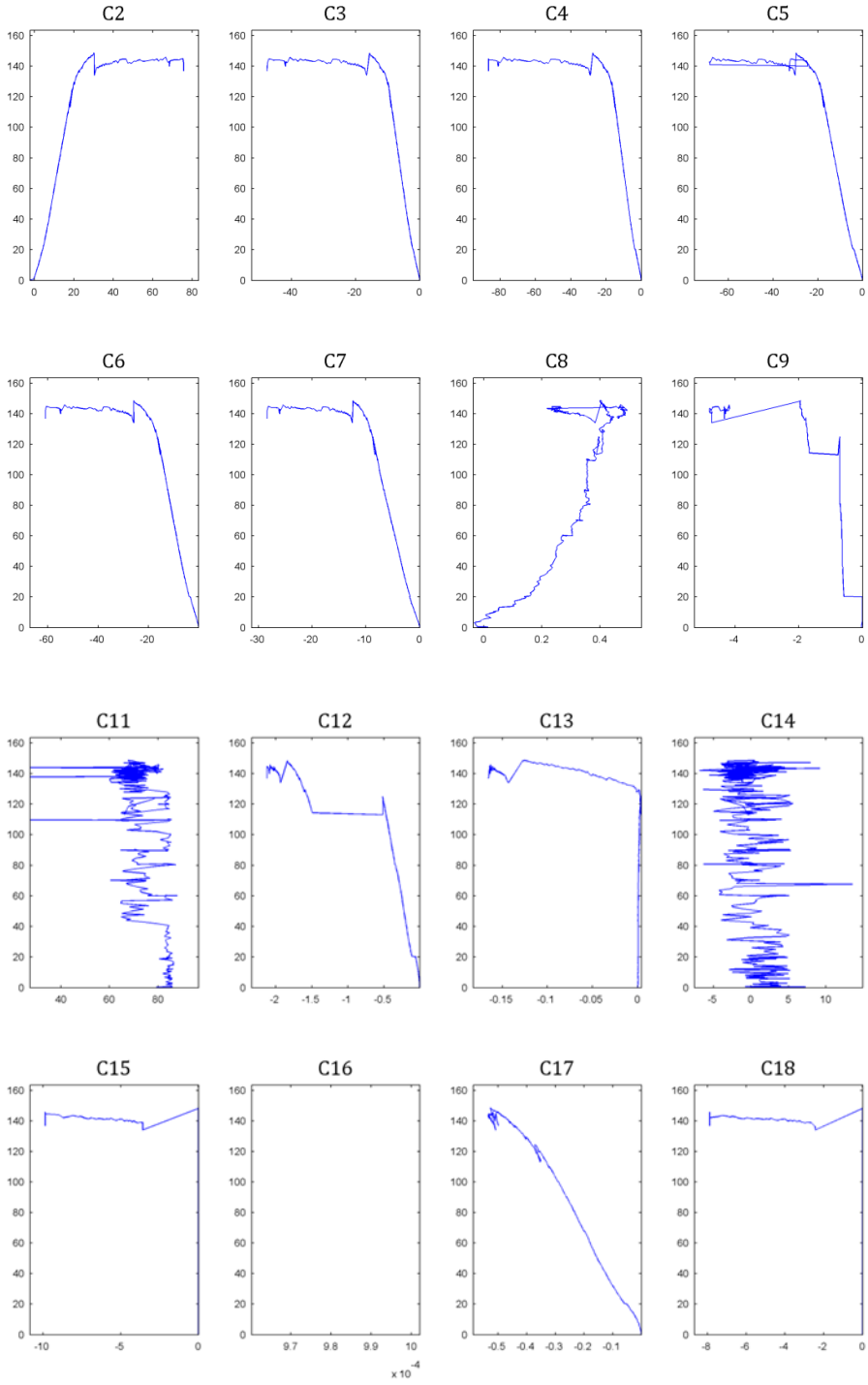

Fig. C5 - 22: Readings of LVDTs (C2 – C18)

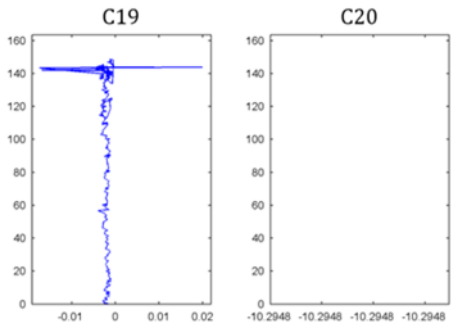

Fig. C5 - 23: Readings of LVDTs (C18 – C20)

C.5.15 FINAL TESTING PHASE-STRAIN READINGS

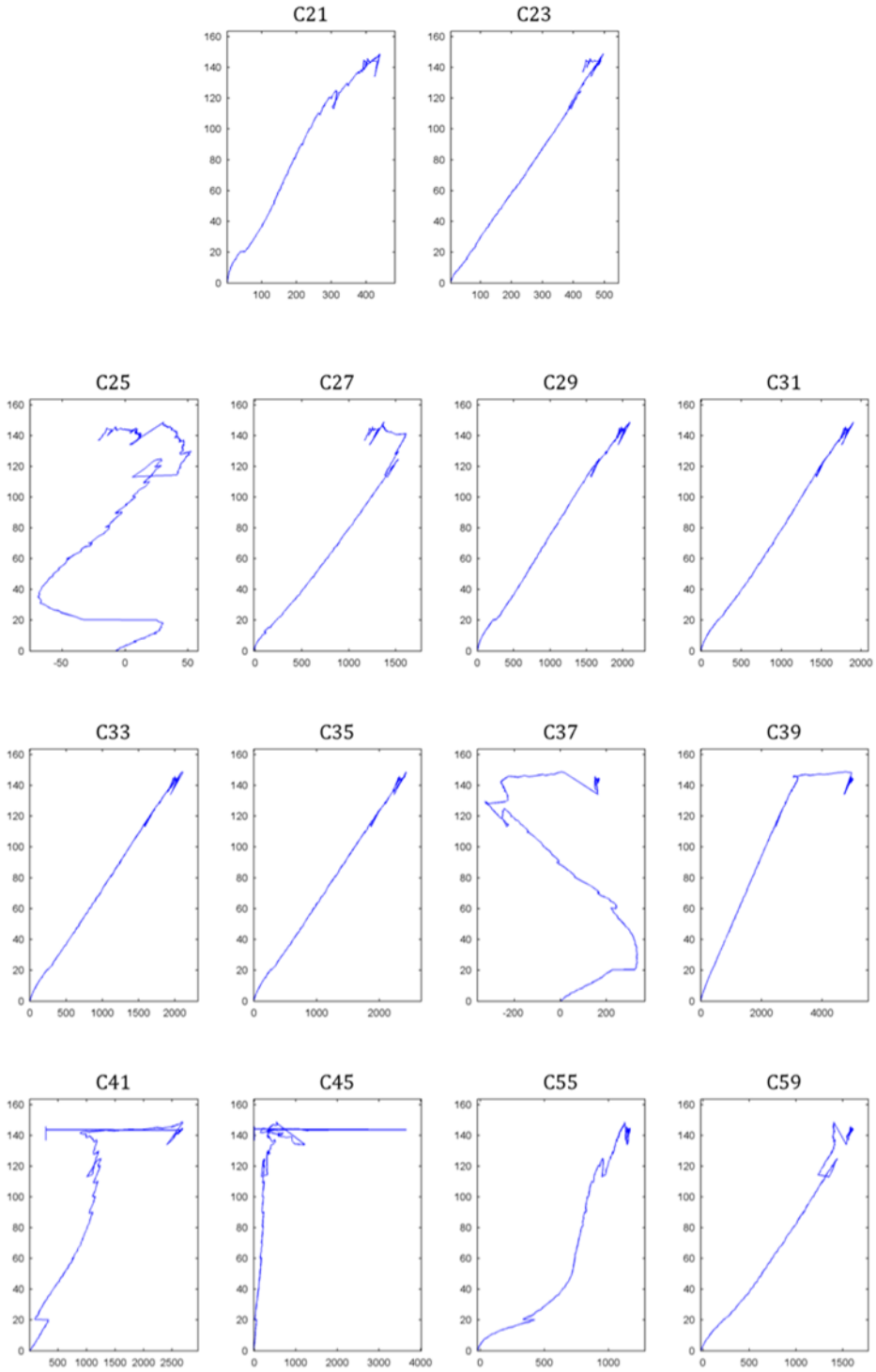

Fig. C5 - 24: Strain readings (C21-C59)

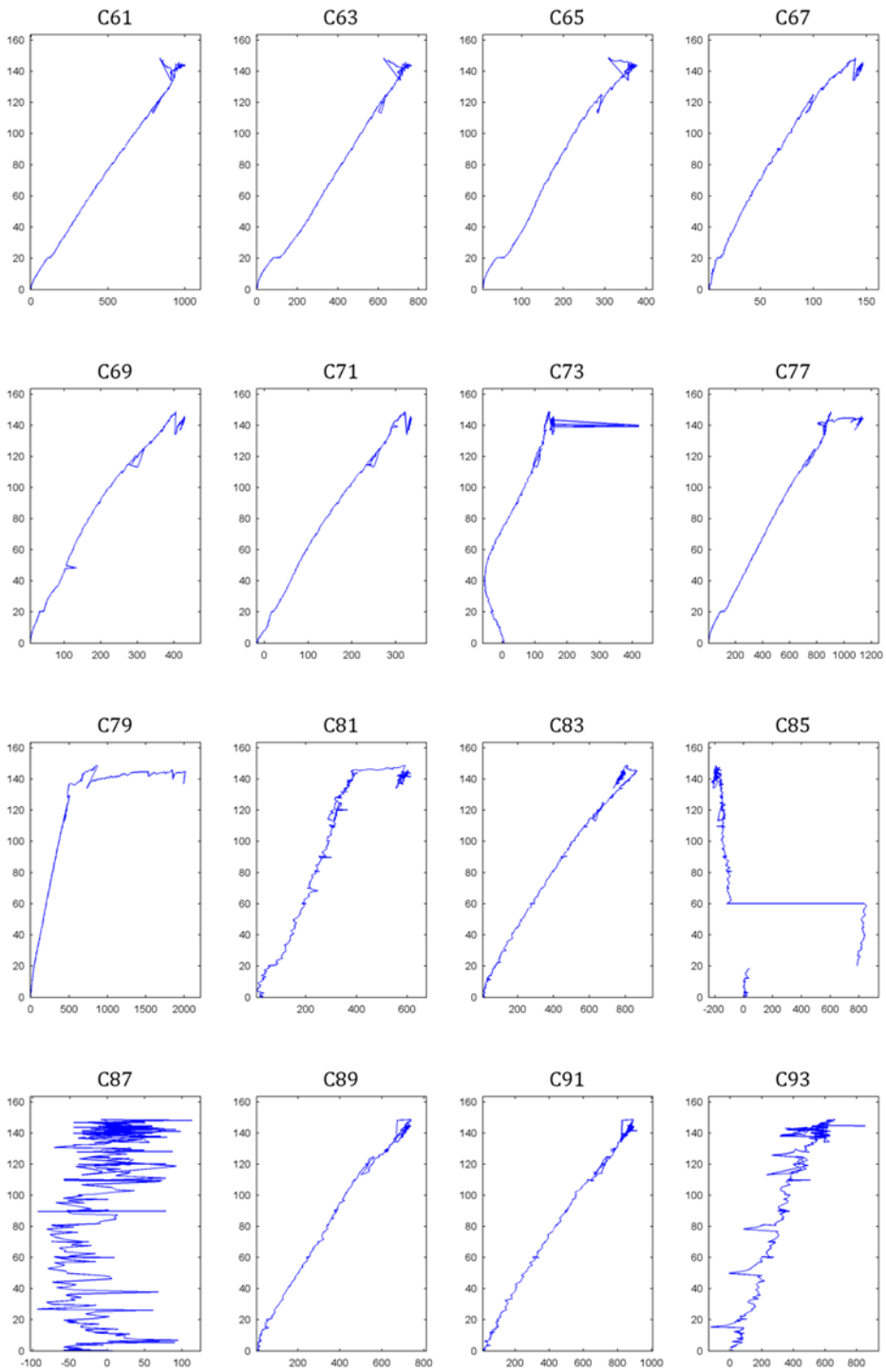

Fig. C5 - 25: Strain readings (C61-C93)

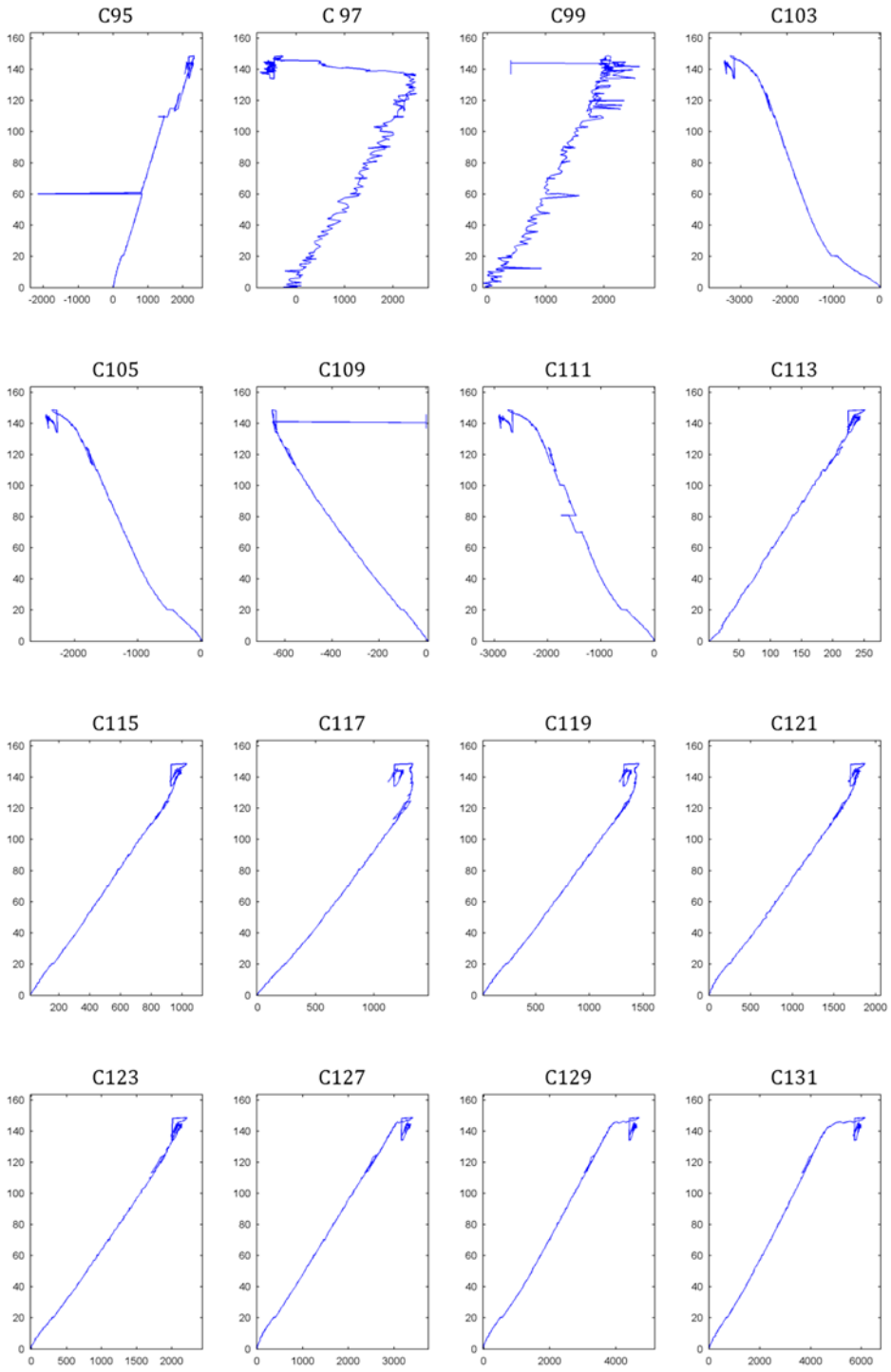

Fig. C5 - 26: Strain readings (C95-C131)

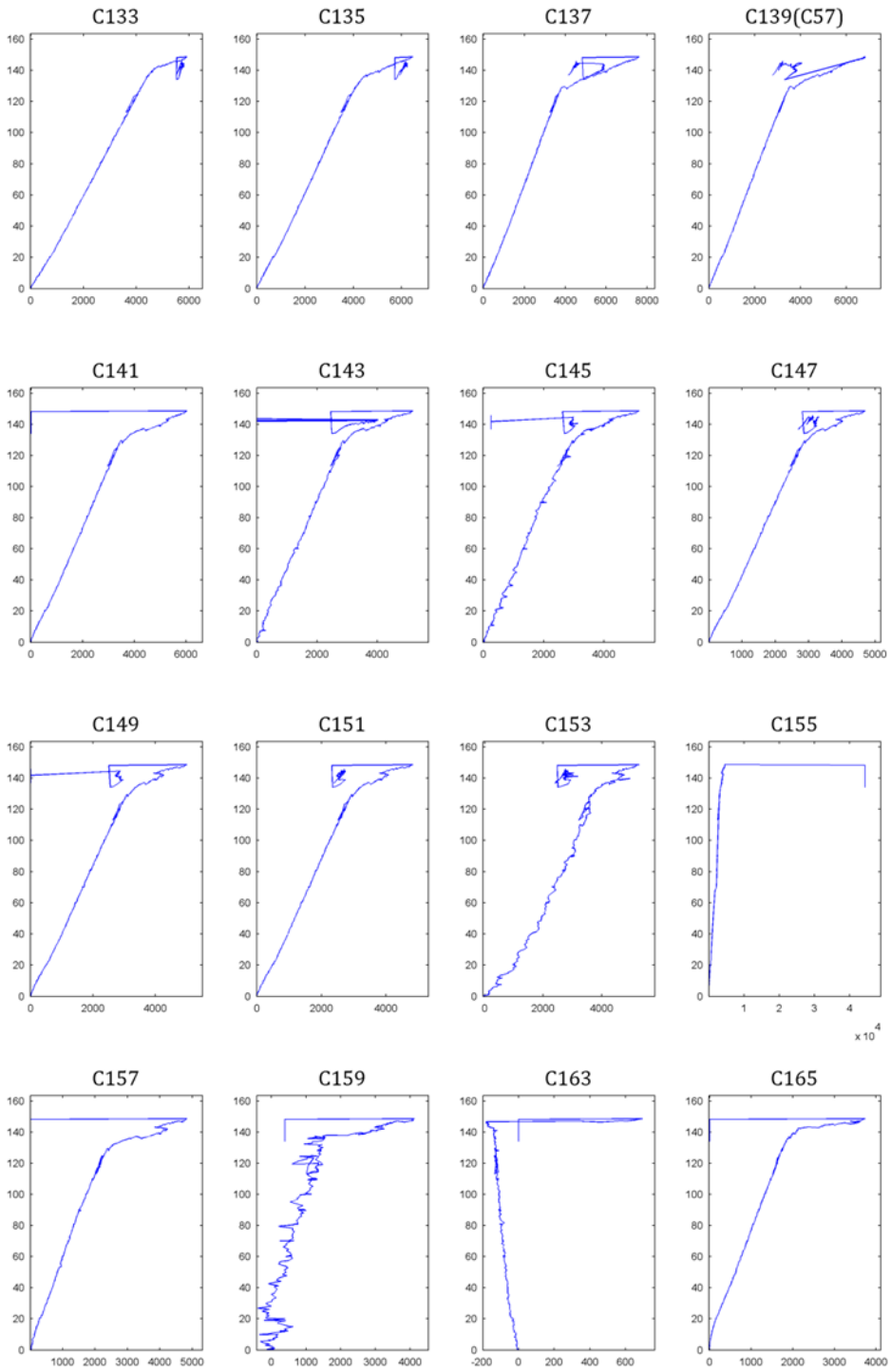

Fig. C5 - 27: Strain readings (C133 – C165)

C.5.16 STRAINS IN THE STEEL REINFORCEMENT AND FRP ALONG THE SPAN

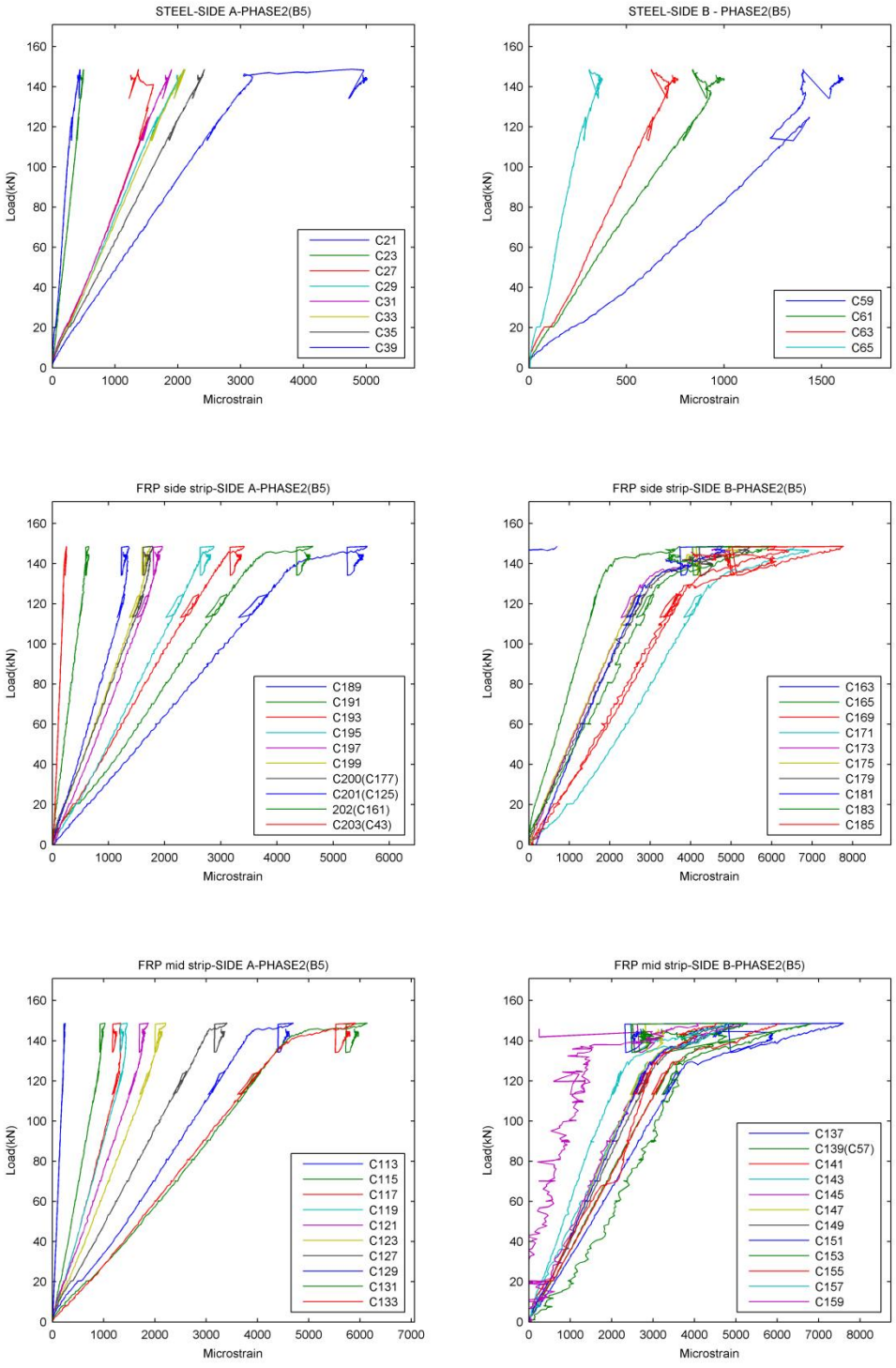

Fig. C5 - 28: Strains in the steel reinforcement and FRP along the span

C.5.17 STRAIN AND BOND STRESS PROFILES

(a)

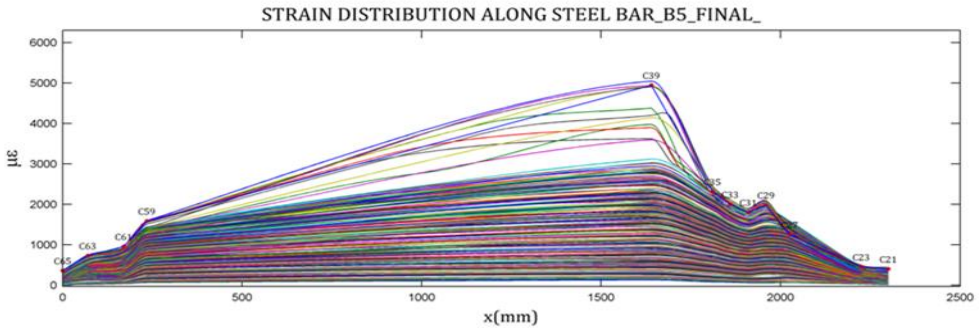

(b)

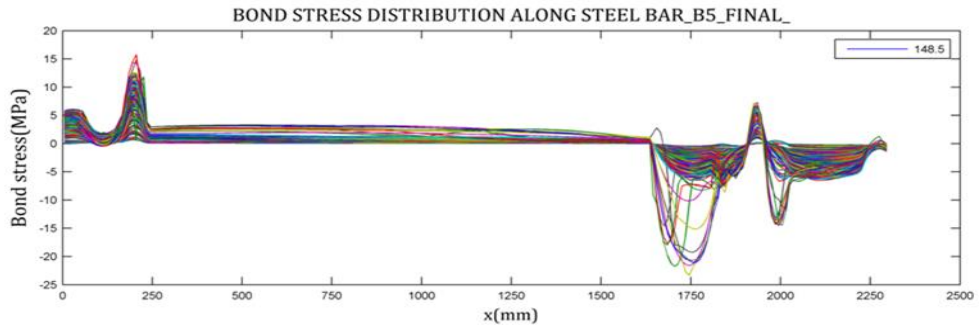

(c)

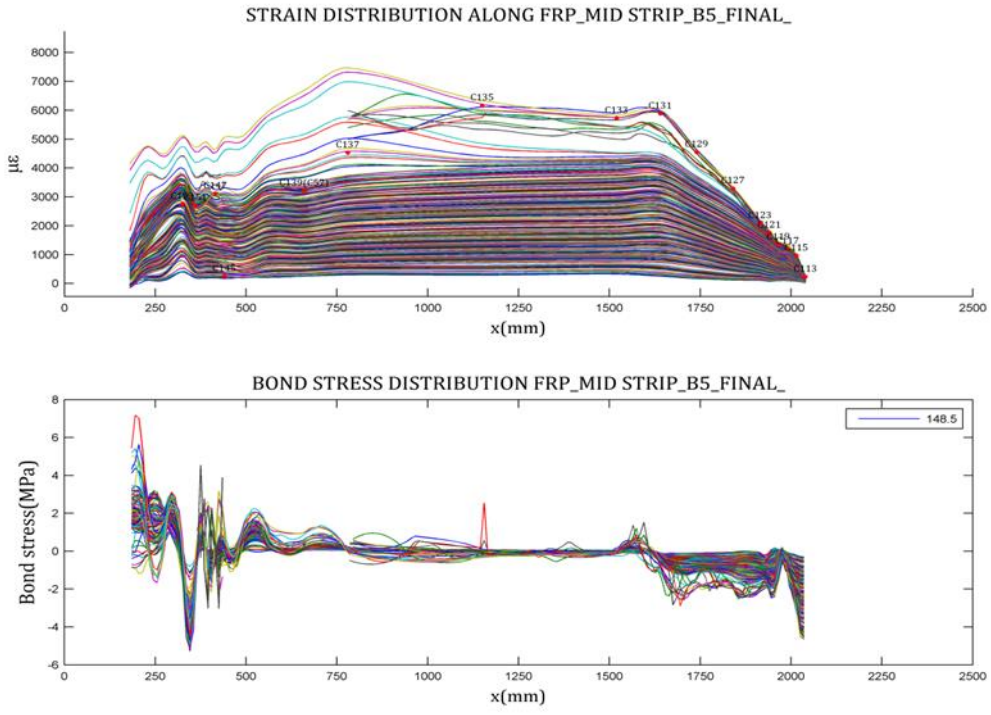

Fig. C5 - 29: Strain and bond stress profiles of (a) Crack pattern of beam NSM2A, (b) FRP, (c) The steel reinforcement

C.5.18 STRAIN AND BOND STRESS PROFILES

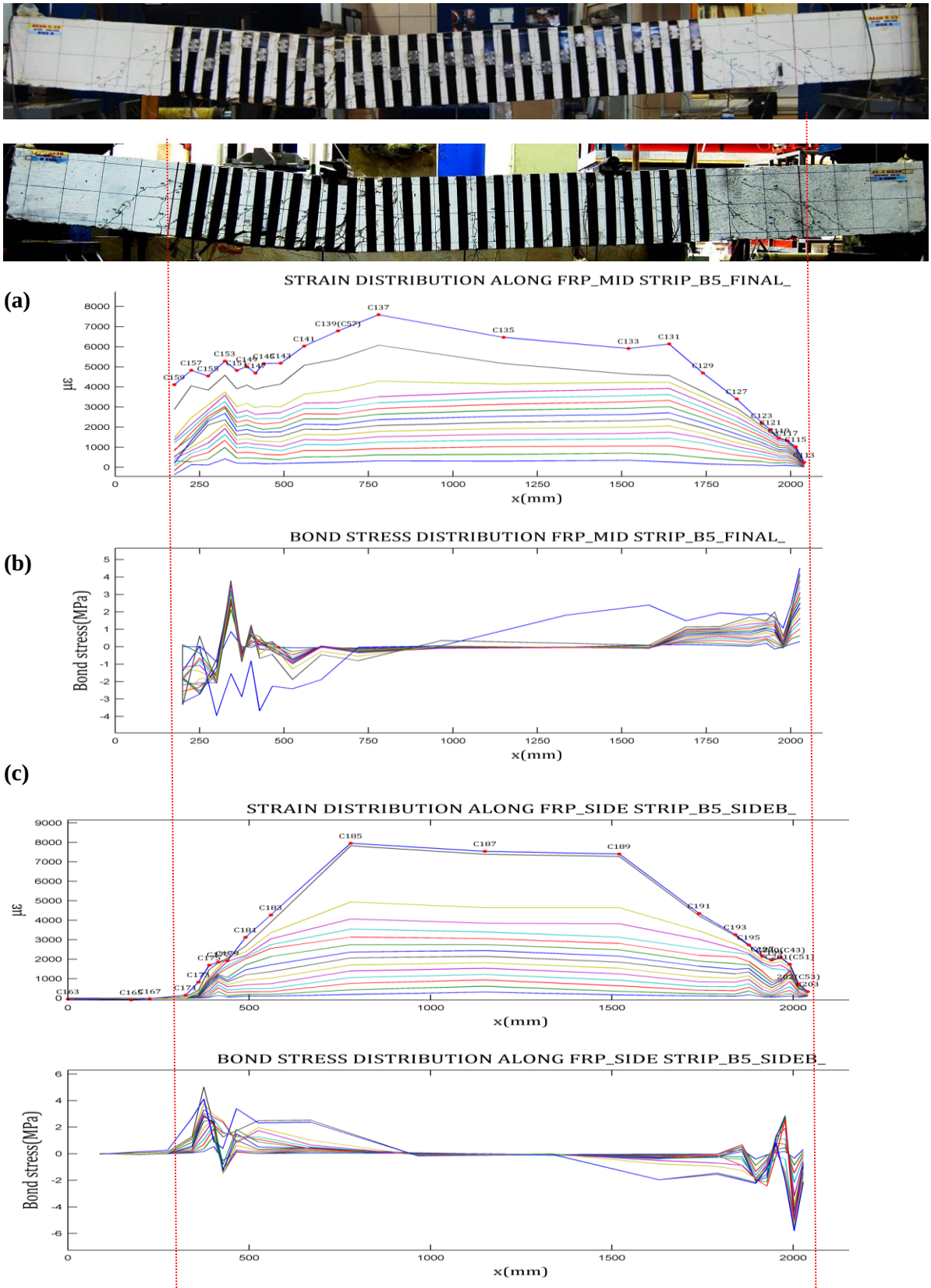

Fig. C5 - 30: Strain and bond stress profiles of (a) Crack pattern of beam NSM2A, (b) FRP, (c) The steel reinforcement

C.5.19 3D PROFILE OF STRAIN AND BOND STRESS

(a)

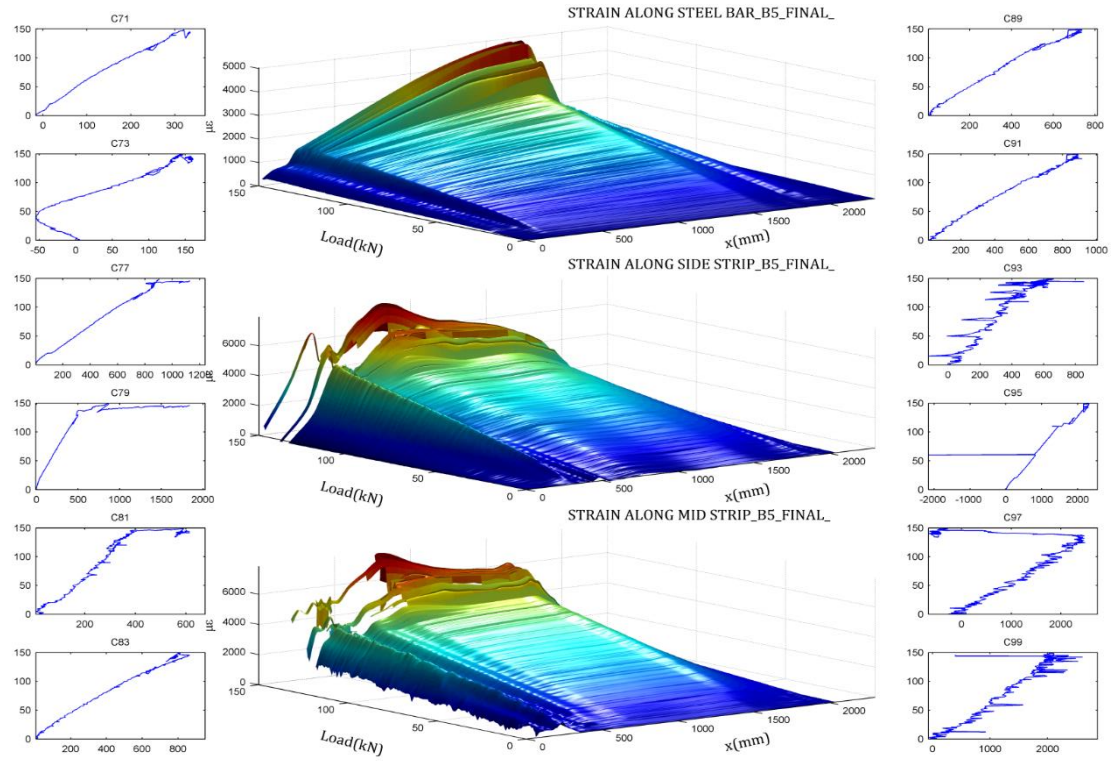

(b)

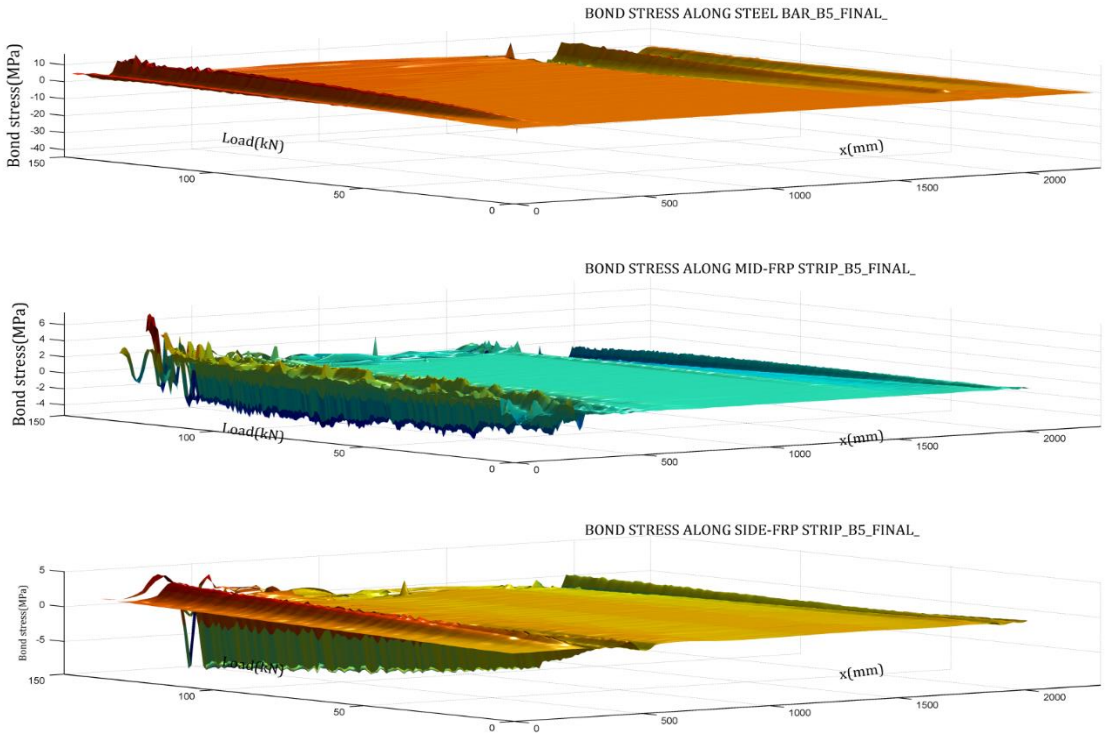

Fig. C5 - 31: Variation of (a) strains and (b) bond stress along the reinforcement and FRP at different load levels

C.6.1 BEAM DESIGN

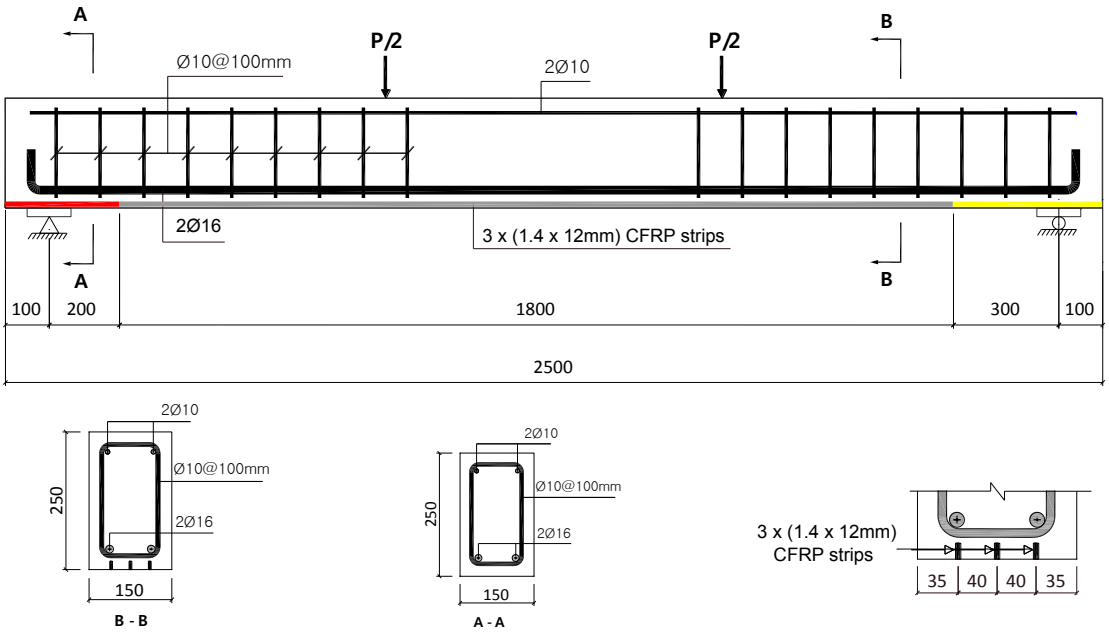

Fig. C6 - 1: Details of specimen

C.6.2 INSTRUMENTATION

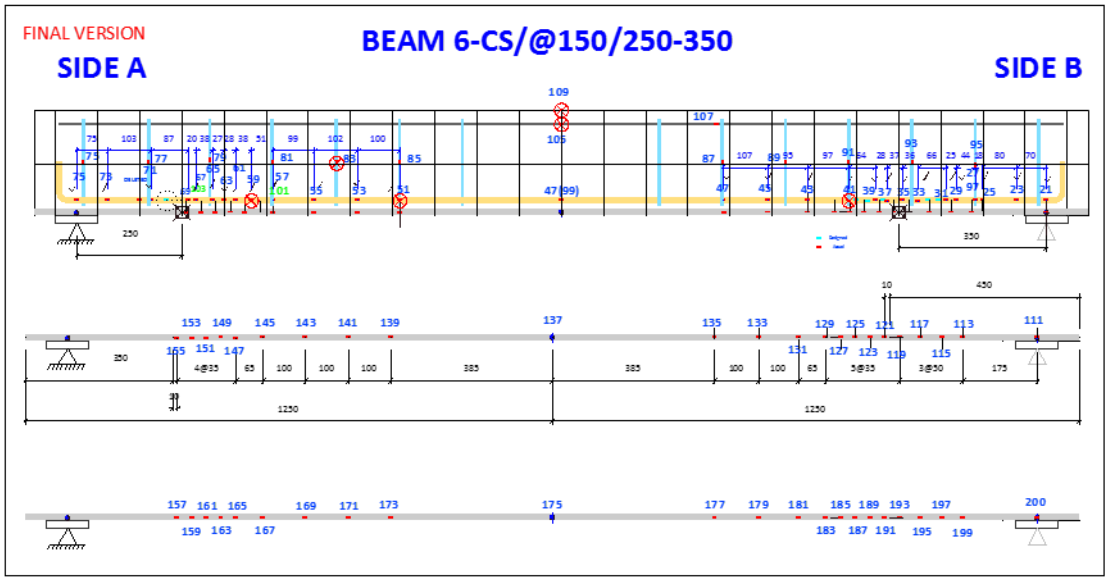

Fig. C6 - 2: Strain gauge arrangement in various components

C.6.3 FIRST TESTING PHASE: PRE-DAMAGING

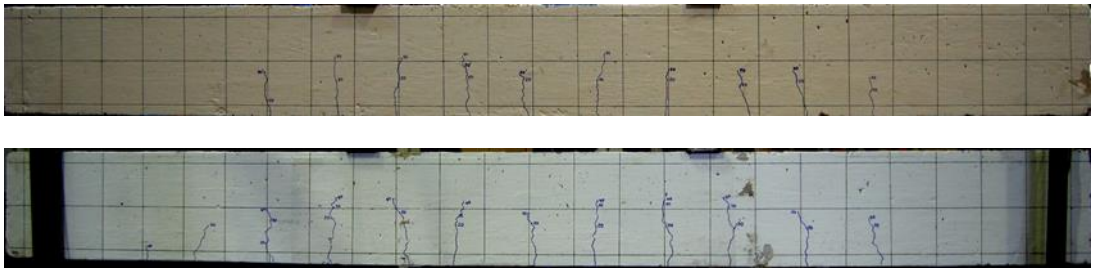

Fig. C6 - 3: Crack pattern of beam NSM6A

C.6.4 FIRST TESTING PHASE: FAILURE ON SIDE B

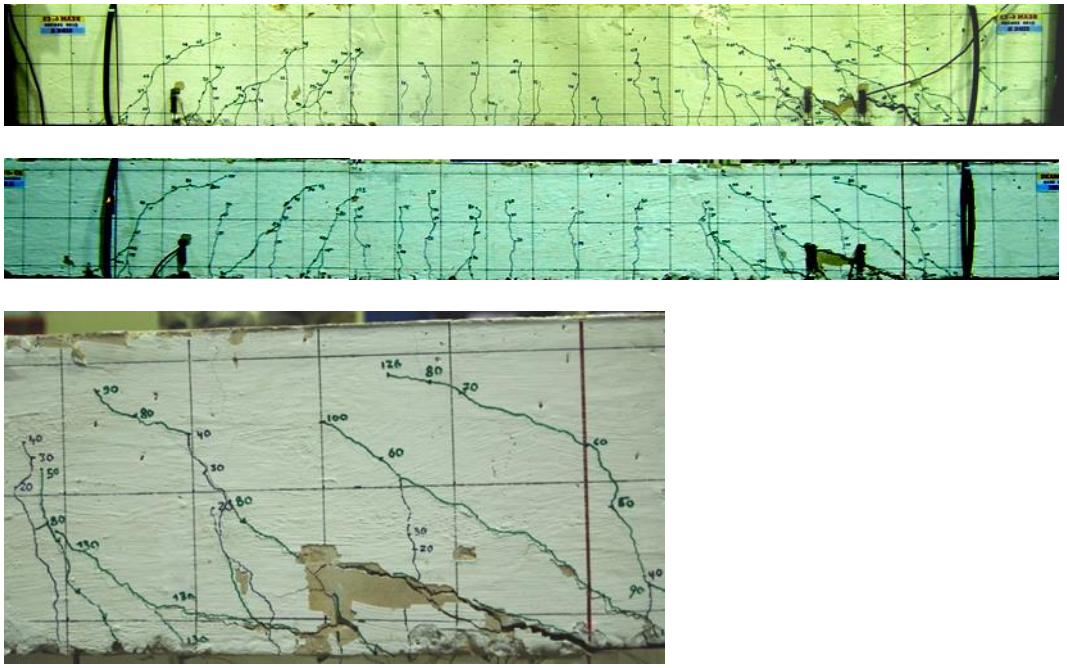

Fig. C6 - 4: Debonding of beam NSM6A

C.6.5 READINGS OF LVDTs

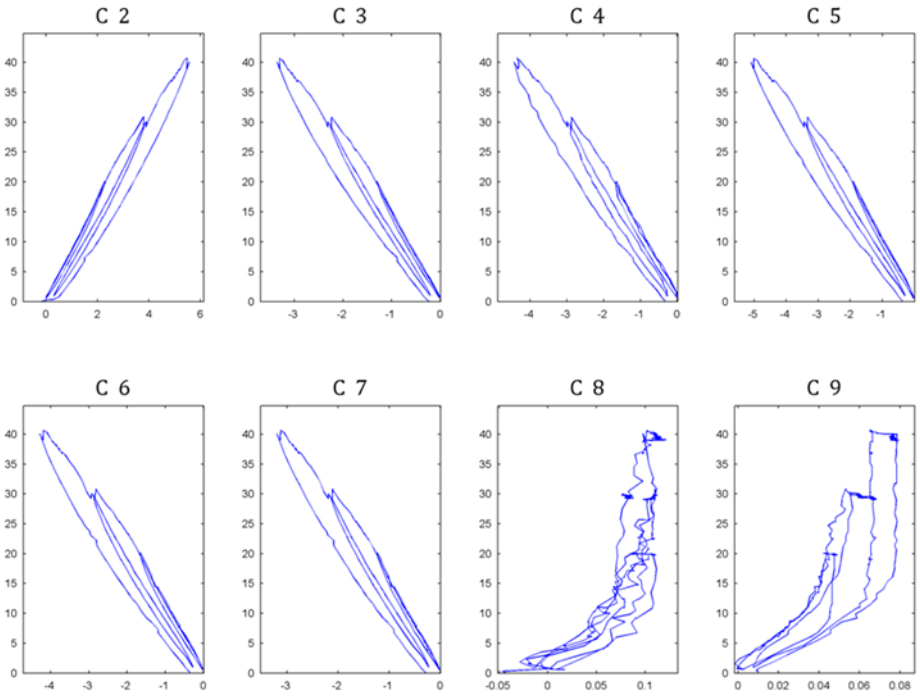

Fig. C6 - 5: Readings of LVDTs (C2 - C9)

C.6.6 STRAIN READINGS

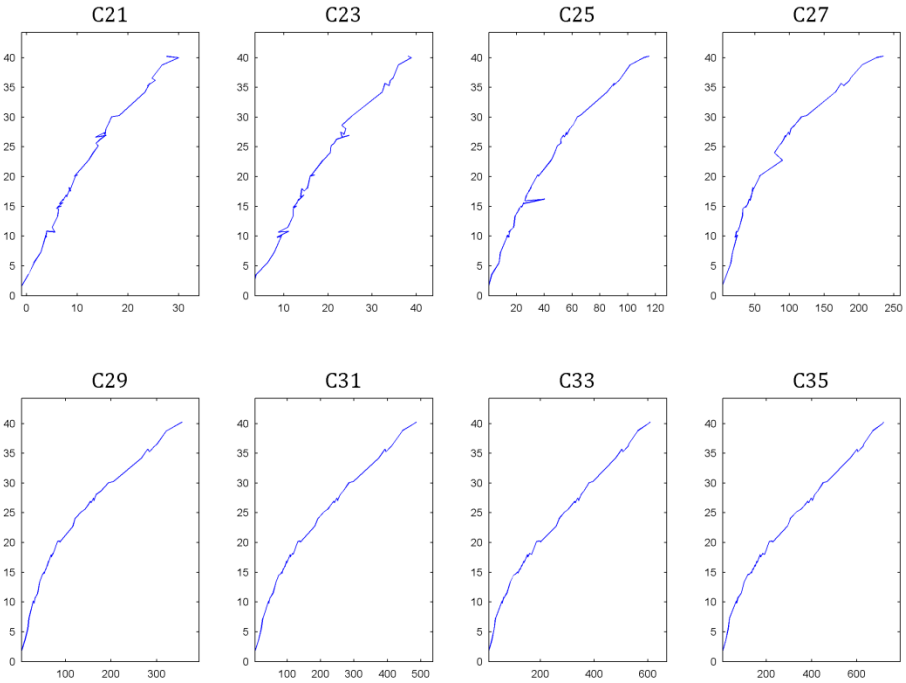

Fig. C6 - 6: Strain readings (C21-C35)

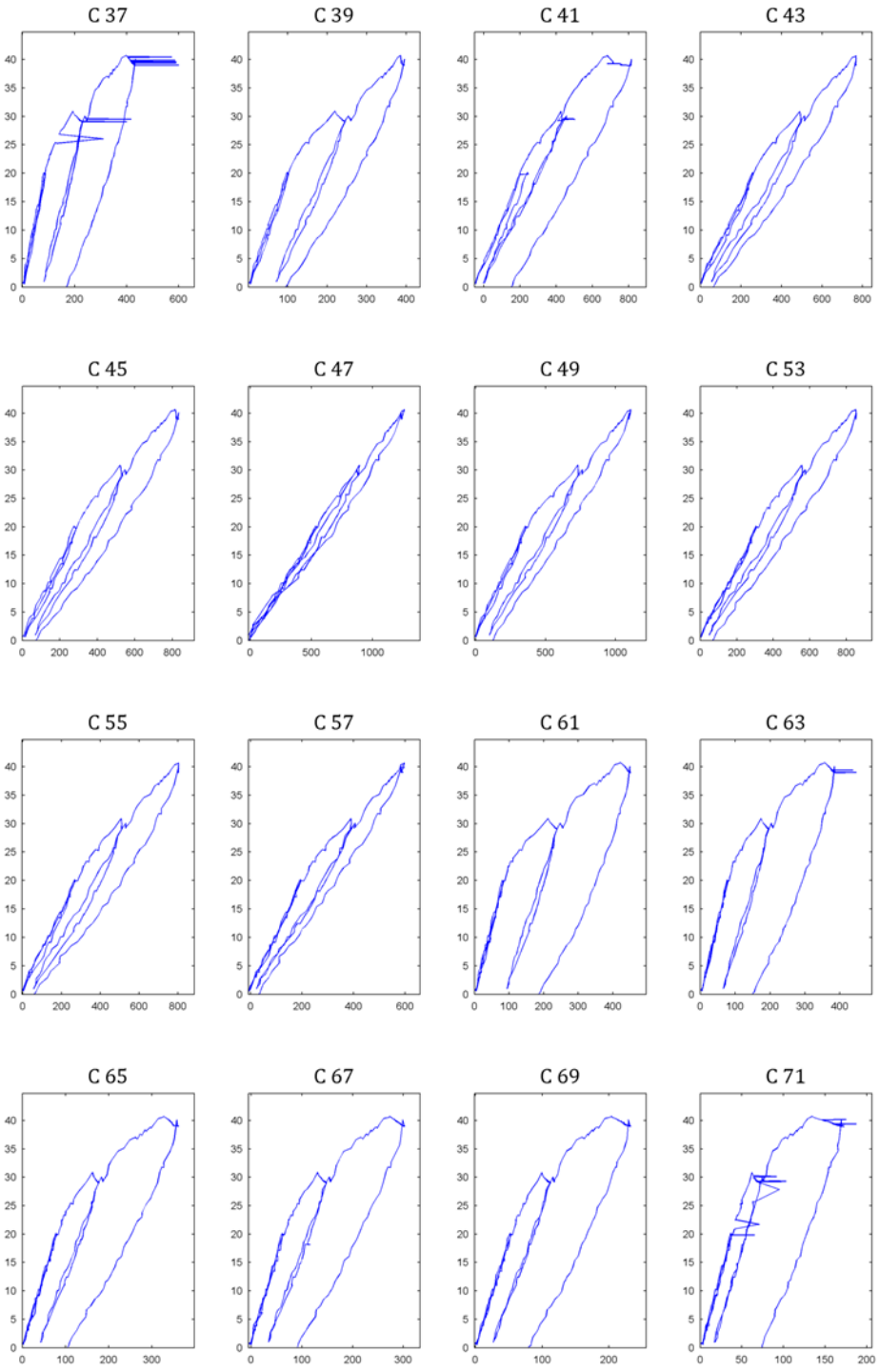

Fig. C6 - 7: Strain readings (C37-C71)

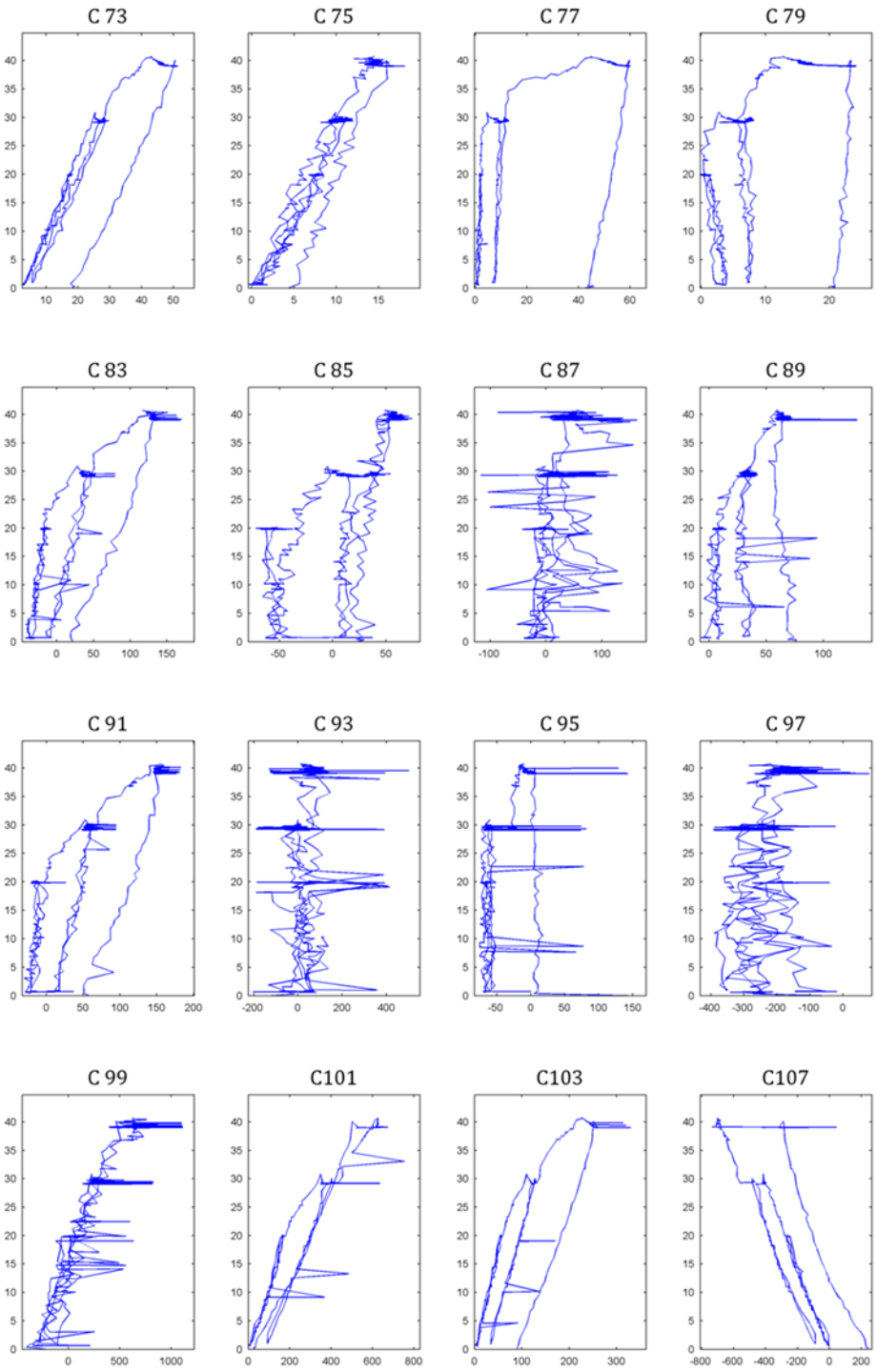

Fig. C6 - 8: Strain readings (C73 – C107)

C.6.7 READINGS OF LVDTs

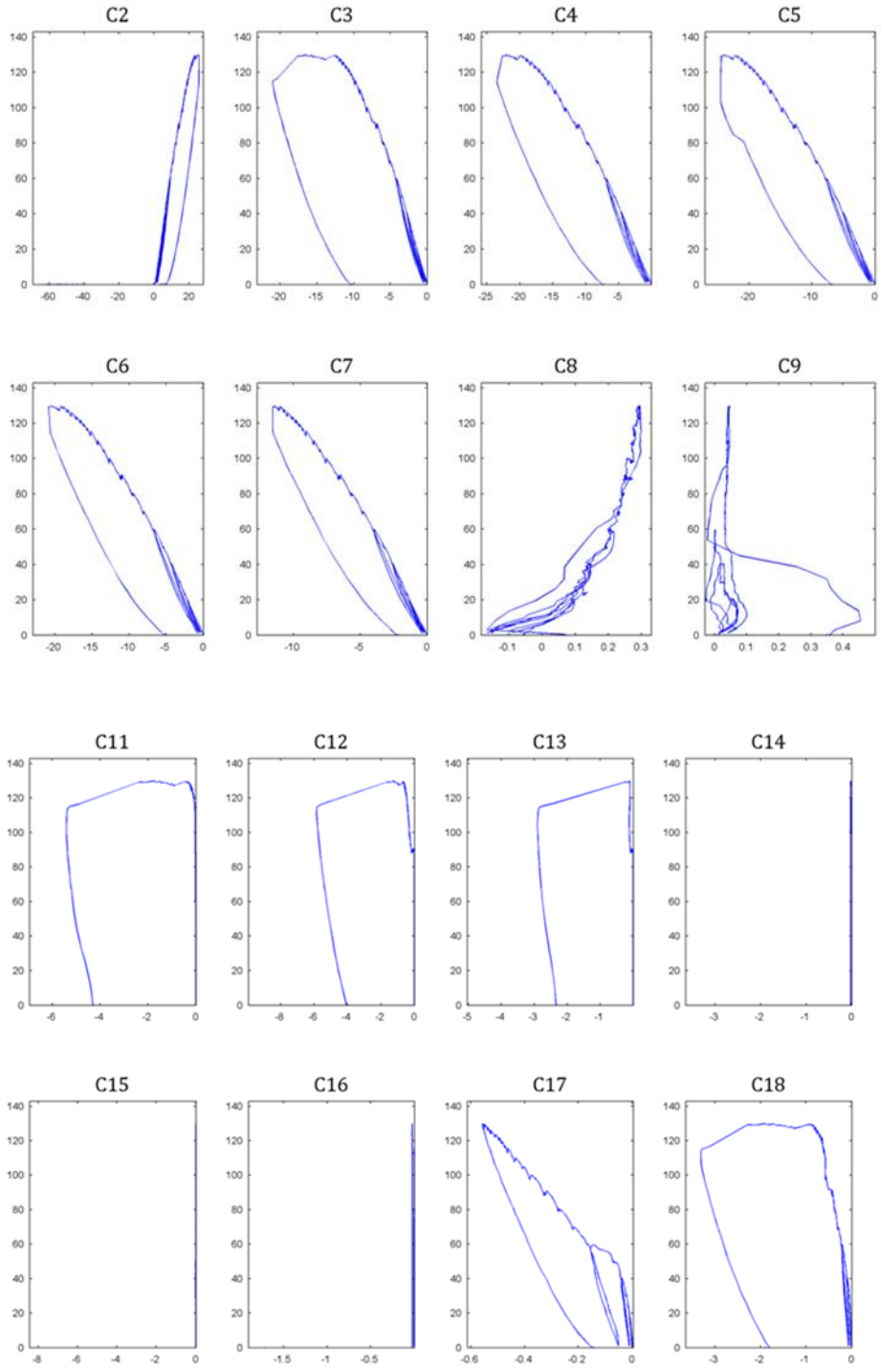

Fig. C6 - 9: Readings of LVDTs (C2-C18)

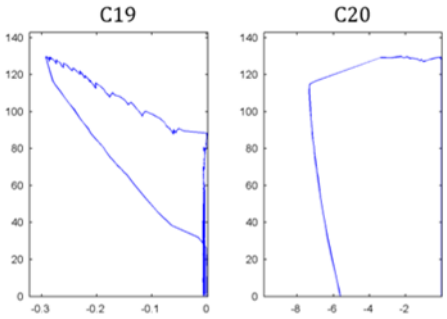

Fig. C6 - 10: Readings of LVDTs (C19 – C20)

C.6.8 STRAIN READINGS

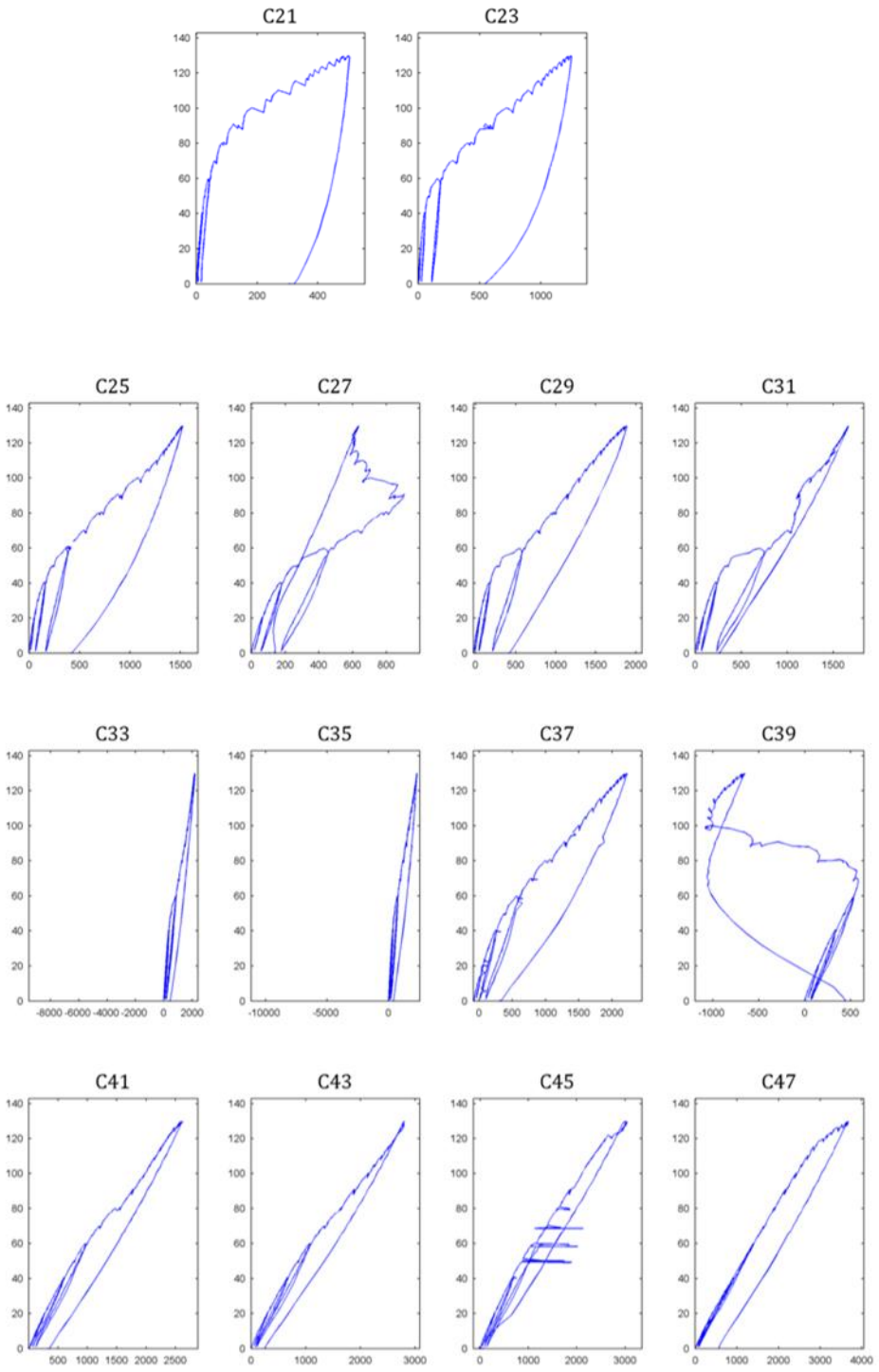

Fig. C6 - 11: Strain readings (C21-C47)

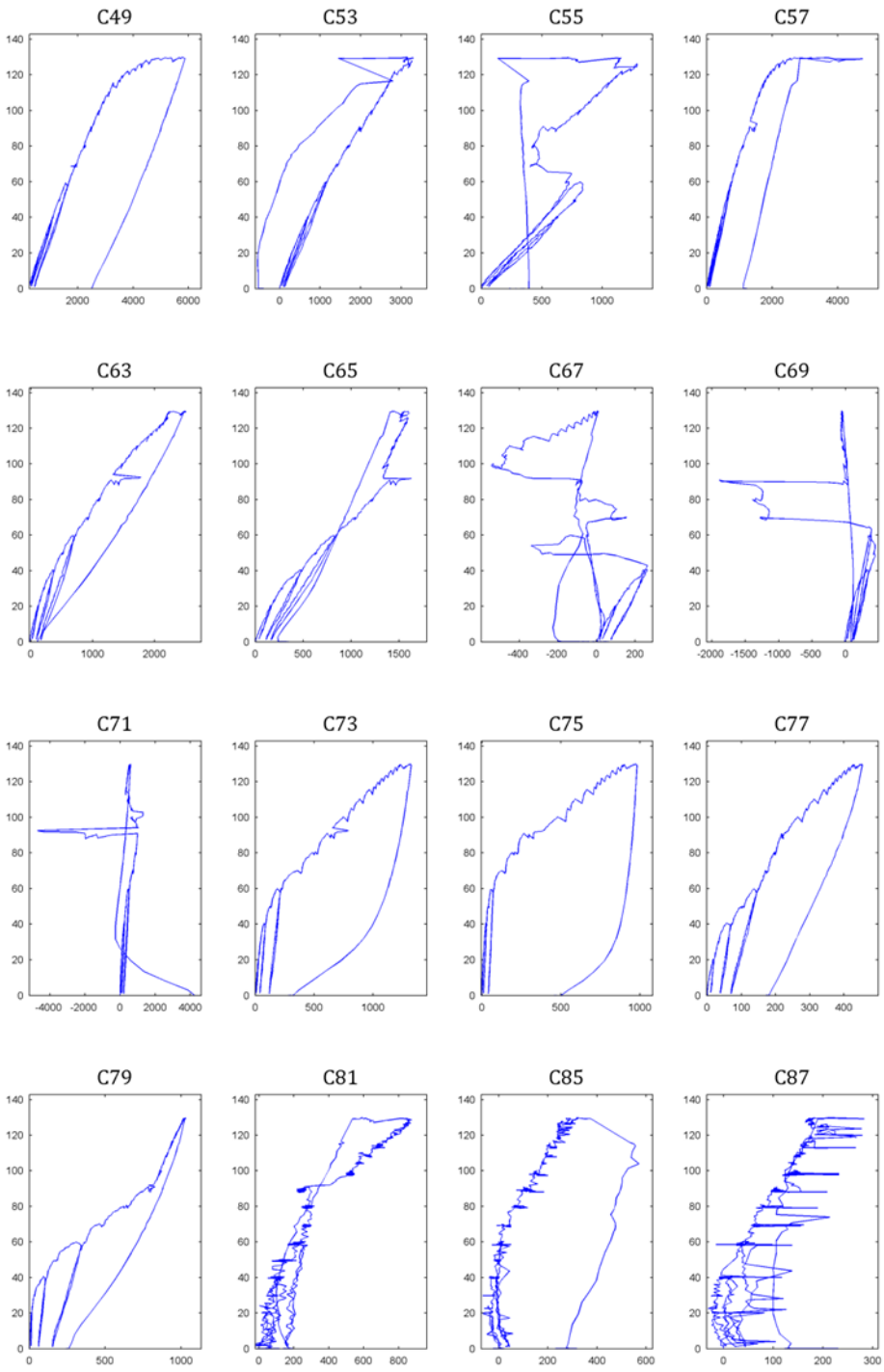

Fig. C6 - 12: Strain readings (C49-C87)

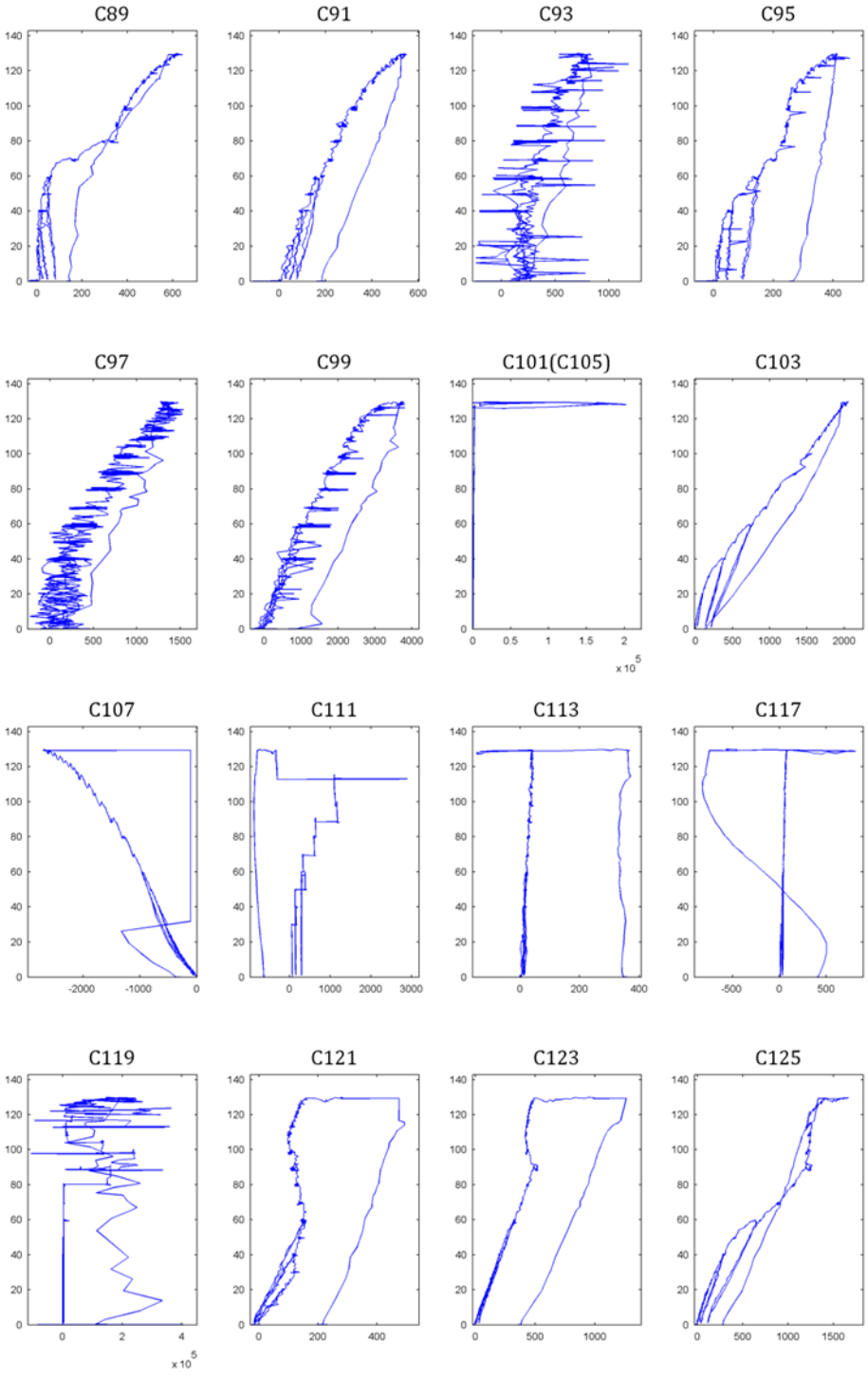

Fig. C6 - 13: Strain readings (C89-C125)

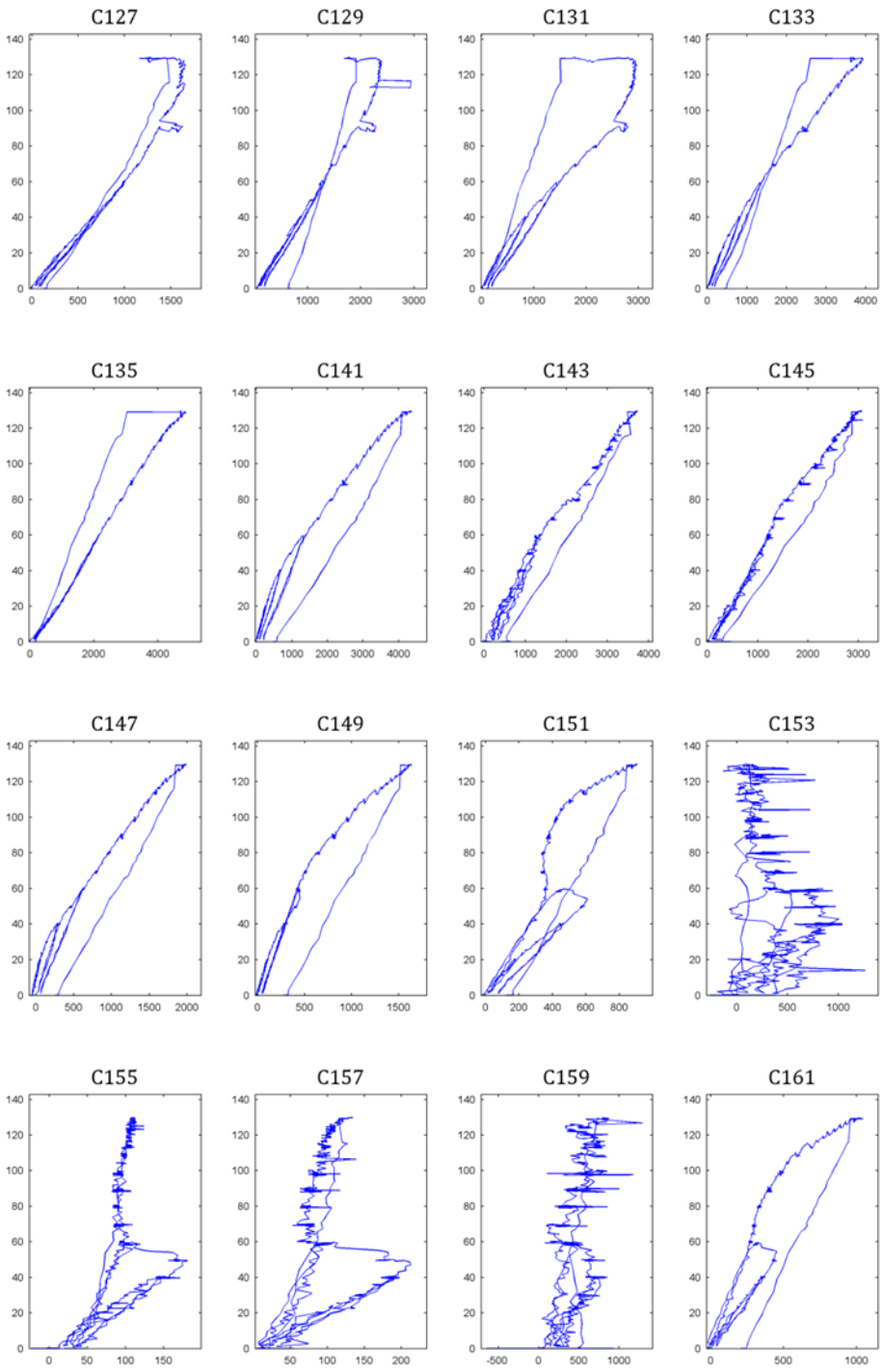

Fig. C6 - 14: Strain readings (C127-161)

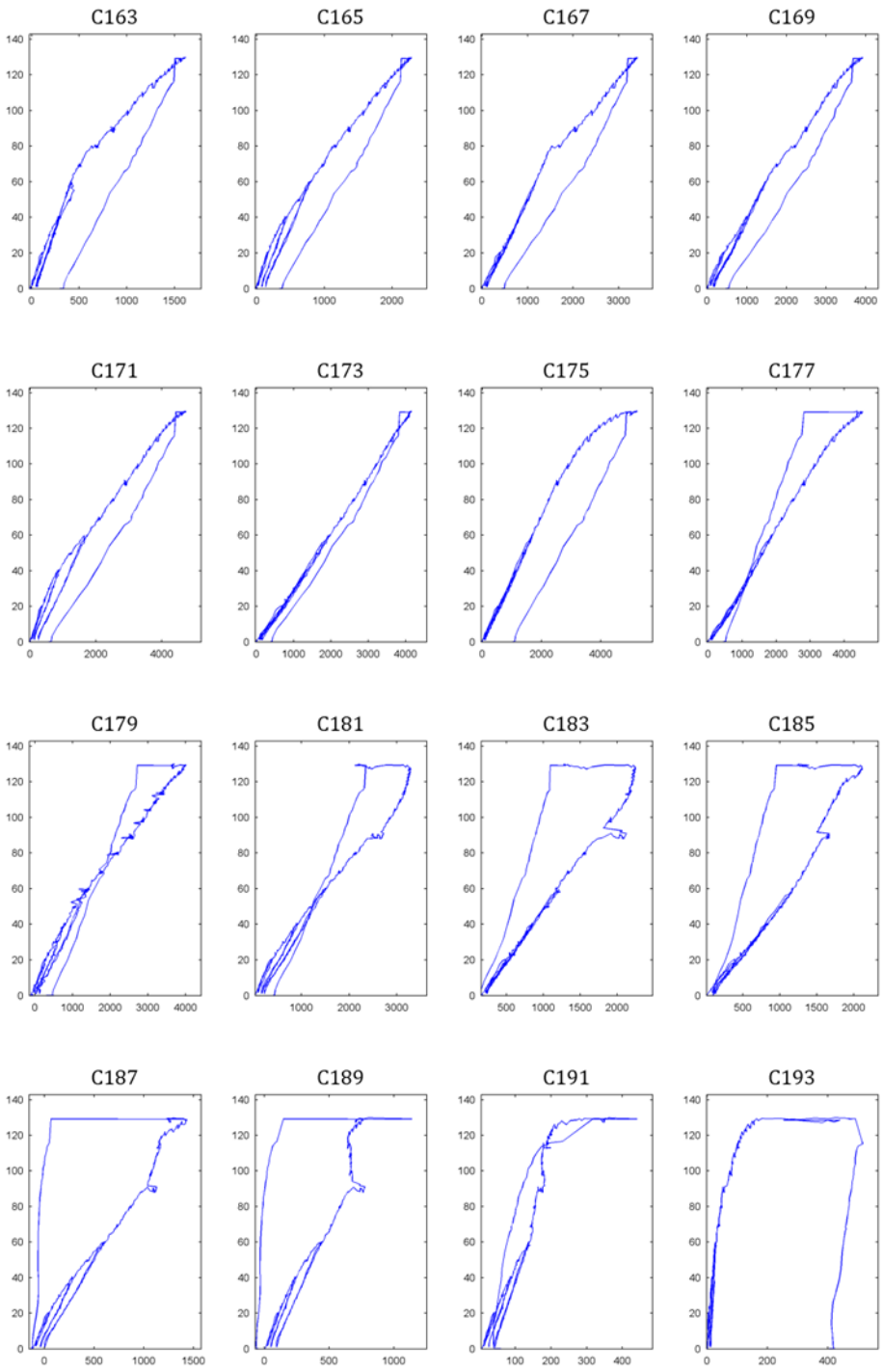

Fig. C6 - 15: Strain readings (C163-C193)

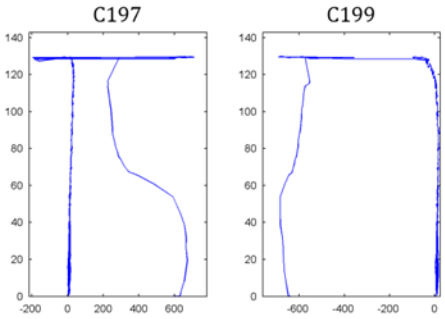

Fig. C6 - 16: Strain readings (C197 – C199)

C.6.9 STRAINS IN THE STEEL REINFORCEMENT AND FRP ALONG THE SPAN

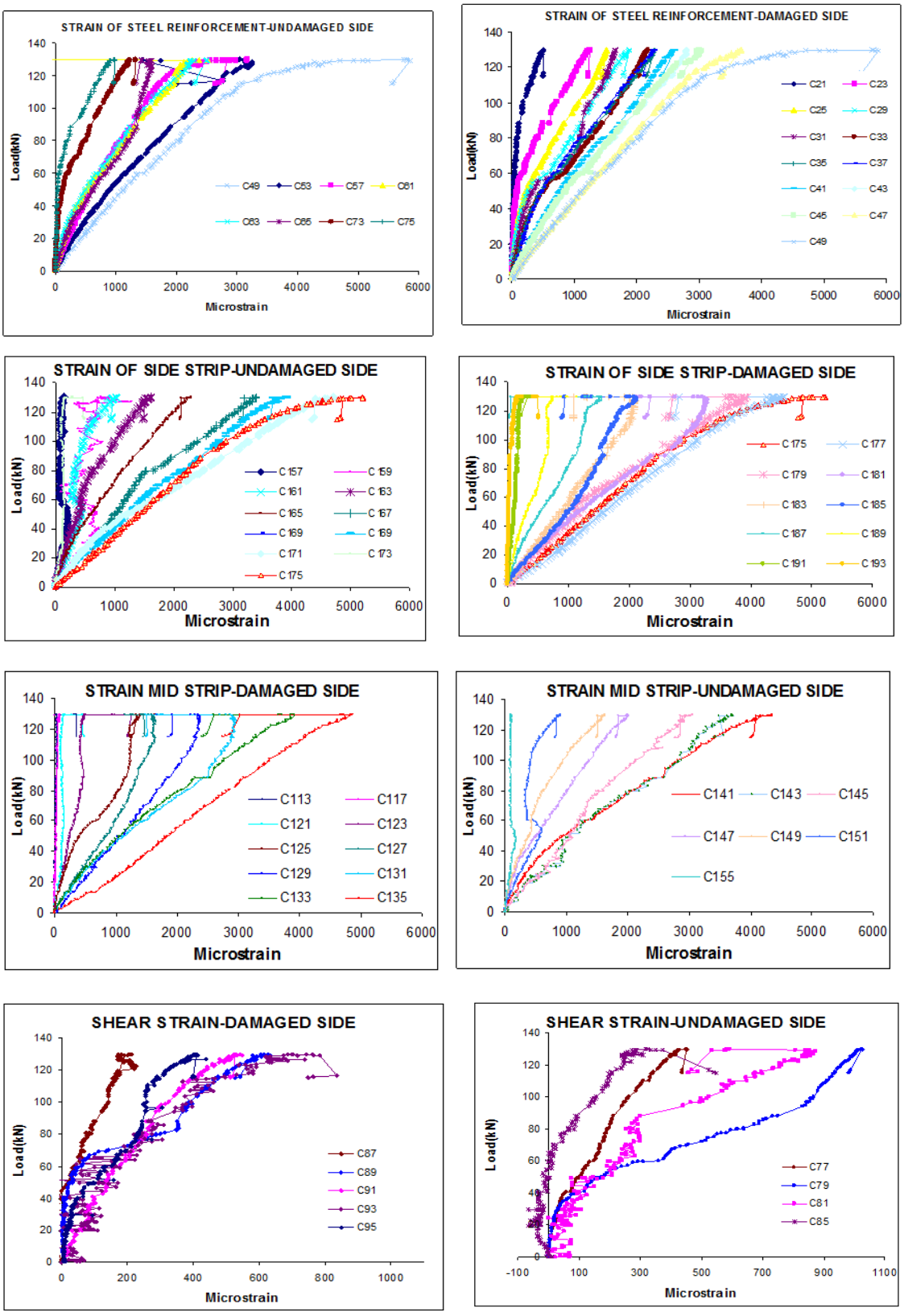

Fig. C6 - 17: Strains in the steel reinforcement and FRP along the span

C.6.10 STRAIN AND BOND STRESS PROFILES

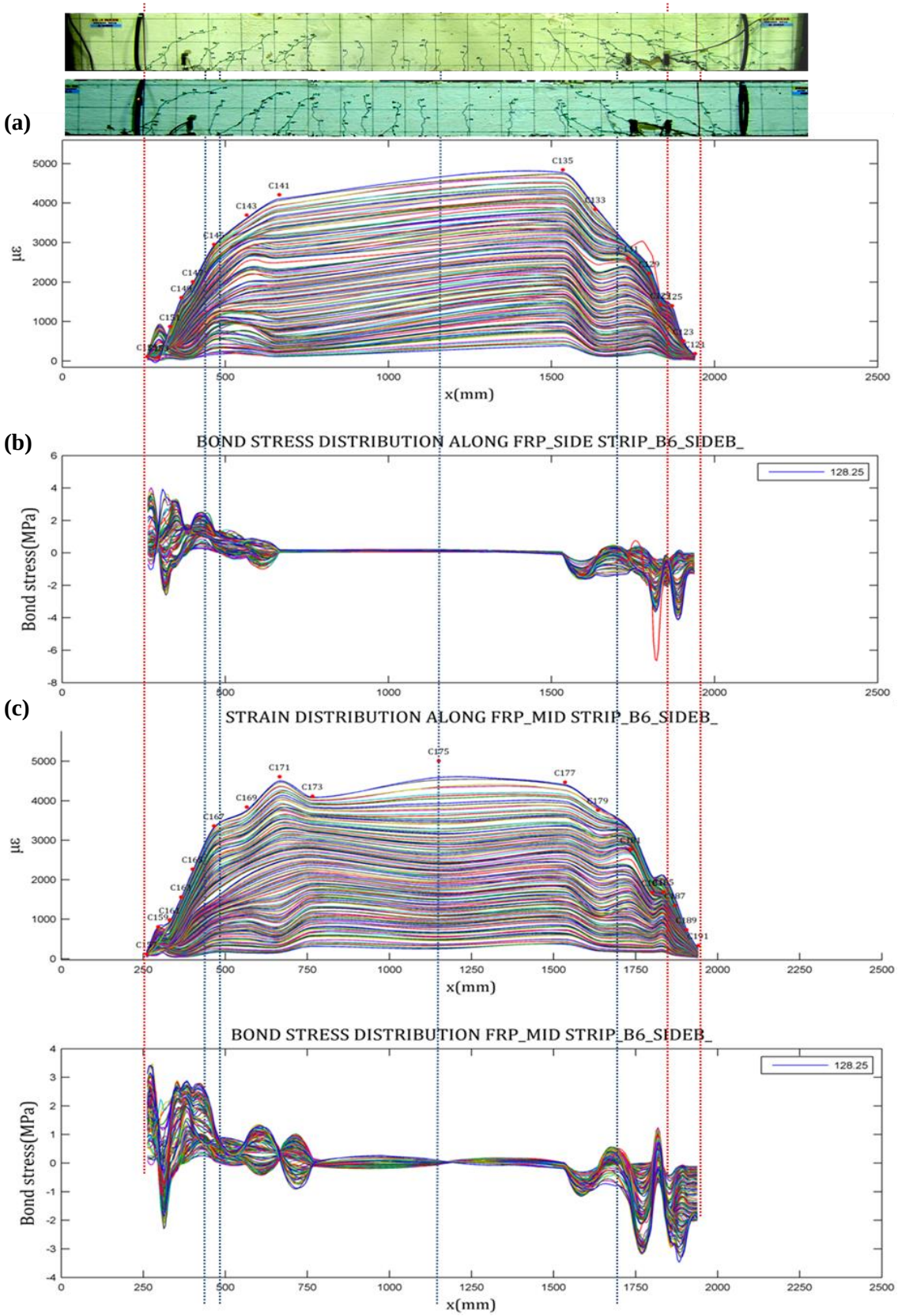

Fig. C6 - 18: Strain and bond stress profiles of (a) Crack pattern of beam NSM2A, (b) FRP, (c) The steel reinforcement

C.6.11 3D PROFILE OF STRAIN AND BOND STRESS

(a)

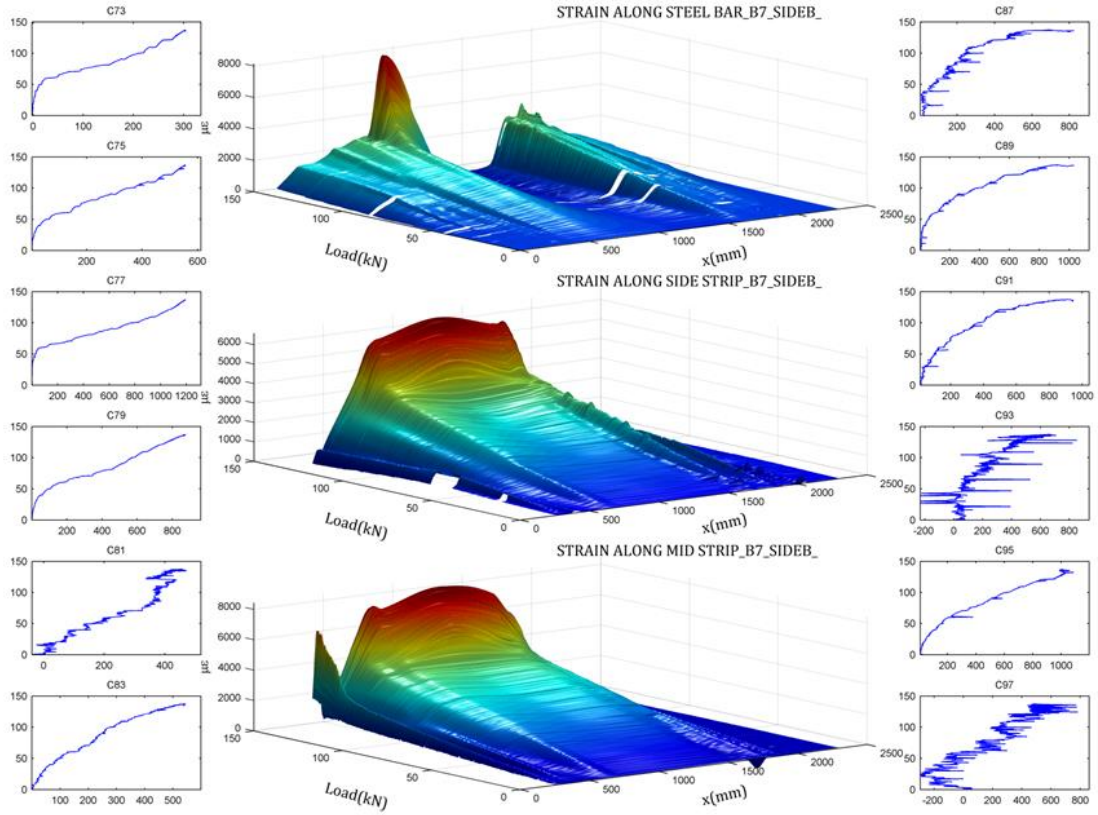

(b)

Fig. C6 - 19: Variation of (a) strains and (b) bond stress along the reinforcement and FRP at different load levels

C.6.12 FINAL TESTING PHASE

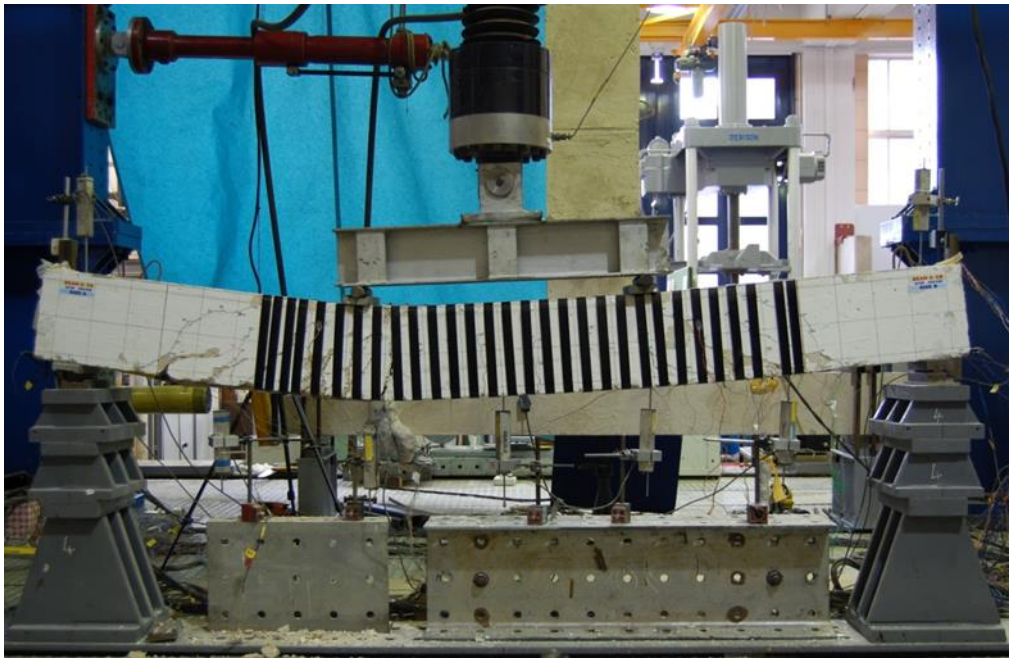

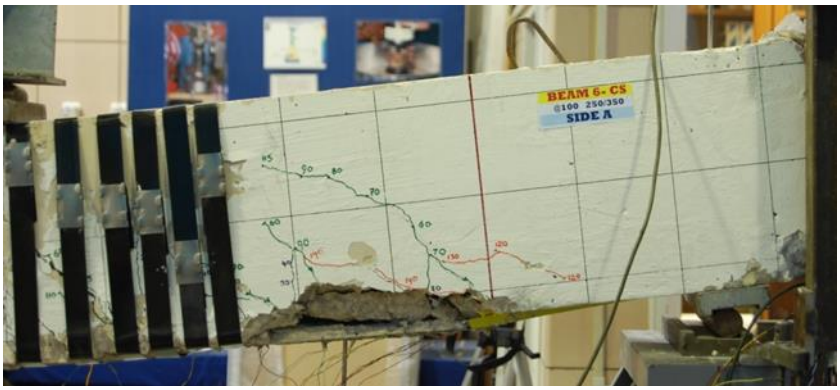

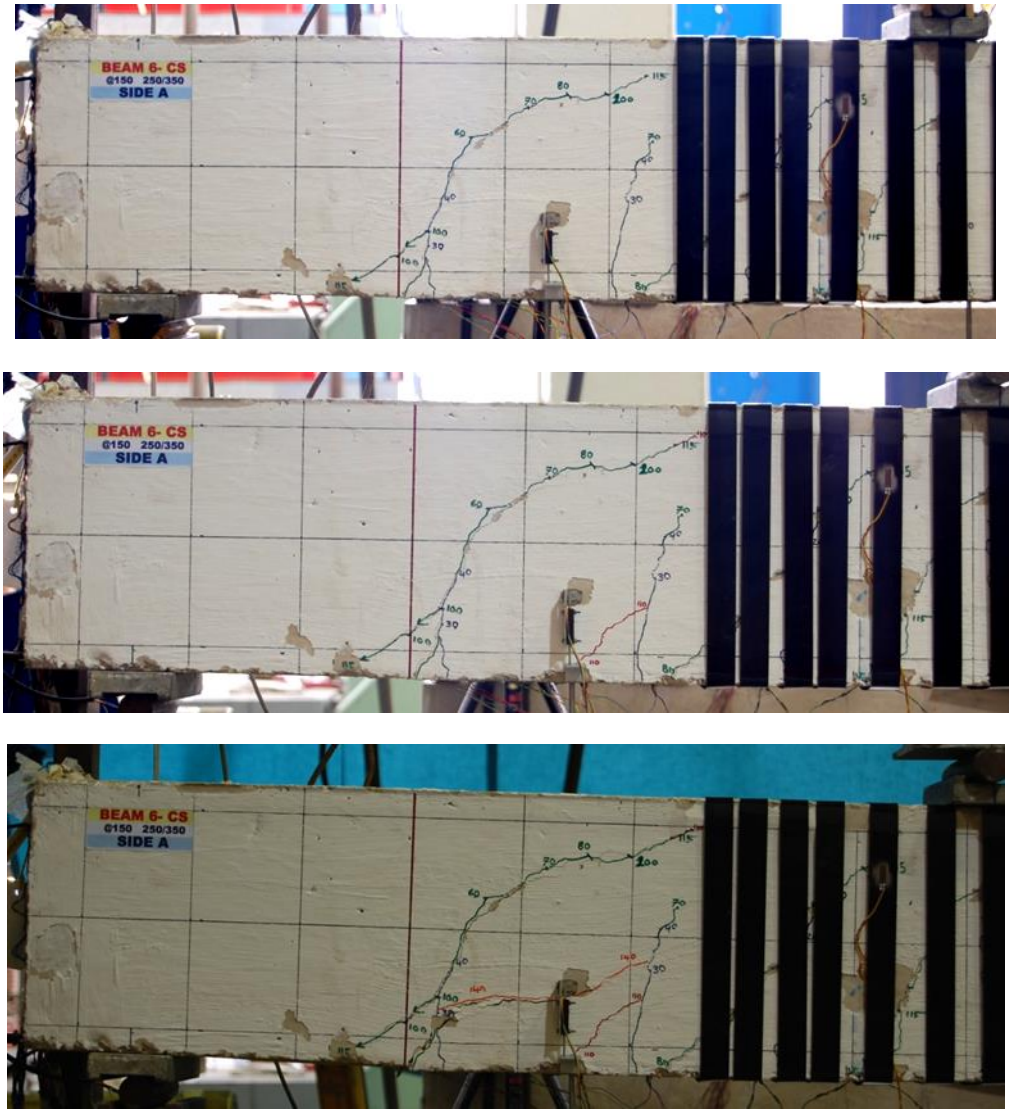

Fig. C6 - 20: Final testing phase of beam NSM6A

C.6.13 READINGS OF LVDTs

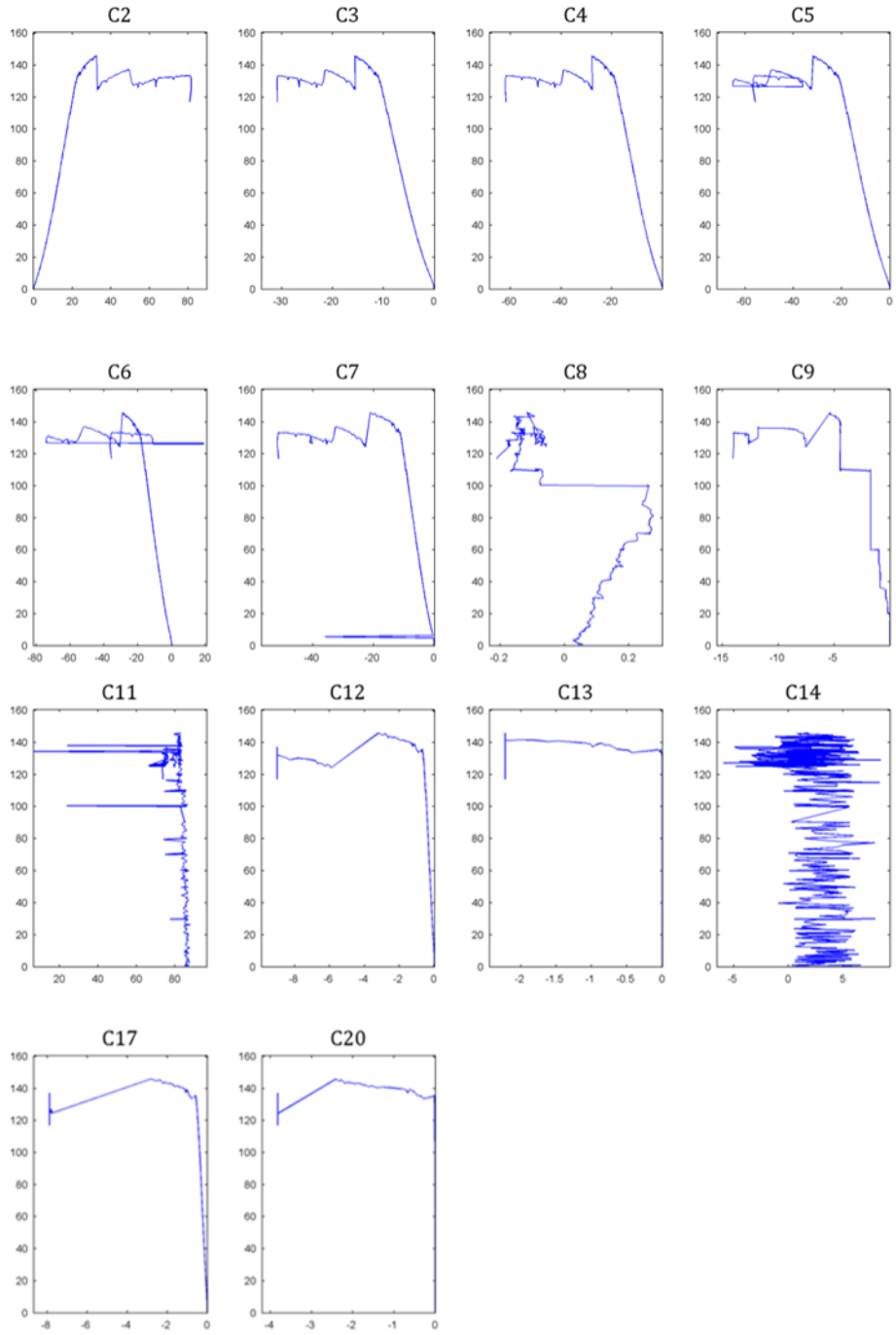

Fig. C6 - 21: Readings of LVDTs (C2 – C20)

C.6.14 STRAIN READINGS

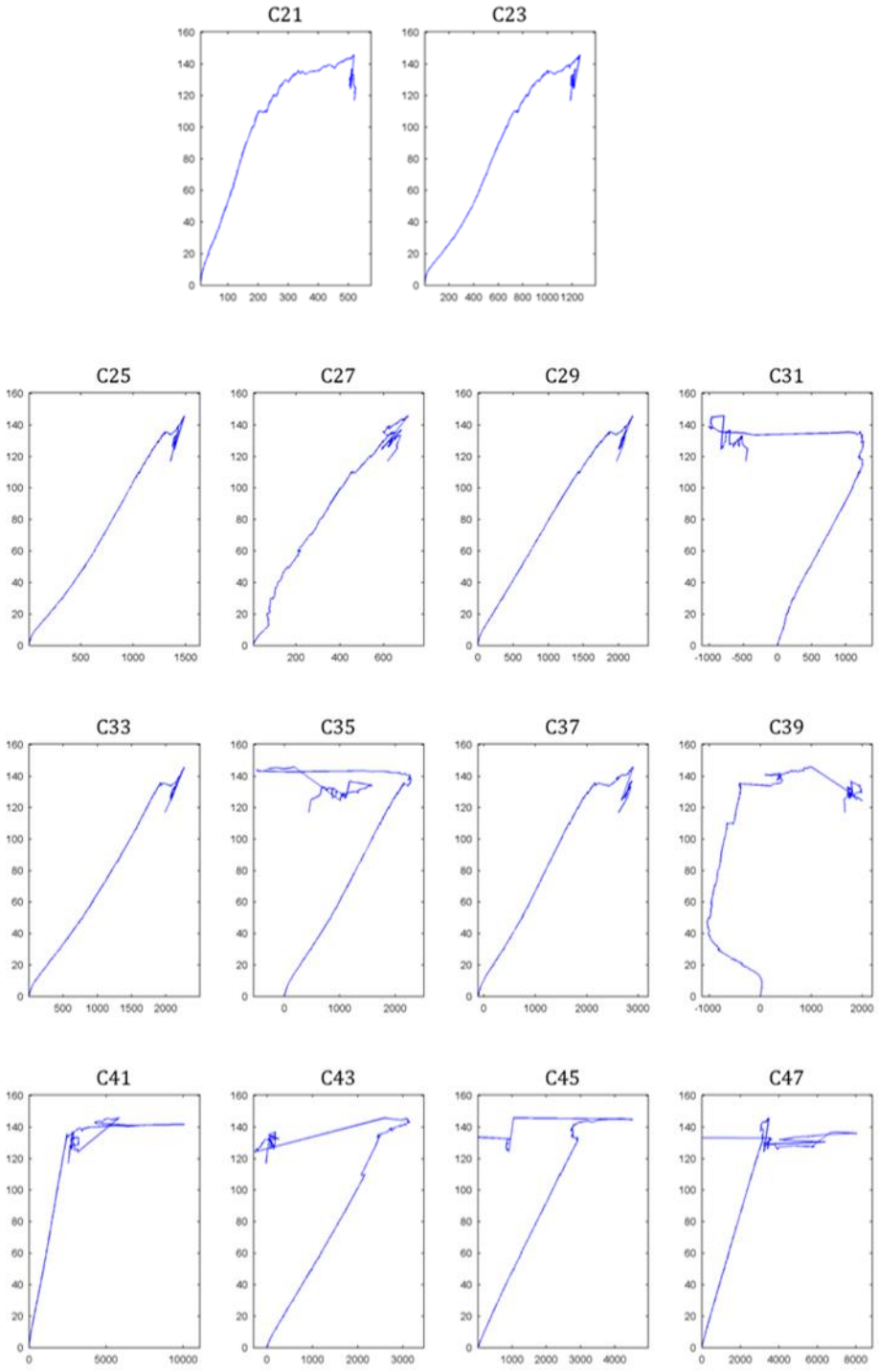

Fig. C6 - 22: Strain readings (C21-C47)

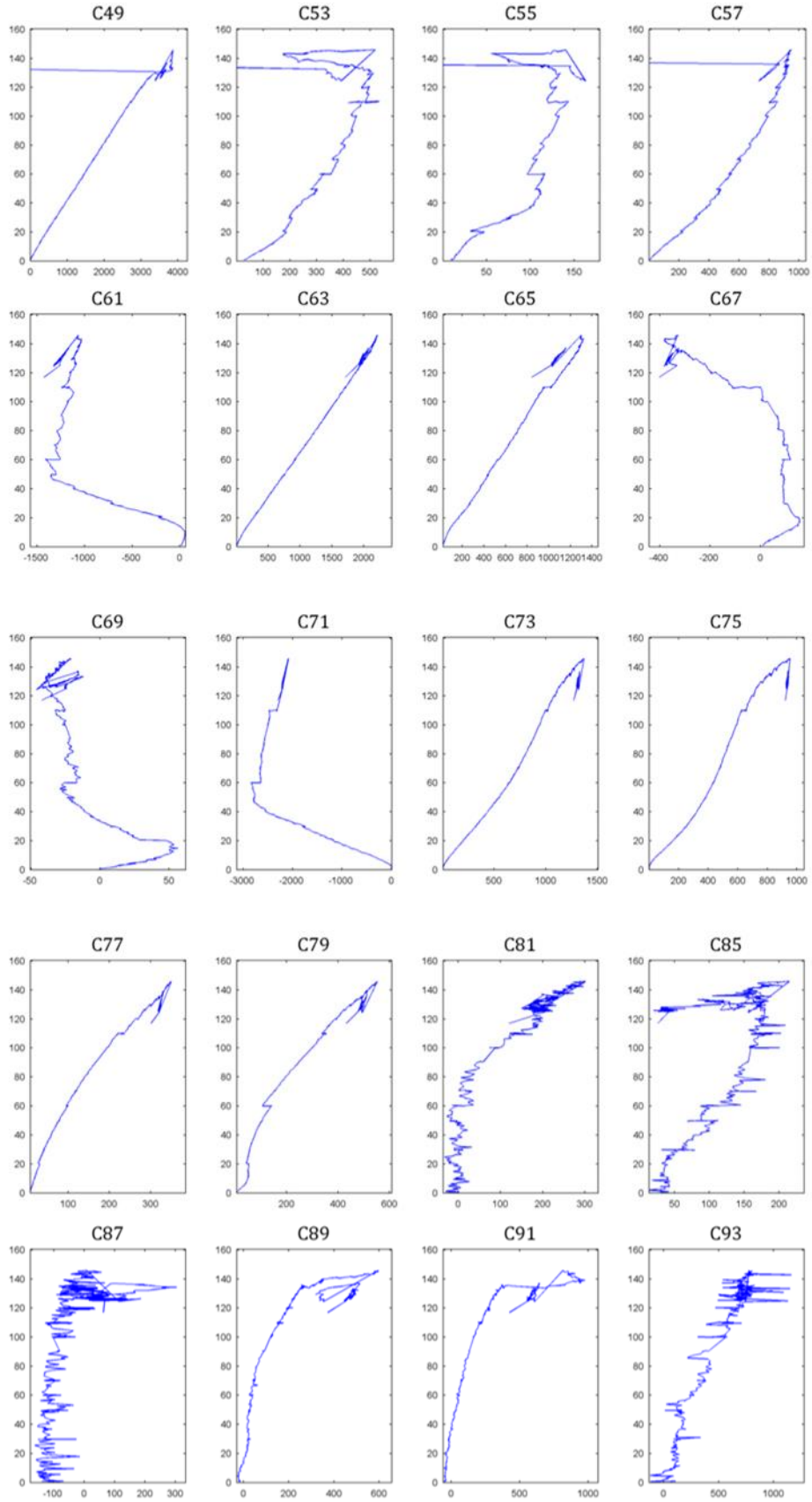

Fig. C6 - 23: Strain readings (C49-C93)

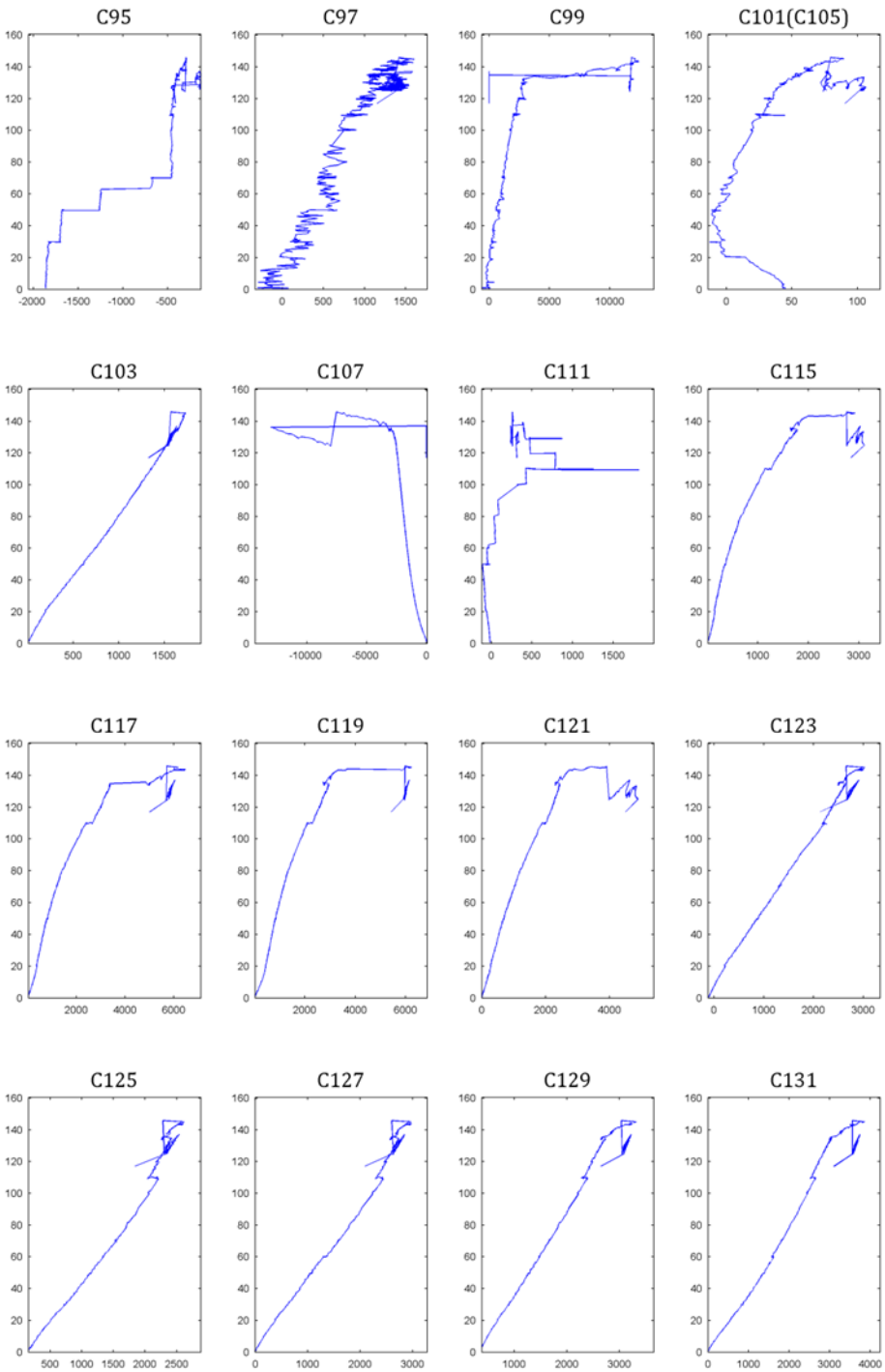

Fig. C6 - 24: Strain readings (C95-C131)

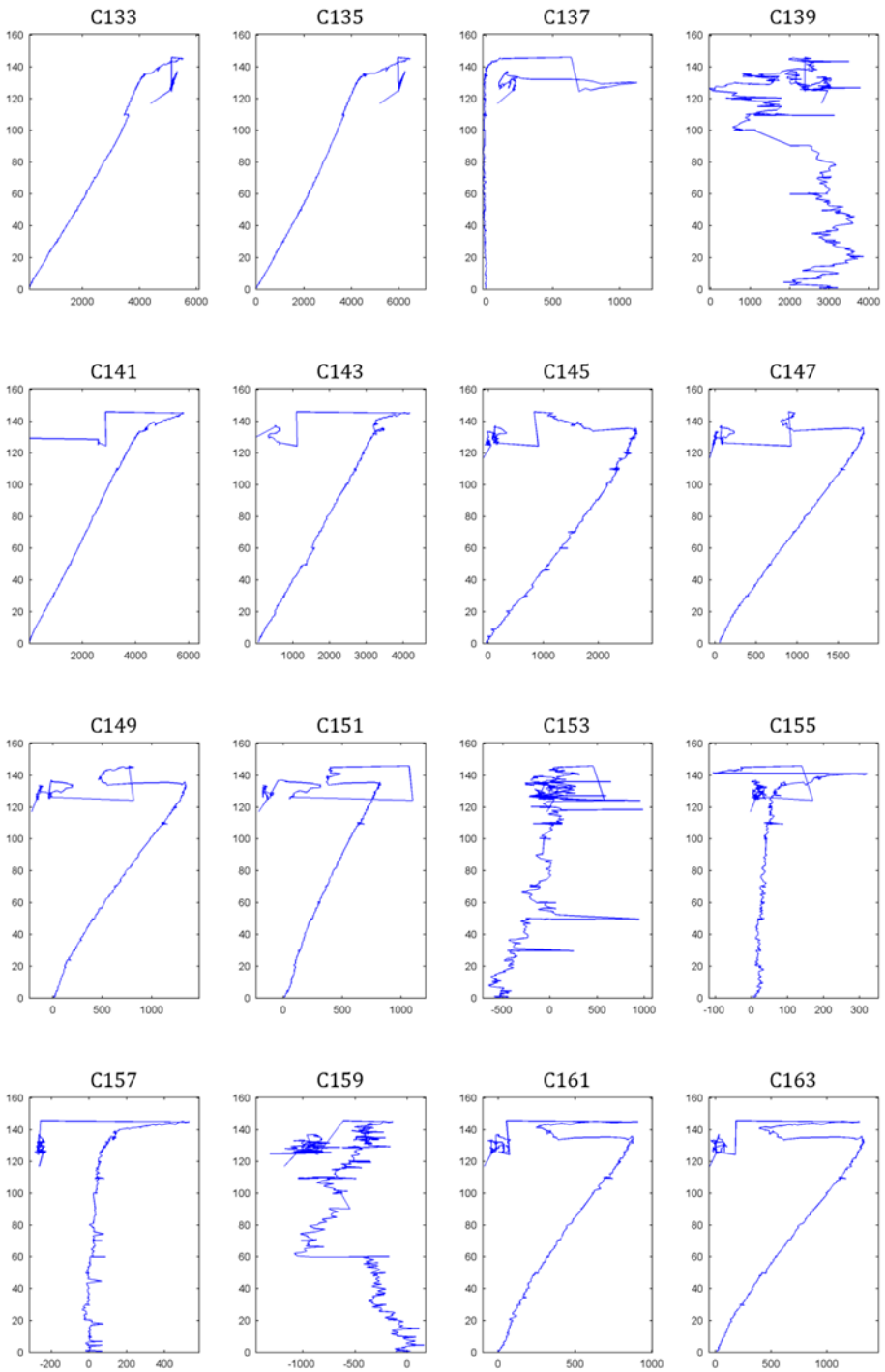

Fig. C6 - 25: Strain readings (C133-C163)

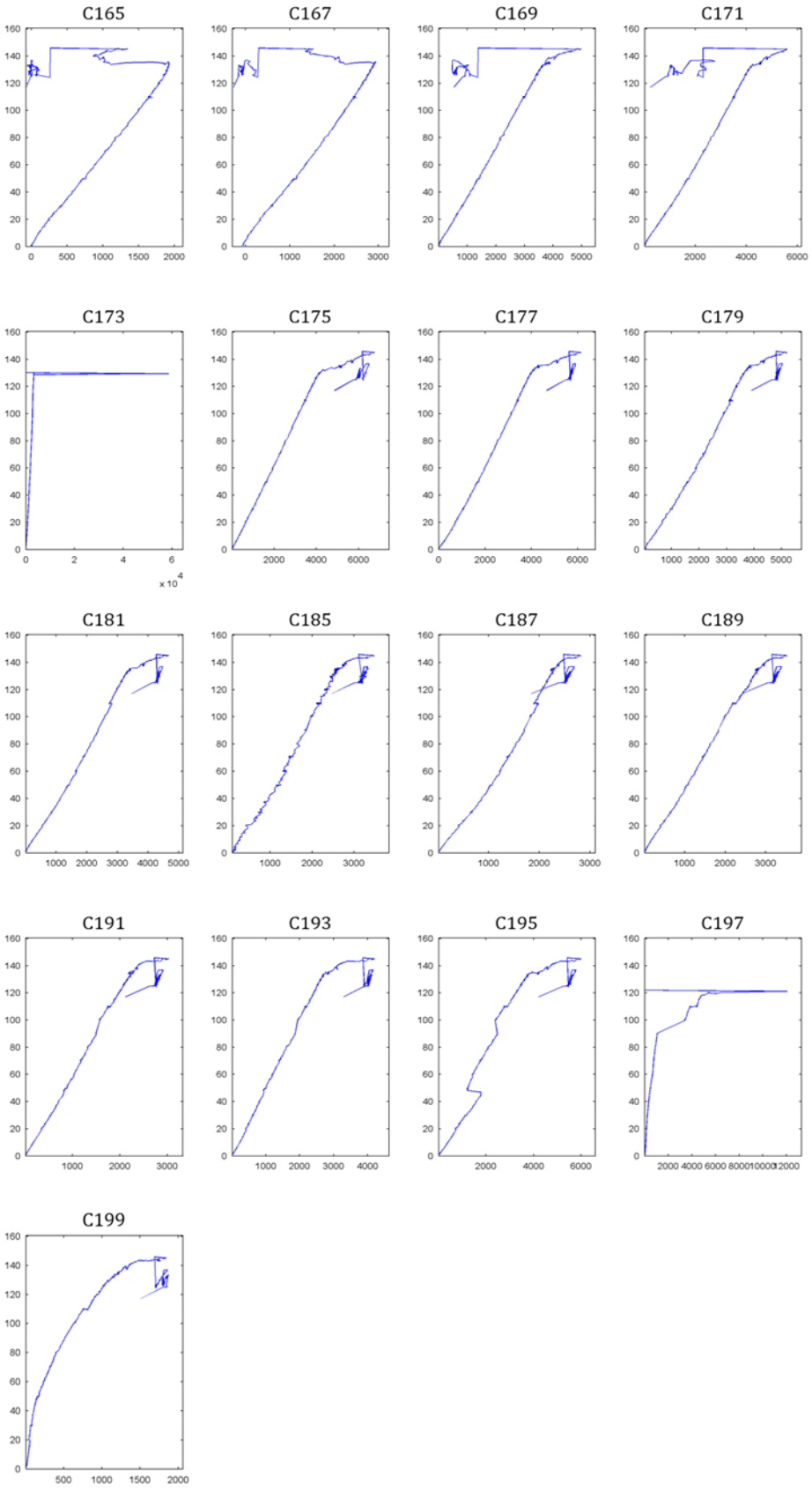

Fig. C6 - 26: Strain readings (C165 – C199)

C.6.15 STRAINS IN THE STEEL REINFORCEMENT AND FRP ALONG THE SPAN

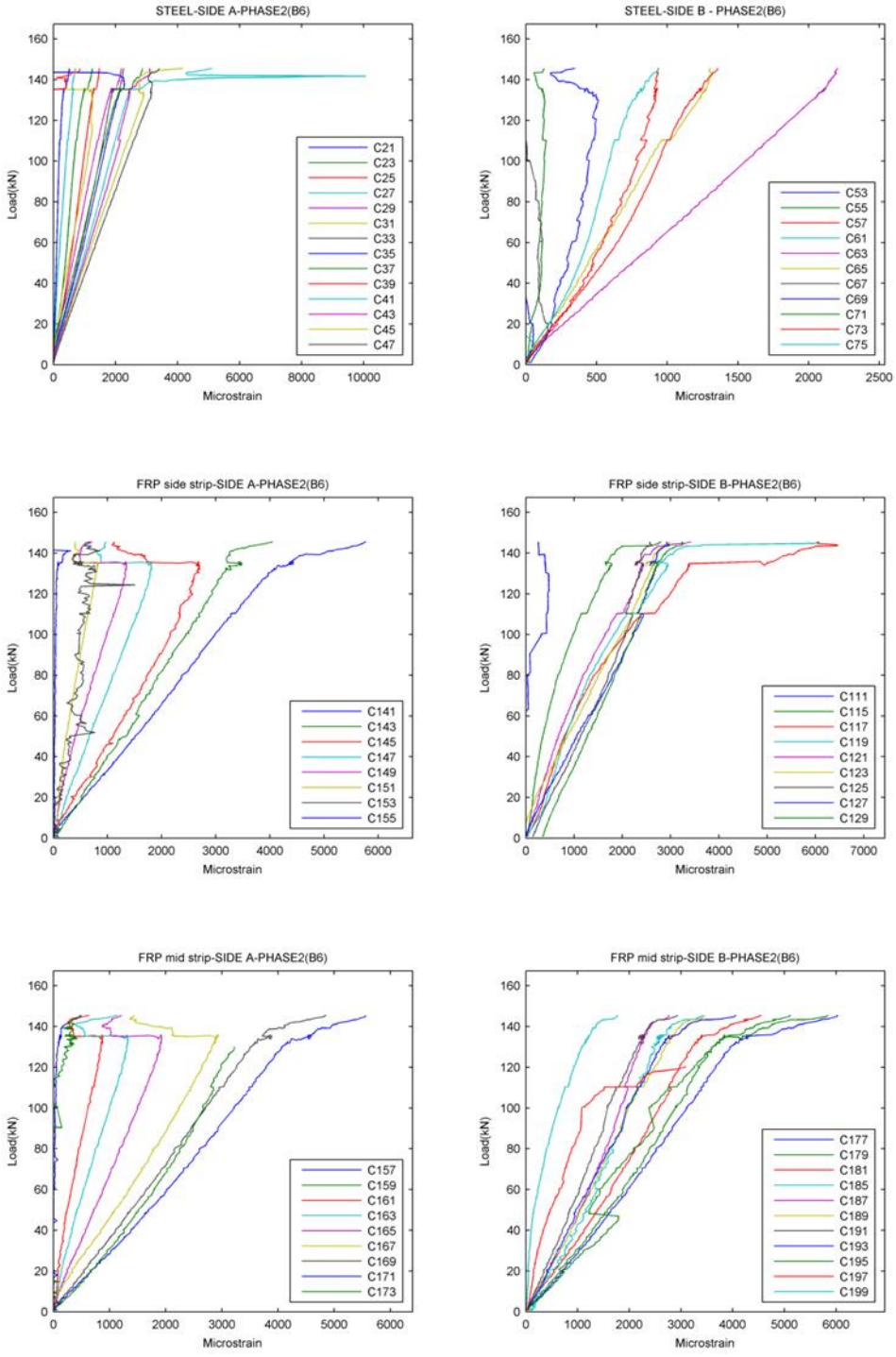

Fig. C6 - 27: Strains in the steel reinforcement and FRP along the span

C.6.16 STRAIN AND BOND STRESS PROFILES

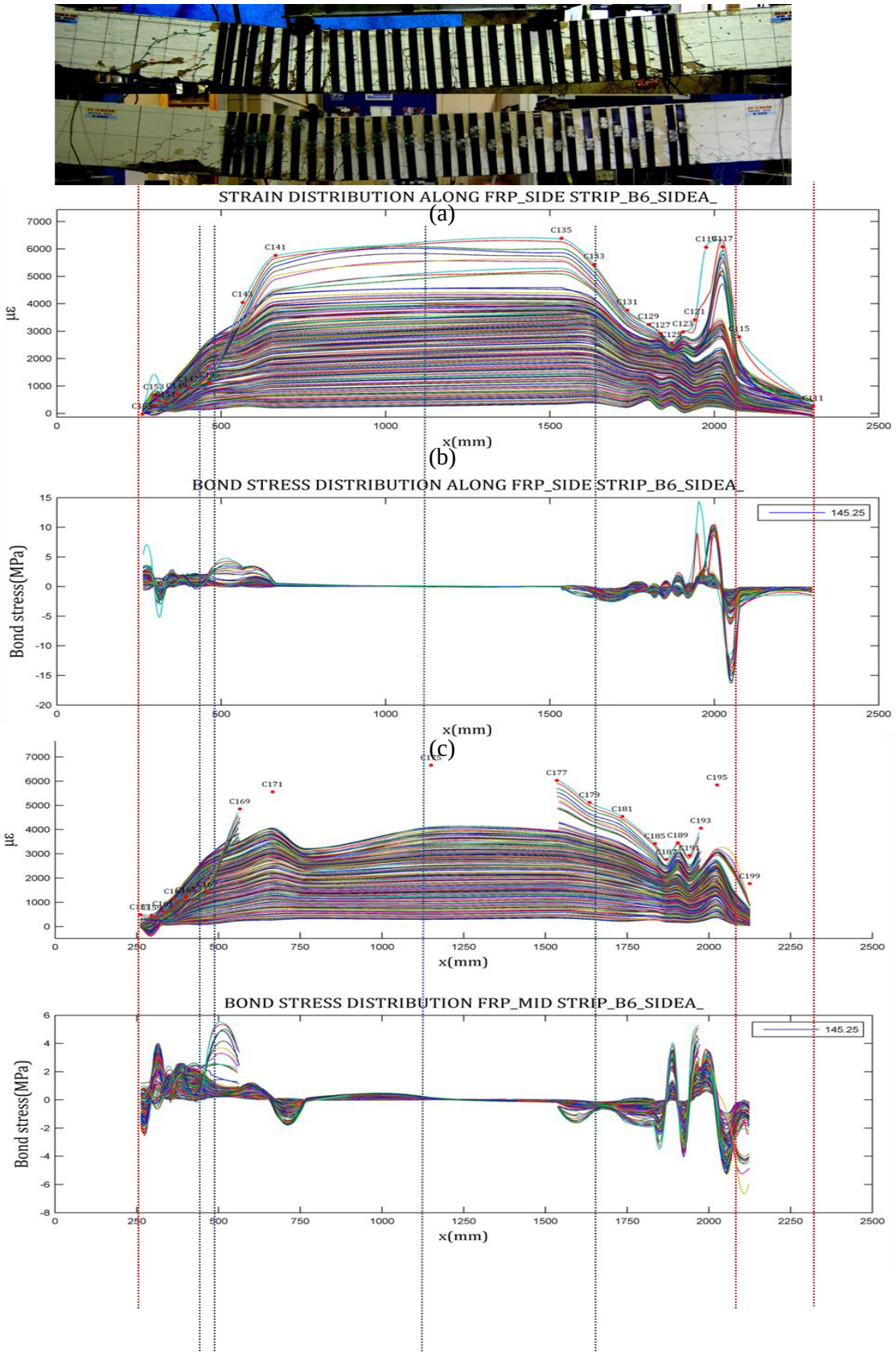

Fig. C6 - 28: Strain and bond stress profiles of (a) Crack pattern of beam NSM2A, (b) FRP, (c) The steel reinforcement

C.6.17 3D PROFILE OF STRAIN AND BOND STRESS

(a)

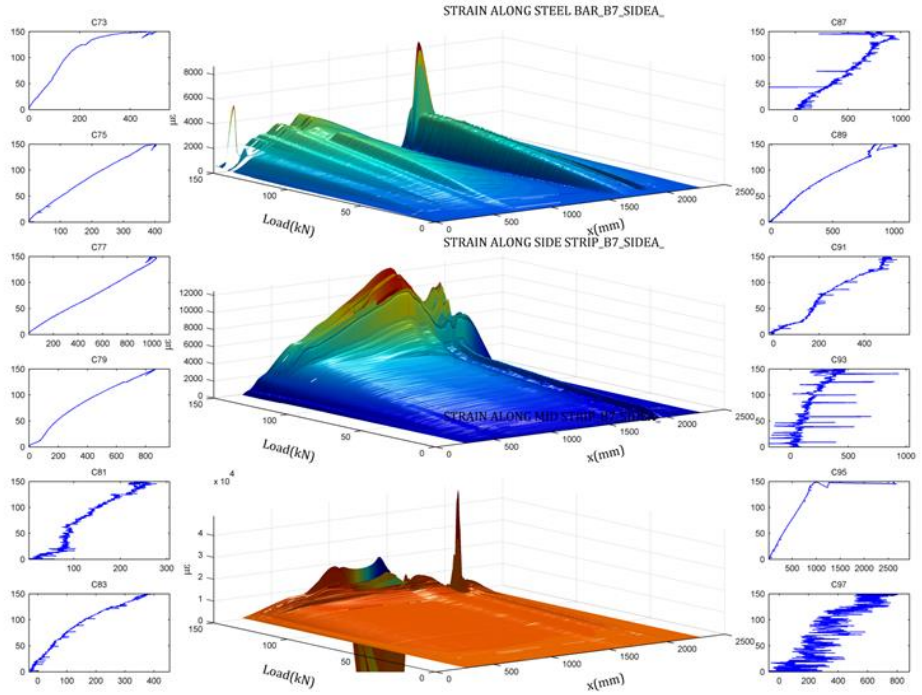

(b)

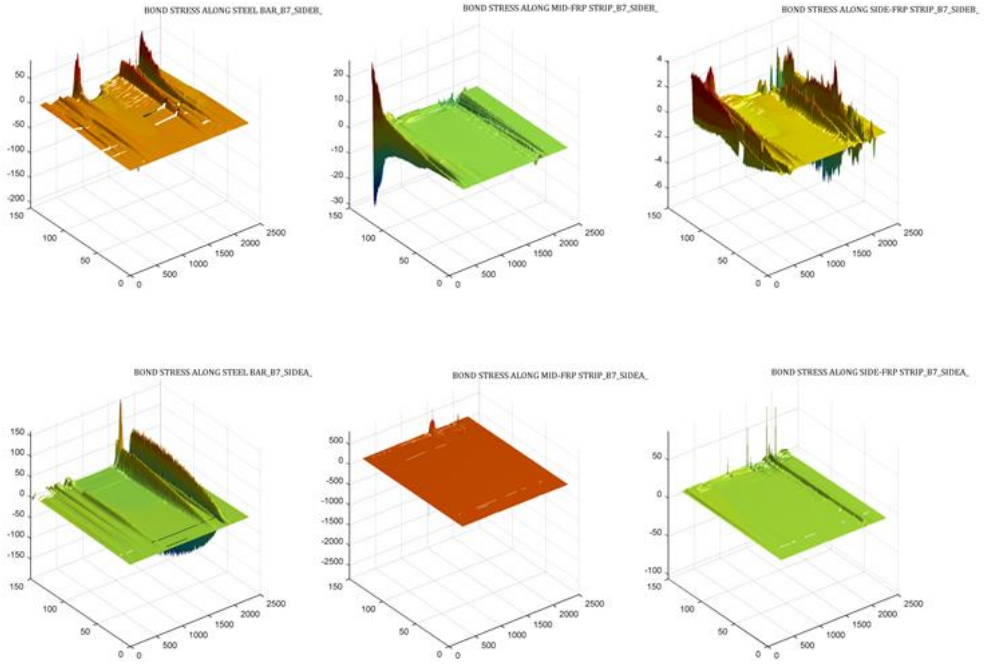

Fig. C6 - 29: Variation of (a) strains and (b) bond stress along the reinforcement and FRP at different load levels

C.7.1 BEAM DESIGN

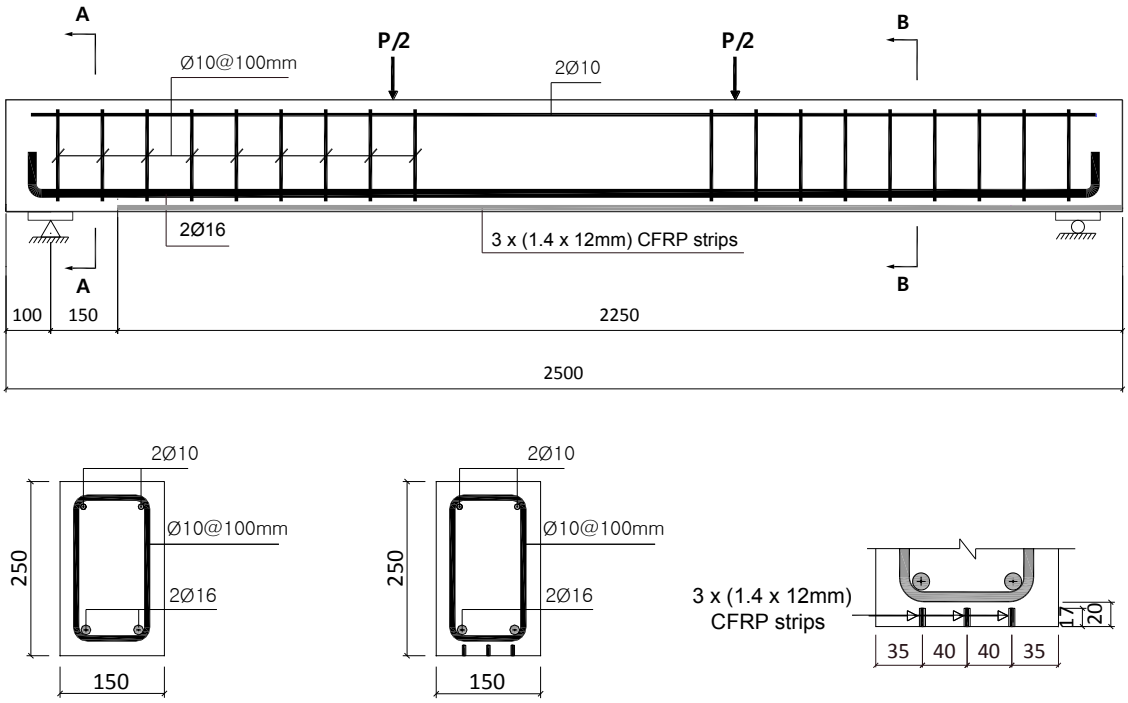

Fig. C7- 1: Details of specimen

C.7.2 INSTRUMENTATION

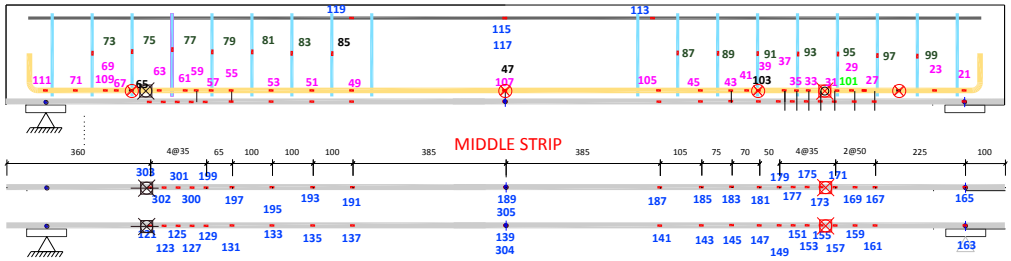

Fig. C7- 2: Strain gauge arrangement in beam components

C.7.3 DAMAGE OF BEAM IN DIFFERENT TESTING PHASES

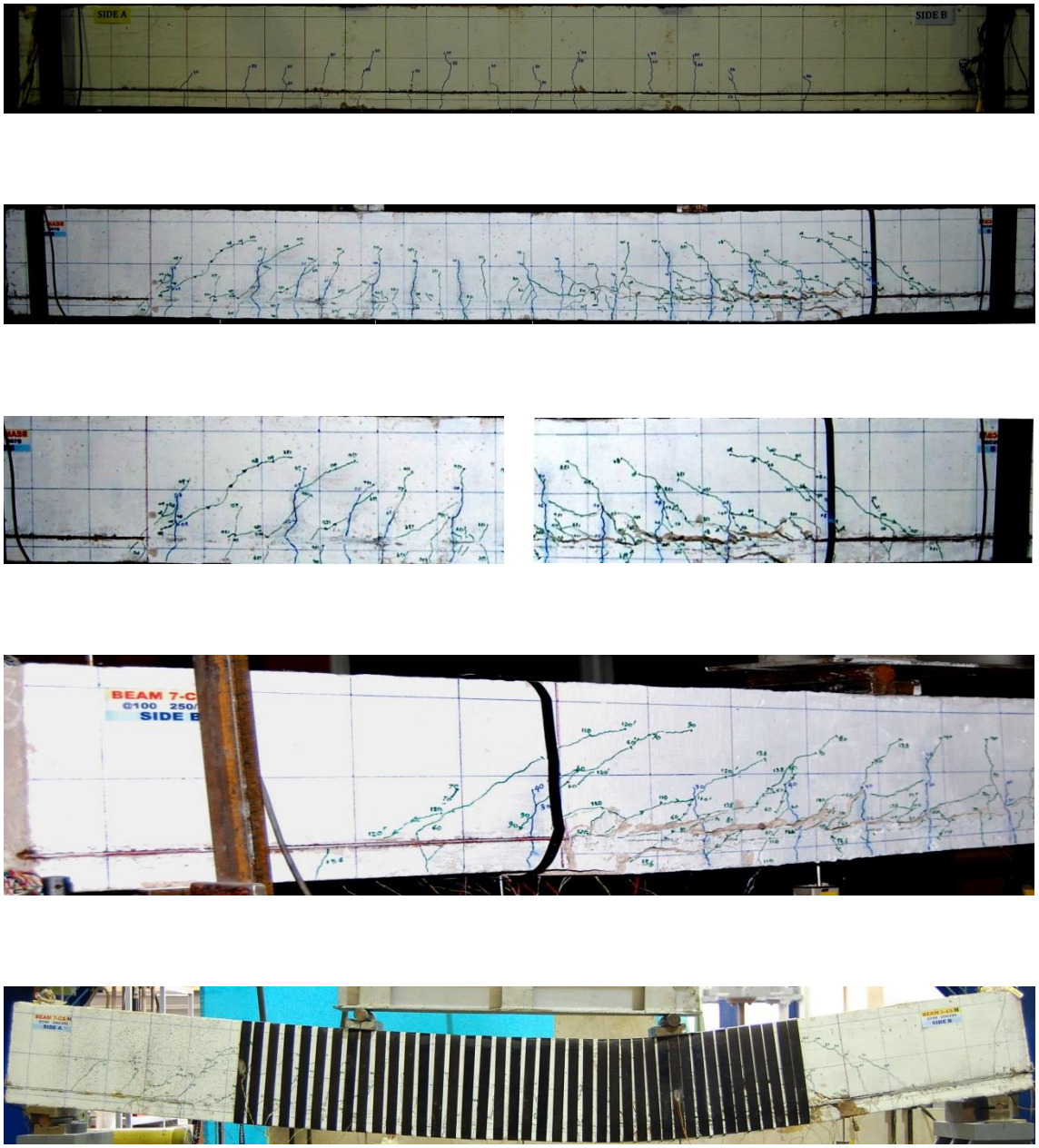

Fig. C7- 3: Crack pattern of beam NSM7A

C.7.4 FIRST TESTING PHASE: PRE-DAMAGING

a. READINGS OF LVDTs

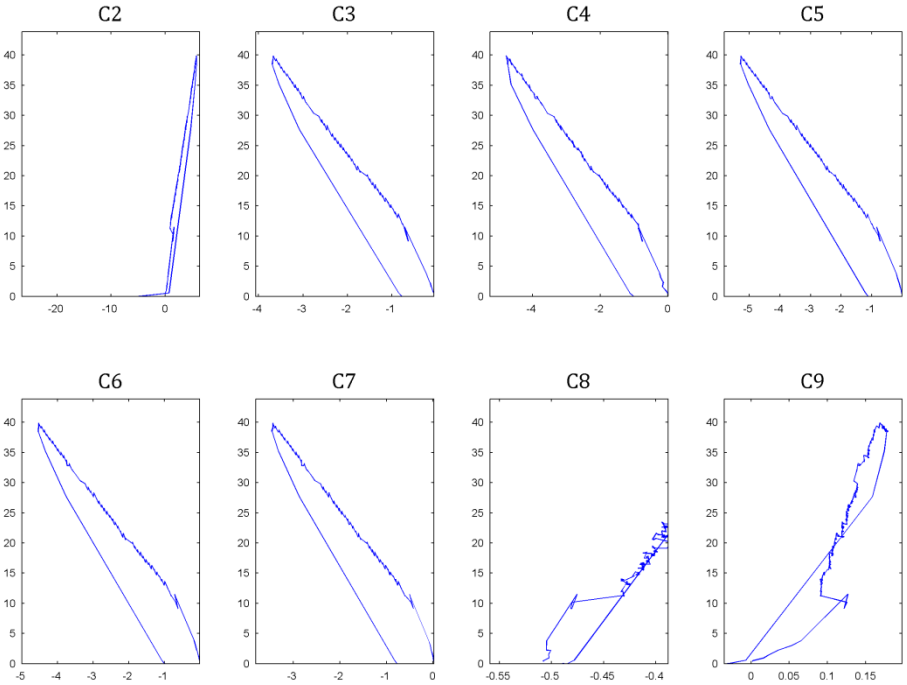

Fig. C7- 4: Readings of LVDTs (C2 – C9)

b. STRAIN READINGS

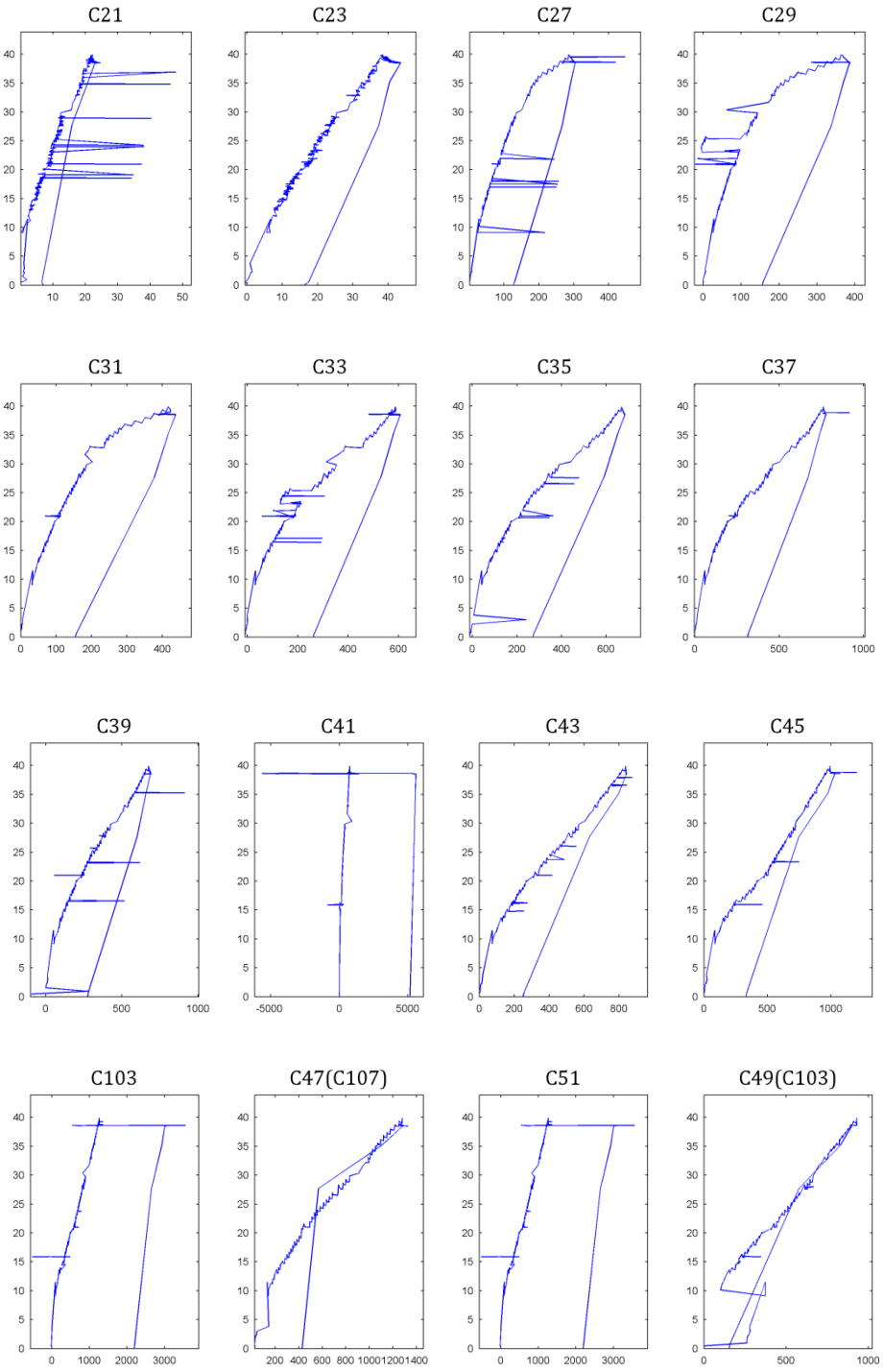

Fig. C7- 5: Strain readings (C21 – C49)

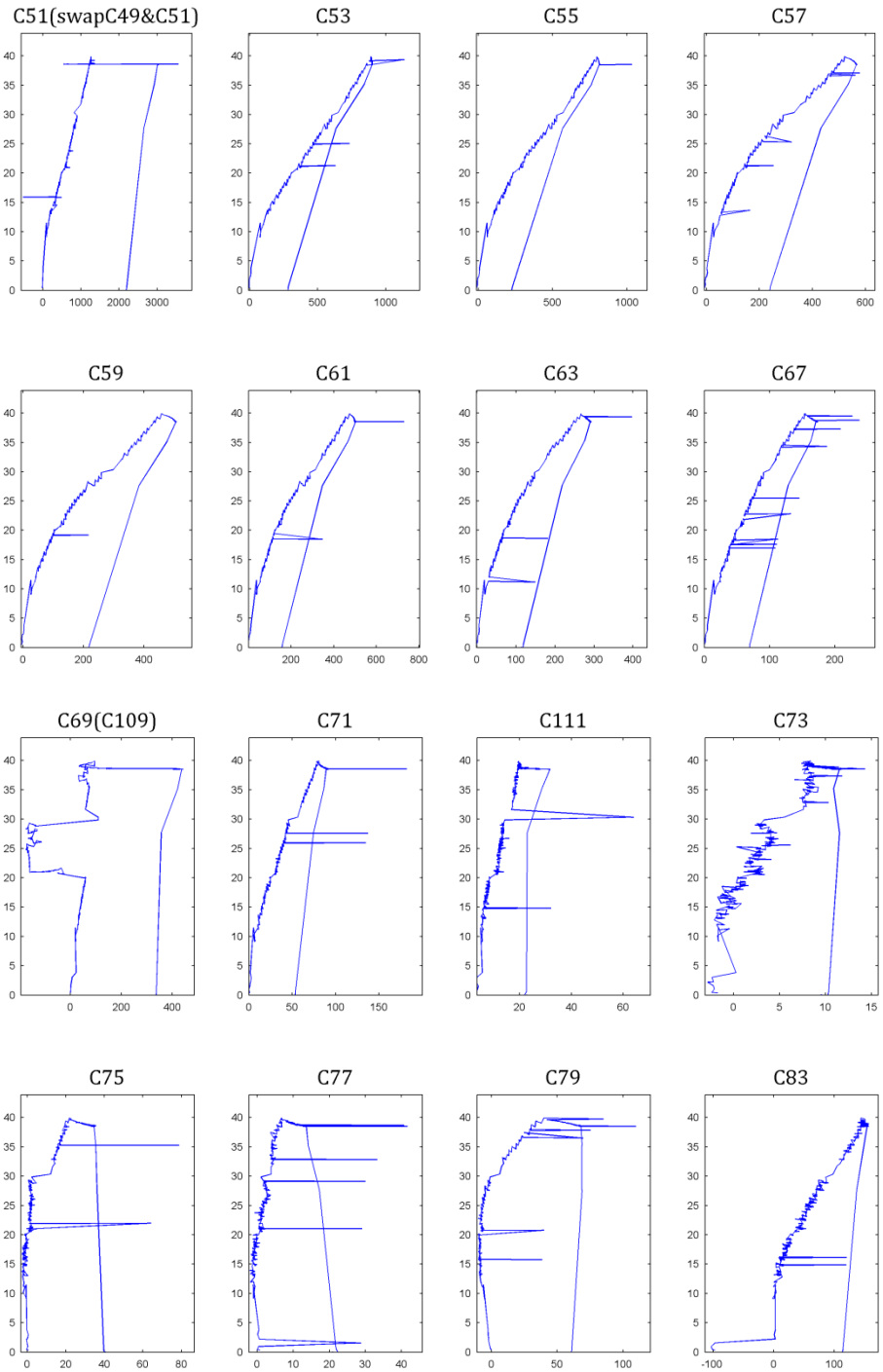

Fig. C7- 6: Strain readings (C51 – C83)

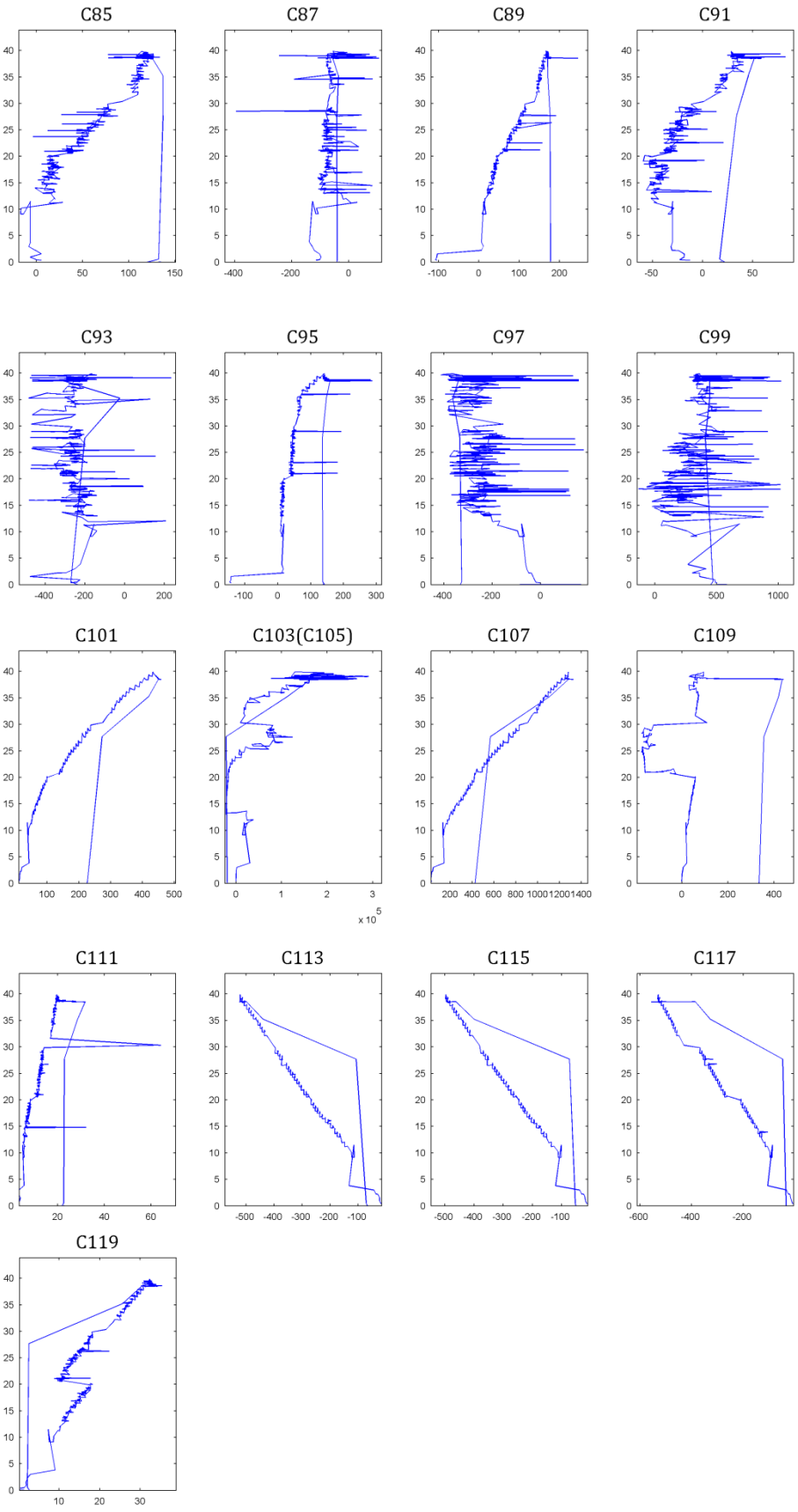

Fig. C7- 7: Strain readings (C85 – C119)

C.7.5 FIRST TESTING PHASE: FAILURE ON SIDE B

a. READINGS OF LVDTs

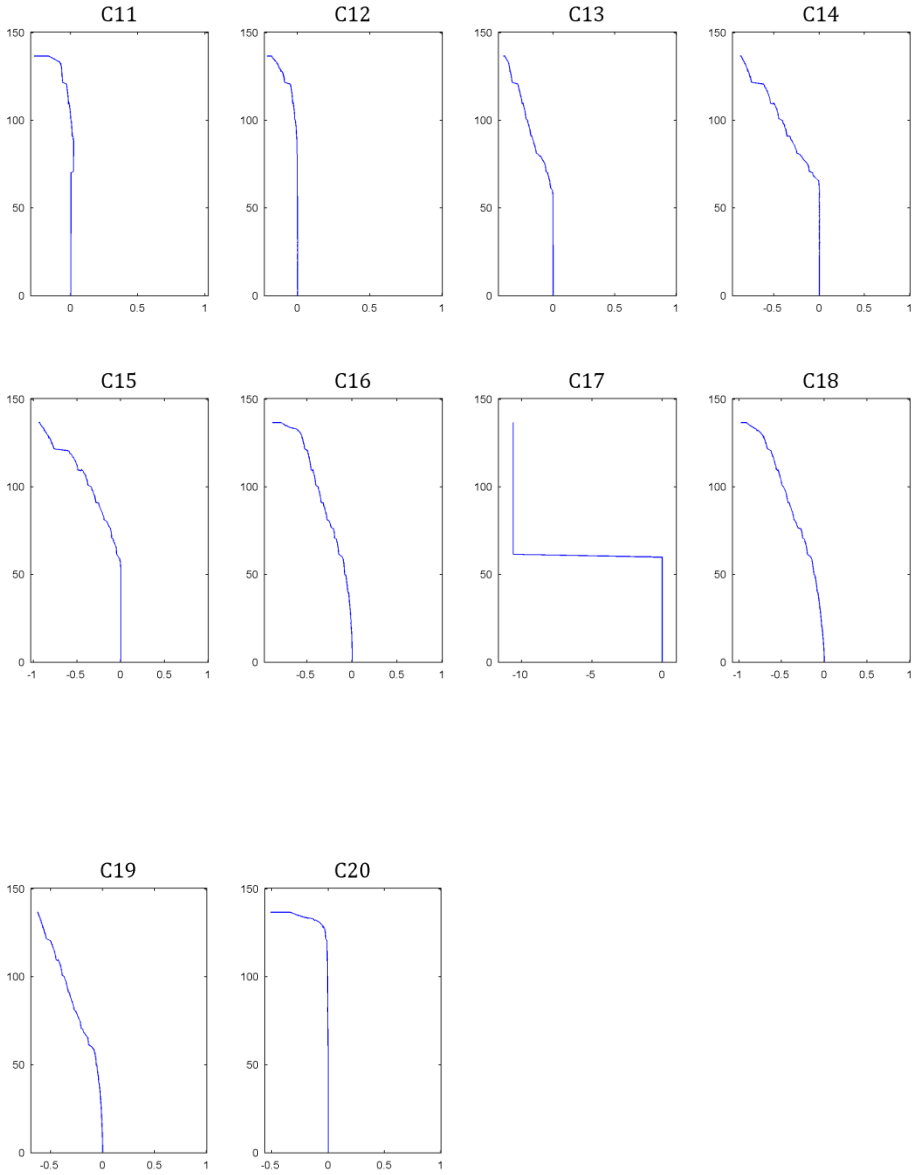

Fig. C7- 8: Readings of LVDTs (C2 – C18)

C.7.6 STRAIN READINGS

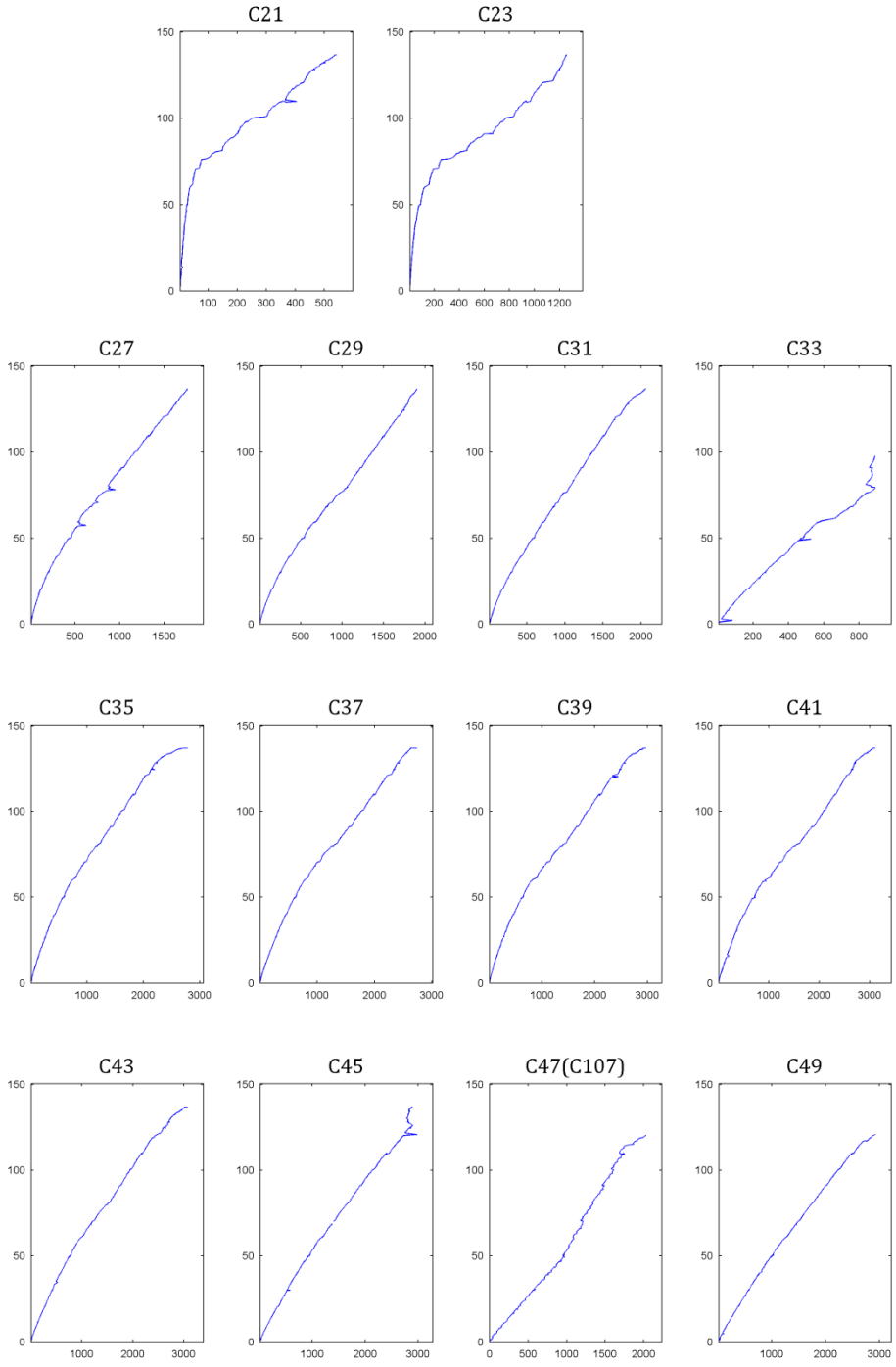

Fig. C7- 9: Strain readings (C21 – C49)

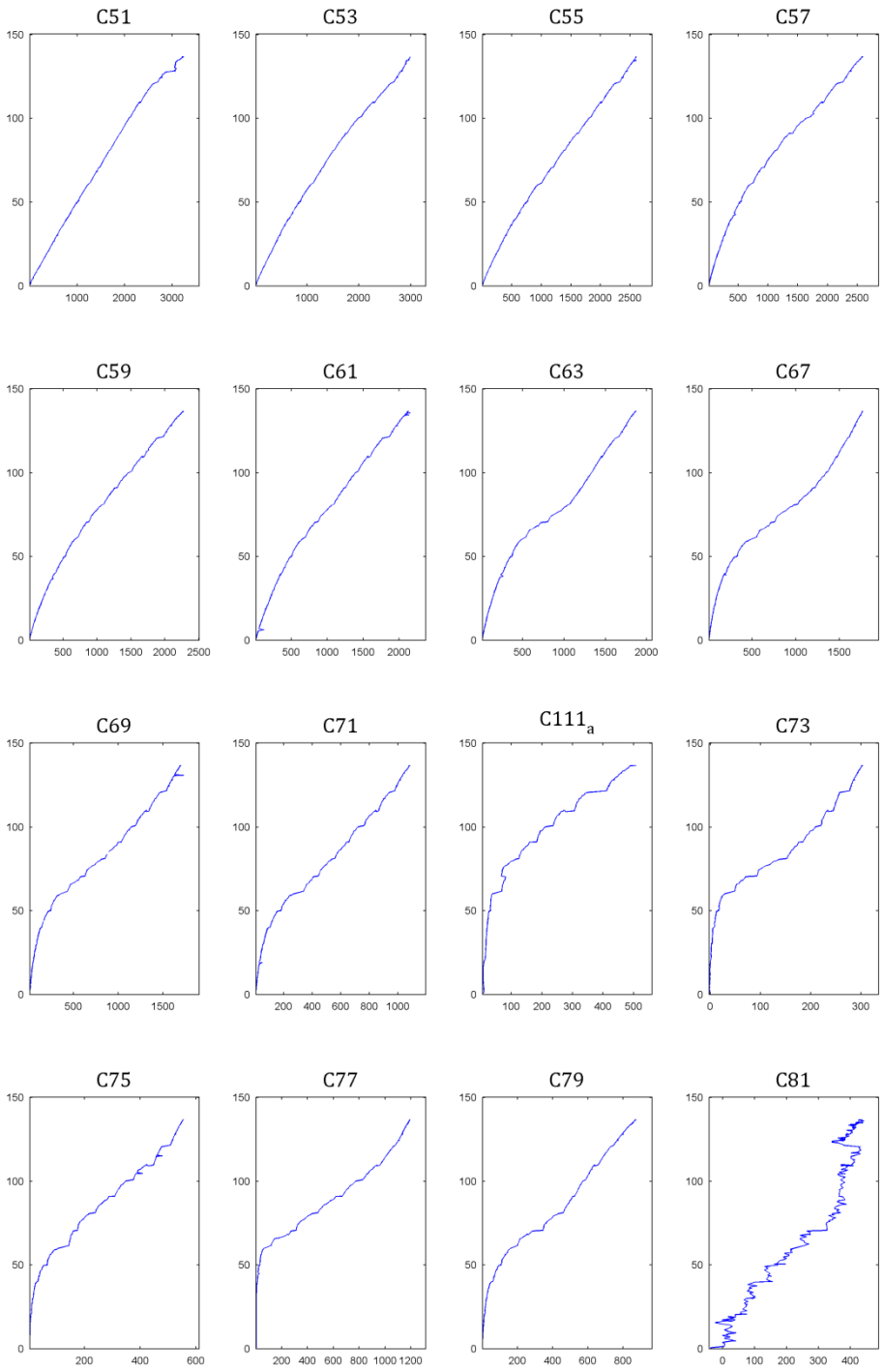

Fig. C7- 10: Strain readings (C51 – C81)

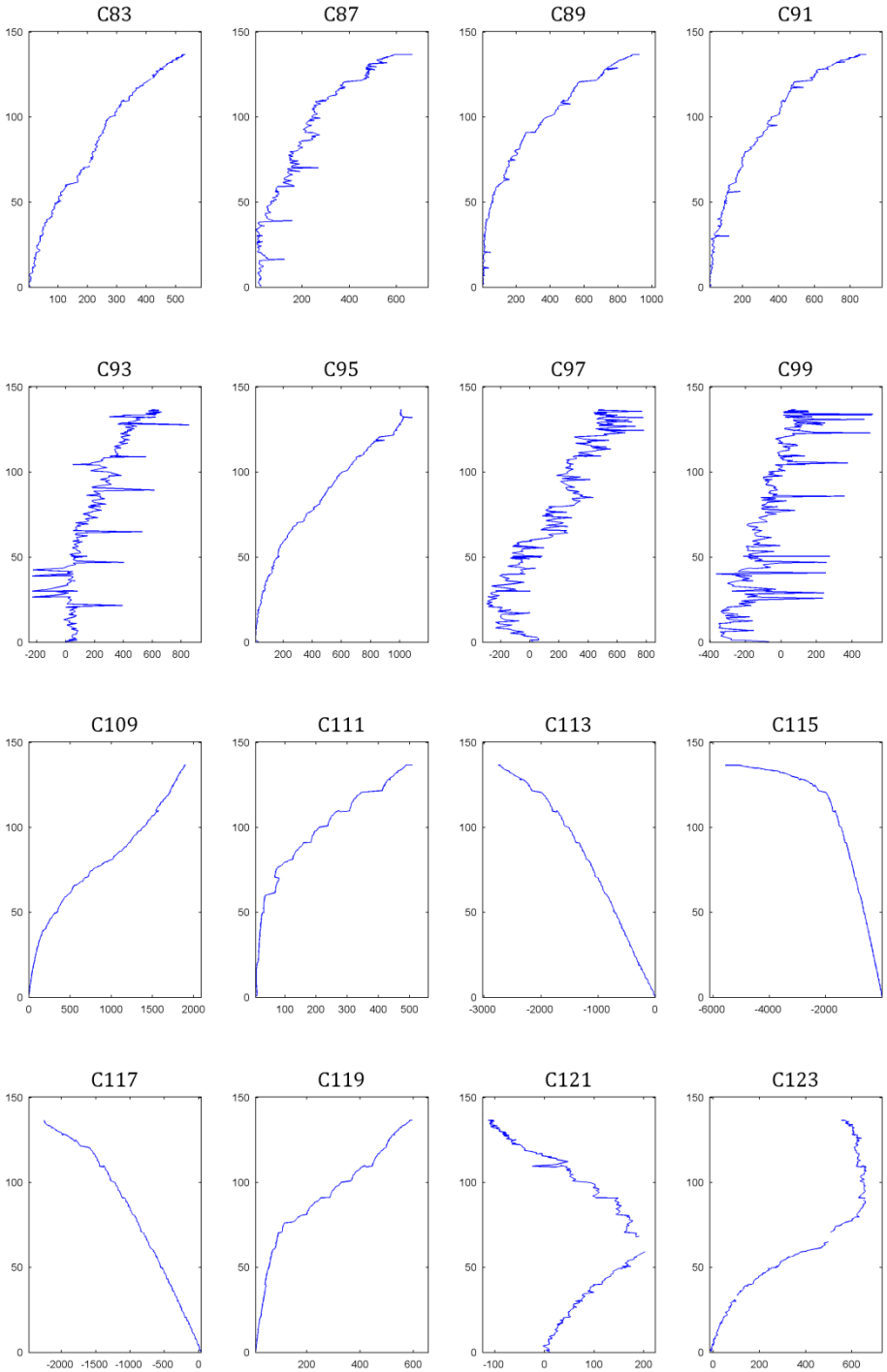

Fig. C7- 11: Strain readings (C83 – C123)

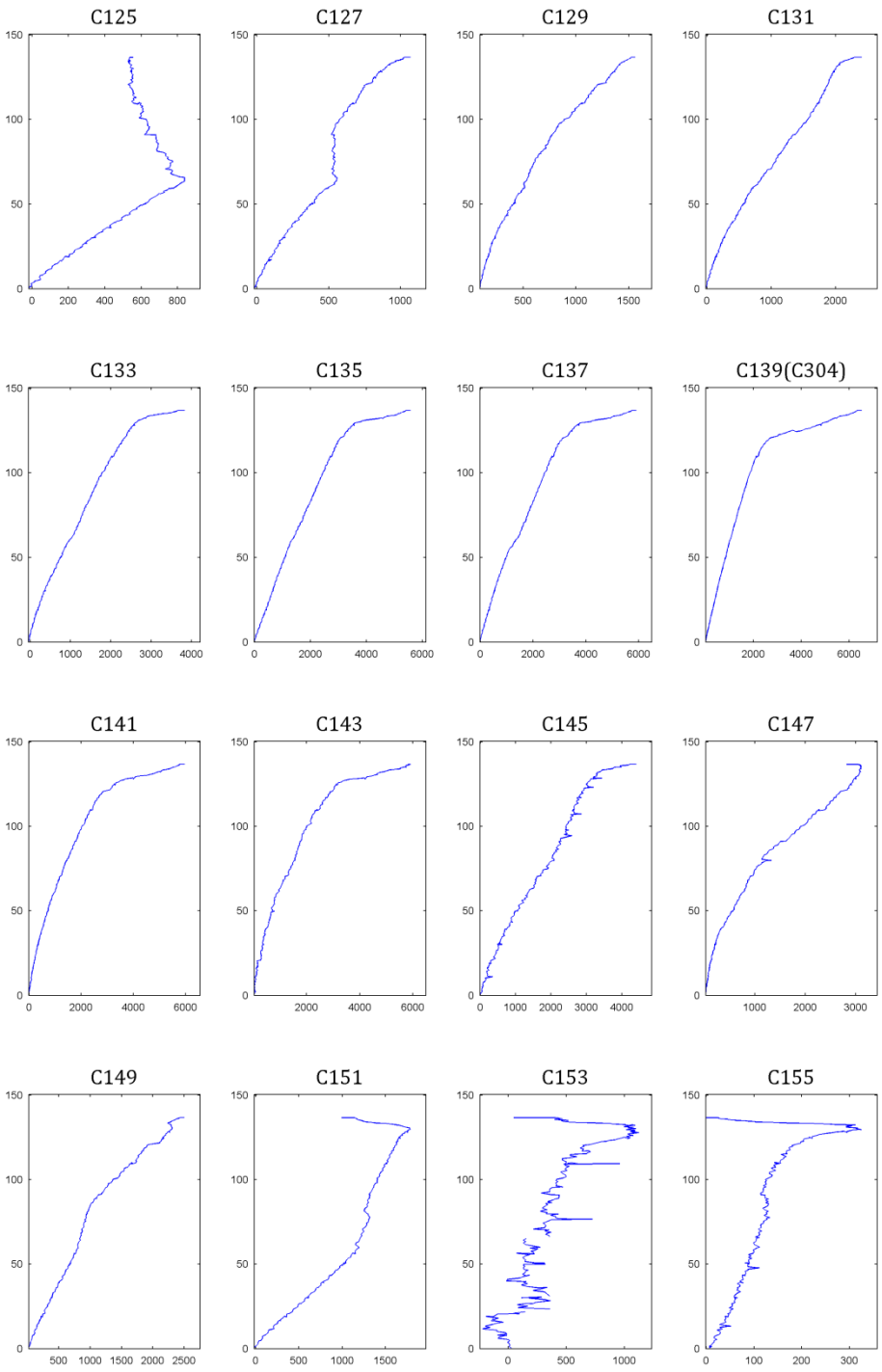

Fig. C7- 12: Strain readings (C125 – C155)

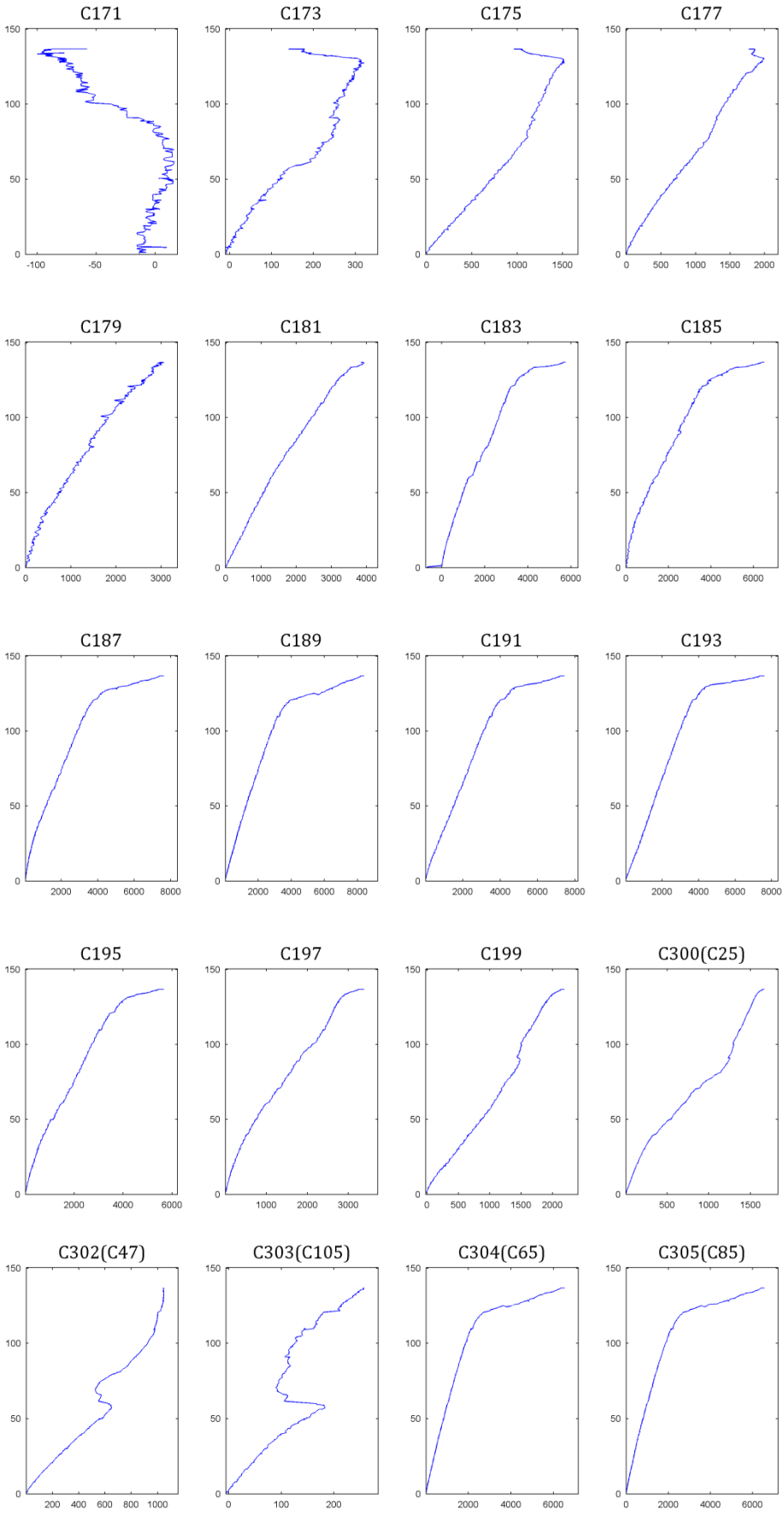

Fig. C7- 13: Strain readings (C171 – C305)

C.7.7 3D PROFILE OF STRAIN AND BOND STRESS

(a)

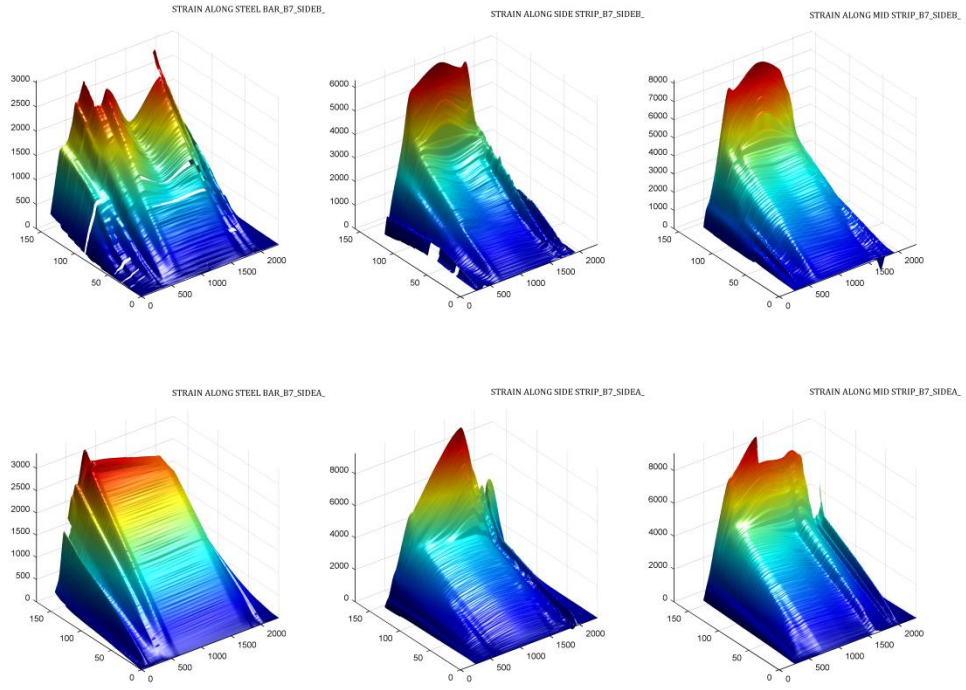

(b)

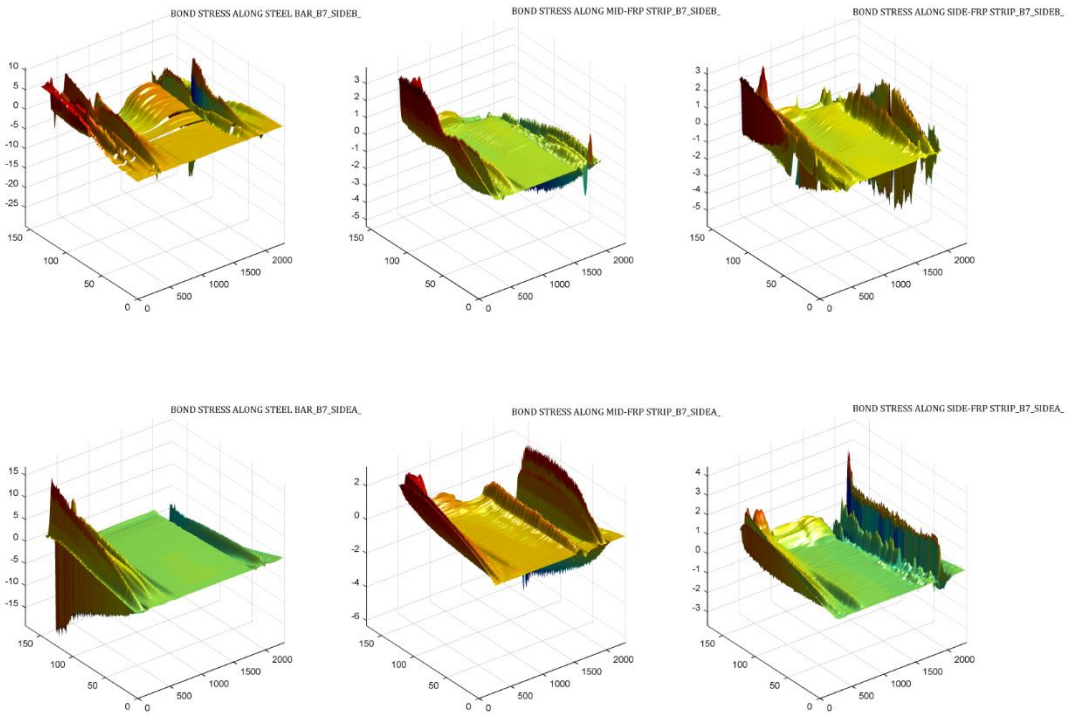

Fig. C7- 14: Variation of (a) strains, (b) bond stress along the steel reinforcement and FRP at different load level

(a)

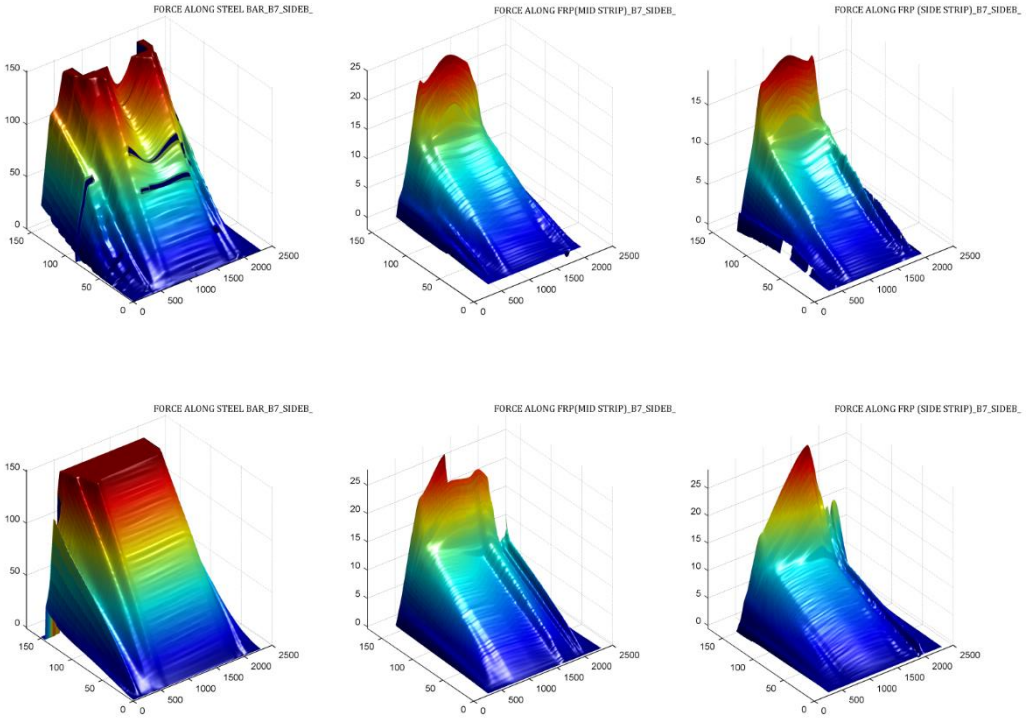

(b)

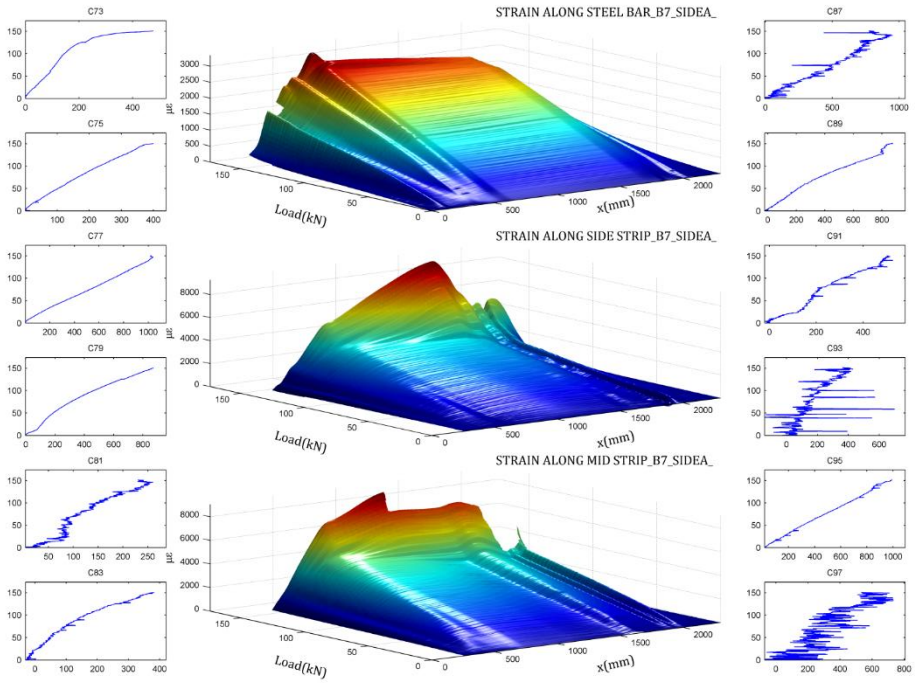

Fig. C7- 15: Variation of (a) Force (b) strains along the steel reinforcement, FRP, shear link at different load level

C.7.8 STRAINS IN THE STEEL REINFORCEMENT AND FRP ALONG THE MID-SPAN REGION

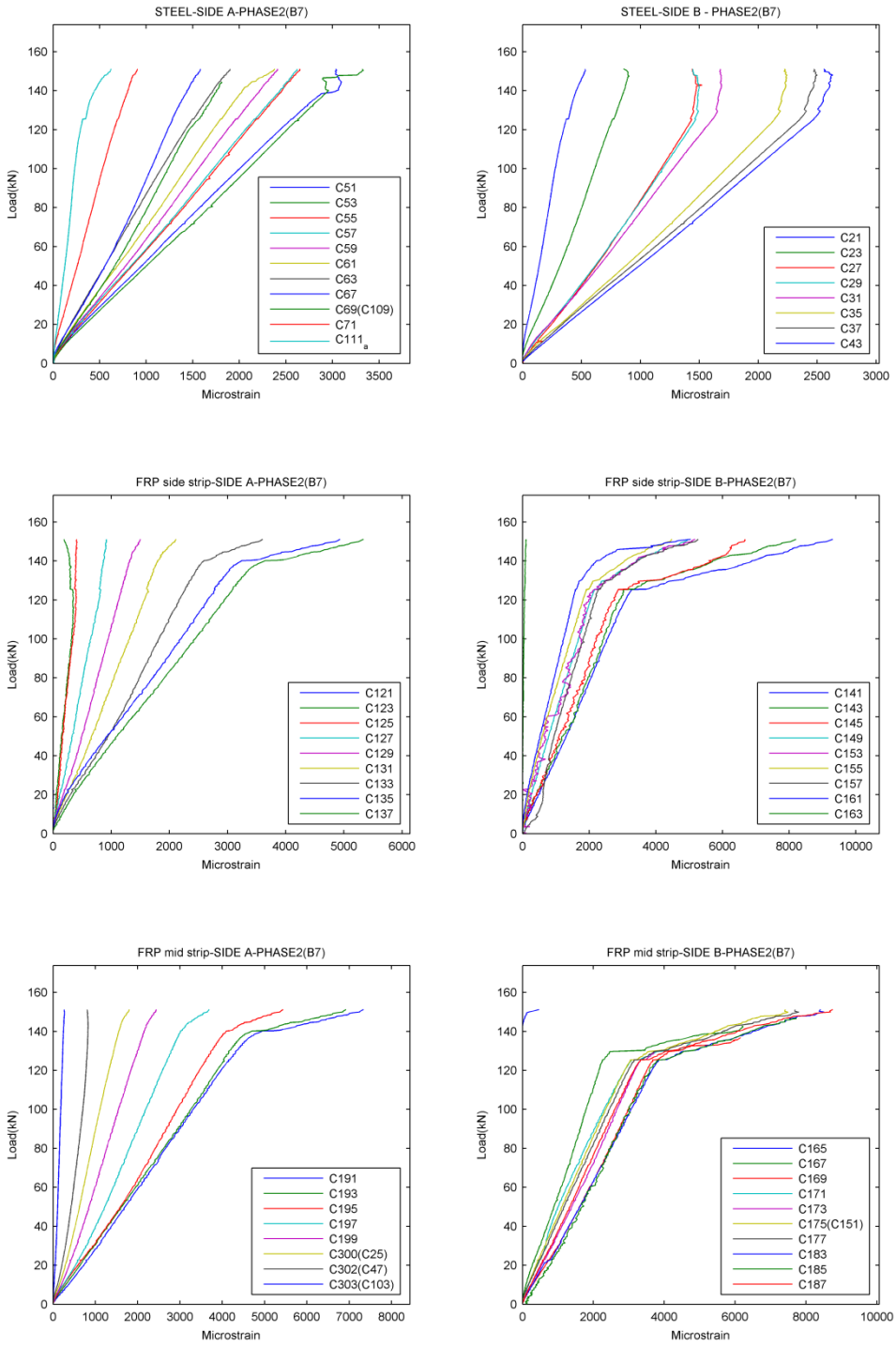

Fig. C7- 16: Strain along steel bar – Phase 2

C.7.9 STRAINS IN THE STEEL REINFORCEMENT AND FRP IN THE REGION AROUND THE COP

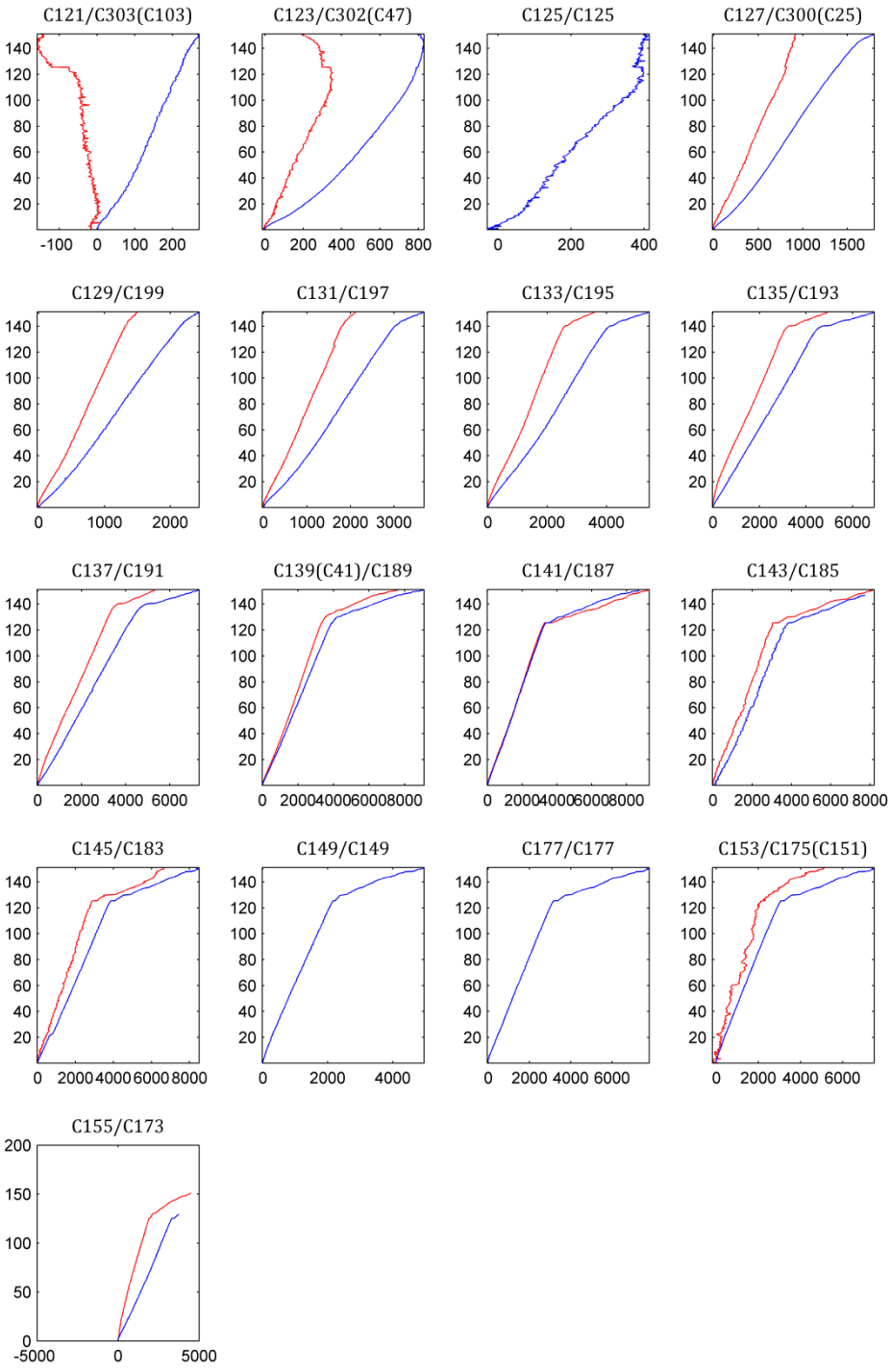

Fig. C7- 17: Strains in the steel reinforcement and FRP in the region around the COP

C.7.10 STRAIN AND BOND STRESS PROFILES

(a)

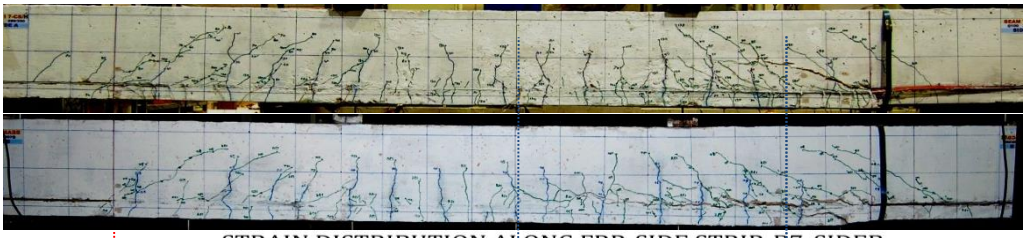

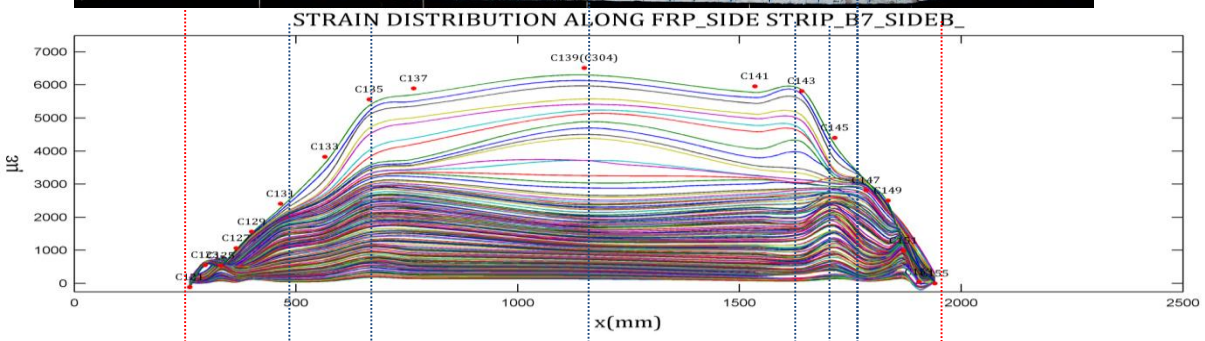

(b)

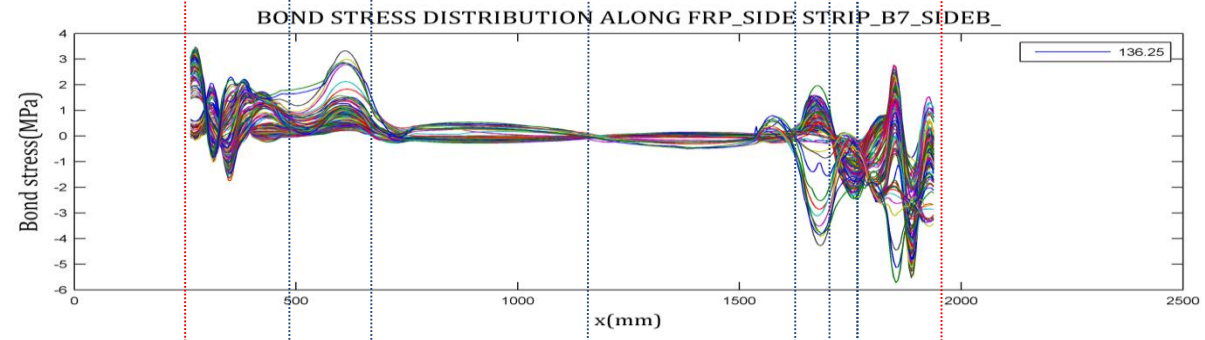

(c)

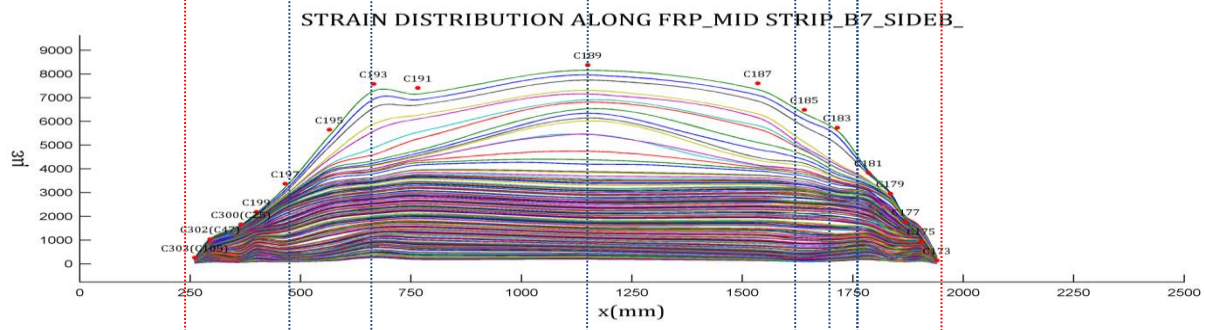

(c)

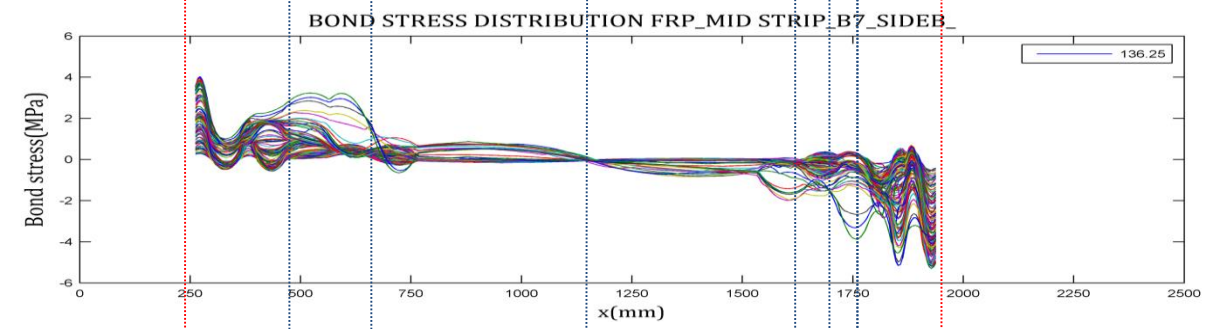

Fig. C7- 18: Strain and bond stress profiles of (a) Crack pattern of beam NSM2A, (b) FRP, (c) The steel reinforcement

C.7.11 FINAL TESTING PHASE

a. READINGS OF LVDTs

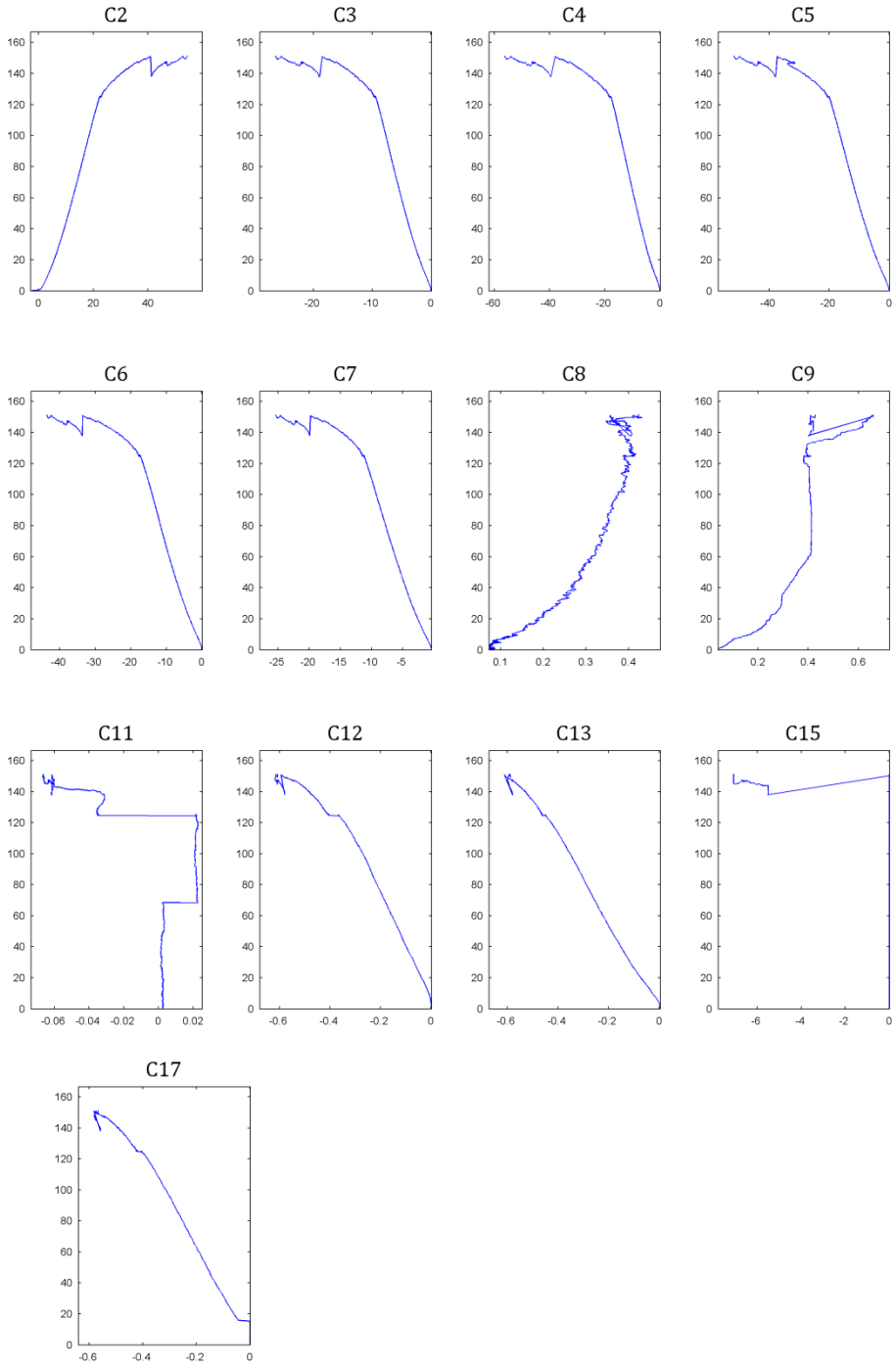

Fig. C7 - 13: Readings of LVDTs (C2 – C17)

C.7.12 STRAIN READINGS

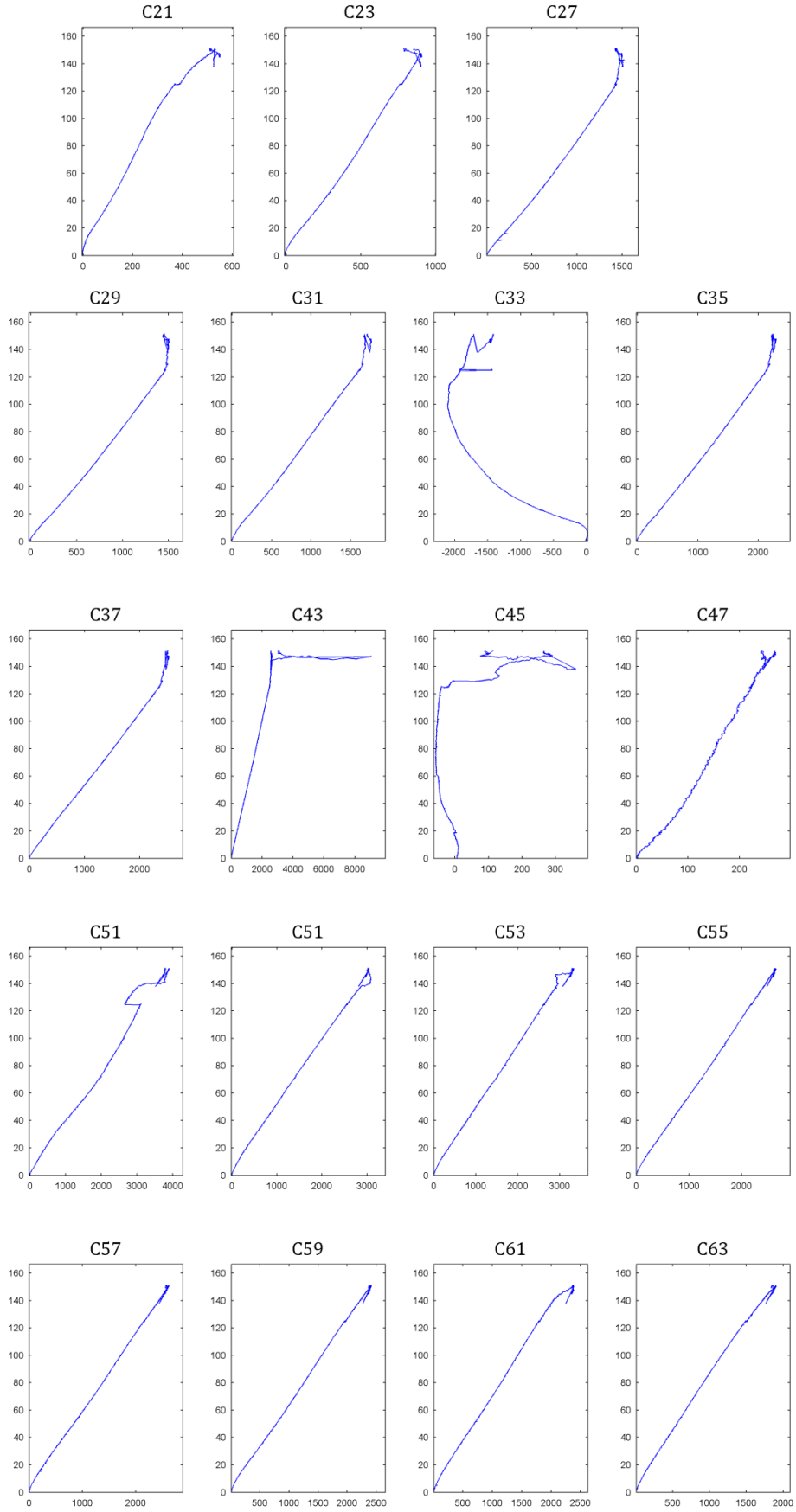

Fig. C7- 19: Strain readings (C21 – C63)

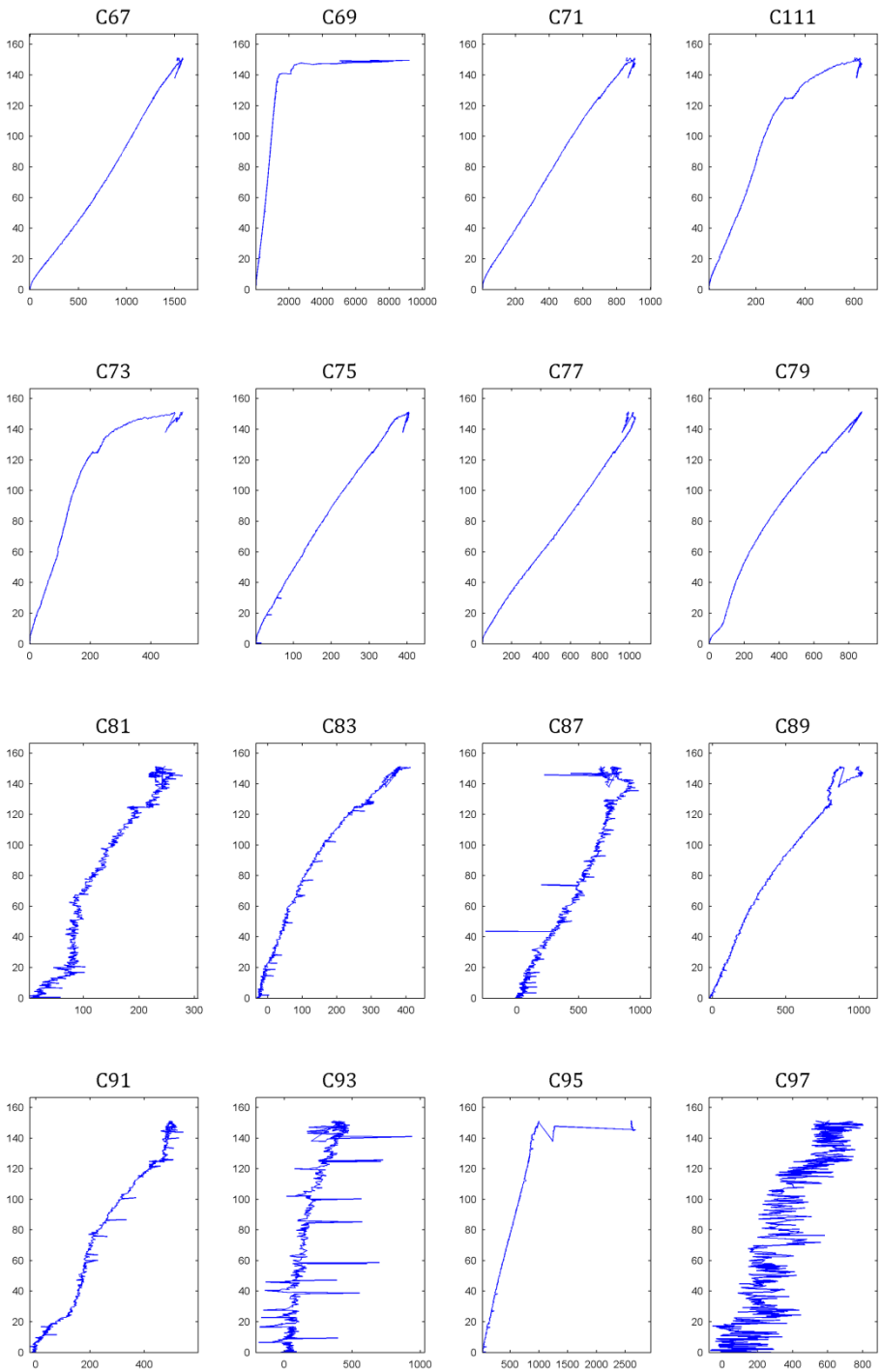

Fig. C7- 20: Strain readings (C67 – C97)

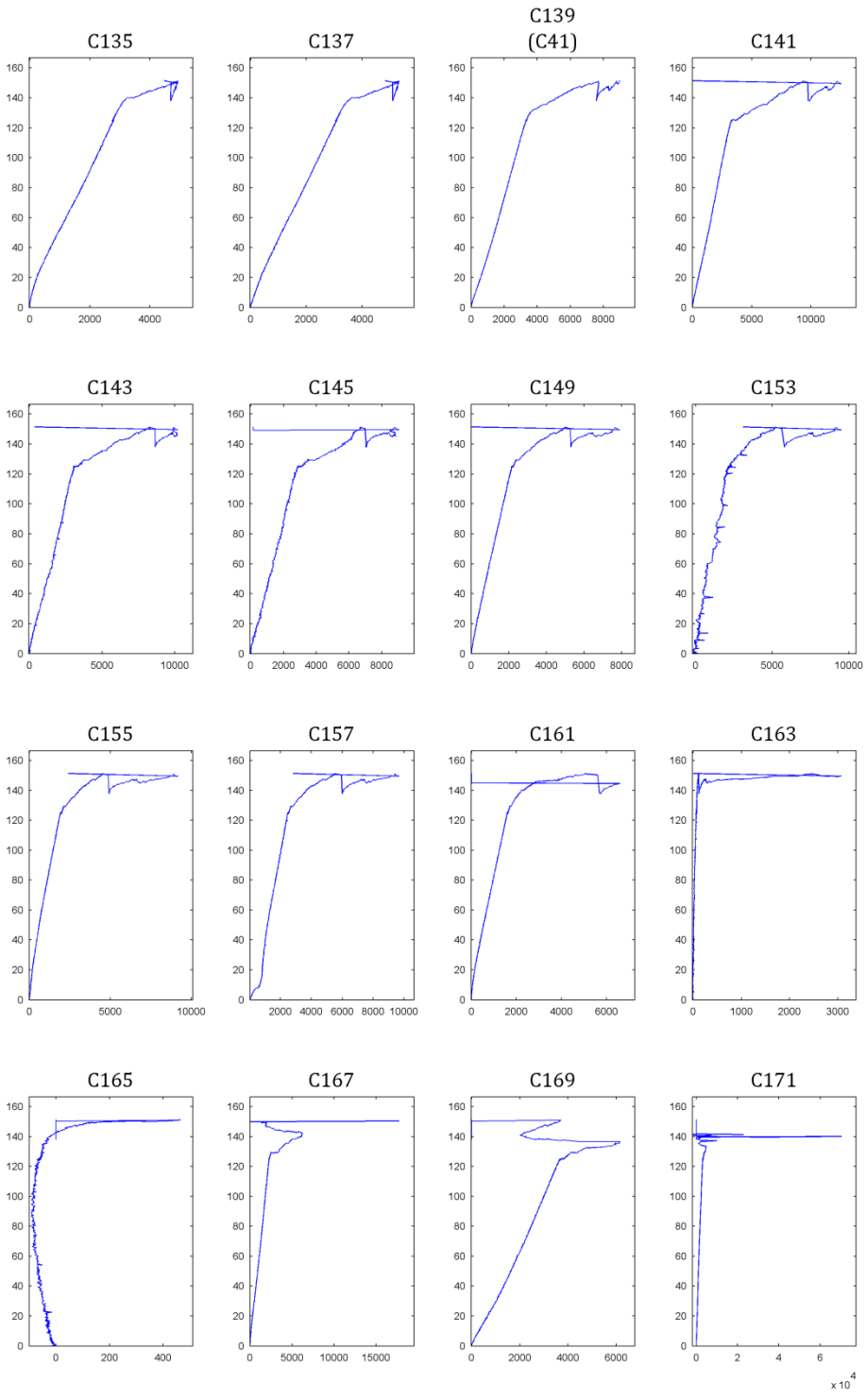

Fig. C7- 21: Strain readings (C135 – C171)

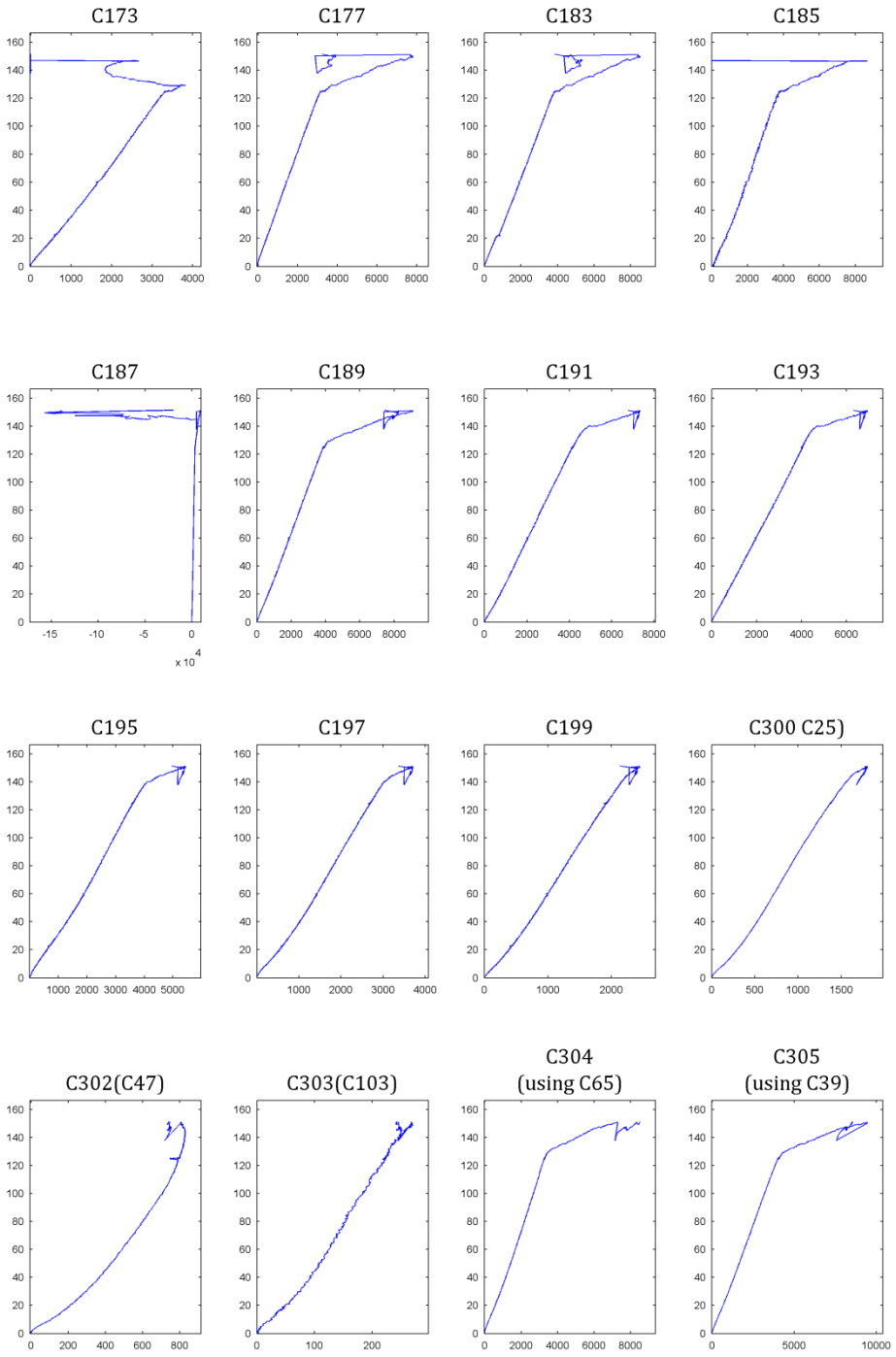

Fig. C7- 22: Strain readings (C173 – C305)

C.7.13 STRAINS IN THE STEEL REINFORCEMENT AND FRP ALONG THE MID-SPAN REGION

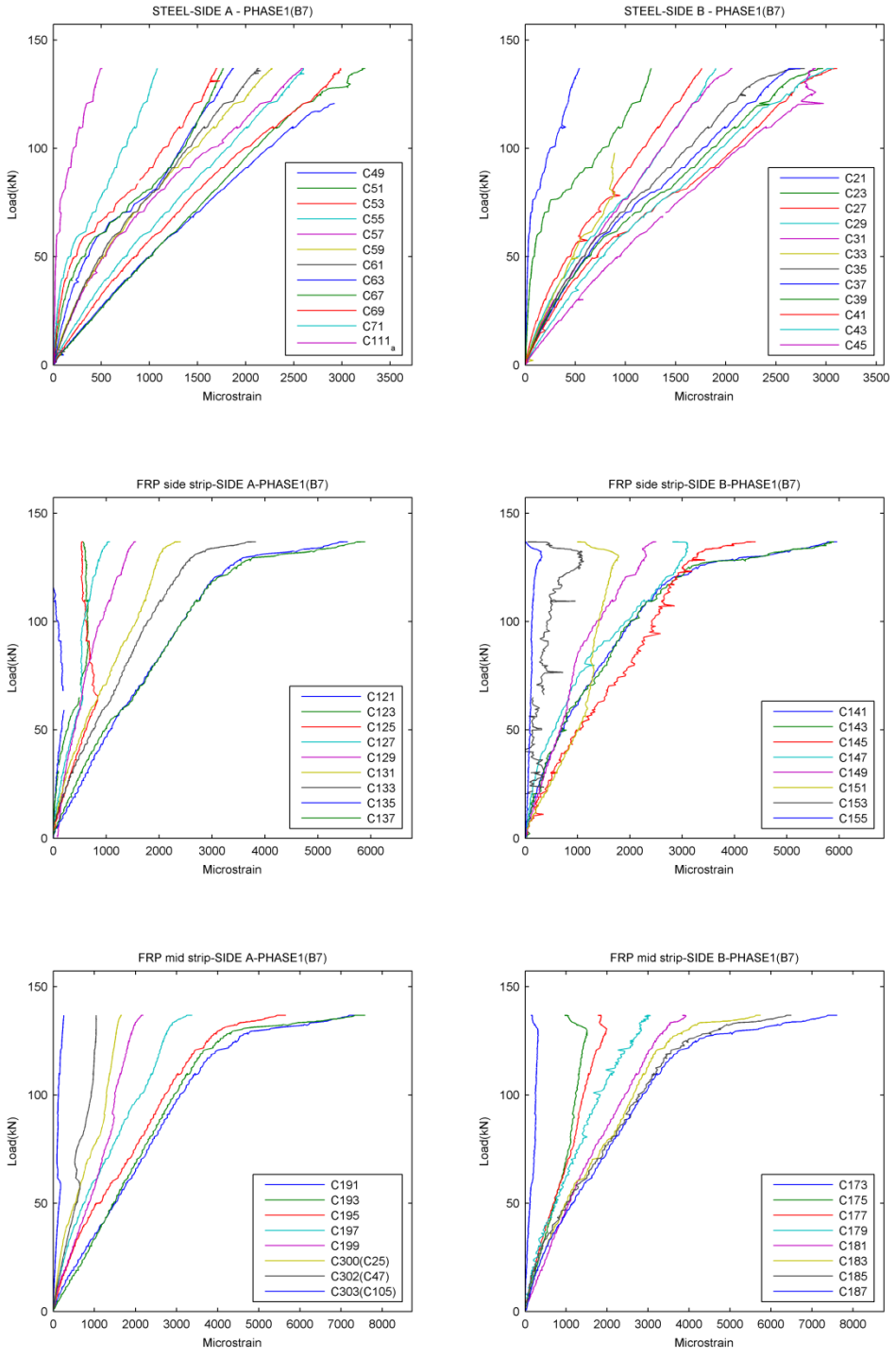

Fig. C7- 23: Strain along the steel bar and FRP – Phase 1

C.7.14 STRAIN AND BOND STRESS PROFILES

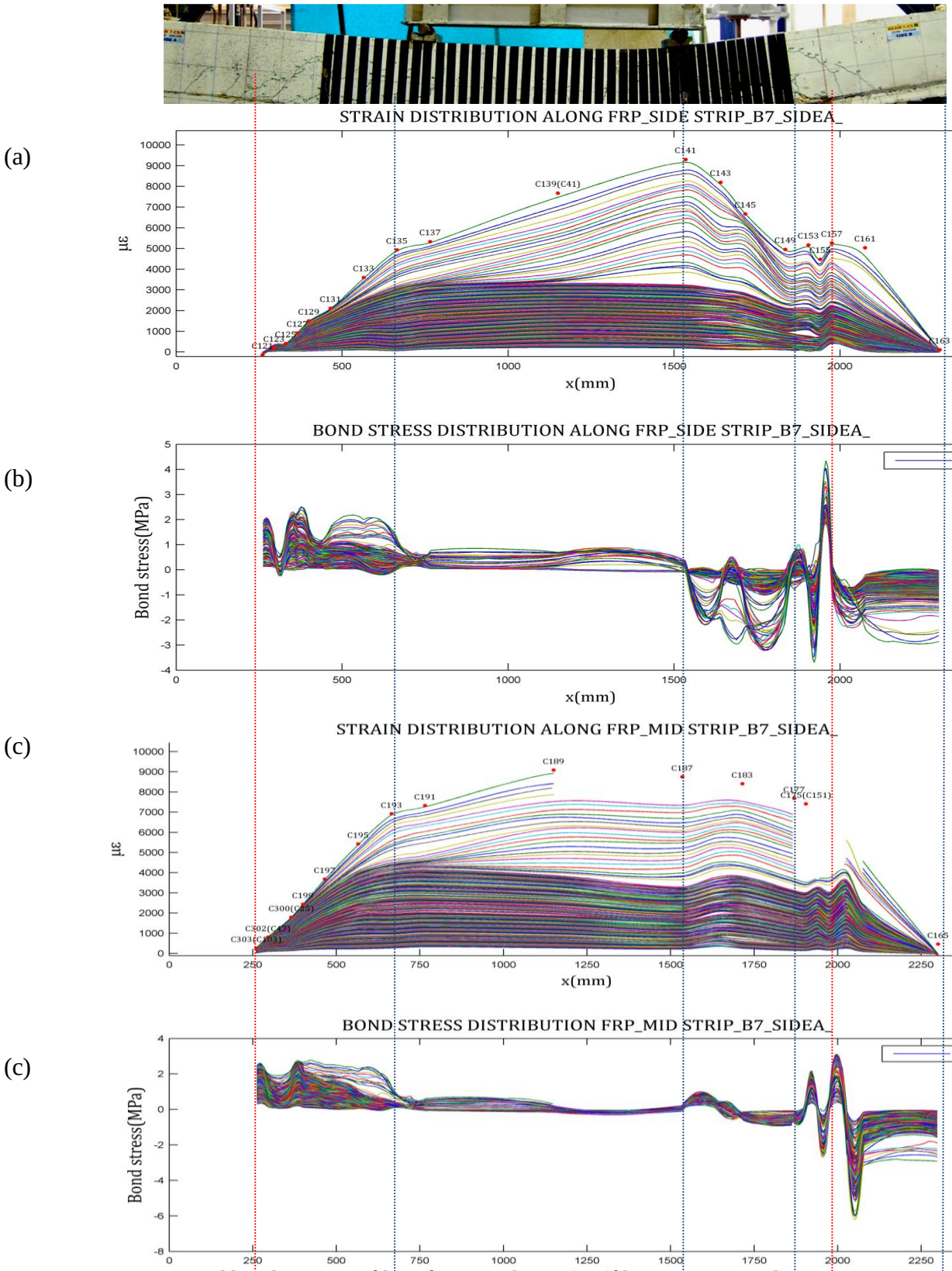

Fig. C7- 24: Strain and bond stress profiles of (a) Crack pattern of beam NSM2A, (b) FRP, (c) steel reinforcement

C.7.15 3D PROFILE OF STRAIN AND BOND STRESS

(a)

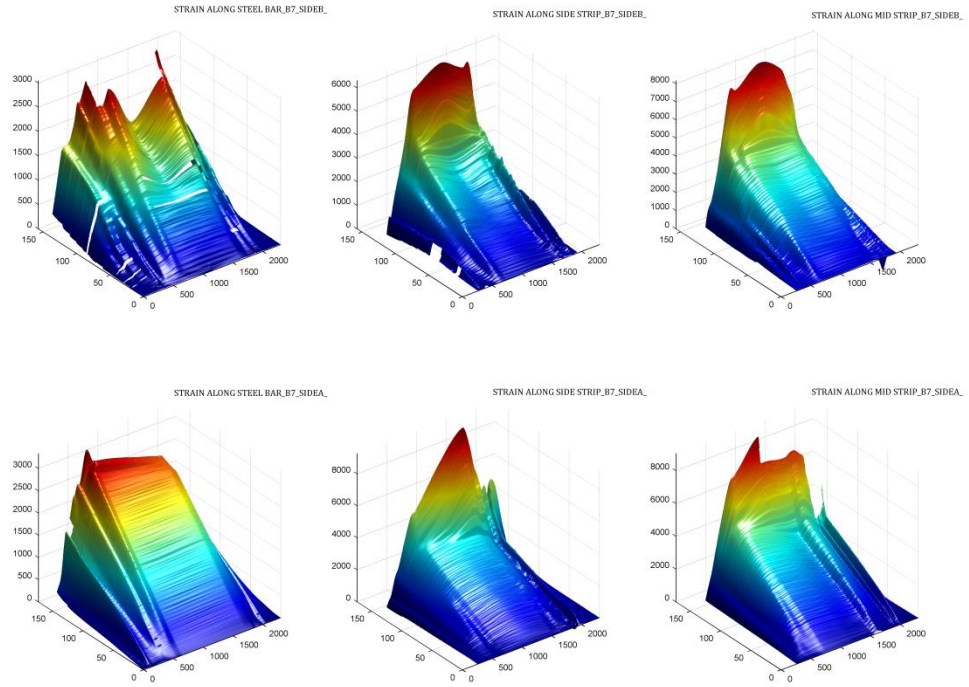

(b)

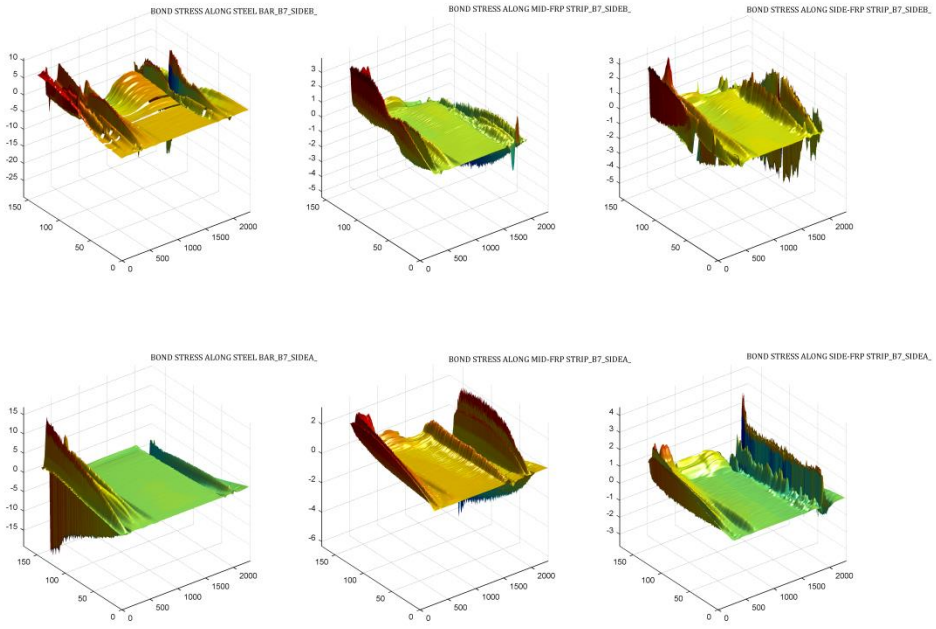

Fig. C7- 25: Variation of (a) strains and (b) bond stress along the reinforcement and FRP at different load levels

C.8.1 INSTRUMENTATION

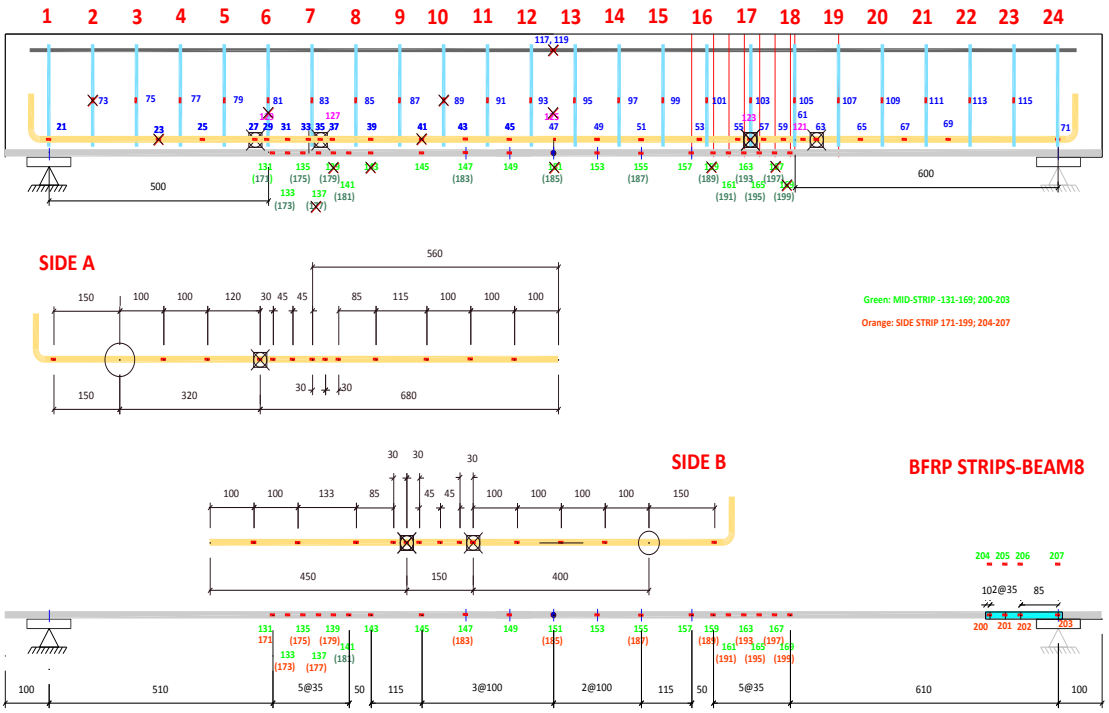

Fig. C8 - 1: Strain gauge arrangement in various components.

C.8.2 THE DAMAGE OF BEAM AT DIFFERENT TESTING PHASES

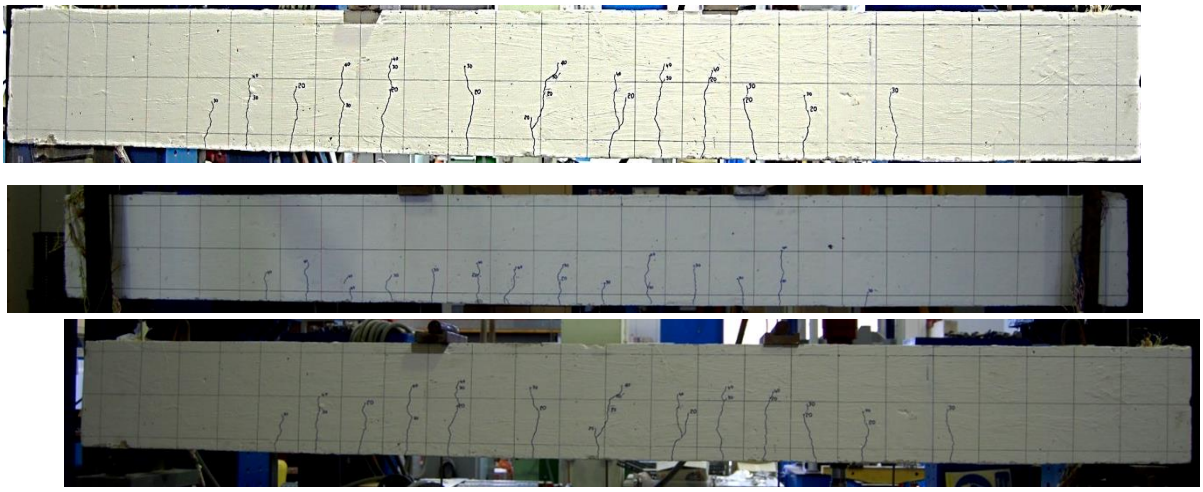

Fig. C8 - 2: Pre-crack stage

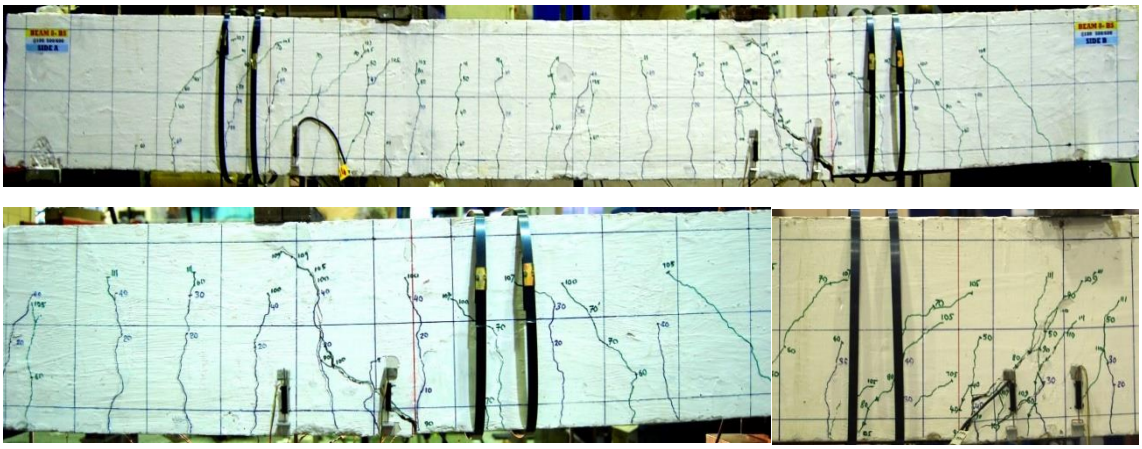

Fig. C8 - 3: Debonding failure of beam in the first testing phase

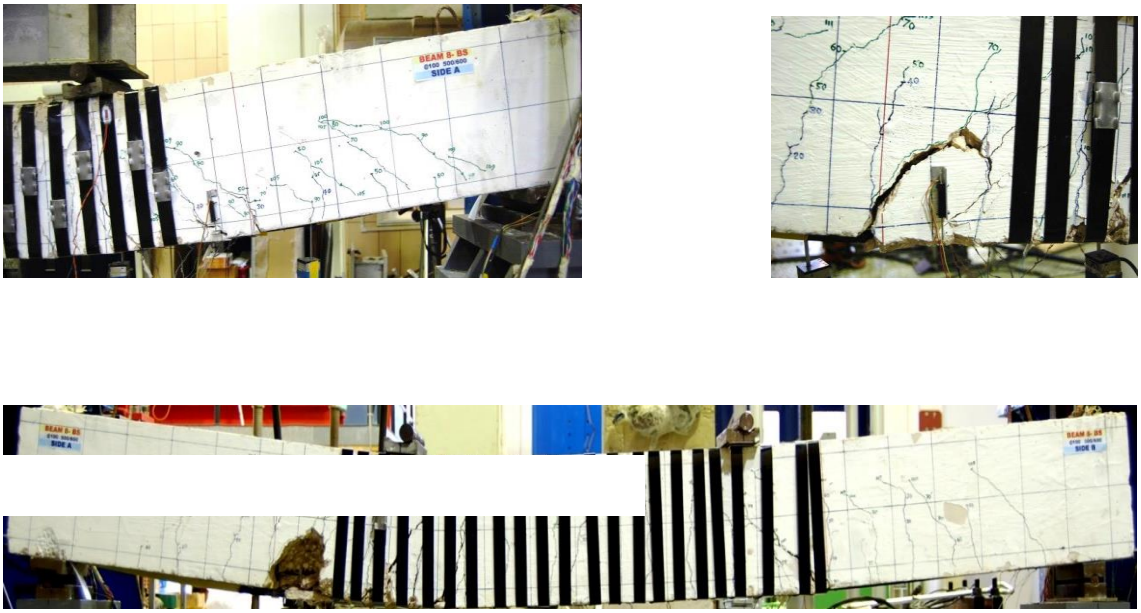

Fig. C8 - 4: Debonding failure of beam in the final testing phase

C.8.3 READINGS OF LVDTs

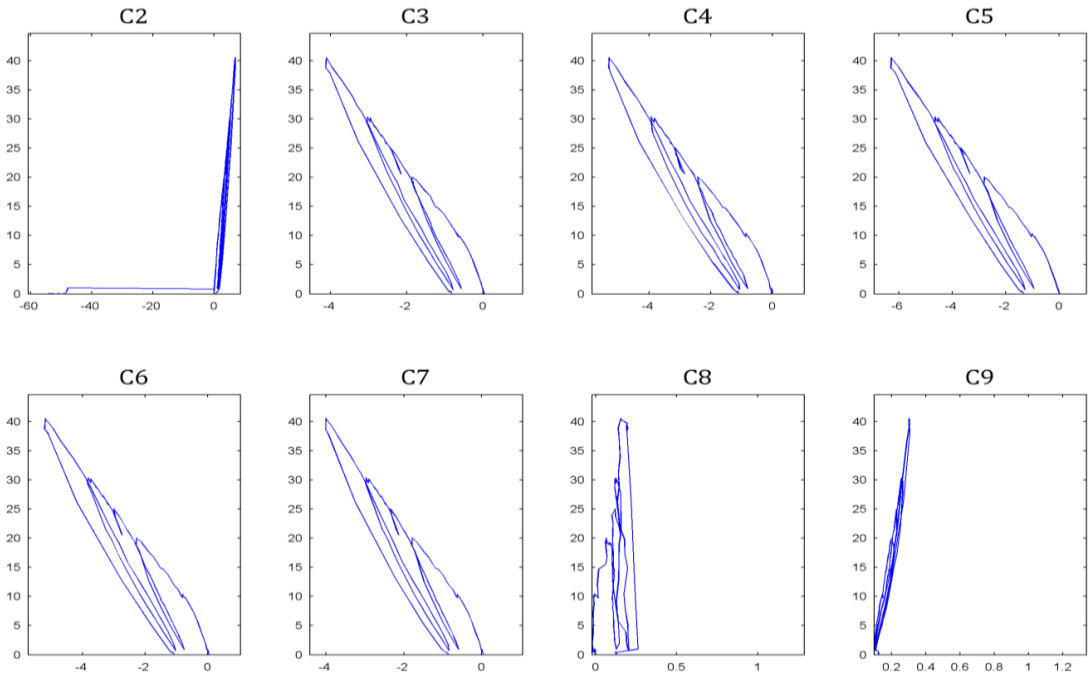

Fig. C8 -5: Readings of LVDTs (C2 - C9)

C.8.4 STRAIN READINGS

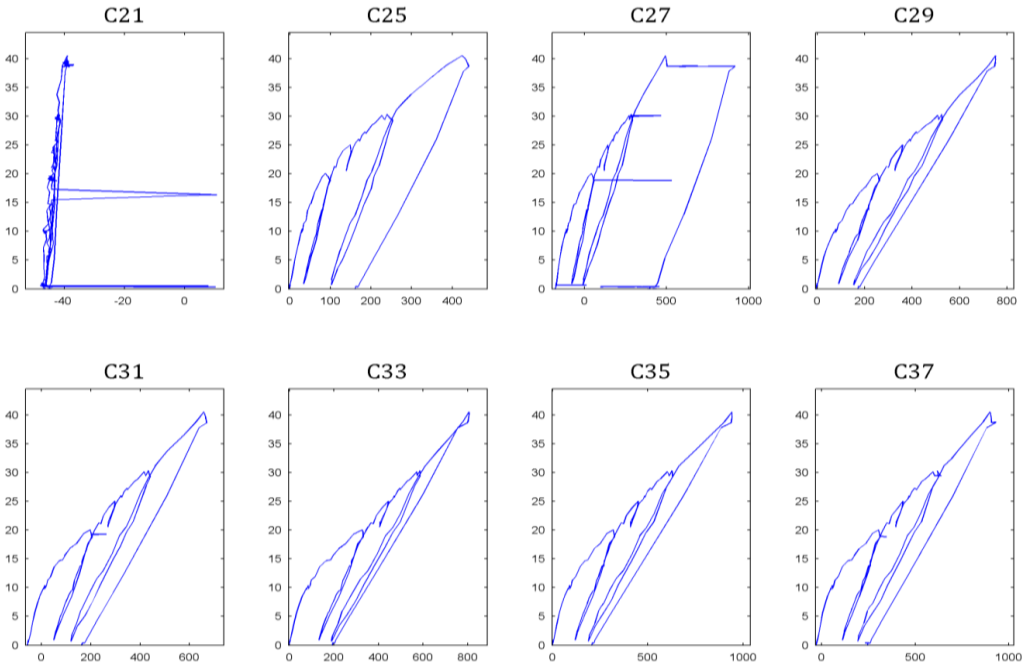

Fig. C8 - 6: Strain readings (C21-37)

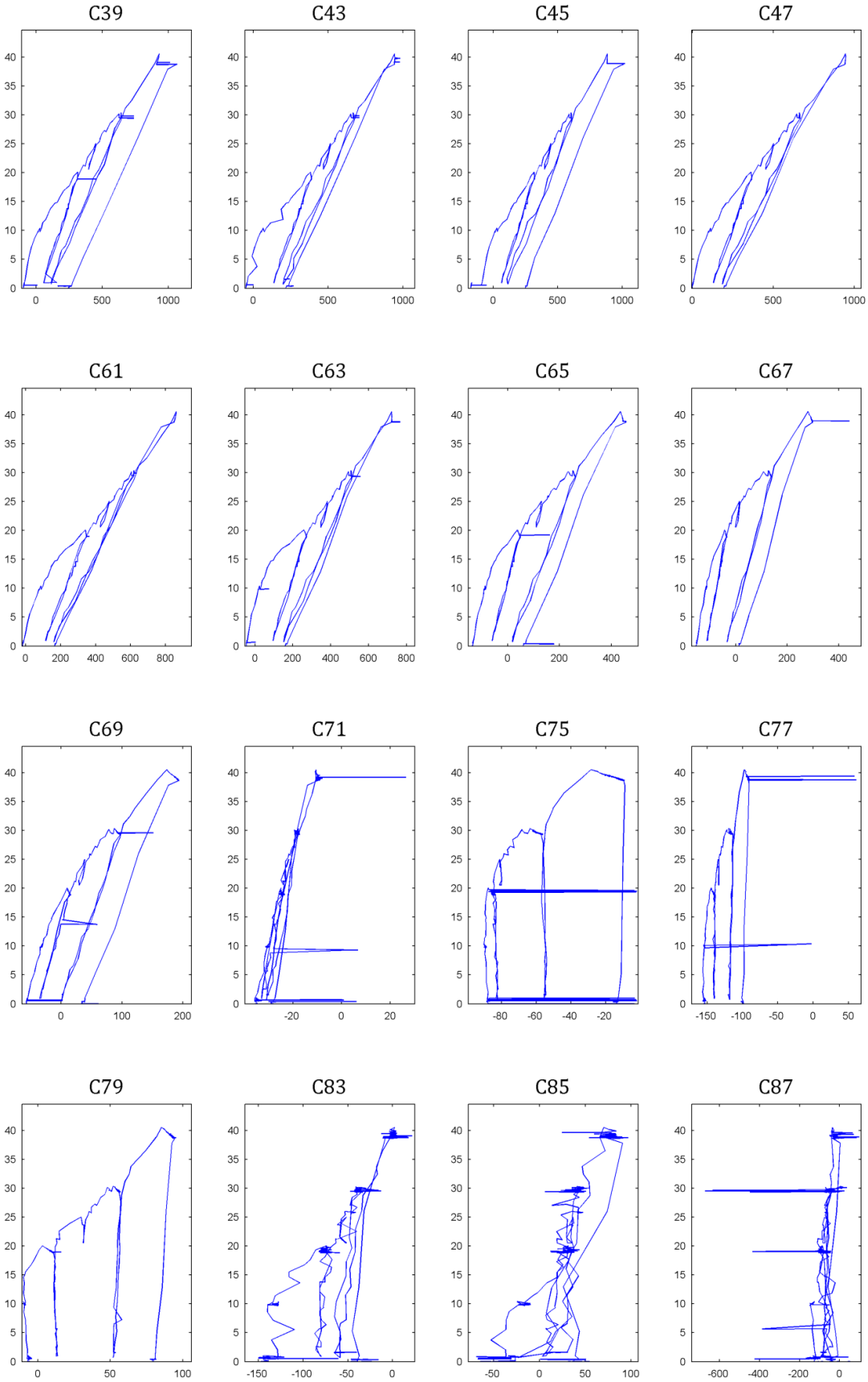

Fig. C8 - 7: Strain readings (C39-C87)

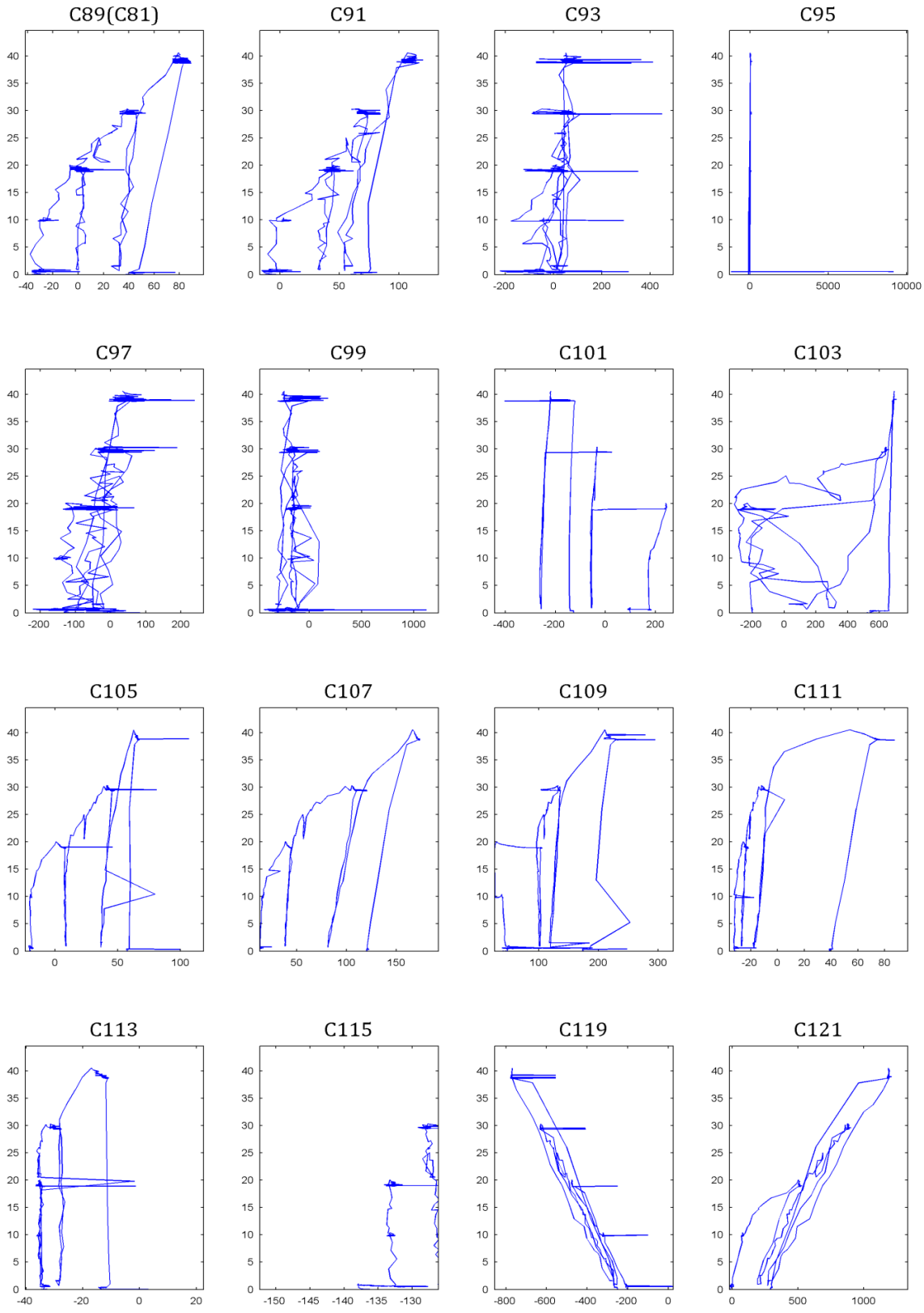

Fig. C8 - 8: Strain readings (C89-C121)

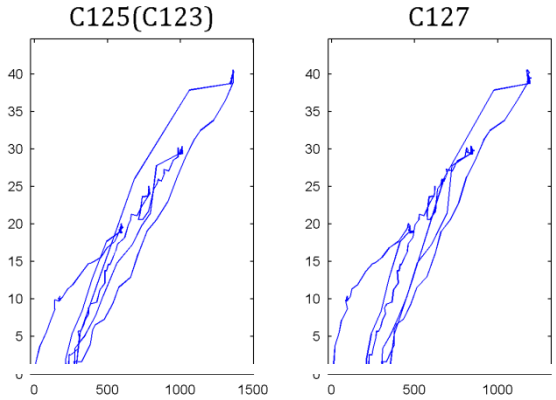

Fig. C8 - 9: Strain readings (C125-C127)

C.8.5 READINGS OF LVDTs

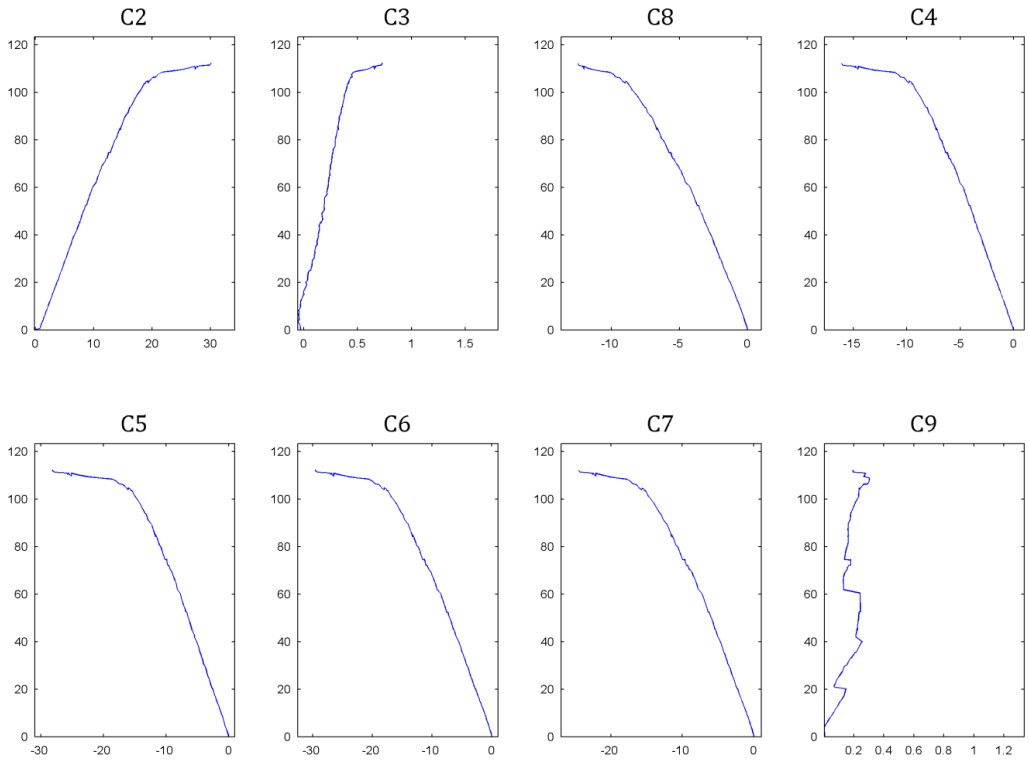

Fig. C8 - 10: Readings of LVDTs (C2-C9)

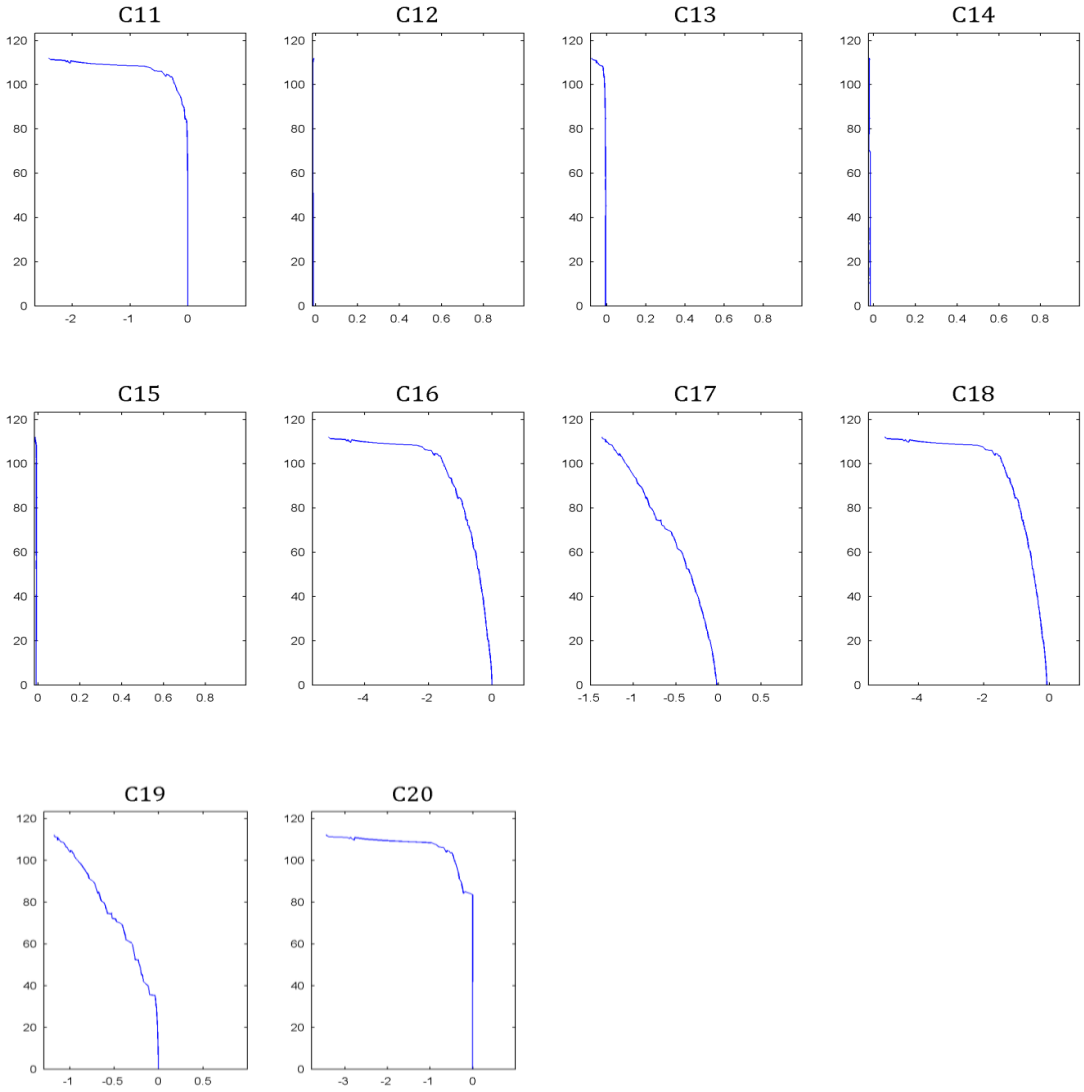

Fig. C8 - 11: Readings of LVDTs (C11 – C20)

C.8.6 STRAIN READINGS

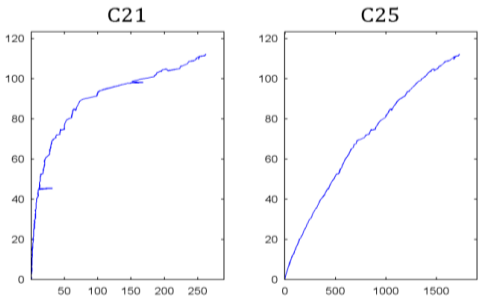

Fig. C8 - 12: Strain readings (C21-C25)

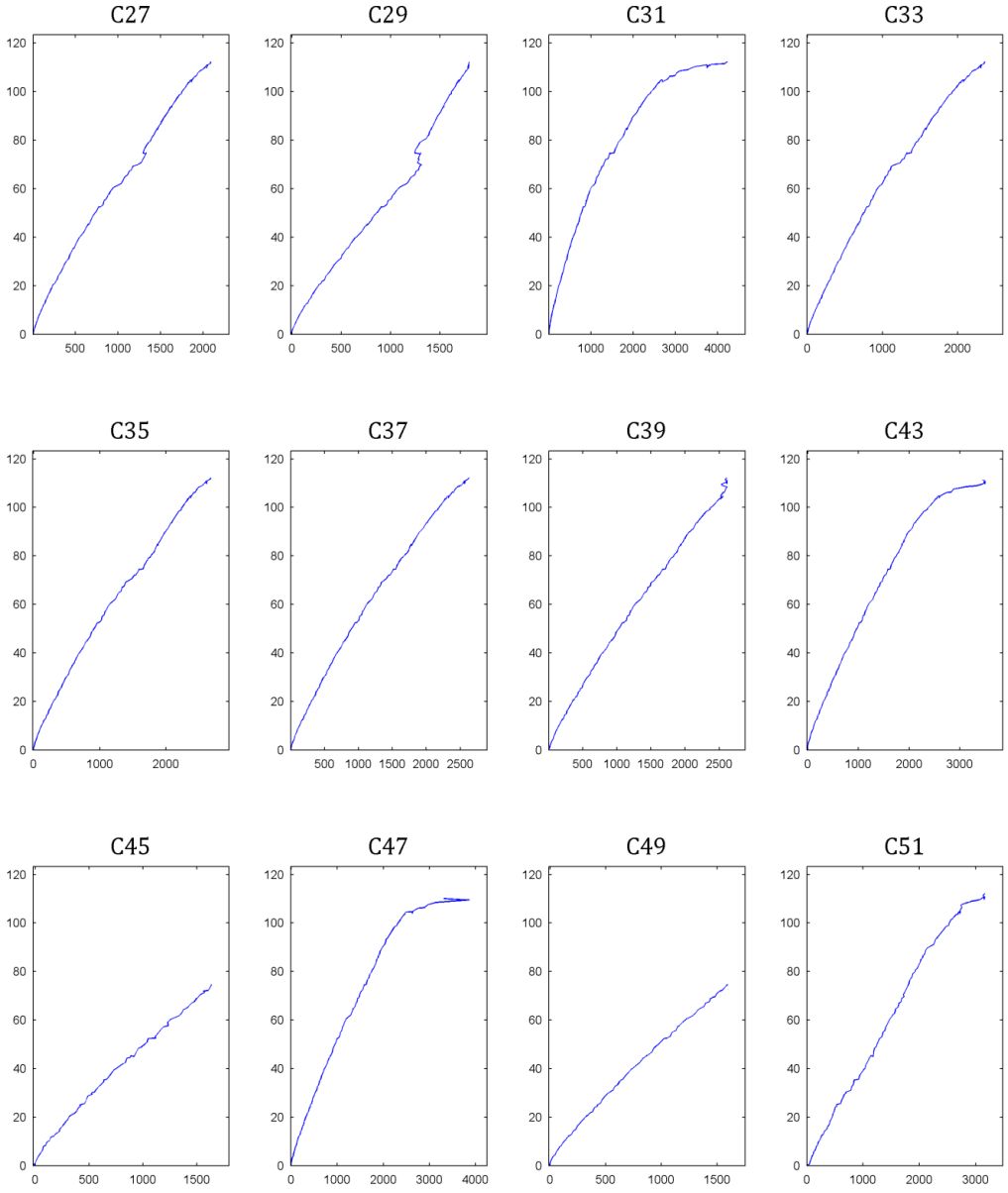

Fig. C8 - 13: Strain readings (C27-C51)

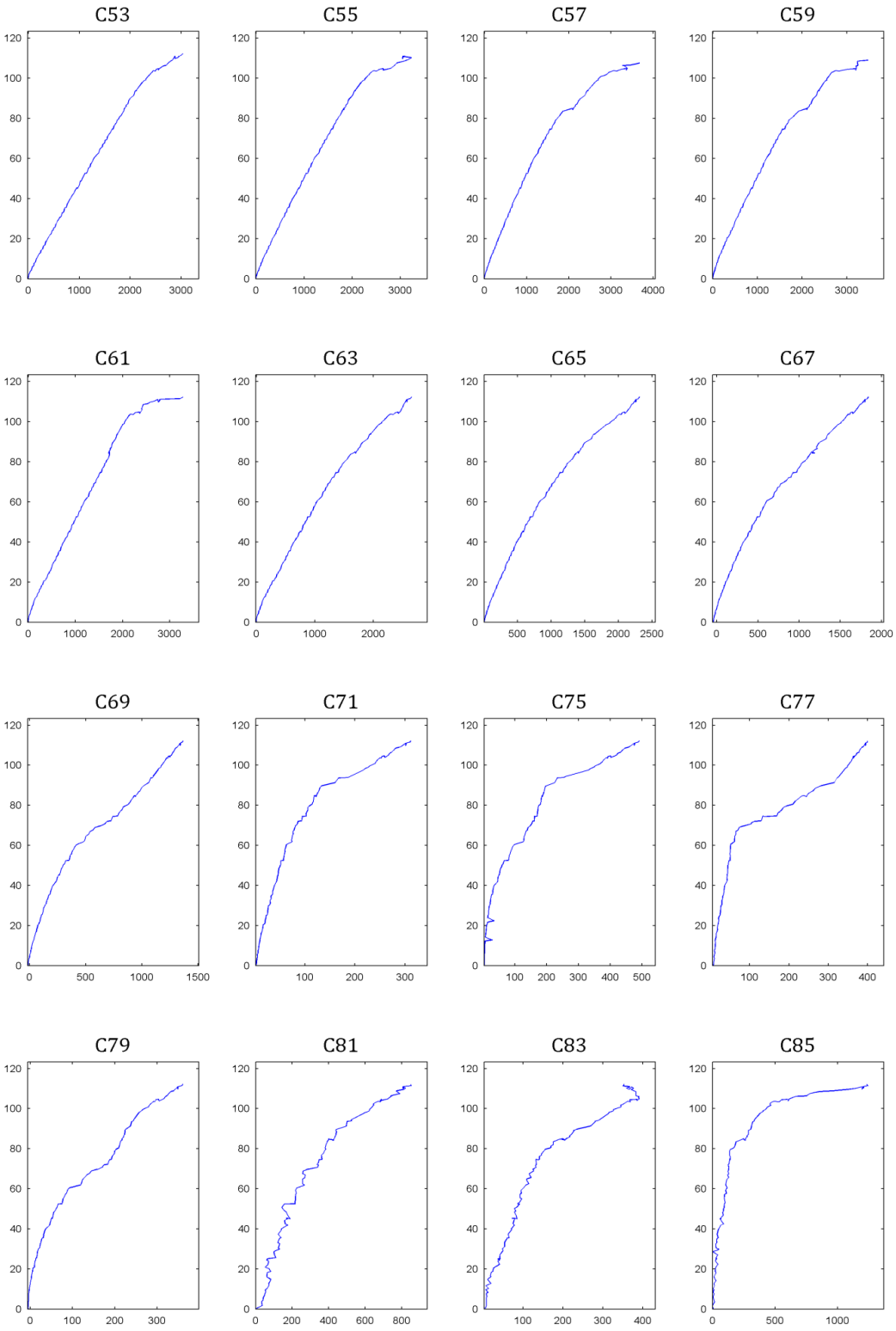

Fig. C8 - 24: Strain readings (C53-C85)

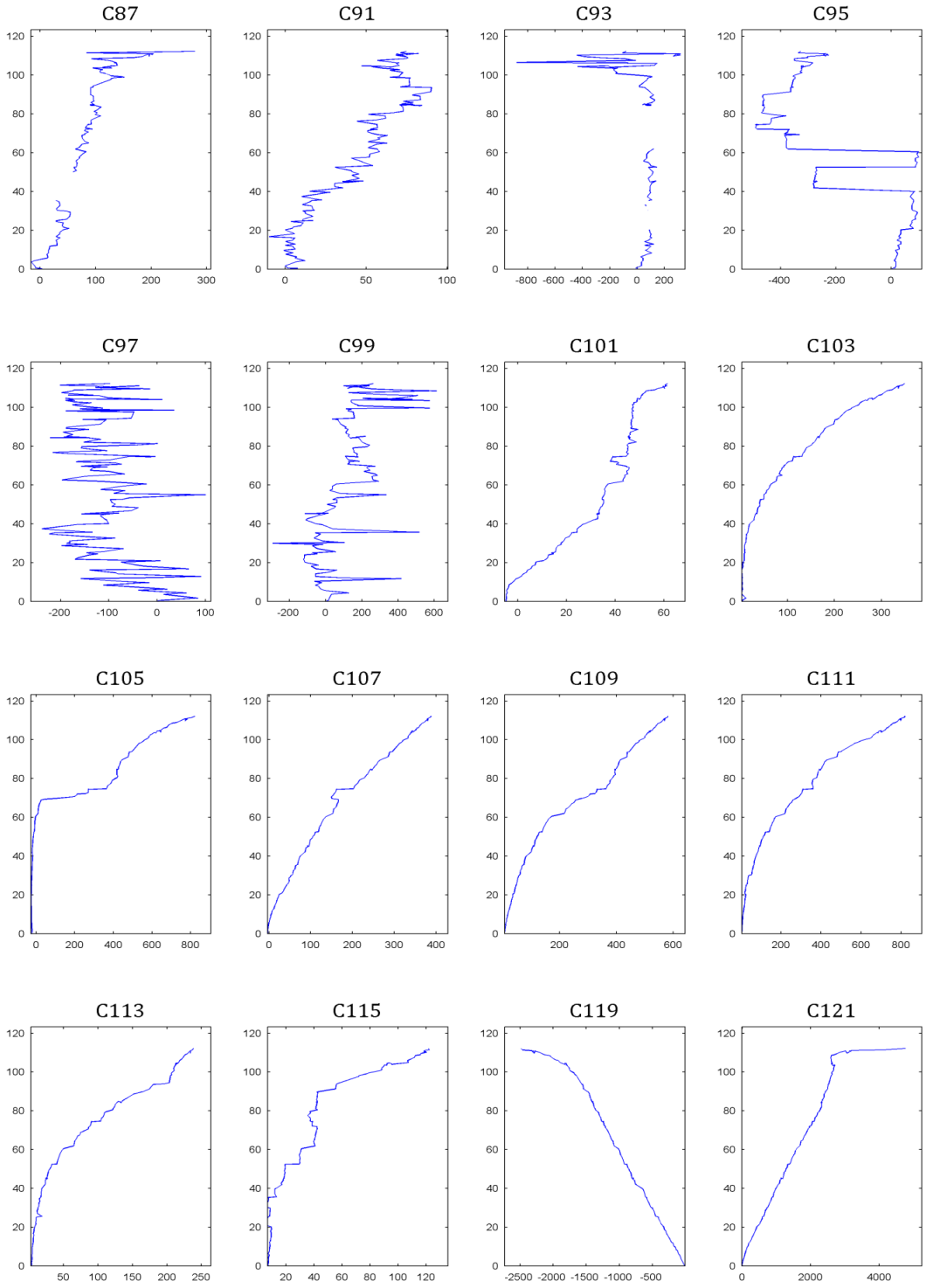

Fig. C8 - 35: Strain readings (C87-C121)

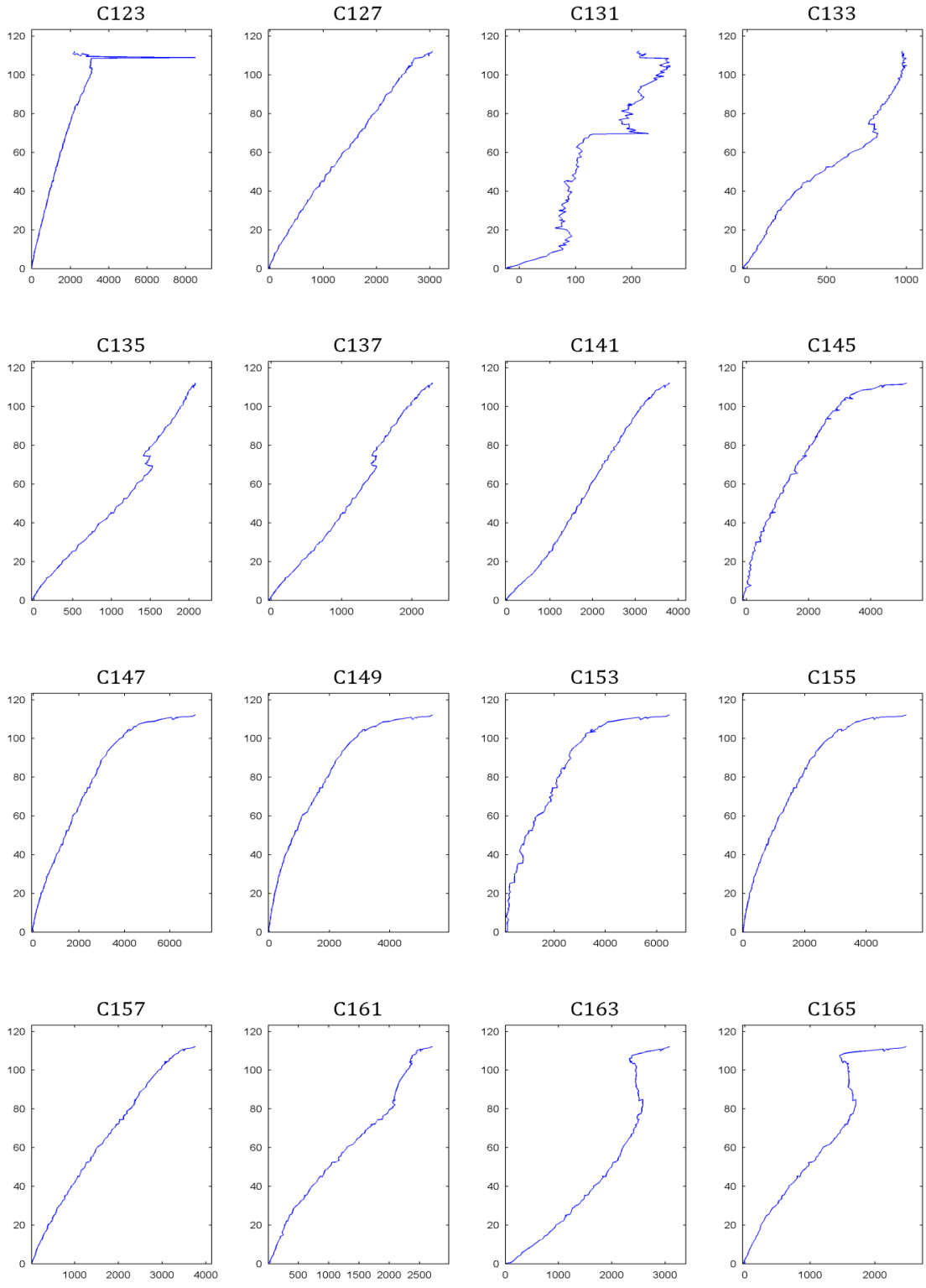

Fig. C8 - 46: Strain readings (C123-C165)

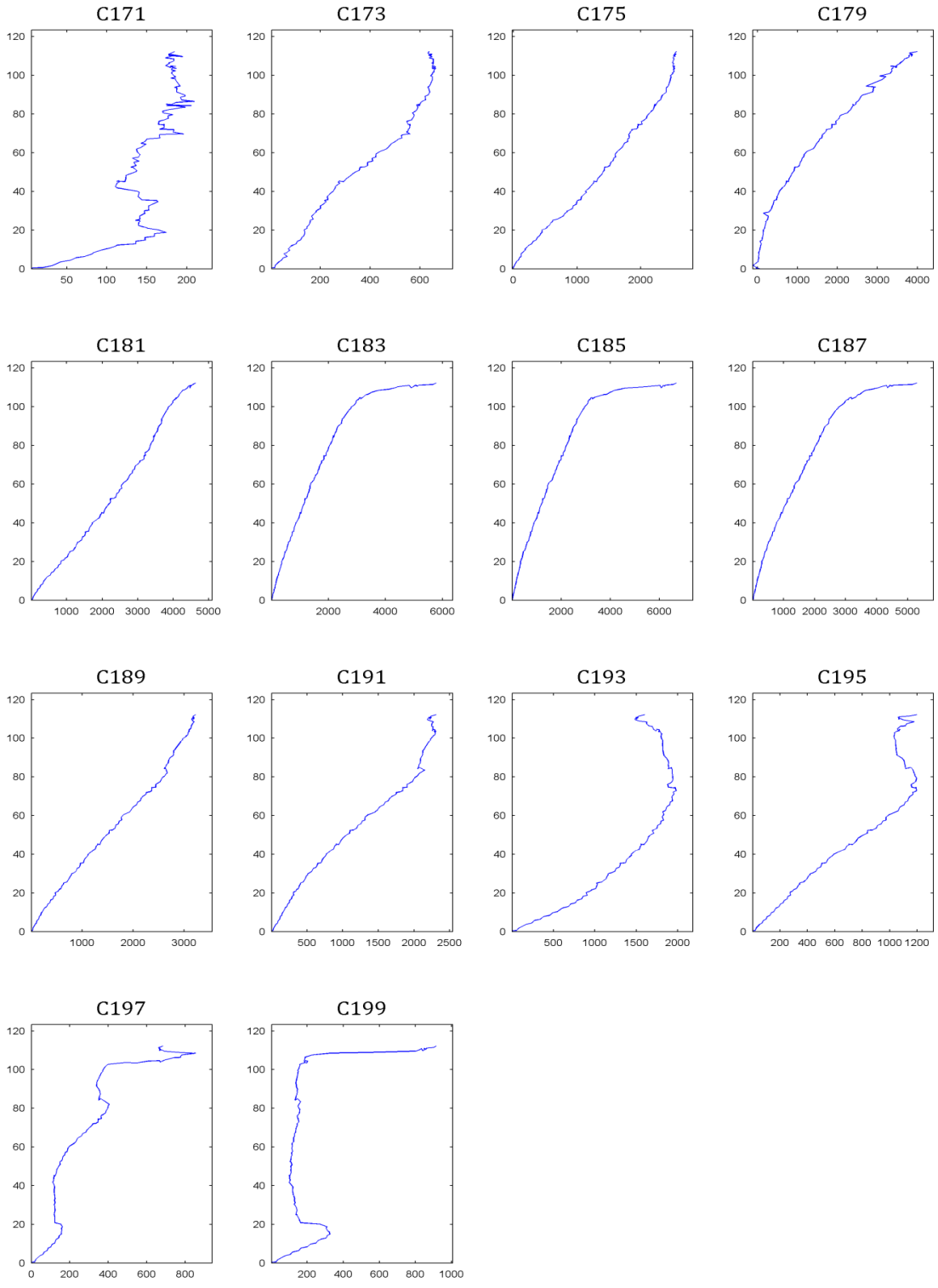

Fig. C8 - 57: Strain readings (C171 – C199)

C.8.7 STRAINS IN THE STEEL REINFORCEMENT AND FRP ALONG THE SPAN

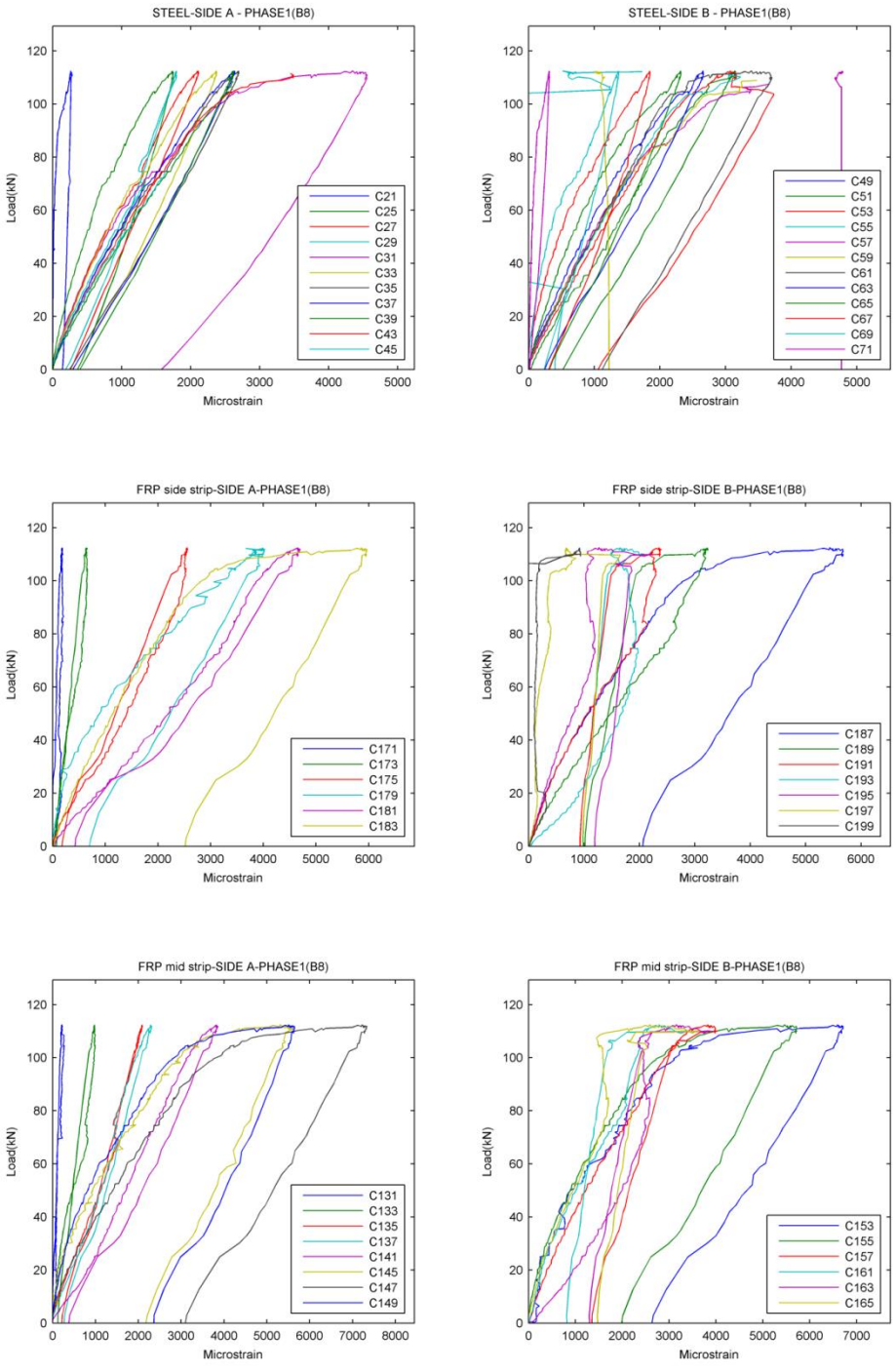

Fig. C8 - 18: Strains in the steel reinforcement and FRP along the span.

C.8.8 STRAIN AND BOND STRESS PROFILES

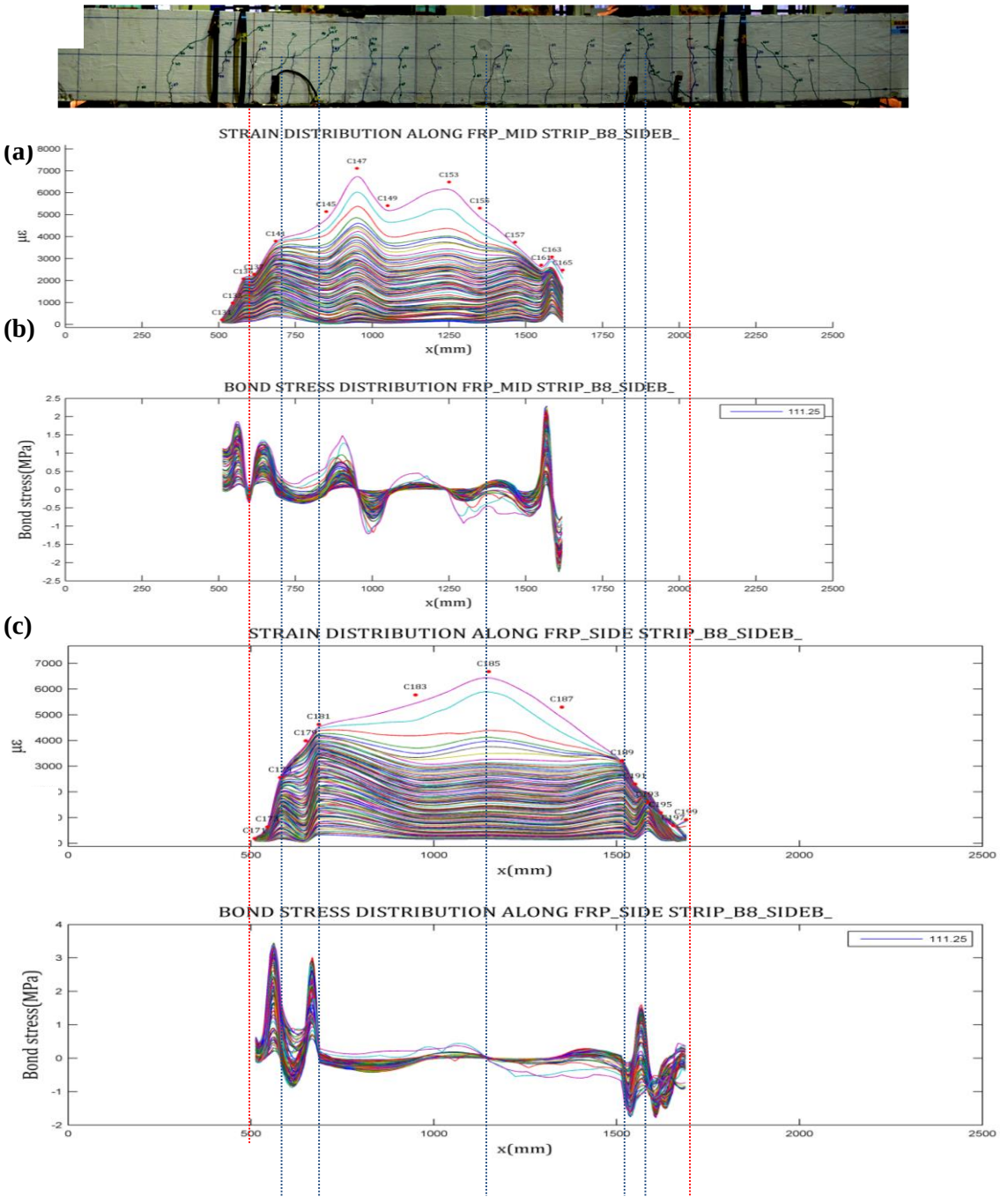

Fig. C8 - 69: Strain and bond stress profiles of (a) Crack pattern of beam NSM2A, (b) FRP, (c) The steel reinforcement.

C.8.9 FINAL TESTING PHASE

a. READINGS OF LVDTs

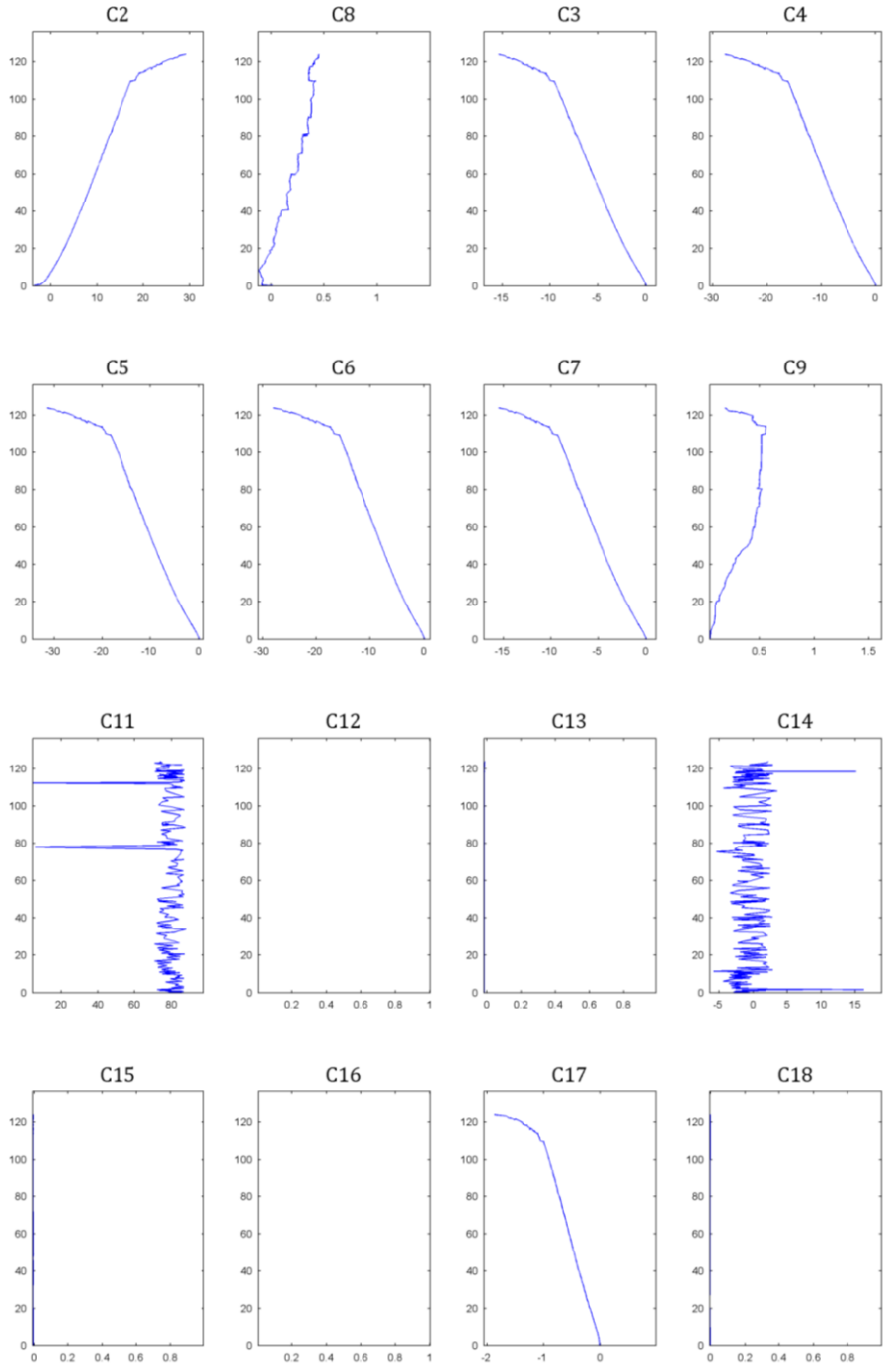

Fig. C8 - 20: Readings of LVDTs (C2-C18)

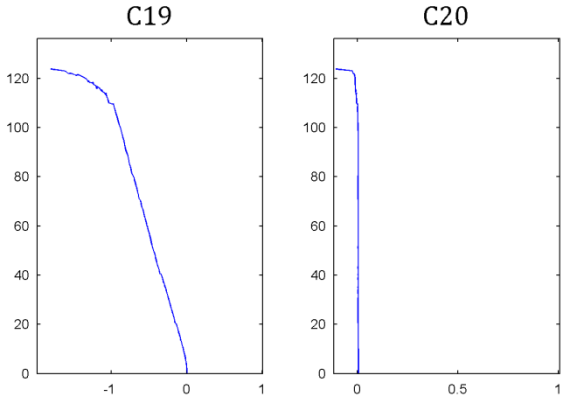

Fig. C8 - 21: Readings of LVDTs (C2 – C20)

C.8.10 STRAIN AND BOND STRESS PROFILES

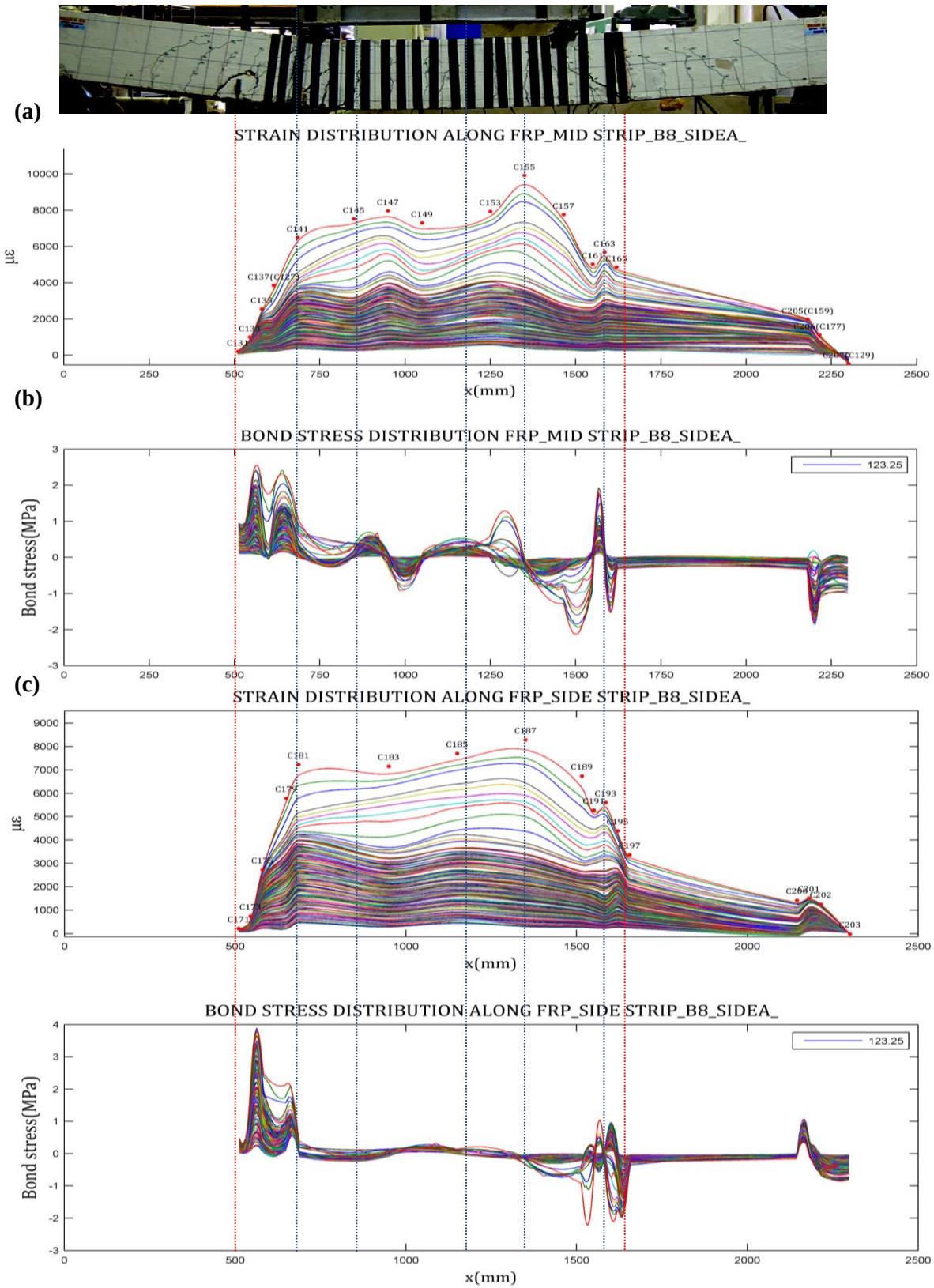

Fig. C8 - 72: Strain and bond stress profiles of (a) Crack pattern of beam NSM2A, (b) FRP, (c) The steel reinforcement

C.9.1 BEAM DESIGN

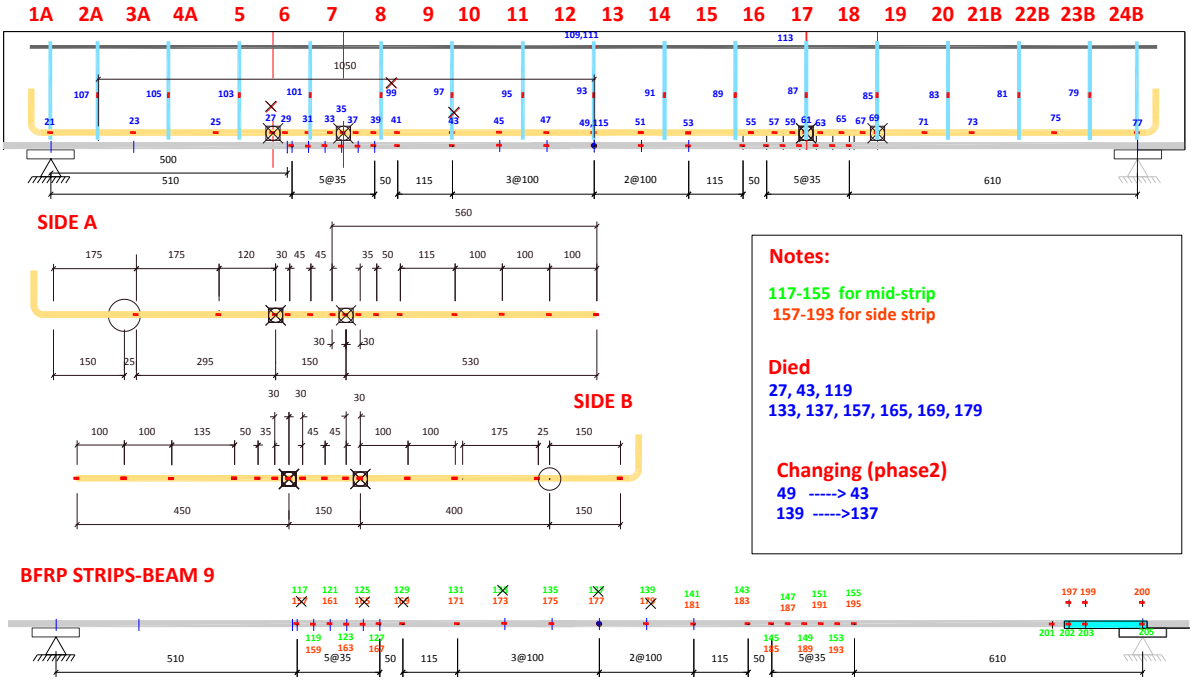

Fig. C9 - 1: Beam NSM B9-BS design

C.9.2 FIRST TESTING PHASE: PRE-DAMAGING

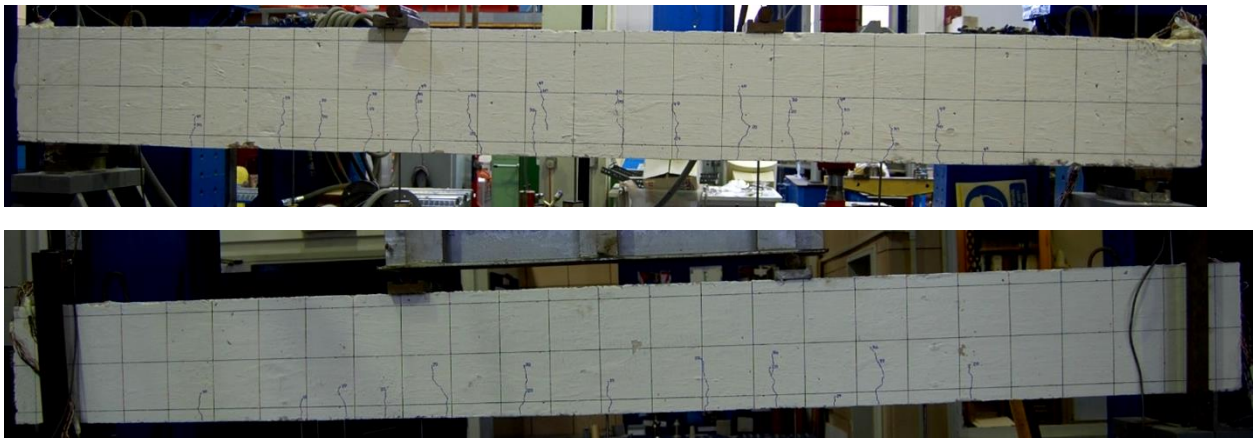

(a)

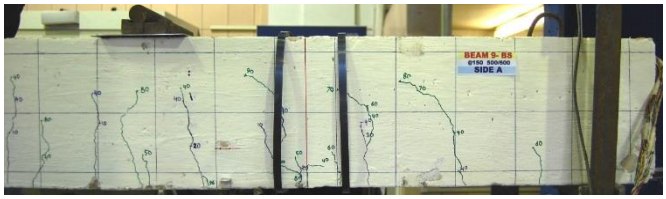

(b)

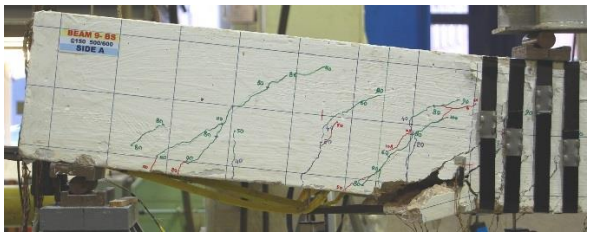

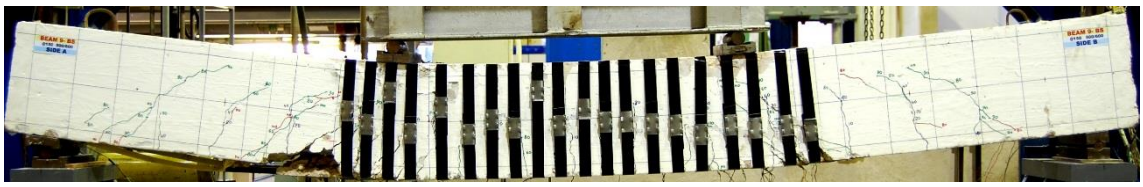

(c)

Fig. C9 - 2: Crack pattern of beam NSM6A

a. LVDTs READINGS

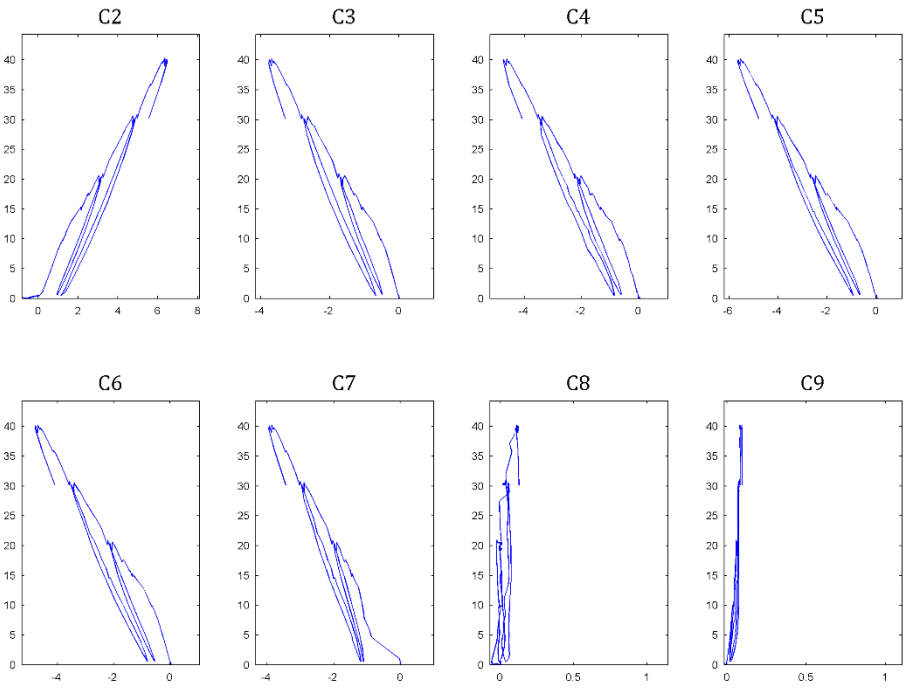

Fig. C9 - 3: Readings of LVDTs (C2 – C9)

b. STRAIN READINGS

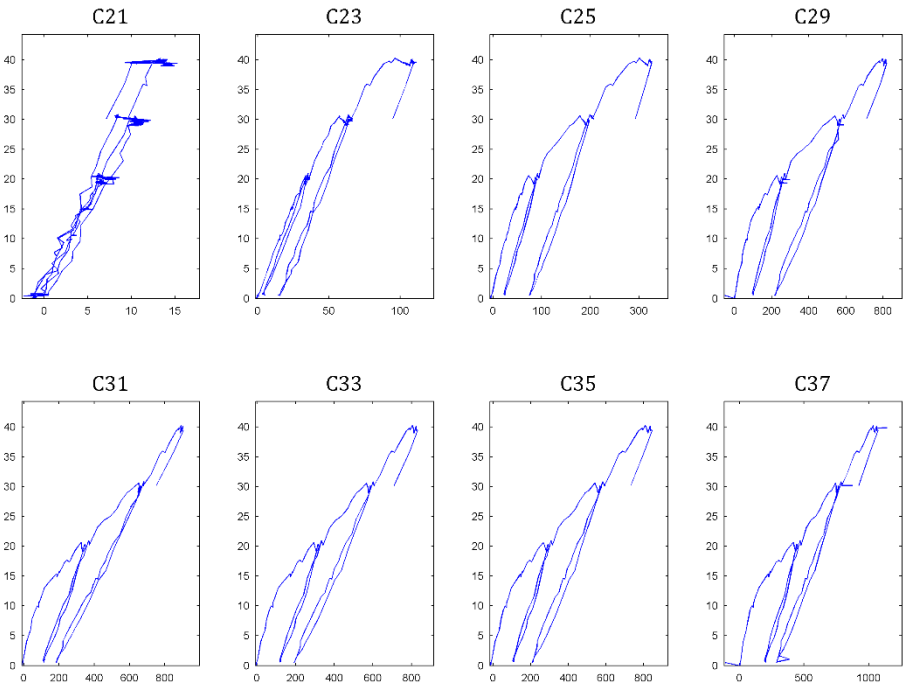

Fig. C9 - 4: Strain readings (C21 – C37)

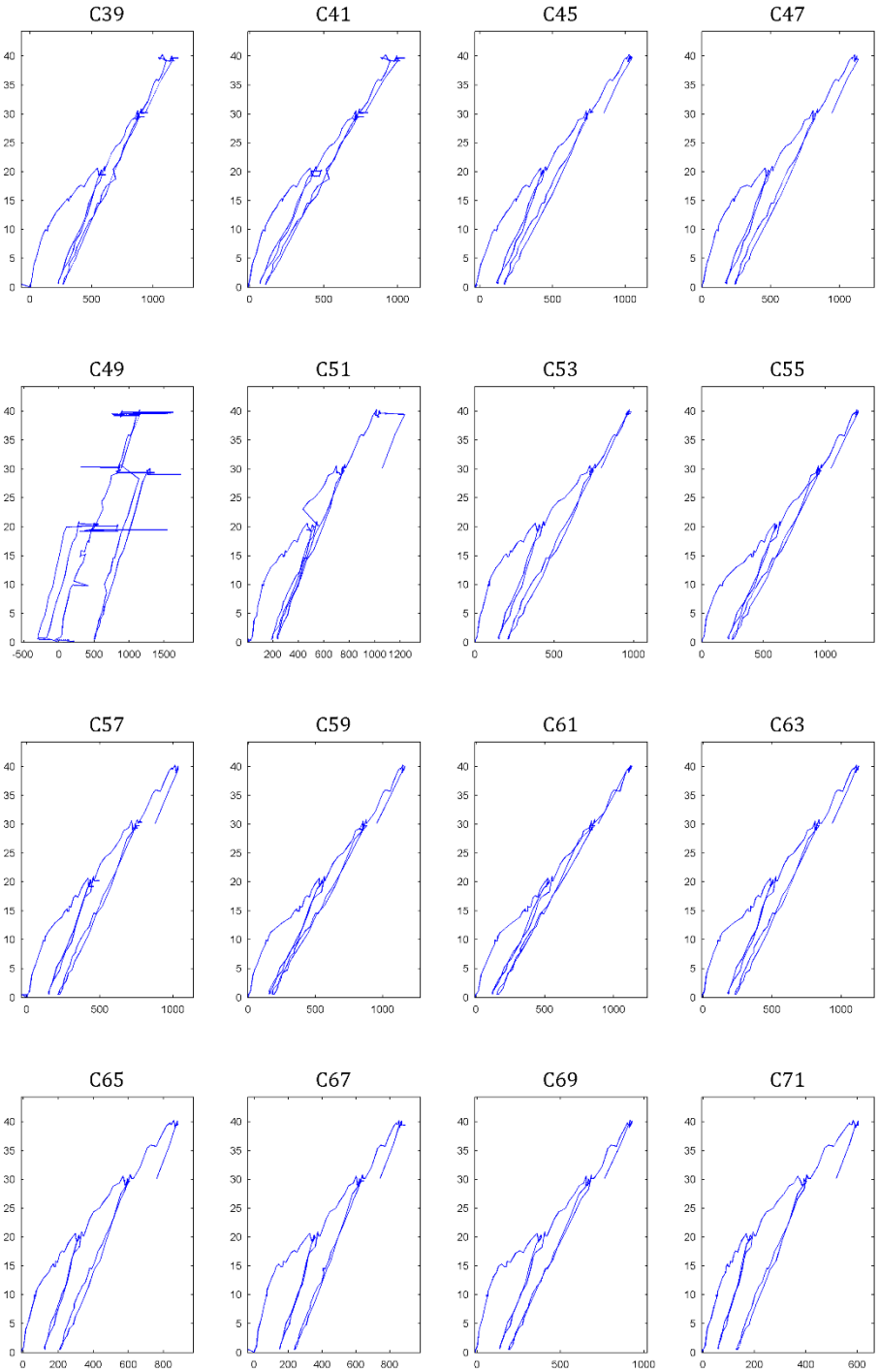

Fig. C9 - 5: Strain readings (C39 – C71)

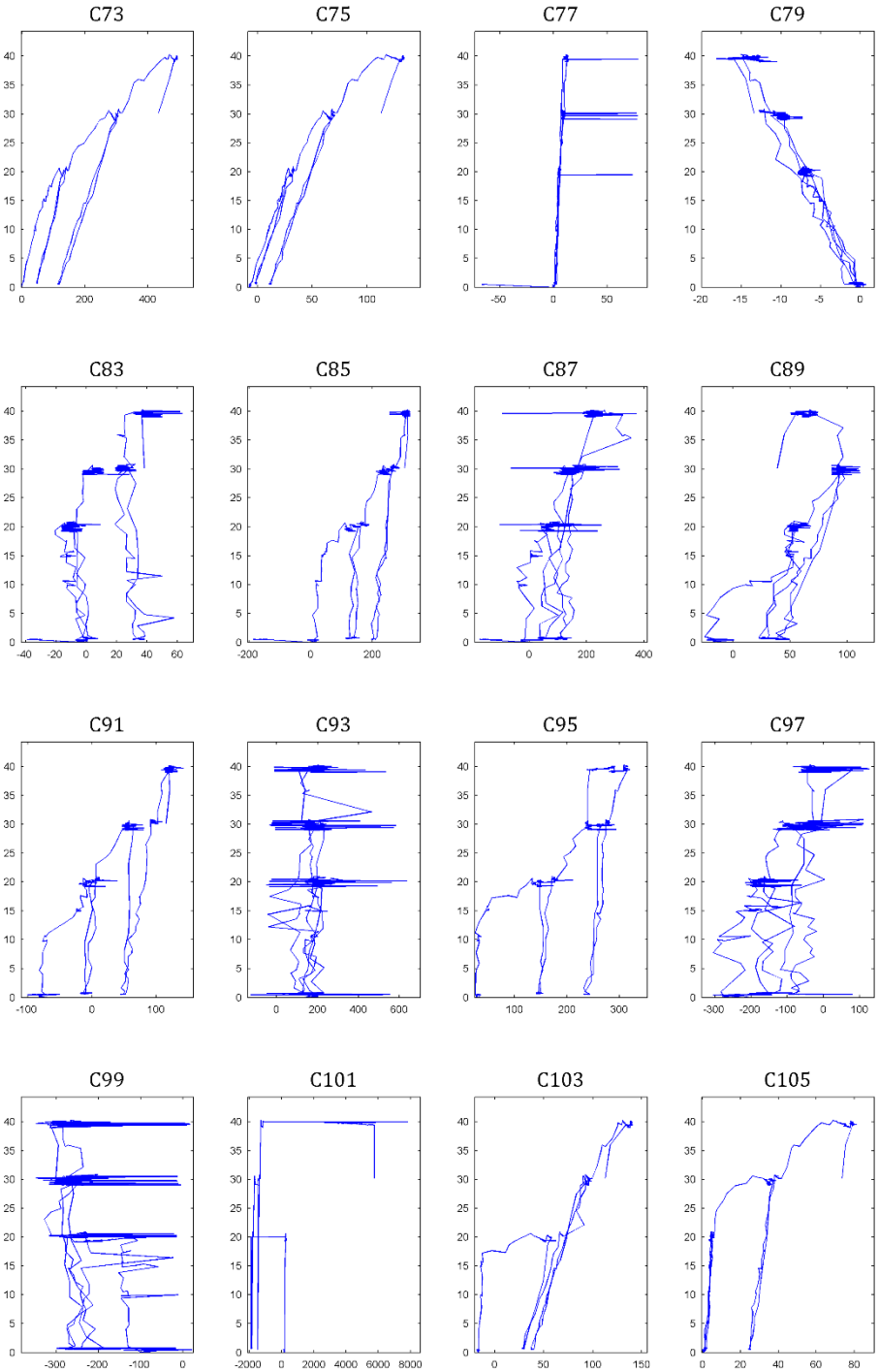

Fig. C9 - 6: Strain readings (C73 – C105)

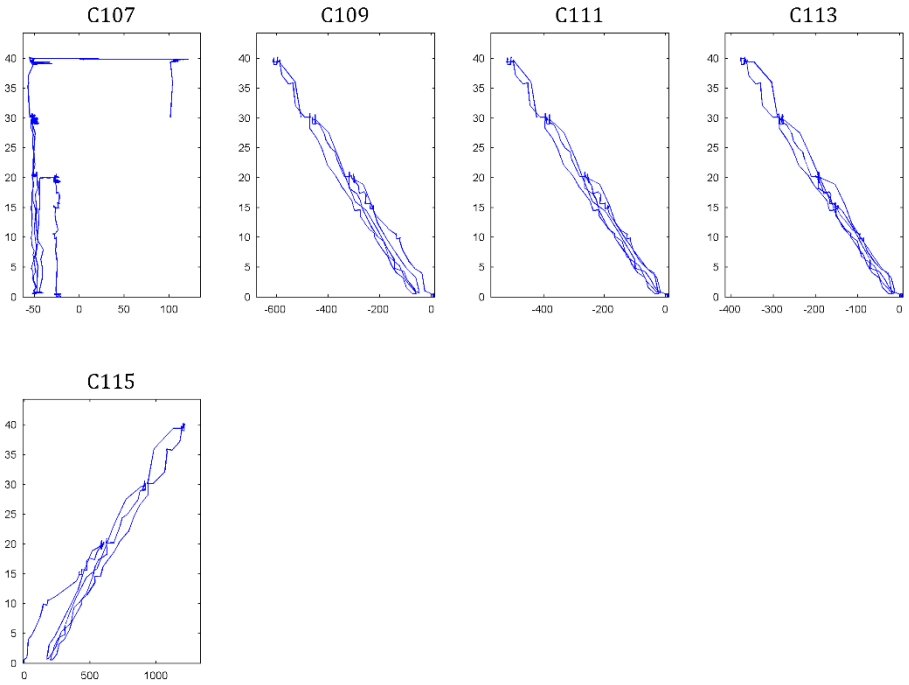

Fig. C9 - 7: Strain readings (C21 – C115)

C.9.3 FIRST TESTING PHASE: FAILURE ON SIDE B

a. LVDTs READINGS

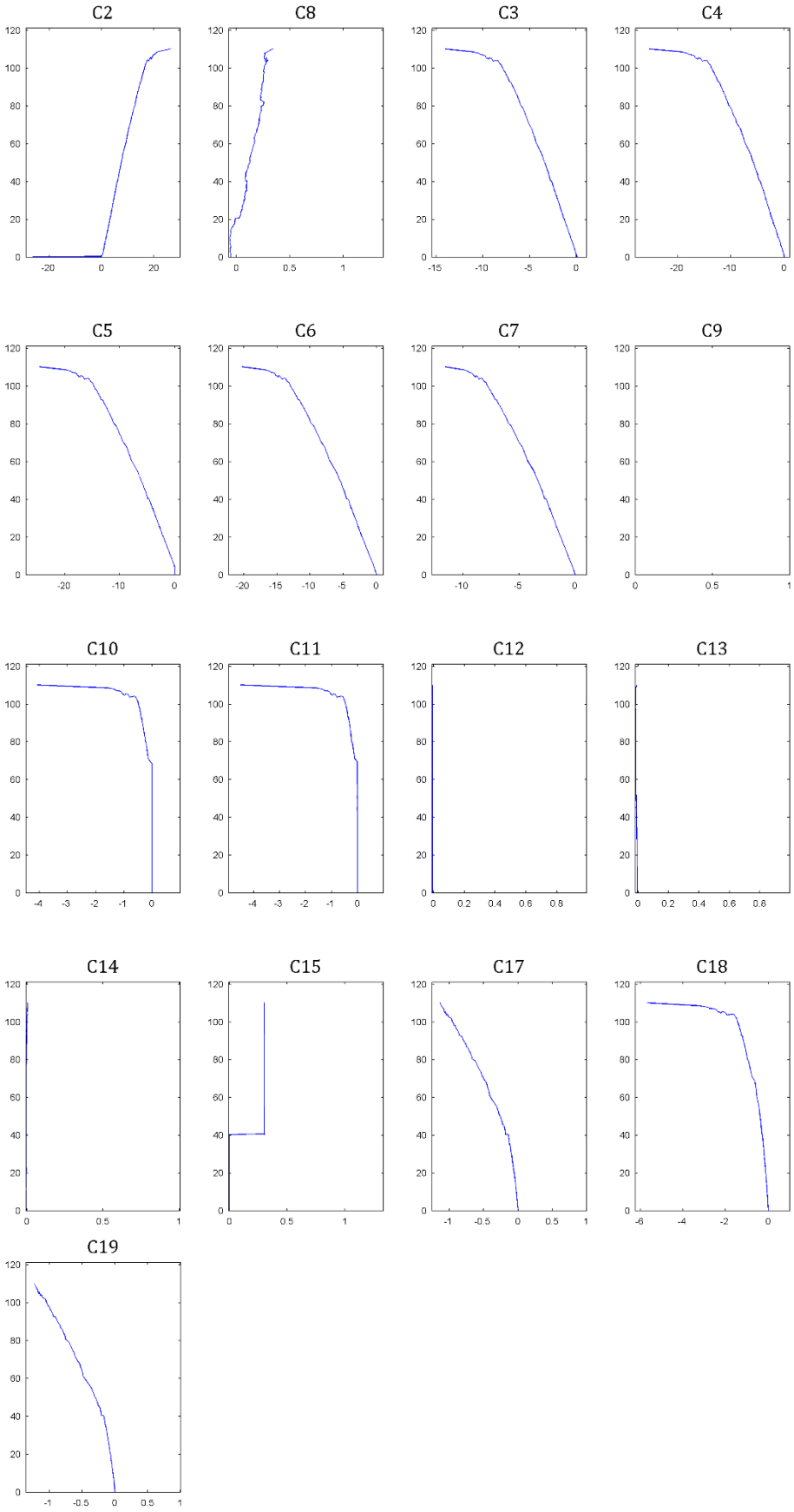

Fig. C9 - 9: Readings of LVDTs (C2 – C19)

b. **STRAIN READINGS**

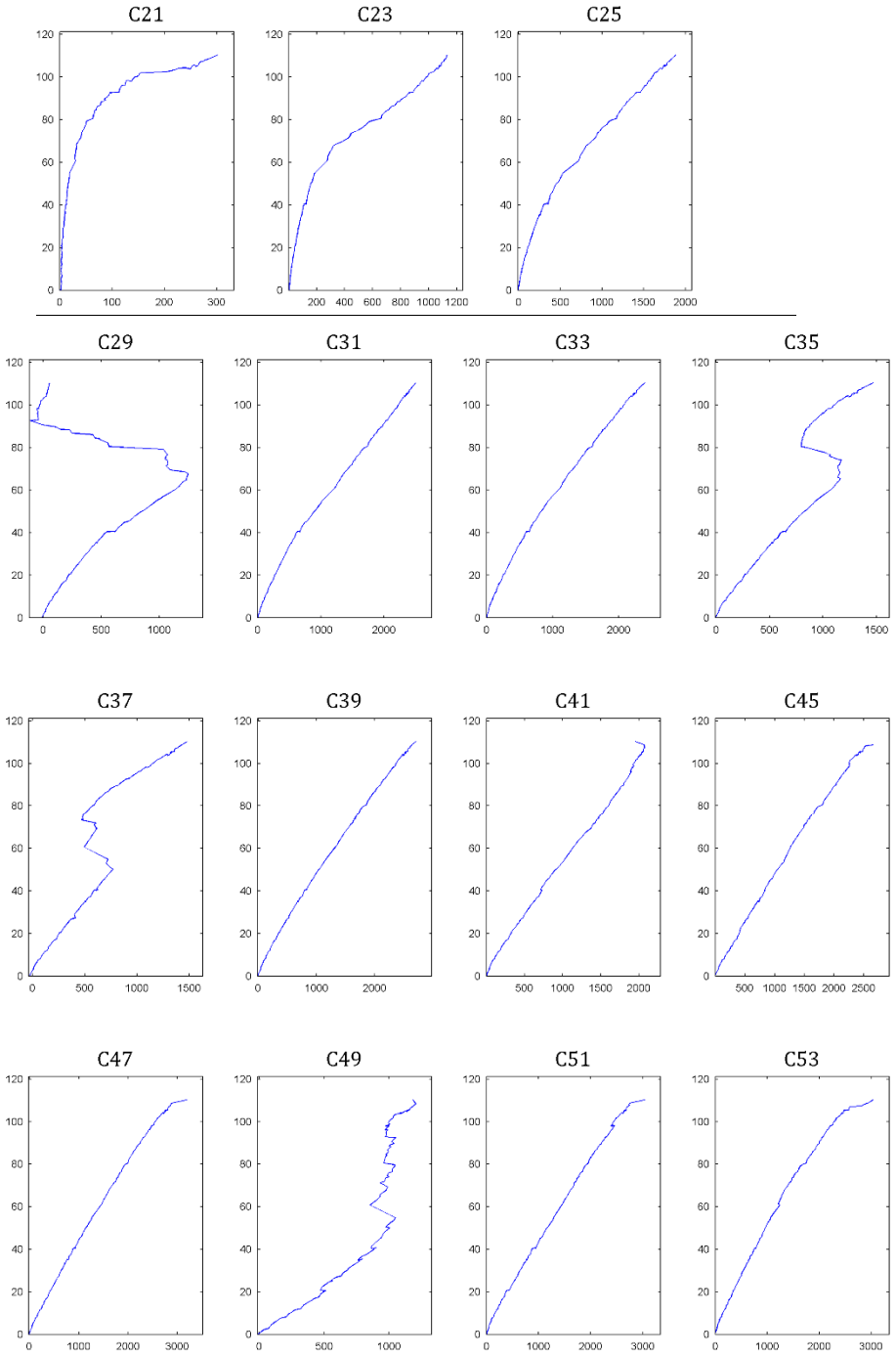

Fig. C9 - 10: Strain readings (C21 – C53)

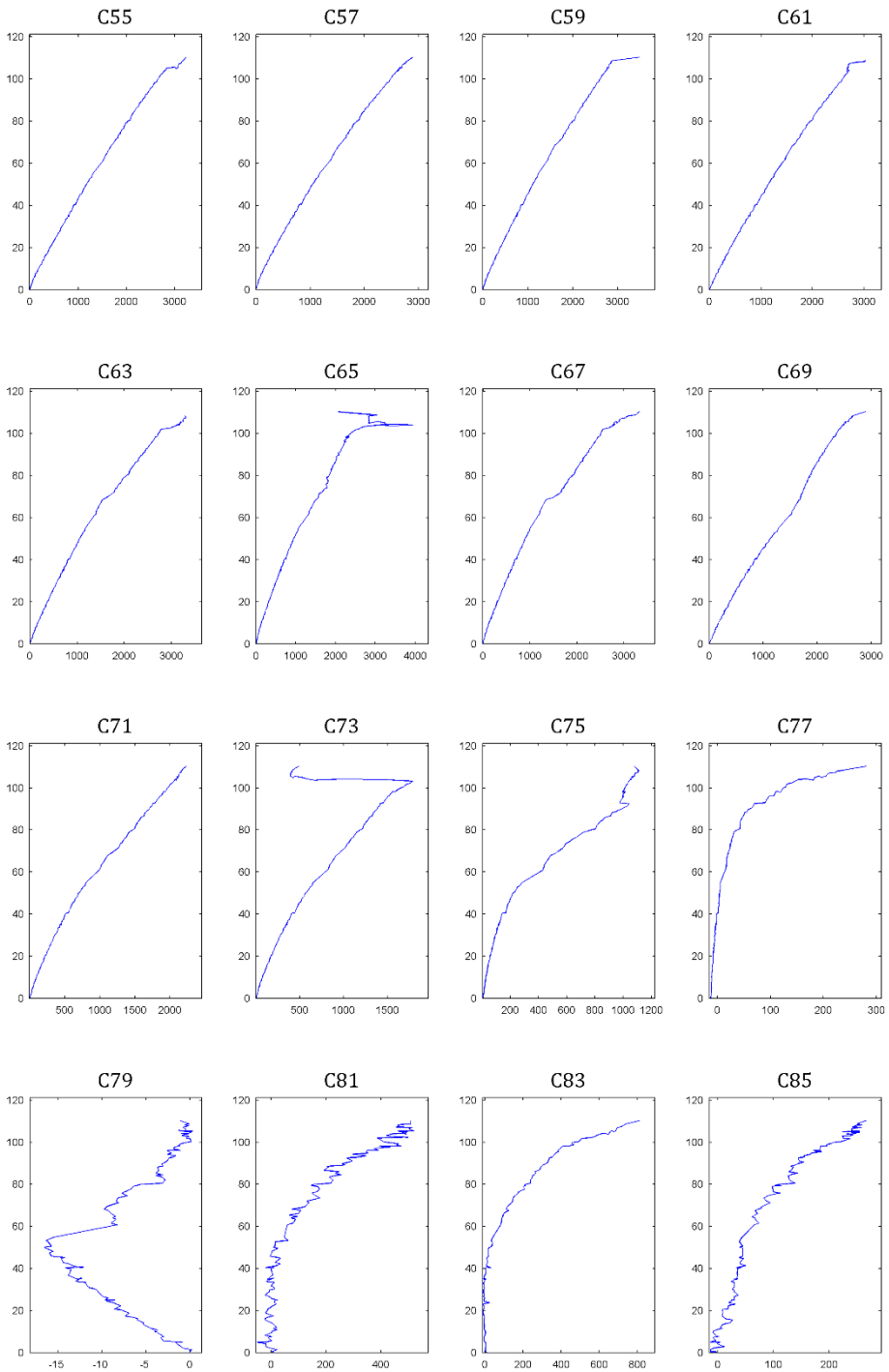

Fig. C9 - 11: Strain readings (C55 – C85)

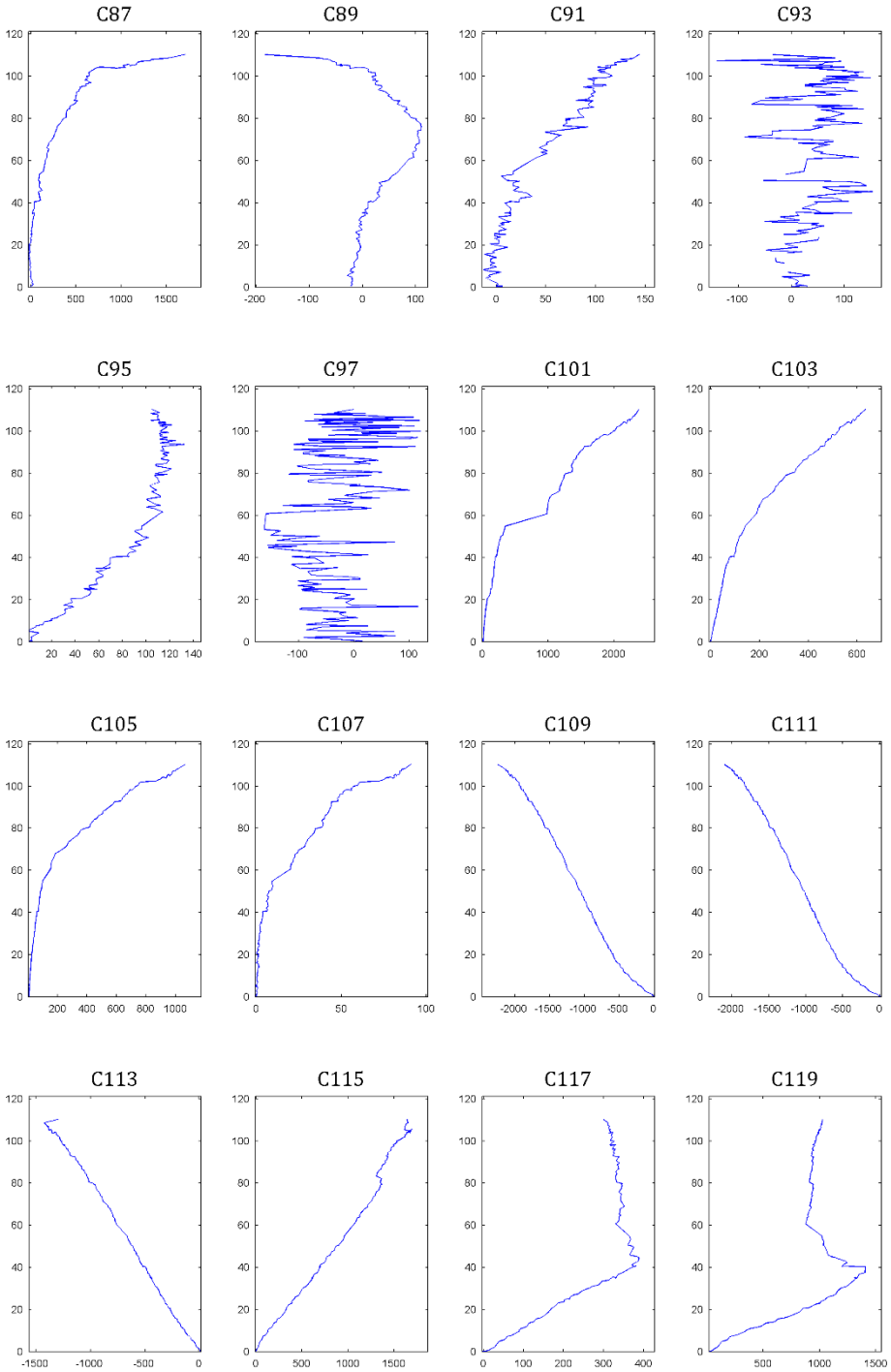

Fig. C9 - 12: Strain readings (C87 – C119)

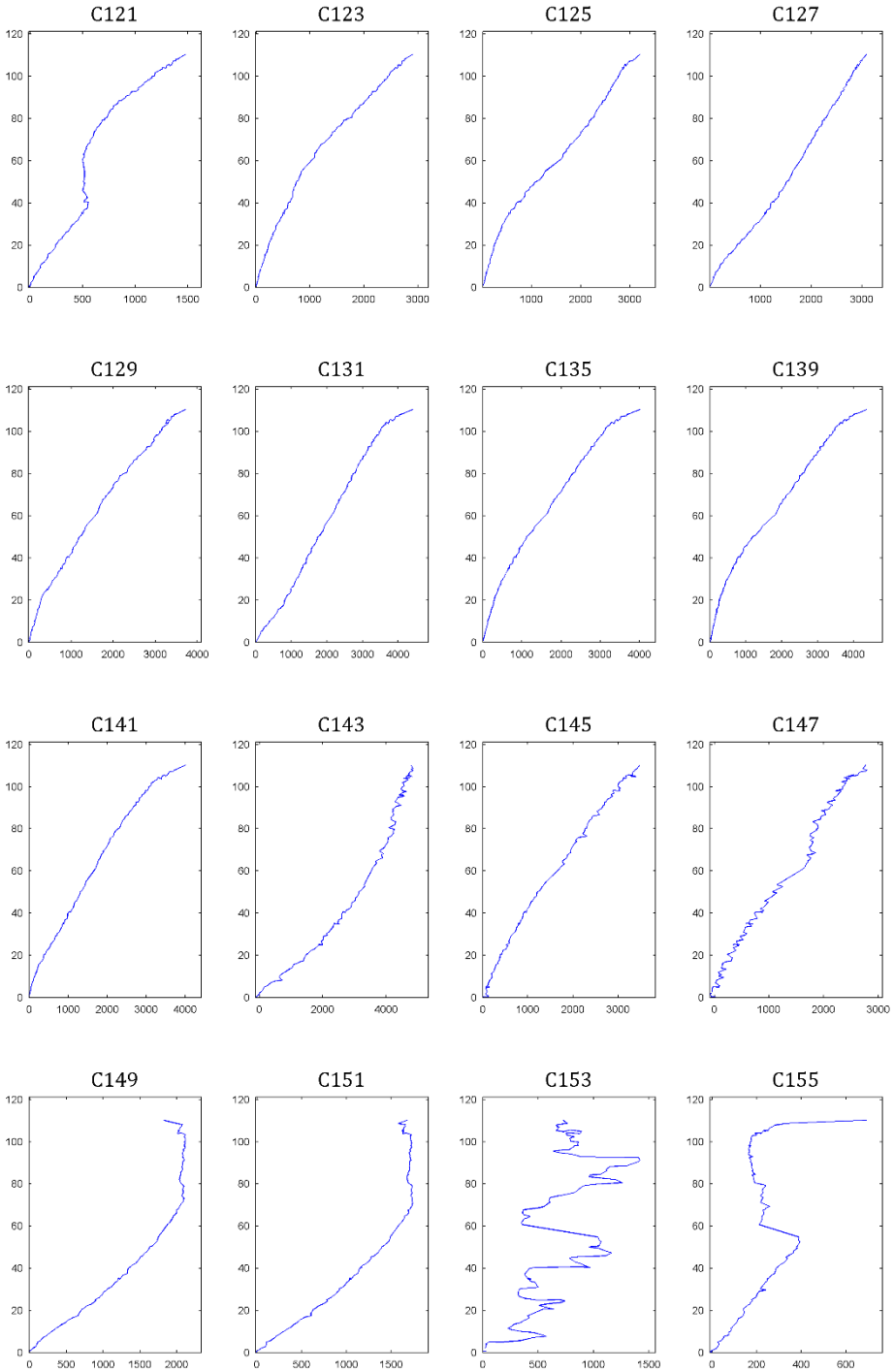

Fig. C9 - 13: Strain readings (C121 – C155)

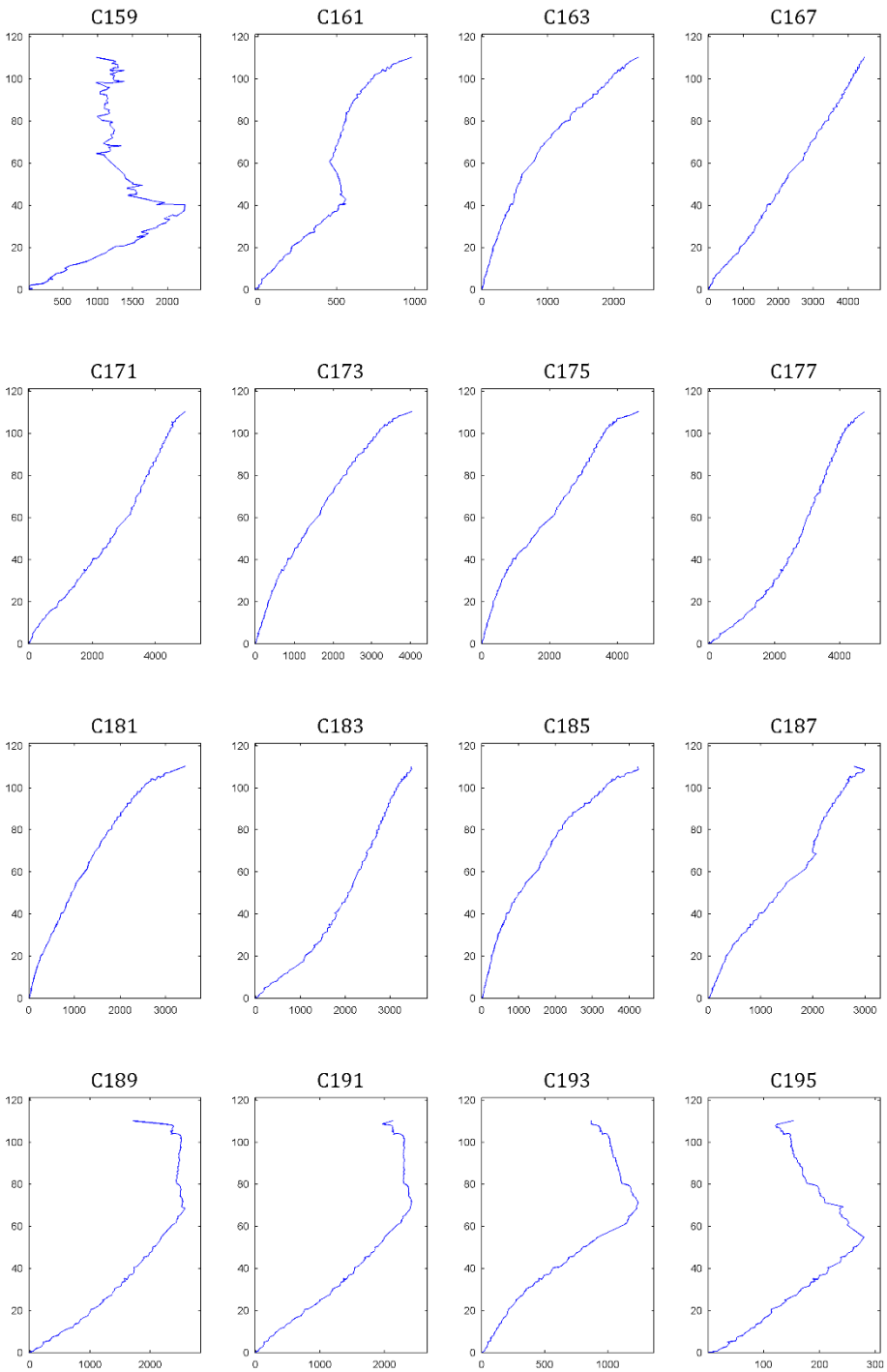

Fig. C9 - 14: Strain readings (C159 – C195)

C.9.4 STRAINS IN THE STEEL REINFORCEMENT AND FRP ALONG THE MID-SPAN REGION

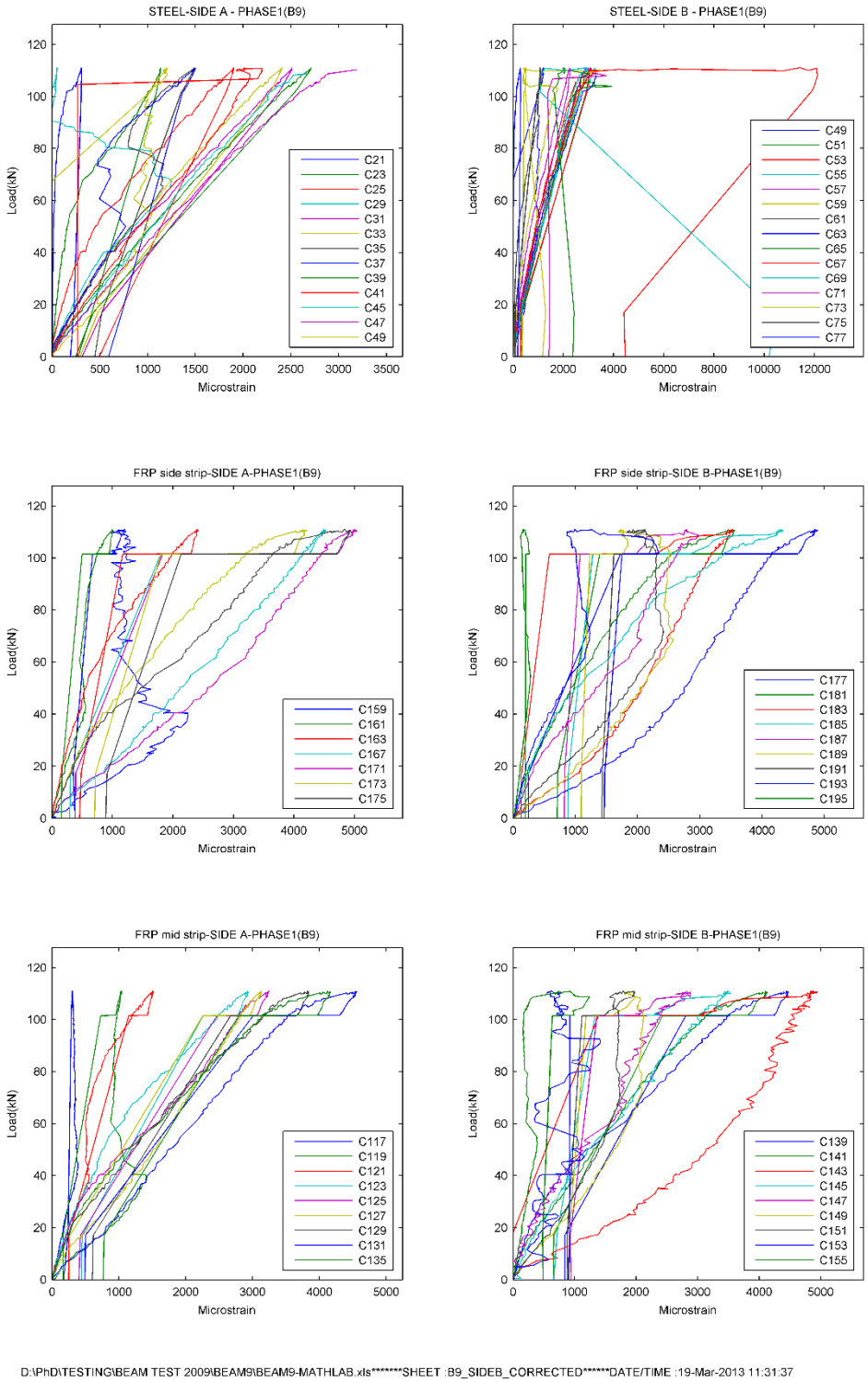

Fig. C9 - 15: Strain along steel bar – Phase 2

C.9.5 STRAIN AND BOND STRESS PROFILES

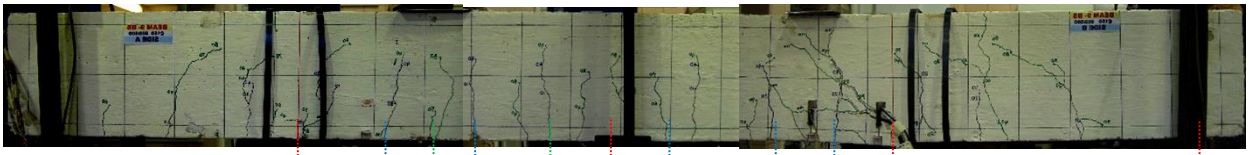

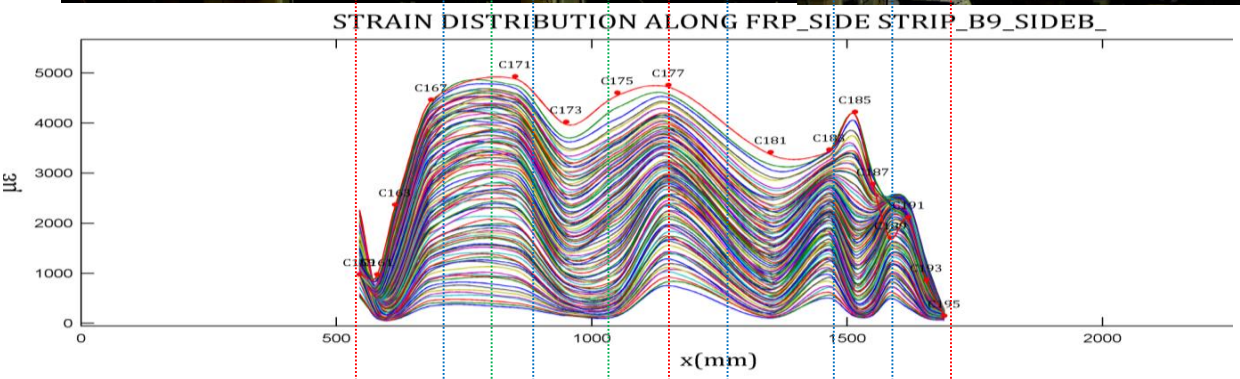

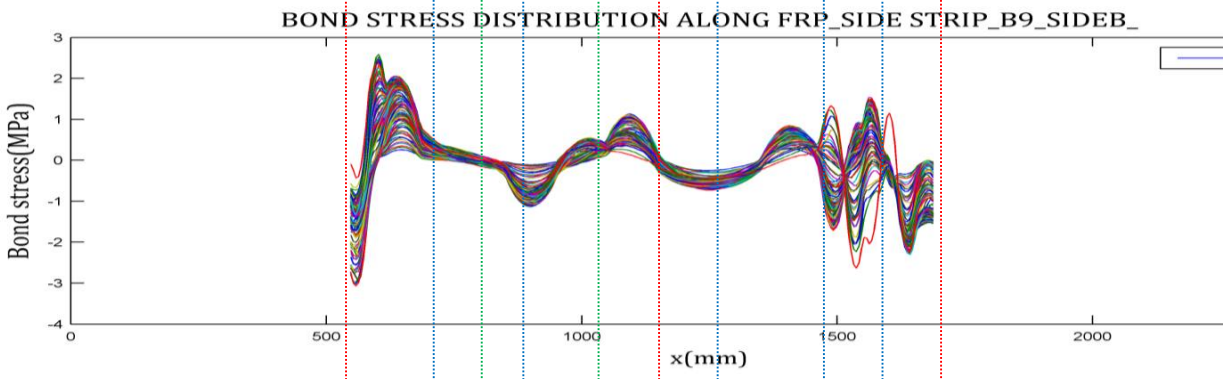

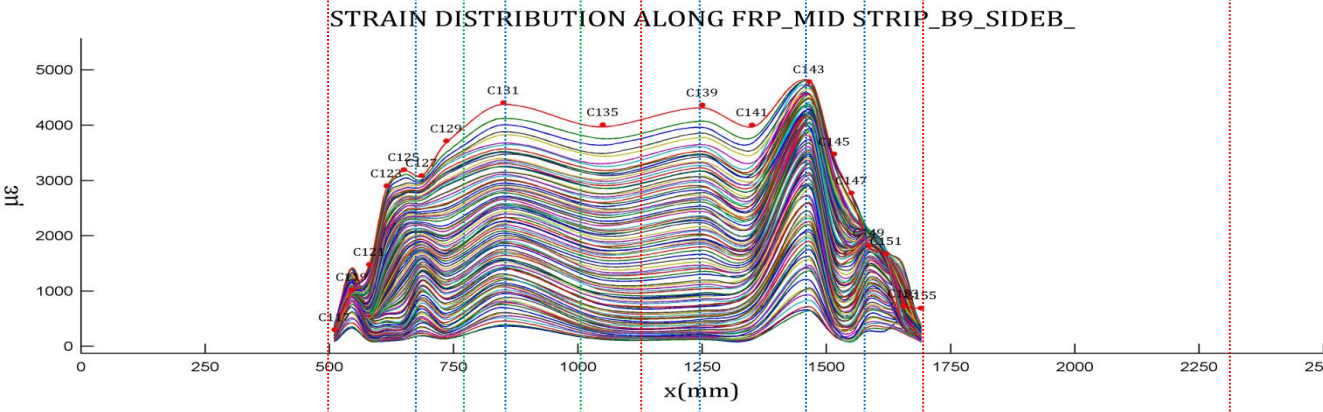

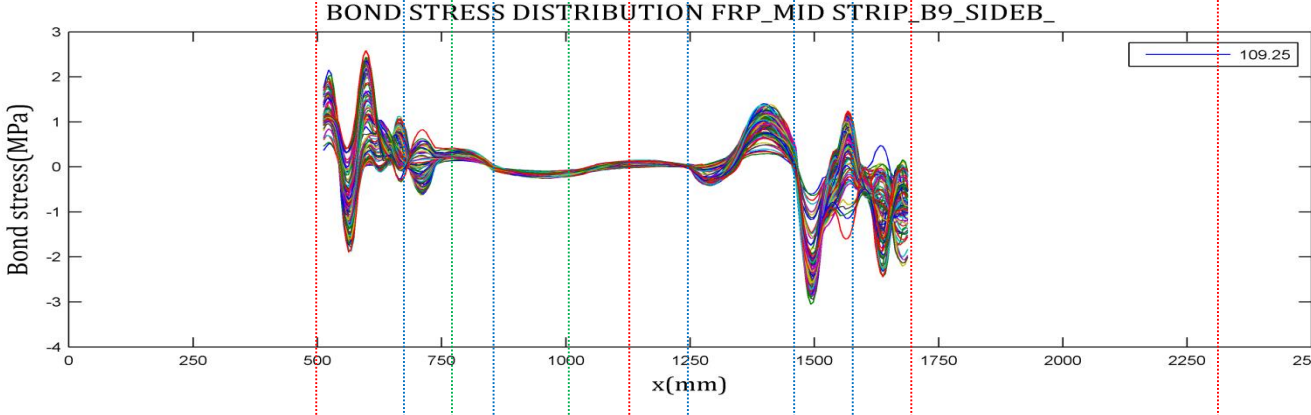

C.9.6 FINAL TESTING PHASE

a. READINGS OF LVDTs

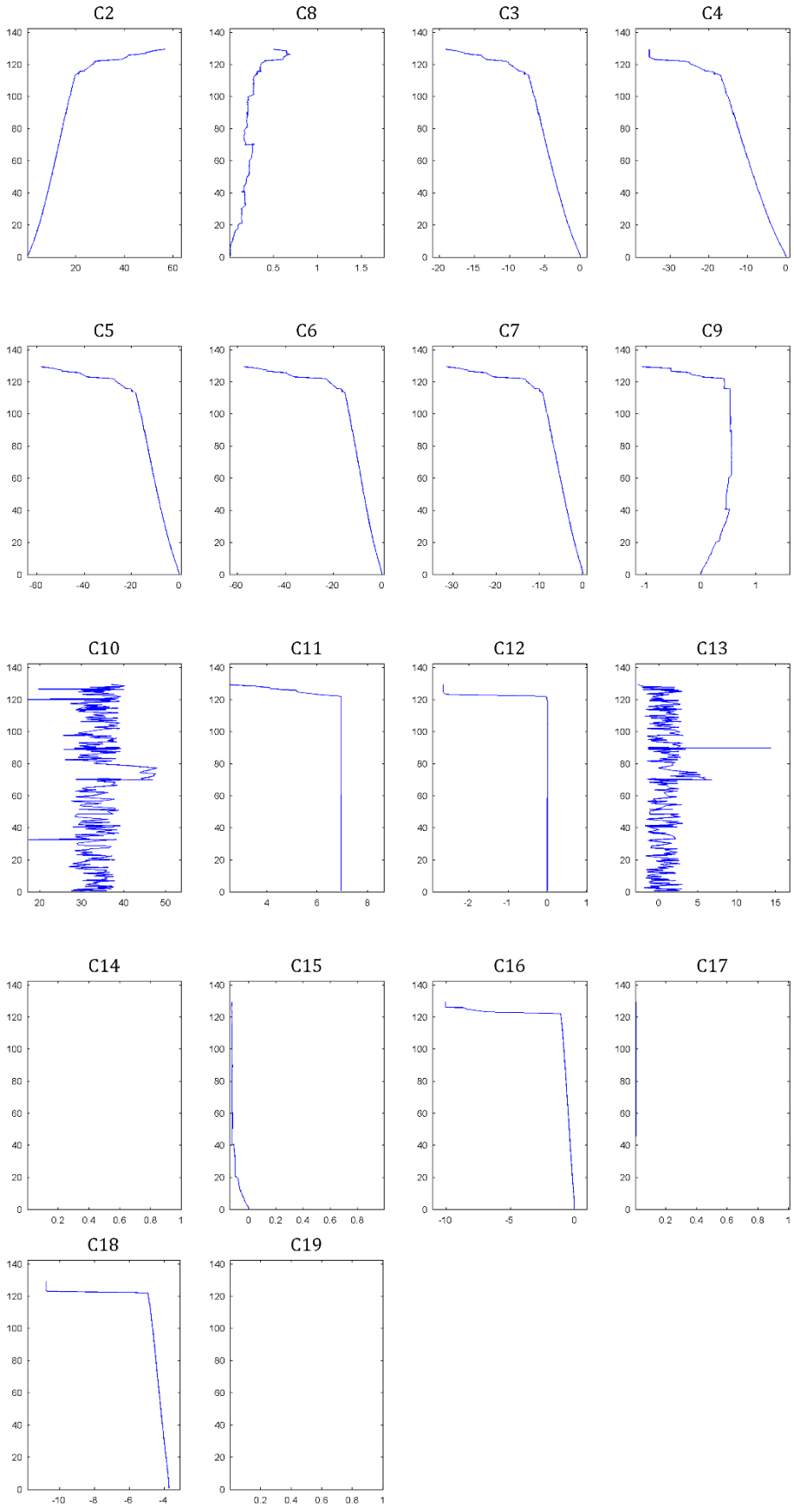

Fig. C9 - 17: Readings of LVDTs (C2 – C19)

C.9.7 STRAIN READINGS

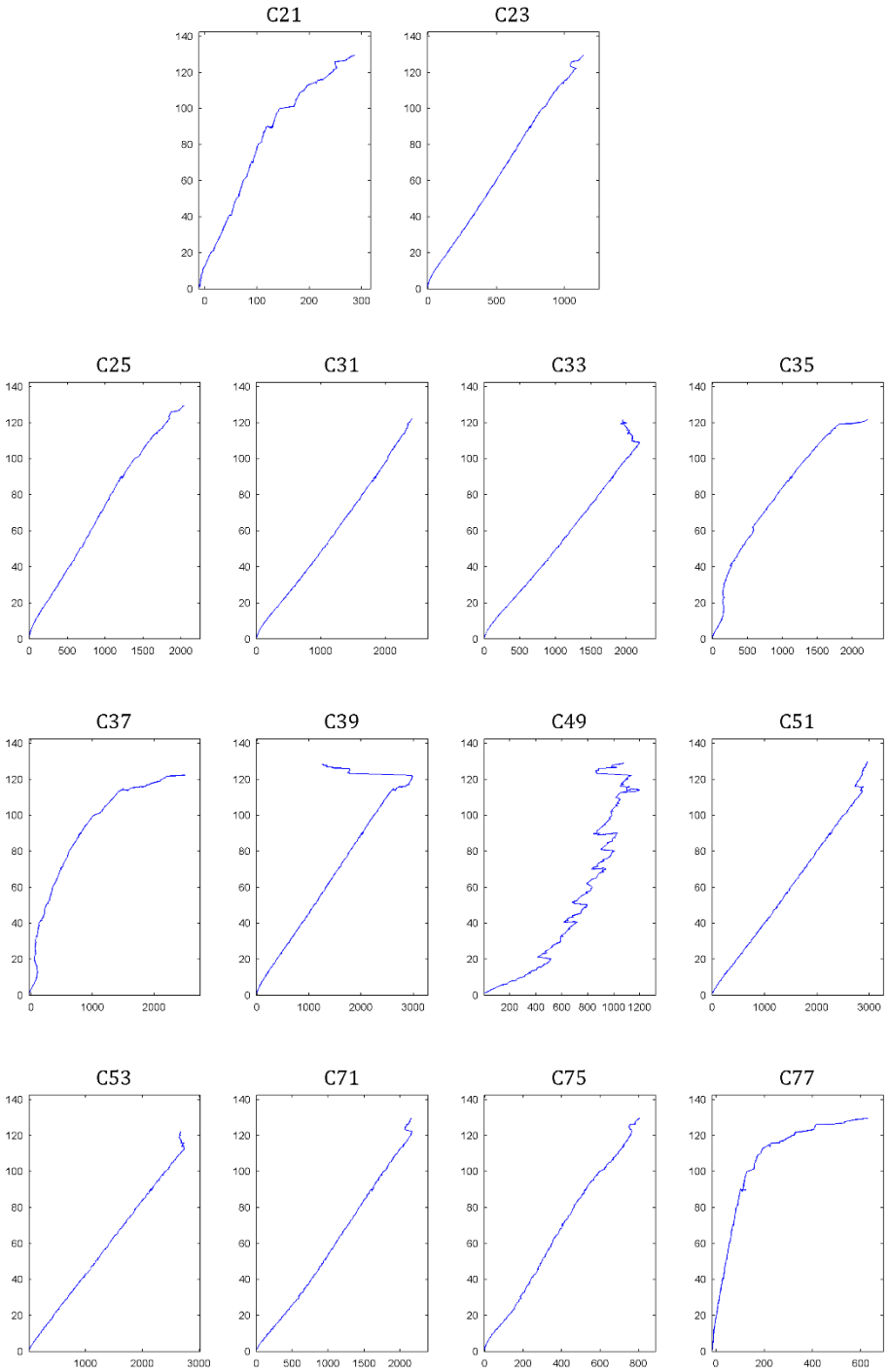

Fig. C9 - 18: Strain readings (C21 – C77)

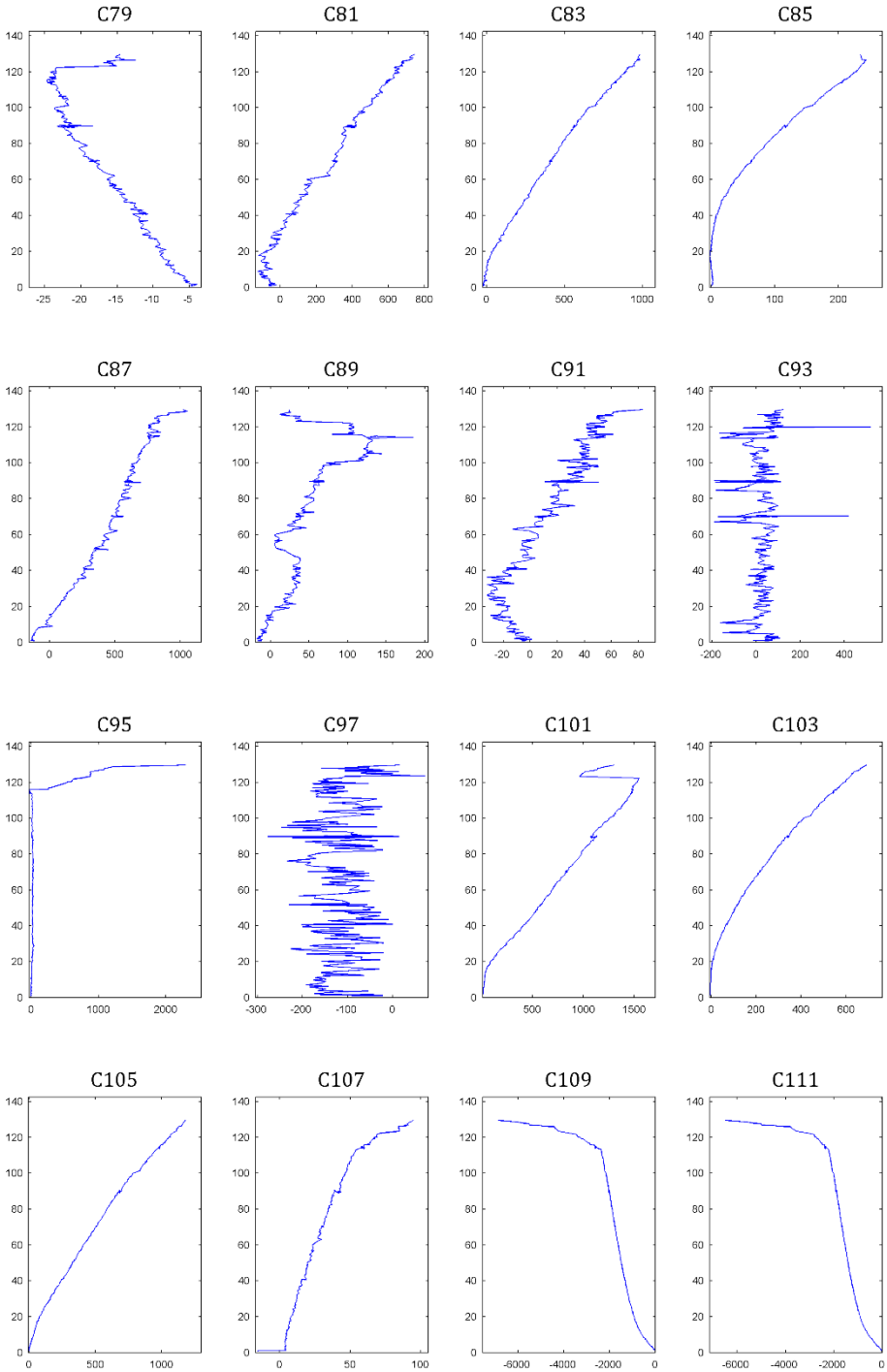

Fig. C9 - 19: Strain readings (C79 – C111)

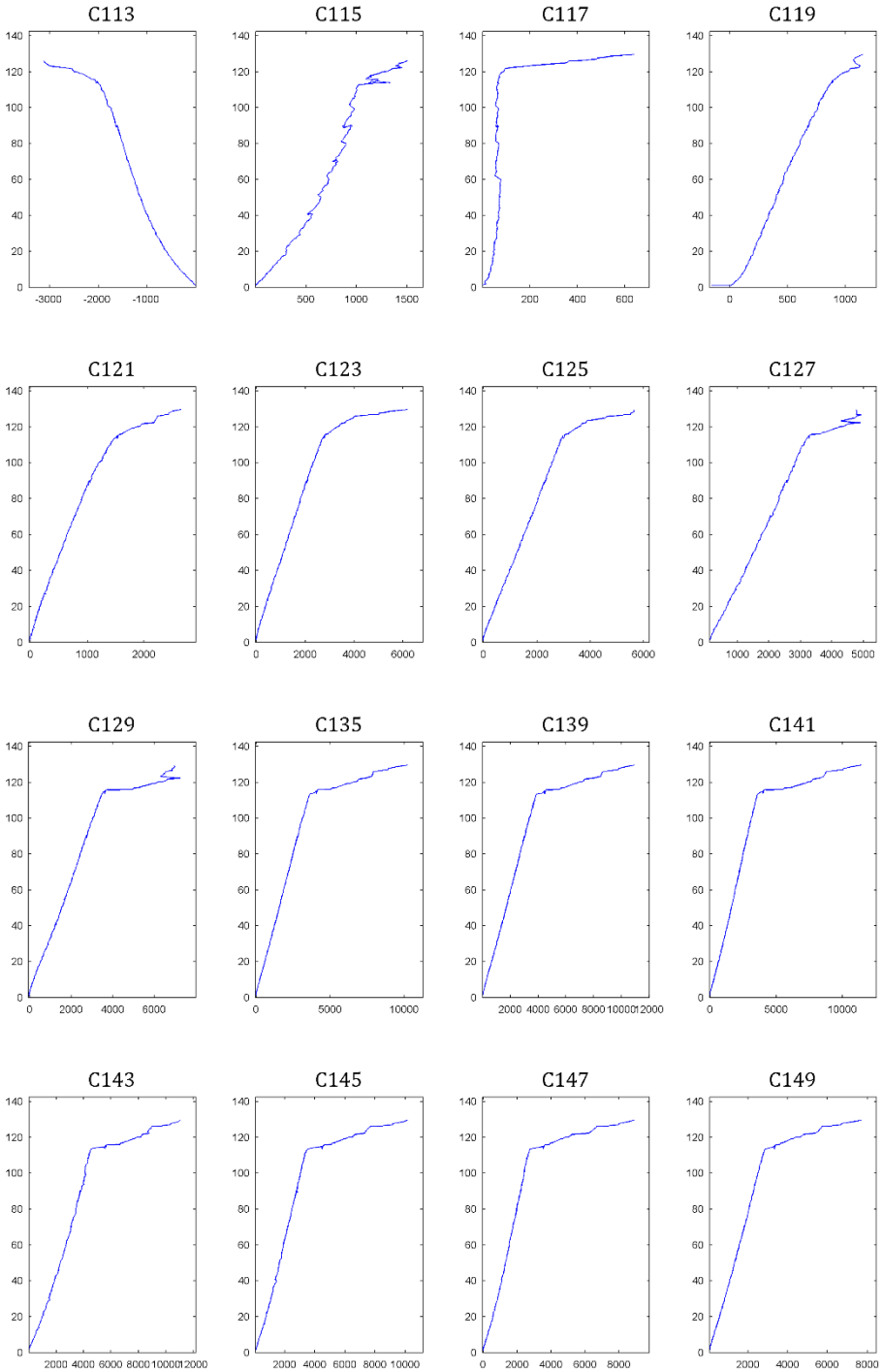

Fig. C9 - 20: Strain readings (C113 – C149)

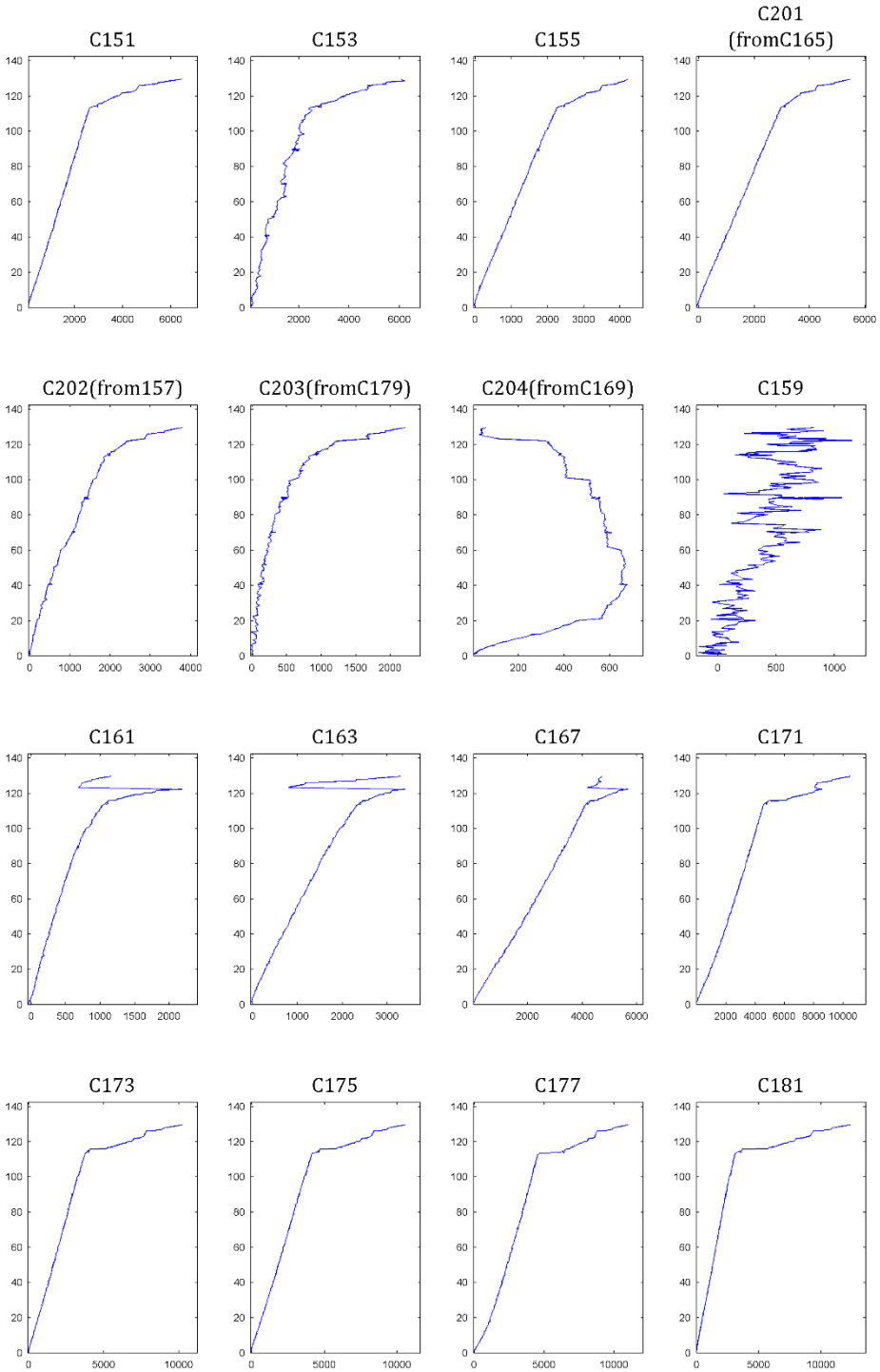

Fig. C9 - 21: Strain readings (C151 – C181)

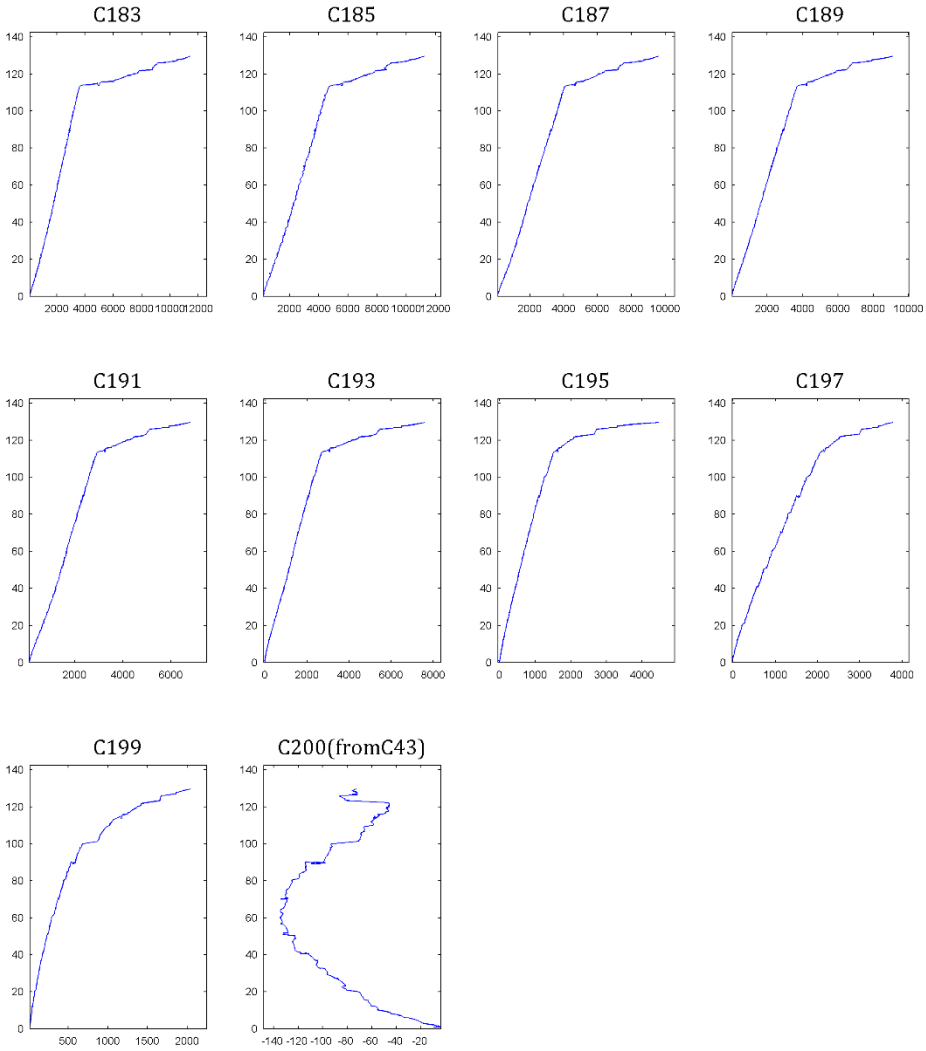

Fig. C9 - 22: Strain readings (C183 – C200)

C.9.8 STRAINS IN THE STEEL REINFORCEMENT AND FRP ALONG THE MID-SPAN REGION

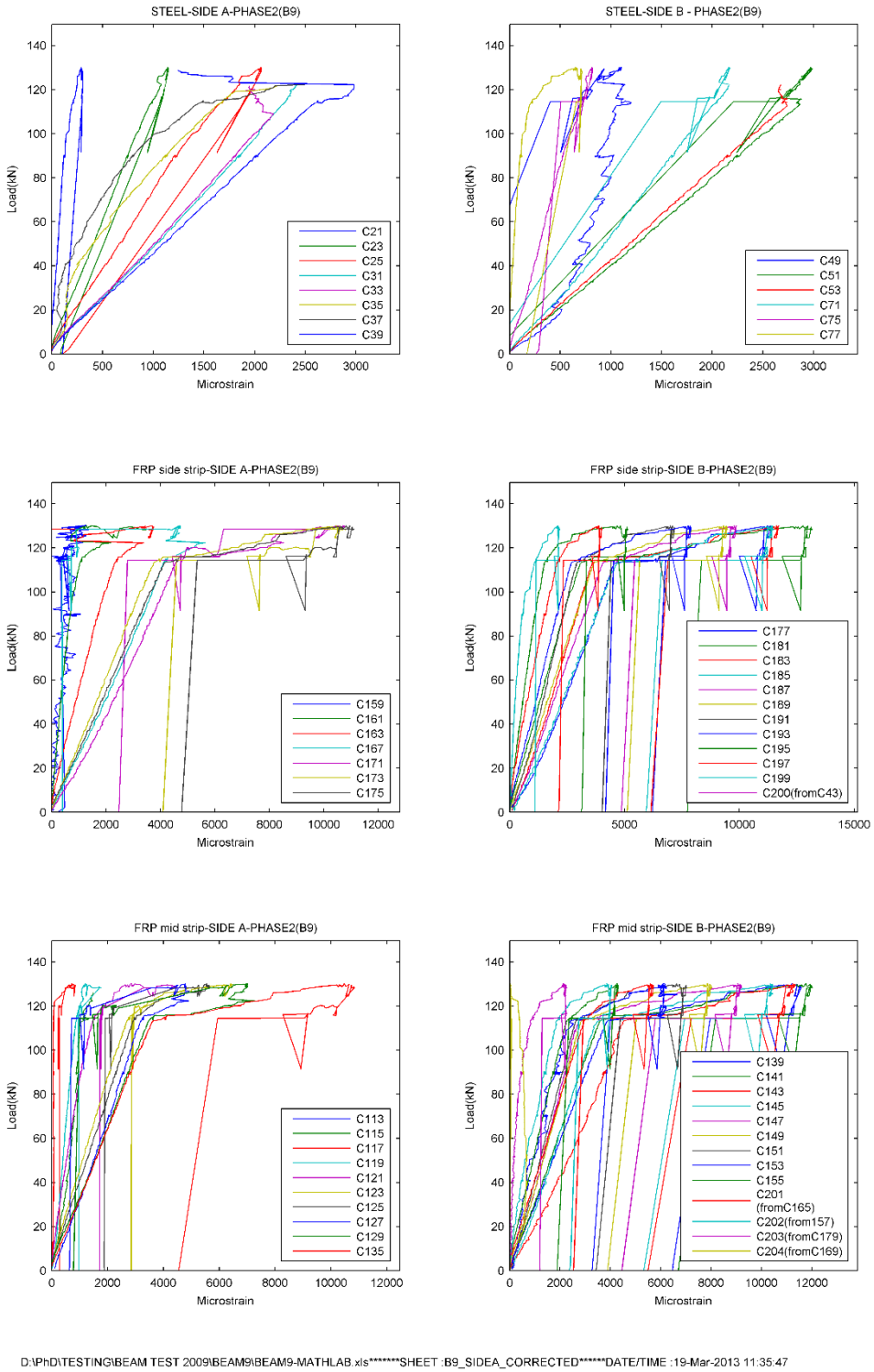

Fig. C9 - 23: Strain along steel bar – Phase 1

C.9.9 STRAIN AND BOND STRESS PROFILES

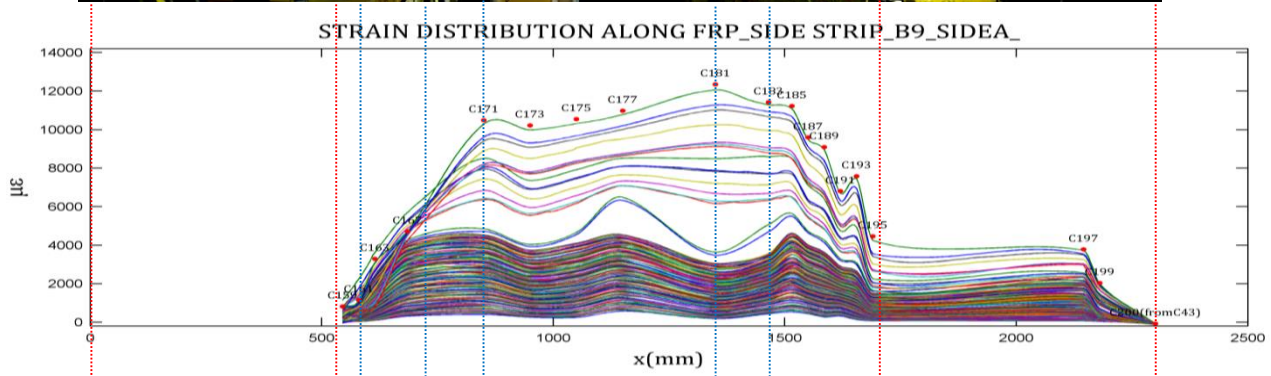

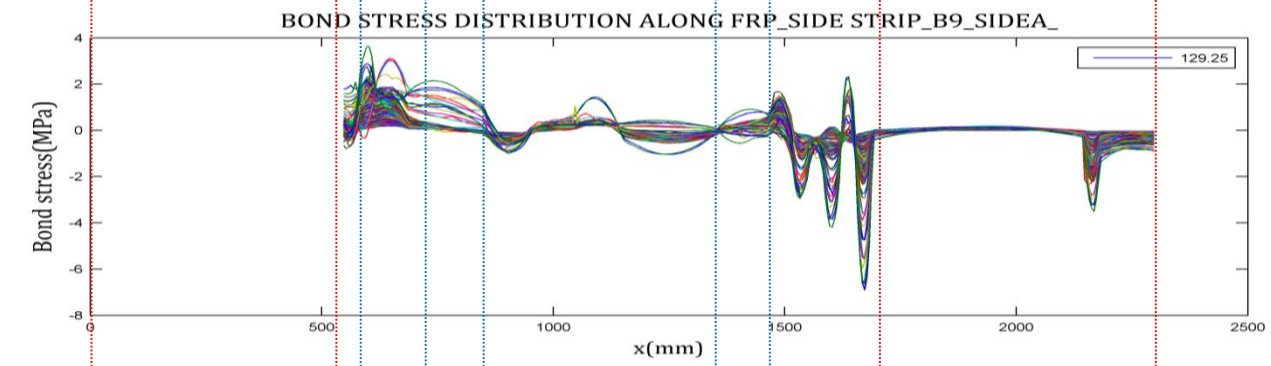

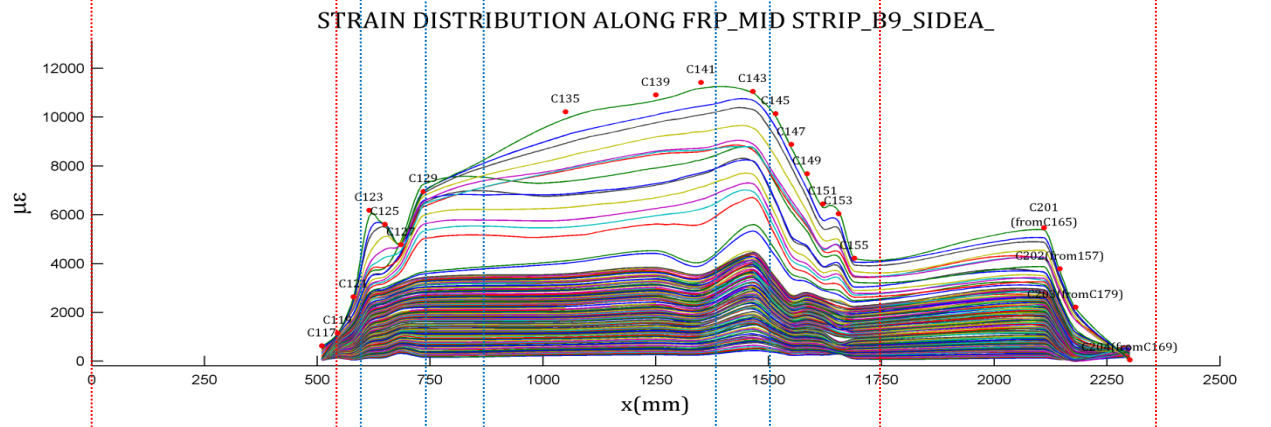

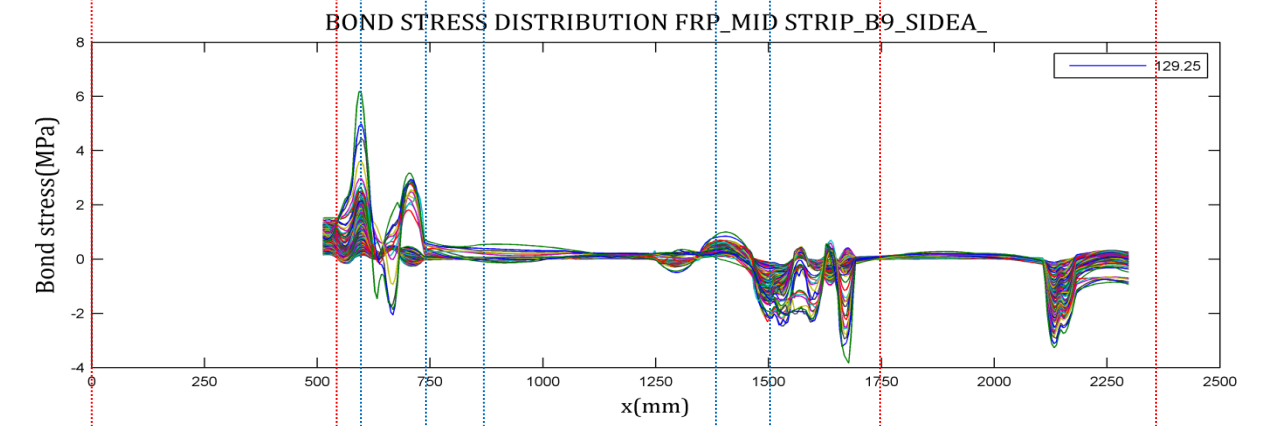

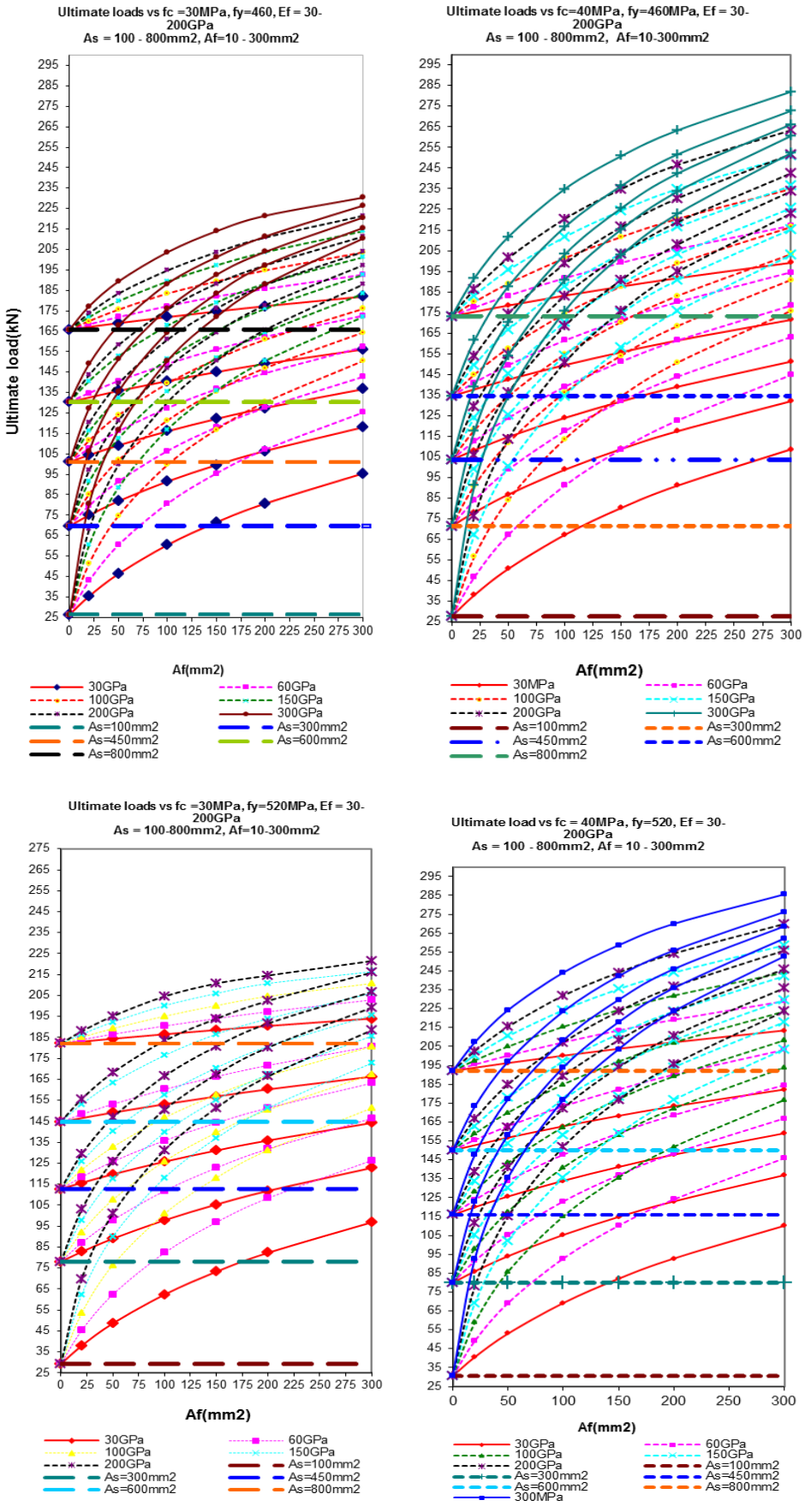

Fig. C10- 1: Parametric study used for design of experimental specimens

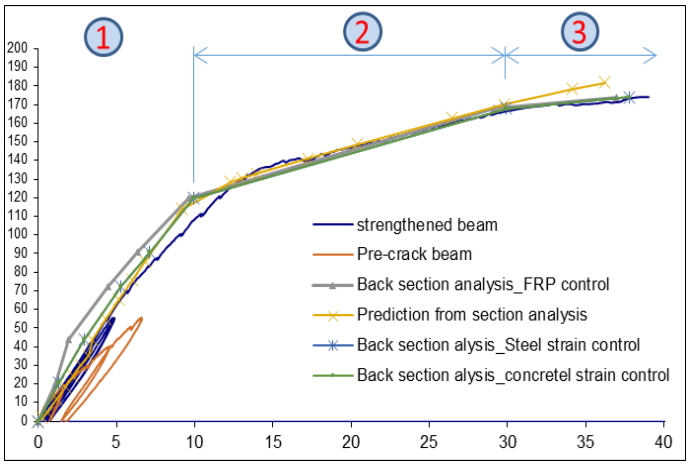

Fig. C10- 2: Comparison of deflection calculated from back section analysis and experimental results

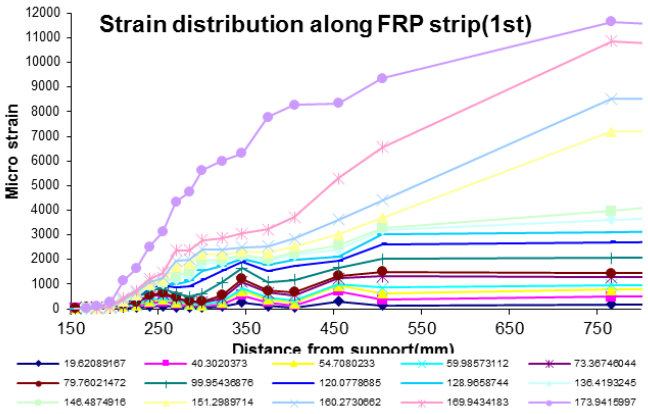

Fig. C10- 3: Strain distribution along FRP strip (1st)

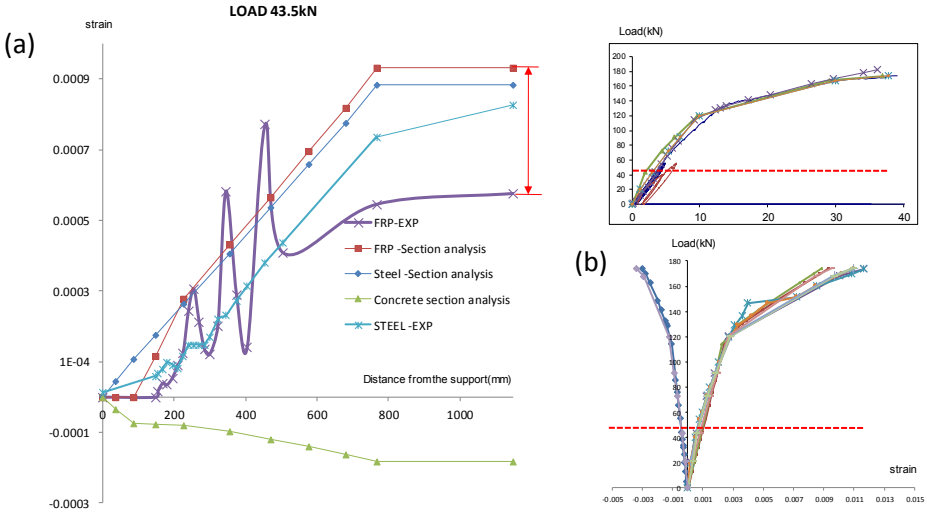

Fig. C10- 4 : (a) Comparison of strain profile in compression and tension for steel reinforcement, (b) Comparison of strain in compression and tension for steel reinforcement

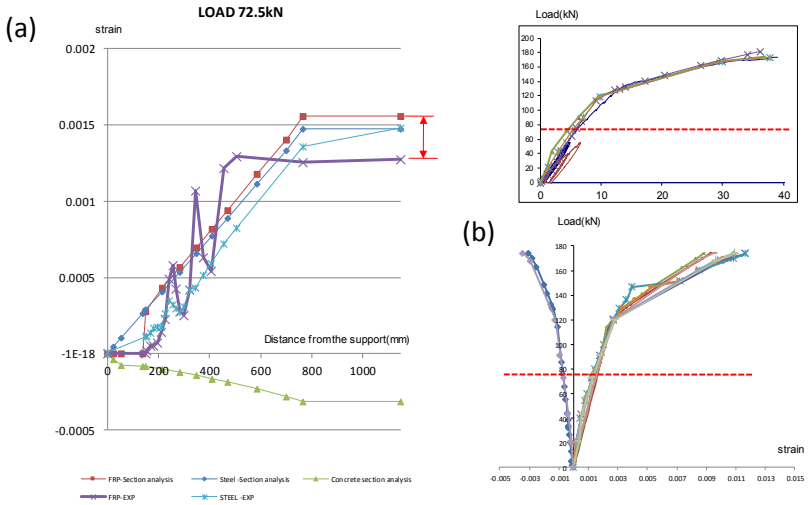

Fig. C10- 5: (a) Comparison of strain profile in compression and tension for steel reinforcement, (b) Comparison of strain in compression and tension for steel reinforcement

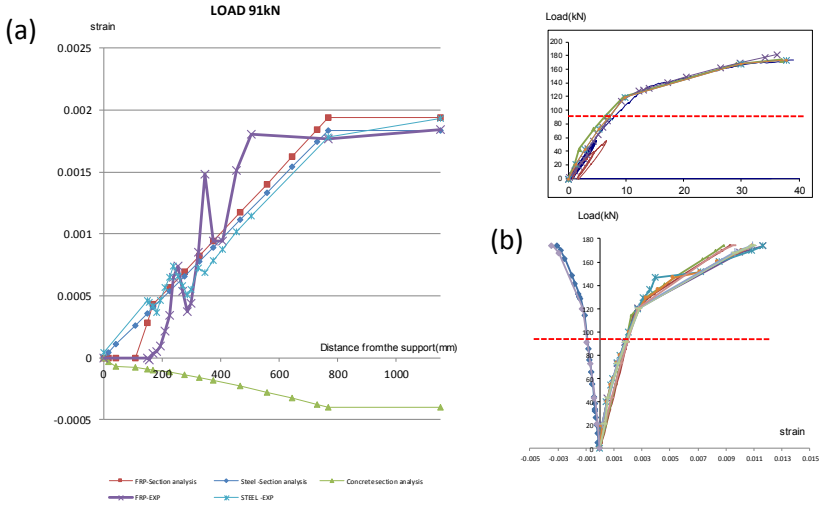

Fig. C10- 6: (a) Comparison of strain profile in compression and tension for steel reinforcement, (b) Comparison of strain in compression and tension for steel reinforcement

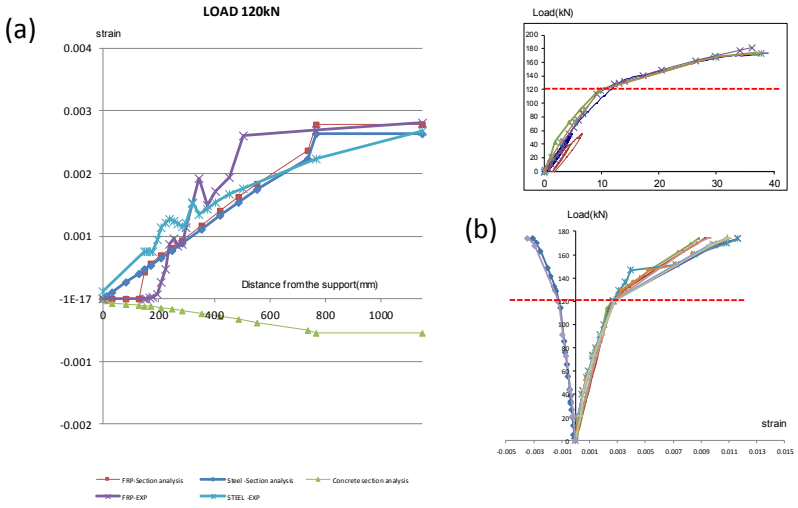

Fig. C10- 7: (a) Comparison of strain profile in compression and tension for steel reinforcement, (b) Comparison of strain in compression and tension for steel reinforcement

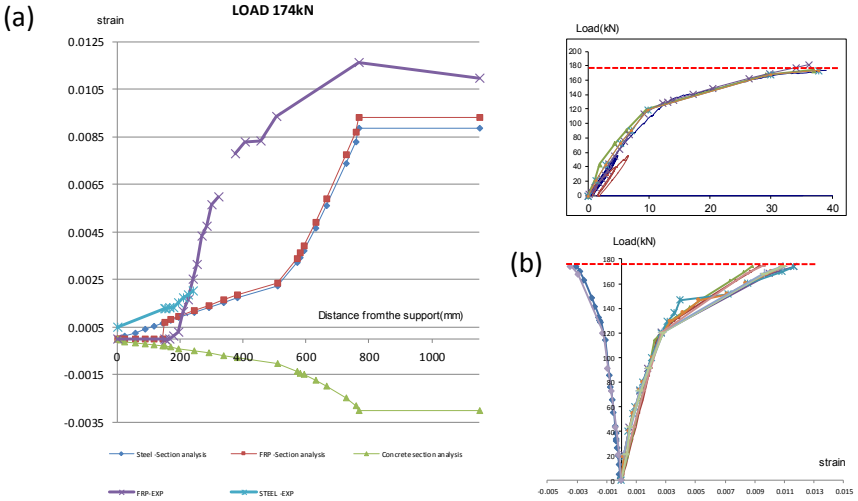

Fig. C10- 8: (a) Comparison of strain profile in compression and tension for steel reinforcement, (b) Comparison of strain in compression and tension for steel reinforcement

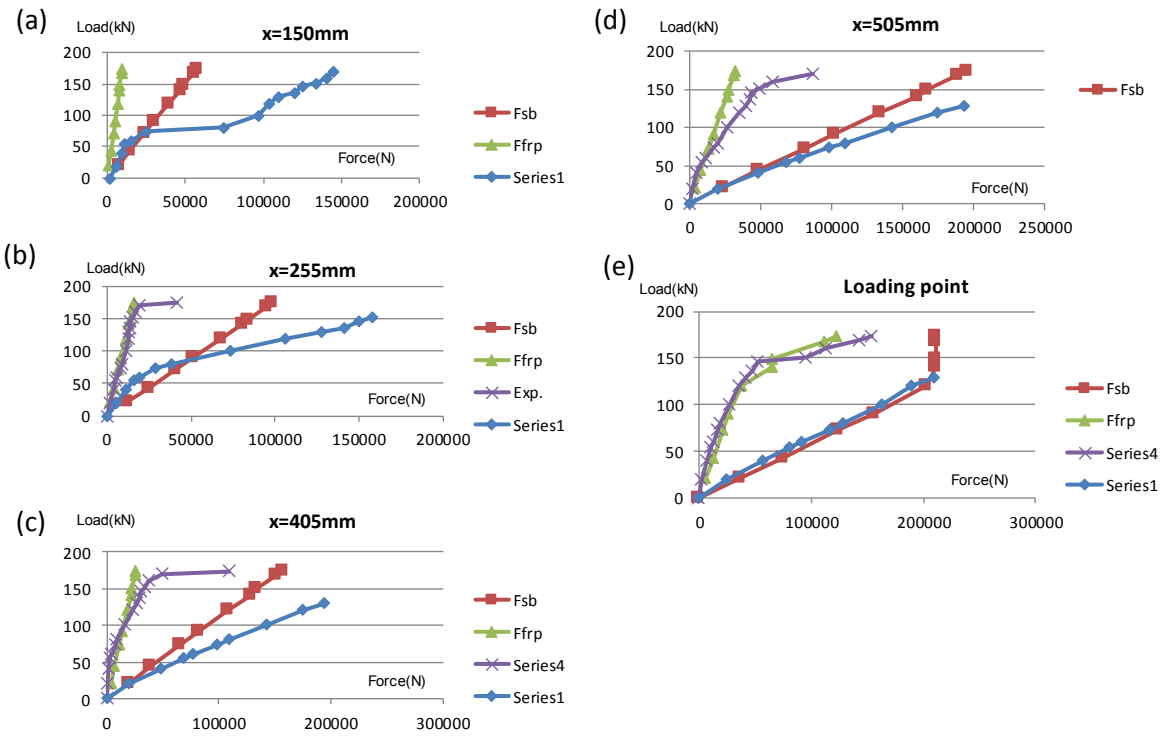

Fig. C10- 9: Comparison forces in FRP & steel reinforcement between experimental result and section analysis at (a)x=150mm, (b)x=255mm, (c)x=405mm, (d)x=505mm, (e)Loading point away from the COP

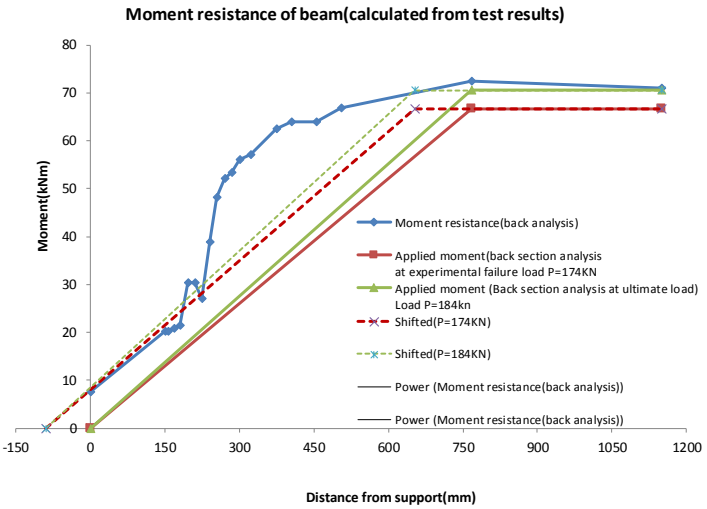

Fig. C10- 10: Comparison of moment resistance of beam BISM3Aa calculated from section analysis and experimental work

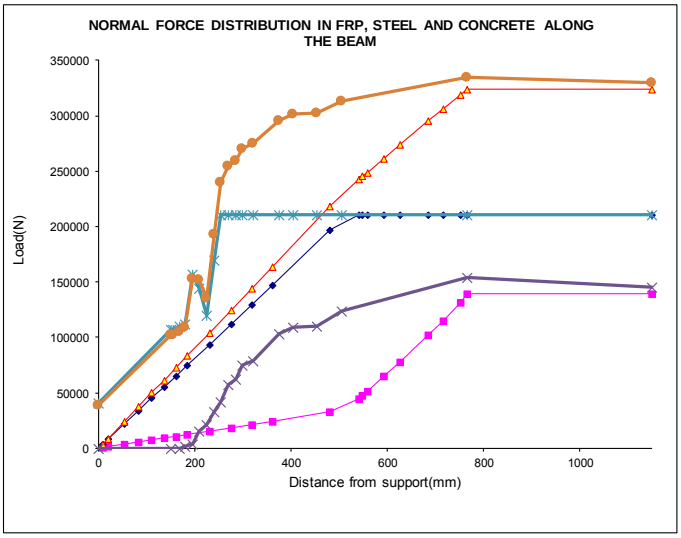

Fig. C10- 11: Comparison profile of force distribution along the steel reinforcement & FRP between experimental results and section analysis

Test No.	At the yielding load		At the peak load			At the ultimate load			Failure type
	Load(kN)	d_y(mm)	Load(kN)	P_p	d_p/d_y	Load(kN)	d_u(mm)	d_f/d_p	
REF-B-0	108.5	13	115.5	40	3.1	115.5	40	3.1	FLX
REF-B-1	94.7	16.1	100	27.5	1.7	100	52.7	3.3	FLX
NSM2-CB/150@100	135	18.2	145.7	18.2	1	145.7	25	1	FLX
NSMR3-PRC	------	------	55	6.3	------	------	------	------	------
NSM3-CS-150@100	140	13.9	173.9	39	2.8	173.9	39	2.8	DB
NSMR4-PRC	------	------	51	6.3	------	------	------	------	------
NSM4-CS-300@100	118	13.1	148.6	30	2.3	148.6	30	2.3	DB
NSM4-CS-200@100	118	17	159.1	38.7	2.3	159.1	38.7	2.3	DB
NSM4-CS-000@100	132.5	21.2	176.5	60.4	2.8	144.8	60.4	2.8	FLX
NSMR5-PRC	------	------	40.2	5.8	------	------	------	------	------
NSM5-CS-350@100	116	15.3	141.2	28	1.8	141.2	28	1.8	DB
NSM5-CS-250@100	125	17.6	148.3	29.9	1.7	144.8	86.7	4.9	FLX
NSMR6-PRC	------	------	41	5.1	------	------	------	------	------
NSM6-CS-350@150	125	19.0	129.5	24.4	1.3	129.5	24.4	1.3	DB
NSM6-CS-250@150	135	18.4	145.5	31.8	1.7	133.6	74.2	4	DB
NSMR7-PRC	40	5.3	------	------	------	------	------	------	------
NSM7-CS350@100	121	17.6	136.8	31.7	1.8	136.8	31.7	1.8	DB
NSM7-CS-250@100	125	17.8	151.2	51.8	2.9	136	77.8	4.4	DEF
NSMR8-PRC	------	------	41	6.3	------	------	------	------	------
NSM8-BS-600@100	107	15.0	112.2	30	2	112.2	30	2.0	SHR
NSM8-BS-500@100	114	16.2	123.9	44.6	2.8	115.9	86.2	5.3	SHR
NSMR9-PRC	------	------	40.1	5.6	------	------	------	------	------
NSM9-BS-600@150	106.4	16.4	111.7	27.4	1.7	102.4	27.4	1.7	SHR
NSM9-BS-500@150	113.4	19.9	129.6	62.9	3.2	117.6	73.8	3.7	SHR

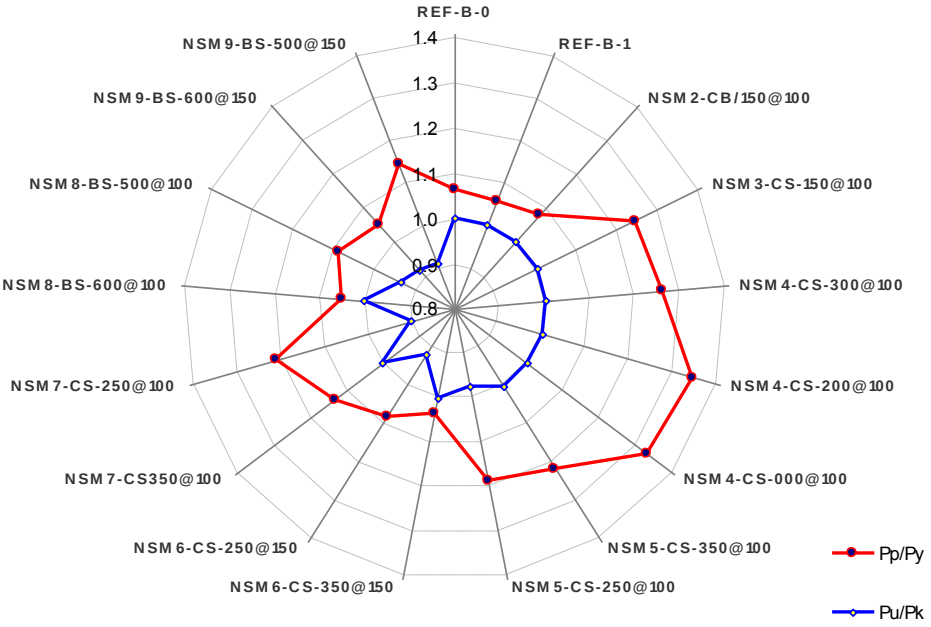

Fig. C10- 12: Ratio of the yielding load, the peak load and the ultimate load of beams.

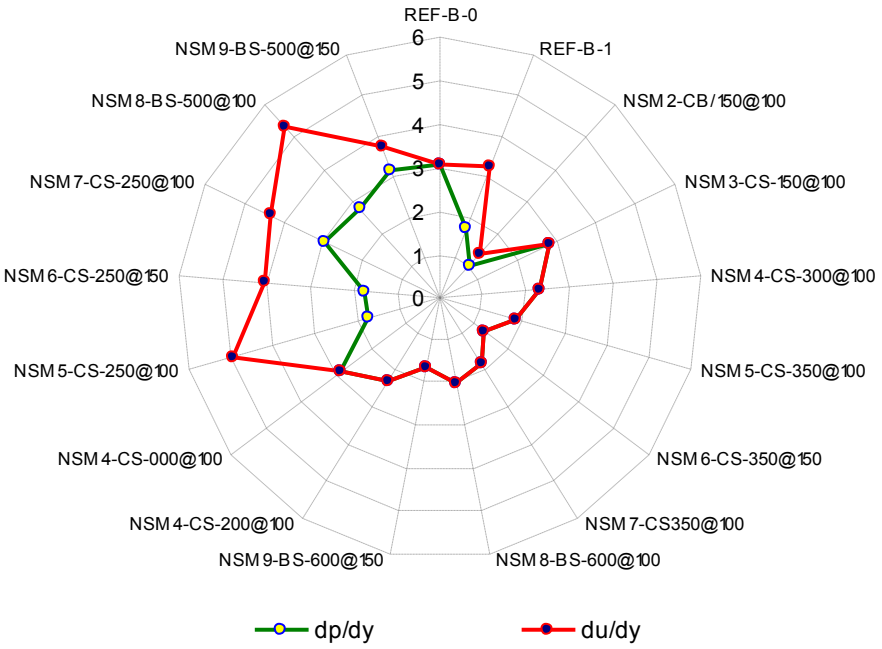

Fig. C10- 13: Shows various types of failures of RC beam specimen retrofitted NSMR which were recorded in testing programme.

Error! Reference source not found. **Yield load and ultimate load of tested beams at different testing phases**

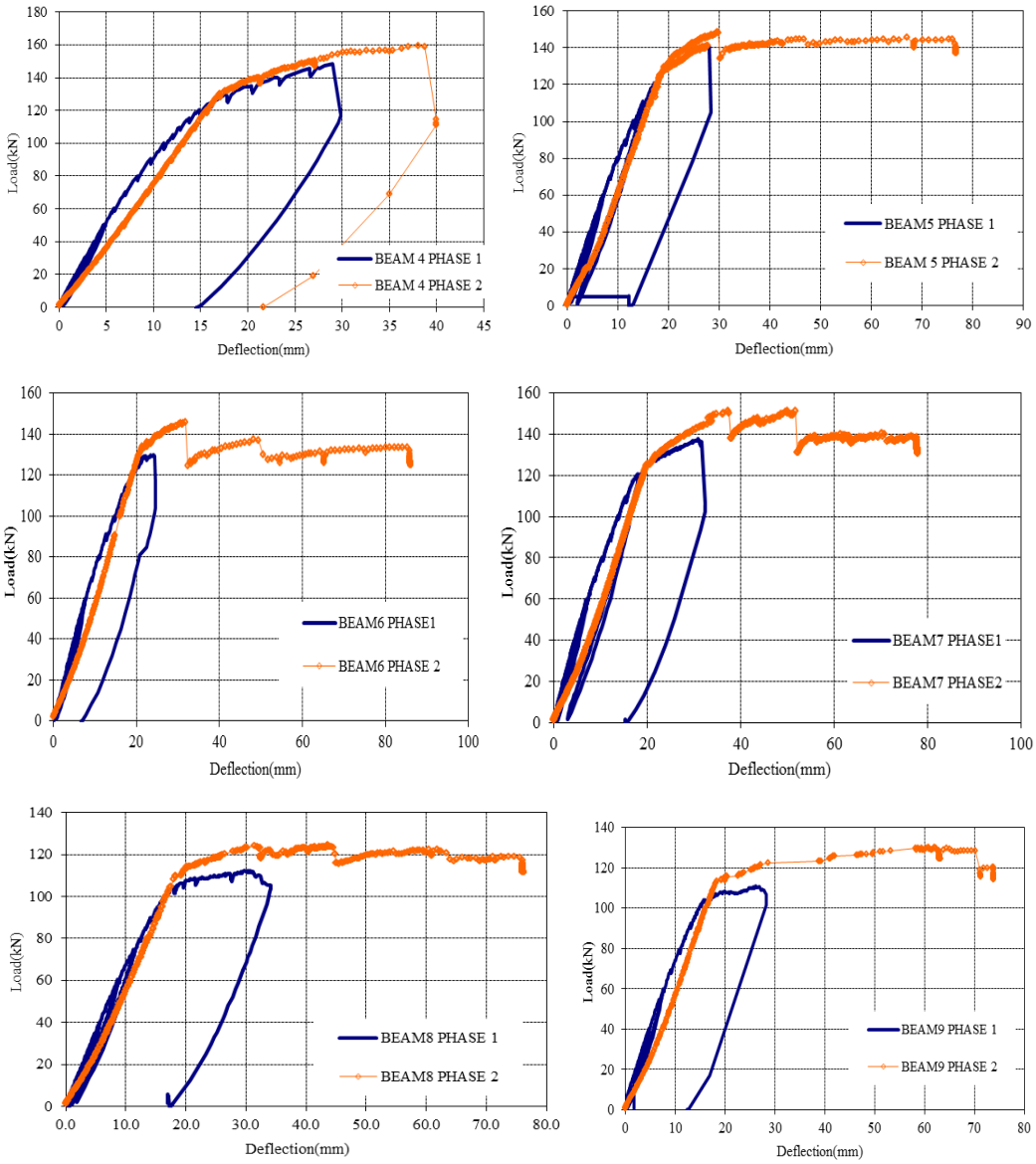

Fig. C10- 14: Maximum deflection of tested beams in the final testing phase

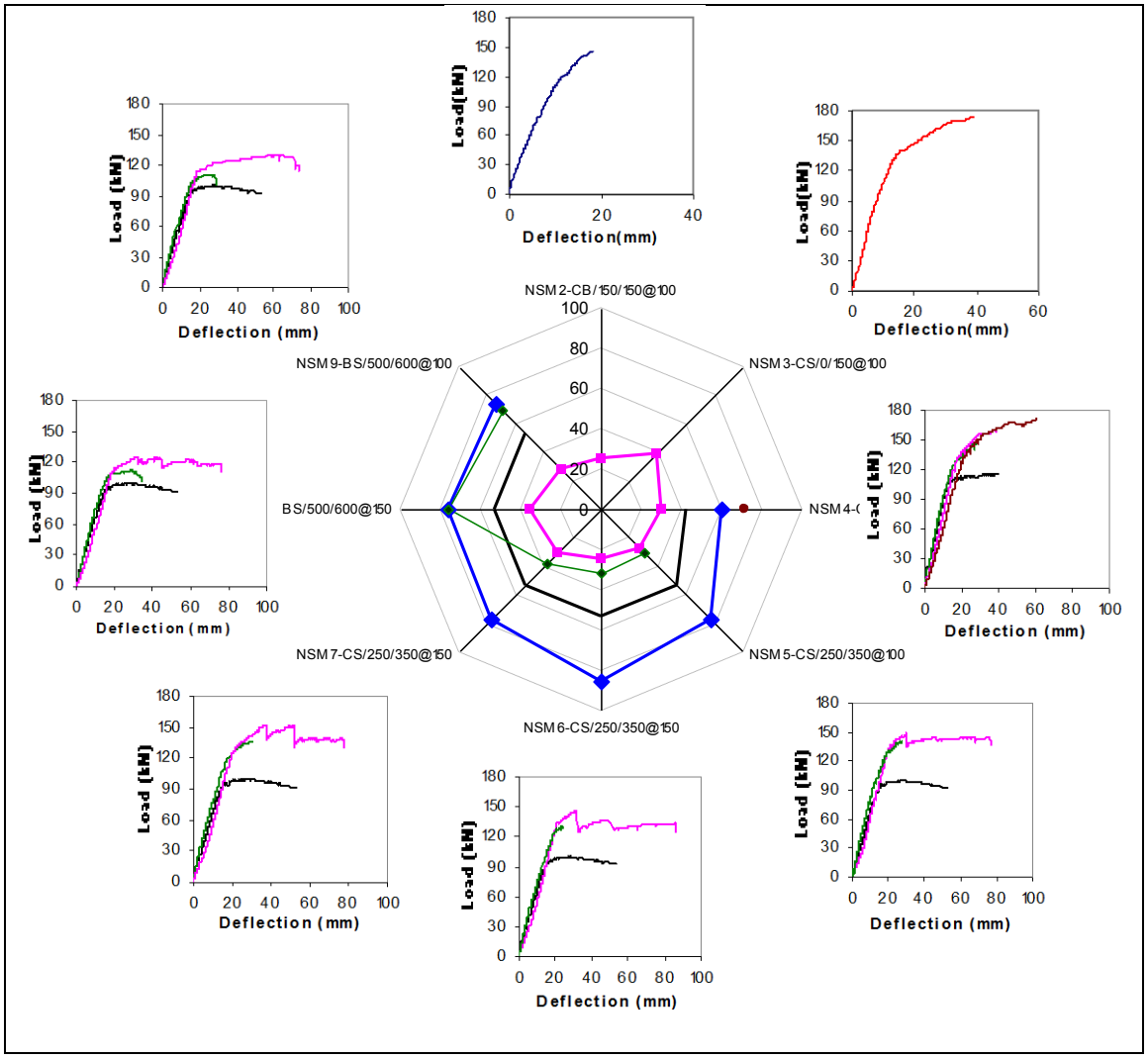

Fig. C10- 15:Maximum deflection of tested beams in the testing phases 2 and 3

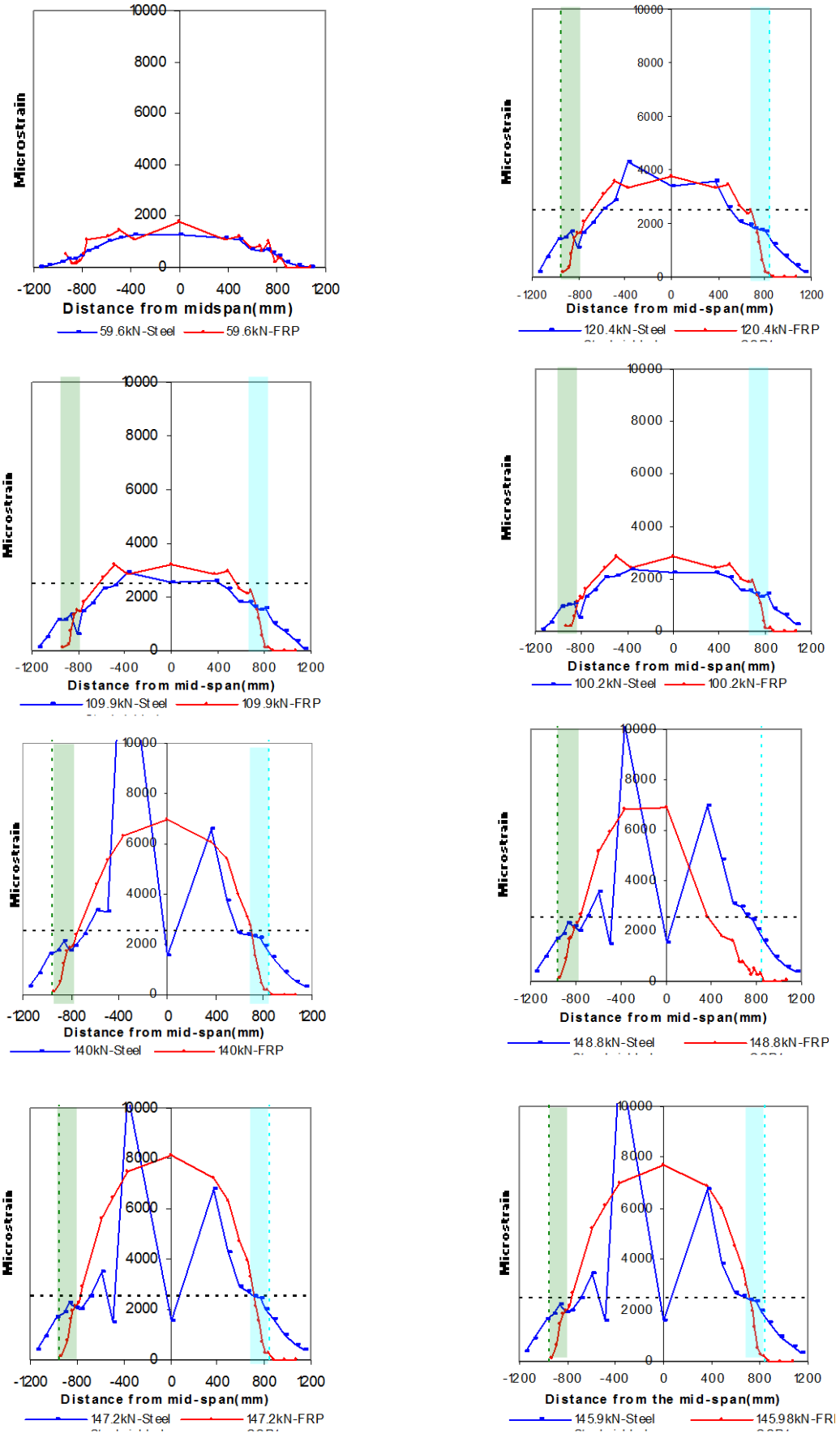

Fig. C10- 16: Evolution of strains along the steel reinforcement and FRP

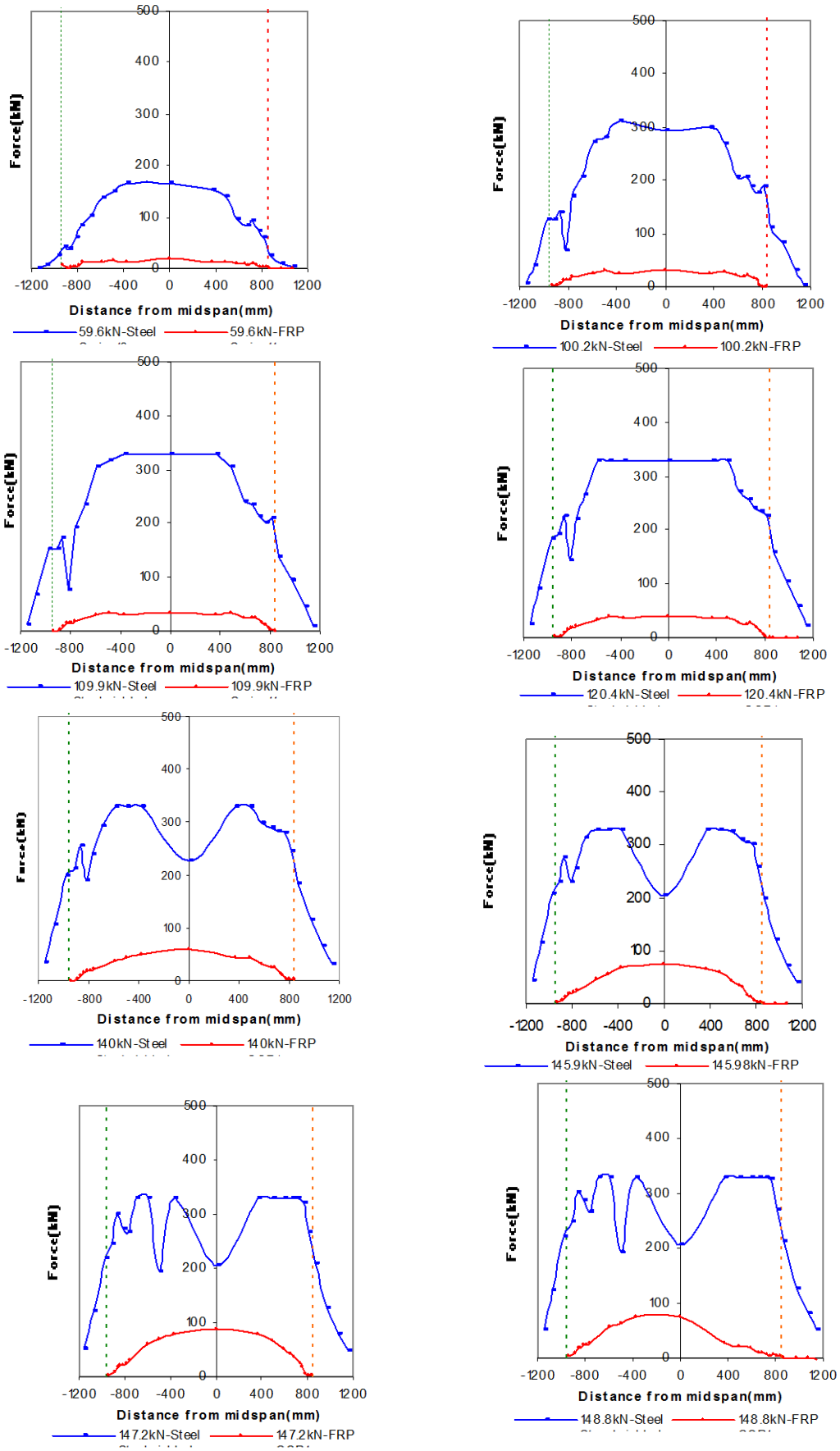

Fig. C10- 17: Evolution of axial forces along the steel reinforcement and FRP.

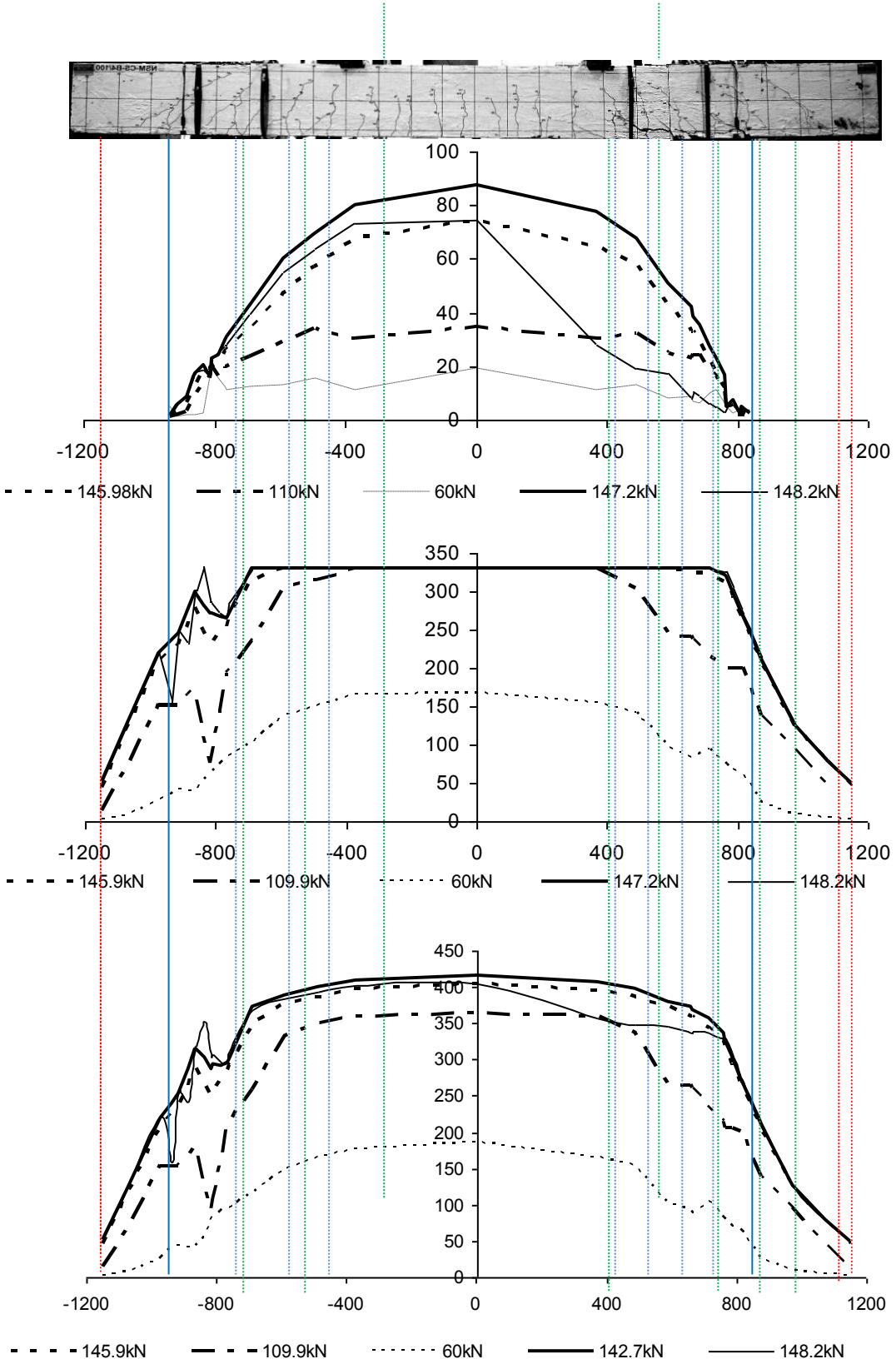
100
80
60
40
20
0
-1200
-800
-400
0
400
800
1200
145.98kN
110kN
60kN
147.2kN
148.2kN
350
300
250
200
150
100
50
0
-1200
-800
-400
0
400
800
1200
145.9kN
109.9kN
60kN
147.2kN
148.2kN
450
400
350
300
250
200
150
100
50
0
-1200
-800
-400
0
400
800
1200
145.9kN
109.9kN
60kN
142.7kN
148.2kN

No.	Reference	Year	Specimen ID	*Beam characteristics*																		
				Span (m)	Shear span	Load type	Geometry							Concrete		Main bars						Top bars
							b	h	b_f	h'	A	Cover	d	f_u	f_t	Dia.	Quan.	Area	f_{sy}	E_s	f_{su}	ρ_s	Dia.
1	Joaquim Barros	Oct-04	V1	1.50	0.50	4P	100	178	0	0	17800	15	154	46.1		6	2	56.5	700	200	760	0.37%	8
2			V1R1	1.50	0.50	4P	100	170	0	0	17000	15	146	46.1		6	2	56.5	700	200	760	0.39%	8
3			V2	1.50	0.50	4P	100	173	0	0	17300	15	149	46.1		6	3	84.8	700	200	760	0.57%	8
4			V2R2	1.50	0.50	4P	100	177	0	0	17700	15	153	46.1		6	3	84.8	700	200	760	0.55%	8
5			V3	1.50	0.50	4P	100	175	0	0	17500	15	150	46.1		6,8	3	106.8	473	200	582	0.71%	8
6			V3R2	1.50	0.50	4P	100	175	0	0	17500	15	150	46.1		6,8	3	106.8	473	200	582	0.71%	8
7			V4	1.50	0.50	4P	100	175	0	0	17500	15	150	46.1		8	3	150.8	473	200	582	1.01%	8
8			V4R3	1.50	0.50	4P	100	180	0	0	18000	15	155	46.1		8	3	150.8	473	200	582	0.97%	8
9	Hassan, Rizkalla	Aug-03	B0	2.5	1.25	3P	150	250	300	50	52500	50	235	48		10	2	157.1	400	200	623	0.45%	mw5.6
10			B1	2.5	1.25	3P	150	250	300	50	52500	50	235	48		10	2	157.1	400	200	623	0.45%	mw5.6
11			B2	2.5	1.25	3P	150	250	300	50	52500	50	235	48		10	2	157.1	400	200	623	0.45%	mw5.6
12			B3	2.5	1.25	3P	150	250	300	50	52500	50	235	48		10	2	157.1	400	200	623	0.45%	mw5.6
13			B4	2.5	1.25	3P	150	250	300	50	52500	50	235	48		10	2	157.1	400	200	623	0.45%	mw5.6
14			B5	2.5	1.25	3P	150	250	300	50	52500	50	235	48		10	2	157.1	400	200	623	0.45%	mw5.6
15			B6	2.5	1.25	3P	150	250	300	50	52500	50	235	48		10	2	157.1	400	200	623	0.45%	mw5.6
16			B7	2.5	1.25	3P	150	250	300	50	52500	50	235	48		10	2	157.1	400	200	623	0.45%	mw5.6
17			B8	2.5	1.25	3P	150	250	300	50	52500	50	235	48		10	2	157.1	400	200	623	0.45%	mw5.6
18	Hassan, Rizkalla	Dec-04	A0	2.5	1.25	3P	150	250	300	50	52500	50	235	48		10	2	157.1	400	200	623	0.45%	mw5.6
19			A1	2.5	1.25	3P	150	250	300	50	52500	50	235	48		10	2	157.1	400	200	623	0.45%	mw5.6
20			A2	2.5	1.25	3P	150	250	300	50	52500	50	235	48		10	2	157.1	400	200	623	0.45%	mw5.6
21			A3	2.5	1.25	3P	150	250	300	50	52500	50	235	48		10	2	157.1	400	200	623	0.45%	mw5.6
22			A4	2.5	1.25	3P	150	250	300	50	52500	50	235	48		10	2	157.1	400	200	623	0.45%	mw5.6
23			A5	2.5	1.25	3P	150	250	300	50	52500	50	235	48		10	2	157.1	400	200	623	0.45%	mw5.6
24			A6	2.5	1.25	3P	150	250	300	50	52500	50	235	48		10	2	157.1	400	200	623	0.45%	mw5.6
25			A7	2.5	1.25	3P	150	250	300	50	52500	50	235	48		10	2	157.1	400	200	623	0.45%	mw5.6
26	J.G.Teng	Apr-06	B0	3	1.2	4P	150	300			45000	30	264	44	3.3	12	2	226.2	532		623	0.57%	8
27			B500	3	1.2	4P	150	300			45000	30	264	44	3.3	12	2	226.2	532		623	0.57%	8
28			B1200	3	1.2	4P	150	300			45000	30	264	44	3.3	12	2	226.2	532		623	0.57%	8
29			B1800	3	1.2	4P	150	300			45000	30	264	44	3.3	12	2	226.2	532		623	0.57%	8
30			B2900	3	1.2	4P	150	300			45000	30	264	44	3.3	12	2	226.2	532		623	0.57%	8
31	J.Y. Kang	2006	B0	3	1.05	4P	200	300			60000	30	253.5	31		10	3	235.6	490		550	0.46%	13
32			TYPE 1-1	3	1.05	4P	200	300			60000	30	253.5	31		10	3	235.6	490		550	0.46%	13
33			TYPE 1-2	3	1.05	4P	200	300			60000	30	253.5	31		10	3	235.6	490		550	0.46%	13
34			TYPE2-1	3	1.05	4P	200	300			60000	30	253.5	31		10	3	235.6	490		550	0.46%	13
35			TYPE 2-2	3	1.05	4P	200	300			60000	30	253.5	31		10	3	235.6	490		550	0.46%	13

No.	Reference	Year	Specimen ID	*Beam characteristics*									*NSMR*											
				Top bars				Shear link					Groove				FRP								
				Quan.	Area	f_{sy}	f_{su}	Dia.	Area	fsy	fsu	s	d	h	s1	s2	Type	Shape	n	h	t	df	Dia.	Area	E_{frp}
1	Joaquim Barros	Oct-04	V1	2	100.5	490	600	6	56.54866776	750	800	100													
2			V1R1	2	100.5	490	600	7	76.96902001	750	800	100	4.5	12	30	35	CFRP	S	1	9.5	1.5			14.25	158
3			V2	2	100.5	490	600	8	100.5309649	750	800	100													
4			V2R2	2	100.5	490	600	9	127.2345025	750	800	100	4.5	12	30	35	CFRP	S	0	9.5	1.5			0	158
5			V3	2	100.5	490	600	10	157.0796327	750	800	100													
6			V3R2	2	100.5	490	600	11	190.0663555	750	800	100	4.5	12	25	25	CFRP	S	0	9.5	1.5			0	158
7			V4	2	100.5	490	600	12	226.1946711	750	800	100													
8			V4R3	2	100.5	490	600	13	265.4645792	750	800	100	4.5	12	25	25	CFRP	S	0	9.5	1.5			0	158
9	Hassan, Rizkalla	Aug-03	B0	mw5.6	mw5.6	mw 5.6	mw 5.6	10	157.0796327			100	5	25											
10			B1	mw5.6	mw5.6	mw 5.6	mw 5.6	10	157.0796327			100	5	25			CFRP	S	1	25	1.2			30	150
11			B2	mw5.6	mw5.6	mw 5.6	mw 5.6	10	157.0796327			100	5	25				S	1	25	1.2			30	150
12			B3	mw5.6	mw5.6	mw 5.6	mw 5.6	10	157.0796327			100	5	25				S	1	25	1.2			30	150
13			B4	mw5.6	mw5.6	mw 5.6	mw 5.6	10	157.0796327			100	5	25				S	1	25	1.2			30	150
14			B5	mw5.6	mw5.6	mw 5.6	mw 5.6	10	157.0796327			100	5	25				S	1	25	1.2			30	150
15			B6	mw5.6	mw5.6	mw 5.6	mw 5.6	10	157.0796327			100	5	25				S	1	25	1.2			30	150
16			B7	mw5.6	mw5.6	mw 5.6	mw 5.6	10	157.0796327			100	5	25				S	1	25	1.2			30	150
17			B8	mw5.6	mw5.6	mw 5.6	mw 5.6	10	157.0796327			100	5	25				S	1	25	1.2			30	150
18	Hassan, Rizkalla	Dec-04	A0	mw5.6	mw5.6	mw 5.6	mw 5.6	10	157.0796327			100	18	30									9.25		
19			A1	mw5.6	mw5.6	mw 5.6	mw 5.6	10	157.0796327			100	18	30			CFRP	B	1	25	1.2		9.25	30	111
20			A2	mw5.6	mw5.6	mw 5.6	mw 5.6	10	157.0796327			100	18	30				B	1	25	1.2		9.25	30	111
21			A3	mw5.6	mw5.6	mw 5.6	mw 5.6	10	157.0796327			100	18	30				B	1	25	1.2		9.25	30	111
22			A4	mw5.6	mw5.6	mw 5.6	mw 5.6	10	157.0796327			100	18	30				B	1	25	1.2		9.25	30	111
23			A5	mw5.6	mw5.6	mw 5.6	mw 5.6	10	157.0796327			100	18	30				B	1	25	1.2		9.25	30	111
24			A6	mw5.6	mw5.6	mw 5.6	mw 5.6	10	157.0796327			100	18	30				B	1	25	1.2		9.25	30	111
25			A7	mw5.6	mw5.6	mw 5.6	mw 5.6	10	157.0796327			100	18	30				B	1	25	1.2		9.25	30	111
26	J.G.Teng	Apr-06	B0	2	100.5	532	623	10	157.0796327	375	503	100	8	22											
27			B500	2	100.5	532	623	10	157.0796327	375	503	100	8	22			CFRP	S	1	16	2			32	131
28			B1200	2	100.5	532	623	10	157.0796327	375	503	100	8	22				S	1	16	2			32	131
29			B1800	2	100.5	532	623	10	157.0796327	375	503	100	8	22				S	1	16	2			32	131
30			B2900	2	100.5	532	623	10	157.0796327	375	503	100	8	22				S	1	16	2			32	131
31	J.Y. Kang	2006	B0	3	398.2	532	623	10	157.0796327	375	503	100													
32			TYPE 1-1	3	398.2	532	623	10	157.0796327	375	503	100						S	1	15	1.2			18	165
33			TYPE 1-2	3	398.2	532	623	10	157.0796327	375	503	100						S	1	25	1.2			30	165
34			TYPE2-1	3	398.2	532	623	10	157.0796327	375	503	100						S	2	25	1.2			60	165
35			TYPE 2-2	3	398.2	532	623	10	157.0796327	375	503	100						S	2	25	1.2			60	165

No.	Reference	Year	Specimen ID	NSMR									FAILURE							
				FRP							Resin		F_u	F_y	$F_{y\text{-}cal}$	$F_{u\text{-}cal}$	ε_s	εf (%)	F_u/F_o	F_y/F_{yo}	$\varepsilon_f/\varepsilon_{fu}$
				f_{frp}	ε_{fu}(%)	$L_f/2$	L_f/h	l	ρ_f	ρ_f/ρ_s	E_{resin}	f_{resin}									
1	Joaquim Barros	Oct-04	V1										28.2	23							
2			V1R1	2700	1.71	700	68.9618	50	0.08%	21.80%	5	16-22	50.3	33				1.55	1.783687943	1.434782609	0.907037037
3			V2										41	37							
4			V2R2	2700	1.71	700	68.9618	50	0.00%	0.00%	5	16-22	78.5	50				1.28	1.914634146	1.351351351	0.749037037
5			V3										41.3	40							
6			V3R2	2700	1.71	700	68.9618	50	0.00%	0.00%	5	16-22	81.9	55				1.28	1.983050847	1.375	0.749037037
7			V4										48.5	45							
8			V4R3	2700	1.71	700	68.9618	50	0.00%	0.00%	5	16-22	94.9	70				1.06	1.956701031	1.555555556	0.620296296
9	Hassan, Rizkalla	Aug-03	B0										52	30							
10			B1	2000	1.33	150	9.20	1100	0.06%	12.82%			53	30				0.17	1.019230769		0.1275
11			B2	2000	1.33	250	15.34	1000	0.06%	12.82%			54	35				0.71	1.038461538		0.5325
12			B3	2000	1.33	500	30.68	750	0.06%	12.82%			60	35				1.18	1.153846154		0.885
13			B4	2000	1.33	750	46.02	500	0.06%	12.82%			74	35				1.27	1.423076923		0.9525
14			B5	2000	1.33	850	52.16	400	0.06%	12.82%			79	35				1.28	1.519230769		0.96
15			B6	2000	1.33	950	58.29	300	0.06%	12.82%			80	40				1.29	1.538461538		0.9675
16			B7	2000	1.33	1050	64.43	200	0.06%	12.82%			80	40				1.31	1.538461538		0.9825
17			B8	2000	1.33	1200	73.63	50	0.06%	12.82%											
18	Hassan, Rizkalla	Dec-04	A0										56								
19			A1	1918	1.73	150	16.22	1100	0.06%	12.82%	3	62	56					0.11	1.076923077		0.063660063
20			A2	1918	1.73	550	59.46	700	0.06%	12.82%	3	62	67					0.63	1.288461538		0.36459854
21			A3	1918	1.73	800	86.49	450	0.06%	12.82%	3	62	73					0.73	1.403846154		0.422471324
22			A4	1918	1.73	1200	129.73	50	0.06%	12.82%	3	62	79					0.78	1.519230769		0.451407716
23			A5	1918	1.73	550	59.46	700	0.06%	12.82%	3	62	59					0.6	1.134615385		0.347236705
24			A6	1918	1.73	800	86.49	450	0.06%	12.82%	3	62	70					0.68	1.346153846		0.393534932
25			A7	1918	1.73	1200	129.73	50	0.06%	12.82%	3	62	76					0.73	1.461538462		0.422471324
26	J.G.Teng	Apr-06	B0										49.5								
27			B500	2068	1.58	250	0.00	1250	0.07%	12.45%	2.6	42.6	49.5					0.2296	1		0.14544294
28			B1200	2068	1.58	600	27.72	900	0.07%	12.45%	2.6	42.6	64.5					0.367	1.303030303		0.232480658
29			B1800	2068	1.58	900	55.44	600	0.07%	12.45%	2.6	42.6	96.8					0.7315	1.955555556		0.46337766
30			B2900	2068	1.58	1450	106.26	50	0.07%	12.45%	2.6	42.6	100.1					0.9707	2.022222222		0.614901838
31	J.Y. Kang	2006	B0										56.2	46.7					1.135353535		
32			TYPE 1-1	2400	1.45	1350	90.62	150	0.03%	6.46%			78.4	57.5					1.583838384	1.231263383	
33			TYPE 1-2	2400	1.45	1350	55.22	150	0.05%	10.76%			86.2	62					1.741414141	1.327623126	
34			TYPE2-1	2400	1.45	1350	55.22	150	0.10%	21.52%			109.7	72					2.216161616	1.541755889	
35			TYPE 2-2	2400	1.45	1350	55.22	150	0.10%	21.52%			107	70.5					2.161616162	1.509635974	

No.	Reference	Year	Specimen ID	FAILURE		
				F_{uc}/F_{oc}	Failure mode	Defl
1	Joaquim Barros	Oct-04	V1			
2			V1R1		Deflection	
3			V2			
4			V2R2		D	
5			V3			
6			V3R2		D	
7			V4			
8			V4R3		D	
9	Hassan, Rizkalla	Aug-03	B0		C	66
10			B1		D	76
11			B2		D	15
12			B3		D	20
13			B4		R	30
14			B5		R	30
15			B6		R	30
16			B7		R	30
17			B8			
18	Hassan, Rizkalla	Dec-04	A0		C	64
19			A1		D	78
20			A2		D	15.3
21			A3		D	21.2
22			A4		D	24.2
23			A5		D	12
24			A6		D	16.5
25			A7		D	25.8
26	J.G.Teng	Apr-06	B0		CC/SY	
27			B500		D	
28			B1200		D	
29			B1800		D	
30			B2900		D	
31	J.Y. Kang	2006	B0			71.68
32			TYPE 1-1			58.9
33			TYPE 1-2			54
34			TYPE2-1			46.9
35			TYPE 2-2			44.4

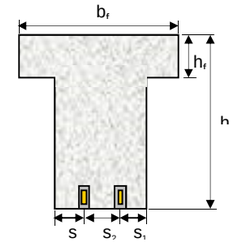

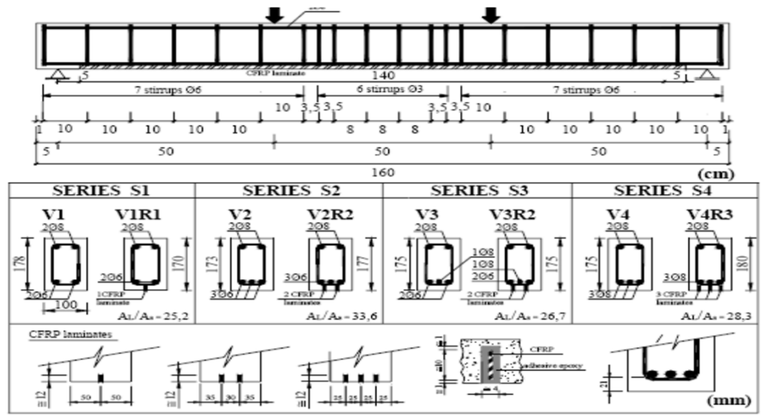

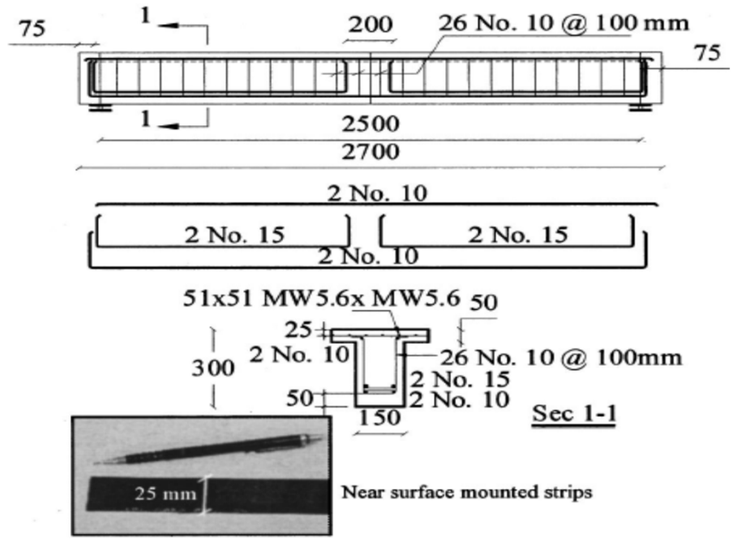

No.	Reference	Year	Specimen ID	*Beam characteristics*																		
				Span (m)	Shear span	Load type	Geometry							Concrete		Main bars						Top bars
							b	h	b_f	h'	A	Cover	d	f_u	f_t	Dia.	Quan.	Area	f_{sy}	E_s	f_{su}	ρ_s	Dia.
36	Joseph Robert Yost	Aug-07	6-C	2.743	1.219	4P	152.4	190			28956	38	161	37.2		16	2	402.1	500	200		1.64%	0
37			6-1Fa	2.743	1.219	4P	152.4	190			28956	38	161	37.2		16	2	402.1	500	200		1.64%	0
38			6-1Fb	2.743	1.219	4P	152.4	190			28956	38	161	37.2		16	2	402.1	500	200		1.64%	0
39			6-2Fa	2.743	1.219	4P	152.4	190			28956	38	161	37.2		16	2	402.1	500	200		1.64%	0
40			6-2Fb	2.743	1.219	4P	152.4	190			28956	38	161	37.2		16	2	402.1	500	200		1.64%	0
41			9-C	2.743	1.219	4P	229	190			43510	38	161	37.2		16	2	402.1	500	200		1.09%	0
42			9-1Fa	2.743	1.219	4P	229	190			43510	38	161	37.2		16	2	402.1	500	200		1.09%	0
43			9-1Fb	2.743	1.219	4P	229	190			43510	38	161	37.2		16	2	402.1	500	200		1.09%	0
44			9-2Fa	2.743	1.219	4P	229	190			43510	38	161	37.2		16	2	402.1	500	200		1.09%	0
45			9-2Fb	2.743	1.219	4P	229	190			43510	38	161	37.2		16	2	402.1	500	200		1.09%	0
46			12-C	2.743	1.219	4P	305	190			57950	38	161	37.2		16	2	402.1	500	200		0.82%	0
47			12-1Fa	2.743	1.219	4P	305	190			57950	38	161	37.2		16	2	402.1	500	200		0.82%	0
48			12-1Fb	2.743	1.219	4P	190	305			57950	38	161	37.2		16	2	402.1	500	200		0.82%	0
49			12-2Fa	2.743	1.219	4P	190	305			57950	38	161	37.2		16	2	402.1	500	200		0.82%	0
50			12-2Fb	2.743	1.219	4P	190	305			57950	38	161	37.2		16	2	402.1	500	200		0.82%	0
51	L. De Lorenzis(Thesis)		BC-a	4	1.75	4P	200	400			80000		370	15		14	2	307.9	496			0.21%	12
52			BC-b	4	1.75	4P	200	400			80000		370	15		18	2	508.9	510			0.34%	12
53			BR1-a	4	1.75	4P	200	400			80000		370	15		14	2	307.9	496			0.21%	12
54			BR1-b	4	1.75	4P	200	400			80000		370	15		18	2	508.9	510			0.34%	12
55			BR2-a	4	1.75	4P	200	400			80000		370	15		14	2	307.9	496			0.21%	12
56			BR2-b	4	1.75	4P	200	400			80000		370	15		18	2	508.9	510			0.34%	12
57			BFV	3.9	1.83	4P	152.4	101.6	381	101.6	54193.44	58.4	348	36		22.2	2	774.2	494			1.46%	12.7
58			BFC3	3.9	1.83	4P	152.4	101.6	381	101.6	54193.44	58.4	348	36		22.2	2	774.2	494			1.46%	12.7
59			BFC4	3.9	1.83	4P	152.4	101.6	381	101.6	54193.44	58.4	348	36		22.2	2	774.2	494			1.46%	12.7
60			BFG4	3.9	1.83	4P	152.4	101.6	381	101.6	54193.44	58.4	348	36		22.2	2	774.2	494			1.46%	12.7
61	I.S.Y. Liu		NS-F1	2 x 2.4			375	120			45000	38	82	37		16	4	804.2	566		656	2.62%	12
62			NS-F2	2 x 2.4			375	120			45000	38	82	37		16	4	804.2	566		656	2.62%	12
63			NS-F3	2 x 2.4			375	120			45000	38	82	37		16	4	804.2	566		656	2.62%	12
64			NS-F4	2 x 2.4			375	120			45000	38	82	37		16	4	804.2	566		656	2.62%	12
65			NS-S1	2 x 2.4			375	120			45000	38	82	37		16	4	804.2	566		656	2.62%	12
66			NS-S2	2 x 2.4			375	120			45000	38	82	37		16	4	804.2	566		656	2.62%	12
67			NB-F1	2 x 2.4			220	240			52800	46/85	161	35		2 x 32+3 x 24	5	2965.7	560		690	8.37%	12
68			NB-F2	2 x 2.4			220	240			52800	46/86	161	35		3 x 32+3 x 24	5	2965.7	560		690	8.37%	12
69			NB-F3	2 x 2.4			220	240			52800	46/87	161	35		4 x 32+3 x 24	5	2965.7	560		690	8.37%	12
70	E. Bonaldo	SL01		1.8	0.6	4P	300	80			24000		57	45.65		6	2	56.5	494		592	0.33%	0
71		SL06		1.8	0.6	4P	300	80			24000		57	49.39		6	2	56.5	494		592	0.33%	0
72		SL03S		1.8	0.6	4P	300	80			24000		57	43.13		6	2	56.5	494		592	0.33%	0
73		SL04S		1.8	0.6	4P	300	80			24000		57	32.41		6	2	56.5	494		592	0.33%	0

No.	Reference	Year	Specimen ID	*Beam characteristics*									*NSMR*											
				Top bars				Shear link					Groove				FRP								
				Quan.	Area	f_{sy}	f_{su}	Dia.	Area	fsy	fsu	s	d	h	s1	s2	Type	Shape	n	h	t	df	Dia.	Area	E_{frp}
36	Joseph Robert Yost	Aug-07	6-C	0	0	0	0	0	0	0	0	0												
37			6-1Fa	0	0	0	0	0	0	0	0	0	6.4	19			CFRP	S	0	15	2.5			0	136
38			6-1Fb	0	0	0	0	0	0	0	0	0	6.4	19			CFRP	S	0	15	2.5			0	136
39			6-2Fa	0	0	0	0	0	0	0	0	0	6.4	19	50.8	50.8	CFRP	S	0	15	2.5			0	136
40			6-2Fb	0	0	0	0	0	0	0	0	0	6.4	19	50.8	50.8	CFRP	S	0	15	2.5			0	136
41			9-C	0	0	0	0	0	0	0	0	0												
42			9-1Fa	0	0	0	0	0	0	0	0	0	6.4	19			CFRP	S	0	15	2.5			0	136
43			9-1Fb	0	0	0	0	0	0	0	0	0	6.4	19			CFRP	S	0	15	2.5			0	136
44			9-2Fa	0	0	0	0	0	0	0	0	0	6.4	19	50.8	50.8	CFRP	S	0	15	2.5			0	136
45			9-2Fb	0	0	0	0	0	0	0	0	0	6.4	19	50.8	50.8	CFRP	S	0	15	2.5			0	136
46			12-C	0	0	0	0	0	0	0	0	0												
47			12-1Fa	0	0	0	0	0	0	0	0	0	6.4	19			CFRP	S	0	15	2.5			0	136
48			12-1Fb	0	0	0	0	0	0	0	0	0	6.4	19			CFRP	S	0	15	2.5			0	136
49			12-2Fa	0	0	0	0	0	0	0	0	0	6.4	19	50.8	50.8	CFRP	S	0	15	2.5			0	136
50			12-2Fb	0	0	0	0	0	0	0	0	0	6.4	19	50.8	50.8	CFRP	S	0	15	2.5			0	136
51	L. De Lorenzis(Thesis)		BC-a	2	226.2	357		8	100.5309649	345		200			46	77	CFRP	RB							
52			BC-b	2	226.2	357		8	100.5309649	345		200			46	77	CFRP	RB							
53			BR1-a	2	226.2	357		8	100.5309649	345		200			46	77	CFRP	RB	1			8	50.2656		130
54			BR1-b	2	226.2	357		8	100.5309649	345		200			46	77	CFRP	RB	1			8	50.2656		130
55			BR2-a	2	226.2	357		8	100.5309649	345		200			46	77	CFRP	RB	2			8	100.5312		130
56			BR2-b	2	226.2	357		8	100.5309649	345		200			46	77	CFRP	RB	2			8	100.5312		130
57			BFV	2	253.4	357		9.5	141.7643685	345		127												
58			BFC3	2	253.4	357		9.5	141.7643685	345		127	19	19			CFRP	RB	2			9.5	141.7647		161.2
59			BFC4	2	253.4	357		9.5	141.7643685	345		127	25.4	25.4			CFRP	RB	2			12.7	253.354332		161.2
60			BFG4	2	253.4	357		9.5	141.7643685	345		127	25.4	25.4			GFRP	RB	2			12.7	253.354332		38.6
61	I.S.Y. Liu		NS-F1	2	226.2	558	546	10	157.0796327			1200	3.3	22	62		CFRP	S	0	20.5	1.22			0	174
62			NS-F2	2	226.2	558	546	11	190.0663555			1200	3.4	17	125		CFRP	S	0	15.5	1.24			0	174
63			NS-F3	2	226.2	558	546	12	226.1946711			1200	3.6	16	188		CFRP	S	0	15.4	1.25			0	174
64			NS-F4	2	226.2	558	546	13	265.4645792			1200	5	16	188		CFRP	S	0	15.2	2.95			0	140
65			NS-S1	2	226.2	558	546	14	307.8760801			1200	3.4	21	75		Steel	S	0	19.1	0.93			0	183
66			NS-S2	2	226.2	558	546	15	353.4291735			1200	5.2	21	125		Steel	S	0	19.1	2.05			0	168
67			NB-F1	2	226.2	558	546	16	402.1238597			70	3.6	16	60		CFRP	S	0	14.8	1.25			0	174
68			NB-F2	2	226.2	558	546	17	453.9601384			70	3.7	17	73		CFRP	S	0	15.2	1.24			0	174
69			NB-F3	2	226.2	558	546	18	508.9380099			70	5.4	17	73		CFRP	S	0	15	2.77			0	140
70	E. Bonaldo	SL01		0	0	0	0	0	0	0	0	0												
71		SL06		0	0	0	0	0	0	0	0	0												
72		SL03S		0	0	0	0	0	0	0	0	0	5	15	150	75	CFRP	S	0	9.4	1.4			0	156.1
73		SL04S		0	0	0	0	0	0	0	0	0	5	15	150	75	CFRP	S	0	9.4	1.4			0	156.1

No.	Reference	Year	Specimen ID	NSMR									FAILURE								
				FRP							Resin										
				f_{frp}	ε_{fu}(%)	$L_f/2$	L_f/h	l	ρ_f	ρ_f/ρ_s	E_{resin}	f_{resin}	F_u	F_y	$F_{y\text{-}cal}$	$F_{u\text{-}cal}$	ε_s	εf (%)	F_u/F_o	F_y/F_{yo}	$\varepsilon_f/\varepsilon_{fu}$
36	Joseph Robert Yost	Aug-07	6-C										21.12	19	18.9						
37			6-1Fa	1648	1.21	1372	117.83	0	0.00%	0.00%			24.83	20.9	21.8			1.175662879	1.1		
38			6-1Fb	1648	1.21	1372	117.83	0	0.00%	0.00%			23.24	21.3	21.8		0.597	1.100378788	1.121052632	0.492669903	
39			6-2Fa	1648	1.21	1372	117.83	0	0.00%	0.00%			24.99	24.4	23.9			1.183238636	1.284210526		
40			6-2Fb	1648	1.21	1372	117.83	0	0.00%	0.00%			26.94	24.7	23.9		0.625	1.275568182	1.3	0.515776699	
41			9-C										25.29	22.4	20.6			1.197443182			
42			9-1Fa	1648	1.21	1372	117.83	0	0.00%	0.00%			28.22	25.3	25.6			1.11585607	1.129464286		
43			9-1Fb	1648	1.21	1372	117.83	0	0.00%	0.00%			27.93	24.5	25.6		0.885	1.104389087	1.09375	0.730339806	
44			9-2Fa	1648	1.21	1372	117.83	0	0.00%	0.00%			37.05	27.7	29			1.465005931	1.236607143		
45			9-2Fb	1648	1.21	1372	117.83	0	0.00%	0.00%			35.82	25	29		0.969	1.416370107	1.116071429	0.799660194	
46			12-C										23.52	21.5	21.2			1.113636364			
47			12-1Fa	1648	1.21	1372	117.83	0	0.00%	0.00%			29.59	24.7	27.9			1.258078231	1.148837209		
48			12-1Fb	1648	1.21	1372	117.83	0	0.00%	0.00%			31.01	25.9	27.9		0.709	1.318452381	1.204651163	0.585097087	
49			12-2Fa	1648	1.21	1372	117.83	0	0.00%	0.00%			33.8	26.5	32.8			1.43707483	1.23255814		
50			12-2Fb	1648	1.21	1372	117.83	0	0.00%	0.00%			41.77	28	32.8		1.17	1.775935374	1.302325581	0.965533981	
51	L. De Lorenzis(Thesis)		BC-a										60.6								
52			BC-b										103.1								
53			BR1-a	2300	1.77	2000	218.75	0	0.06%	30.20%			84.7					1.397689769			
54			BR1-b	2300	1.77	2000	218.75	0	0.06%	18.27%			125.1				1.05	1.213385063		0.593478261	
55			BR2-a	2300	1.77	2000	218.75	0	0.13%	36.54%			97.3				0.715	1.605610561		0.404130435	
56			BR2-b	2300	1.77	2000	218.75	0	0.13%	60.41%			135.4				0.71	1.31328807		0.401304348	
57			BFV										156.6		154.1						
58			BFC3	2515	1.56	1950	192.63	0	0.26%	17.92%	2.8	13.8	203.6		223.9		0.77			0.493534791	
59			BFC4	2515	1.56	1950	144.09	0	0.47%	32.03%	2.8	13.8	226		290.7		0.525			0.336500994	
60			BFG4	773	2.00	1950	144.09	0	0.47%	32.03%	2.8	13.8	196.9		216						
61	I.S.Y. Liu		NS-F1	2800	1.61	1100	81.85		0.00%	0.00%			25.3	25.3			0.720			0.447428571	
62			NS-F2	2800	1.61	1100	107.19	100	0.00%	0.00%			27.9	19.8			1.300			0.807857143	
63			NS-F3	2800	1.61	1100	107.82	100	0.00%	0.00%			27.4	19			1.500			0.932142857	
64			NS-F4	2330	1.66	1100	103.62	100	0.00%	0.00%			26.9	17.4			0.840			0.50472103	
65			NS-S1	933	0.51	1100	88.31	100	0.00%	0.00%			28	16.4		4.2				8.237942122	
66			NS-S2	846	0.50	1100	85.86	100	0.00%	0.00%			26.7	18.4		3.5				6.95035461	
67			NB-F1	2800	1.61	1100	112.02	100	0.00%	0.00%			113	65.5			0.950			0.590357143	
68			NB-F2	2800	1.61	1100	109.22	100	0.00%	0.00%			113	67.3			1.020			0.633857143	
69			NB-F3	2330	1.66	1100	105.45	100	0.00%	0.00%			111	73.2			0.830			0.498712446	
70	E. Bonaldo		SL01										5.35								
71			SL06										4.71								
72			SL03S	2880	1.84	850	85.54	50	0.00%	0.00%	5	16-22	24.38				1.410			0.764239583	
73			SL04S	2880	1.84	850	85.54	50	0.00%	0.00%	6	16-23	24.91								

No.	Reference	Year	Specimen ID	FAILURE		
				F_{uc}/F_{oc}	Failure mode	Defl
36	Joseph Robert Yost	Aug-07	6-C		SY/CC	
37			6-1Fa		CC	
38			6-1Fb		CC	
39			6-2Fa		CC	
40			6-2Fb		CC	
41			9-C		SY/CC	
42			9-1Fa		CC	
43			9-1Fb		CC	
44			9-2Fa		CC	
45			9-2Fb		CC	
46			12-C		SY/CC	
47			12-1Fa		R	
48			12-1Fb		R	
49			12-2Fa		CC	
50			12-2Fb		CC	
51	L. De Lorenzis(Thesis)		BC-a		CC/SY	
52			BC-b		CC/SY	
53			BR1-a		CC/SY	
54			BR1-b		CC/SY	
55			BR2-a		CC/SY	
56			BR2-b		CC/SY	
57			BFV		CC/SY	
58			BFC3		R	
59			BFC4		R	
60			BFG4		CC/SY	
61	I.S.Y. Liu		NS-F1		SF/s	
62			NS-F2		CC/s	
63			NS-F3		CC/s	
64			NS-F4		D	
65			NS-S1		CC/s	
66			NS-S2		SF/s	
67			NB-F1		CC/s	
68			NB-F2		D	
69			NB-F3		D	
70	E. Bonaldo		SL01		Flexure	
71			SL06		Flexure	
72			SL03S		Shear/Flexure	
73			SL04S		Flexure	

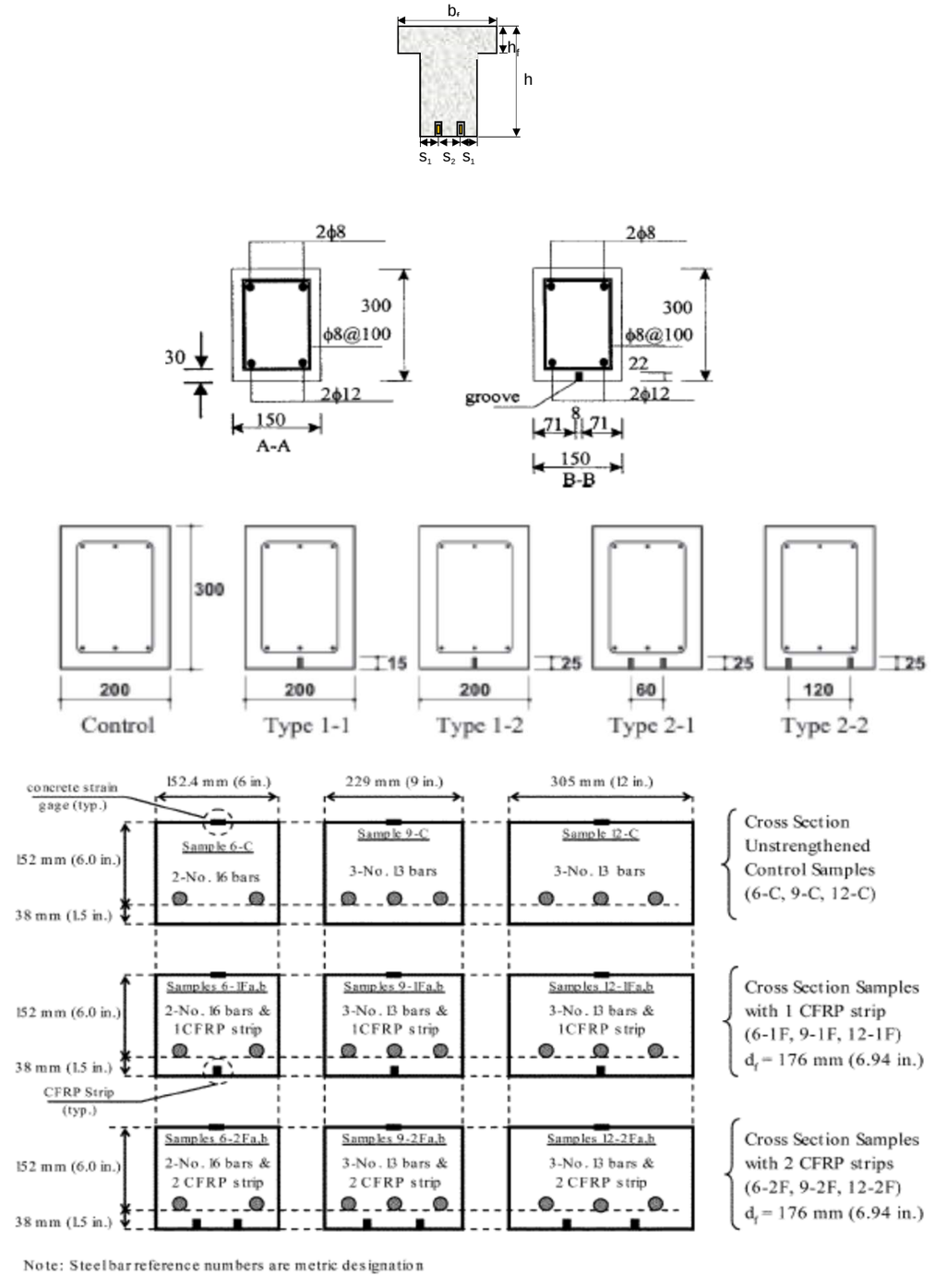

No.	Reference	Year	Specimen ID	Beam characteristics																		
				Span (m)	Shear span	Load type	Geometry							Concrete		Main bars						Top bars
							b	h	b_f	h'	A	Cover	d	f_u	f_t	Dia.	Quan.	Area	f_{sy}	E_s	f_{su}	ρ_s	Dia.
74	E. Bonaldo		SL08S	1.8	0.6	4P	300	80			24000		57	49.35		6	2	56.5	494		592	0.33%	0
75	Van Hien Nguyen	Jul-07	NSM2	2.3	0.766667	4P	150	250			37500		210	32		20	2	628.3	460	210	592	1.99%	10
76			NSM3	2.3	0.766667	4P	150	250			37500		210			16	2	402.1	525	210	625	1.28%	8
77			NSM4	2.3	0.766667	4P	150	250			37500		210			16	2	402.1	525	210	625	1.28%	8
78			NSM5	2.3	0.766667	4P	150	250			37500		210			16	2	402.1	525	210	625	1.28%	8
79			NSM6	2.3	0.766667	4P	150	250			37500		210			16	2	402.1	525	210	625	1.28%	8
80			NSM7	2.3	0.766667	4P	150	250			37500		210			16	2	402.1	525	210	625	1.28%	8
81			NSM8	2.3	0.766667	4P	150	250			37500		210			16	2	402.1	525	210	625	1.28%	8
82			NSM9	2.3	0.766667	4P	150	250			37500		210			16	2	402.1	525	210	625	1.28%	8
83	Joshua B. Quattlebaum	Dec-05	U-S	4.572	2.286	3P	152	254			38608	32	222	29.5		13	3	398.2	446		735	1.18%	na
84			N-S	4.572	2.286	3P	152	254			38608	33	222	29.5		13	3	398.2	446		736	1.18%	na
85	Everaldo Bonaldo	Mar-08	SL1	1.8	0.6	4P	300	80			24000		56	26	2.9	8	3	150.8	466	200.3	557.1	0.90%	na
86			SL4S	1.8	0.6	4P	300	80			24000		56	26	2.9	8	3	150.8	466	200.3	557.1	0.90%	na
87			SL2	1.8	0.6	4P	300	80			24000		56	26.4	3.3	8	3	150.8	466	200.3	557.1	0.90%	na
88			SL3S	1.8	0.6	4P	300	80			24000		56	26.4	3.3	8	3	150.8	466	200.3	557.1	0.90%	na
89	Gang Wu	Aug-14	Control	1.8	0.6	4P	150	300			45000		253	34.4(Cylinder)	na	14	3	461.8	340	na	na	1.22%	6
90			B11	1.8	0.6	4P	150	300			45000		253	34.4(Cylinder)	na	14	3	461.8	340	na	na	1.22%	6
91			B21	1.8	0.6	4P	150	300			45000		253	34.4(Cylinder)	na	14	3	461.8	340	na	na	1.22%	6
92			B22	1.8	0.6	4P	150	300			45000		253	34.4(Cylinder)	na	14	3	461.8	340	na	na	1.22%	6
93	Firas Al-Mahmoud , Arnaud Castel	May-09	Controlbeam	2.8	0.8	4P	150	280			42000		238	37.4	3.0	12	2	226.2	600	210		0.63%	6
94	, Raoul François , Christian		S-C6(VC30)	2.8	0.8	4P	150	280			42000		238	37.5	3.4	12	2	226.2	600	210		0.63%	6
95	Tourneur		S-C6(270-R)	2.8	0.8	4P	150	280			42000		238	36.5	3.2	12	2	226.2	600	210		0.63%	6
96			S-C6(210-R)	2.8	0.8	4P	150	280			42000		238	36.7	3.2	12	2	226.2	600	210		0.63%	6
97			S-C6(VC60)	2.8	0.8	4P	150	280			42000		238	66.5	5.4	12	2	226.2	600	210		0.63%	6
98			S-C6(270-M)	2.8	0.8	4P	150	280			42000		238	38.1	3.3	12	2	226.2	600	210		0.63%	6
99			S-C12(VC30)	2.8	0.8	4P	150	280			42000		238	35.1	3.4	12	2	226.2	600	210		0.63%	6
100			S-C12(VC60)	2.8	0.8	4P	150	280			42000		238	67.2	5.6	12	2	226.2	600	210		0.63%	6
101	R. El-Hacha, J.N. da Silva Filho and G.S.	Jul-04	B0	2.5	1.25	3P	150	250	300	50	52500	50	215	na	na	2D16+2D13	4	667.6	na	na	na	2.07%	2D13+mw5.6
102	Melo, S.H. Rizkalla		B1	2.5	1.25	3P	150	250	300	50	52500	50	215	na	na	2D16+2D14	4	667.6	na	na	na	2.07%	2D13+mw5.7
103			B2	2.5	1.25	3P	150	250	300	50	52500	50	215	na	na	2D16+2D15	4	667.6	na	na	na	2.07%	2D13+mw5.8
104			B3	2.5	1.25	3P	150	250	300	50	52500	50	215	na	na	2D16+2D16	4	667.6	na	na	na	2.07%	2D13+mw5.9
105			B4	2.5	1.25	3P	150	250	300	50	52500	50	215	na	na	2D16+2D17	4	667.6	na	na	na	2.07%	2D13+mw5.10
106			B2a(EBR)	2.5	1.25	3P	150	250	300	50	52500	50	215	na	na	2D16+2D18	4	667.6	na	na	na	2.07%	2D13+mw5.11
107			B3a(EBR)	2.5	1.25	3P	150	250	300	50	52500	50	215	na	na	2D16+2D19	4	667.6	na	na	na	2.07%	2D13+mw5.12
108			B4a(EBR)	2.5	1.25	3P	150	250	300	50	52500	50	215	na	na	2D16+2D20	4	667.6	na	na	na	2.07%	2D13+mw5.13
109			Ref_c_no_1																			
110	A. Balsamo, A. Bilotta,		Ref_d_no_1																			
111	F. Ceroni, E. Nigro, M. Pecce		EBR_c_1.4x40_1																			

No.	Reference	Year	Specimen ID	*Beam characteristics*									*NSMR*											
				Top bars				Shear link					Groove				FRP								
				Quan.	Area	f_{sy}	f_{su}	Dia.	Area	fsy	fsu	s	d	h	s1	s2	Type	Shape	n	h	t	df	Dia.	Area	E_{frp}
74	E. Bonaldo		SL08S	0	0	0	0	0	0	0	0	0	5	15	150	75	CFRP	S	0	9.4	1.4			0	156.1
75	Van Hien Nguyen	Jul-07	NSM2	2	157.1	460	546	10	157.0796327			100	6	18			CFRP	RB	3				6.35	133.25885	133
													12											
76			NSM3	2	100.5309649	460	546	8	100.5309649															
77			NSM4	2	100.5309649	460	546	8	100.5309649															
78			NSM5	2	100.5309649	460	546	8	100.5309649															
79			NSM6	2	100.5309649	460	546	8	100.5309649															
80			NSM7	2	100.5309649	460	546	8	100.5309649															
81			NSM8	2	100.5309649	460	546	8	100.5309649															
82			NSM9	2	100.5309649	460	546	8	100.5309649															
83	Joshua B. Quattlebaum	Dec-05	U-S	na	na	na	na	na	na	na	na	na												
84			N-S	na	na	na	na	na	na	na	na	na	6.4	32	44	54	CFRP	S	2	25	1.4			70	215
85	Everaldo Bonaldo	Mar-08	SL1	na	na	na	na	na	na	na	na	na	4	15	75	37.5	CFRP	S	4	9.4	1.4			52.64	156.1
86			SL4S	na	na	na	na	na	na	na	na	na	4	15	75	37.5	CFRP	S	4	9.4	1.4			52.64	156.1
87			SL2	na	na	na	na	na	na	na	na	na	4	15	75	37.5	CFRP	S	4	9.4	1.4			52.64	156.1
88			SL3S	na	na	na	na	na	na	na	na	na	4	15	75	37.5	CFRP	S	4	9.4	1.4			52.64	156.1
89	Gang Wu	Aug-14	Control	2	56.5	240	na	10	157.0796327	275	na	80							0						
90			B11	2	56.5	240	na	10	157.0796327	275	na	80	20	20		75	CFRP	RB	1				7.9	49.016814	170
91			B21	2	56.5	240	na	10	157.0796327	275	na	80	20	20	70	40	CFRP	RB	2				7.9	98.033628	170
92			B22	2	56.5	240	na	10	157.0796327	275	na	80	20	20	70	40	CFRP	RB	2				7.9	98.033628	170
93	Firas Al-Mahmoud , Arnaud Castel	May-09	Controlbeam	2	56.5	na		6	56.54866776	na	na	150	12	12	88	62	CFRP	RB	2				6	56.5488	146
94	, Raoul François , Christian		S-C6(VC30)	2	56.5	na		7	76.96902001	na	na	151	12	12	88	62	CFRP	RB	2				6	56.5488	146
95	Tourneur		S-C6(270-R)	2	56.5	na		8	100.5309649	na	na	152	12	12	88	62	CFRP	RB	2				6	56.5488	146
96			S-C6(210-R)	2	56.5	na		9	127.2345025	na	na	153	12	12	88	62	CFRP	RB	2				6	56.5488	146
97			S-C6(VC60)	2	56.5	na		10	157.0796327	na	na	154	12	12	88	62	CFRP	RB	2				6	56.5488	146
98			S-C6(270-M)	2	56.5	na		11	190.0663555	na	na	155	12	12	88	62	CFRP	RB	2				6	56.5488	146
99			S-C12(VC30)	2	56.5	na		12	226.1946711	na	na	156	24	24	na	75	CFRP	RB	1				12	113.0976	146
100			S-C12(VC60)	2	56.5	na		13	265.4645792	na	na	157	24	24	na	75	CFRP	RB	1				12	113.0976	146
101	R. El-Hacha, J.N. da Silva Filho and G.S.	Jul-04	B0			na	na	13	265.4645792	na	na	100													
102	Melo, S.H. Rizkalla		B1			na	na	13	265.4645792	na	na	100	18	30	0	75	CFRP	RB	1			285	9.5	70.88235	122.5
103			B2			na	na	13	265.4645792	na	na	100	6.4	19	75	37.5	CFRP	S	2	16	2	290.5		64	140
104			B3			na	na	13	265.4645792	na	na	100	6.4	25	76	38	CFRP	S	2	25	1.2	287.5		60	150
105			B4			na	na	13	265.4645792	na	na	100	6.4	25	38	37	GFRP	S	3	20	2	287.5		120	45
106			B2a(EBR)			na	na	13	265.4645792	na	na	100	na	na								300		64	140
107			B3a(EBR)			na	na	13	265.4645792	na	na	100	na	na								300		60	150
108			B4a(EBR)			na	na	13	265.4645792	na	na	100	na	na								300		120	45
109			Ref_c_no_1																						
110	A. Balsamo, A. Bilotta,		Ref_d_no_1																						
111	F. Ceroni, E. Nigro, M. Pecce		EBR_c_1.4x40_1																						

No.	Reference	Year	Specimen ID	NSMR									FAILURE							
				FRP							Resin		F_u	F_y	$F_{y\text{-}cal}$	$F_{u\text{-}cal}$	ε_s	εf (%)	F_u/F_o	F_y/F_{yo}	$\varepsilon_f/\varepsilon_{fu}$
				f_{frp}	ε_{fu}(%)	$L_f/2$	L_f/h	l	ρ_f	ρ_f/ρ_s	E_{resin}	f_{resin}									
74	E. Bonaldo		SL08S	2880	1.84	850	85.54	50	0.00%	0.00%	7	16-24	24.15					1.270			0.688357639
75	Van Hien Nguyen	Jul-07	NSM2	1452.521465	1.09	1000	97.11	50	0.36%	17.82%	7	16-24	146					0.50			0.45782456
76			NSM3																		
77			NSM4																		
78			NSM5																		
79			NSM6																		
80			NSM7																		
81			NSM8																		
82			NSM9																		
83	Joshua B. Quattlebaum	Dec-05	U-S										37.1	26.7/32.6							
84			N-S	2676.75	1.8	2.134		152.5	0.18%	15.36%	na	na	49.4	35.5/40.8							
85	Everaldo Bonaldo	Mar-08	SL1	2879	1.85	850	85.54	50	0.22%	24.44%	7.5	33	14.3	10.6							
86			SL4S	2879	1.85	850	85.54	50	0.22%	24.44%	7.5	33	17.9	69.6							
87			SL2	2879	1.85	850	85.54	50	0.22%	24.44%	7.5	33	15.1	12.1							
88			SL3S	2879	1.85	850	85.54	50	0.22%	24.44%	7.5	33	19.2	79.5							
89	Gang Wu	Aug-14	Control										168.7								
90			B11	2629	1.55	850		50	0.11%	8.95%	3.5(tensile)	30(tensile)	170.8								
91			B21	2629	1.55	850		50	0.22%	17.90%	3.5(tensile)	30(tensile)	190								
92			B22	2629	1.55	850		50	0.22%	17.90%	3.5(tensile)	30(tensile)	190								
93	Firas Al-Mahmoud , Arnaud Castel	May-09	Controlbeam	1875	1.28%				0.13%	21.25%	4.94	83	76.5	71.25							
94	, Raoul François , Christian		S-C6(VC30)	1875	1.28%	1500		0	0.13%	21.25%	4.94	83	145.25	88							
95	Tourneur		S-C6(270-R)	1875	1.28%	1350		50	0.13%	21.25%	4.94	83	142.75	92							
96			S-C6(210-R)	1875	1.28%	1050		350	0.13%	21.25%	4.94	83	143	95.5							
97			S-C6(VC60)	1875	1.28%	1500		-100	0.13%	21.25%	4.94	83	167.25	119.25							
98			S-C6(270-M)	1875	1.28%	1350		50	0.13%	21.25%	31.4(Mortar)	74.6	235	112							
99			S-C12(VC30)	1875	1.28%	1500		-100	0.27%	42.50%	4.94	83	187.75	92.25							
100			S-C12(VC60)	1875	1.28%	1500		-100	0.27%	42.50%	4.94	83	145.5	88.25							
101	R. El-Hacha, J.N. da Silva Filho and G.S.	Jul-04	B0										55.4	38.11							
102	Melo, S.H. Rizkalla		B1	1408	1.14	1200		50	0.14%	6.52%	na	na	93.8	47.94							
103			B2	1525	1.08	1200		50	0.12%	5.89%	na	na	99.3	48.62							
104			B3	2000	1.33	1200		50	0.11%	5.52%	na	na	110.2	49.16							
105			B4	1000	2.22	1200		50	0.23%	11.04%	na	na	102.7	48.17							
106			B2a(EBR)	1525	1.08	1200		50	0.12%	5.89%	na	na	64.6	44.88							
107			B3a(EBR)	2000	1.33	1200		50	0.11%	5.52%	na	na	69.3	61.0							
108			B4a(EBR)	1000	2.22	1200		50	0.23%	11.04%	na	na	71.1	48.16							
109			Ref_c_no_1																		
110	A. Balsamo, A. Bilotta,		Ref_d_no_1																		
111	F. Ceroni, E. Nigro, M. Pecce		EBR_c_1.4x40_1																		

No.	Reference	Year	Specimen ID	FAILURE		
				F_{uc}/F_{oc}	Failure mode	Defl
74	E. Bonaldo		SL08S		Flexure	
75	Van Hien Nguyen	Jul-07	NSM2		CC	
76			NSM3			
77			NSM4			
78			NSM5			
79			NSM6			
80			NSM7			
81			NSM8			
82			NSM9			
83	Joshua B. Quattlebaum	Dec-05	U-S			
84			N-S			
85	Everaldo Bonaldo	Mar-08	SL1		Flexure	
86			SL4S		Flexure	
87			SL2		Flexure	
88			SL3S		Flexure	
89	Gang Wu	Aug-14	Control		Flexure	
90			B11		IC debonding	
91			B21		Flexure	
92			B22		Flexure	
93	Firas Al-Mahmoud , Arnaud Castel	May-09	Controlbeam		Crushingofcompressedconcrete	
94	, Raoul François , Christian		S-C6(VC30)		CFRProdpull-out	
95	Tourneur		S-C6(270-R)		CFRProdpull-out	
96			S-C6(210-R)		Concretepeeling-offattheendofCFRProds	
97			S-C6(VC60)		Crushingofcompressedconcrete	
98			S-C6(270-M)		CFRProdpull-out	
99			S-C12(VC30)		CFRProdpull-out	
100			S-C12(VC60)		Debondingatthemortar–concreteinterface	
101	R. El-Hacha, J.N. da Silva Filho and G.S.	Jul-04	B0		Crushing of concrete	64.4
102	Melo, S.H. Rizkalla		B1		DB	29.2
103			B2		Rupture of the NSM	30.5
104			B3		Rupture of the NSM	50.8
105			B4		DB	44.3
106			B2a(EBR)		DB	43.7
107			B3a(EBR)		DB	16.3
108			B4a(EBR)		DB	22.2
109			Ref_c_no_1			
110			Ref_d_no_1			
111	A. Balsamo, A. Bilotta, F. Ceroni, E. Nigro, M. Pecce		EBR_c_1.4x40_1			

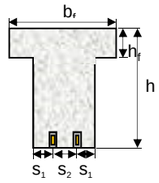

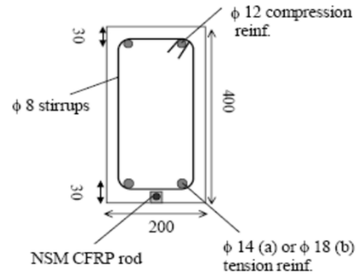

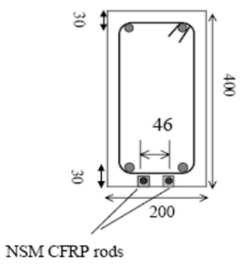

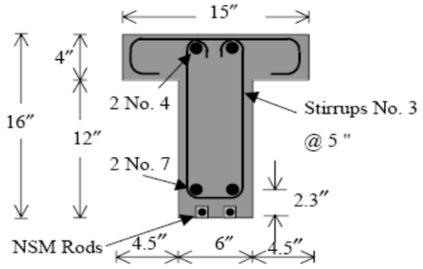

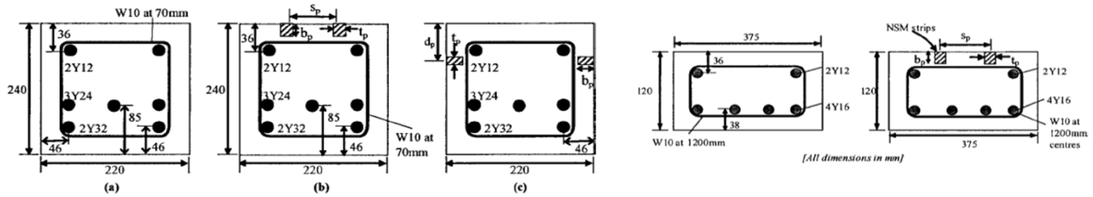

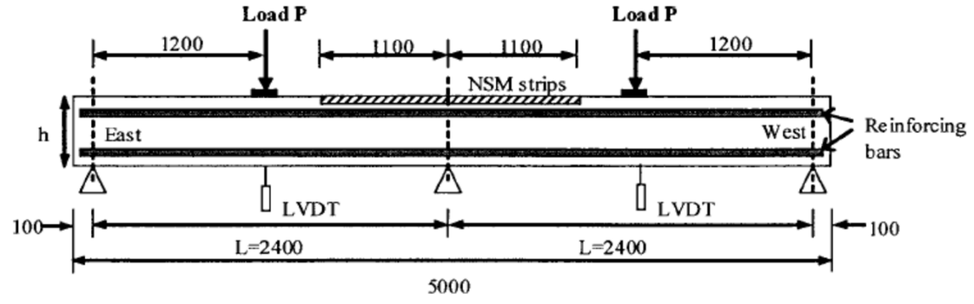

No.	Reference	Year	Specimen ID	Beam characteristics																		
				Span (m)	Shear span	Load type	Geometry							Concrete		Main bars						Top bars
							b	h	b_f	h'	A	Cover	d	f_u	f_t	Dia.	Quan.	Area	f_{sy}	E_s	f_{su}	ρ_s	Dia.
112	A. Balsamo, A. Bilotta, F. Ceroni, E. Nigro, M. Pecce		EBR_c_1.4x40_2																			
113			EBR_d_1.4x40_1																			
114			EBR_d_1.4x40_2																			
115			NSM_d_2x1.4x10_1																			
116			NSM_d_3x1.4x10_1																			
117	Tarek H. Almusallam, Hussein M. Elsanadedy Yousef A. Al-Salloum, Saleh H. Alsayed	12-Dec	CS	2	0.9	4P	150	200			30000	30	157	36.6		10	3	235.6	408	200	na	1.00%	6
118			CF	2	0.9	4P	150	200			30000	30	157	36.6		10	3	235.6	408			1.00%	6
119			RW1S	2	0.9	4P	150	200			30000	30	157	36.6		10	2	157.1	408			0.67%	6
120			RW1Ø14S	2	0.9	4P	150	200			30000	30	157	36.6		10	2	157.1	408			0.67%	6
121			RW1F	2	0.9	4P	150	200			30000	30	157	36.6		10	2	157.1	408			0.67%	6
122			RW2S	2	0.9	4P	150	200			30000	30	157	36.6		10	1	78.5	408			0.33%	6
123			RW2Ø14S	2	0.9	4P	150	200			30000	30	157	36.6		10	1	78.5	408			0.33%	6
124			RW2F	2	0.9	4P	150	200			30000	30	157	36.6		10	1	78.5	408			0.33%	6

No.	Reference	Year	Specimen ID	*Beam characteristics*									*NSMR*											
				Top bars				Shear link					Groove				FRP								
				Quan.	Area	f_{sy}	f_{su}	Dia.	Area	fsy	fsu	s	d	h	s1	s2	Type	Shape	n	h	t	df	Dia.	Area	E_{frp}
112	A. Balsamo, A. Bilotta, F. Ceroni, E. Nigro, M. Pecce		EBR_c_1.4x40_2																					
113			EBR_d_1.4x40_1																					
114			EBR_d_1.4x40_2																					
115			NSM_d_2x1.4x10_1																					
116			NSM_d_3x1.4x10_1																					
117	Tarek H. Almusallam, Hussein M. Elsanadedy Yousef A. Al-Salloum, Saleh H. Alsayed	12-Dec	CS	1	28.3	334	na	8	100.5309649	374		100							0		185	0	0	
118			CF	1	28.3	335	na	8	100.5309649	374		100							0		185	0		
119			RW1S	1	28.3	336	na	8	100.5309649	374		100	30	30	0	75	Steel	RB	0		185	10	0	200
120			RW1Ø14S	1	28.3	337	na	8	100.5309649	374		100	30	30	0	75	Steel	RB	1		185	14	153.9384	200
121			RW1F	1	28.3	338	na	8	100.5309649	374		100	30	30	0	75	GFRP	RB	0		185	10	0	40
122			RW2S	1	28.3	339	na	8	100.5309649	374		100	30	30	60	30	Steel	RB	0		185	10	0	200
123			RW2Ø14S	1	28.3	340	na	8	100.5309649	374		100	30	30	60	30	Steel	RB	0		185	14	0	200
124			RW2F	1	28.3	341	na	8	100.5309649	374		100	30	30	60	30	GFRP	RB	0		185	10	0	40

No.	Reference	Year	Specimen ID	NSMR									FAILURE							
				FRP							Resin		F_u	F_y	$F_{y\text{-}cal}$	$F_{u\text{-}cal}$	ε_s	εf (%)	F_u/F_o	F_y/F_{yo}	$\varepsilon_f/\varepsilon_{fu}$
				f_{frp}	ε_{fu}(%)	$L_f/2$	L_f/h	l	ρ_f	ρ_f/ρ_s	E_{resin}	f_{resin}									
112	A. Balsamo, A. Bilotta, F. Ceroni, E. Nigro, M. Pecce	12-Dec	EBR_c_1.4x40_2																	
113			EBR_d_1.4x40_1																	
114			EBR_d_1.4x40_2																	
115			NSM_d_2x1.4x10_1																	
116			NSM_d_3x1.4x10_1																	
117			CS										40.5							
118			CF										52.8							
119	Tarek H. Almusallam, Hussein M. Elsanadedy Yousef A. Al-Salloum, Saleh H. Alsayed		RW1S	408		1000		-100	0.00%	0.00%	4.3	na	41.9							
120			RW1Ø14S	550		1000		-100	0.51%	76.93%	4.3	na	57.5							
121			RW1F	743	1.86	1000		-100	0.00%	0.00%	4.3	na	48.5							
122			RW2S	408		1000		-100	0.00%	0.00%	4.3	na	45.8							
123			RW2Ø14S	550		1000		-100	0.00%	0.00%	4.3	na	79							
124			RW2F	743	1.86	1000		-100	0.00%	0.00%	4.3	na	51.2							

No.	Reference	Year	Specimen ID	FAILURE		
				F_{uc}/F_{oc}	Failure mode	Defl
112	A. Balsamo, A. Bilotta, F. Ceroni, E. Nigro, M. Pecce	12-Dec	EBR_c_1.4x40_2			
113			EBR_d_1.4x40_1			
114			EBR_d_1.4x40_2			
115			NSM_d_2x1.4x10_1			
116			NSM_d_3x1.4x10_1			
117	Tarek H. Almusallam, Hussein M. Elsanadedy Yousef A. Al-Salloum, Saleh H. Alsayed		CS			
118			CF			
119			RW1S			
120			RW1Ø14S			
121			RW1F			
122			RW2S			
123			RW2Ø14S			
124			RW2F			

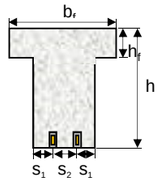

No.	References	Beam ID	Experimental	TR-55		ACI		NGUYEN		Theoretical Yielding	Theoretical Ultimate
			P_{exp}	P_{TR-55}	P_{TR-55}/P_{exp}	P_{ACI}	P_{ACI}/P_{exp}	P_{NGUYEN}	P_{NGUYEN}/P_{exp}	P_y	$P_{the.}$
			(kN)	(kN)		(kN)		(kN)		(kN)	(kN)
1	Teng (2006)	B0	49.5							46.9	49.1
2		B500	49.5	65	1.32	47.0	0.95	49.1	0.99	57.7	100.3
3		B1200	64.5	65	1.01	80.3	1.24	49.3	0.76	57.7	100.3
4		B1800	96.8	65	0.68	95.0	0.98	66.8	0.69	57.7	100.3
5		B2900	100.1	65	0.65	95.0	0.95	100.3	1.00	57.7	100.3
6	Nguyen(2009)	B0	116.1							103.7	109.0
7		B1	100							102.9	104.8
8		NSM2	145.2	114.4	0.79	140.0	0.96	145.2	1.00	141.7	145.2
9		NSM3Aa	173.9	118.5	0.68	166.9	0.96	176.4	1.01	121.5	176.4
10		NSM4Aa	148.6	114.3	0.77	140.6	0.95	143.8	0.97	120.7	145.7
11		NSM5Aa	141.2	114.3	0.81	140.7	1.00	131.8	0.93	120.7	145.7
12		NSM6Aa	129.9	114.3	0.88	140.7	1.08	131.8	1.01	120.7	145.7
13		NSM7Aa	137.6	113.5	0.83	133.4	0.97	131.8	0.96	116.6	137.7
14		NSM8Ba	112.5	111.4	0.99	121.9	1.08	104.8	0.93	110.1	125.7
15		NSM9Ba	111.1	111.4	1.00	121.9	1.10	104.8	0.94	110.1	125.7
16	Barros(2004)	V1	28.2							26.0	27.0
17		V1R1	50.3	31.7	0.63	48.9	0.97	53.4	1.06	30.3	53.4
18		V2	41							37.3	38.6
19		V2R2	78.5	47.8	0.61	73.2	0.93	73.8	0.94	49.0	77.2
20		V3	41.3							41.0	42.6
21		V3R2	81.9	51.9	0.63	75.2	0.92	79.1	0.97	52.3	79.1
22		V4	48.5							45.1	47.1
23		V4R3	94.9	57.0	0.60	85.8	0.90	88.2	0.93	59.3	90.5

No.	References	Beam ID	Experimental	TR-55		ACI		NGUYEN		Theoretical	
										Yielding	Ultimate
			P_{exp}	P_{TR-55}	P_{TR-55}/P_{exp}	P_{ACI}	P_{ACI}/P_{exp}	P_{NGUYEN}	P_{NGUYEN}/P_{exp}	P_y	$P_{the.}$
			(kN)	(kN)		(kN)		(kN)		(kN)	(kN)
24	Al-Mahmoud(2009)	Controlbeam	73.75							73.7	76.6
25		S-C6(270-R)	133.3	91.5	0.69	134.9	1.01	143.1	1.07	91.0	143.1
26		S-C6(210-R)	110.0	63.2	0.57	110.0	1.00	93.1	0.85	91.0	143.5
27		S-C6(VC60)	133.25	62.7	0.47	139.0		188.3		91.7	188.3
28		S-C6(270-M) -Mota	109.75		0.00	135.3	1.23			91.1	145.9
29		S-C12(VC30)				168.4				108.4	178.1
30		S-C12(VC60)				210.3				109.1	239.7
31	Al-Mahmoud(2010)	C	36.1							24.5	25.5
32		S-C(CR)(240)	71.4	61.1	0.86	45.5	0.64	47.9	0.67	30.3	47.9
33		S-C(CR)(190)	62.0	61.0	0.98	45.3	0.73	47.7	0.77	30.3	47.7
34		S-C(CR)(150)	43.2	61.1	1.41	45.8	1.06	48.2	1.12	30.3	48.2
35		C(FPT)	43.2	90.8	2.10	134.9		143.5		91.0	143.5
36		S-C(FPT)(270)	133.3	91.5	0.69	134.9	1.01	143.1	1.07	91.0	143.1
37		S-C(FPT)(210)	110	91.6	0.83	134.9	1.23	143.5	1.30	91.0	143.5
38	Bonaldo (2008)	SL1	14.3							11.8	12.1
39		SL4s	37.7	18.8	0.50	25.1	0.66	26.3	0.70	21.3	26.3
40	E. Bonaldo	SL2	15.1							14.1	14.2
41		SL3s	35.6	18.8	0.53	15.5	0.43	26.3	0.74	21.0	26.3
42	Bonaldo(2005)	SL01	5.4							5.0	5.2
43	E. Bonaldo	SL06	4.7							5.0	5.2

No.	References	Beam ID	Experimental	TR-55		ACI		NGUYEN		Theoretical	
										Yielding	Ultimate
			P_{exp}	P_{TR-55}	P_{TR-55}/P_{exp}	P_{ACI}	P_{ACI}/P_{exp}	P_{NGUYEN}	P_{NGUYEN}/P_{exp}	P_y	$P_{the.}$
			(kN)	(kN)		(kN)		(kN)		(kN)	(kN)
44		SL03S	24.4	6.5	0.27	21.5	0.88	25.3	1.04	8.3	25.3
45		SL04S	24.9	6.6	0.26	20.6	0.83	22.0	0.89	8.4	22.0
46		SL08S	24.2	6.5	0.27	23.8	0.98	28.2	1.16	8.5	28.2
47	A. Balsamo	Ref_d_no_1	46.1							31.1	31.9
48		NSM_d_2x1.4x10_1	71.3	18.3	0.26	19.0	0.27	41.1	0.58	40.3	41.1
49		NSM_d_3x1.4x10_1	67.6	18.9	0.28	20.2	0.30	44.0	0.65	45.0	44.0
50	Quattlebaum(2005)	U-S	37.1							31.8	32.7
51		N-S	49.4	38.3	0.77	47.9	0.97	49.9	1.01	38.6	49.9
52	Wu(2014)	Control	168.7							176.0	180.7
53		B11	256.7	212.7	0.83	239.9	0.93	248.6	0.97	199.6	248.6
54		B21	260.9	206.6	0.79	250.9	0.96	274.6	1.05	223.2	287.8
55		B22	288.3	206.6	0.72	250.9	0.87	274.6	0.95	223.2	287.8
56	Sharaky(2014)	CB	70.4							66.9	69.1
57		LB1C1	109.1	91.3	0.84	126.3	1.16	111.4	1.02	82.5	133.1
58		LB1G1	99.2	83.3	0.84	99.4	1.00	111.4	1.12	72.9	100.9
59		LB2C1	117.2	90.9	0.78	127.6	1.09	111.4	0.95	98.1	163.5
60		LB2G1	112.2	82.9	0.74	117.9	1.05	111.4	0.99	79.0	123.8
61		LA2C1	114.5	90.9	0.79	127.6	1.11	111.4	0.97	98.1	163.5
62		LA2G1	110.6	82.9	0.75	117.9	1.07	111.4	1.01	79.0	123.8

No.	References	Beam ID	Experimental	TR-55		ACI		NGUYEN		Theoretical	
										Yielding	Ultimate
			P_{exp}	P_{TR-55}	P_{TR-55}/P_{exp}	P_{ACI}	P_{ACI}/P_{exp}	P_{NGUYEN}	P_{NGUYEN}/P_{exp}	P_y	$P_{the.}$
			(kN)	(kN)		(kN)		(kN)		(kN)	(kN)
63		LB1G2	105.8	91.7	0.87	121.7	1.15	111.4	1.05	80.5	128.0
64	Sharaky(2015)	CB	70.4							66.1	68.2
65		F2C1	117.2	90.7	0.77	127.2	1.09	109.9	0.94	66.1	162.1
66		F2S1	111.7	86.4	0.77	146.2	1.31	109.7	0.98	66.1	134.3
67		F2G1	122.2	82.3	0.67	115.9	0.95	109.5	0.90	66.1	121.8
68		F1G2	105.8	90.8	0.86	118.2	1.12	109.3	1.03	66.1	124.3
69	Soliman(2010)	A0	55.0							52.8	55.5
70		AC1	67.0	88.5	1.32	67.9	1.01	55.5	0.83	69.2	181.0
71		AC2	73.0	88.5	1.21	85.2	1.17	55.5	0.76	69.2	181.0
72		AC3	94.0	88.5	0.94	118.6	1.26	65.4	0.70	69.2	181.0
73		AC4	96.0	88.5	0.92	132.8	1.38	79.5	0.83	69.2	181.0
74		AC5	88.0	81.5	0.93	85.2	0.97	55.5	0.63	69.2	181.0
75		AC6	94.0	81.5	0.87	118.6	1.26	65.4	0.70	69.2	181.0
76		AC7	102.0	88.5	0.87	132.8	1.30	79.5	0.78	69.2	181.0
77		AC8	74.0	100.9	1.36	109.5	1.48	55.5	0.75	84.6	231.7
78		AC9	109.0	100.9	0.93	162.3	1.49	85.9	0.79	84.6	231.7
79		AG10	75.0	82.2	1.10	121.5	1.62	55.5	0.74	63.5	154.3
80		AG11	112.0	82.2	0.73	121.5	1.08	85.9	0.77	63.5	154.3
81		B0	130.0							104.2	109.8

No.	References	Beam ID	Experimental	TR-55		ACI		NGUYEN		Theoretical	
										Yielding	Ultimate
			P_{exp}	P_{TR-55}	P_{TR-55}/P_{exp}	P_{ACI}	P_{ACI}/P_{exp}	P_{NGUYEN}	P_{NGUYEN}/P_{exp}	P_y	$P_{the.}$
			(kN)	(kN)		(kN)		(kN)		(kN)	(kN)
82		BC1	135.0	140.3	1.04	136.3	1.01	109.8	0.81	120.7	207.1
83		BC2	154.0	140.3	0.91	170.4	1.11	129.2	0.84	120.7	207.1
84		C0	233.0							201.6	209.4
85		CC1	227.0	237.1	1.04	209.6	0.92	209.4	0.92	217.9	268.3
86		CC2	229.0	237.1	1.04	221.8	0.97	209.4	0.91	217.9	268.3
87		CC3	234.0	237.1	1.01	232.2	0.99	209.4	0.89	217.9	268.3
88		CC4	254.0	237.1	0.93	266.3	1.05	249.7	0.98	217.9	268.3
89	Ceroni(2010)	A1						0.0		21.1	22.0
90		A9	50.7	30.0	0.59	45.0	0.89	47.4	0.94	31.0	47.4
91		A10				45.0		47.4		0.0	47.4
91	Wang(2008)	B0	59.7							50.5	52.7
92		B2600	81.5	61.9	0.76	70.2	0.86	72.5	0.89	53.6	72.5
93		B2800	80.6	52.5	0.65	70.2	0.87	72.5	0.90	53.6	72.5
94		B3200	81.9	52.5	0.64	70.2	0.86	72.5	0.89	53.6	72.5
95	EL-Hacha(2004)	B0	55.4							79.5	83.6
96		B1	93.8	99.4	1.06	117.0	1.25	121.8	1.30	89.7	121.8
97		B2	99.3	92.2	0.93	118.9	1.20	124.0	1.25	90.5	124.0
98		B3	110.2	92.2	0.84	118.5	1.08	123.5	1.12	90.3	123.5
99		B4	102.7	85.6	0.83	118.5	1.15	123.5	1.20	90.3	123.5

CALCULATION SHEET FOR DATABASE CHECK
VAN HIEN'S BEAM (NSM4Aa-NSM6Aa)

Geometry data $b := 150$ $h := 250$ $d_s := 210$ $d_f := 243$

$a_b := 4$ $b_b := 20$ $L_s := 767$ $L := 2300$

Materials

$f_c := 32.3$ $\varepsilon_{c\_max} := 0.0035$ $E_c := 22 \cdot \left(\frac{f_c}{10}\right)^{0.3} \cdot 1000 = 3.13 \cdot 10^4$

$E_s := 210000$ $\sigma_y := 525$ $n_s := \frac{E_s}{E_c} = 6.71$ $A_s := 402$

$E_f := 214000$ $\varepsilon_{f\_max} := 0.013$ $n_f := \frac{E_f}{E_c} = 6.84$ $A_f := 50$ $\sigma_f := E_f \cdot \varepsilon_{f\_max} = 2.78 \cdot 10^3$

1-Yield load and the ultimate load of the *unstrengthened beam*

1.1Neutral axis depth at yield load

$$y_{y\_unstr} := \frac{-(n_s \cdot A_s) + \sqrt{(n_s \cdot A_s)^2 + 2 \cdot b \cdot (n_s \cdot A_s \cdot d_s)}}{b} = 70.8$$

1.2 Neutral axis depth at ultimate load $y_{u\_unstr} := \frac{(A_s \cdot \sigma_y)}{0.8 \cdot b \cdot f_c} = 54.5$

1.3 Strain in the steel reinforcement at ultimate load

$$\varepsilon_{su\_unstr} := \frac{d_s - y_{u\_unstr}}{y_{u\_unstr}} \cdot \varepsilon_{c\_max} = 10 \cdot 10^{-3}$$

1.4 Equivalent moment of inertia

$$I_c := \frac{b \cdot y_{y\_unstr}^3}{3} + n_s \cdot A_s \cdot (d_s - y_{y\_unstr})^2 = 7 \cdot 10^7$$

1.5Yielding moment $M_{y\_unstr} := \frac{\sigma_y \cdot I_c}{n_s \cdot (d_s - y_{y\_unstr})} \cdot 10^{-6} = 39.34$

$$P_{y\_unstr} := 2 \cdot \frac{M_{y\_unstr}}{L_s} \cdot 10^3 = 102.58$$

1.6 Ultimate moment resistance

$$M_{u\_unstr} := A_s \cdot \sigma_y \cdot \left(d_s - 0.4 \cdot y_{u\_unstr}\right) \cdot 10^{-6} = 39.7$$

2 Yield and ultimate load of strengthened beam

$$P_{u\_unstr} := 2 \cdot \frac{M_{u\_unstr}}{L_s} \cdot 10^{3} = 103.58$$

2.1Neutral axis depth

$$y_{u\_str} := \frac{\left(A_s \cdot \sigma_y - \varepsilon_{c\_max} \cdot E_f \cdot A_f\right) + \sqrt{\left(A_s \cdot \sigma_y - \varepsilon_{c\_max} \cdot E_f \cdot A_f\right)^2 + 3.2 \cdot b \cdot f_c \cdot \varepsilon_{c\_max} \cdot E_f \cdot A_f \cdot d_f}}{1.6 \cdot b \cdot f_c}$$

$$y_{u\_str} = 75.77$$

2.2 Strain in the steel $$\varepsilon_{su\_str} := \frac{d_s - y_{u\_str}}{y_{u\_str}} \cdot \varepsilon_{c\_max} = 6.2 \cdot 10^{-3}$$

2.3 Strain in the FRP $$\varepsilon_{fu\_str} := \frac{d_f - y_{u\_str}}{y_{u\_str}} \cdot \varepsilon_{c\_max} = 7.72 \cdot 10^{-3}$$

2.4 Ultimate moment resistance

$$M_{u\_str} := \left(A_s \cdot \sigma_y \cdot \left(d_s - 0.4 \cdot y_{u\_str}\right) + E_f \cdot A_f \cdot \varepsilon_{fu\_str} \cdot \left(d_f - 0.4 \cdot y_{u\_str}\right)\right) \cdot 10^{-6} = 55.5$$

2.5 Increase of ultimate moment resistance after strengthening

$$\frac{M_{u\_str}}{M_{u\_unstr}} = 1.4 \qquad P_{u\_str} := 2 \cdot \frac{M_{u\_str}}{L_s} \cdot 10^{3} = 144.73$$

Guess Values

$$x := \frac{h}{4}$$

$$\varepsilon_c(x) := \frac{x \cdot \varepsilon_{f\_max}}{d_f - x}$$

$$\alpha(x) := -68711 \cdot \varepsilon_c(x)^2 + 464.79 \cdot \varepsilon_c(x) + 0.01$$

$$\gamma(x) := \left(1962.6 \cdot \varepsilon_c(x)^2 + 17.89 \cdot \varepsilon_c(x) + 0.33\right)$$

Given

Constraints

$$f_c \cdot b \cdot x \cdot \alpha(x) - A_f \cdot E_f \cdot \varepsilon_{f\_max} - A_s \cdot \sigma_y = 0$$

Solve for x

$$a := \text{find}(x)$$

$$a = -51.53$$

$$M_{u\_str2} := \left(A_s \cdot \sigma_y \cdot \left(d_s - 0.4 \cdot a\right) + E_f \cdot A_f \cdot \varepsilon_{fu\_str} \cdot \left(d_f - 0.4 \cdot a\right)\right) \cdot 10^{-6}$$

$$M_{u\_str2} = 70.46 \qquad P_{u\_str2} := 2 \cdot \frac{M_{u\_str2}}{L_s} \cdot 1000 = 183.72$$

$$M_{u\_str} := \text{if } \left(\varepsilon_{fu\_str} - \varepsilon_{f\_max}\right) > 0 \quad \| \text{bb} \ldots M$$

$$M_{u\_str} = 55.5$$

else

$bb \leftarrow M_{u\_str}$

$$P_{u\_str} := 2 \cdot \frac{M_{u\_str}}{L_s} \cdot 10^3 = 144.73$$

VAN HIEN'S METHOD

3-Calcualte the embedment length of the NSMR

3.1 Yield load

3.1.1 Neutral axis depth

$$y_{yield\_str} := \frac{-(n_s \cdot A_s + n_f \cdot A_f) + \sqrt{(n_s \cdot A_s + n_f \cdot A_f)^2 + 2 \cdot b \cdot (n_s \cdot A_s \cdot d_s + n_f \cdot A_f \cdot d_f)}}{b} = 75$$

3.1.2 Equivalent moment of inertia

$$I_{onc} := \frac{b \cdot y_{yield\_str}^3}{3} + n_s \cdot A_s \cdot (d_s - y_{yield\_str})^2 + n_f \cdot A_f \cdot (d_f - y_{yield\_str})^2$$

3.1.3 Yield moment resistance

$$M_{y\_str} := \frac{\sigma_y \cdot I_{onc}}{(d_s - y_{yield\_str}) \cdot n_s} \cdot 10^{-6} = 46.3$$

3.2-Calcualte the yield length $L_y := \frac{M_{u\_str} - M_{y\_str}}{M_{u\_str}} \cdot L_s = 127$

3.3 Calculate the shear shift $S := 1 \quad d_f = 243 \qquad t := 50$

3.4 Total embedment length $L_f := \text{ceil}\left(\frac{L_y + S + t}{10}\right) \cdot 10 = 430$

$L_{COP\_VHIEN} := L_s - L_f = 337$

3-Calculate debonding load corresponding to provided embedment length

Beam NSM4Aa $L_{COP1} := 300$

Beam NSM5Aa-NSM6Aa $L_{COP2} := 350$

$$\lambda_2 := \frac{L_s}{L_{COP2} + t + S} = 1.19$$

$$M_{COP2} := \lambda_2 \cdot M_{y\_str} = 55.23$$

$P_{db2} :=$ if $M_{COP2} \geq M_{u\_str}$

$\quad P_{u\_str}$

else if $M_{COP2} \leq M_{u\_unstr}$

$\quad P_{u\_unstr}$

else

$P_{db2} = 144 \quad kN$

$$\left\| 2 \cdot \frac{M_{COP2}}{L_s} \cdot 10^3 \right\|$$

Beam NSM6Aa $L_{COP3} := 350$

$$\lambda_3 := \frac{L_s}{L_{COP3} + t + S} = 1.19 \qquad M_{COP3} := \lambda_3 \cdot M_{y\_str} = 55.23$$

$$P_{db3} := \begin{cases} P_{u\_str} & \text{if } M_{COP3} \geq M_{u\_str} \\ P_{u\_unstr} & \text{else if } M_{COP3} \leq M_{u\_unstr} \\ \left\| 2 \cdot \frac{M_{COP3}}{L_s} \cdot 10^3 \right\| & \text{else} \end{cases}$$

$P_{db3} = 144 \quad kN$

Distance from support to COP to avoid end debonding

$$L_{COP} := \frac{L - \langle 2 \cdot L_f + \langle L - 2 \cdot L_s \rangle \rangle}{2} = 337\,mm$$

ACI's prediction

$$L_{ACI} := \frac{a_b \cdot b_b}{2 \cdot \langle a_b + b_b \rangle \cdot 6.9} \cdot \sigma_f = 672 \quad mm$$

$$L_{COP\_ACI} := L_s - L_{ACI} = 95 \quad mm$$

TR55's prediction

Mean tensile strength of concrete $f_{ctm} := 0.3 \cdot \langle f_c \rangle^{\frac{2}{3}} = 3.04 \quad MPa$

Characteristic tensile strength of concrete $f_{ctk} := 0.7 \cdot f_{ctm} = 2.13 \quad MPa$

Number of grooves $n := 1$

Effective perimeter of groove $b_{nothperim} := \langle a_b + 2\ b_b \rangle = 44 \quad mm$

1- Maximum tensile force the bond joint can bear

$$T_{nsm\_max} := 10 \cdot b_{nothperim} \sqrt{E_f \cdot A_f \cdot f_{ctk} \cdot 10^{-3}} \cdot 10^{-3} = 66.4 \quad kN$$

Minimum length of FRP corresponding to maximum tensile force the

$$L_{nsm\_max} := 0.135 \cdot b_{nothperim} \cdot \sqrt{\frac{E_f \cdot A_f \cdot 10^{-3}}{f_{ctk}}} = 421 \quad mm$$

2- Allowable tensile force to avoid concrete cover separarion

$$T_{nsm\_max\_lim} := 38 \cdot \sqrt{\frac{b}{n} \cdot E_f \cdot A_f \cdot f_{ctk} \cdot 10^{-3}} \cdot 10^{-3} = 70.3 \quad kN$$

3- Force in the FRP at rupture $T_{rupture} := A_f \cdot \sigma_f \cdot 10^{-3} = 139.1 \quad kN$

4- Maximum force allows to develop in the NSMR

$$T_{min} := min\left(T_{nsm\_max}, T_{nsm\_max\_lim}, T_{rupture}\right) = 66.42$$

$$l_{nsm}(T) := L_{nsm\_max} \cdot \left(1 - \sqrt{1 - \frac{T}{T_{nsm\_max}}}\right)$$

$$T_{nsm}\left(l_{nsm}\right) := T_{nsm\_max} \cdot \frac{l_{nsm}}{L_{nsm\_max}} \cdot \left(2 - \frac{l_{nsm}}{L_{nsm\_max}}\right)$$

However, due to $T_{nsm\_max\_lim} < T_{rupture}$, the force in FRP can not exceed $T_{nsm\_max\_lim}$. The failure of beam is controlled by concrete cover separation and the maximum strain in FRP cannot exceed

$$\varepsilon_{f\_failure} := \frac{T_{min}}{T_{rupture}} \cdot \varepsilon_{f\_max} = 0.0062$$

$$L_{f\_TR55a} := l_{nsm}\left(T_{nsm\_max\_lim}\right) \qquad l_{nsm} := 0, 10 .. L_{nsm\_max}$$

Guess Values

$x := y_{u\_str}$

$\varepsilon_c(x) := \frac{x \cdot \varepsilon_{f\_max}}{d_f - x}$

$\alpha(x) := -68711 \cdot \varepsilon_c(x)^2 + 464.79 \cdot \varepsilon_c(x) + 0.01$

$\gamma(x) := \left(1962.6 \cdot \varepsilon_c(x)^2 + 17.89 \cdot \varepsilon_c(x) + 0.33\right)$

Constraints

$f_c \cdot b \cdot x \cdot \alpha(x) - A_f \cdot E_f \cdot \varepsilon_{f\_failure} - A_s \cdot \sigma_y = 0$

Solve for

$y_{u\_str\_failure} := \text{find}(x)$

$y_{u\_str\_failure} = -46$

$$M_{u\_str\_TR55} := \left(A_s \cdot \sigma_y \cdot \left(d_s - 0.4 \cdot y_{u\_str\_failure}\right) + E_f \cdot A_f \cdot \varepsilon_{f\_failure} \cdot \left(d_f - 0.4 \cdot y_{u\_str\_failure}\right)\right) \cdot 10^{-6}$$

$M_{u\_str\_TR55} = 65.57 \quad kN.m$

Beam fails at load level

$$P_{u\_str\_TR55} := 2 \cdot \frac{M_{u\_str\_TR55}}{L_s} \cdot 1000 = 171 \quad kN$$

5- Calculation termination point

5a- At the maximum moment point

To avoid the end debonding the minimum L_{COP} need to be provided:

$$L_{f\_TR55a} = 421 - 101\mathrm{i} \qquad mm$$

Actual termination point from the support must smaller than

$$L_{COP\_TR55a} := L_s - S - L_{f\_TR55a} = 103 + 101\mathrm{i} \qquad mm$$

$$T_{nsm\_b} := \frac{M_{u\_unstr}}{M_{u\_str\_TR55}} \cdot \varepsilon_{f\_failure} \cdot A_f \cdot E_f \cdot 10^{-3} = 40.24 \quad kN$$

At the theoretical termination point

$$L_{f\_TR55b} := L_{nsm\_max} \cdot \left(1 - \sqrt{1 - \frac{T_{nsm\_b}}{T_{nsm\_max}}}\right) = 157 \quad mm$$

Theoretical termination point

$$L_t := \frac{M_{u\_str\_TR55} - M_{u\_unstr}}{M_{u\_str\_TR55}} \cdot L_s = 302.3 \quad mm$$

Distance from the termination point to the support

$$L_{COP\_TR55b} := L_s - \left(L_t + S + L_{f\_TR55b}\right) = 65 \qquad mm$$

The actual termination point of the NSMR is selected with the longest embedment length

$$L_{COP\_TR55} := min\left(L_{COP\_TR55a}, L_{COP\_TR55b}\right) = 65 + 101\mathrm{i} \qquad mm$$

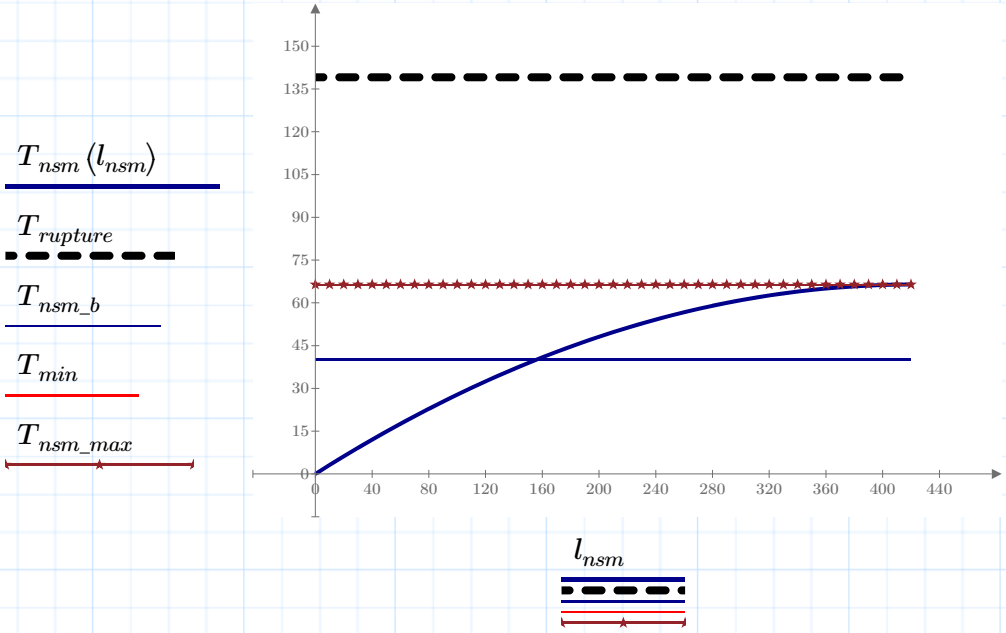

$$l_{nsm}(T) := L_{nsm\_max} \cdot \left(1 - \sqrt{1 - \frac{T}{T_{nsm\_max}}}\right)$$

$$T_{nsm}(l_{nsm}) := T_{nsm\_max} \cdot \frac{l_{nsm}}{L_{nsm\_max}} \cdot \left(2 - \frac{l_{nsm}}{L_{nsm\_max}}\right)$$

BeamNSM4Aa $L_{COP2} = 350$

$$T_{f\_NSM4Aa} := \frac{900 + S}{L_s} \cdot T_{nsm\_max} = 98.99$$

If rupture of the FRP occurs, the forces at the termination points (including the shear shift)

$$T_{max\_NSM4Aa} := \frac{L_{COP2} + S}{L_s} \cdot T_{rupture} = 107.5 \qquad l_{nsm}(T_{max\_NSM4Aa}) = 421.02 - 331.26\text{i}$$

$$T_{max\_NSM5Aa} := \frac{L_{COP3} + S}{L_s} \cdot T_{rupture} = 107.5 \qquad l_{nsm}(T_{max\_NSM5Aa}) = 421 - 331\text{i}\ mm$$

CALCULATION SHEET FOR DEBONDING CALCULATION

Input data

$b := 200$ $d_s := 250$ $d_f := 290$ $A_s := 500$ $h := 300$ $L_s := 1000$

$E_f := 150000$ $E_s := 210000$ $f_c := 35$ $\varepsilon_{c\_max} := 0.0035$ $E_c := 22 \cdot \left(\frac{f_c}{10}\right)^{0.3}$ $\sigma_y := 520$ $\varepsilon_{f\_max} := 0.01$

$n_s := \frac{E_s}{1000\ E_c}$ $n_s = 6.6$ $n_f := \frac{E_f}{1000\ E_c}$ $n_f = 4.7$

Strengthening level $\alpha := 1.6$

Calculate: AREA OF FRP

EMBEDMENT LENGTH

Constrains:

(a) Attain the requirement strengthening level

(b) Not allow IC debonding

(c) Not allow end debonding failure

(d) Not allow rupture of FRP before concrete crushing

(e) Provide sufficient ductility

(f) Service load of strengthened must be lower than the ultimate load of unstrengthened ones

---

1-Calculate the yield load and the ultimate load of the *unstrengthened beam*

2.1.1 Neutral axis depth at yield load $y_{y\_unstr} := \frac{-(n_s \cdot A_s) + \sqrt{(n_s \cdot A_s)^2 + 2 \cdot b \cdot (n_s \cdot A_s \cdot d_s)}}{b} = 75.6$

2.1.1 Neutral axis depth at ultimate load $y_{u\_unstr} := \frac{(A_s \cdot \sigma_y)}{0.8 \cdot b \cdot f_c} = 46.4$

2.1.2 Strain in the steel reinforcement at ultimate load

$\varepsilon_{su\_unstr} := \frac{d_s - y_{u\_unstr}}{y_{u\_unstr}} \cdot \varepsilon_{c\_max} = 0.015$

2.1.3 Equivalent moment of inertia $I_c := \frac{b \cdot y_{y\_unstr}^3}{3} + n_s \cdot A_s \cdot (d_s - y_{y\_unstr})^2 = 1.285 \cdot 10^8$

2.1.4 Yielding moment $M_{y\_unstr} := \frac{\sigma_y \cdot I_c}{n_s \cdot (d_s - y_{y\_unstr})} \cdot 10^{-6} = 58.45$

2.1.5 Ultimate moment resistance $M_{u\_unstr} := A_s \cdot \sigma_y \cdot (d_s - 0.4 \cdot y_{u\_unstr}) \cdot 10^{-6} = 60.2$

New required moment resistance $M_{u\_str\_design} := \alpha \cdot M_{u\_unstr} = 96.3$

3. Lower limit of FRP area to prevent IC debonding failure / rupture of FRP (constrains b, d)

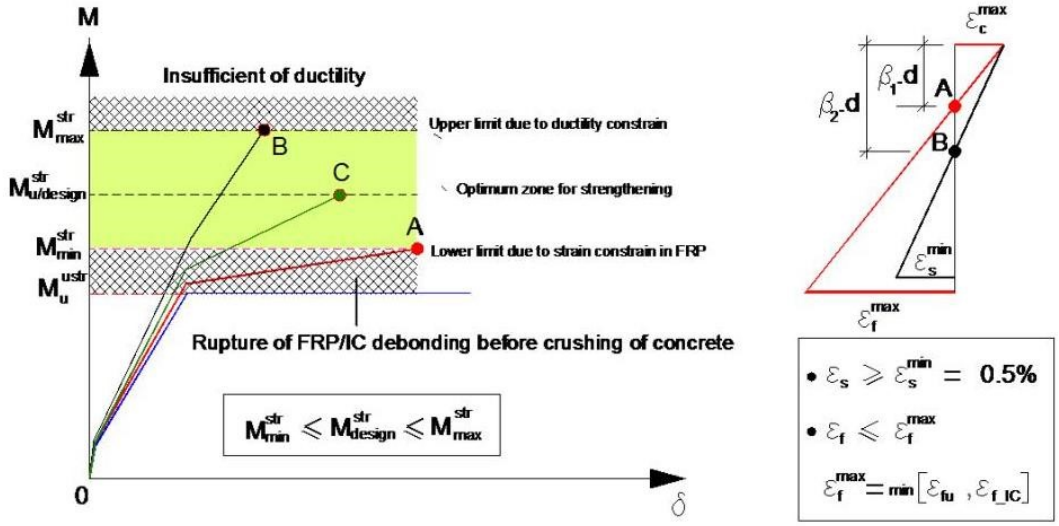

$$\beta_{min} := \frac{\varepsilon_{c\_max}}{\varepsilon_{f\_max} + \varepsilon_{c\_max}} = 0.259$$

3.1 Area of FRP

$$A_{fmin} := \text{root}\left(\frac{\left(A_s \cdot \sigma_y - \varepsilon_{c\_max} \cdot E_f \cdot A_f\right) + \sqrt{\left(A_s \cdot \sigma_y - \varepsilon_{c\_max} \cdot E_f \cdot A_f\right)^2 + 3.2 \cdot b \cdot f_c \cdot \varepsilon_{c\_max} \cdot E_f \cdot A_f \cdot d_f}}{1.6 \cdot b \cdot f_c} - \beta_{min} \cdot d_f, A_f\right)$$

$$A_{fmin} = 107.358$$

3.2 Moment resistance corresponding to the lower limits of FRP area

3.2.1 Neutral axis depth $y_{u\_str1} := \beta_{min} \cdot d_f = 75.185$

3.2.2 Strain in the FRP $\varepsilon_{f1} := \frac{d_f - y_{u\_str1}}{y_{u\_str1}} \cdot \varepsilon_{c\_max} = 0.01$

3.2.3 Ultimate moment resistance

$$M_{u\_str1} := \left(A_s \cdot \sigma_y \cdot \left(d_s - 0.4 \cdot y_{u\_str1}\right) + E_f \cdot A_{fmin} \cdot \varepsilon_{f1} \cdot \left(d_f - 0.4 \cdot y_{u\_str1}\right)\right) \cdot 10^{-6} = 99$$

3.2.4 Minimum strengthening level $\alpha_{min} := \frac{M_{u\_str1}}{M_{u\_unstr}} = 1.65$

$A_{fmin} :=$ if $A_{fmin} \le 0$, $bb \leftarrow 0$; else A_{fmin}

$\alpha_{min} :=$ if $A_{fmin} \le 0$, $bb \leftarrow 1$; else α_{min}

$$A_{fmin} = 107.358$$

4. Upper limit of the FRP area to maintain ductility of structures - constrain (e)

ε_{c_max}

$$\beta_{max} := \frac{\varepsilon_{c\_max}}{0.005 + \varepsilon_{c\_max}} = 0.412$$

4.1 Area of FRP

$$A_{fmax} := \text{root}\left(\frac{\left(A_s \cdot \sigma_y - \varepsilon_{c\_max} \cdot E_f \cdot A_f\right) + \sqrt{\left(A_s \cdot \sigma_y - \varepsilon_{c\_max} \cdot E_f \cdot A_f\right)^2 + 3.2 \cdot b \cdot f_c \cdot \varepsilon_{c\_max} \cdot E_f \cdot A_f \cdot d_f}}{1.6 \cdot b \cdot f_c} - \beta_{max} \cdot d_s, A_f\right)$$

$$A_{fmax} = 331.73$$

4.2 Moment resistance corresponding to the upper limits of FRP area

4.2.1 Neutral axis depth $y_{u\_str2} := \beta_{max} \cdot d_s = 102.941$

4.2.2 Strain in the FRP $\varepsilon_{f2} := \frac{d_f - y_{u\_str2}}{y_{u\_str2}} \cdot \varepsilon_{c\_max} = 0.006$

4.2.3 Ultimate moment resistance

$$M_{u\_str2} := \left(A_s \cdot \sigma_y \cdot \left(d_s - 0.4 \cdot y_{u\_str2}\right) + E_f \cdot A_{fmax} \cdot \varepsilon_{f2} \cdot \left(d_f - 0.4 \cdot y_{u\_str2}\right)\right) \cdot 10^{-6} = 133$$

4.2.4 Maximum strengthening level $\alpha_{max} := \frac{M_{u\_str2}}{M_{u\_unstr}} = 2.21$

---

5. Area of FRP $A_{f1} < A_f < A_{f2}$ attain the strengthening level-constrain (a)

5.1 Area of FRP

$$A_f := \frac{\left(A_{fmax} - A_{fmin}\right)}{2} \cdot \left(\frac{\left(\alpha - \alpha_{min}\right)^2}{\left(\alpha_{max} - \alpha_{min}\right)^2} + 1.2\,\frac{\alpha - \alpha_{min}}{\alpha_{max} - \alpha_{min}}\right) + A_{fmin} = 97.155$$

Select 3 strips 16mmx2mm

5.2 Check if the ultimate load of strengthened beam attains the required value

5.2.1 Neutral axis depth

$$y_{u\_str} := \frac{\left(A_s \cdot \sigma_y - \varepsilon_{c\_max} \cdot E_f \cdot A_f\right) + \sqrt{\left(A_s \cdot \sigma_y - \varepsilon_{c\_max} \cdot E_f \cdot A_f\right)^2 + 3.2 \cdot b \cdot f_c \cdot \varepsilon_{c\_max} \cdot E_f \cdot A_f \cdot d_f}}{1.6 \cdot b \cdot f_c} = 73.337$$

5.2.2 Strain in the steel

5.2.2 Strain in the steel

$$\varepsilon_{su\_str} := \frac{d_s - y_{u\_str}}{y_{u\_str}} \cdot \varepsilon_{c\_max} = 0.008$$

5.2.3 Strain in the FRP

$$\varepsilon_{fu\_str} := \frac{d_f - y_{u\_str}}{y_{u\_str}} \cdot \varepsilon_{c\_max} = 0.01$$

5.2.4 Ultimate moment resistance

$$M_{u\_str} := \left(A_s \cdot \sigma_y \cdot \left(d_s - 0.4 \cdot y_{u\_str}\right) + E_f \cdot A_f \cdot \varepsilon_{fu\_str} \cdot \left(d_f - 0.4 \cdot y_{u\_str}\right)\right) \cdot 10^{-6} = 96.7$$

6.2.5 Actual increase of ultimate moment resistance after strengthening

$$\frac{M_{u\_str}}{M_{u\_unstr}} = 1.606 \ > \ \alpha = 1.6 \qquad \text{OK}$$

7-Calcualte the embedment length of the NSMR, constrain (c)

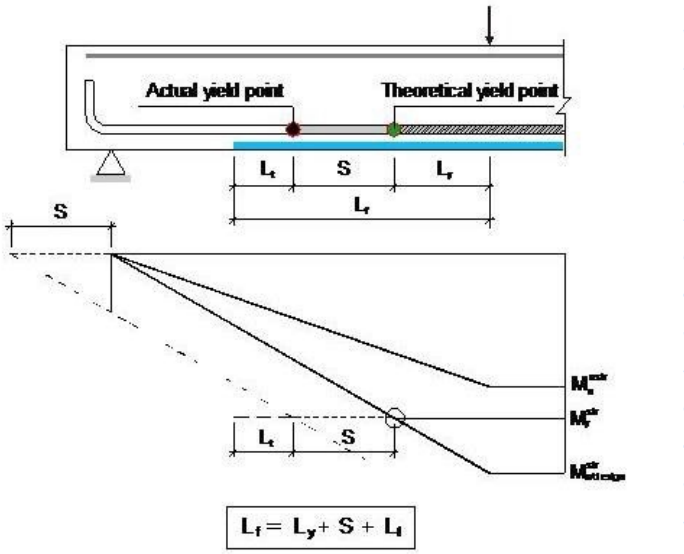

7.1 Yield load

7.1.1 Neutral axis depth

$$n_s = 6.555$$

$$y_{yield\_str} := \frac{-\left(n_s \cdot A_s + n_f \cdot A_f\right) + \sqrt{\left(n_s \cdot A_s + n_f \cdot A_f\right)^2 + 2 \cdot b \cdot \left(n_s \cdot A_s \cdot d_s + n_f \cdot A_f \cdot d_f\right)}}{b} = 80.6$$

7.1.2 Equivalent moment of inertia

$$y_{yield\_str} = 80.642$$

$$I_{onc} := \frac{b \cdot y_{yield\_str}^3}{3} + n_s \cdot A_s \cdot \left(d_s - y_{yield\_str}\right)^2 + n_f \cdot A_f \cdot \left(d_f - y_{yield\_str}\right)^2$$

7.1.3 Yield moment resistance

$$M_{y\_str} := \frac{\sigma_y \cdot I_{onc}}{\left(d_s - y_{yield\_str}\right) \cdot n_s} \cdot 10^{-6} = 69.75$$

7.2-Calcualte the yield length

$$L_y := \frac{M_{u\_str\_design} - M_{y\_str}}{M_{u\_str\_design}} \cdot L_s = 276$$

7.3 Calculate the shear shift $S := 1.2 \cdot d_f = 348$

7.4 Total embedment length $L_f := \text{ceil}\left(\frac{L_y + S + 150}{10}\right) \cdot 10 = 780$

$$L_f := \text{ceil}\left(\frac{L_y + 2 \cdot d_s}{10}\right) \cdot 10 = 780$$

---

8. Calculate the service load of the unstrengthened and strengthened beam-constrain (f)

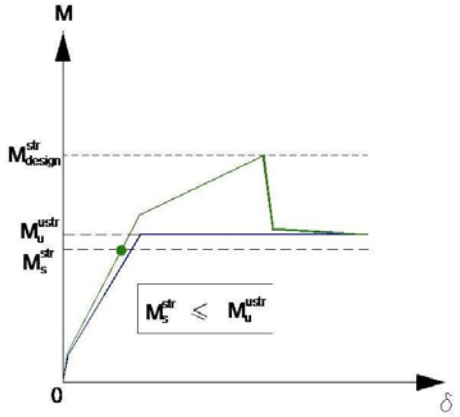

8.1 Calculate strain of concrete at service load fcs= 0.45fc

$x := 0$ $\varepsilon_{cs} := \text{root}\left(x \cdot \left(2 - \frac{x}{0.002}\right) - 0.0009, x\right) = 5.168 \cdot 10^{-4}$ $x_c := 0.5 \cdot d_s$

8.2 Un-strengthened beam

8.2.1 Neutral axis depth $y_{cs\_unstr} := \text{root}\left(\frac{0.45 \cdot f_c \cdot b \cdot x_c}{2} - A_s \cdot E_s \cdot \frac{d_s - x_c}{x_c} \cdot \varepsilon_{cs}, x_c\right) = 77.2$

8.2.2 Strain in the steel reinforcement

$$\varepsilon_{ss\_unstr} := \frac{d_s - y_{cs\_unstr}}{y_{cs\_unstr}} \cdot \varepsilon_{cs} = 0.0012$$

8.2.3 Service moment

$$M_{s\_unstr} := \left(A_s \cdot E_s \cdot \varepsilon_{ss\_unstr} \cdot \left(d_s - \frac{1}{3} \cdot y_{cs\_unstr}\right)\right) \cdot 10^{-6} = 27.3$$

8.3 Strengthened beam

3.3.1 Neutral axis depth

8.3.1 Neutral axis depth

$$y_{cs\_str} := \mathbf{root}\left(\frac{0.45 \cdot f_c \cdot b \cdot x_c}{2} - A_s \cdot E_s \cdot \frac{d_s - x_c}{x_c} \cdot \varepsilon_{cs} - A_f \cdot E_f \cdot \frac{d_f - x_c}{x_c} \cdot \varepsilon_{cs}, x_c\right) = 82.3$$

8.3.2 Strain in the steel reinforcement

$$\varepsilon_{ss\_str} := \frac{d_s - y_{cs\_str}}{y_{cs\_str}} \cdot \varepsilon_{cs} = 0.0011$$

8.3.2 Strain in FRP

$$\varepsilon_{fs\_str} := \frac{d_f - y_{cs\_str}}{y_{cs\_str}} \cdot \varepsilon_{cs} = 0.0013$$

8.3.2 Service moment

$$M_{s\_str} := \left(A_s \cdot E_s \cdot \varepsilon_{ss\_str} \cdot \left(d_s - \frac{1}{3} \cdot y_{cs\_str}\right) + E_f \cdot A_f \cdot \varepsilon_{fs\_str} \cdot \left(d_f - \frac{1}{3} \cdot y_{cs\_str}\right)\right) \cdot 10^{-6} = 29.61$$

8.4 Increase of service moment

$$\frac{M_{s\_str}}{M_{s\_unstr}} = 1.086$$

8.5 Check of if service moment is smaller than the ultimate moment of the unstrengthed beam

$$\frac{M_{s\_str}}{M_{u\_unstr}} = 0.492$$

8.6 For the case fracture of FRP/IC debonding before crushing of concrete

$$M_{u\_str\_design} = 96.274$$

To attain the desirable strengthening level, the area of FRP can be calculated by following equations

$$\alpha = 1.6 \qquad n := \frac{\alpha}{\alpha_{min}} = 0.972$$

Guess Values

$$A_f := n \cdot A_{fmin} \qquad x := 70 \qquad \varepsilon_c(x) := \frac{x \cdot \varepsilon_{f\_max}}{d_f - x}$$

$$\alpha(x) := -68711 \cdot \varepsilon_c(x)^2 + 464.79 \cdot \varepsilon_c(x) + 0.01$$

$$\gamma(x) := \left(1962.6 \cdot \varepsilon_c(x)^2 + 17.89 \cdot \varepsilon_c(x) + 0.33\right)$$

Constraints

$$f_c \cdot b \cdot x \cdot \alpha(x) - A_f \cdot E_f \cdot \varepsilon_{f\_max} - A_s \cdot \sigma_y = 0$$

$$A_f \cdot E_f \cdot \varepsilon_{f\_max} \cdot (d_f - x \cdot \gamma(x)) + A_s \cdot \sigma_y \cdot (d_s - x \cdot \gamma(x)) - M_{u\_str\_design} \cdot 10^6 = 0$$

Solver

$$a := \text{find}(A_f, x)$$

$$A_f := a_0 = 100.765 \qquad x := a_1 = 73.793$$

$$\frac{x \cdot \varepsilon_{f\_max}}{d_f - x} = 0.003$$

$$\alpha = 1.6 \qquad \alpha_{min} = 1.646$$

Approximation calculation

$$A_f := \frac{\langle A_{fmin} \rangle}{2} \cdot \left[\frac{(0.9\ \alpha - 1)^2}{(\alpha - 1)^2} + 1.5\ \frac{\alpha - 1}{\alpha_{min} - 1} \right] = 103.66$$

$$x := \text{root}\left[f_c \cdot b \cdot x \cdot \left[-68711 \cdot \left(\frac{x \cdot \varepsilon_{f\_max}}{d_f - x} \right)^2 + 464.79 \cdot \left(\frac{x \cdot \varepsilon_{f\_max}}{d_f - x} \right) + 0.01 \right] - A_f \cdot E_f \cdot \varepsilon_{f\_max} - A_s \cdot \sigma_y, x \right]$$

$$x = 74.61 \qquad \varepsilon_c := \frac{x \cdot \varepsilon_{f\_max}}{d_f - x} = 0.003$$

$$\gamma := \left(1962.6 \cdot \varepsilon_c^2 + 17.89 \cdot \varepsilon_c + 0.33\right)$$

$$M_{u\_str\_design} = 96.274$$

$$M := \left(A_f \cdot E_f \cdot \varepsilon_{f\_max} \cdot (d_f - x \cdot \gamma) + A_s \cdot \sigma_y \cdot (d_s - x \cdot \gamma)\right) \cdot 10^{-6} = 97.211$$